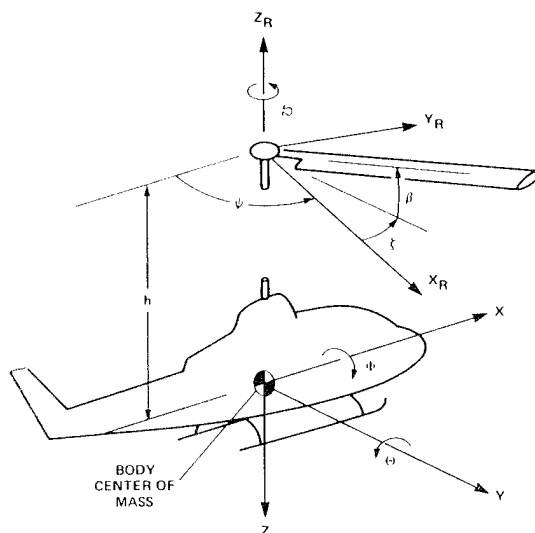
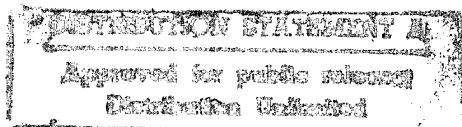


*Volume II—Materials and Structures,
Propulsion and Drive Systems, Flight
Dynamics and Control, and Acoustics*



19951215 082

*Proceedings of a conference held at
Ames Research Center
Moffett Field, California
March 17-19, 1987*



DPIC QUALITY INSPECTED 1

01 01
1 1
2 2
3 3
4 4
5 5
6 6
7 7

DISCLAIMER NOTICE



THIS DOCUMENT IS BEST QUALITY AVAILABLE. THE COPY FURNISHED TO DTIC CONTAINED A SIGNIFICANT NUMBER OF PAGES WHICH DO NOT REPRODUCE LEGIBLY.

NASA Conference Publication 2495

NASA/Army Rotorcraft Technology

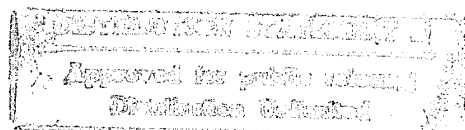
*Volume II—Materials and Structures,
Propulsion and Drive Systems, Flight
Dynamics and Control, and Acoustics*

Proceedings of a conference sponsored by
the Department of the Army and the National
Aeronautics and Space Administration and held at
Ames Research Center
Moffett Field, California
March 17-19, 1987



National Aeronautics
and Space Administration

Scientific and Technical
Information Division



1988

CONTENTS

Volume I

Introduction.....	1
Aerodynamics	
Summary.....	5
Accomplishments at NASA Langley Research Center in Rotorcraft Aerodynamics Technology.....	7
John C. Wilson	
The Developmeny of CFD Methods for Rotor Applications.....	34
F.X. Caradonna and W.J. McCroskey	
Dynamics and Aeroelasticity	
Summary.....	69
A Summary of Recent NASA/Army Contributions to Rotorcraft Vibrations and Structural Dynamics Technology.....	71
Raymond G. Kvaternik, Felton D. Bartlett, Jr. and John H. Cline	
A Review of Research in Rotor Loads.....	180
William G. Bousman and Wayne R. Mantay	
Comprehensive Rotorcraft Analysis Methods.....	312
Wendell B. Stephens and Edward E. Austin	
Rotorcraft Aeroelastic Stability.....	353
Robert A. Ormiston, William G. Warmbrodt, Dewey H. Hodges, and David A. Peters	

Volume II

Materials and Structures

Summary.....	533
Review of Fatigue and Fracture Research at NASA Langley Research Center.....	535
R.A. Everett, Jr.	
Delamination Durability of Composite Materials for Rotorcraft....	573
T. Kevin O'Brien	
Helicopter Crashworthiness Research Program.....	606
Gary L. Farley, Richard L. Boitnott, and Huey D. Carden	

For	
<input checked="" type="checkbox"/>	<input type="checkbox"/>
<input type="checkbox"/>	<input type="checkbox"/>
on	
on/	
ty Codes	
and/or	
dist	special
A-1	

Contents (continued)

Materials and Structures (continued)

Advanced Composite Airframe Program - Today's Technology.....	656
Danny E. Good and L. Thomas Mazza	

Propulsion and Drive Systems

Summary.....	681
Technology Developments for a Compound Cycle Engine.....	683
G.A. Bobula, W.T. Wintucky, and J.G. Castor	
Small Gas Turbine Engine Technology.....	698
Richard W. Niedzwiecki and Peter L. Meitner	
The Convertible Engine: A Dual-Mode Propulsion System for Advanced Rotorcraft.....	737
Jack G. McArdle	
Results of NASA/Army Transmission Research.....	769
John J. Coy, Dennis P. Townsend, and Harold H. Coe	
NASA's Rotorcraft Icing Research Program.....	802
Robert J. Shaw, John J. Reinmann, and Thomas L. Miller	

Flight Dynamics and Control

Summary.....	835
Helicopter Mathematical Models and Control Law Development for Handling Qualities Research.....	837
Robert T.N. Chen, J. Victor Lebacqz, Edwin W. Aiken, and Mark B. Tischler	
Rotorcraft Flight-Propulsion Control Integration.....	900
James R. Mihalow, Mark G. Ballin, and D.G.C. Rutledge	
Helicopter Human Factors Research.....	929
David C. Nagel and Sandra G. Hart	
Rotorcraft Handling-Qualities Design Criteria Development.....	948
Edwin W. Aiken, J. Victor Lebacqz, Robert T.N. Chen, and David L. Key	

Acoustics

Summary.....	1001
Recent Langley Helicopter Acoustics Contributions.....	1003
H.G. Morgan, S.P. Pao, and C.A. Powell	

Contents (continued)

Acoustics (continued)

Identification and Proposed Control of Helicopter Transmission Noise at the Source.....	1045
John J. Coy, Robert F. Handschuh, David G. Lewicki, Ronald G. Huff, Eugene A Krejsa, and Allan M. Karchmer	
A Decade of Aeroacoustic Research at NASA Ames Research Center...	1066
F.H. Schmitz, M. Mosher, C. Kitaplioglu, J. Cross, and I. Chang	
Aeroacoustic Research Programs at the Army Aviation Research and Technology Activity.....	1091
Yung H. Yu, Fredric H. Schmitz, and H. Andrew Morse	

Volume III

Systems Integration

Summary.....	1117
Status of NASA/Army Rotorcraft Research and Development Piloted Flight Simulation.....	1119
Gregory W. Condon and Terrence D. Gossett	
System Analysis in Rotorcraft Design - The Past Decade.....	1154
Thomas L. Galloway	
An Integrated Approach to Rotorcraft Human Factors Research.....	1167
Sandra G. Hart, E. James Hartzell, James W. Voorhees, Nancy M. Bucher, and R. Jay Shively	
Avionics Systems Integration Technology.....	1189
George Stech and James R. Williams	
Integrated Diagnostics.....	1211
Roger J. Hunthausen	

Research Aircraft

Summary.....	1233
Rotorcraft Flight Research with Emphasis on Rotor Systems.....	1234
W.J. Snyder	

Industry

Summary.....	1277
--------------	------

Contents (continued)

Industry (continued)

An Overview of Key Technology Thrusts at Bell Helicopter Textron.....	1279
Jim Harse, Jing G. Yen, and Rod Taylor	
Rotorcraft Technology at Boeing Vertol: Recent Advances.....	1341
John Shaw, Leo Dadone, and Robert Wiesner	
Recent Sikorsky R&D Progress.....	1395
Sikorsky Aircraft Division, United Technologies Corporation	
McDonnell Douglas Helicopter Company Independent Research and Development - Preparing for the Future.....	1450
A.C. Haggerty	
List of Conference Attendees.....	1485

MATERIALS AND STRUCTURES

Session Cochairmen:

H. Benson Dexter, NASA

T. Kevin O'Brien, Department of the Army

MATERIALS AND STRUCTURES SESSION

SUMMARY

The session opened with an overview of Materials and Structures Technology. Primary emphasis was on advanced composite materials because of their high performance potential. Recent developments in advanced aluminum-lithium alloys and superplastically forming of aluminum were also discussed. The overview indicated that up to 40 percent weight savings can be achieved with advanced composites in the next generation rotorcraft. However, composites technology is not mature and additional research is required to develop affordable, damage tolerant materials. In addition, advanced material forms and fabrication techniques that lend themselves to producibility and affordability must be developed.

Because of the fatigue failures commonly found in helicopter dynamic components, a review of metal fatigue and fracture research at NASA Langley was presented. Primary focus was on correlation of experimental fatigue and fracture data with various predictive methods. Additional research is required to accurately predict the response of advanced metallic materials under a variety of load spectra.

Since delamination is the most commonly observed failure mode in composite dynamic components of rotorcraft, a talk was presented on the delamination behavior of composite materials. A fracture mechanics approach for analyzing and characterizing composite delamination was presented. Strain energy release rate associated with delamination growth was shown to be useful in understanding and characterizing delamination of composites. Current efforts by government and industry to develop ASTM standard test methods for measuring interlaminar fracture toughness of composite materials were discussed. Results were presented that indicated that interlaminar fracture toughness of composite materials may be degraded due to cyclic fatigue loading.

Improved safety is a major concern for the next generation rotorcraft. Energy absorption capability and crashworthiness of composite fuselage structures were reviewed. Recent studies indicate that brittle composite materials can be configured to absorb more energy than comparable metallic materials. Results were presented for graphite and Kevlar composite materials and comparisons were made with aluminum. Composite sub-floor beam concepts that provide good energy absorption capability and post-crushing integrity were discussed. A simple analytical procedure that relates energy absorption of composite materials to the energy absorption of composite beam elements was presented.

A review of the U. S. Army Advanced Composite Airframe Program (ACAP) was presented. Design, fabrication, and testing methodologies utilized by Bell Helicopter Textron and Sikorsky Aircraft were discussed. Based on today's technology, both designs met the weight and cost goals developed by the U. S. Army. The results of ground flight tests were presented and a review of militarization test and evaluation efforts were presented. Additional tests are planned to determine crashworthiness of the composite airframes.

REVIEW OF FATIGUE AND FRACTURE RESEARCH AT
NASA LANGLEY RESEARCH CENTER

R. A. Everett, Jr.

U.S. Army Aerostructures Directorate, ARTA (AVSCOM)
NASA Langley Research Center

Most dynamic components in helicopters are designed with a safe-life, constant-amplitude testing approach that has not changed in many years. In contrast, the fatigue methodology in other industries has advanced significantly in the last two decades. Perhaps the helicopter industry should take a closer look at design methodology in other industries and at recent research findings to see if changes in their design methodology are warranted. The purpose of the current paper is to review recent research at the NASA Langley Research Center and U.S. Army Aerostructures Directorate at Langley relating to fatigue and fracture design methodology for metallic components. Most of the Langley research has been directed towards the damage tolerance design approach, but some work has been done that is applicable to the safe-life approach. The research areas to be discussed are identified in the following two paragraphs.

In the area of testing, damage tolerance concepts are concentrating on the "small-crack" effect in crack growth and the measurement of crack opening stresses. Current safe-life test programs pertain to developing correction factors to Miner's rule to account for the damage caused by ground-air-ground load cycles and using the local strain approach for determining fatigue life. Tests have also been conducted to determine the effects of a machining scratch on the fatigue life of a high strength steel.

In the area of analysis, work is concentrated on developing a crack closure model that will predict fatigue life under spectrum loading for several different metal alloys including a high strength steel that is often used in the dynamic components of helicopters. Work is also continuing in developing a three-dimensional, finite-element stress analysis for cracked and uncracked structures, as well as developing a boundary element method for cracked isotropic and anisotropic structures. A numerical technique for solving simultaneous equations called the multigrid method is being pursued to enhance the solution schemes in both finite-element analysis and boundary element analysis. Finally, a fracture mechanics project involving an elastic-plastic finite element analysis of the J-resistance curve is also being pursued.

Under the two major headings of testing and analysis, each of the above topics will be briefly discussed.

TESTING

Small-Crack Effect

The possibility of a "small-crack" effect in the crack growth process in metals was first revealed when Pearson (ref. 1) published his paper on the growth of very short cracks in aluminum alloys in 1971. In his work, he showed that the linear elastic stress intensity range(ΔK) did not correlate crack growth rate data for very small cracks(6 to 500 μm). In fact, his data showed that for the same ΔK values the so-called "small cracks" propagated at a much faster rate than the large cracks. Today, some researchers believe that this is an area where fracture mechanics breaks down and that a probabilistic approach using stress as a correlating factor is the best approach (ref. 2 and 3). However, other researchers believe that it just takes a proper analysis of this problem for fracture mechanics to work.

At NASA Langley, work has been done showing the effectiveness of fracture mechanics in the "small crack" regime with 2024-T3 aluminum alloy(ref. 4). The testing portion of this work has monitored the initiation and growth of small cracks(5 to 500 μm) at a semi-circular notch in 2024-T3 under constant-amplitude loading at a stress ratio of -1. Typical results from these tests are shown in figure 1 where data is presented in the form of crack growth rates versus ΔK for cyclic tests at a maximum gross stress of 80 MPa. As stated previously, these data show that at a given value of ΔK , crack growth rates for small cracks are much faster than the large crack data represented by the dashed line. The solid line in this figure represents an analytical prediction of these data calculated from a crack growth model developed by Newman(ref. 5). The Newman model uses large-crack growth rate data that has been adjusted to account for the effects of crack closure. In using this model to predict growth rates in the short-crack regime, the large-crack threshold behavior was ignored and an effective ΔK threshold behavior was defined as shown by the dash-dot line in Figure 1 (ref. 4). From photomicrographs, crack initiation was viewed to generally occur at inclusion particle clusters. These cracks appear to have initiated from defects caused by the separation of the alloy matrix material from an inclusion cluster(ref. 4).

Further tests generated life-to-failure data for constant-amplitude loading at stress ratios of -2,0, and 0.5 as well as under spectrum loading. Figure 2 shows the results at a stress ratio of 0.5 and the prediction made by the crack closure model of Newman. Very good agreement is shown between the experimental data and the analytical predictions.

Finally, in figure 3 experimental life-to-failure data generated under a fighter spectrum called FALSTAFF (ref. 6) shows good agreement for loading conditions that are more like an aircraft would experience. Again the solid curve is the life prediction made by the crack closure model (ref. 5).

The small-crack effect is also presently being studied using 4340 steel and 7075-T6 aluminum alloy. In the test program on 4340 steel, a helicopter load spectrum known as HELIX(ref. 7) is being used to generate crack growth data for loads more like the actual loading environment experienced by a hinged rotor helicopter. Study of the small-crack effect

in metals has a potentially large payoff, in that the fatigue process is being examined in the crack length regime where components spend most of their fatigue life.

Crack Opening Stress Measurements

In the study of crack growth in metallic structures, concepts from fracture mechanics have become the principle tools for analyzing cracked configurations. The use of concepts like stress intensity factors from fracture mechanics were first used to describe the behavior of fatigue crack growth when a fatigue crack was modeled by a zero-width saw cut. An elastoplastic analysis by Rice(ref. 8) of this idealised crack under cyclic tensile loading showed that the crack would not be fully closed upon unloading until the applied load was zero. However, experimental work by Elber(refs. 9 and 10) showed that a fatigue crack under cyclic loading would close upon unloading before the applied load reached zero. The stress level at which the crack will proceed to grow again is called the crack opening stress and is often different than zero. These crack opening stresses can be determined by experimental measurements and it is these measurements which are generally believed to be essential in the process of crack growth predictions(ref. 11). The crack opening stress is used in the calculation of the effective stress intensity range, ΔK_{eff} , which is believed to be the appropriate parameter for correlating crack growth rates under various loading conditions. An excellent review paper on fatigue crack closure by Schijve is given in reference 11.

In the determination of the large-crack stress intensity threshold, ΔK_{th} , it has been shown that ΔK_{th} is a function of the material and other test variables, the most significant of these being the stress ratio, R , and the environment(ref. 12). Previous work(ref. 13 and 14) has shown that this R dependency of ΔK_{th} is dramatically reduced if ΔK_{eff} is used as the appropriate concept of the stress intensity range. Recent tests at NASA Langley by Phillips(ref. 12) were conducted to evaluate the capability of ΔK_{eff} to correlate the large-crack stress intensity threshold using crack opening measurements to define ΔK_{eff} .

In these tests, near-threshold crack growth rates were generated using a manually-controlled, discrete-step load shedding method. In this method, after every increment of crack growth of 0.5 mm, the load was reduced by a fixed percentage of the previous value. The percentage load reductions were 6, 18, and 30 percent. These tests were conducted at stress ratios over a range of -2 to 0.7. Figure 4 shows the crack growth rate plotted against ΔK for several R values using the 6 percent load step reduction procedure. These data show the expected dependency of growth rates on R . In order to use ΔK_{eff} as the correlating parameter, opening loads were determined from load-displacement plots using a "reduced displacement" method(ref. 15). These data are shown in figure 5 as a function of the maximum fatigue cyclic load. When the data in figure 4 are replotted using ΔK_{eff} which is determined from the opening stress, the

data as shown in figure 6 do not show the systematic layering with R. The data in this figure also show a smaller scatter for ΔK . The difference in the capabilities of ΔK and ΔK_{eff} to correlate the threshold data is shown quite clearly in figure 7, where ΔK_{th} is plotted against the stress ratio. The $\Delta K_{eff_{th}}$ values are shown by the cross symbols which show a very small variation with R, whereas the square symbols which represent the ΔK_{th} values without stress opening considerations show an obvious dependency on R. In future tests the scatter in the measurements of the opening loads must be kept to a minimum in order to show the true capability of ΔK_{eff} in correlating crack growth results.

The accuracy of opening stress measurements will be the subject of future work conducted at Langley and a round-robin test program sponsored under task group E24.04.04 of ASTM. Other future work at Langley on stress opening measurements will measure crack opening stresses during spectrum loading. In this work, load spectra representative of both transport and fighter aircraft will be used in the testing of aluminum alloy specimens.

In the current understanding of fracture mechanics, K_{eff} appears to be a good parameter for correlating crack growth data. Therefore, accurate measurements of crack opening stresses as well as a thorough understanding of the role of these stresses in the fatigue process is an important part of the damage tolerant design methodology. If fracture mechanics concepts are going to enhance the fatigue design of helicopter components, the study of crack opening stresses must be pursued.

Fatigue Life of a Material With a Machining Scratch

As stated previously, the fatigue life of dynamic parts of helicopters is currently determined by a safe life analysis where stress versus life cycle curves are determined from constant amplitude tests on actual components. Because of the complex configuration of some components, machining scratches can be left on the surface of finished parts. If parts without scratches are used to define S-N curves and failures occur in service as a result of these scratches, the statistical validity of the predicted fatigue life is questionable.

To assess the effect of machining scratches on the fatigue life of 4340 high strength steel, constant amplitude fatigue tests were run on unnotched specimens with and without a 0.05mm (0.002 inch) deep machining scratch. Specimens with scratches that had been shot peened were also tested to see if the compressive residual stresses from the shot peening would provide any relief from the stress concentration caused by the scratch. The magnitude of the residual stresses produced by the shot peening was determined by x-ray diffraction measurements. To assess the effect of shot peening on the fatigue life of materials without machining imperfections, tests were also run on specimens that had been shot peened but contained no scratches.

Figure 8 shows some of the results of these tests where the alternating stress level, S_a , is plotted against fatigue life, N. As can be seen in this

figure the machining scratch caused about a 40% reduction in the material endurance limit. The tests on the specimens that had been shot peened showed that the compressive residual stresses produced by the shot peening almost eliminated the effects of the stress concentration caused by the scratch. For the specimens without machining imperfections that had been shot peened, only about a 10% increase in the endurance limit was noted. The x-ray diffraction measurements of the compressive residual stresses produced by the shot peening ranged from 414 MPa to 621 MPa (60 to 90 ksi). The compressive residual stresses reached a zero stress level at about 0.152 mm (0.006 inches) below the specimen surface.

These tests have shown that a machining scratch significantly reduces the fatigue strength of a high strength steel. However, shot peening was shown to negate the effects of the scratch. Analytically predicting the effects of residual stresses on fatigue life of components is still difficult due mainly to the difficulty in experimentally determining the level of residual stress. The X-ray diffraction technique is showing great promise in improving this situation, but before life predictions that account for residual stresses can be made with a high degree of confidence, joint analytical and experimental programs need to be undertaken that will prove the reliability of the X-ray diffraction measurements.

Ground-Air-Ground Correction Factor for Miner's Rule

In the safe life analysis of aircraft structures, a linear cumulative damage rule like the Miner rule is usually used to predict fatigue life. In spite of the many inadequacies in this type of analysis (ref. 16 to 19), no new theory has replaced the Miner analysis with any significant improvement. Various techniques have been used with the basic concept developed by Miner, in the hope of eliminating some of these inadequacies (ref. 20 to 22). One of the deficiencies of this analysis is its inability to account for sequence effects (load interaction) which are usually present in spectrum loading (ref. 17). In a recent survey of the helicopter industry a hypothetical fatigue life problem was posed that sought the calculation of the fatigue life of a component called the pitch link (ref. 23). In all of the proposed solutions (ref. 24 to 30), the linear cumulative damage theory formed the basis of the life predictions. Both cycle counting and peak value analysis of the flight loads were used to calculate fatigue life. However, because of the significant dissimilarities in methodology in the industry, ground-air-ground (GAG) cycles were not included in the problem.

Current research is being aimed at aiding the safe life designer with a method for including a correction factor in the Miner cumulative damage rule to account for the damage caused by GAG cycles. Simple spectrum block loading similar to that shown in figure 9 will initially be used to assess the upper bounds of the damage caused by these cycles. In an attempt to generalize these correction factors to more realistic load spectra, tests will also be conducted using the standardized helicopter load spectra known as HELIX and FELIX (ref. 7). Previous work has shown that when Miner's rule was used to predict the fatigue life of test coupons tested using the HELIX/FELIX spectra, the fatigue life was overestimated (ref. 31).

Local Strain Method for Predicting Fatigue Life

Over the last two decades a technique has been developed to predict fatigue life using safe-life methodology but concentrating on the area of the structure where maximum damage is actually being accumulated. This technique, called the local strain approach, calculates fatigue life based on the local strains at a notch(ref. 22 and 32). This method takes into account such factors as the mean stress, state of stress, and the effect of local notch plasticity. These factors are still combined into a linear cumulative damage analysis.

Tests are currently being conducted on 4340 steel using the load spectra called HELIX(ref. 7) to simulate the variable cyclic loading usually experienced by dynamic helicopter components. Actual air-to-air combat spectra will also be used as test loads. Test lives will be compared to lives predicted using the local strain approach.

These series of tests are concentrating on using load spectra as opposed to constant amplitude loads since a great weakness in the present design of helicopters is the lack of spectrum tests in the design process. For future work, actual load spectra from various helicopter components must be obtained, since as noted by Dowling(ref. 32), the uncertainties in predictions associated with the choice of a life estimation method may be small compared to the uncertainties which now exist in the definition of helicopter load spectra.

ANALYSIS

Crack Closure Model for Predicting Fatigue Life

As stated previously, the design of most fixed-wing aircraft structures is based on a damage tolerance approach where crack growth analysis is an essential part of the design process. Since about 1970, many crack growth models have been proposed to predict the life of structures. All of these models recognize the need to account for load interaction effects which cause such crack growth phenomena as retardation and acceleration and almost all are based on either crack tip plasticity or crack closure concepts(ref. 33). Two models based on the crack tip plasticity concept are those by Wheeler(ref. 34) and Willenborg(ref. 35). Almost all models based on the plasticity concept use one of these two models as their basis. The Wheeler model accounts for crack growth retardation by employing the concept of yield zone interaction. In this concept, crack growth is retarded if the yield zone of current loads lie within the boundaries of the yield zone of previous high loads. The Wheeler model uses a crack growth retardation parameter that includes an empirically determined constant which is dependent on the material and loading. The Willenborg model accounts for retardation by using the yield zone interaction concepts conceived by Wheeler to determine a so-called "effective" stress that reflects the stress reduction that occurs as a result of overloads. Neither of these models account for the possible counteracting effect on

retardation caused by negative peak loads. A model first developed by Johnson(ref. 36) in 1975 to account for retardation and acceleration, uses Forman's crack growth equation(ref. 37), but uses an "effective" stress ratio which is adjusted for each load cycle to account for load interaction. This model is known as the Multi-Parameter Yield Zone(MPYZ) model.

Crack growth models which account for the concept of the physical crack actually closing before the applied load reaches zero are known as crack closure models. The crack closure phenomena was first noted as a result of the non-linear load displacement behavior of a cracked sheet thus suggesting that the structure has a varying geometry which could only be explained by the crack closing prior to complete unloading(ref. 9). The crack closure crack growth models not only account for retardation and acceleration, but also for delayed retardation. As stated previously in this paper, a crack closure model developed by Newman(ref. 5) has also been used to model the behavior of the so-called "small-crack" effect(ref. 4).

The closure model developed by Newman(ref. 5) at NASA Langley, uses Elber's basic concept of the closure phenomena which states that only that portion of the cyclic load which is above the crack opening load causes the crack to grow. Thus the form of the stress intensity factor that is used to correlate crack growth data is called the effective stress intensity range, ΔK_{eff} , and is essentially calculated by using the difference between the maximum stress in the load cycle and the crack opening stress.

Newman's model uses a modified form of Dugdale's elastic-plastic solution(ref. 38) for stresses and displacements in a cracked body. In Newman's modification of Dugdale's model, plastic deformations at the crack tip are retained in the wake of the crack as it grows. This plastic wake is shown schematically in figure 10, where the shaded regions indicate material that has been plastically deformed. The plastic deformations in the wake cause the crack surfaces to come in contact before the unloading reaches zero. When the load is increased again, the applied stress at which the crack surfaces become fully separated(zero contact stress) is characteristically called the "crack opening stress". For a detailed description of Newman's closure model and how crack growth rates are calculated, see reference 5.

As an illustration of the ability of this model to correlate crack growth data under constant amplitude loading, figure 11 shows crack growth rates for 2219-T851 aluminum alloy at various stress ratios. The solid lines in this figure are a result of calculations using Newman's closure model and the dots are the experimental data points. The predicted crack growth curves are in good agreement with the experimental data. As an example of this model's ability to correlate data from spectrum load tests, figure 12 shows crack-length against load cycle data for a typical fighter spectrum. The specimens were subjected to the same spectrum, but with different load amplification factors(0.2, 0.3, and 0.4) applied to the spectrum loads. Again good agreement is shown between the predicted curves(dashed and solid lines) and the experimental data points when the α factor, which indicates the stress state, is accounted for. For further comparisons between experimental data and closure model predictions, see references 5 and 39.

The crack closure model is an excellent example of the ability of an analytical tool to predict the fatigue life of aircraft structures. As stated previously, this model is currently being used in the investigation of the small-crack effect in 4340 steel, a material often used in the design of helicopter dynamic rotor components.

Boundary-Force Method For Stress Analysis Of Cracked Plates

During the design process, stress analyses are performed to calculate stress concentration factors for holes or notches or stress intensity factors for cracks. Among today's analysis tools, the finite element method (FEM) appears to be the most widely used numerical analysis method. However, recently a new form of an indirect boundary element method (BEM) developed by Tan(ref. 40) at NASA Langley is seeing more widespread use because of its efficiency in modeling the structure which is being analysed. As opposed to the FEM, where usually a relative large number of elements are needed to accurately model the entire structure, in the BEM only the boundaries of the region of interest are modeled.

Two earlier BEMs proposed by Nisitani(ref. 41) and Isida(ref. 42) were called "body force" methods since the unknowns were body force densities in the x- and y- directions and a crack was modeled as a very slender elliptical notch. Tan's Boundary Force Method (BFM) uses Erodogan's analytical solution for concentrated forces and a moment in an infinite plate with a crack(ref. 43), thus, eliminating the need to model the crack. In the BFM, the unknowns are not only the concentrated forces in the x- and y- directions, but also the moments on each segment of the discretized boundaries. The essential differences between Tan's BFM and the other BEM's mentioned are in the fundamental solutions, the treatment of the boundary conditions, and the treatment of the crack faces. For a more detailed account of these differences see reference 40.

To compare the accuracy obtained by satisfying the boundary conditions in terms of resultant forces and moments to that of resultant forces only, a center crack tension specimen was analyzed using the two methods. Figure 13 shows the relative error of these two methods where the relative error is defined as

$$\text{Relative error} = \frac{K_{\text{computed}} - K_{\text{ref}}}{K_{\text{ref}}}$$

where K_{computed} is the stress intensity factor computed by either method and K_{ref} is the reference value taken from the literature. These data show that for the same number of degrees of freedom, Tan's "force and moment" formulation gives a solution which is more accurate. The data in figure 13 shows that Tan's method gives a solution within 1% of the reference solution with as few as 24 degrees of freedom.

Figure 14 shows the BFM solution of the stress-intensity factor for a crack located between four holes. This configuration simulates the effect of a stringer on a propagating crack. This is a rather complex configuration where few stress-intensity solutions are available. The solution shown in figure 14 predicts that the stress intensity will increase until the crack reaches the center-line of the hole at which point it decreases thus simulating the effect of the stringer on the propagating crack and showing the probable retarding of the crack growth and possibly its arrest.

Three-Dimensional Finite-Element Analysis for Cracked and Uncracked Bodies

Prior to the late 1970's, two-dimensional elastic analyses were usually used to calculate stress intensity factors. These analyses approximated the real crack environment being analysed by assuming the two-dimensional states of stress of either plane-stress or plane-strain. Since these states of stress are an engineering approximation of the actual three-dimensional problem, researchers have attempted to solve Navier's equations of equilibrium for the stress field near the crack front. Only a few successful solutions have been developed and these were limited to such crack configurations as the penny-shaped and elliptical crack in an infinite solid(ref. 44). Since the closed-form solutions proved to be very difficult to obtain, several numerical approximations were developed(ref. 45 to 47).

Of these approximate methods, the finite-element method has been the most widely used. However, in most of the finite-element solutions the stress intensity factors were calculated by using the crack-opening displacements and two-dimensional plane-strain assumptions. This approach is again an approximation of the real three-dimensional situation and is justified only near the middle of the specimen thickness where plane-strain conditions may exist. In 1977, Raju and Newman at NASA Langley published a paper on three-dimensional finite-element analysis using a nodal force method to calculate the mode I stress intensity factors along the crack front(ref. 48). This method does not require any prior assumptions of plane-strain or plane-stress. In this paper, Raju and Newman investigated the stress-intensity factor across the thickness for such commonly used fracture specimens as the center-crack tension, single- and double-edge-crack tension, and the compact tension specimen(shown in figure 15). An example of some of the results from this paper is shown in figure 16 for the single-edge-crack tension specimen. The figure shows that the stress-intensity factors are nearly uniform over most of the specimen thickness, but are lower than the plane-strain value near the free surface where the plane-strain assumptions would be questionable. For the rest of the results obtained by Raju and Newman, see reference 48.

In 1979 Raju and Newman continued their work on the analysis of the three-dimensional problem by developing stress-intensity factors for surface cracks(ref. 49). In this work, they modeled shallow and deep semi-elliptical surface cracks in plates subjected to uniform tension. Figure 17 shows the results of a convergence study for a deep semi-elliptic surface

crack. The two finest models give stress-intensity factors within about 1% of each other. In this work they also compared their finite-element results for an embedded elliptical crack with an exact solution developed by Green and Sneddon(ref. 50). In general, Raju and Newman's solution agreed with the exact solution within 1% along most of the crack front.

More recently, Newman and Raju(ref. 51) have presented a paper where stress-intensity-factor equations were developed for several crack configurations from stress-intensity-factors determined from three-dimensional finite-element analysis. Prior to this paper, most of the stress-intensity solutions for cracks have been from approximate analytical solutions where most of the results were for limited ranges of parameters and were presented in the form of curves or tables(ref. 52 to 54). Obviously, an equational form for the stress-intensity factors is preferred because it is easier to use than curves and tables. These equations were developed for tension and bending loads over a wide range of crack configuration parameters such as the ratio of the crack depth to plate thickness(a/t), the ratio of crack depth to crack length(a/c), the ratio of hole radius to plate thickness(r/t), and the effect of plate width, b . The crack configurations considered are shown in figure 18. These include an embedded semi-elliptical crack, a semi-elliptical surface crack, a quarter-elliptical corner crack, a semi-elliptical surface crack at a circular hole, and a quarter-elliptical corner crack at a circular hole in finite thickness plates. An example of the equational form for the embedded semi-elliptical crack is

$$K = S_t (\pi a/Q)^{1/2} F_e(a/c, a/t, c/b, \phi)$$

where S_t is the remotely applied stress, a is the crack depth, and Q is the shape factor for an ellipse and is given by the square of the complete elliptic integral of the second kind. The function F_e accounts for the influence of the crack shape(a/c), crack size(a/t), finite width(c/b), and the angular location(ϕ).

Multigrid Methods In Structural Mechanics

In the finite element method of structural analysis, it is necessary to solve large systems of simultaneous equations. Currently, these equations are usually solved using a direct solution technique such as Gaussian elimination or Cholesky decomposition. These solution techniques are essentially like solving the equation of a straight line, $y=mx+b$. For a structural problem with many degrees of freedom this can involve a large amount of computational time.

Recently, a paper published by Raju et al(ref. 55) at NASA Langley proposed the use of a solution technique called the multigrid method which has been used to solve certain classes of partial differential equations in the field of fluid mechanics(ref. 56 and 57). This method is an iterative technique which assumes an initial answer for the unknown nodal

displacements and iterates through an algorithm until the current estimate of the unknowns are within a predetermined tolerance (or error).

One of the main purposes in Raju's paper was to gain an understanding of the multigrid method for use in structural mechanics applications. Hence, in this paper the multigrid technique was applied to the finite element analysis of the deflections of a simply supported Bernoulli-Euler beam(ref. 55).

This work on the simply supported beam has laid the foundation for extending this work to two- and three-dimensional problems and to include problems in structural analysis where singularities exist such as those at the tip of a crack. The final goal is a black box algebraic multigrid solution package for finite element analysis that could be 10 times faster than the direct solution techniques currently used in finite element analysis.

J-Integral Resistance Curve for Ductile Materials

The stress intensity factor range, ΔK , which has been used effectively to correlate crack growth data in metal structures is generally limited to use in situations that can be described as small-scale yielding at the crack tip. This will be the case for most aircraft structures. However, in a situation where large amounts of plastic deformation occur a parameter called the J-integral is often used to correlate crack growth and fracture data(ref. 58 and 59). The J-integral is defined as the rate of change of the total potential energy of the specimen with respect to the crack length(ref. 60). In contrast to K, the J-integral depends on the amount of crack growth.

Currently, the test procedures for determining J-R curves (crack-growth resistance curves based on the J-integral) show a dependency on specimen type(ref. 61). Two specimens which are often used in determining J-R curves are the three-point bend specimen and the compact specimen, shown in figure 19. Because of the J-R curves dependency on specimen type a task group from ASTM Committee E24 was initiated to develop a test procedure that would give J-R curves that were not dependent on specimen configuration(ref. 62).

In 1980, a round robin test program was conducted in 19 laboratories to measure J-R curves on HY-130 steel plate to evaluate the tentative test procedure developed by the ASTM task group. Figure 20 shows curves from one of these laboratories for both the compact and the bend specimen. The lack of uniqueness shown by these data showed the need for further investigations.

Recent work at NASA Langley was initiated to analyze numerically the discrepancy between the compact and bend specimen J-R curves. The approach taken was to model the fracture process in the two specimens using a two-dimensional, elastic-plastic, finite-element computer program(ref. 63) with a critical crack-tip-opening displacement failure criterion(ref. 64). The results from the analysis are shown in figure 21. As seen in this figure,

up to the maximum load, the J curves calculated from this analysis agreed well for both specimen configurations.

CONCLUDING REMARKS

Most dynamic components in helicopters are designed with a safe-life, constant amplitude testing approach that has not changed in many years. In contrast, the fatigue methodology in other industries has advanced significantly in the last two decades. In this paper a review is presented of the current research at the NASA Langley Research Center and U.S. Army Aerostructures Directorate at Langley which might aid the helicopter industry in enhancing the fatigue and fracture design methodology for metallic components.

In the area of testing, Langley research has shown that "small" cracks do grow at stress intensity ranges below the so-called large crack threshold. Crack opening stress measurements have shown that when the stress intensity range is calculated using only the stress range above the crack opening stress, a good correlation of crack growth data is obtained. Further work has shown that a machining scratch (0.05 mm deep) can reduce the fatigue life of a high strength steel by 40%, but shot peening can almost eliminate the effects of the stress concentration caused by a scratch.

In the area of analysis, a crack closure model for predicting fatigue life has been developed and used to predict fatigue life for both constant-amplitude and spectrum loading. Since the ability of the crack closure model to predict fatigue life is dependent upon an accurate stress analysis, a three-dimensional finite element program has been developed to calculate the stress intensity factors needed in the closure model. A boundary force method for calculating stress intensity factors has also been developed. This method is more efficient in modeling the structure being analysed than the finite element method, since only the boundary of the structure needs to be modeled.

REFERENCES

1. Pearson, S.: "Initiation of Fatigue Cracks in Commercial Aluminum Alloys and the Subsequent Propagation of Very Short Cracks," Engineering Fracture Mechanics, Vol. 7, No. 2, 1975, pp. 235-247.
2. Ritchie, R. O. and Lankford, J.: "Overview of the Small Crack Problem", Proceedings of the Second Engineering Foundation International Conference/Workshop on Small Fatigue Cracks, 1986, pp. 1-5.

3. Nisitai, H.: "Behavior of Small Cracks in Fatigue and Relating Phenomena," Current Research on Fatigue Cracks, The Society of Materials Science, Japan, pp. 1-22.
4. Newman, J. C., Jr.; Swain, M. H.; and Phillips, E. P.: "An Assessment of the Small-Crack Effect for 2024-T3 Aluminum Alloy," Proceedings of the Second Engineering Foundation International Conference/Workshop on "Small Fatigue Cracks", 1986, pp. 427-452.
5. Newman, J. C., Jr.: "A Crack-Closure Model for Predicting Fatigue Crack Growth Under Aircraft Spectrum Loading," Methods and Models for Predicting Fatigue Crack Growth Under Random Loading, ASTM STP 748, eds. J.B. Chang and C.M. Hudson, 1981, pp. 53-84.
6. van Dijk, G. M. and de Jonge, J. B.: "Introduction to a Fighter Aircraft Loading Standard for Fatigue Evaluation FALSTAFF," NLR MP 75017U, May 1975.
7. Edwards, P. R. and Darts, J.: "Standardised Fatigue Loading Sequences for Helicopter Rotors (HELIX and FELIX) Part 1: Background and Fatigue Evaluation," Royal Aircraft Establishment, TR 84084, 1984.
8. Rice, J. R.: in Fatigue Crack Propagation, ASTM STP 415, 1967, p. 247.
9. Elber, W.: "Fatigue Crack Propagation," Ph.D. thesis, University of South Wales, Australia, 1968.
10. Elber, W.: "Fatigue Crack Closure Under Cyclic Tension," Engineering Fracture Mechanics, Vol. 2, No. 1, 1970, pp. 37-45.
11. Schijve, J.: "Fatigue Crack Closure, Observations and Technical Significance," keynote paper at the ASTM International Symposium on Fatigue Crack Closure, Charleston, S.C., May 1986.
12. Phillips, E.P.: "The Influence of Crack Closure on Fatigue Crack Growth Thresholds in 2024-T3 Aluminum Alloy," presented at the ASTM International Symposium on Fatigue Crack Closure in Charleston, S.C., May 1986.
13. Liaw, P.K.; Leax, T.R.; Swaminathan, V.P.; and Donald, J.K.: "Influence of Load Ratio on Near-Threshold Fatigue Crack Propagation Behavior," Scripta Metallurgica, Vol. 16, 1982, pp. 871-876.
14. Ohta, A.; Kosuge, M.; and Sasaki, E.: "Fatigue Crack Closure Over the Range of Stress Ratios from -1 to 0.8 Down to Stress Intensity Threshold Level in HT80 Steel and SUS304 Stainless Steel," International Journal of Fracture, Vol. 14, No. 3, June 1978, pp. 251-264.
15. Elber, W.: "Crack-Closure and Crack-Growth Measurements in Surface-Flawed Titanium Alloy Ti-6Al-4V", NASA TN D-8010, National Aeronautics and Space Administration, Washington, D.C., Sept. 1975.

16. Jacoby, G.: "Comparison of Fatigue Life Estimation Processes for Irregularly Varying Loads," Proceedings of the Third Conference on Dimensioning, Budapest, 1968.
17. Gassner, E. and Lipp W.: "Long Life Random Fatigue Behavior of Notched Specimens in Service, in Service Duplication Tests, and in Program Tests," ASTM STP 671, Nov. 1977.
18. Shutz, W.: "The Prediction of Fatigue Life in the Crack Initiation and Propagation Stages - A State of the Art Survey," Engineering Fracture Mechanics, Vol. 11, No. 2, 1979.
19. Ryan, J.P.; Berens, A.P.; Coy, R.G.; and Roth, G.J.: "Helicopter Fatigue Load and Life Determination Methods," U.S. Army Air Mobility Research and Development Laboratory, Ft. Eustis, Va., USAAMRDL-TR-75-27, 1975.
20. Haibach, E.: "Fatigue Life Prediction By Amplitude Transformation," Fracture 1977, Vol. 2, ICF4.
21. Buch, A.: "Improvement of Fatigue Life Prediction Accuracy for Various Loading Spectra By Use of Correction Factors," Technion Israel Institute of Technology, TAE No. 581, Nov. 1985.
22. Dowling, N.E.: "A Discussion of Methods for Estimating Fatigue Life," proceedings of SAE Fatigue Conference, Fatigue Conference and Exposition, April 1982.
23. Arden, R.W.: "Hypothetical Fatigue Life Problem," American Helicopter Society Specialists Meeting on Helicopter Fatigue Methodology sponsored by the Midwest Region, preprint no. 18, 1980.
24. Stievenard, G.: "Hypothetical Fatigue Life Problem Application of Aerospace Method," American Helicopter Society Specialists Meeting on Helicopter Fatigue Methodology sponsored by the Midwest Region, preprint no. 19, 1980.
25. Aldinio, G. and Alli, A.: "The Agusta's Solution of AHS'S Hypothetical Fatigue Life Problem," American Helicopter Society Specialists Meeting on Helicopter Fatigue Methodology sponsored by the Midwest Region, preprint no. 20, 1980.
26. McCloud, G.W.: "A Method of Determining Safe Service Life for Helicopter Components," American Helicopter Society Specialists Meeting on Helicopter Fatigue Methodology sponsored by the Midwest Region, preprint no. 21, 1980.
27. Thompson, G.H.: "Boeing Vertol Fatigue Life Methodology," American Helicopter Society Specialists Meeting on Helicopter Fatigue Methodology sponsored by the Midwest Region, preprint no. 22, 1980.
28. McDermott, J.: "Hughes Helicopters-Fatigue Life Methodology," American Helicopter Society Specialists Meeting on Helicopter Fatigue Methodology sponsored by the Midwest Region, preprint no. 23, 1980.

29. Hardensen, L.P.: "Fatigue Life Prediction of Helicopter Pitch Link Using Kaman Life Calculation Methods," American Helicopter Society Specialists Meeting on Helicopter Fatigue Methodolgy sponsored by the Midwest Region, preprint no. 24, 1980.
30. Altman, B. and Pratt, J.: "The Challenge of Standardizing Fatigue Methodology," American Helicopter Society Specialists Meeting on Helicopter Fatigue Methodology sponsored by the Midwest Region, preprint no. 25, 1980.
31. Edwards, P.R.: "A Description of Helix and Felix, Standard Fatigue Loading Sequence for Helicopters, and of Related Fatigue Tests Used to Assess Them," Ninth European Rotorcraft Forum, Stresa Italy, 1983.
32. Dowling, N.E.: "Fatigue Failure Predictions for Complicated Stress-Strain Histories," Journal of Materials, Vol. 7, No.1, 1972, pp. 71-87.
33. Ewalds, H.L. and Wanhill, R.J.H.: Fracture Mechanics, Edward Arnold and Delftse Uitgevers Maatschappij Ltd, The Netherlands, 1984.
34. Wheeler, O.E.: Journal of Basic Engineering, Transactions of American Society of Mechanical Engineers, Series D, Vol. 94, No.1, 1972, p. 181.
35. Willenborg, J.D.; Engle, R.M., Jr.; and Wood, H.A.,: "A Crack Growth Retardation Model Using Effective Stress Concept," AFFDL-TM-71-1-FBR, Jan. 1971.
36. Johnson, W.S.: "CGR, An Improved Computerized Model to Predict Fatigue Crack Growth Under Spectrum Loading, NSRDC Report 4577, Jan. 1975.
37. Foreman, R.G.; Kearney, V.E.; and Engle, R.M.: Journal of Basic Engineering, Transactions of American Society of Mechanical Engineers, Series D, Vol. 89, No. 3, Sept. 1967, pp. 459-464.
38. Dugdale, D.S.: "Yielding of Steel Sheets Containing Slits," Journal of the Mechanics of the Physics of Solids, Vol. 8, 1960.
39. Newman, J.C., Jr.: "Prediction of Fatigue Crack Growth under Variable-Amplitude and Spectrum Loading Using a Closure Model," ASTM STP 761, 1982, pp. 255-277.
40. Tan, P.W.; Raju, I.S.; and Newman, J.C., Jr.: "Boundary Force Method for Analyzing Two-Dimensional Cracked Bodies," NASA TM-87725, May 1986.
41. Nisitani, H.: "Two-Dimensional Problems Solved Using A Digital Computer," Journal of Jap. Soc. Mech. Engrs., Vol. 70, No. 580, 1967, pp. 627-635.
42. Isida, M.: "A New Procedure of the Body Force Method with Applications to Fracture Mechanics," Numerical Methods in Fracture Mechanics; Proceedings of the First International Conferences, Swansea, Wales, Jan. 1978, pp. 81-94.

43. Erodogan, F.: "On the Stress Distribution in a Plate with Collinear Cuts Under Arbitrary Loads," Proceedings of the Fourth U.S. National Congress of Applied Mechanics, 1962, pp. 547-553.
44. Kassir, M.K. and Sih, G.C.: "Three Dimensional Stress Distribution Around an Elliptical Crack Under Arbitrary Loadings," Trans. ASME, Ser. E, Journal of Applied Mechanics, Vol. 33, No. 3, Sept. 1966, pp. 601-611.
45. Cruse, T.A. and Vanburen, W.: "Three-Dimensional Elastic Analysis of a Fracture Specimen With an Edge Crack," International Journal of Fracture Mechanics, Vol. 7, No. 1, March 1971, pp. 1-15.
46. Tracey, D.M.: "Finite Elements for Three-Dimensional Elastic Crack Analysis," Nuclear Engineering and Design, Vol. 26, No. 2, 1974, pp. 282-290.
47. Atluri, S. and Kathiresan, K.: "An Assumed Displacement Hybrid Finite Element Model for Three-Dimensional Linear-Fracture-Mechanics Analysis," proceedings off the 12th Annual Meeting of the Society of Engineering Science, 1975, pp. 391-399.
48. Raju, I.S. and Newman, J.C., Jr.: "Three-Dimensional Finite-Element Analysis of Finite-Thickness Fracture Specimens," NASA TN D-8414, 1977.
49. Raju, I.S. and Newman, J.C., Jr.: "Stress-Intensity Factors for a Wide Range of Semi-Elliptical Surface Cracks in Finite-Thickness Plates," Engineering Fracture Mechanics, Vol. 11, No. 4, 1979, pp. 817-829.
50. Green, S.E. and Sneddon, I.N.: "The distribution of Stress in the Neighborhood of a Flat Elliptical Crack in an Elastic Solid," proceedings of Cambridge Phil. Soc. 46, 1959.
51. Newman, J.C., Jr. and Raju I.S.: "Stress-Intensity Factor Equations for Cracks in Three-Dimensional Finite Bodies Subjected to Tension and Bending Loads," Computation Methods in the Mechanics of Fracture, Vol. 2 in Computational Methods in Mechanics, (ed.) Atluri, S.N., 1986.
52. Smith, F.W.; Emery, A.F.; and Kobayashi, A.S.: "Stress Intensity Factors for Semi-Circular Cracks, Part 2-Semi-Infinite Solid," Journal of Applied Mechanics 34, No.4, Trans. ASME, Vol. 89, Series E, 1967, pp. 953-959.
53. Heliot, J.; Labbens, R.; and Pellissier-Tanon, A.: "Benchmark Problem No. 1 - Semi-Elliptical Surface Crack," Int. Journal of Fracture 15, 1979, R197-R202.
54. Nishioka, T. and Atluri, S.N.: "Analytical Solution for Embedded Elliptical Cracks, and Finite Element-Alternating Method for Elliptical Surface Cracks, Subjected to Arbitrary Loadings," Engineering Fracture Mechanics, 17 1983, pp.247-268.
55. Raju, I.S.; Bigelow, C.A.; Ta'asan, A.; and Hussaini, M.Y.: "Multigrid Methods in Structural Mechanics," NASA TM-87761, July 1986.

56. Brandt, A.: "Multigrid Techniques: 1984 Guide with Applications to Fluid Dynamics," Monograph, Available as GMD-Studie No. 85 form GMD-FlT, Postfach 1240, D-5205, St. Augustin 1, W. Germany.
57. Jameson, A.: "Solution of the Euler Equations for Two Dimensional Transonic Flow by a Multigrid Method," Applied Math. and Comp., Vol. 13, 1983, pp.327-355.
58. Irwin, G.R.: "Fracture", Encyclopedia of Physics, S. Flugge (ed.), Vol. 6, Springer, Berlin, 1958, pp. 551-590.
59. Rice, J.R.: "A Path Independent Integral and the Aproximate Analysis of Strain Concentrations by Notches and Cracks," Journal of Applied Mechanics, Transactions of ASME, Vol. 90, Series E, No. 2, 1968, pp. 379-386.
60. Broek, D.: Elementary Engineering Fracture Mechanics, Martinus Nijhoff Publishers, The Hague, 1983.
61. Newman, J.C., Jr.; Booth, B.C.; and Shivakumar, K.N.; "An Elastic-Plastic Finite-Element Analysis of the J-Resistance Curve Using A CTOD Criterion," presented at the Eighteenth National Symposium on Fracture Mechanics, Univ. of Colorado, 1985.
62. Albrecht, P.; Andrews, W.R.; Gudas, J.P.; Joyce, J.A.; Loss, F.J.; McCage, D.E.; Schmidt, D.W.; and VanDerSlugs, W.A.; "Tentative Test Procedure for Determining the Plane Strain J(I)-R Curve," Journal of Testing and Evaluation, JTEVA, Vol. 10, No. 6, Nov. 1982, pp. 252-262.
63. Newman, J.C., Jr.: "Finite-Element Analysis of Fatigue Crack Propagation - Including the Effects of Crack Closure," Ph.D. Thesis, Virginia Polytechnic Institute and State University, May 1974.
64. Newman, J.C., Jr.: "Finite-Element Analysis of Initiation, Stable Crack Growth, and Instability Using a Crack-Tip-Opening Displacement Criterion," NASA TM-84564, Oct. 1982.

CRACK-GROWTH RATES FOR SMALL CRACKS

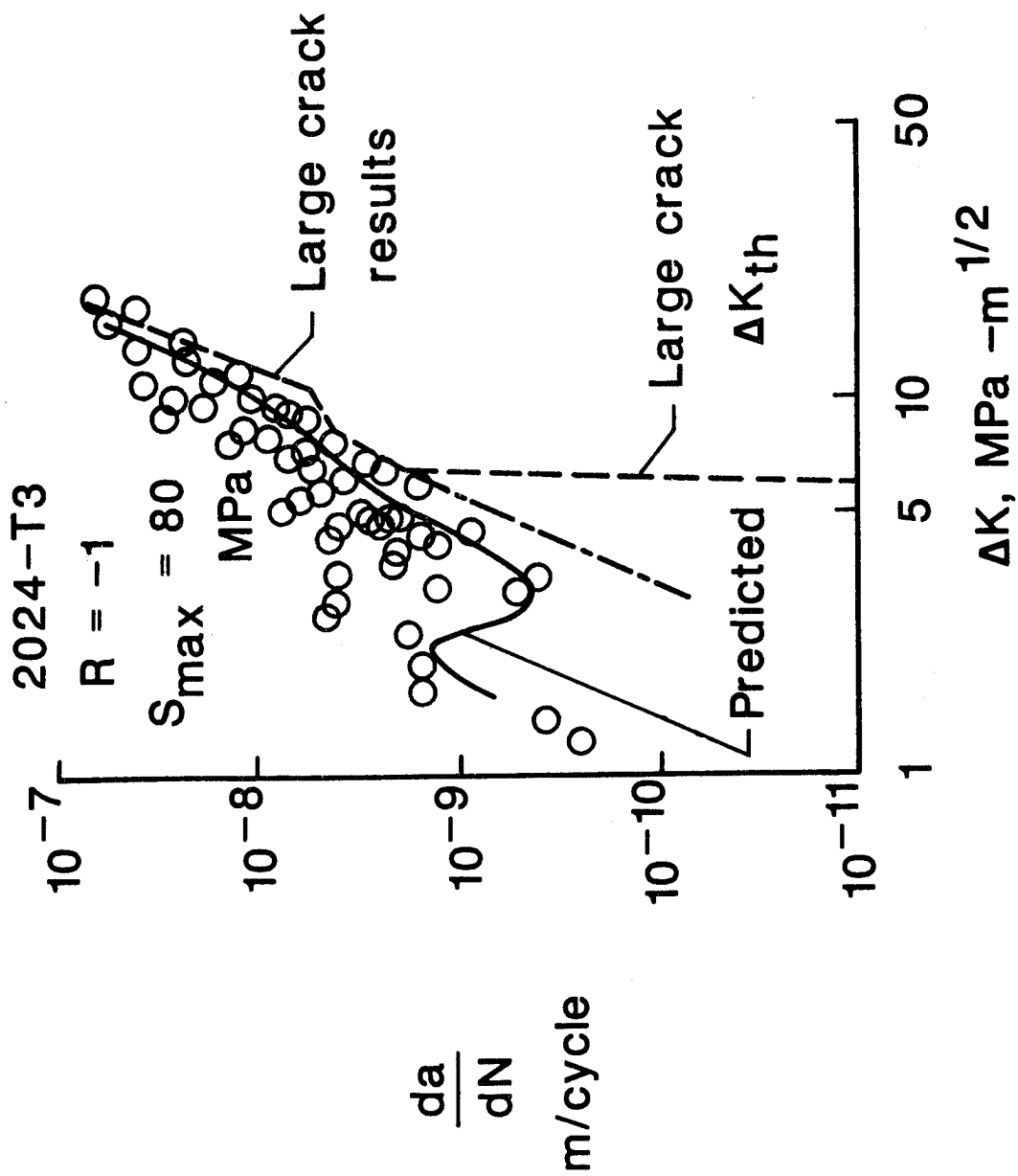


Figure 1.

LIFE-TO-FAILURE DATA FOR NOTCHED SPECIMENS

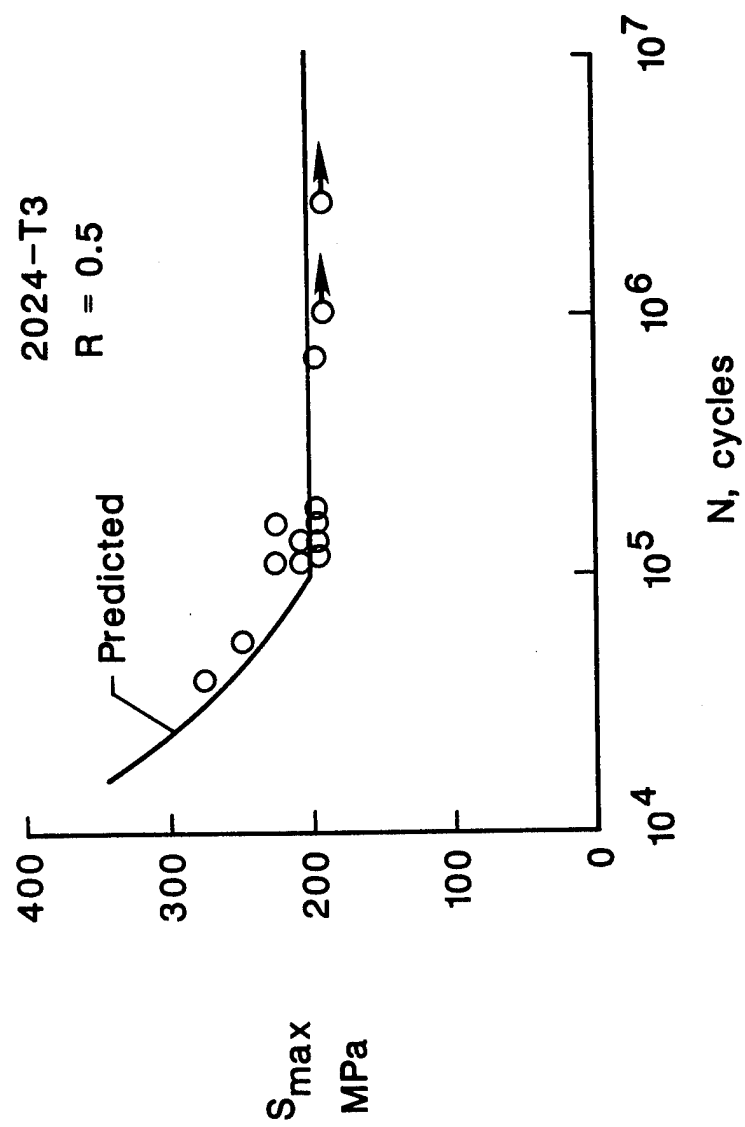


Figure 2.

LIFE-TO-FAILURE DATA FOR A FIGHTER SPECTRUM

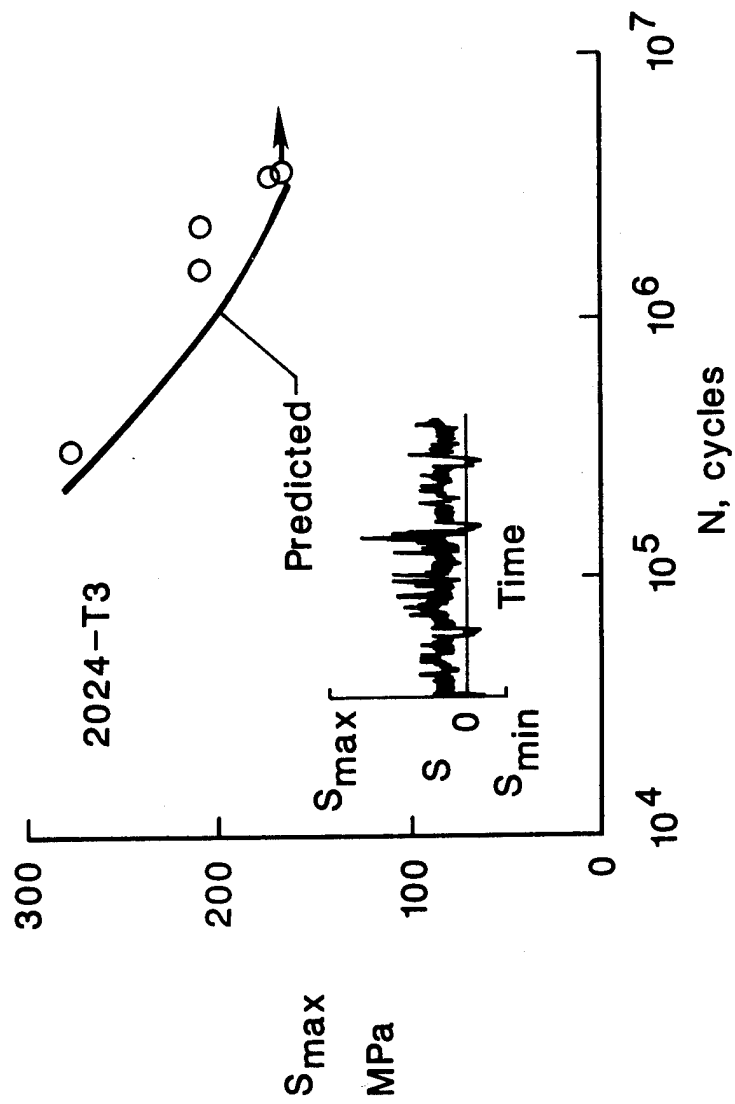


Figure 3.

CRACK GROWTH RATES AT SEVERAL STRESS RATIOS **6% LOAD REDUCTION**

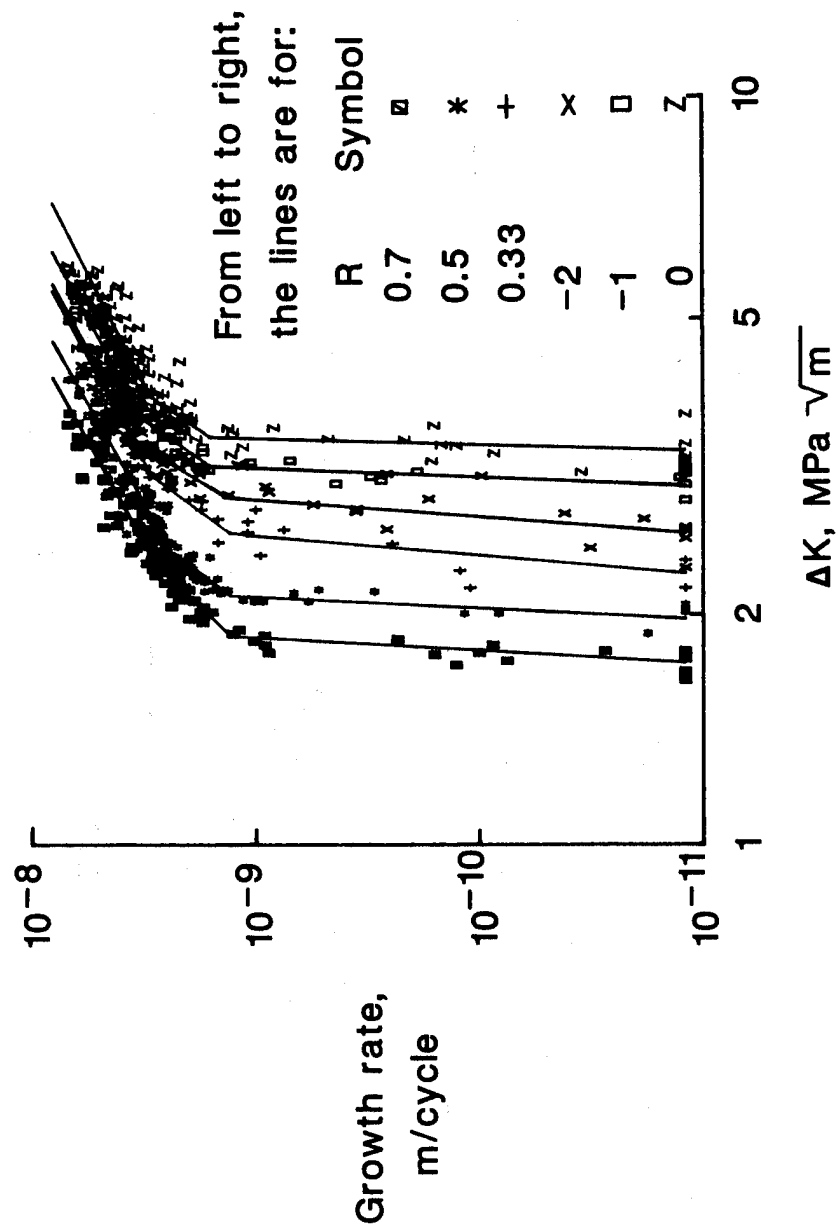


Figure 4.

CRACK OPENING LOADS AT SEVERAL STRESS RATIOS

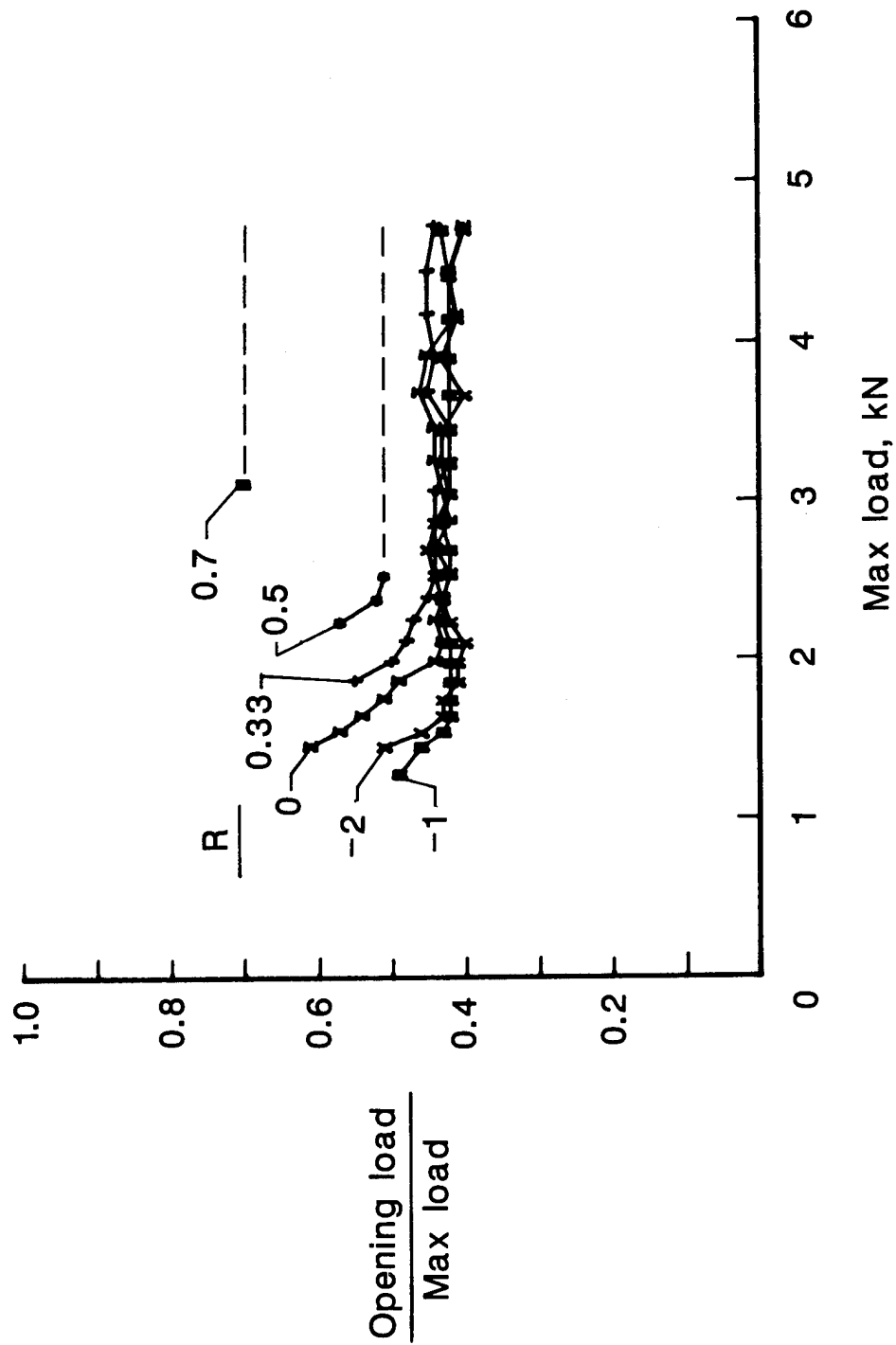


Figure 5.

CRACK GROWTH RATES AT SEVERAL STRESS RATIOS

USING ΔK_{eff}

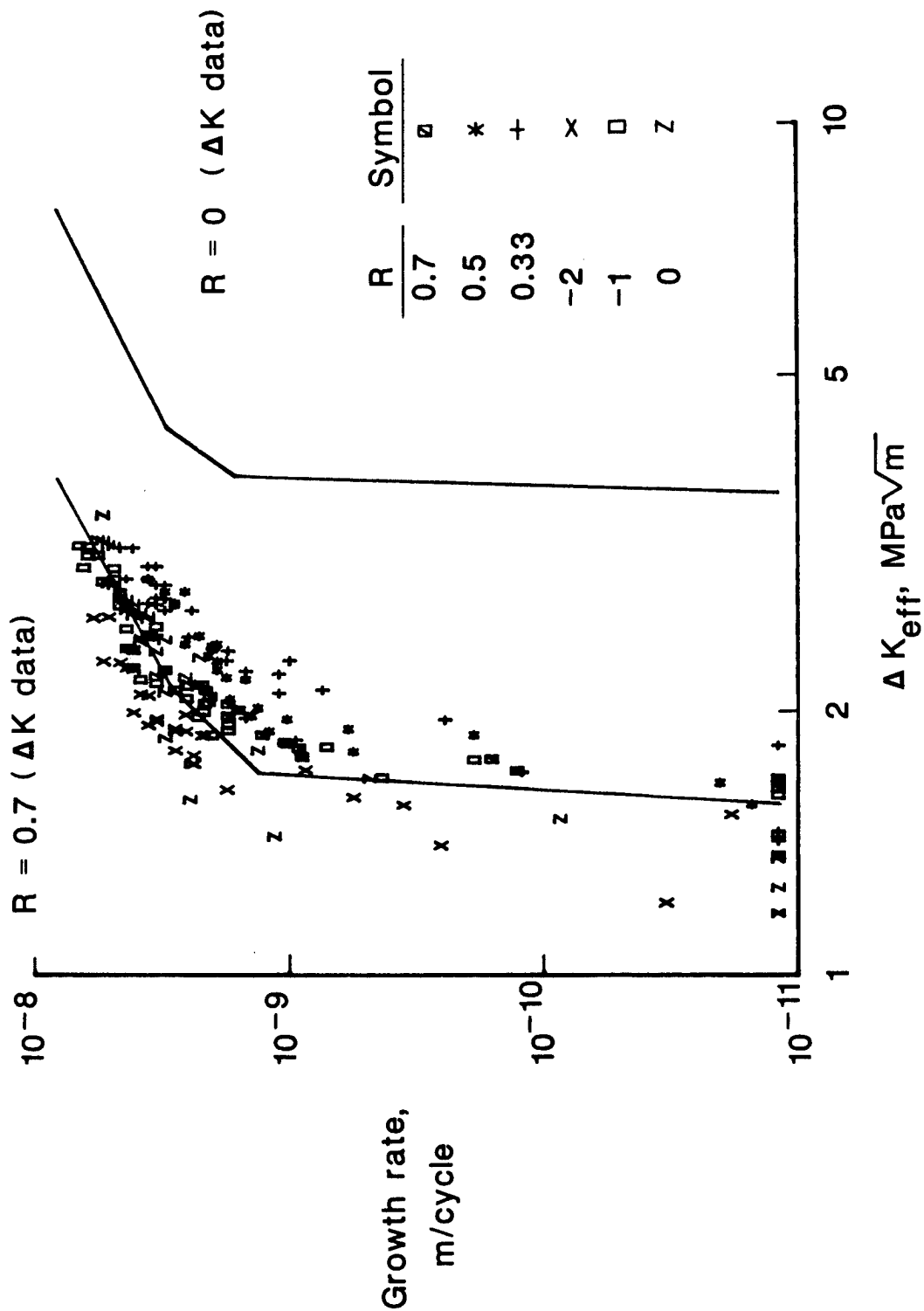


Figure 6.

THRESHOLD ΔK AND ΔK_{eff} VALUES WITH STRESS RATIO

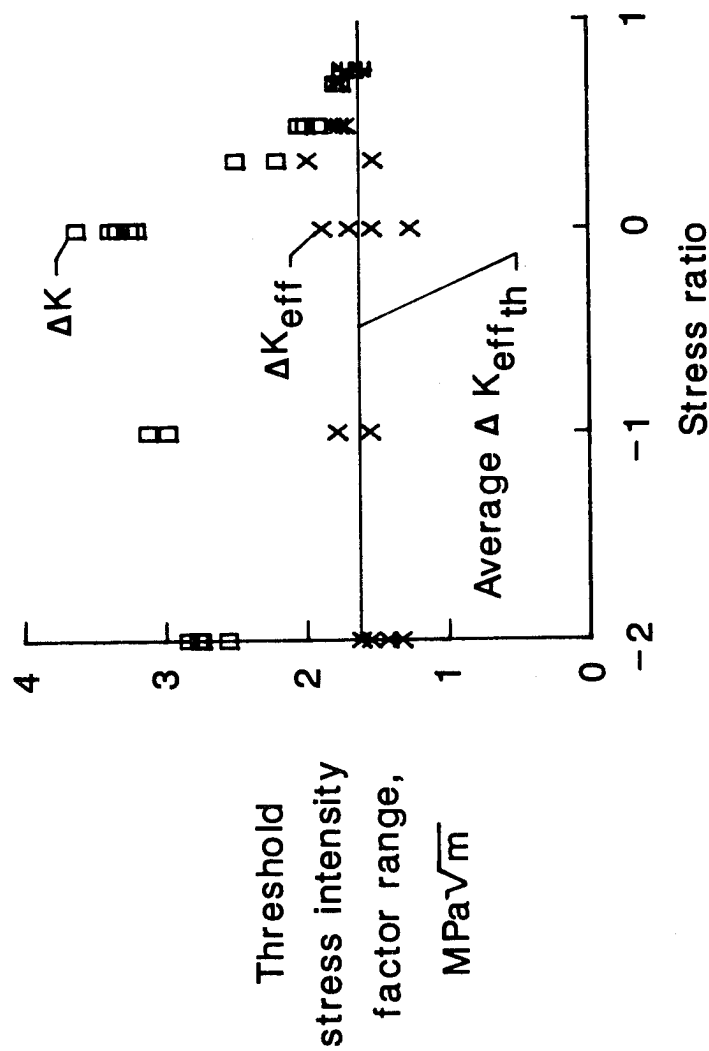


Figure 7.

EFFECT OF MACHINING SCRATCH ON LIFE-CYCLES-TO FAILURE

4340 STEEL

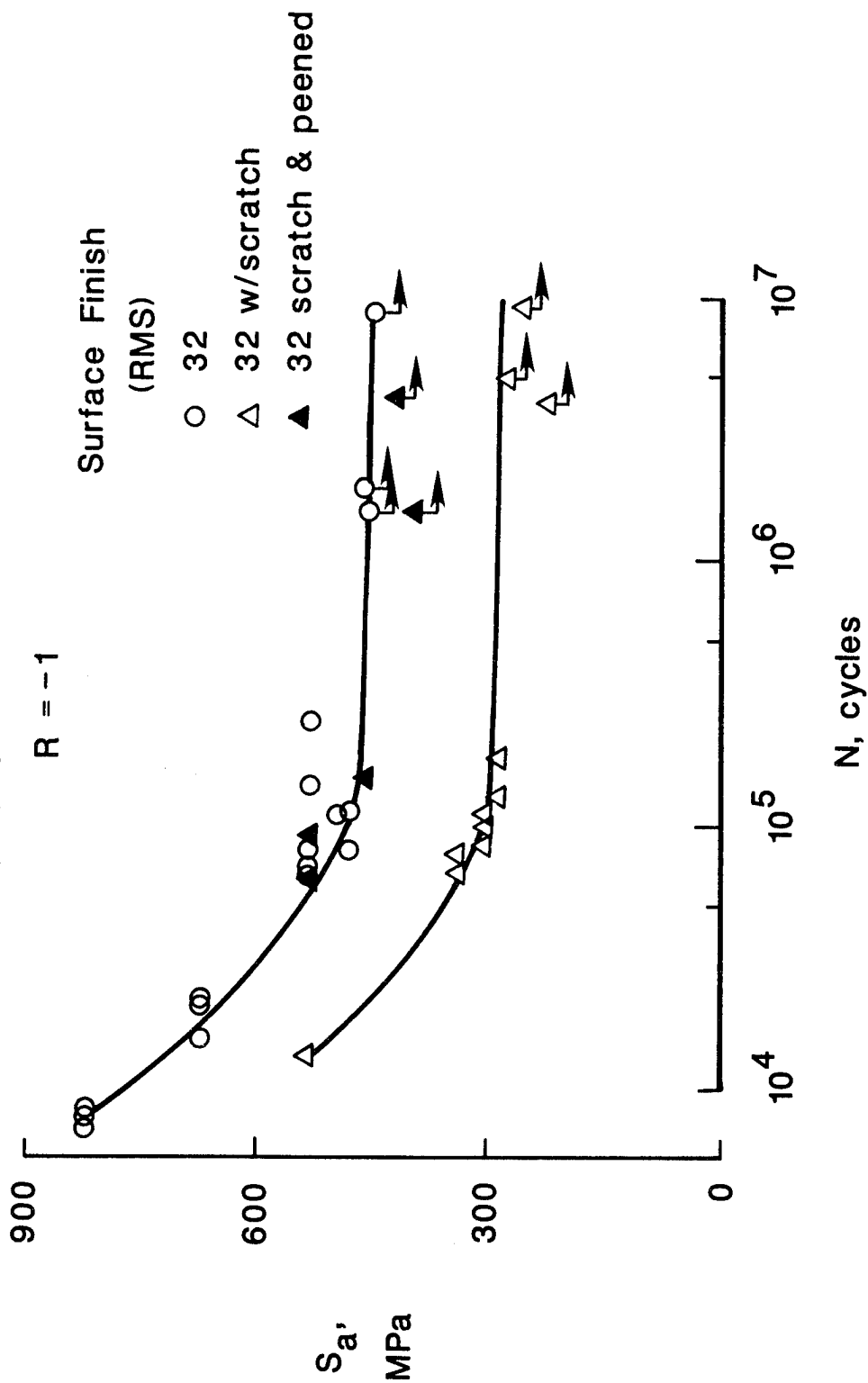
$$\frac{1}{R}$$


Figure 8.

GROUND-AIR-GROUND (GAG) CYCLES IN BLOCK LOADING

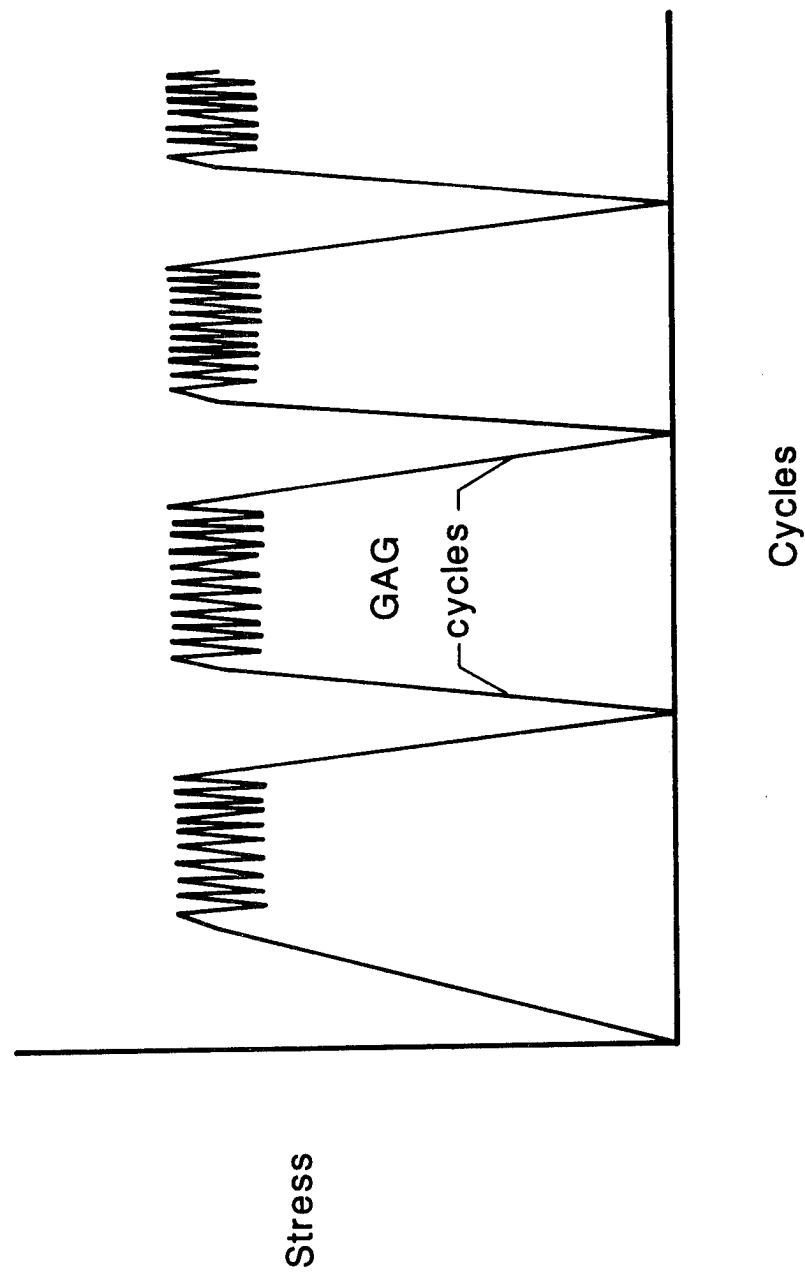


Figure 9.

PLASTIC WAKE IN NEWMAN'S CRACK-CLOSURE MODEL

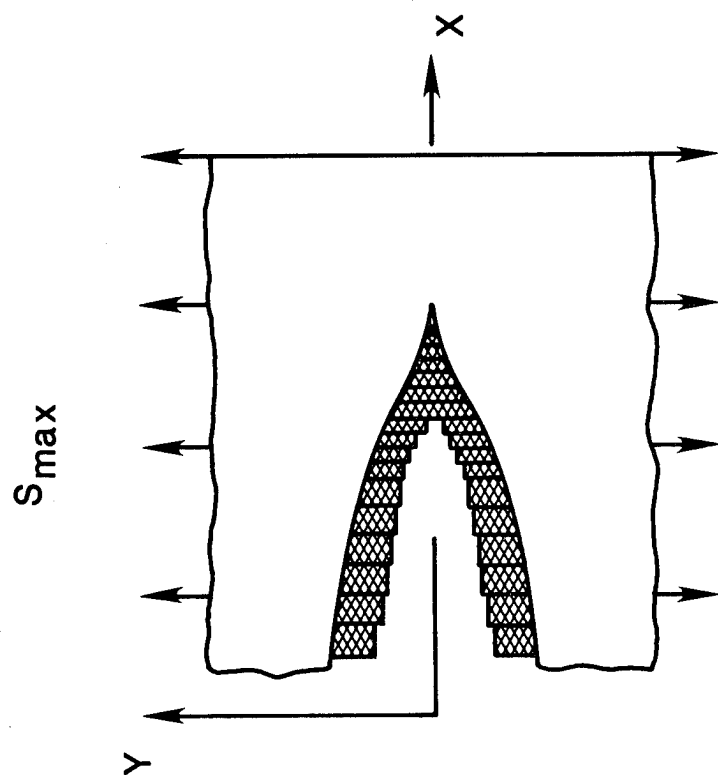


Figure 10.

CLOSURE MODEL PREDICTION OF CRACK GROWTH TESTS CONSTANT AMPLITUDE TESTS

2219-T851

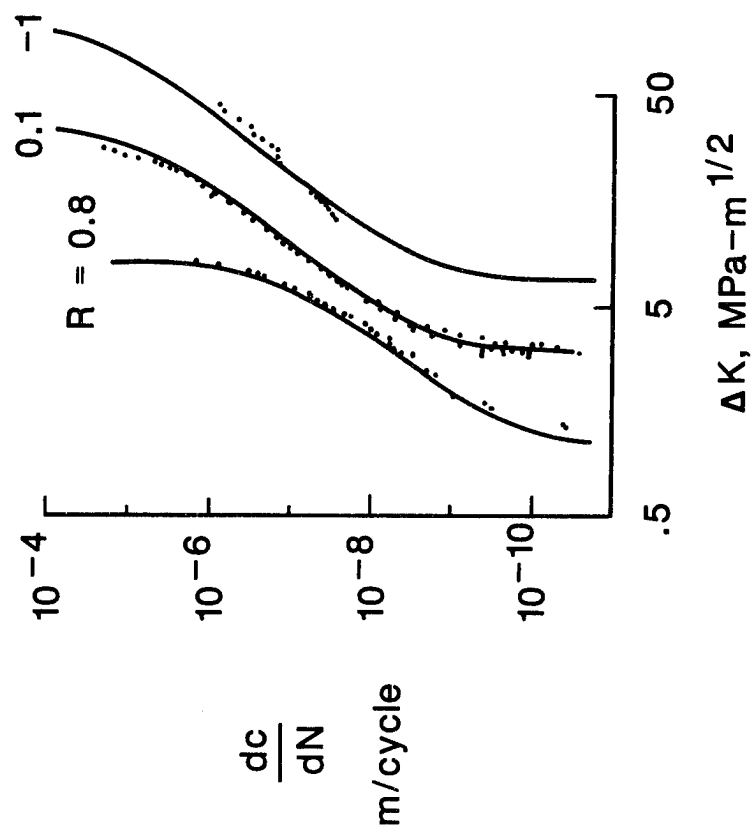


Figure 11.

CLOSURE MODEL PREDICTION OF SPECTRUM LOADING TESTS

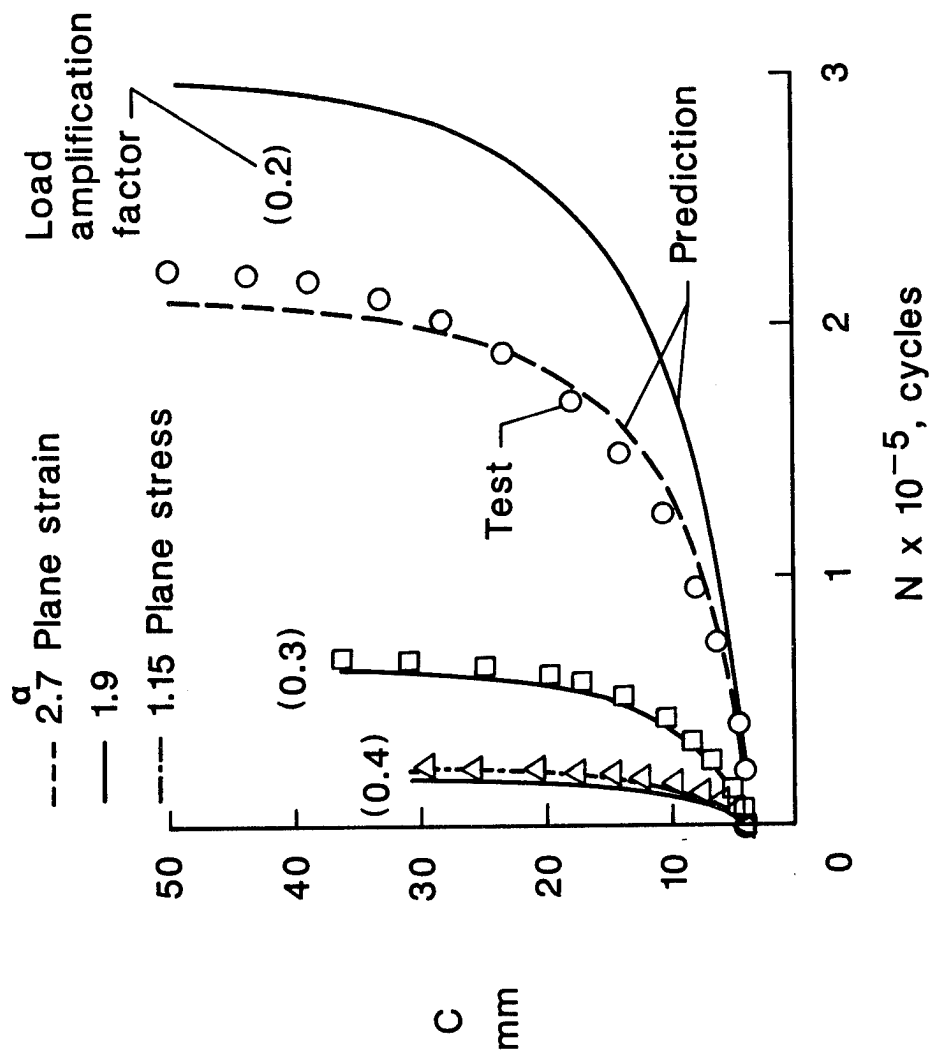


Figure 12.

RELATIVE ERROR IN K FROM TWO BOUNDARY ELEMENT METHODS

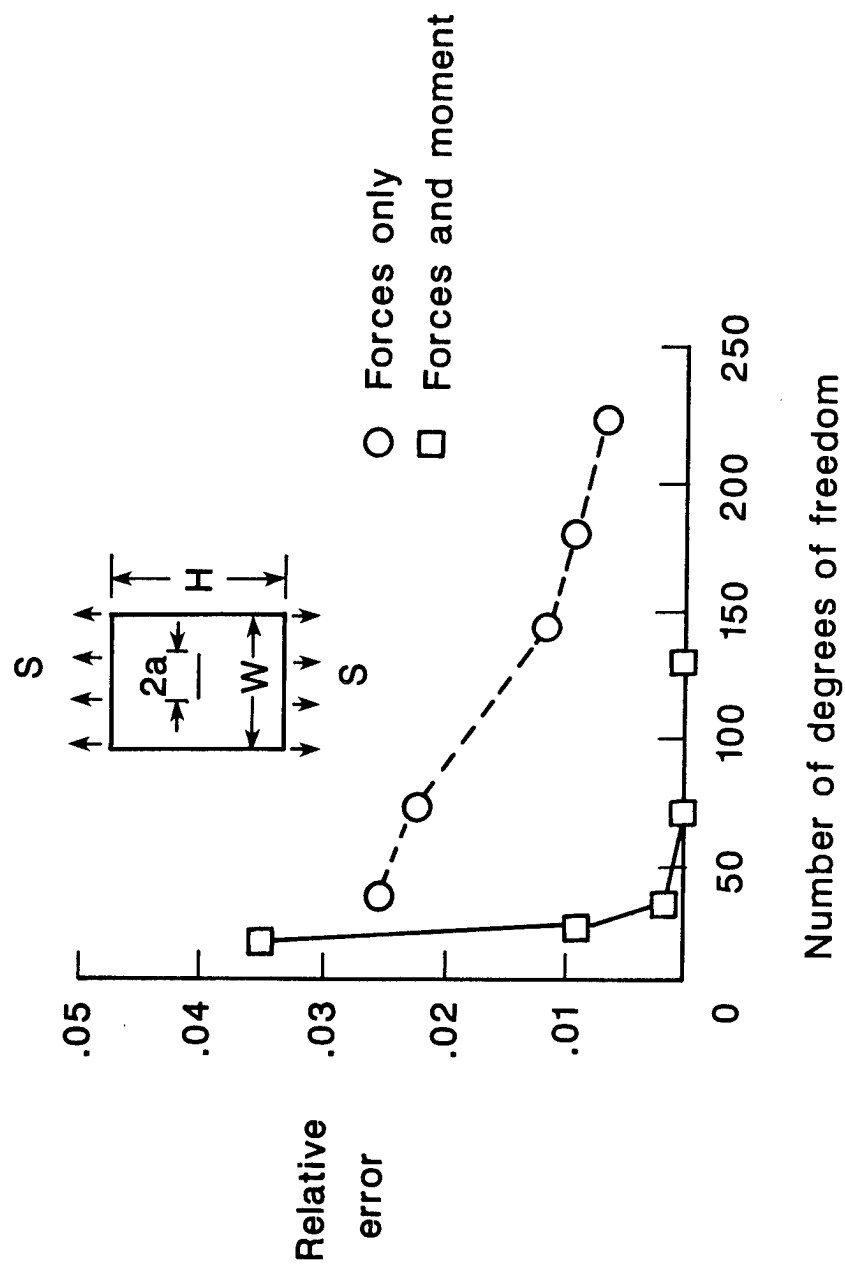


Figure 13.

STRESS INTENSITY FACTOR FROM THE BOUNDARY FORCE METHOD

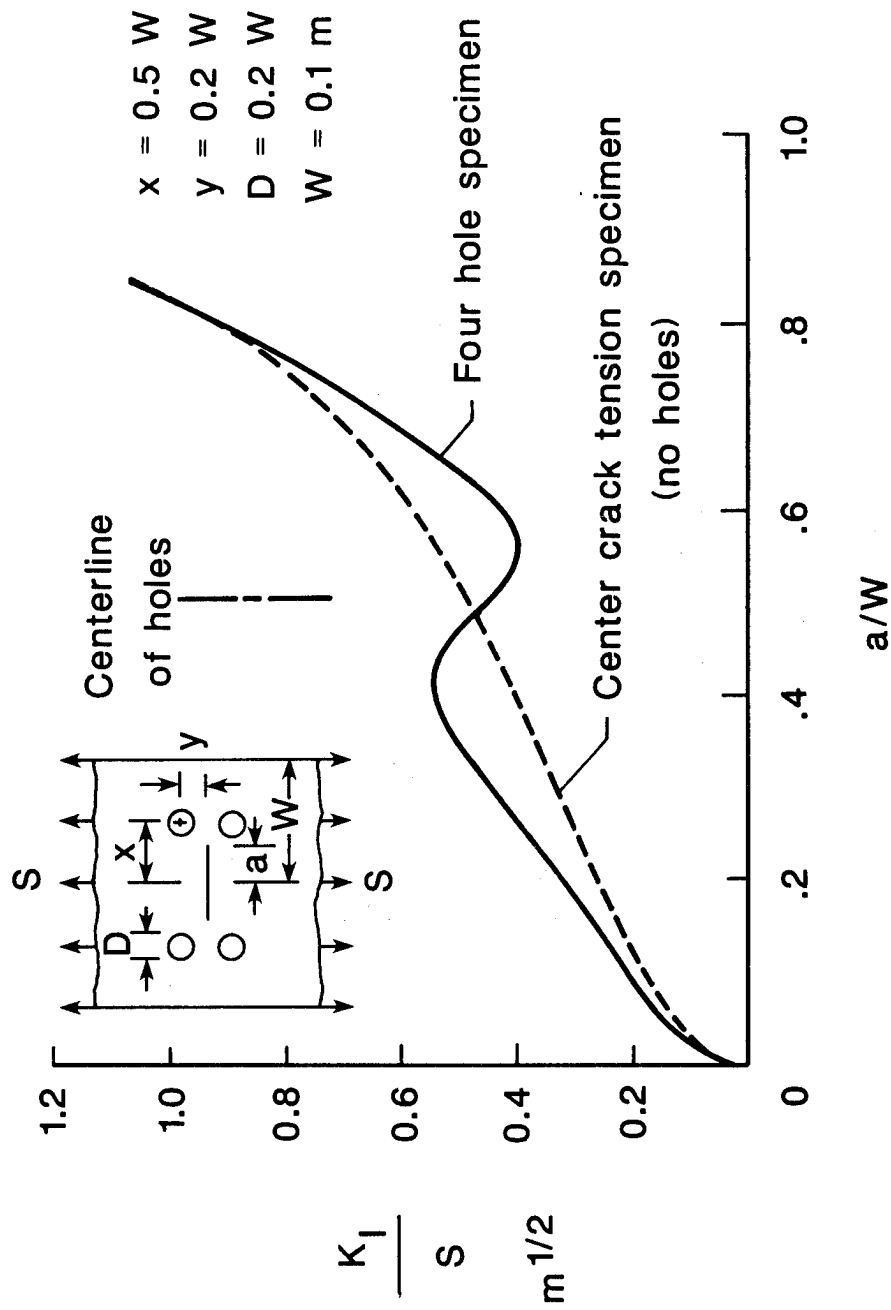


Figure 14.

THREE-DIMENSIONAL FRACTURE SPECIMENS

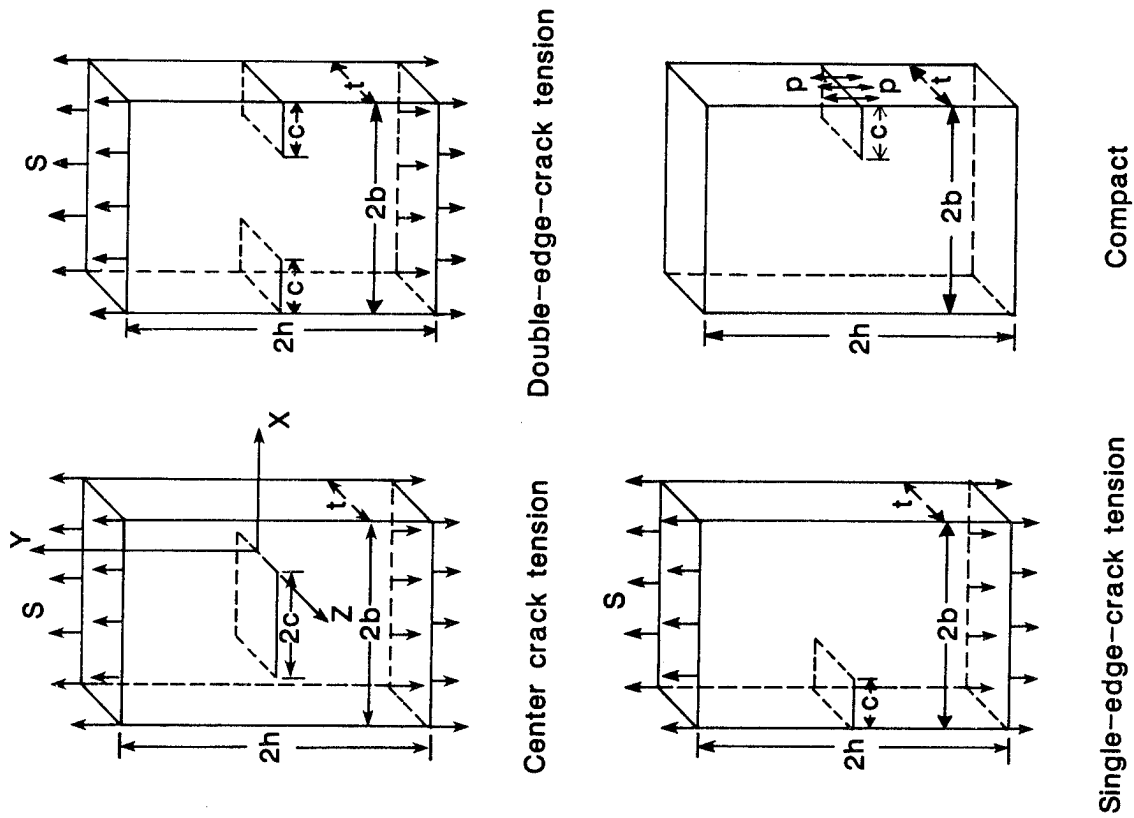


Figure 15.

STRESS-INTENSITY FACTORS FROM 3-D ANALYSIS

SINGLE-EDGE-CRACK-TENSION SPECIMEN

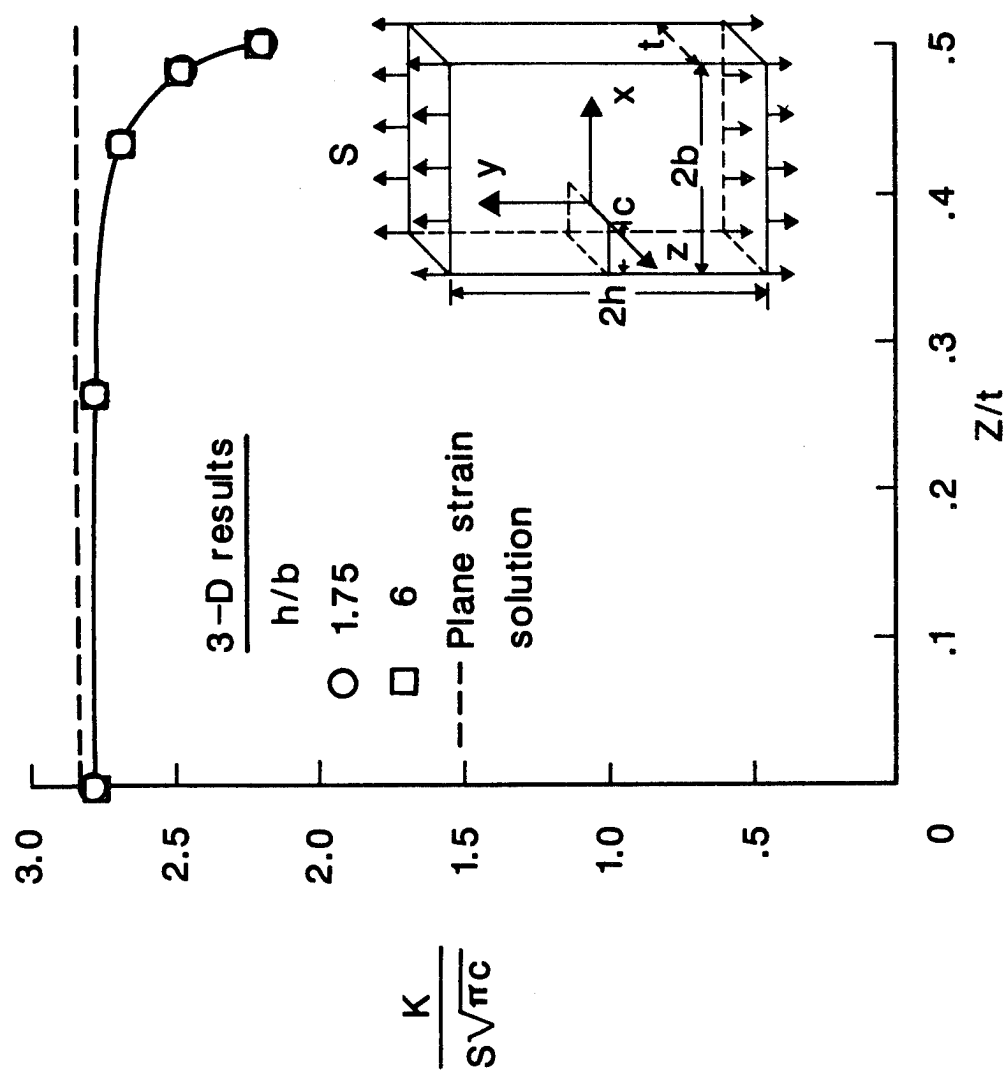


Figure 16.

CONVERGENCE STUDY FOR 3-D STRESS-INTENSITY FACTORS DEEP SEMI-ELLIPTICAL SURFACE CRACK

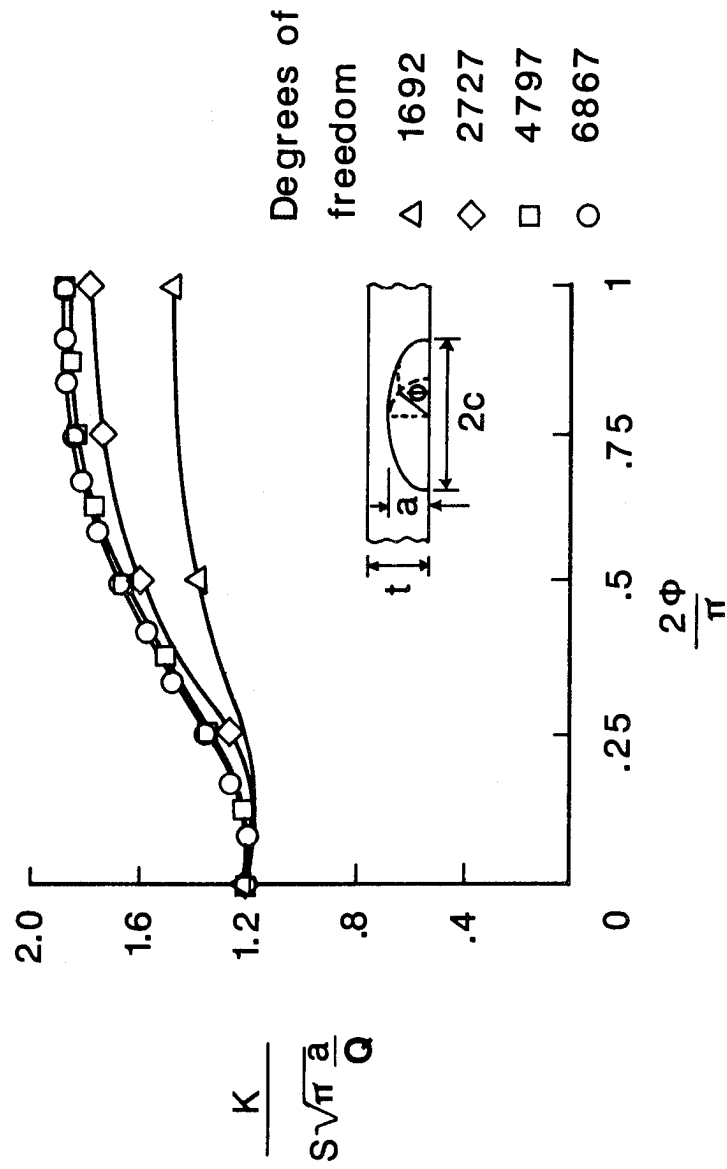


Figure 17.

CRACK CONFIGURATIONS FOR THREE DIMENSIONAL K SOLUTIONS

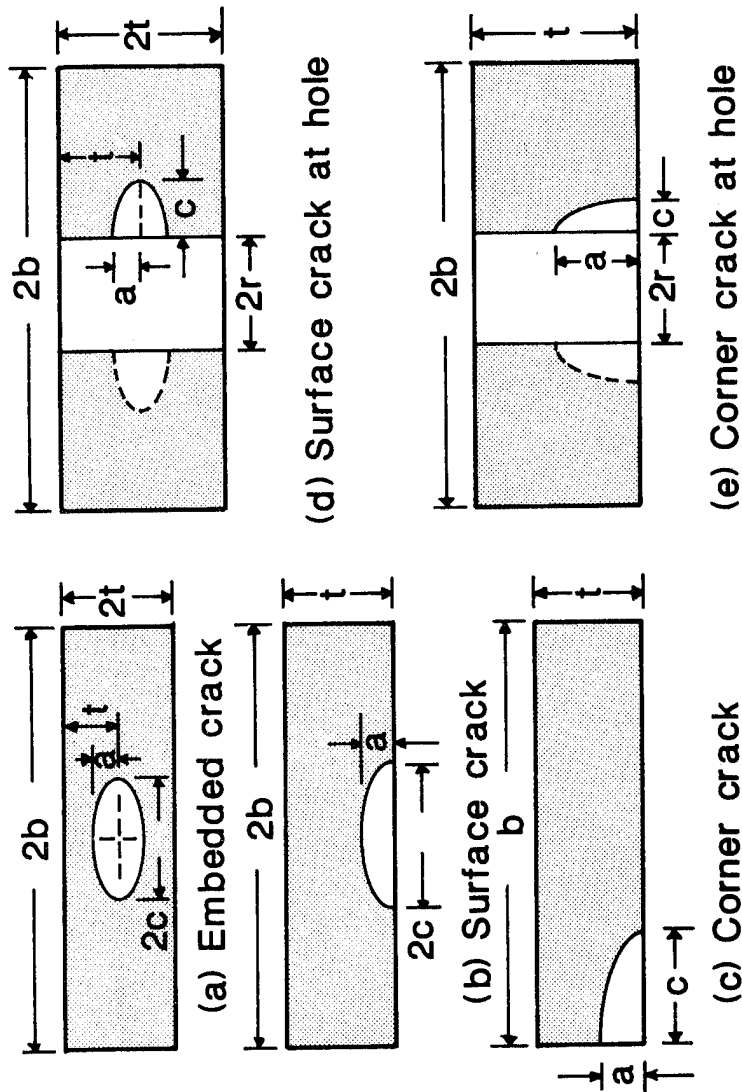
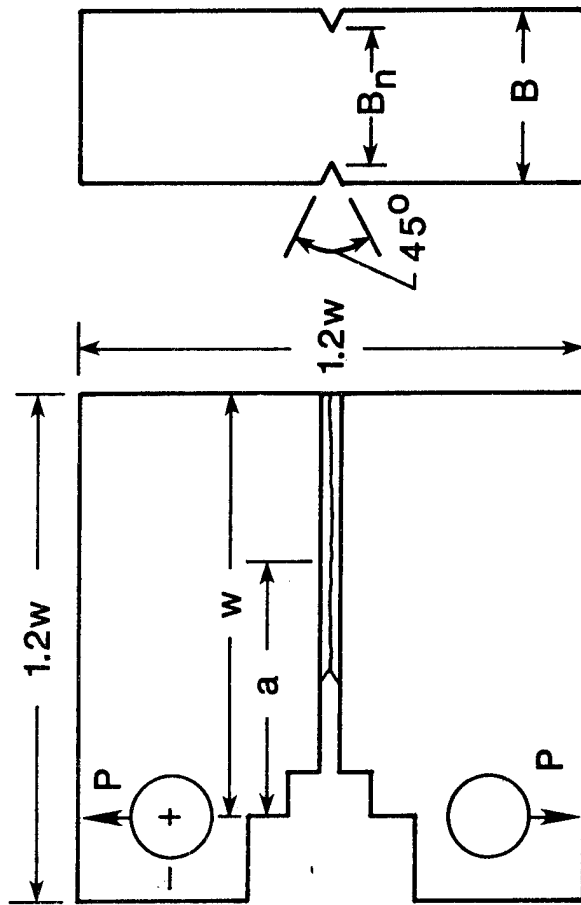
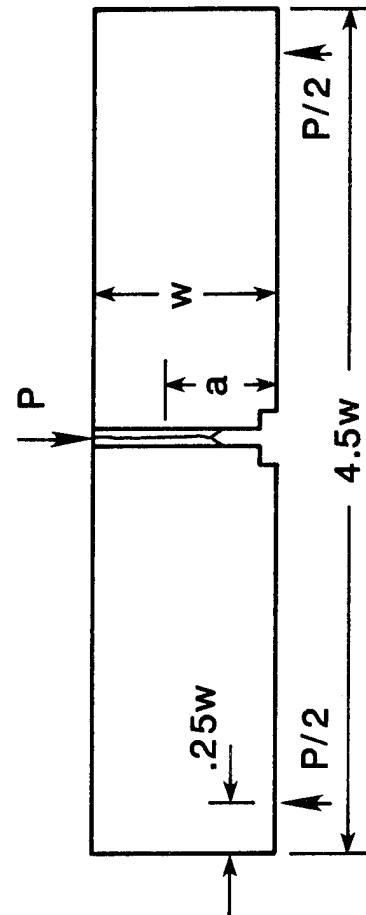


Figure 18.

SPECIMENS FOR DETERMINING J-INTEGRAL RESISTANCE CURVES



(a) J-compact specimen



(b) Bend specimen

Figure 19.

J-INTEGRAL RESISTANCE DATA

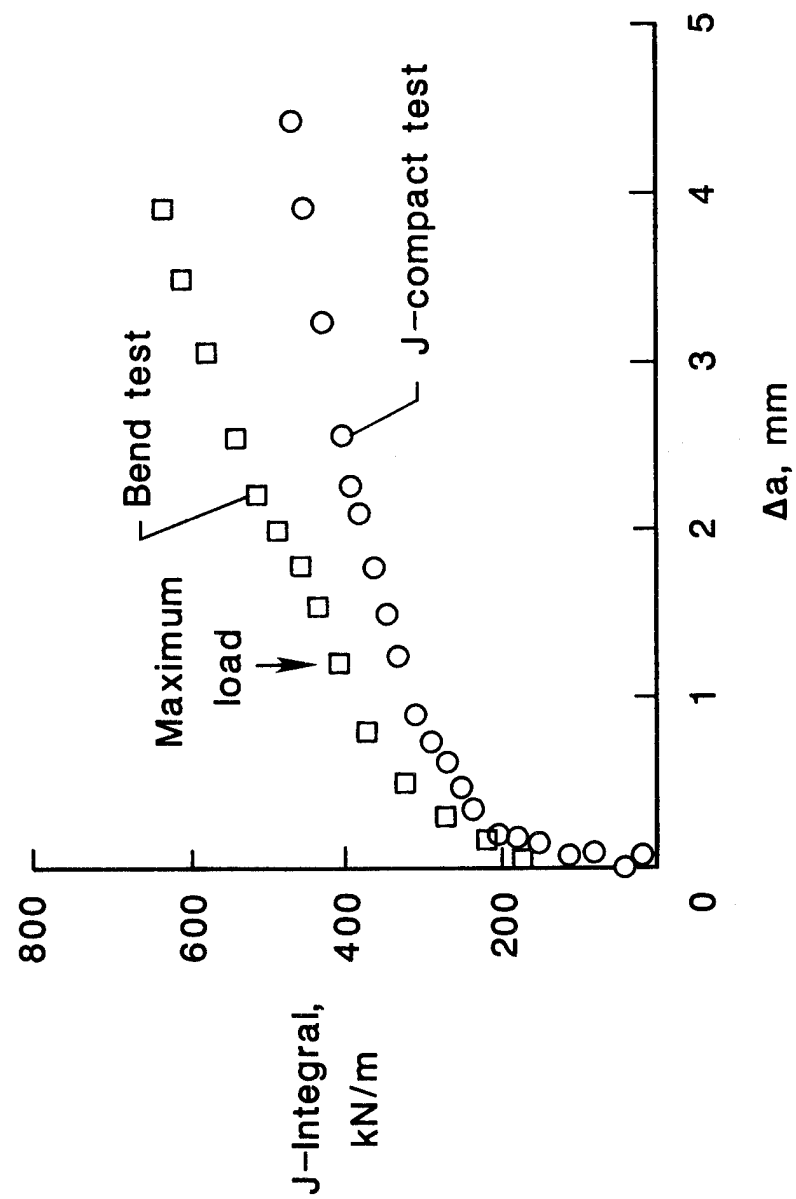


Figure 20.

COMPUTED J-INTEGRAL RESISTANCE CURVES

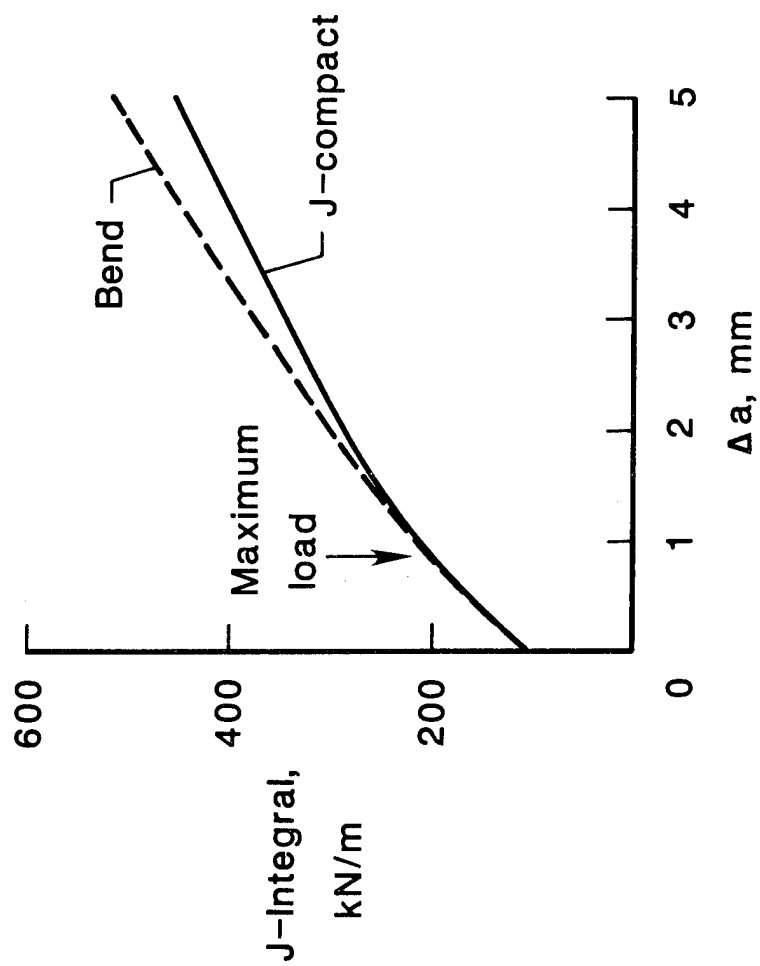


Figure 21.

DELAMINATION DURABILITY OF
COMPOSITE MATERIALS FOR ROTORCRAFT

T. Kevin O'Brien

Aerostructures Directorate

U.S. Army Research and Technology Activity (AVSCOM)

NASA Langley Research Center

Hampton, Virginia

Delamination is the most commonly observed failure mode in composite rotorcraft dynamic components. Although delamination may not cause immediate failure of the composite part, it often precipitates component repair or replacement, which inhibits fleet readiness, and results in increased life cycle costs. In this paper, a fracture mechanics approach for analyzing, characterizing, and designing against delamination will be outlined. Examples of delamination problems will be illustrated where the strain energy release rate associated with delamination growth has been found to be a useful generic parameter, independent of thickness, layup, and delamination source, for characterizing delamination failure. Several analysis techniques for calculating strain energy release rates for delaminations from a variety of sources will be outlined. Current efforts to develop ASTM standard test methods for measuring interlaminar fracture toughness and developing delamination failure criteria will be reviewed. A technique for quantifying delamination durability due to cyclic

loading will be presented. The use of this technique for predicting fatigue life of composite laminates and developing a fatigue design philosophy for composite structural components will be reviewed.

FRACTURE MECHANICS ANALYSIS OF DELAMINATION

Potential delamination sites exist in composite structures wherever a discontinuity exists in the load path (ref. 1). These discontinuities give rise to interlaminar stresses even when the remote loading is in-plane. Discontinuities may occur at (1) a straight edge with a stress-free boundary (often called a "free-edge"), (2) a curved stress-free boundary, such as the edge of a drilled hole, (3) a drop-off of the interior plies of a laminate to taper thickness, (4) a bonded or co-cured joint, and (5) a bolted joint (fig. 1). Of these cases, the free-edge delamination problem has been studied most extensively, and illustrates the benefits of fracture mechanics for characterizing delamination behavior.

Army and NASA investigators have analysed the strain energy release rate, G , associated with edge delamination growth (refs. 2-6). From finite element analyses they have found that once the delamination is modeled beyond a few ply thicknesses from the straight edge, G reaches a constant plateau given by the equation shown in figure 2. This equation, derived from a rule of mixtures and laminated plate theory, shows that G is independent of delamination size and depends only on the remote strain, ϵ , the laminate thickness, t , and two modulus terms, E_{LAM} and E^* , that correspond to the laminate modulus before and after delamination. In reference 2, the critical strain, ϵ_c , measured at the onset of

delamination at the $-30/90$ interfaces of eleven-ply $(\pm 30/\pm 30/90/90)_s$ laminates was substituted into the edge delamination equation in fig. 2 to determine a critical G_c for Thornel 300/ Narmco 5208 graphite epoxy composites. This G_c was then used to predict the onset strains for edge delamination in the $0/90$ interfaces of $(45_n/-45_n/0_n/90_n)_s$ laminates of the same material, where $n=1,2,3$ corresponds to an 8-, 16-, and 24-ply laminate. Figure 3 shows that the predictions agreed well with experimental data, and captured the trend of decreasing delamination onset strain with increasing thickness. An analysis based on the critical values of the interlaminar stresses at the straight edge would not account for this thickness dependence because the interlaminar stresses at the straight edge are independent of thickness (ref. 7).

Finite Element Analysis

Because a delamination is constrained to grow between individual plies, both interlaminar tension and shear stresses are commonly present at the delamination front. Therefore, delamination is often a mixed-mode fracture process. A boundary value problem must be formulated and solved to determine the strain energy release rate components at the crack tip: G_I due to interlaminar tension, G_{II} due to sliding shear, and G_{III} due to scissoring shear. A virtual crack extension technique was used in combination with a quasi-three dimensional finite element analysis to calculate the various G components (refs. 2-6). Figure 4 shows the results of such an analysis for delaminations between the 90 -deg and neighboring ply in a family of three quasi-isotropic laminates. The 90 -deg plies were in the center of each layup, but the 45 ,- 45 , and 0 -deg plies were permuted to yield three unique stacking sequences. As noted earlier, the total G rises to a constant plateau when the delamination progresses beyond a

few ply thicknesses from the edge. The total G values calculated by the rule of mixtures and by summing the G components from the finite element analysis were nearly identical for all three layups. However, the mixture of the G components was different for each layup. For example, figure 4 shows that the G_I components for the various layups have values ranging from nearly 90% of the total G to less than 30% of the total G . The G_{III} component calculated for each layup was negligible. Hence the difference in the G_I component and total G for each case was the G_{II} contribution. Furthermore, like the total G , the G components are independent of delamination size. As illustrated in a later section, tests conducted on three similar layups, where the ± 45 -deg plies were changed to ± 35 -deg based on a parametric study conducted in ref. 4 to minimize the ϵ_c required to measure a given G_c , were used to develop mixed-mode interlaminar fracture criteria for composite materials (ref. 5).

Residual Thermal Stress Contributions to G

Composite laminates are manufactured, or cured, under temperature and pressure and then cooled to room temperature for testing. During cooling from the cure temperature, the plies of the laminate that are oriented at different angles would like to contract differently, but they are forced to contract equally. This constraint leads to the development of residual thermal stresses in the individual plies. When a composite delaminates, part of the strain energy released may be attributed to these residual thermal stresses. A previously developed analysis for the strain energy release rate associated with edge delamination in composite laminates was modified to include the contribution of residual thermal stresses (ref. 6). This analysis was performed for several materials to determine the influence of the residual thermal stresses on

delamination formation and growth. Figure 5 shows the strain energy release rate, G^{M+T} , for edge delamination in a $(25/-25/90)_s$ laminate due to a combination of mechanical (M) and thermal (T) loads, as a function of the thermal gradient, ΔT , between the cure or consolidation temperature and room temperature. The value of G calculated for mechanical loading only is shown on the ordinate where $\Delta T=0$. The other value indicated by a symbol corresponds to G where both the mechanical load and the appropriate ΔT for the material were included in the analysis. For a graphite fiber composite with a brittle epoxy matrix, delaminations occur at mechanical strains around 0.004, and the contribution of residual thermal stresses to G is small. However, for a high modulus graphite fiber composite with a brittle bismaleimide (BMI) matrix that is cured at a higher temperature than epoxy, nearly one half of the strain energy released at a strain of 0.004 is attributed to the residual thermal stresses. Composite laminates made with thermoplastic matrices are typically much tougher, delaminating at mechanical strains of nearly 0.01. However, thermoplastic matrix composites are manufactured at extremely high temperatures, resulting in a significant residual thermal stress contribution to the strain energy release rate for delamination (ref. 8). Hence, the influence of residual thermal stresses on delamination is significant for materials manufactured at high temperatures.

DELAMINATION ANALYSIS OF STRUCTURAL DETAILS

Delamination Around an Open Hole

A rotated straight edge technique has been used to determine delamination onset around an open hole in a composite laminate (ref. 9). This technique, which is

illustrated in figure 6, involves analysing each angular position, θ , around the hole boundary as if it was the straight edge of a laminate whose plies were rotated from the original orientation by θ degrees. The rotated layup was assumed to be subjected to a uniaxial strain equal to the circumferential strain at the hole boundary. Using these assumptions the equation for strain energy release rate associated with straight edge delamination may be used as shown in figure 6, where the strain and modulus terms are functions of θ , to generate G distributions around the hole boundary for each unique interface in the laminate. Figure 7 shows a radial plot of a nondimensionalized G parameter in the 45/90 interface of a quasi-isotropic (45/90/-45/0)_s laminate. The position of the maximum G on the hole boundary is located using this technique. Furthermore, finite element analyses may be performed using the techniques described earlier for straight edge delaminations to determine the G_I distribution around the hole boundary, shown by the shaded region in figure 7.

Higher order plate theory analysis of delamination

Previously, a finite element analysis was required to determine the relative contributions of G_I , G_{II} , and G_{III} to the total strain energy release rate for delamination. Although these finite element analyses are useful, they are typically not performed during the design of the structure until the final design stage or until a problem has arisen during qualification testing or in service. Because delamination failures may depend on the ratio of these fracture modes, calculations of G_I , G_{II} , and G_{III} may be needed to accurately anticipate delamination failures. A simple "desk-top" computer analysis for calculating the strain energy release rate, G , components for edge delamination has been

developed by Georgia Tech under an Army/NASA Grant (NAG-1-558). The analysis models the two shearing modes using shear deformation theory to calculate G_{II} and G_{III} directly, then G_I is determined by subtracting the two shear components from the total G . Results from this analysis were compared to finite element results calculated for delamination around an open hole using the rotated straight edge technique. Figure 8 shows results for delamination in the 90/-45 interface of a (45/90/-45/0)_s laminate with a circular hole. As shown in the figure, the higher order plate theory (HPT) yields results that are similar to the finite element (FEM) results; however, the HPT analysis may be performed quickly using a desk top computer. The simple nature of the HPT method makes it suitable for preliminary design analyses which require the evaluation of a large number of configurations, quickly and economically.

Delamination Due to Internal Ply-Drops

Composite rotor hubs, currently being designed and manufactured, are hingeless and bearingless to reduce weight, drag, and the total number of parts. These composite hubs typically have a flapping flexure region where the laminate thickness is reduced by dropping internal plies. Delamination failures are often observed at these ply drops due to the combined centrifugal tension and bending loads applied at the flexure regions of the hub. Although these delaminations may not cause component failure, and therefor yield a desirable benign failure mode, the low delamination durability of current composite materials may result in high repair or replacement costs for the composite hubs. In order to design these composite hubs for delamination durability, analyses are needed that model the delamination failure mode observed. To this end, a simple model was developed for the strain energy release rate associated with delamination growth

from internal ply drops in laminates subjected to tension loads (ref. 10). The delamination was assumed to occur at the first transition from the thin section into the tapered region, labeled point A in figure 9. A simple free body diagram revealed that the maximum interlaminar tensile stress resultant would occur at this point. As shown in figure 9, this local transition region was idealized as a flat laminate with a stiffness discontinuity in the outer "belt" plies and a continuous stiffness in the internal "core" plies. The belt stiffness in the tapered region, E_2 , was obtained from a tensor transformation of the belt stiffness in the thin region, E_1 , transformed through the taper angle, β . The resulting equation for the strain energy release rate, G , shown in figure 9, is a function of the thicknesses and moduli of the core plies and the belt plies in the tapered region compared to the original thickness, t , and modulus, E_{LAM} , of the thin section of the laminate where the internal plies have been dropped. Furthermore, G was independent of the delamination length, a . Because the belt stiffness in the tapered region is a function of the taper angle, β , G will increase as β increases. Figure 9 shows the increase in G , normalized by the applied tensile load per unit width squared, N_x^2 , as the taper angle is increased for a $[0_9/(\pm 45)_2]_S$ glass epoxy laminate. Therefore, the taper angle and ply thicknesses must be considered along with the layup to optimize the rotor hub design for the desired structural performance while minimizing the probability of a delamination failure.

DELAMINATION FAILURE CRITERIA

Interlaminar Fracture Toughness Characterization

Because delamination is the most commonly observed composite failure mode, the need for standard test methods to develop delamination failure criteria has become paramount. To meet this need, a round robin test program has been organized within ASTM committee D30 on High Modulus Fibers and Their Composites to develop standard tests for measuring the interlaminar fracture toughness of composites. Four test methods are being evaluated for their ability to rank materials for improved delamination resistance, to compare toughness measurements between the various tests, and to check the repeatability of measurements between laboratories. The four tests included in the round robin are the double cantilever beam (DCB) test, the edge delamination tension (EDT) test, the cracked lap shear (CLS) test, and the end-notched flexure (ENF) test. These four tests measure critical values of the strain energy release rate, G , for delamination that range from a pure opening mode due to interlaminar tension, G_I , to a pure interlaminar shear mode, G_{II} . The data from these four tests may be used to generate delamination failure criteria for composite materials. As depicted in figure 10, all four test methods will be conducted with three different composite materials with the same AS4 graphite fiber, but with polymer matrices that range from very brittle to very tough. The matrices chosen were (1) Hercules 3501-6, (2) Cyanamid BP 907, and (3) ICI Polyetheretherketone (PEEK). A total of thirty-two laboratories, from five different countries, will be participating in the round robin. Each test will be conducted by at least nine participants. The results of this round robin will be

used to develop ASTM test standards for interlaminar fracture toughness measurement.

Results from edge delamination tension (EDT) tests, pure mode I double cantilever beam (DCB) tests, pure mode II end-notched flexure (ENF) tests, and mixed-mode cracked-lap-shear (CLS) tests have already been used to determine delamination failure criteria for several composite materials (ref. 11). Data are plotted in figure 11, where the G_I component at failure is plotted versus the G_{II} component at failure, for graphite reinforced composite laminates with matrices ranging from very brittle (3501-6, 5208) to very tough (PEEK, F185). In all cases, a linear failure criterion of the form $(G_I/G_{Ic} + G_{II}/G_{IIc}) = 1$ fit the data well. However, for the brittle matrix composites, G_{Ic} is much less than G_{IIc} ; whereas for the toughened matrix composites, G_{Ic} is nearly equal to G_{IIc} .

Delamination Durability Under Cyclic Loading

Delamination may occur at cyclic strain levels corresponding to cyclic G levels well below the interlaminar fracture toughness of the composite (ref. 4,8,12,13). Delaminations form at these lower cyclic strains after a certain number of cycles, N . In ref.4, cyclic edge delamination tests were conducted where the G_c values calculated from maximum cyclic strains were plotted as a function of the number of cycles to edge delamination onset (figure 12). These G_c values drop sharply in the first 200,000 cycles until they reach a plateau tantamount to a threshold for delamination onset in fatigue. A finite element analysis of the $(35/-35/0/90)_s$ and $(0/35/-35/90)_s$ laminates tested yielded an identical total G for a given nominal strain, but the G_I

components were very high and low, respectively. As shown in figure 12, the G_c for these two layups measured in static tests ($N=1$) were different. However, the G_c thresholds under cyclic loading were nearly identical. Hence, the total G does not determine the delamination onset under static loading, but the total G does appear to control the delamination onset in fatigue. Furthermore, a comparison of the relatively tough Hexcel 205 matrix composites to the brittle 5208 matrix composites shows a significant improvement in the static G_c , but the magnitude of this improvement for the G_c threshold in fatigue is much less, as shown in figure 12. A similar trend is shown in figure 13 where the maximum cyclic G_c is plotted as a function of log-cycles to delamination onset for four materials with a wide range of static toughnesses. The matrix materials were (1) Narmco 5208, a 350°F brittle epoxy, (2) Hexcel H205, a 250°F epoxy, (3) Cyanamid HST7, a 350°F epoxy with a tough adhesive interleaf between each ply, and (4) ICI Polyetheretherketone (PEEK), a semicrystalline thermoplastic. When cycles to delamination onset are plotted on a log scale as in figure 13, continued degradation appears possible beyond the 10^6 -cycle "threshold" seen earlier, so it may be more appropriate to think of these thresholds at 10^6 cycles as endurance limits. As figure 13 indicates, there is a large difference in the static interlaminar fracture toughnesses of these materials, shown on the ordinate at $N=1$, but the cyclic strain energy release rate endurance limits at 10^6 cycles are similar.

Delamination Growth

Although the data in figure 13 shows little difference in delamination durability between brittle and toughened matrix composites, the tough matrix composites will typically exhibit slower delamination growth. Figure 14 shows a

schematic of a log-log plot of delamination growth rate, da/dN , as a function of cyclic strain energy release rates. For the brittle matrix composite, G_c will be low, with an even lower cyclic threshold, G_{th} . Any stable delamination growth under cyclic loading must occur between these two values. Because G_c and G_{th} are very low, delamination growth rates in brittle matrix composites are typically very high compared to crack growth rates in metals. For the toughened matrix composite, G_c will be much higher than for the brittle matrix composite, but G_{th} will be only slightly higher. Because G_c values are much higher than G_{th} values for the toughened matrix composites, slower delamination growth rates are observed. If G_c values are high enough, these growth rates may become comparable to crack growth rates in metals.

FATIGUE ANALYSIS OF COMPOSITE LAMINATES

Composite laminates containing plies of several orientations may experience fatigue failures below their static tensile strength. Figure 15 shows the maximum cyclic load at failure (solid symbols) as a function of fatigue cycles, N , for a $(45/-45/0/90)_s$ graphite epoxy laminate (ref. 12). A fatigue endurance limit was observed around 70 percent of the static tensile strength. The open symbols in figure 15 indicate the onset of 0/90 interface edge delamination, which reaches a plateau around 40 percent of the static tensile strength. Above this threshold, stiffness loss is observed as the edge delamination grows, but fatigue failure does not occur even though the edge delamination may propagate across the width of the laminate. Fatigue failures occur, however, when local delaminations form at matrix ply cracks in the ± 45 -deg plies. These local delaminations cause isolation of the cracked plies that results in local strain concentrations in the uncracked plies (ref. 14,15). Because of these local

strain concentrations, fatigue failures occur at nominal strain levels below the static failure strain, as illustrated in figure 15 for a quasi-isotropic graphite epoxy laminate.

One technique for estimating the fatigue life of such laminates is being pursued in a joint research program on fatigue of composite materials between the U.S. Army Aerostructures Directorate at NASA Langley and Agusta Helicopter Company under the U.S. Army/ Italian Memorandum of Understanding (MOU). This technique, which is illustrated in figure 16, involves two steps. First, cyclic edge delamination data are used to generate fatigue delamination onset criteria as shown in figures 12,13. This information is then used in the appropriate equations relating applied load to strain energy release rate for local delamination onset to estimate the fatigue failure load as a function of cycles to the onset of local delamination. Under the MOU, this technique will be applied to a variety of composite layups, ranging from orthotropic to quasi-isotropic, for a variety of materials including graphite-epoxy, glass-epoxy, and glass/graphite hybrids.

FATIGUE DESIGN PHILOSOPHY FOR COMPOSITES STRUCTURAL COMPONENTS

Because fatigue failure is a result of the accumulation of delamination sites through the laminate thickness, and because delaminations grow rapidly for most brittle epoxy matrix materials, a no-growth delamination threshold approach for infinite delamination life has been proposed (ref. 12). One concern with this approach in the past has been the uncertainty inherent in predicting service loads which could exceed no-growth thresholds and lead to catastrophic propagation. However, unlike crack growth in metals, catastrophic delamination

growth does not necessarily equate to material or structural failure. Delaminated composites may have inherent redundant load paths that prevent failure and provide a degree of fail safety. This was the case for edge delaminations in the tensile loaded laminates discussed earlier. This degree of fail safety has led designers to think of composite delamination as a relatively benign failure mode. Unfortunately, delaminations may occur from several sources in a given component or structure. Even simple laminates subjected to only cyclic tension loads, experienced an edge delamination first that was relatively benign, followed by local delamination from matrix cracks that caused fatigue failures. Structural components with complex shapes subjected to complex loadings, such as bearingless rotor hubs subjected to combined tension, bending, and torsion loadings, may have a multitude of potential delamination sites. An iterative composite mechanics analysis that considers each of these potential sites must be performed to insure fail safety of the structure. Such an analysis could also be used to identify changes in design details that inhibit delamination. Delamination suppression techniques such as replacement of brittle matrices with toughened matrices, use of adhesive strips in critical interfaces, use of through-the-thickness stitching, and wrapping of the laminate with a reinforced cloth have all suppressed delamination in composites under static loads, but have not been as successful under cyclic loads. Hence, the need for a delamination threshold/fail safety analysis as proposed in ref. 12 is still evident.

CONCLUDING REMARKS

Fracture mechanics has been found to be a useful tool for understanding and characterizing composite delamination. Analyses for calculating the strain

energy release rate associated with delamination growth have been developed for several common delamination sources. The strain energy release rate has been found to be a useful generic parameter, independent of layup, thickness, or delamination source, for characterizing delamination failure. ASTM test standards for interlaminar fracture toughness are being developed and have already been used to generate delamination failure criteria. A technique for quantifying delamination durability due to cyclic loading has been developed and is being used to predict fatigue life of composite laminates and to develop a fatigue design philosophy for composite structural components.

REFERENCES

1. O'Brien, T.K., "Interlaminar Fracture of Composites", NASA TM-85768, 1984, (Also in J. of the Aeronautical Society of India, Vol. 37, No.1, Part III, 1985, p.61.)
2. O'Brien, T.K., "Characterization of delamination onset and growth in a Composite Laminate," in Damage in Composite Materials, ASTM STP 775, June, 1982, p.140.
3. O'Brien, T.K., Johnston, N.J., Morris, D.H., and Simonds, R.A., "A Simple Test for the Interlaminar Fracture Toughness of Composites," SAMPE Journal, Vol.18, No.4, July/August 1982, p.8.
4. O'Brien, T.K., "Mixed-Mode Strain-Energy-Release-Rate Effects on Edge Delamination of Composites," in Effects of Defects in Composite Materials, ASTM STP 836, 1984, p.125.

5. O'Brien, T.K., Johnston, N.J., Morris, D.H., and Simonds, R.A., "Determination of Interlaminar Fracture Toughness and Fracture Mode Dependence of Composites using the Edge Delamination Test," Proceedings of the International Conference on Testing, Evaluation, and Quality Assurance of Composites, University of Surrey, Guildford, England, September, 1983, p.223.
6. O'Brien, T.K., Raju, I.S., and Garber, D.P., "Residual Thermal and Moisture Influences on the Strain Energy Release Rate Analysis of Edge Delamination," Journal of Composites Technology and Research, Vol.8, No.2, Summer, 1986, p.37.
7. Crossman, F.W., Warren, W.T., Wang, A.S.D., and Law, G.E., "Initiation and Growth of Transverse Cracks and Edge Delamination in Composite Laminates", J. of Composite Materials, Supplemental Volume (1980), pp. 88-106.
8. O'Brien, T.K., "Fatigue Delamination Behavior of PEEK Thermoplastic Composite Laminates," Proceedings of the American Society for Composites (ASC) First Conference on Composite Materials, Dayton, Ohio, October, 1986., pp. 404-420.
9. O'Brien, T.K., and Raju, I.S., "Strain Energy Release Rate Analysis of Delamination Around an Open Hole in Composite Laminates," AIAA-84-0961, Proceedings of the 25th AIAA/ASME/ASCE/AHS Structures, Structural Dynamics, and Materials Conference, Palm Springs, Ca., 1984, p.526.

10. O'Brien, T.K., "Delamination of Tapered Composite Laminates Containing Internal Ply Drops," to be presented at the 28th AIAA/ASME/ASCE/AHS Structures, Structural Dynamics, and Materials Conference, Monterey, California, April 6-8, 1987.
11. Johnson, W.S., and Mangalgari, P.D., "Influence of Resin on Interlaminar Fracture," in Toughened Composites, ASTM STP 937, 1987.
12. O'Brien, T.K., "Generic Aspects of Delamination in Fatigue of Composite Materials," J. of the American Helicopter Society, Vol. 32, No. 1, January, 1987.
13. Adams, D.F., Zimmerman, R.S., and Odem, E.M., "Determining Frequency and Load Ratio Effects on the Edge Delamination Test in Graphite Epoxy Composites," in Toughened Composites, ASTM STP 937, 1987.
14. O'Brien, T.K., "The Effect of Delamination on the Tensile Strength of Unnotched, Quasi-isotropic, Graphite/Epoxy Laminates," in Proceedings of the SESA/JSME 1982 Joint Conference on Experimental Mechanics, Hawaii, Part I, Society for Experimental Stress Analysis, Brookfield, Conn., May, 1982, p.236.
15. Ryder, J.T., and Crossman, F.W., "A Study of Stiffness, Strength, and Fatigue Life Relationships for Composite Laminates," NASA CR-172211, October, 1983.

SOURCES OF OUT-OF-PLANE LOADS FROM LOAD PATH DISCONTINUITIES

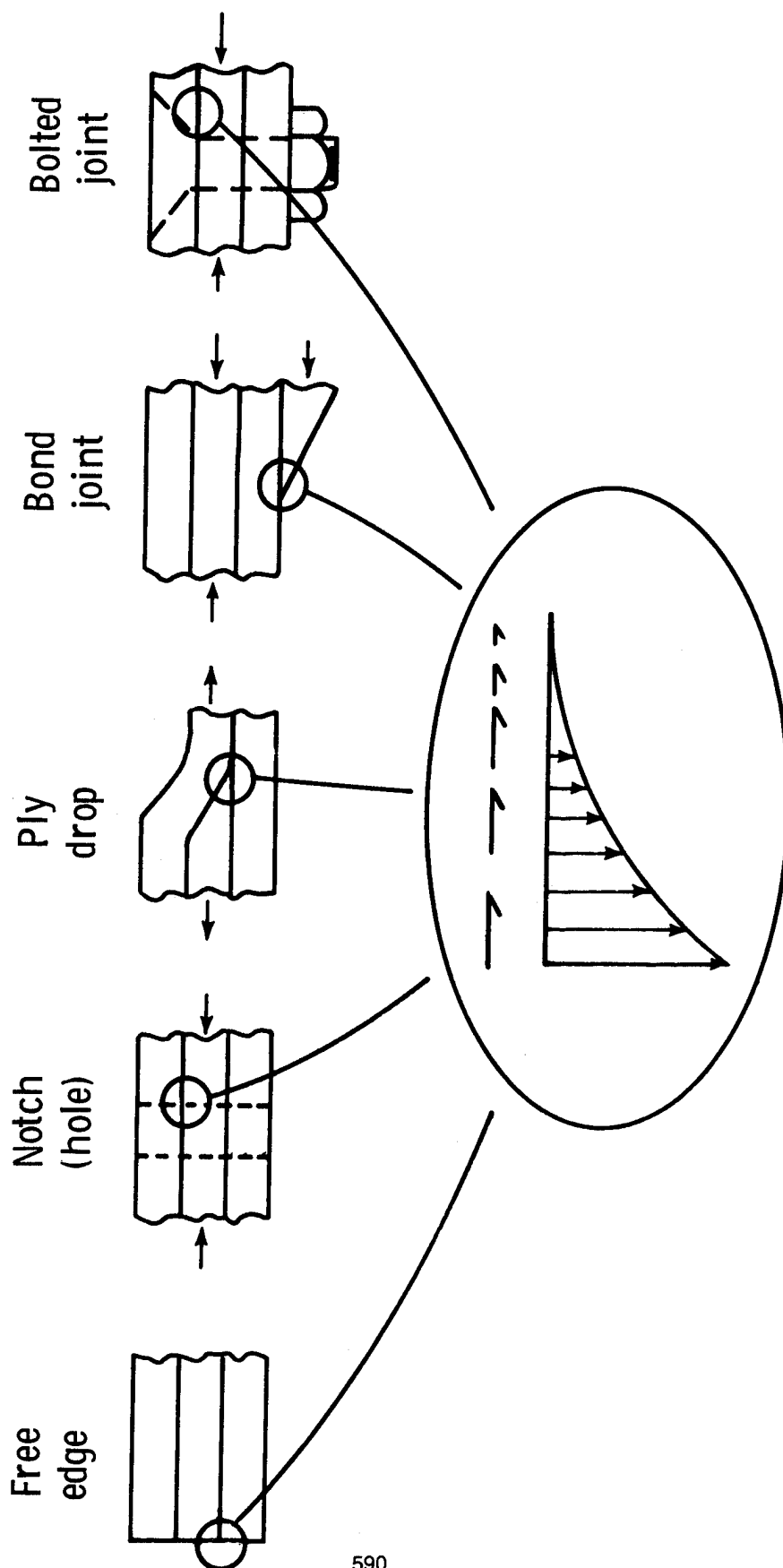


Figure 1.

STRAIN ENERGY RELEASE RATE FOR DELAMINATION GROWTH

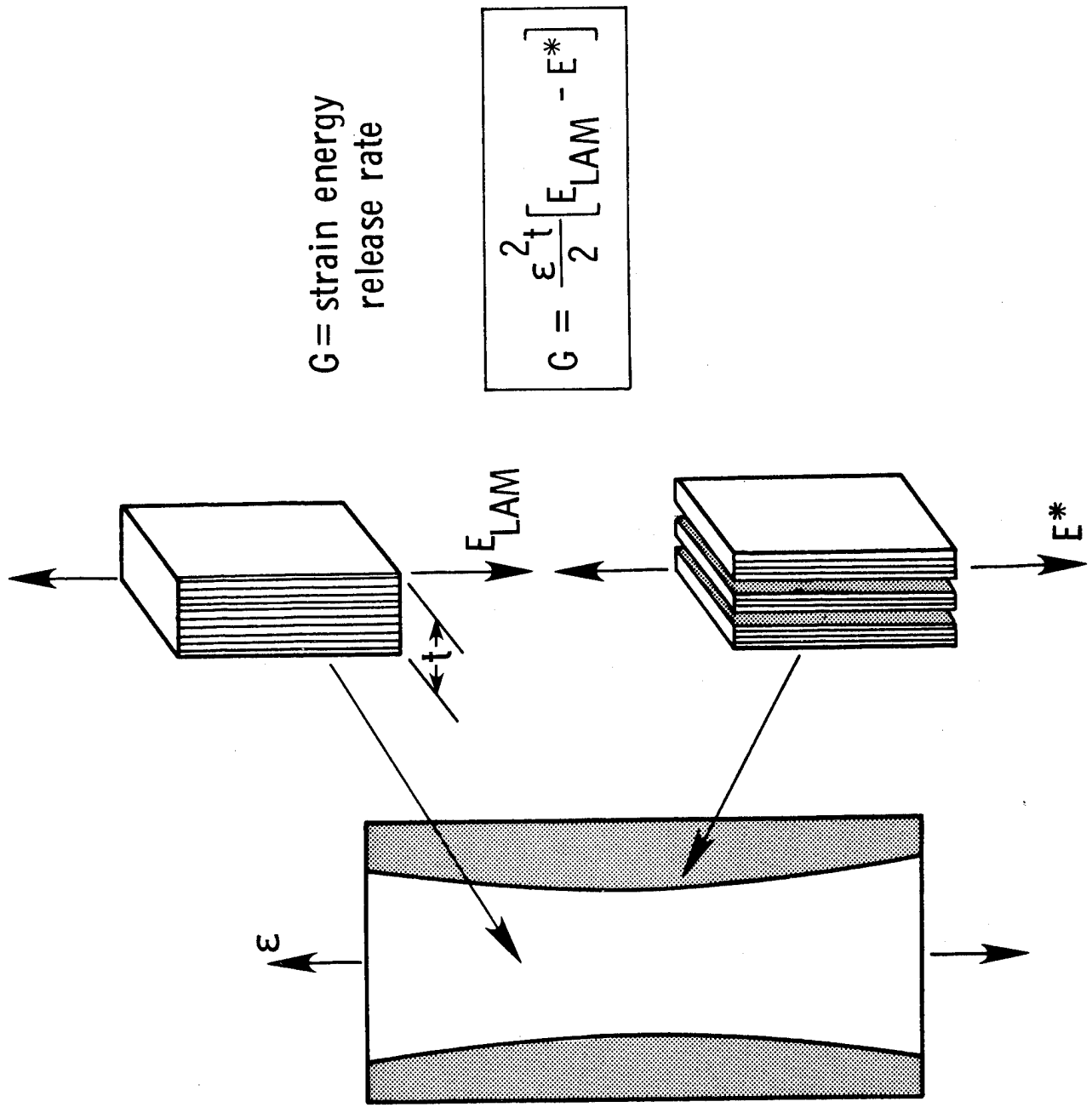
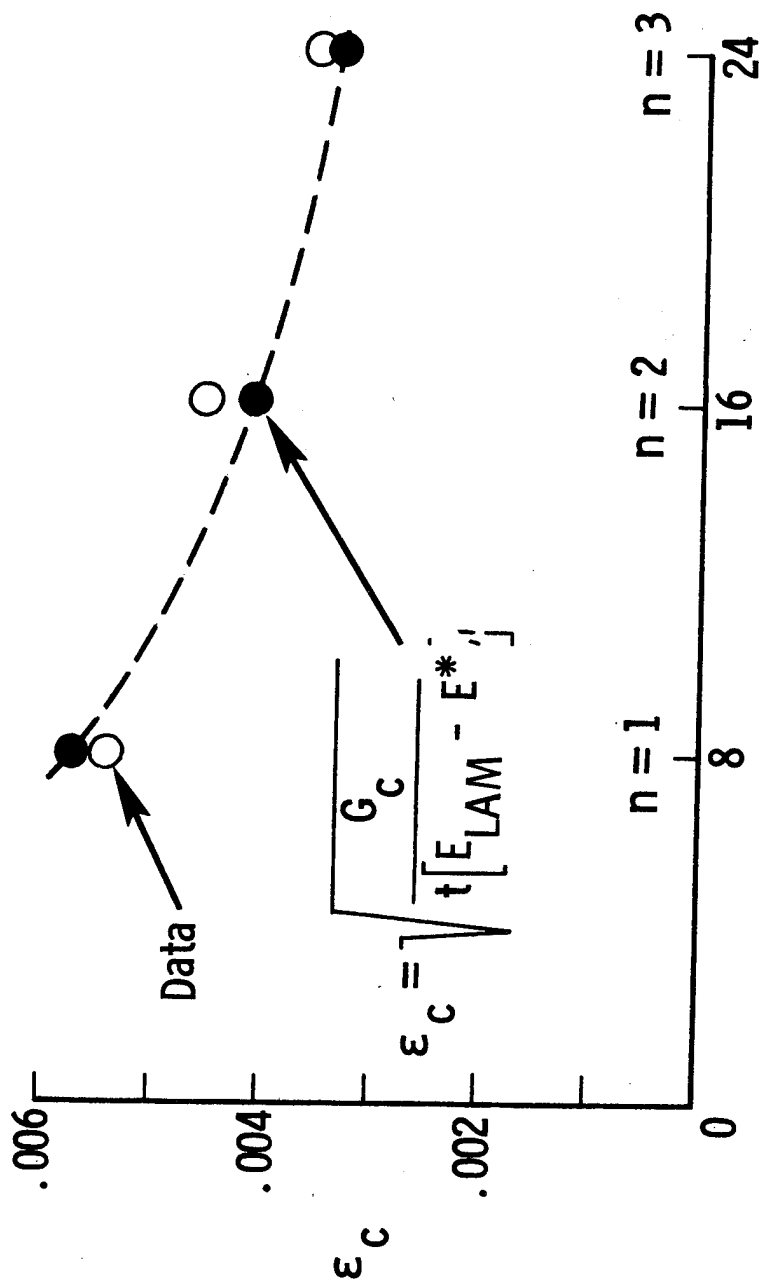


Figure 2.

DELAMINATION ONSET PREDICTION

Graphite epoxy
 $[\pm 45_n / 0_n / 90_n]_s$



Numbers of plies

Figure 3.

FINITE ELEMENT ANALYSIS OF STRAIN ENERGY RELEASE RATES

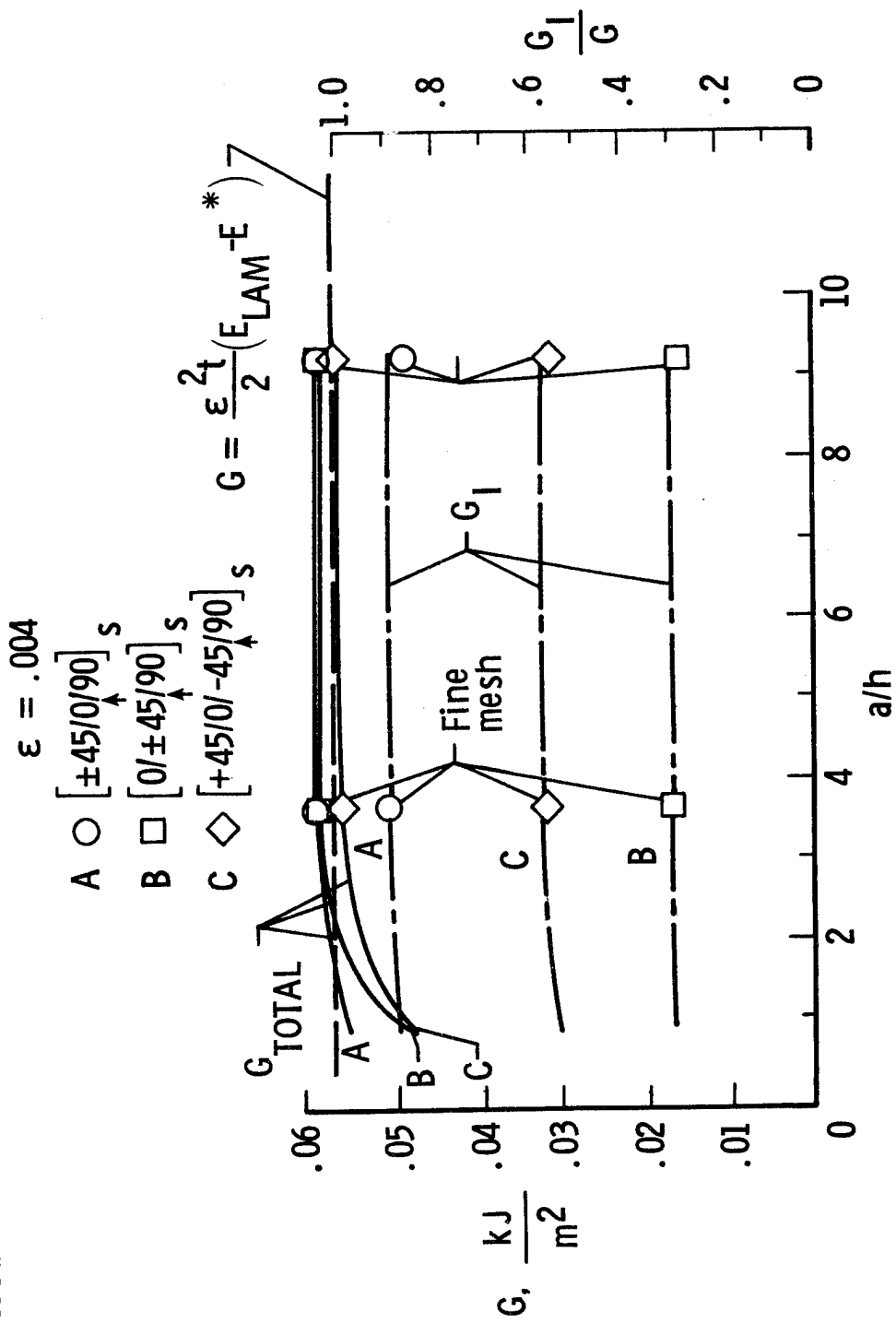


Figure 4.

INFLUENCE OF RESIDUAL THERMAL STRESS ON G FOR EDGE DELAMINATION

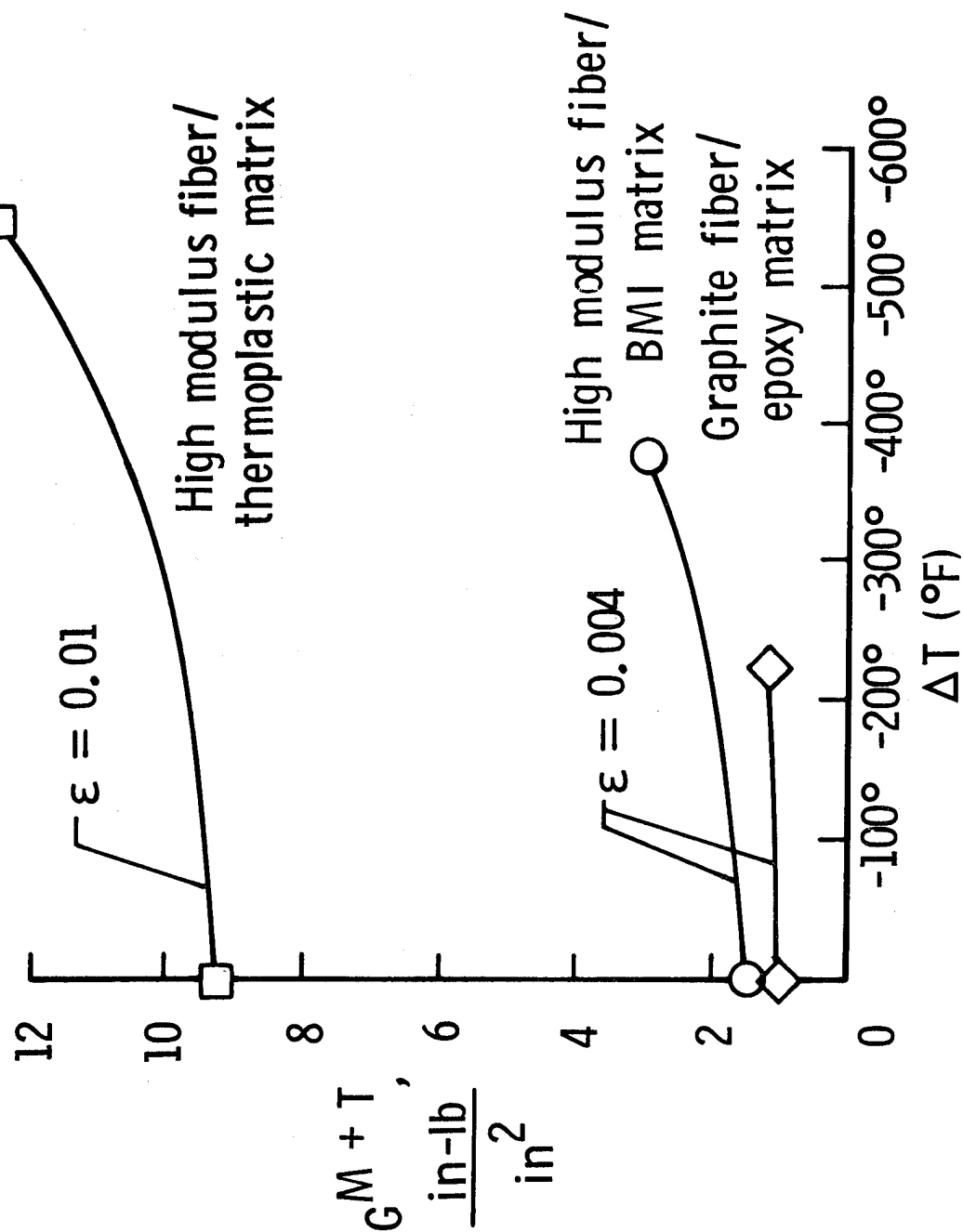
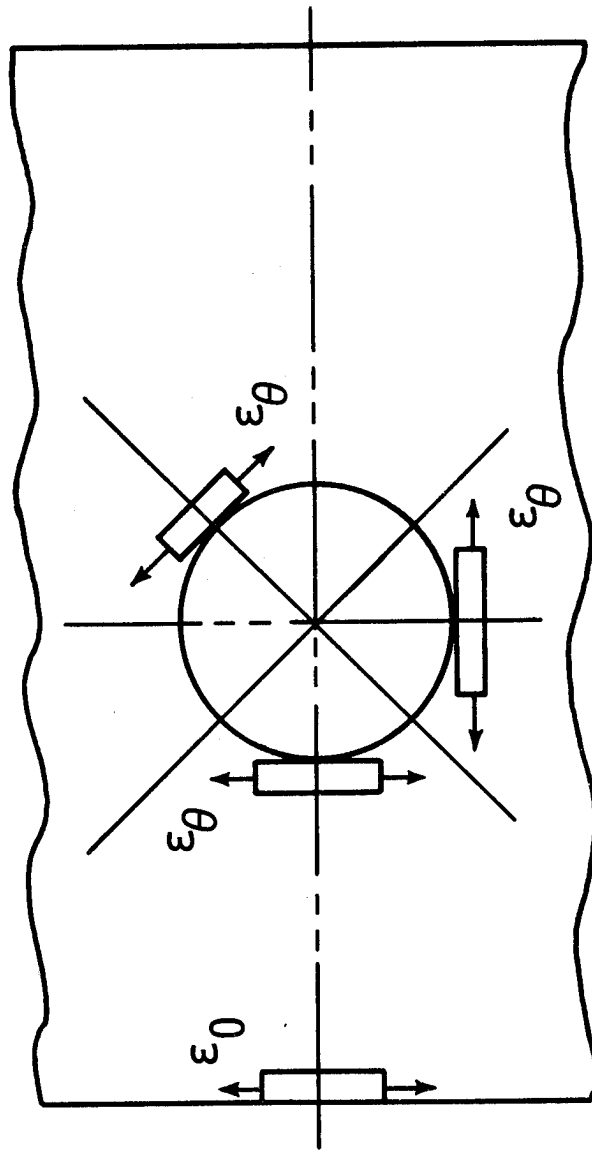
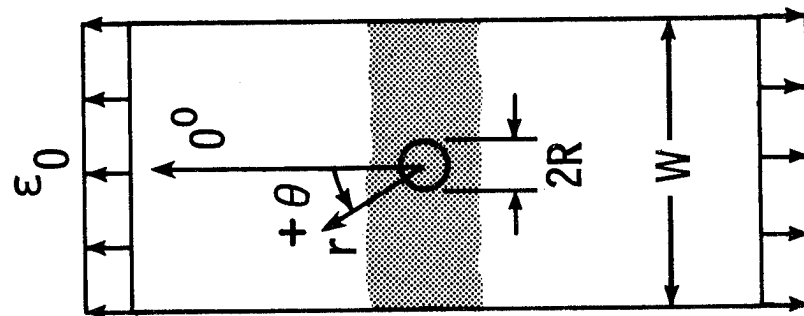


Figure 5.

ROTATED STRAIGHT EDGE ANALYSIS OF STRAIN ENERGY RELEASE RATE AROUND AN OPEN HOLE



$$G = \frac{\epsilon_{\theta}^2 t}{2m} [E_{LAM} - E^*(\theta)]$$

Figure 6.

**NORMALIZED STRAIN ENERGY RELEASE RATE DISTRIBUTION
IN 45/90 INTERFACE OF (45/90/-45/0)_S LAMINATE
NEAR HOLE BOUNDARY (SHADED REGION IS G_I)**

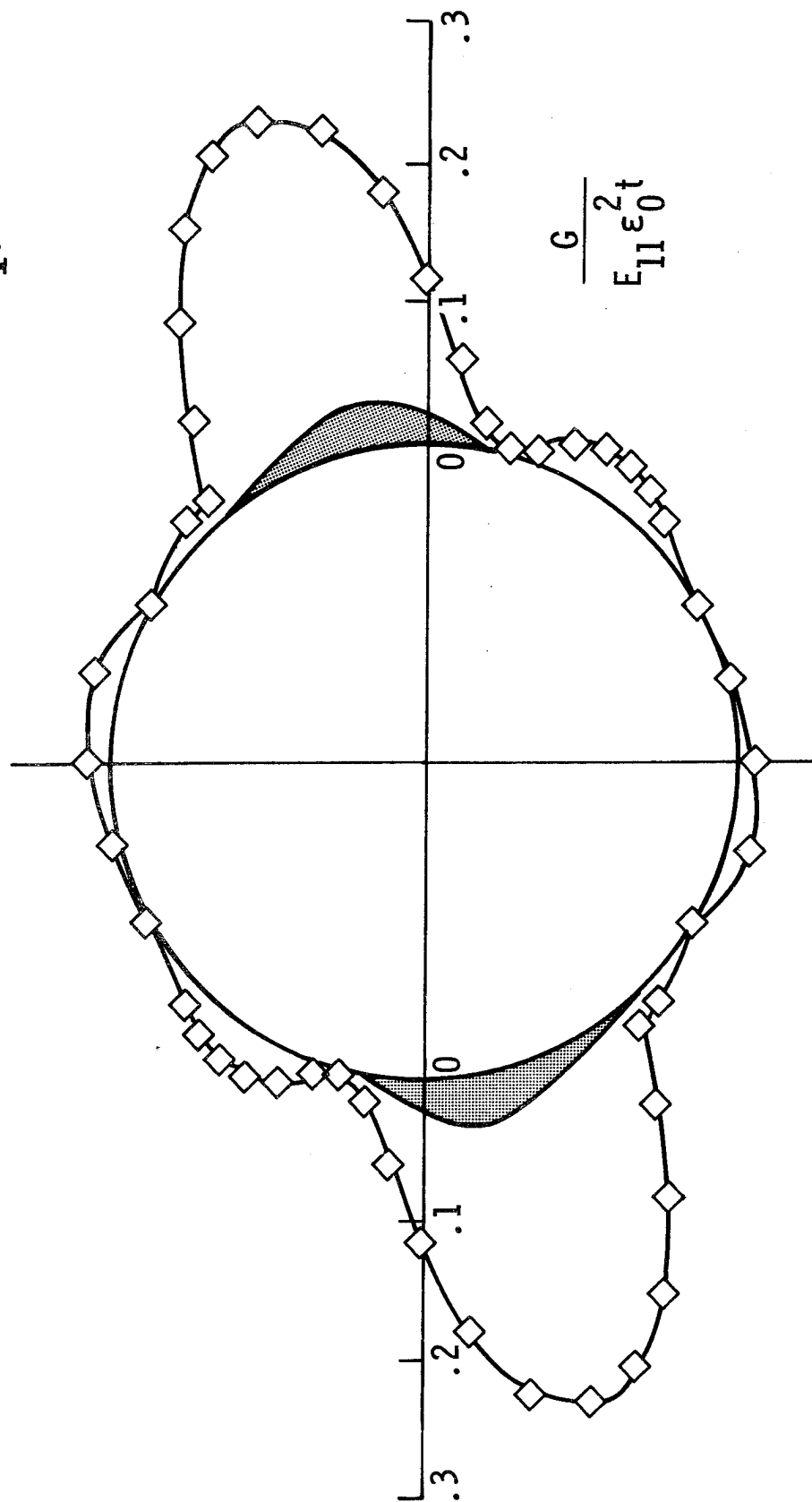


Figure 7.

COMPARISON OF DELAMINATION ANALYSES FOR STRAIN ENERGY RELEASE RATE COMPONENTS

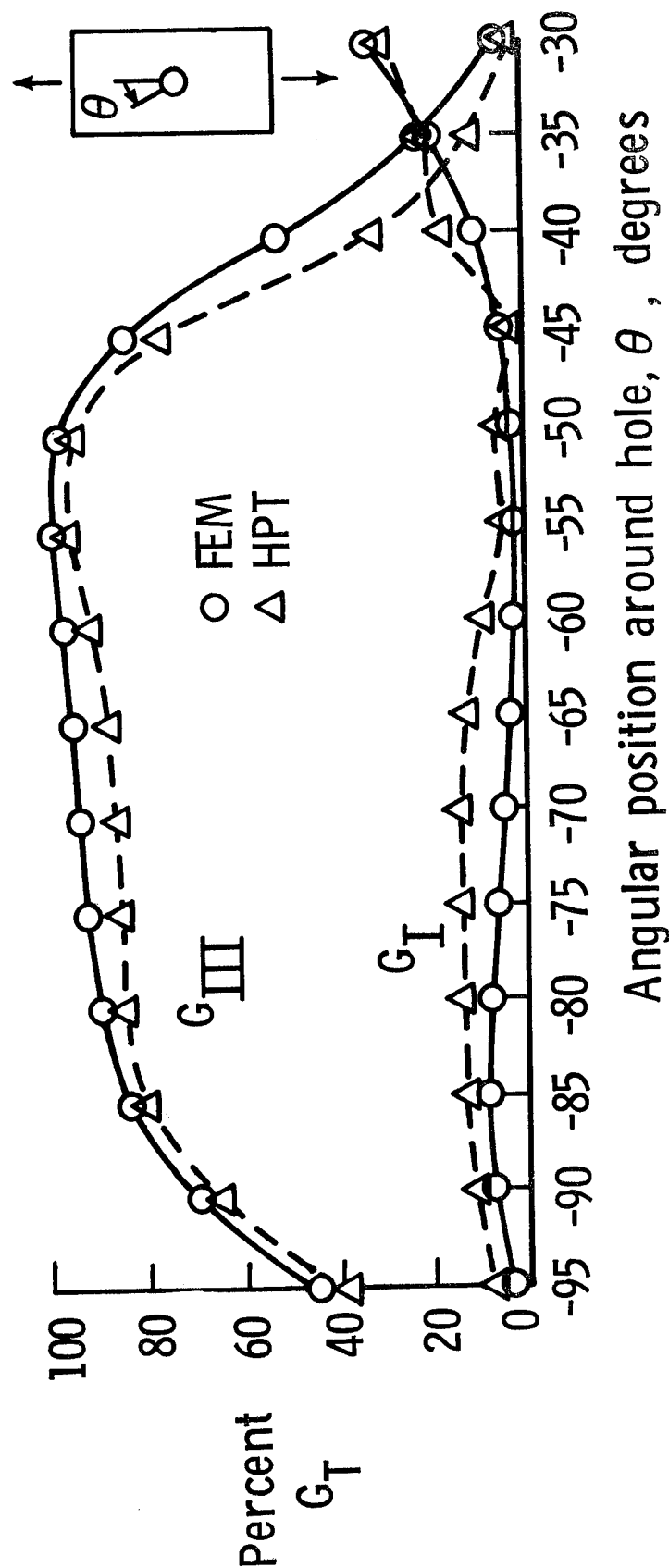


Figure 8.

STRAIN ENERGY RELEASED RATE ANALYSIS OF

DELAMINATION IN A TAPERED LAMINATE

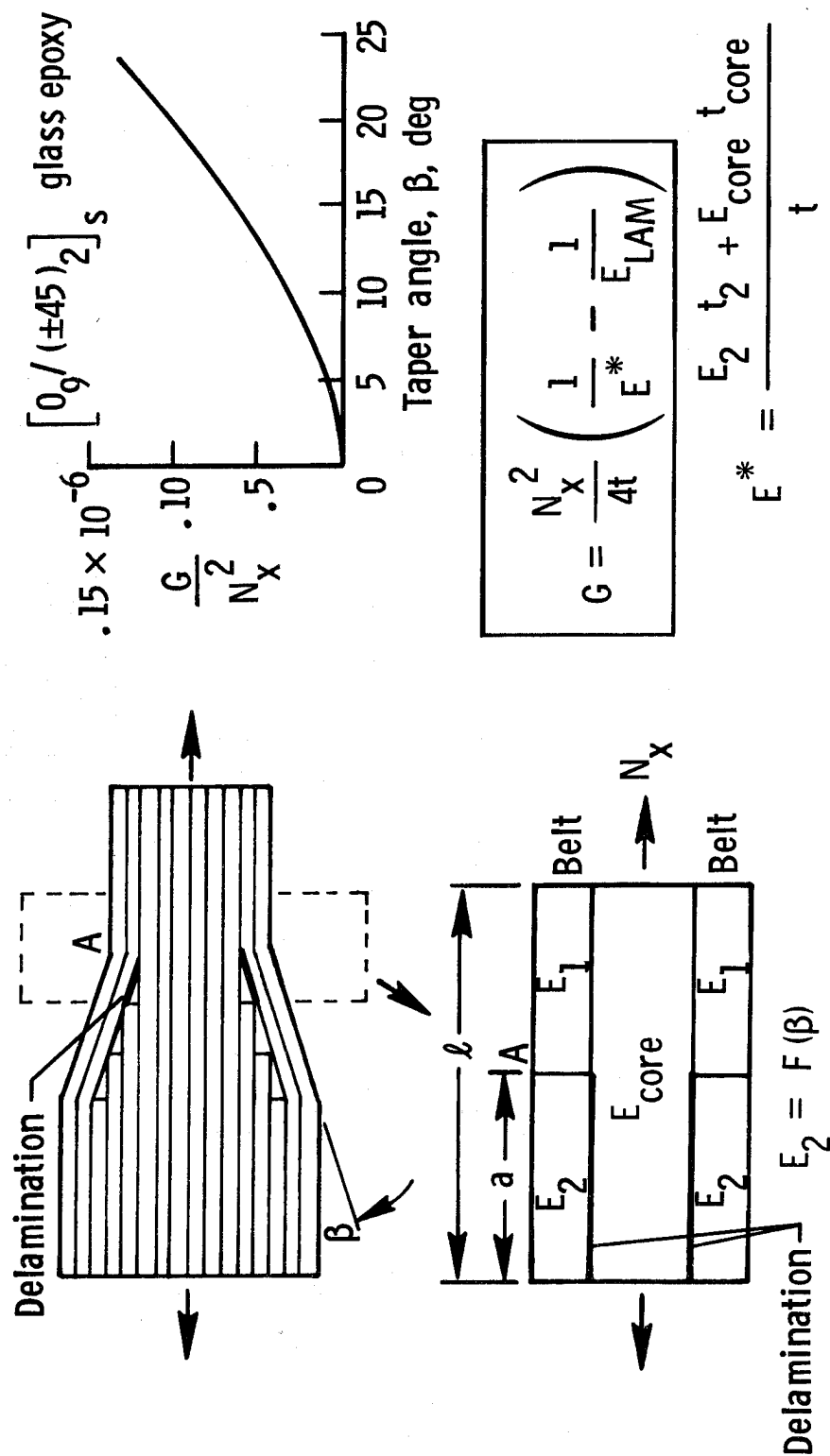
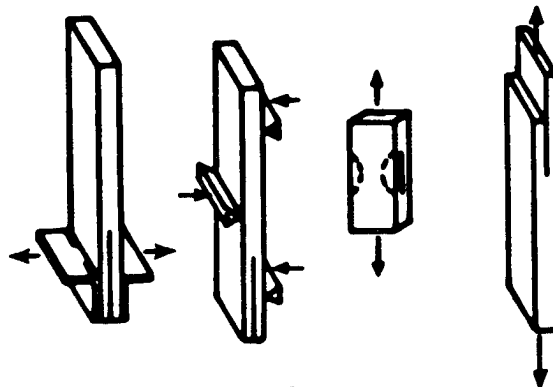


Figure 9.

ASTM ROUND ROBIN INTERLAMINAR FRACTURE TOUGHNESS TESTING

Brittle ← → Tough

Test \ Material	AS4/3501-6	AS4/BP907	AS4/PEEK
DCB - Mode I			
ENF - Mode II			
EDT - Mode I and mixed mode			
CLS - Mixed mode			



- 32 laboratories included
- 5 countries represented
- Each participant limited to two tests
- Between 9 and 16 participants per test

Figure 10.

MIXED MODE FRACTURE TOUGHNESS

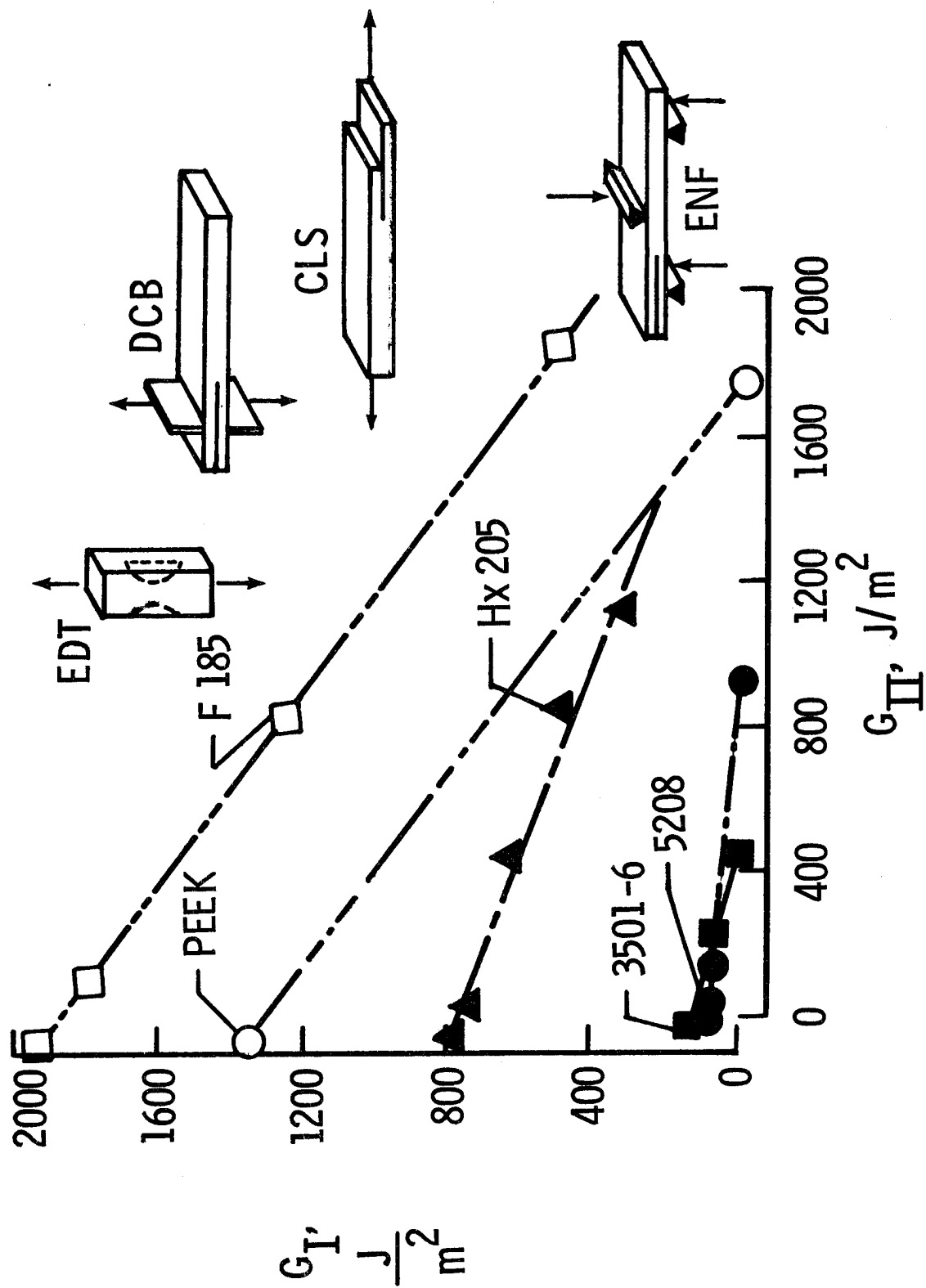


Figure 11.

G_c AS A FUNCTION OF FATIGUE CYCLES

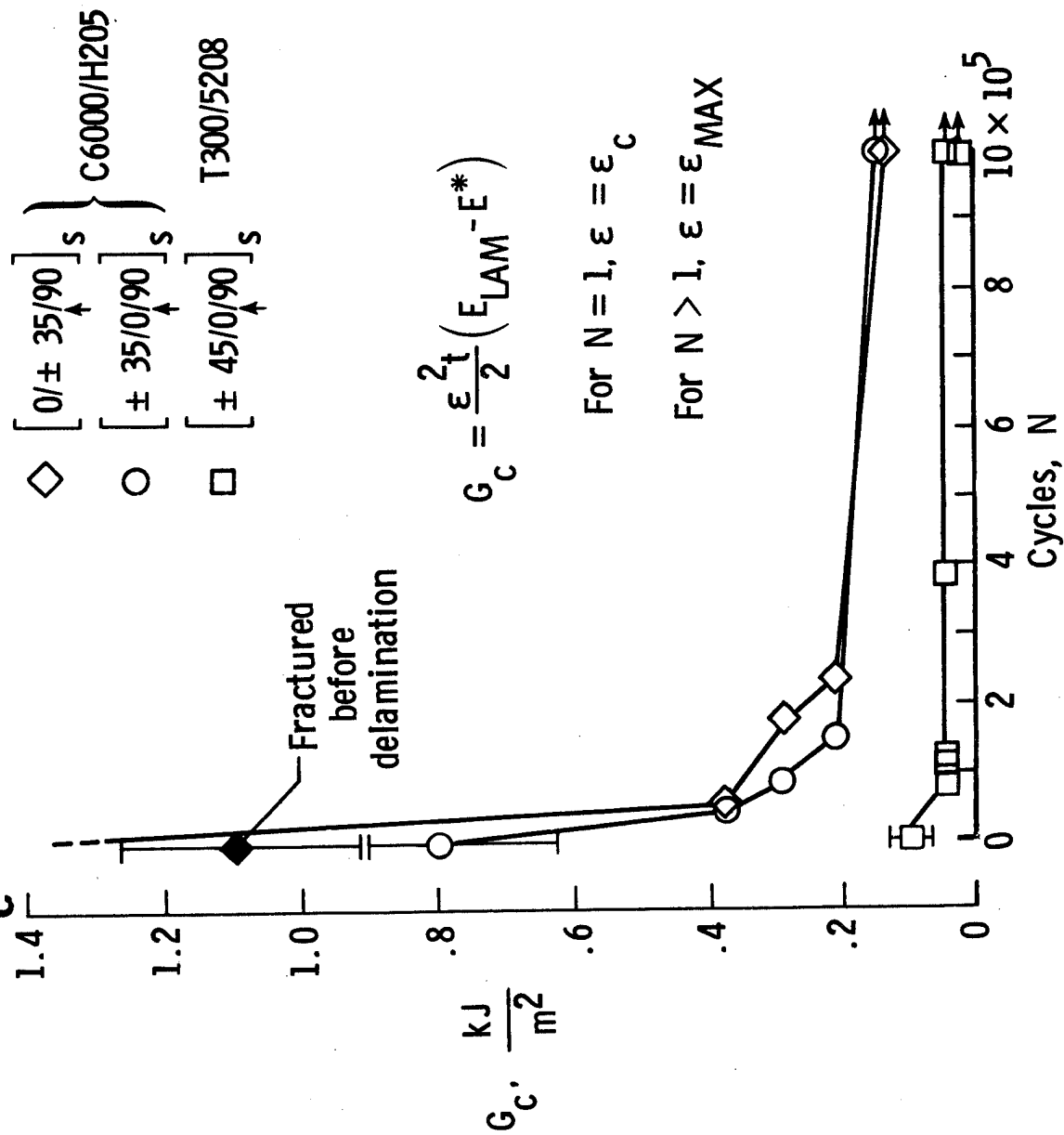


Figure 12.

MECHANICAL STRAIN ENERGY RELEASE RATE AT DELAMINATION ONSET AS A FUNCTION OF FATIGUE CYCLES

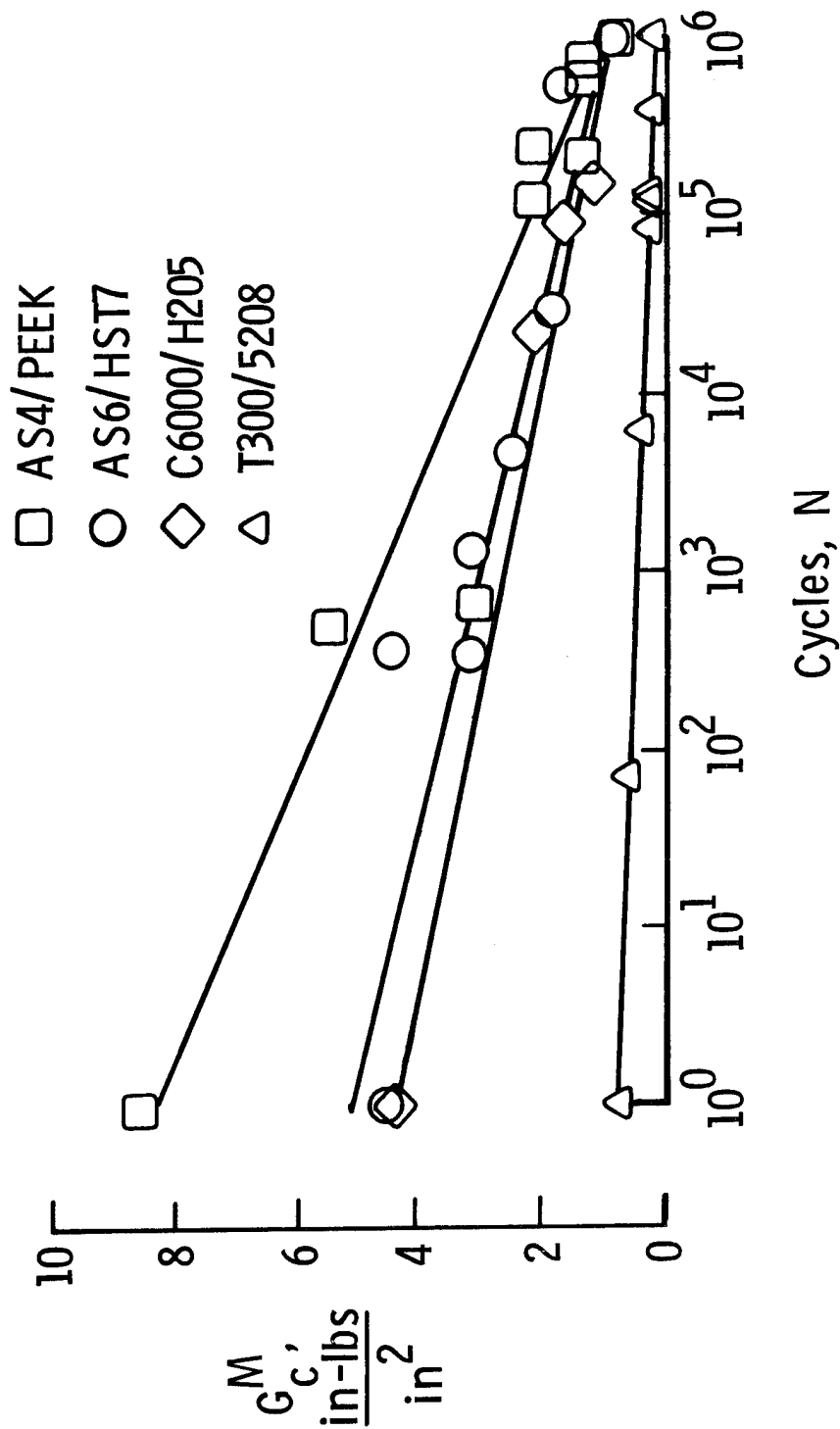


Figure 13.

COMPARISON OF DELAMINATION GROWTH RATES FOR COMPOSITES WITH BRITTLE AND TOUGH MATRICES

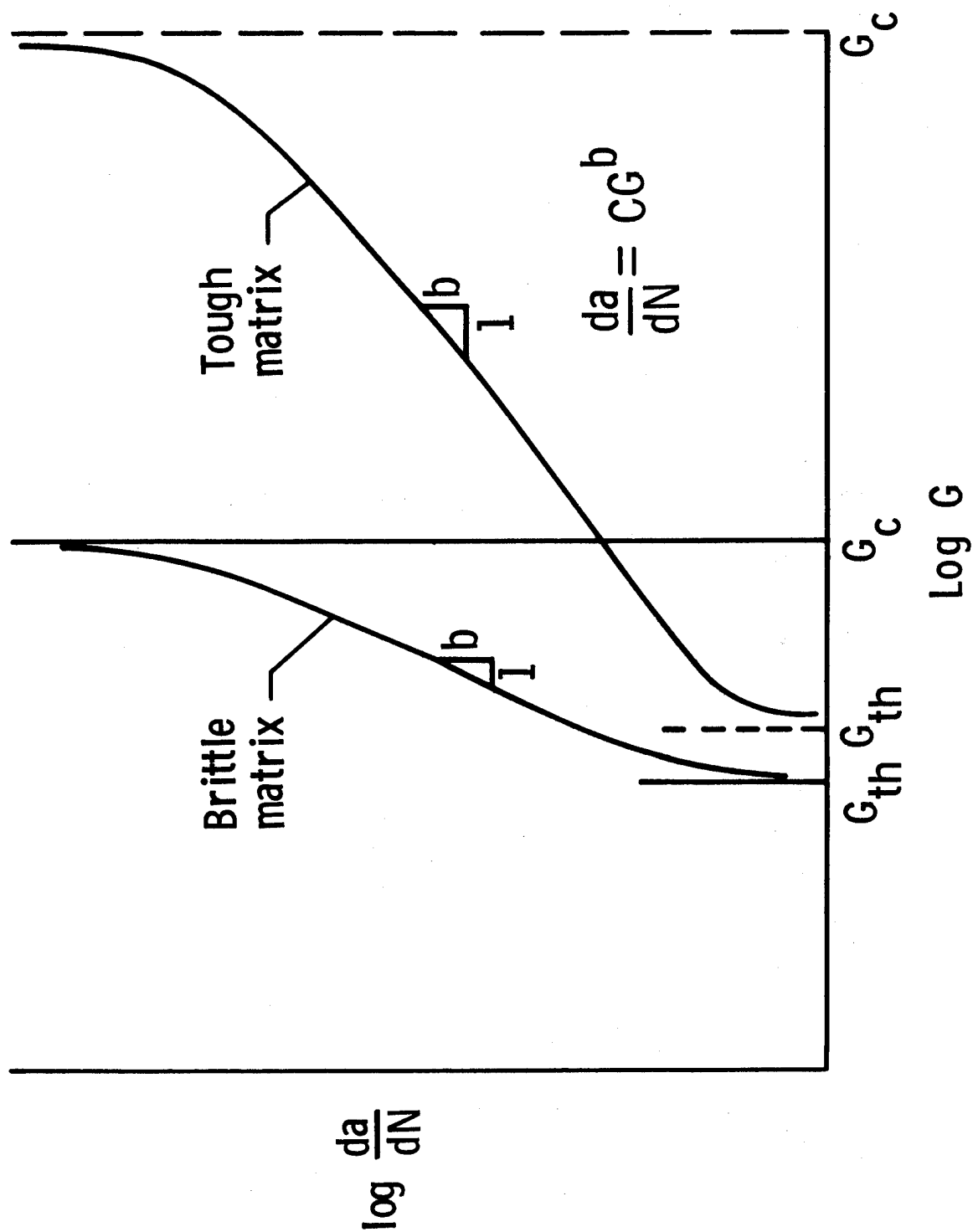


Figure 14.

TENSILE FATIGUE BEHAVIOR OF UNNOTCHED $[\pm 45/0/90]_s$ GRAPHITE EPOXY LAMINATES

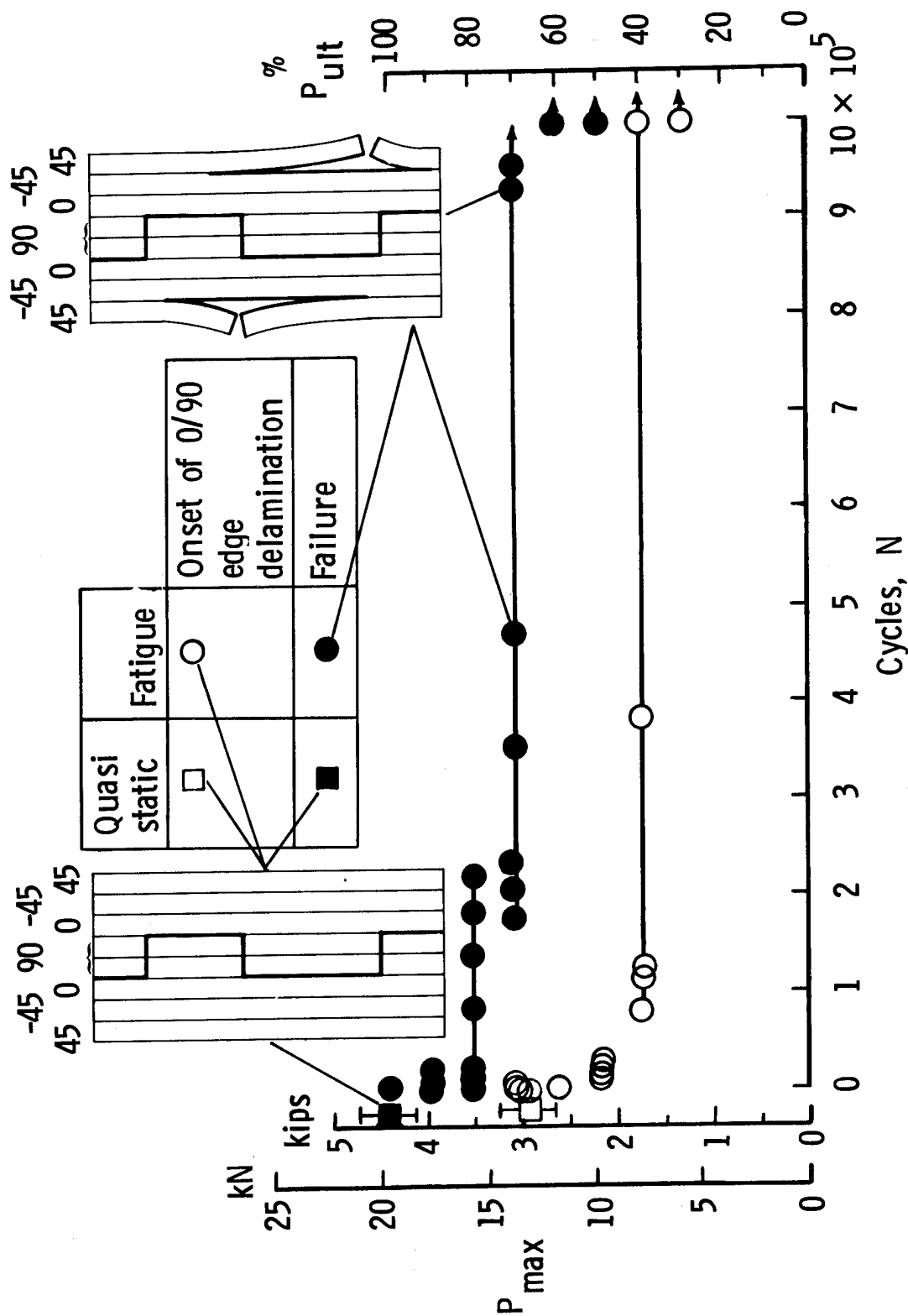


Figure 15.

FATIGUE LIFE ESTIMATION TECHNIQUE FOR COMPOSITE LAMINATES

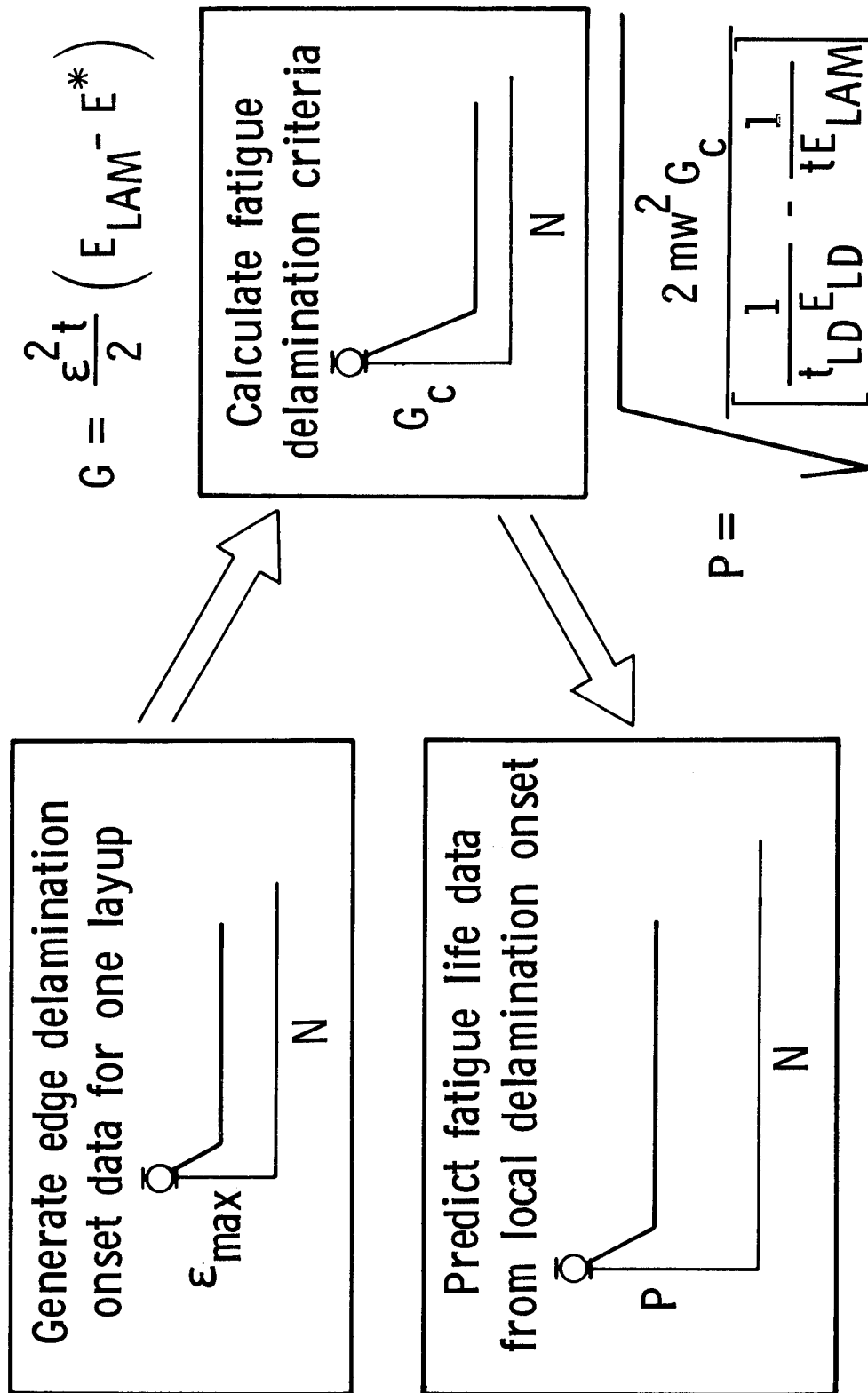


Figure 16.

HELICOPTER CRASHWORTHINESS RESEARCH PROGRAM

Gary L. Farley and Richard L. Boitnott

Aerostructures Directorate
USAARTA-AVSCOM

National Aeronautics and Space Administration
Langley Research Center

and

Huey D. Carden

National Aeronautics and Space Administration
Langley Research Center

Results are presented from the U.S. Army-Aerostructures Directorate/NASA-Langley Research Center joint research program on helicopter crashworthiness. Through the on-going research program an in-depth understanding has been developed on the cause/effect relationships between material and architectural variables and the energy-absorption capability of composite material and structure. Composite materials were found to be efficient energy absorbers. Graphite/epoxy subfloor structures were more efficient energy absorbers than comparable structures fabricated from Kevlar or aluminum. An accurate method of predicting the energy-absorption capability of beams was developed.

INTRODUCTION

The design requirements in Mil-Std-1290, reference 1, define the crash scenarios that must be survivable for the occupants of U.S. Army helicopters. Vehicle crashworthiness, as specified in Mil-Std-1290, requires the maintenance of a protective shell around the occupants in addition to absorbing vehicle kinetic energy. In the case of a helicopter the protective shell is the fuselage structure. The crash induced loads in the helicopter fuselage structure, per the requirements of Mil-Std-1290, are generally greater than loads from other flight or ground conditions.

In the next generation of military helicopters, composite materials will be used extensively in all primary structure. Composite materials offer considerable potential advantages over metallic materials from the perspective of weight and fabrication cost. However, composite materials and structures exhibit brittle failure characteristics, in contrast to the benign ductile failure characteristics of most metallic structures.

Prior to the design of the next generation of military helicopters, sufficient technology must be developed to design crashworthy fuselage structure utilizing composite materials. This technology includes understanding the cause/effect relationships of energy absorption in composite materials and developing analysis tools and design methodology. Once the material response is understood, efficient energy absorbing structural subfloor concepts can be developed.

The U.S. Army Aerostructures Directorate and NASA's Langley Research Center formed a joint research program to develop the technology required to design crashworthy composite helicopter structure. This program consists of a material characterization phase, a structural element phase, and a fuselage section demonstration phase. The material characterization phase consists of investigations to understand how composite materials absorb energy and how the numerous material and architectural variables effect energy-absorption capability. The structural element phase consists of two parts: subfloor structure and fuselage structural integrity. Investigations conducted in the structural element phase include the development of energy absorbing subfloor beam concepts, analysis methods, and fuselage structural integrity. The final phase, a fuselage section demonstration, includes the design and fabrication, of representative floor and fuselage sections. These sections will be tested using static load and dynamic impact conditions.

This paper presents the results obtained to date in the material characterization and structural element phases. Recent developments in energy absorbing composite materials and structures are described. Finally, results are presented from composite fuselage frame investigations.

SYMBOLS

A	cross sectional area, cm^2 .
D	internal diameter of circular cross section tubes, cm.
E	epoxy matrix.
F	woven fabric material.
G1	glass fiber reinforcement.
Gr	graphite fiber reinforcement.
H	graphite/Kevlar hybrid 24 by 24 balanced woven fabric material.
i.C.E.	ith characteristic element.
K	Kevlar fiber reinforcement.
N	number of plies.
n	number of characteristic elements.
S	symmetric ply layup.
S.E.	structural element.
T	tape material.
t	tube wall thickness, cm.
W	internal width of square cross section tubes, cm.
D/t	diameter-to-thickness ratio of circular cross section tubes.
W/t	width-to-thickness ratio of square cross section tubes.
σ	average crushing stress, Pa.
ρ	material density, gr/cm^3 .
θ	ply orientation angle.
σ/ρ	specific sustained crushing stress, Nm/gr .

TERMINOLOGY

Specific sustained crushing stress - average crushing load divided by the product of the specimen cross sectional area and the material density.

Characteristic crushing length - the nominal length of the crushed material.

Bias ply - composite ply oriented at any direction other than along the longitudinal or transverse axis of the specimen.

DYCAST - finite element computer code, Dynamic Crash Analysis of Structures, reference 2.

ENERGY ABSORPTION CHARACTERISTICS OF COMPOSITE MATERIAL

Design of efficient energy absorbing structure requires understanding the cause/effect relationship between the material and architectural variables and the energy-absorption capability of composite materials. Composite materials and structures absorb energy in modes that are considerably different than those of metallic materials and structures. Tailoring the mechanical response of composites using material property variables (fiber and matrix stiffness and failure strain) and architectural variables (ply orientation, stacking sequence, hybridization, fiber volume fraction, and specimen geometry) is well understood. However, the manner in which these variables affect the energy-absorption capability of composite materials is not well understood. Studies were conducted to further define the energy absorption process of composite materials. These studies included definition of the crushing process and crushing modes and the energy absorption efficiency of several composite materials and an investigation of what effect material property variables, architectural variables, and crushing speed have on the energy-absorption capability of composite materials.

In the following discussion, data are presented in terms of the specific sustained crushing stress (σ/ρ). Specific sustained crushing stress is a measure of energy-absorption capability.

Crushing Modes/Processes

Four different crushing modes and combinations of the four modes have been identified for composite materials, as reported in references 3-8 and depicted in figure 1. These four modes are 1) local buckling, 2) transverse shearing, 3) brittle fracturing, and 4) lamina bending. The local buckling mode is similar to that exhibited by ductile metals. This crushing mode has been demonstrated by both ductile (Kevlar) and brittle (graphite and glass) fiber reinforced composites. Ductile fiber composites always exhibit the local buckling crushing mode. Ductile fibers plastically deform at the buckle site along the compression side of the buckled fibers. The fibers can also split into small fibrils along the tension side of the buckled fibers. Ductile fiber reinforced composites remain intact after being crushed and thereby demonstrating post-crushing integrity. The post-crushing integrity of ductile fiber reinforced composites is a result of fiber plasticity and fiber splitting. Brittle fiber composites only exhibit the local buckling crushing mode when the ply orientations are such that interlaminar stresses which are small relative to the strength of the matrix and when the matrix is a high failure strain and low stiffness material. The combination of a high failure strain/low stiffness matrix with certain ply orientations reduces or prevents interlaminar cracking from occurring in the crushing process. If the interlaminar cracks are eliminated the tube crushes in the local buckling mode or fails catastrophically and is unable to carry load.

The brittle fracturing, lamina bending, and transverse shearing modes are exhibited exclusively by brittle fiber reinforced composites. These crushing modes are a function of the mechanical properties of the constituent materials. Generally, one or multiple interlaminar cracks are formed through the thickness of the composite. The number, location, and length of the cracks are a function of architecture and constituent material properties. The interlaminar cracks form lamina bundles which can act as columns. As the load is applied the interlaminar cracks grow until the column buckles and either the edges of the column are sheared away forming a conical shaped cross section (transverse shearing mode), fractured (brittle fracturing mode), or bent (lamina bending mode).

Just as strain rate can effect the mechanical response of a material, crushing speed can effect the energy-absorption capability of composite materials. To understand how crushing speed influences energy-absorption capability it is necessary to determine how crushing speed affects the mechanisms that control the crushing process.

The controlling mechanisms in the four crushing modes are: transverse laminate strength (transverse shearing crushing mode), matrix strength (brittle fracturing and lamina bending crushing modes), lamina bundle bending strength (brittle fracturing crushing mode), and fiber/matrix yield strength (local buckling crushing mode). The transverse strength of a laminates typically used in helicopter structural applications is primarily a function of fiber strength. Therefore, if the fiber's mechanical response is a function of strain rate then the energy-absorption capability of specimens that crush in a transverse shearing mode can be a function of crushing speed.

Matrix strength controls the interlaminar crack growth in both the brittle fracturing and lamina bending crushing modes. Many polymeric matrix materials exhibit mechanical responses that are a function of strain rate. Therefore, a specimen that exhibits either the brittle fracturing mode or lamina bending mode can exhibit energy-absorption capability that is a function of crushing speed. Crushing speed will effect energy-absorption capability when the percentage of energy absorbed by the interlaminar crack growth is a significant part of the total energy absorbed. For that reason, specimens that crush in the lamina bending mode will be more affected than specimens that crush in the brittle fracturing mode. In the lamina bending crushing mode a significant portion of the total energy absorbed is by interlaminar crack growth, whereas the converse is true for the brittle fracturing mode.

The bending strength of the lamina bundle controls the fracturing of the lamina bundle in the brittle fracturing crushing mode. The mechanical response of the lamina bundle is primarily a function of either fiber (e.g., 0 degree lamina bundle) or matrix (e.g., 90 degree lamina bundle or low fiber volume fraction material). Therefore, if the mechanical response of the dominant property (fiber or matrix) is a function of strain rate then the energy-absorption capability of the lamina bundle can be a function of crushing speed.

The mechanism that controls the local buckling crushing mode is the yield strength of the fiber and/or matrix. Brittle fiber reinforced composites can produce the local buckling crushing mode only if the matrix has a low stiffness and high failure strain. If the matrix mechanical response is a function of strain rate then the energy-absorption capability can be a func-

tion of crushing speed. Ductile fiber reinforced composites crush in the local buckling mode because of either the fiber or matrix properties. Therefore, if either the fiber or matrix mechanical response is a function of strain rate then the energy-absorption capability can be a function of crushing speed.

ENERGY-ABSORPTION EFFICIENCY

Debris size of crushed material (characteristic crushing length) is a qualitative measure of energy-absorption efficiency. The characteristic crushing length of specimens that exhibit transverse shearing mode, brittle fracturing mode, lamina bending mode, and local buckling mode are on the order of a lamina thickness, a laminate thickness, 10-100 laminate thicknesses, and 10-50 laminate thicknesses, respectively. The smaller the characteristic crushing length the greater the energy-absorption efficiency. This ordering of energy-absorption crushing efficiency is applicable only to specimens of the same material. Different materials have different energy-absorption potential. A specimen fabricated from a material that has a high energy-absorption potential can have a greater energy-absorption capability despite a less efficient crushing mode than a specimen fabricated from a material that has a lower energy-absorption potential but crushes in a more efficient mode.

EFFECT OF MATERIAL PROPERTIES

Fiber and Matrix Failure Strain

A series of studies, references 9 and 10, were performed to determine the effect of fiber and matrix failure strain on energy-absorption capability of graphite and Kevlar reinforced composites. These studies were conducted using low failure strain (T300), intermediate failure strain (AS4) and high failure strain (AS6) graphite, and with Kevlar fibers. These fibers were embedded into low failure strain (934), intermediate failure strain (5245 and 974), high failure strain (F185), and toughened interleaved (HST-7) matrices. Table 1 presents the combinations of these fibers and matrices used in this study. Based upon the results of these studies, as shown in figures 2 and 3, composite materials composed of low and intermediate failure strain graphite fibers and matrices (T300/934, AS4/934, T300/5245, and AS4/5245) generally exhibit an increase in energy-absorption capability as failure strain increased. The predominant crushing mode of the materials was a brittle fracturing mode with lamina bending. The energy-absorption trends for the low and intermediate failure strain material are generally consistent with mechanical response trends of these composites. However, these trends do not hold for high strain fiber and matrix material (AS6/F185) and the high strain fibers in a toughened matrix material (AS6/HST-7) as shown in figure 4. The crushing mode of the high strain material changed from a predominantly brittle fracturing to a predominantly lamina bending mode or to a local buckling crushing mode. The energy-absorption capability of the high strain and toughened composites were substantially less than the intermediate strain (AS4/5245) material. The crushing mode of the toughened material was a mixture of brittle fracturing and lamina bending and energy-absorption capability was similar to that exhibited by the AS4/934 material. The toughened interleaved material consists of a low failure strain matrix, similar to the 934 matrix, with a high failure strain adhesive between the plies. The adhesive

layer was ineffective in stopping the interlaminar cracks because the cracks formed in the low failure strain matrix adjacent to the adhesive layer.

Similar studies were conducted using Kevlar-49 in 934 and 974 matrices to determine the effect of matrix failure strain on the energy-absorption capability of a ductile fiber reinforced composite material. As shown in figure 5, a 5 to 15 percent decrease in energy-absorption capability occurred as matrix failure strain increased from 1 to 2 percent. The crushing mode and crushing load level are primarily controlled by the compression characteristics of the fiber. Kevlar fibers exhibit an inherent failure mechanism related to its plastic deformation. Therefore, matrix failure strain would have little effect on altering the fiber failure load or mode.

Effect of Fiber Stiffness

The effects of fiber stiffness, reference 10, on the energy-absorption capability were evaluated for brittle fiber reinforcements using T300, P55, and P75 graphite fibers in a common matrix (934). It is difficult in studies of this type to isolate the effects of a single property on energy-absorption capability. Two cases were cited in the previous section where a change in a secondary material property altered the crushing response. In this evaluation the effects of fiber stiffness were studied. However, the fibers have significantly different failure strains. The failure strain of the T300, P55, and P75 graphite fibers are 0.012, 0.005, and 0.004, respectively.

Figures 6 and 7 show that energy-absorption capability decreased nonlinearly with respect to increasing fiber stiffness. The difference in energy-absorption capabilities demonstrated by the material systems is proportional to the difference in fiber failure strain. This proportionality between energy absorption and fiber failure strain is apparent upon examining the energy-absorption trends for ply orientations where fibers are principally oriented in the direction of the applied load such as $[0/\pm 15]_4$ and $[\pm 15]_6$. These results suggest that changes in fiber stiffness affect energy-absorption capability less than changes in fiber failure strain, provided the different materials crush in the same mode. The P55/934 and P75/934 material exhibited a progressive transverse shearing crushing mode. The residue formed by crushing the P55/934 and P75/934 was like powder whereas residue from the T300/934 material was coarser. These results indicate that the high failure strain brittle fibers, such as glass, have significant potential for absorbing energy provided the load carrying fibers can be sufficiently stabilized to crush in a transverse shearing or a brittle fracturing mode.

EFFECT OF SPECIMEN ARCHITECTURE

Effects of Ply Orientation and Material Form

Ply orientation is one of the most important variables available to the composite structural designer to tailor the mechanical response of a composite laminate. The stiffness and strength of a laminate are a direct function of the ply orientation. However, energy-absorption capability is not as well defined. The effects of ply orientation on the crushing response of tube specimens was investigated.

Tests were conducted, reference 3, on T300/934 (Gr/E), E-G1/934 (G1/E), and K/934 (K/E) tube specimens, as shown in figure 8, to determine the effect of ply orientation on energy-absorption capability. Only the results from the $[0/\pm\theta]_4$ specimens will be discussed. The energy-absorption trends for the materials differed significantly. As the ply angle increased, the energy-absorption capability of the Gr/E material decreased. This trend is consistent with the general mechanical response of such composites. However, the opposite trend occurred for the G1/E and K/E material. Energy-absorption capability generally increased with increasing ply angle. The difference in energy-absorption trends can be explained by examination of the crushing modes.

The Gr/E specimens crushed in a brittle fracturing mode while the G1/E and K/E specimens crushed in a lamina bending and local buckling mode, respectively. As previously discussed, the brittle fracturing mode exhibited by the Gr/E is a more efficient energy-absorption mode than the lamina bending or the local buckling modes. These energy-absorption trends can be related to the constituent properties of the fiber and matrix.

In the case of the Gr/E specimens, the matrix is sufficiently stiff and has sufficient failure strain to stabilize the axially oriented Gr fibers. Therefore, the crushing load, hence energy-absorption capability, is a function of axial stiffness. At bias ply orientations greater than 45 degrees, the bias plies began to provide lateral support to the axially oriented fibers. That is, the bias plies helped the matrix. Beyond 60 degrees the loss of axial stiffness balanced out the increased lateral support provided by the bias plies and resulted in a relatively constant energy-absorption capability.

The glass fibers in tube specimens that have fibers oriented in the direction of the applied load are not adequately stabilized by the matrix which results in a less efficient energy-absorption mode (lamina bending). As the bias plies become more circumferentially oriented the energy-absorption capability increased even though the axial stiffness decreased. At bias ply angles greater than 45 degrees, the bias plies provide lateral support to stabilize the axial fibers. Further increase in circumferential fiber angle beyond 60 degrees provided no additional support to the axial fibers. A similar crushing scenario applies to the K/E specimens except that the K/E specimens crushed in a local buckling mode.

Another important parameter influencing energy-absorption capability is the material form, such as tape, planar woven, or filament wound material. The majority of the studies have been performed with specimens fabricated using tape and planar woven composite prepreg material. The characteristic crushing length of the tape material is a function of the fiber and matrix mechanical properties and ply orientation as previously discussed. The woven material has a built-in failure initiator at each undulation of the reinforcement tow. These undulations can predetermine the characteristic crushing length of the material. In the case of glass reinforced composites, the undulations of the woven material can change the crushing modes from lamina bending to a brittle fracturing mode. Changes of this type can influence the energy-absorption capability. If the characteristic crushing length of a specimen is less than the spacing of undulations, then the woven material will have a lower energy-absorption capability than the nonwoven material. In this case, the undulation reduces the bending stiffness of the lamina bundles resulting in a lower

energy-absorption capability for the woven material. Filament wound specimens typically crush in modes similar to those of specimens fabricated using tape prepreg provided the interleave spacing is greater than the characteristic crushing length.

Effects of Stacking Sequence

Lamina stacking sequence can be an important variable in tailoring the bending stiffness of a composite laminate and, therefore, will have significant implications with respect to energy-absorption capability, as reported in reference 10. Figure 9 shows the effect of stacking sequence on a hybrid composite and figure 10 examines this same effect on Gr/E and K/E [± 45] composites.

Figure 9 shows the effect of stacking sequence on the energy-absorption capability of [$+45^\circ_F/0^\circ_{Gr_{10T}}/-45^\circ_F$] and [$0^\circ_{Gr_{5T}}/\pm 45^\circ_F/0^\circ_{Gr_{5T}}$] tube specimens. The difference between these two stacking sequences is the position of the 0 degree Gr/E plies. In the first specimen the 0 degree Gr/E plies are in the center of the layup, whereas, the 0 degree Gr/E plies are on the outside in the second specimen. A 300 percent difference in energy-absorption capability was obtained for these hybrid composite specimens. The difference in energy-absorption capability is attributed to the crushing mode of the 0 degree plies. The 0 degree graphite plies of the [$+45^\circ_F/0^\circ_{Gr_{10T}}/-45^\circ_F$] specimens crushed in a brittle fracturing mode while the 0 degree graphite plies of the [$0^\circ_{Gr_{5T}}/\pm 45^\circ_F/0^\circ_{Gr_{5T}}$] specimens crushed in a lamina bending mode. Both types of specimens exhibited post-crushing integrity as a result of the hybrid woven fabric plies. Current composite design practice would avoid layups concentrating all the 0 degree plies either in the center or on the outer surfaces. From an energy absorption consideration the 0 degree plies should not be located on the outer surfaces.

Stacking sequence does not always have as significant effect on energy-absorption capability. In figure 10 the test results of two different combinations of [± 45] Gr/E plies and three different combinations of [± 45] K/E plies are presented. Only a 5 percent change in energy-absorption capability was demonstrated by the [± 45]₆ and [$\pm 45_3/+45_3$] Gr/E specimens. Both [± 45]₆ and [$\pm 45_3/+45_3$] Gr/E specimens exhibited the characteristic brittle fracturing mode. The energy-absorption capability of the [$+45_6/-45_6$] K/E specimens was approximately 30 percent lower than the [± 45]₆ and [$\pm 45_3/+45_3$] K/E specimens. The [$+45_6/-45_6$] specimens exhibited the characteristic buckling crushing mode although more extensive interlaminar delaminations occurred than in the [± 45]₆ or [$\pm 45_3/+45_3$] specimens. Conventional manufacturing practices typically do not allow the segregation of plies in a manner representative of the [$+45_6/-45_6$] layup. Therefore, for most practical combinations of 45 degree plies stacking sequence has negligible effect on energy absorption.

A third example will demonstrate how concentrating all the plies in the center of the laminate can lead to unexpected results. A series of tests were conducted on [$\pm 45^\circ_K/0^\circ_{Gr_N}$]_S ply orientations where N=3, 6, 9, and 12. The test results are shown in figure 11 and typical crushed tubes are shown in figure 12. In this study, the ply orientations of the K/E plies were at ± 45 degrees which is representative of typical ply orientations in helicopter subfloor beams. The unidirectional Gr/E plies were oriented such that the fibers were in the direction of the applied crushing load, i.e., in the direction to achieve maximum energy-absorption capability.

Previous tests had shown that increasing the percentage of graphite plies oriented in the direction of applied load would produce higher energy-absorption capability. The test results shown in figure 11 exhibit the opposite trend. The reason for this trend is evident upon examination of the crushing modes shown in figure 12. As N (the number of 0 degree plies) increased, the crushing mode of the Gr/E plies changed from a brittle fracturing mode, to a predominantly lamina bending mode. However, in all cases the energy-absorption capability of $[\pm 45^K/0^{Gr}_N]_S$ exceeds the energy-absorption capability of aluminum. Ideally the circumferentially oriented plies (i.e., the K/E plies) should be interspersed through the laminate which would insure the Gr/E plies crush in a brittle fracturing mode.

Effect of Fiber Volume Fraction

The effect of fiber volume fraction, reference 10, on the energy-absorption characteristics of Gr/E and K/E composites is shown in figures 13 and 14, respectively. Prepreg materials with different percentages, between 40 and 70 percent, of fiber (by volume) were used to make tube specimens. As shown in figure 13, the $[\pm 45]_6$ and $[0/\pm 15]_4$ specimens exhibited an approximate 10 percent decrease in energy-absorption capability while the $[0/\pm 75]_4$ specimens exhibited an insignificant change in energy-absorption capability as fiber volume fraction increased between 40 and 55 percent. As the volume of matrix between fibers decreases, the interlaminar strength of the composite typically decreases. As the interlaminar strength decreases, interlaminar cracks form at lower loads, resulting in a reduction in energy-absorption capability. Also, as fiber volume fraction increases the density of the composite increases which results in a lower energy-absorption capability.

The effect of fiber volume fraction on energy-absorption capability of Kevlar reinforced composites is shown in figure 14. Between fiber volume fractions of 46 and 55 percent, the change in energy absorption was negligible for all ply orientations. The densities of the Kevlar fiber and the matrix are similar, therefore fiber volume fraction has little effect on energy-absorption capability provided the reduction in matrix between fibers does not affect the crushing mode. Both the $[\pm 45]_6$ and $[0/\pm 75]_4$ ply orientations exhibited approximately a 10 percent decrease in energy-absorption capability between fiber volume fractions of 54 and 70 percent. The energy-absorption capability of the $[0/\pm 15]_4$ ply orientation increased approximately 10 percent between fiber volume fractions of 55 and 66 percent.

Effects of Material Hybridization

The term hybrid composite material encompasses a large class of composite materials. Hybrids include both combinations of different reinforcement fibers in a laminate or a combinations of different material forms of the same fiber system such as tape and fabric. Most of the specimens that were fabricated with hybrid materials had different reinforcement fibers such as graphite-Kevlar or graphite-glass. Kevlar exhibits a local buckling crushing mode and has post-crushing integrity, which may be advantageous for certain structural applications. However, Kevlar composites are not as efficient energy absorbers as graphite composites. There are applications, such as the subfloor structure, where combining the post-crushing integrity characteristics of Kevlar with the high energy-absorption capability of graphite can

be beneficial.

A number of studies, references 3 and 10, have been conducted to evaluate the energy-absorption potential of hybrid materials. Only two of these materials will be discussed here. Figure 15 depicts the energy-absorption capability of $[\pm 45^\circ \text{H}_\text{F}]_2$ Gr-K/E and $[\pm 45^\circ \text{H}_\text{F}/0^\circ \text{Gr}_5 \text{T}]_5$ materials. The $[\pm 45^\circ \text{H}_\text{F}]_2$ hybrid woven fabric material is a balance weave fabric composed of alternating tows of graphite and Kevlar reinforcement. The $[\pm 45^\circ \text{H}_\text{F}/0^\circ \text{Gr}_5 \text{T}]_5$ hybrid consists of the aforementioned hybrid woven fabric enclosing 10 plies of unidirectional graphite tape. The energy-absorption capability of the $[\pm 45^\circ \text{H}_\text{F}]_2$ is approximately the average of the $[\pm 45^\circ \text{T}]_6$ Gr/E and K/E materials and the hybrid material also has post-crushing integrity. These results suggest that the hybrid material could be a direct replacement for Kevlar, both improving the energy-absorption capability and possessing post-crushing integrity. The $[\pm 45^\circ \text{H}_\text{F}/0^\circ \text{Gr}_5 \text{T}]_5$ hybrid material has an energy-absorption capability that exceeds all Gr/E layups evaluated and is 25 percent greater than 6061-T6 aluminum. This hybrid also has post-crushing integrity.

Effects of Specimen Geometry and Scalability

To date there is no standard test specimen or test method for characterizing the energy-absorption capabilities of composite materials. To quantify the energy-absorption capability of composites tubular specimens have been employed. However, the geometry (i.e., characteristic dimension, wall thickness, and cross sectional shape) of these specimens can significantly affect energy-absorption capability. Understanding the effects of specimen geometry is important for predicting the energy-absorption capability of subfloor beam structure.

A series of studies, references 11 and 12, were conducted using circular and square cross section tube specimens fabricated with Gr/E and K/E. Tube ply orientations were $[\pm 45^\circ]_\text{N}$. This ply orientation is used in typical subfloor beam structure. Circular cross section tube diameters ranged from 1.27 cm to 10.16 cm. The number of $\pm 45^\circ$ ply pairs (N) was between 2 and 24 resulting in internal diameter-to-wall thickness (D/t) ratios of 1.4 to 125. The energy-absorption trends for the circular cross section tube specimens are shown in figures 16 and 17. The energy-absorption capability of Gr/E circular cross section tubes is a nonlinear function of tube D/t ratio. All Gr/E tubes exhibited a progressive brittle fracturing crushing mode. A significant finding was that each diameter tube produced a different nonlinear response. A reduction in tube D/t ratio results in an increase in energy-absorption capability. This increase in energy-absorption capability is related to a reduction in interlaminar cracking in the crushed region of the tube. As the length and number of interlaminar cracks decreases, the buckling load of the associated lamina bundles increases. These results suggest that as D/t ratio decreases the sustained crushing stress approaches the compressive strength of the material. Therefore, the energy-absorption potential of a composite material is its compressive strength.

The K/E circular cross section tubes also exhibited a nonlinear energy-absorption capability as a function of tube D/t ratio as depicted in figure 17. Unlike the Gr/E tube results, the K/E test results do not show a different energy-absorption capability as a function of tube inside diameter. When

crushed, all K/E tubes, exhibited the characteristic local buckling crushing mode. The buckle wave length varied with tube geometry (tube diameter and wall thickness).

The nonlinear variation in energy-absorption capability with D/t ratio is similar to the classic short wave length buckling response of axially compressed metallic cylinders. Closed form buckling equations for metallic cylinders predict a linear variation in buckling load with D/t ratio, although tests yield a quadratic behavior. The differences between test and analytical predictions are generally attributed to inelastic behavior of the material and local imperfections.

Kevlar fibers exhibit inelastic compressive behavior similar to that of metallic materials. The nonlinear response with respect to D/t ratio is partially attributed to the fibers' inelastic response and tube imperfection. The increase in energy-absorption capability as D/t ratio decreases is related to a decrease in interlaminar cracking. The decreased interlaminar cracking reduces the magnitude of the local imperfections which directly affects the buckling load and, hence, the energy-absorption capability.

Square cross section Gr/E and K/E tubes with ply orientations of $[\pm 45]_N$ were also evaluated. The results are depicted in figures 18 and 19. The inside tube widths ranged from 1.27 cm to 7.62 cm. The number of ± 45 ply pairs (N) were between 2 and 8 resulting in tube width-to-wall thickness ratios of between 6 and 125. The energy-absorption capability of Gr/E tubes is a nonlinear function of W/t ratio. Generally, as W/t ratio decreased the energy-absorption capability increased and reached a maximum between W/t ratio of 20 and 55. With further decreases in W/t the energy-absorption capability decreased. The predominant crushing mode was a lamina bending mode or a combined brittle fracturing and lamina bending mode. All Gr/E tubes also exhibited a laminate tearing mode at the corners of the tubes. Square cross section tubes had lower energy-absorption capability than comparable size circular cross section tubes.

The energy-absorption capability of K/E square cross section tube specimens is a nonlinear function of tube W/t ratio as depicted in figure 19. This trend is similar to that of circular cross section tube specimens. The increase in energy-absorption capability with respect to decreasing W/t ratio is related to the reduced interlaminar cracking and is consistent with the buckling load characteristic of edge supported plates.

All of the K/E specimens crushed in a progressive local buckling mode. The buckle wave length is a function of tube geometry (width and wall thickness). The magnitude of the variation of the crushing force was a function of W/t ratio. The greater the W/t ratio the greater the variation in crushing force.

Tube specimens were geometrically scaled by proportionally changing tube inside diameter or width and wall thickness. If the energy-absorption capability of these tubes were geometrically scalable, tube specimens that have the same D/t or W/t ratio, although different diameters or widths and thicknesses, should have similar energy-absorption capabilities. The test results shown in figures 16-19 suggest the energy-absorption capability of Gr/E tubes was not geometrically scalable while the energy-absorption capability of K/E tubes was scalable.

Effects of Crushing Speed

Tests were conducted, reference 4, to investigate whether the energy-absorption capability of Gr/E and K/E composite materials is a function of crushing speed. Tube specimen ply orientations were $[0/\pm\theta]_2$ and $[\pm\theta]_3$. Figures 20 and 21 present the test results for crushing speeds between 10^{-5} m/sec and 12 m/sec. The energy-absorption trends varied for the different materials and ply orientations evaluated.

The energy-absorption capability of $[0/\pm\theta]_2$ Gr/E specimens was not influenced by crushing speed. All specimens crushed in a brittle fracturing mode. In the brittle fracturing mode the energy associated with the fracturing of the lamina bundles is considerably more than the energy associated with inter-laminar crack growth. The 0 degree plies reduced strain rate effects in the mechanical response of the lamina bundles. Therefore, the energy-absorption capability of $[0/\pm\theta]_2$ specimens should not be a function of the crushing speed.

The energy-absorption capability of $[\pm\theta]_3$ Gr/E specimens was a function of crushing speed. As ply orientation angle, θ , increased from 15 to 75 degrees the magnitude of the effects of crushing speed on energy-absorption capability increased. Energy-absorption capability increased as much as 15 percent over the speed range tested. All $[\pm\theta]_3$ specimens crushed in predominantly a brittle fracturing mode. As the ply orientation angle increased from 15 to 75 degrees the mechanical response of the lamina bundles became more strongly influenced by the matrix properties than by the fiber properties. Correspondingly, the percent of the total energy absorbed by the fracturing of the lamina bundles decreased. Therefore, the energy absorbed by the interlaminar crack growth relative to the total energy absorbed increased. Thus, the energy-absorption capability of the $[\pm\theta]_3$ Gr/E specimens are a function of crushing speed and ply orientation.

Figure 21 shows the effect of crushing speed on the energy-absorption capability of $[0/\pm\theta]_2$ and $[\pm\theta]_3$ K/E tube specimens. All K/E tube specimens crushed in the local buckling mode. The energy-absorption capability of K/E is a function of crushing speed, particularly between 6 m/sec and 12 m/sec. Energy-absorption capability increased between 20 and 40 percent for both $[0/\pm\theta]_2$ and $[\pm\theta]_3$ specimens between crushing speeds of 10^{-5} m/sec and 12 m/sec. Specimens with fibers predominantly oriented in the direction of the applied load (e.g., $[0/\pm 15]_2$ and $[\pm 15]_3$) exhibited the most significant increase in energy-absorption capability as crushing speed increased from 6 m/sec to 12 m/sec. The mechanical response of Kevlar fibers is a function of strain rate, therefore, the observed changes in energy-absorption capability are reasonable.

The results describing the effect of crushing speed are consistent with the crushing process described in a previous section. Energy-absorption capability is a function of crushing speed when the mechanical response of the controlling crushing mechanisms is a function of strain rate.

COMPOSITE SUBFLOOR BEAM CONCEPTS FOR ENERGY ABSORPTION

Four different subfloor beam concepts have been evaluated; sandwich, sine wave and two integrally stiffened concepts. The subfloor beam concepts are shown

in figure 22 and details are available in reference 13. In this section the relative energy-absorption capabilities of the different concepts are discussed. The energy-absorption trends of the beams are compared with the material response based upon tube tests. Finally, a method to predict the energy-absorption capability of composite subfloor beams is presented.

Energy Absorbing Subfloor Beam Concepts

The sandwich beams evaluated were fabricated using Nomex honeycomb core co-cured to K/E woven fabric face sheets oriented at ± 45 degrees. Different through-the-thickness stitching concepts were also evaluated. The energy-absorption capability test results are shown in figure 23. The stitching did not significantly affect the energy-absorption capability. However, the stitching did improve crushing load uniformity. The sandwich concepts crushed in the characteristic local buckling mode and they exhibited post-crushing integrity. The combinations of stitching parameters (i.e., stitch spacing, stitch pattern, and thread size) investigated was not exhaustive. Other stitching parameters might improve energy-absorption capability. However, the energy-absorption capability of the sandwich beams was significantly lower than other concepts.

The evaluation of sine-wave beams involved many different materials, material forms, hybridization, ply orientations and geometries (D/t). The sine-wave concepts were tangent half tube (included angles of 180 degrees) designs. A limited number of results will be presented here. The energy-absorption trends of sine-wave beams are similar to those trends found for circular cross section tube specimens. The effects of beam geometry for K/E beams are compared with tube data in figure 24. The agreement between beam and tube results is excellent. Beam and tube results for hybrid materials, as shown in figure 25, were equally good. The crushing modes of Gr/E and K/E beams are shown in figure 26. These crushing modes are similar to crushing modes of comparable tube specimens. The sine-wave beam concept was the most efficient energy absorbing concept evaluated. The energy-absorption efficiency is related to the relative efficiency between the circular and flat sections.

Both circular and rectangular tube stiffened beams were evaluated. Beams were fabricated from Gr/E, K/E and 6061-T6 aluminum. Ply orientation of the composite beams were $[(\pm 45)_4]_S$ and beam thickness was comparable for composite and aluminum beams. Different geometry stiffened beams were evaluated to compare energy-absorption trends with results from tube data. Figures 27 and 28 depict the test results for these beam concepts. For beams of comparable geometry the Gr/E beams had higher energy-absorption capability than Kevlar or aluminum beams. Energy-absorption capability as a function of beam geometry for both Gr/E and K/E was consistent with that determined from tube tests. That is, as D/t or W/t increased the energy-absorption capability decreased. The crushing modes of the beams were also consistent with the modes of tube specimens of the same material. As seen in figure 29 the K/E specimens crushed in a local buckling mode while the Gr/E specimens exhibited a brittle fracturing mode along the curved sections and a lamina bending mode in the flat sections.

Method of Predicting Energy Absorption Capability

Tests established that the crushing characteristics and energy-absorption trends of beams and tube specimens are similar. These results suggest that the energy-absorption capability of a beam can be predicted using tube data.

A method was formulated, reference 14, for predicting the energy-absorption capability of structural elements. The hypothesis is: the crash energy-absorption capability of a structural element is the sum of the weighted average of the energy-absorption capability of its characteristic elements. Mathematically, in terms of the specific sustained crushing stress (σ/ρ), this can be expressed as

$$(\sigma/\rho)_{S.E.} = \sum_{i=1}^n \frac{A_{i C.E.}}{A_{S.E.}} * (\sigma/\rho)_{i C.E.} \quad (1)$$

This hypothesis assumes the structure is properly designed to crush prior to catastrophic failure. Other requirements are that the tube specimens must have the same D/t or W/t ratio as the characteristic elements of the beam, the same ply orientation and stacking sequence, and have the same material form (e.g., tape, woven, filament wound).

This prediction method has been verified using several Gr/E, K/E and hybrid sine wave and stiffened beams. A detail example of this prediction method is given for a circular cross section tube stiffened beam fabricated with K/E. Figure 30 shows the beam configuration and dimensions. Web width between tube stiffeners was 3.81 cm and web thickness was 0.20 cm resulting in a W/t ratio of 19. The cross sectional area of each web was 0.76 cm². The web extended beyond the stiffeners 1.27 cm on each side of the beam. The W/t ratio of the web beyond the stiffeners was 6 and cross sectional area was 0.25 cm². The composite layup in the web region was $[\pm 45]_3 S$. The stiffener was a circular tube with an inside diameter of 2.54 cm and a wall thickness of 0.09 cm resulting in a D/t ratio of 28.2. The layup of the tube was $[\pm 45]_3$, and the cross-sectional area was 0.78 cm². Using equation 1 to compute the energy-absorption capability of the beam with the appropriate circular and square cross section tube data results in

$$\begin{aligned} (\sigma/\rho)_{S.E.} &= (4 * A_{Tube} * (\sigma/\rho)_{Tube} + 3 * A_{Web} * (\sigma/\rho)_{Web} \\ &\quad + 2 * A_{End} * (\sigma/\rho)_{End}) / A_{S.E.} \\ &\quad \text{of Web} \quad \text{of Web} \\ (\sigma/\rho)_{S.E.} &= 30 \text{ Nm/gr.} \end{aligned}$$

The measured energy-absorption capability of the beam was 28 Nm/gr. The difference between the predicted and measured values was approximately 7 percent.

Development of efficient energy absorbing concepts requiring a minimum number of design support tests for validation should now be readily achievable using the previously described prediction method. The application of the prediction method should result in a reduction in design cost and result in a lighter structure.

Composite material and structure can be tailored for efficient energy-absorption. However, additional work is required to advance this technology to the existing level for other composite structure. Further development of energy absorbing subfloor beam intersections and crushing initiators is required. Also, studies are needed, similar to those in references 15 and 16, are needed to incorporate energy absorbing structural concepts into fuselage sections to reduce manufacturing cost and reduce other development risks.

COMPOSITE FUSELAGE FRAME STRUCTURE

The subfloor structure previously discussed absorbs the energy in a crash but does not insure the structural integrity of the fuselage. The integrity of the fuselage must be maintained by the frames, bulkheads, and longerons in the structure. This integrity is important because it provides a protective shell around the occupants preventing foreign object intrusion and collapse of the fuselage. As part of the fuselage structural integrity investigation research on fuselage frames was conducted, reference 17. Drop tests of two aluminum and three Gr/E frames was conducted to investigate the impact acceleration levels and failure mechanisms.

The frame specimens were Z cross section frames approximately two meters in inside diameter. Frame dimensions are shown in figure 31. Each frame was fabricated in quarters and assembled with bolted splice plates. Ten pound masses were attached to both the left and right sides of the frames. Frames were instrumented with accelerometers and strain gages. Frames were dropped from a height of approximately four meters, producing an approximate impact speed of 8.2 m/sec.

Upon impact, the aluminum frames exhibited three sites of significant deformation. A plastic hinge formed to the left of the initial impact point which was on a splice plate. Significant section rotation occurred in the entire frame below the attachment points of the ten pound masses. The failure mechanisms of the aluminum frames were very similar to those of actual fuselage sections. The initial acceleration pulses at the impact point and at the floor frame intersection were on the order of 400 G's and 20 G's, respectively. Durations of the initial pulses were 0.0025 sec. and 0.010 sec. for the impact and the floor intersection points, respectively.

Two of the Gr/E frames were tested in an identical manner to the aluminum frames. Failure in the first two specimens occurred at 15 degrees in a counter clockwise direction from the impact point. The sequence of failure events was failure of the outside flange, failure across the web and finally failure of the inside flange. This complete section fracture might have been avoided by using one of the materials which exhibit post-crushing integrity such as Kevlar or a Kevlar-graphite hybrid. The third Gr/E frame was rotated 45 degrees, to impact halfway between the splice plates. The masses were attached in a similar fashion to the attachments on the first two Gr/E frames. Failure occurred at the point of impact. Overall deformations and

shape of frame were similar to the previous Gr/E frames. Typical accelerations at the impact points were approximately 650 G's and 65 G's at the floor-frame intersections. These accelerations are between 2 and 3 times those of the aluminum frames. Initial impact pulse durations were 0.001 sec. and 0.01 sec. at the impact point and the floor-frame intersection points.

A DYCAST finite element model was developed to predict the dynamic response of the frame structures. The calculated and measured strains agree in the general shape of the distribution; however, the measured strains near the splice plate are lower in magnitude than the predicted strains, as seen in figure 32. At angles below -22.5 degrees and above +22.5 degrees, good strain correlation were obtained between prediction and experiment.

The results of these tests provide needed insight into the failure characteristics of fuselage frames when subjected to simulated crash impacts. The good correlation between analysis and experiment is encouraging because it will allow the designer to reduce the support tests required to validate a concept.

CONCLUDING REMARKS

The U.S. Army-Aerostructures Directorate/NASA Langley Research Center joint research program on crashworthiness of composite helicopter structures has made good progress in understanding how composite materials and structures absorb energy and how structures fail under simulated crash conditions. Through this research program an understanding of the cause/effect relationship of composite material and specimen architectural properties on energy-absorption capability has been developed. Efficient energy absorbing structure can be achieved with graphite/epoxy despite the brittle nature of the material. However, careful attention must be given to design details. Graphite/epoxy structures can be more efficient energy absorbers than either Kevlar or aluminum structures. Sine-wave beams were the most efficient energy absorbing sub-floor concepts evaluated. An accurate, yet simple, method of predicting the energy-absorption capability of beams was developed.

Additional developments related to beam intersections, crushing initiators and fuselage integration are still needed. Further enhancements of analysis techniques to predict material and global structural response are also necessary.

REFERENCES

1. Light Fixed and Rotary Wing Aircraft Crashworthiness. Mil-Std-1290, Jan. 1974.
2. Winter, R., Pifko, A. B., and Cronkhite, J. D.: Crash Simulation of Composite and Aluminum Helicopter Fuselages Using a Finite Element Program. AIAA Paper 79-0781, 20 SDM Conference, Apr. 1979.
3. Farley, G. L.: Energy Absorption of Composite Materials. Journal of Composite Materials, vol. 17, May 1983.
4. Farley, G. L.: The Effects of Crushing speed On the Energy Absorption Capability of Composite Material. To be published as a NASA TM 1987.

5. Thornton, P. H.: Energy Absorption in Composite Structures. Journal of Composite Materials, vol. 13, July 1979.
6. Hull, D.: Research on Composite Materials at Liverpool University, Part 2: Energy Absorbing Composite Materials. Physics Technology, vol. 14, 1983.
7. Berry, J. and Hull, D.: Effect of Speed on Progressive Crushing of Epoxy-Glass Cloth Tubes. Institute Physics Conference on the Mechanical Properties at High Rates of Strain, 1984.
8. Cronkhite, J. D., Hass, T. J., Berry, V. L. and Winter, R.: Investigation of the Crash Impact Characteristics of Advanced Airframe Structure. USARTL-TR-79-11, Sept. 1979.
9. Farley, G. L.: Effect of Fiber and Matrix Maximum Strain on the Energy Absorption of Composite Materials. Journal of Composite Materials, vol. 20, July 1986.
10. Farley, G. L., Bird, R. K., and Modlin, J. T.: The Role of Fiber and Matrix in Crash Energy Absorption of Composite Materials. Proceedings of the AHS National Specialists' Meeting on Crashworthy Design of Rotorcraft, April 1986.
11. Farley, G. L.: Effect of Specimen Geometry on the Energy-Absorption Capability of Composite Materials. Journal of Composite Materials, vol. 20, July 1986.
12. Farley, G. L.: Energy-Absorption Capability and Scalability of Square Cross Section Composite Tube Specimens. To be published as a NASA TM, 1987.
13. Farley, G. L.: Crash Energy Absorbing Composite Sub-Floor Structure. Submitted to the American Helicopter Society for publication, 1986.
14. Farley, G. L.: A Method of Predicting the Energy-Absorption Capability of Composite Sub-Floor Beams. To be published as a NASA TM, 1987.
15. Jackson, A. C., Balena, F. J., LaBarge, W. L., Pei, G., Pitman, W. A., and Wittlin, G.: Transport Composite Fuselage Technology - Impact Dynamics and Acoustic Transmission. NASA-CR-4035, Dec. 1986.
16. Cronkhite, J. D. and Berry, V. L.: Investigation of the Crash Impact Characteristics of helicopter Composite Structure. USAAVRADCOM-TR-82-D-14, Feb. 1983.
17. Boitnott, R. L., and Carden, H. D.: Drop Testing and Analysis of Six Foot Diameter Graphite-Epoxy Frames. Proceedings of the AHS National Specialists' Meeting on Crashworthy Design of Rotorcraft, April 1986.

TABLE 1. COMPOSITE MATERIALS USED TO INVESTIGATE EFFECTS OF FAILURE STRAIN ON ENERGY-ABSORPTION CAPABILITIES.

Matrix Fiber	934	974	5245	F185	HST-7
T300	X	X	X		
AS4			X		
AS6				X	X
K-49	X	X			

FOUR CRUSHING MODES EXHIBITED BY COMPOSITE MATERIAL

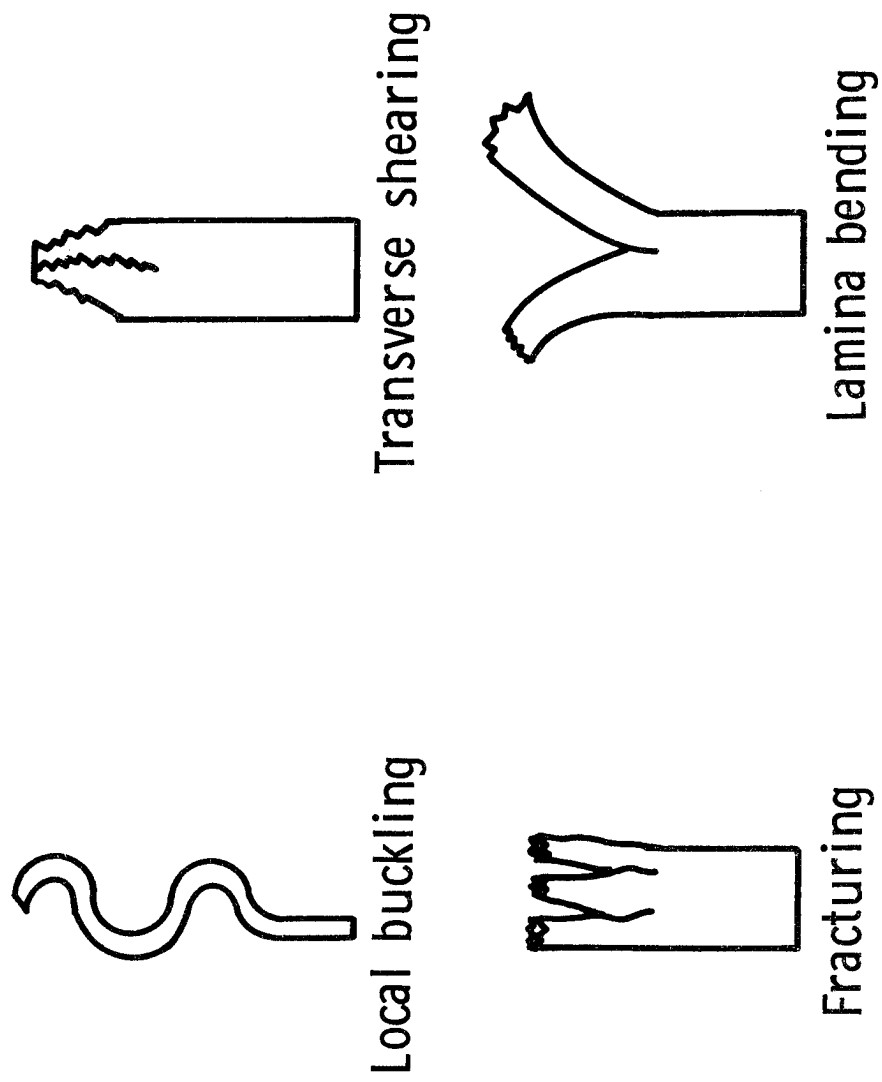


Figure 1

EFFECT OF FIBER FAILURE STRAIN ON THE ENERGY ABSORPTION OF GRAPHITE REINFORCED COMPOSITE MATERIALS

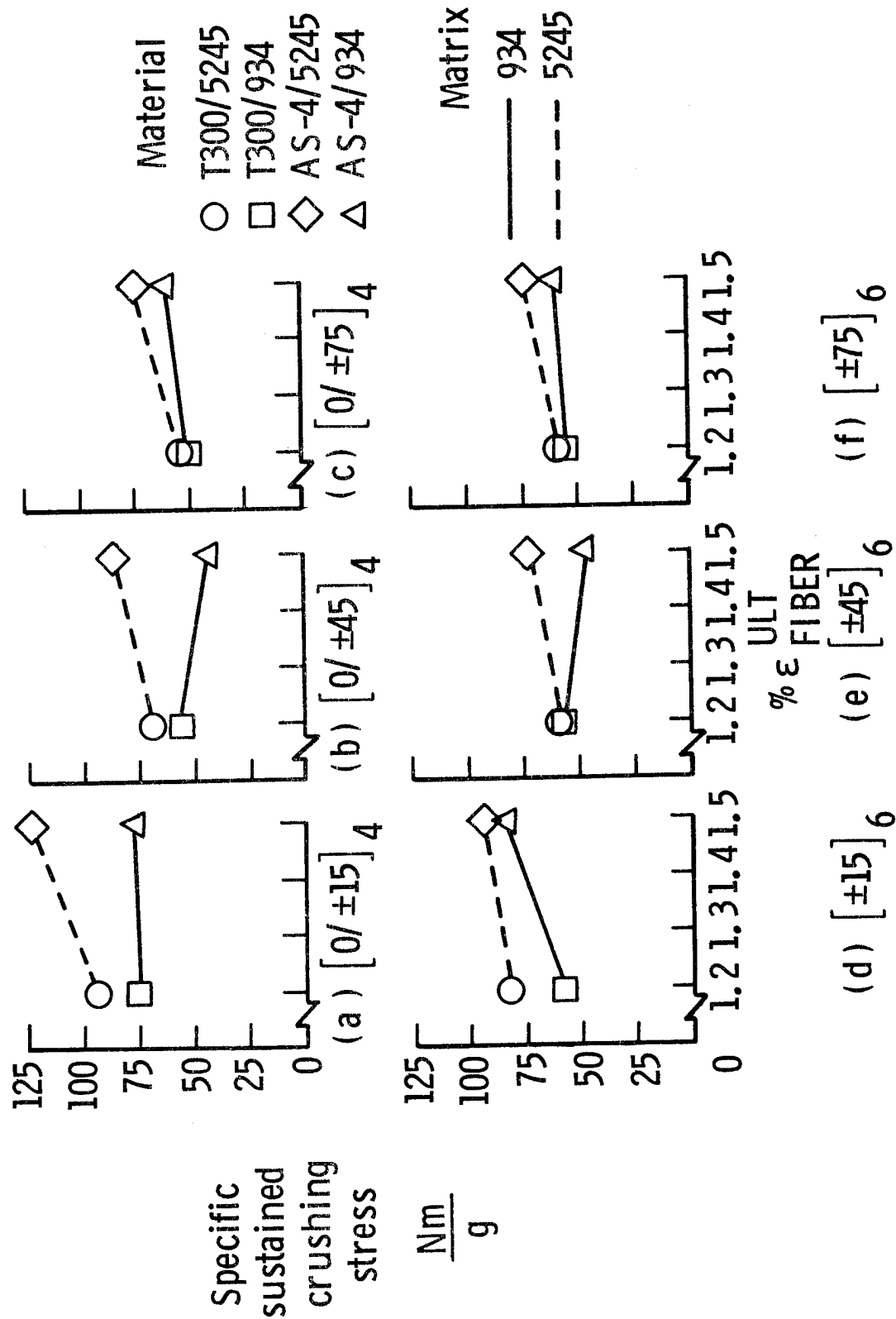


Figure 2

EFFECT OF MATRIX FAILURE STRAIN ON THE ENERGY ABSORPTION OF GRAPHITE REINFORCED COMPOSITE MATERIALS

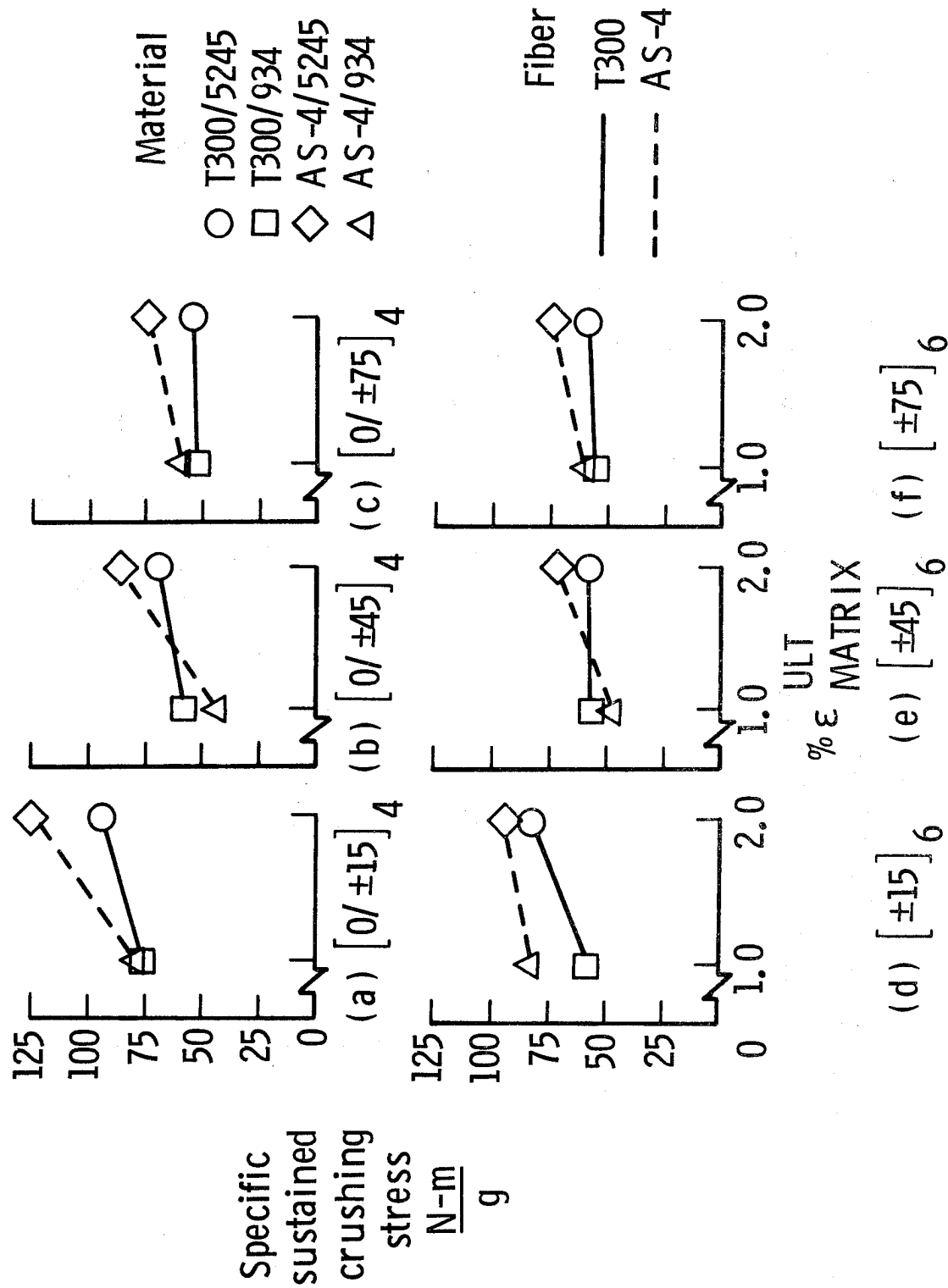


Figure 3

EFFECTS OF FIBER STIFFNESS ON ENERGY ABSORPTION OF $[\pm\Theta]_6$ GRAPHITE/EPOXY COMPOSITE MATERIAL

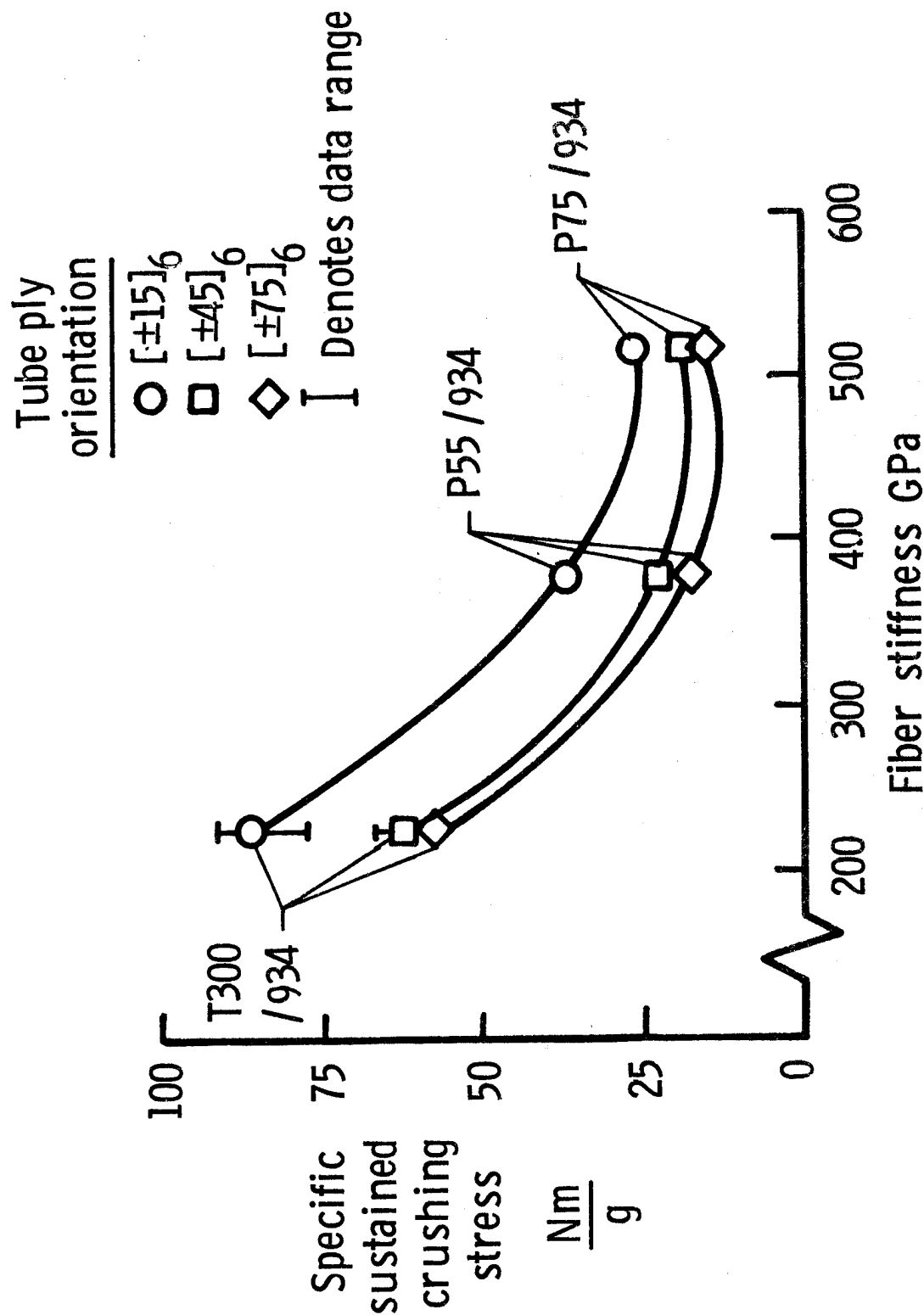


Figure 7

EFFECTS OF MATRIX FAILURE STRAIN ON THE ENERGY ABSORPTION CAPABILITY OF KEVLAR REINFORCED COMPOSITE MATERIAL

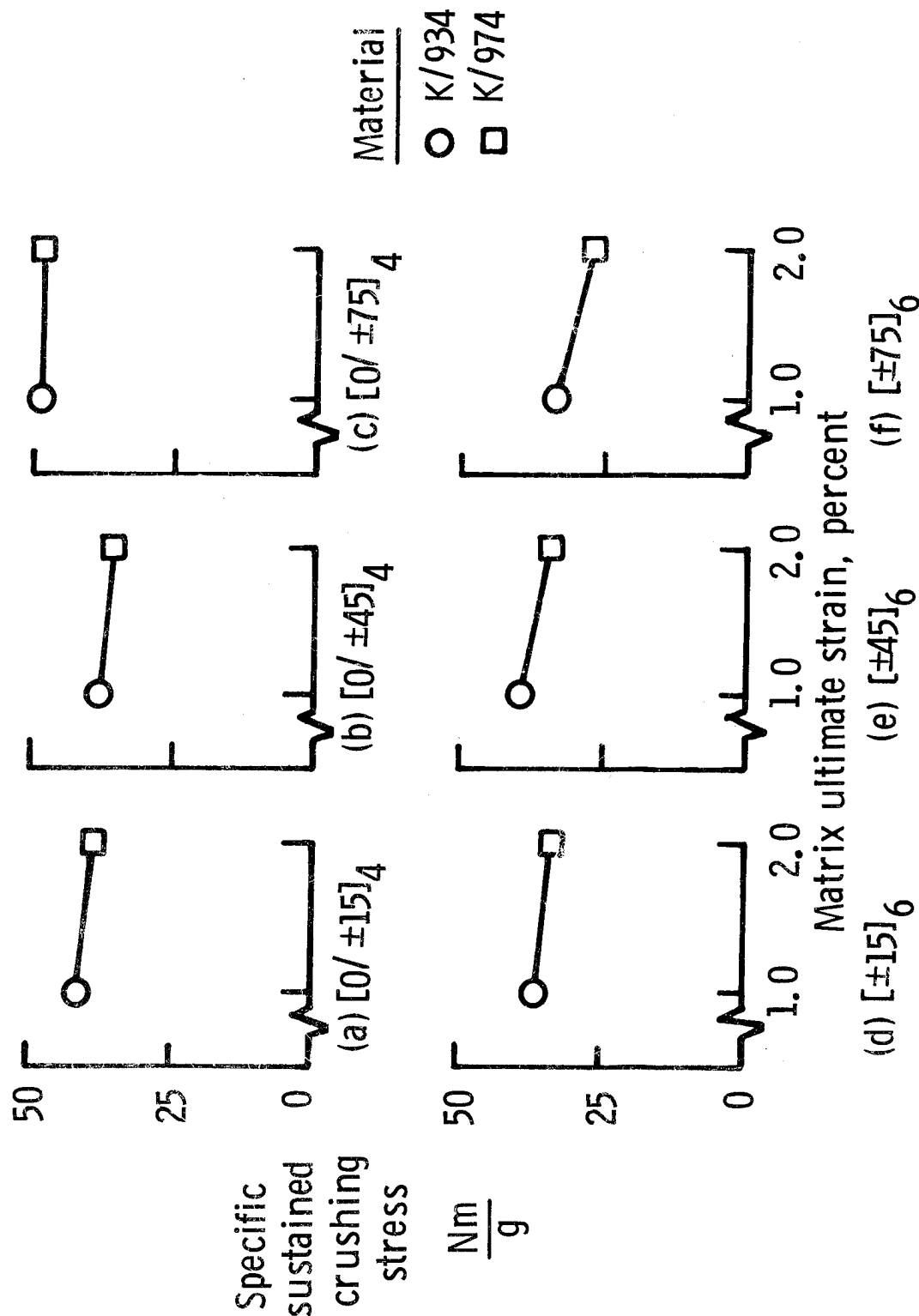


Figure 5

EFFECT OF FIBER AND MATRIX FAILURE STRAIN ON ENERGY ABSORPTION

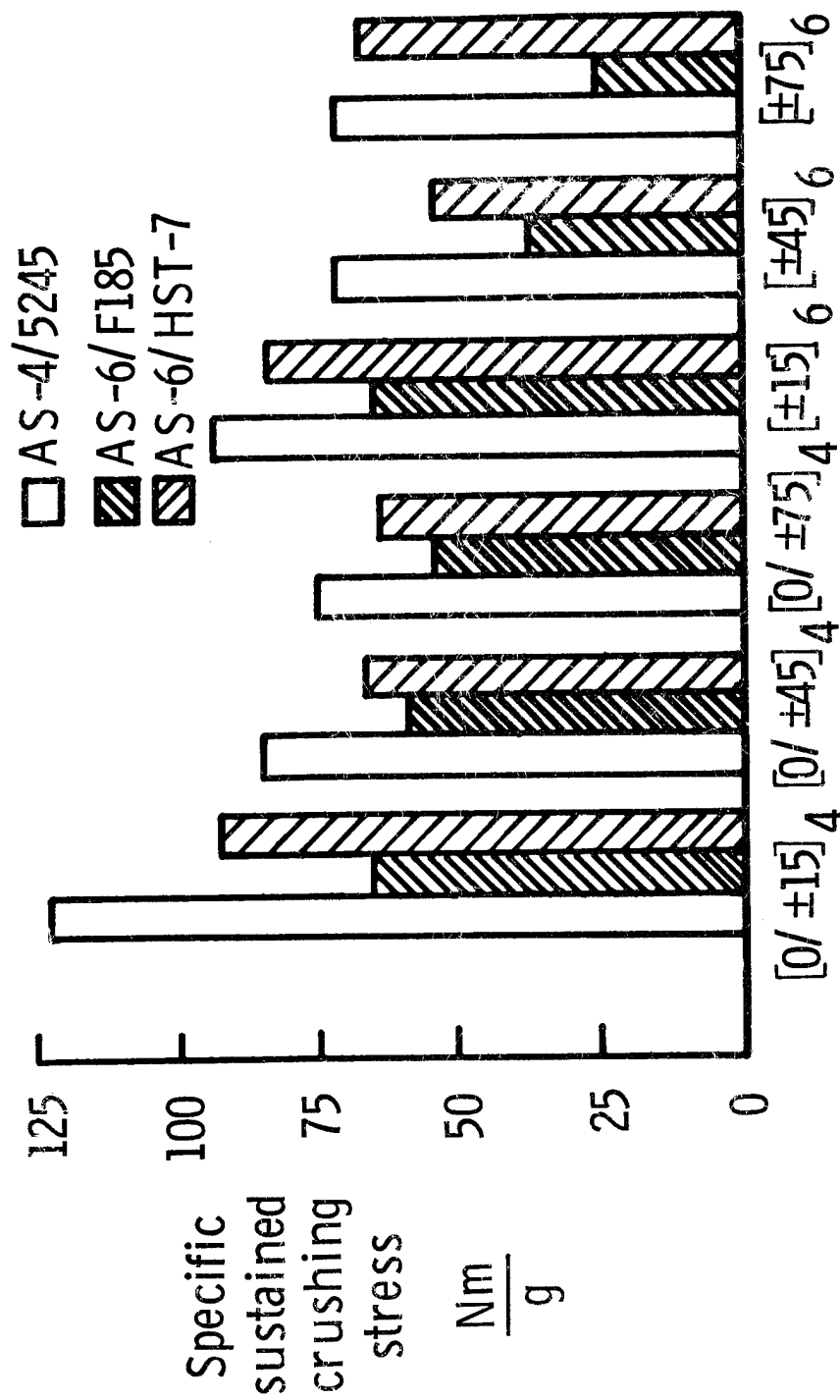


Figure 4

EFFECTS OF FIBER STIFFNESS ON ENERGY ABSORPTION OF $[0/\pm\Theta]_4$ GRAPHITE/EPOXY COMPOSITE MATERIAL

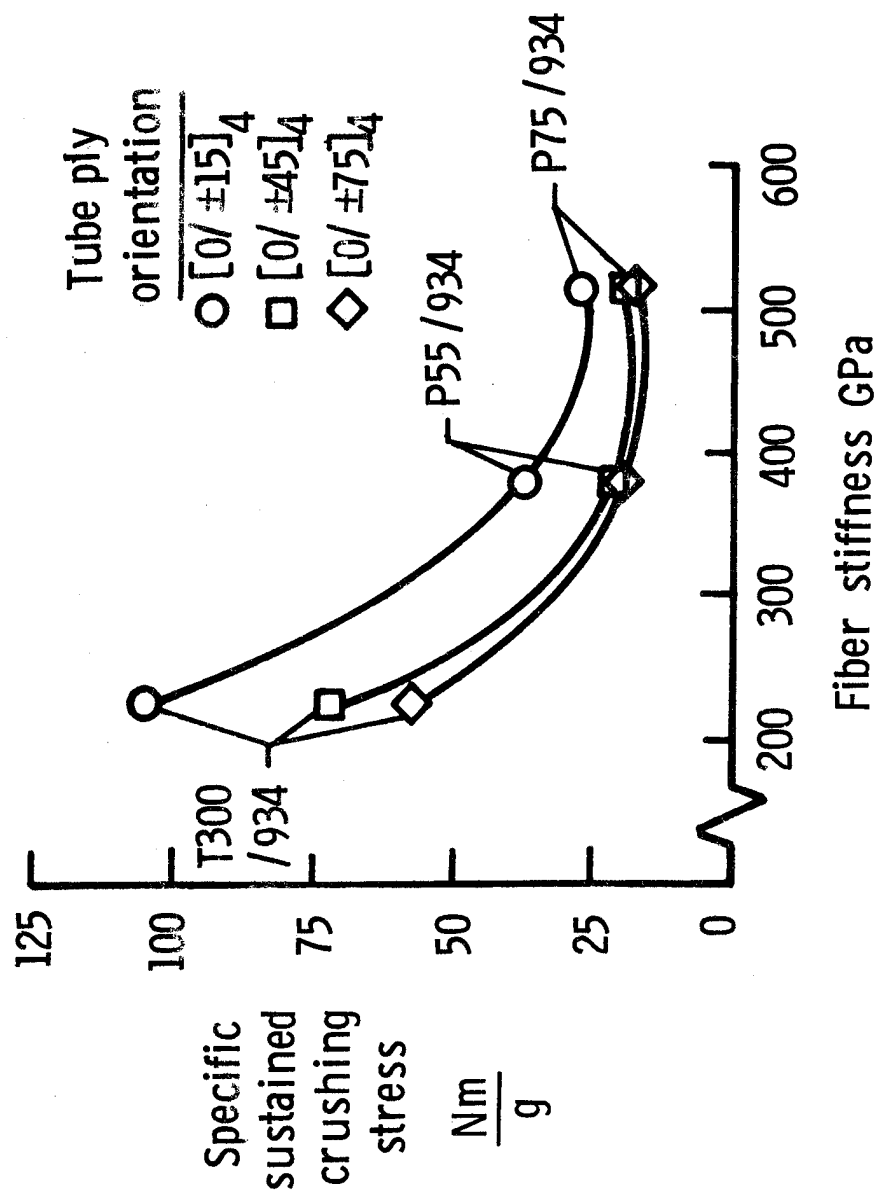


Figure 6

ENERGY ABSORPTION OF Gr/E, K/E, AND Gl/E $[0/\pm\theta]_4$ TUBES

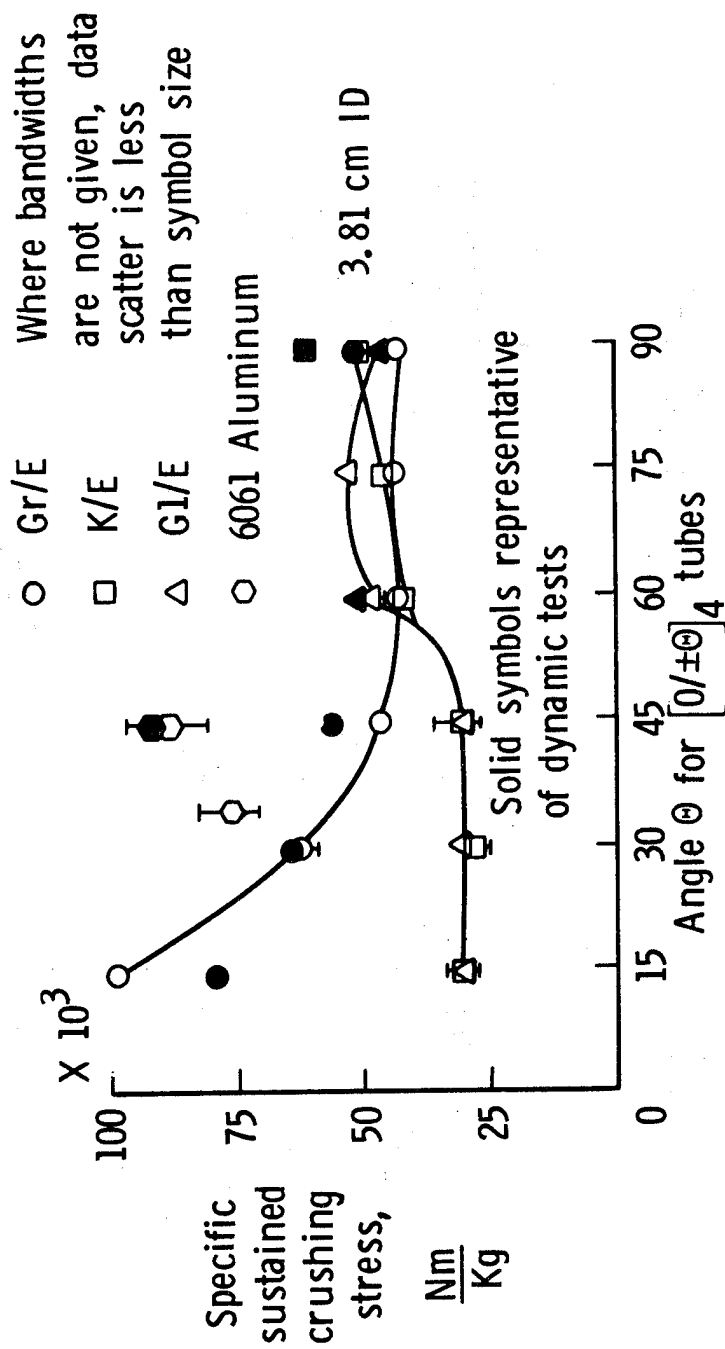


Figure 8

THE EFFECT OF STACKING SEQUENCE ON ENERGY ABSORPTION

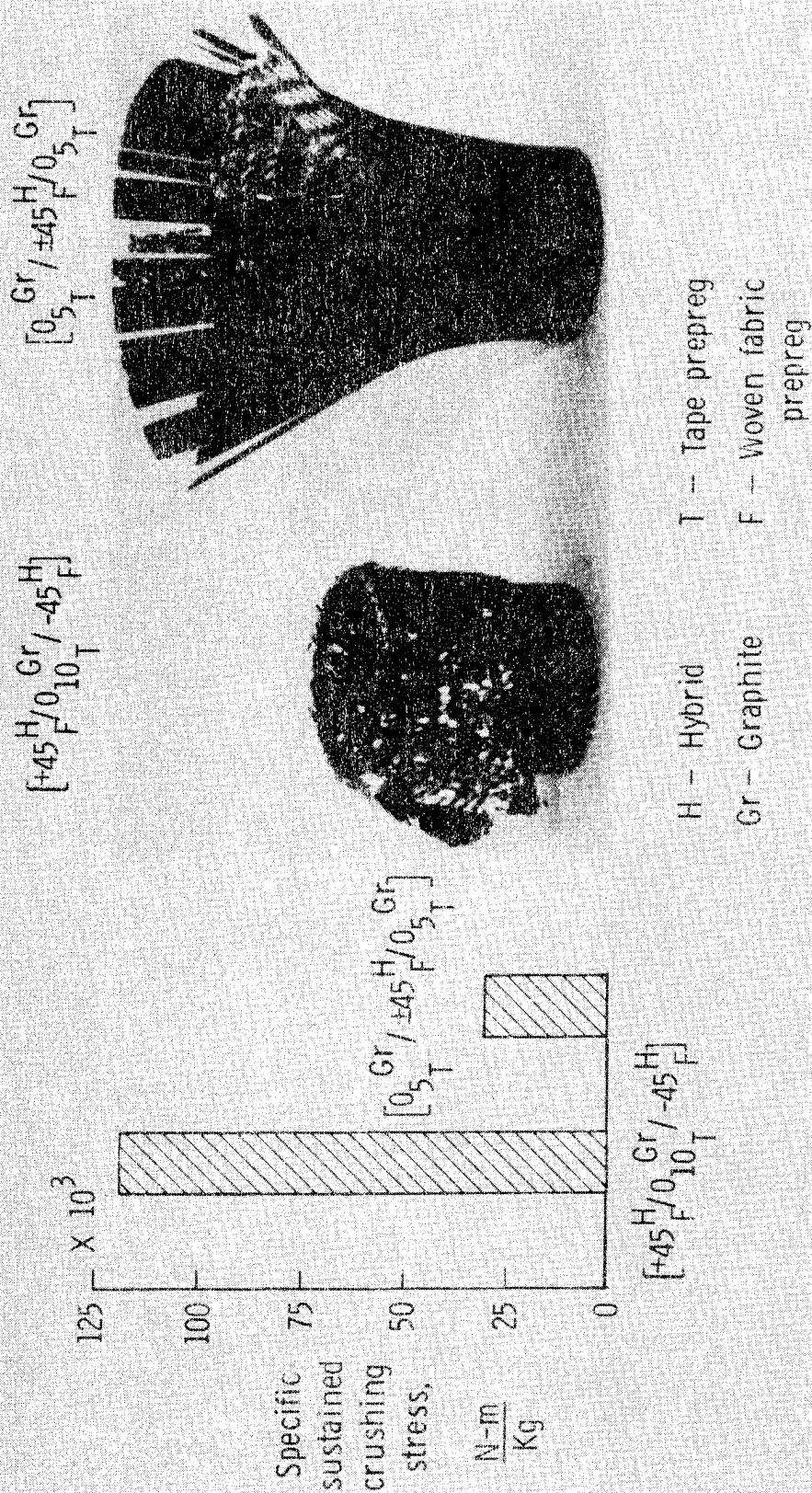


Figure 9

EFFECT OF STACKING SEQUENCE ON THE ENERGY ABSORPTION OF $[\pm 45]$ COMPOSITE TUBE

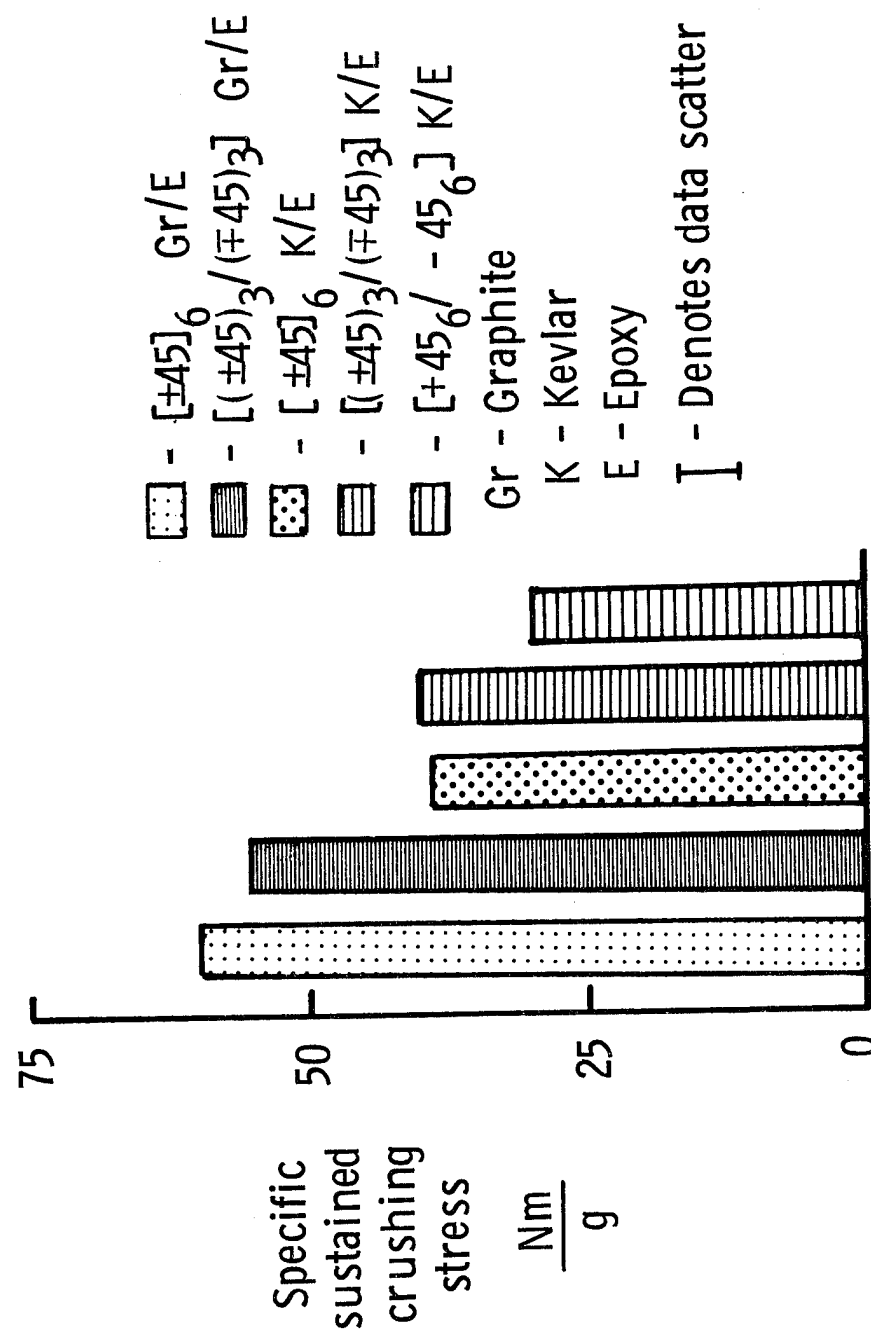


Figure 10

ENERGY ABSORPTION OF $[\pm 45^\circ \text{K/O}^\text{Gr}_\text{N}]_s$ GRAPHITE-KEVLAR/EPOXY COMPOSITES

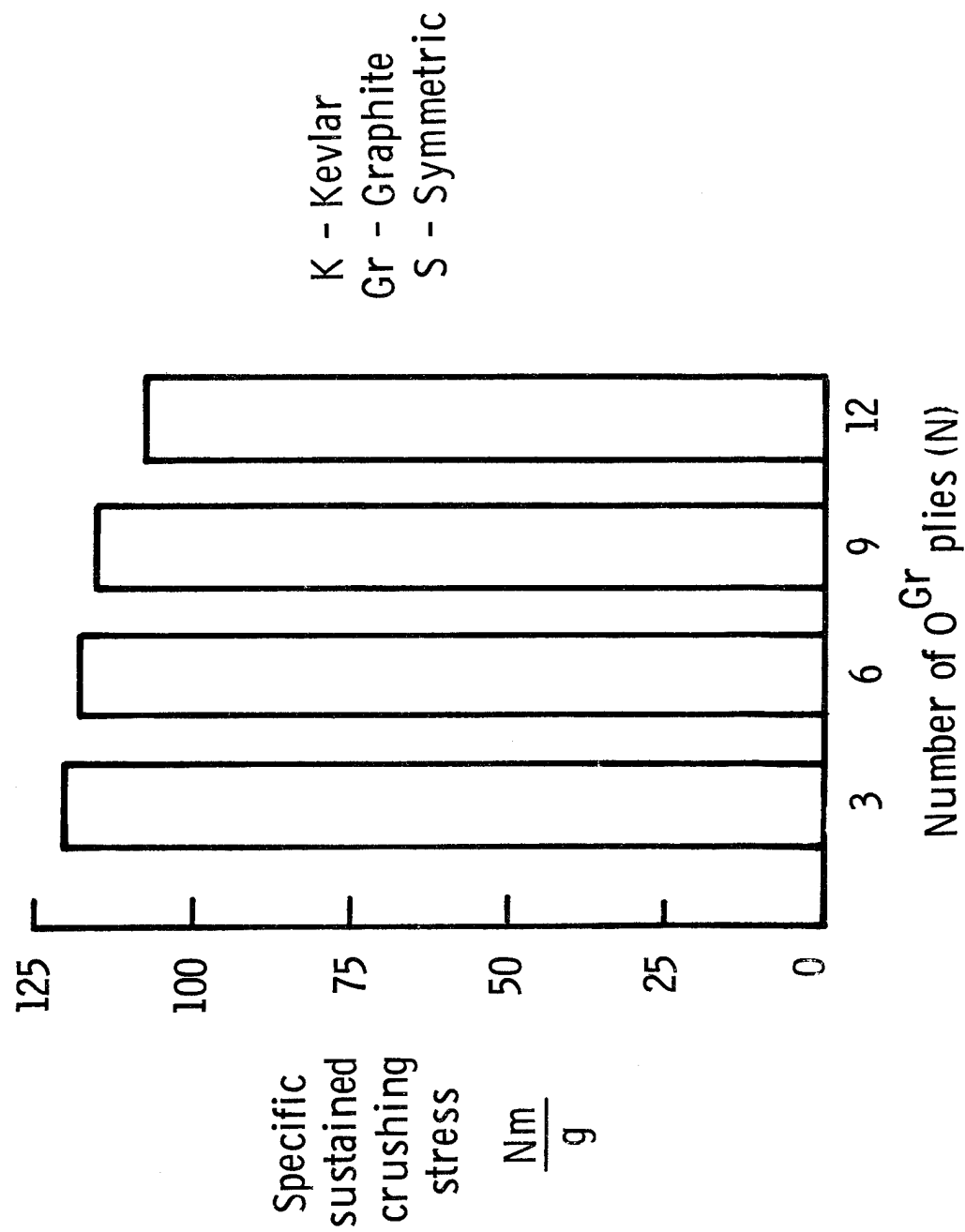


Figure 11

**CRUSHED GRAPHITE-KEVLAR/EPOXY UNIDIRECTIONAL
HYBRID TUBE SPECIMENS**

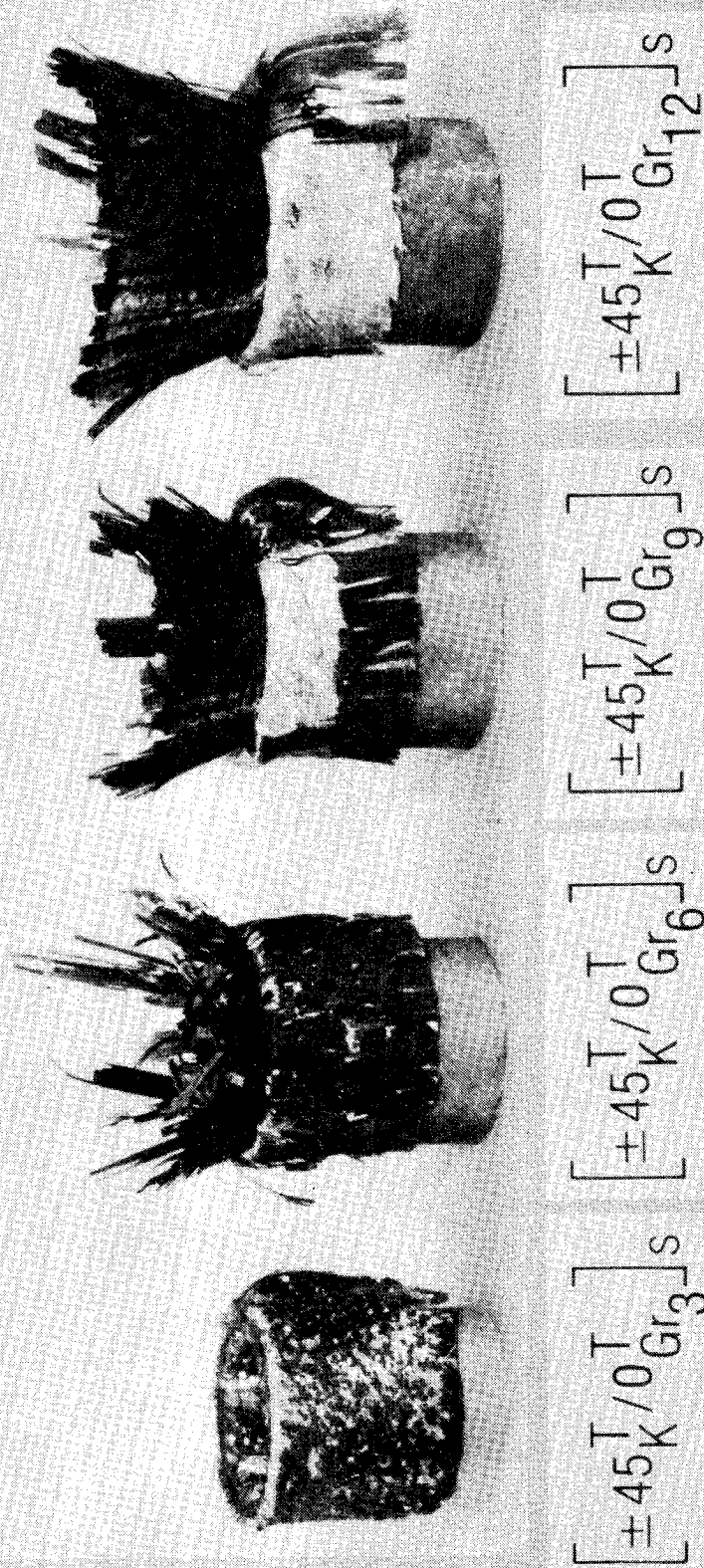


Figure 12

EFFECTS OF FIBER VOLUME FRACTION ON THE ENERGY ABSORPTION CAPABILITY OF T300/934 COMPOSITE MATERIAL

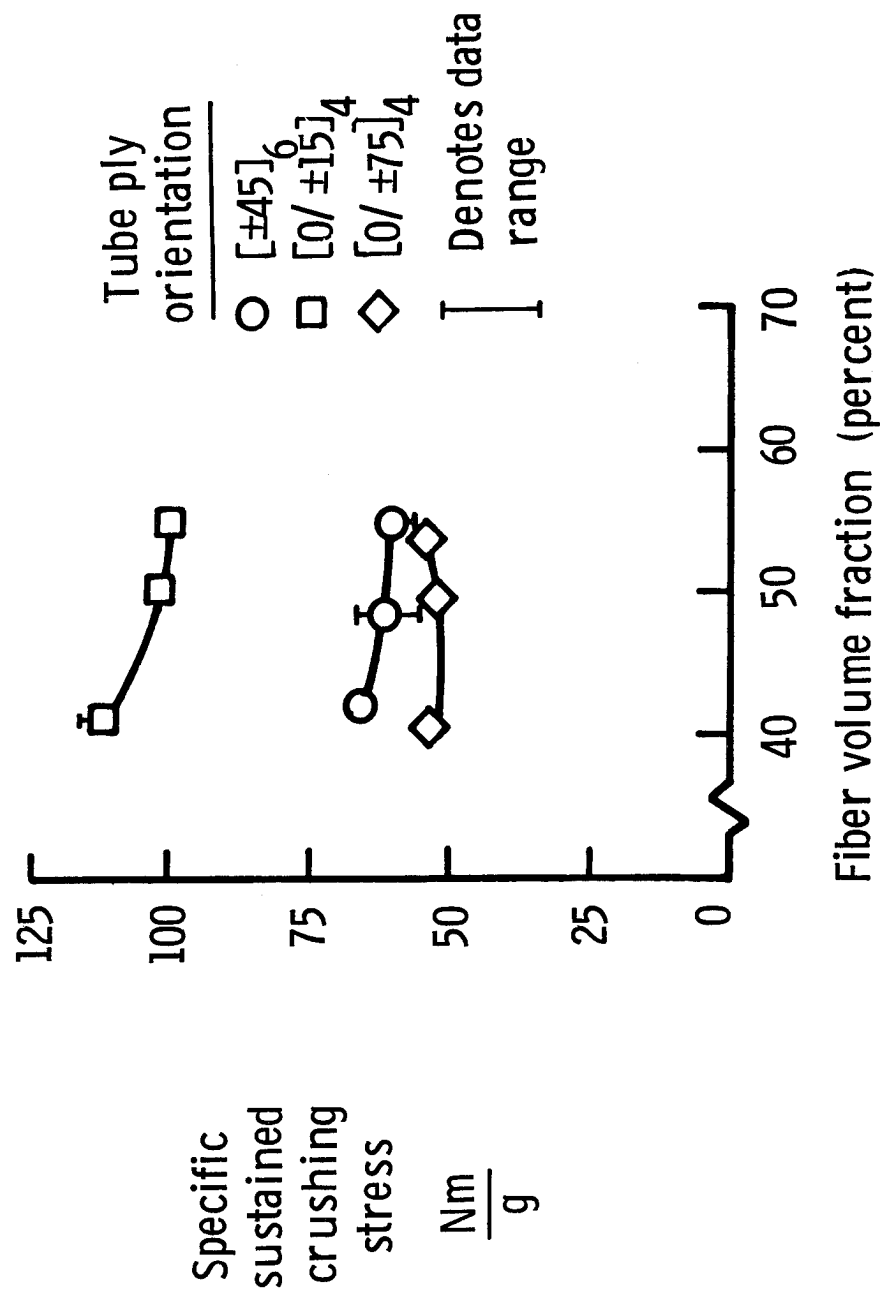


Figure 13

EFFECT OF FIBER VOLUME FRACTION ON THE ENERGY ABSORPTION CAPABILITY OF KEVLAR-49/934 COMPOSITE MATERIAL

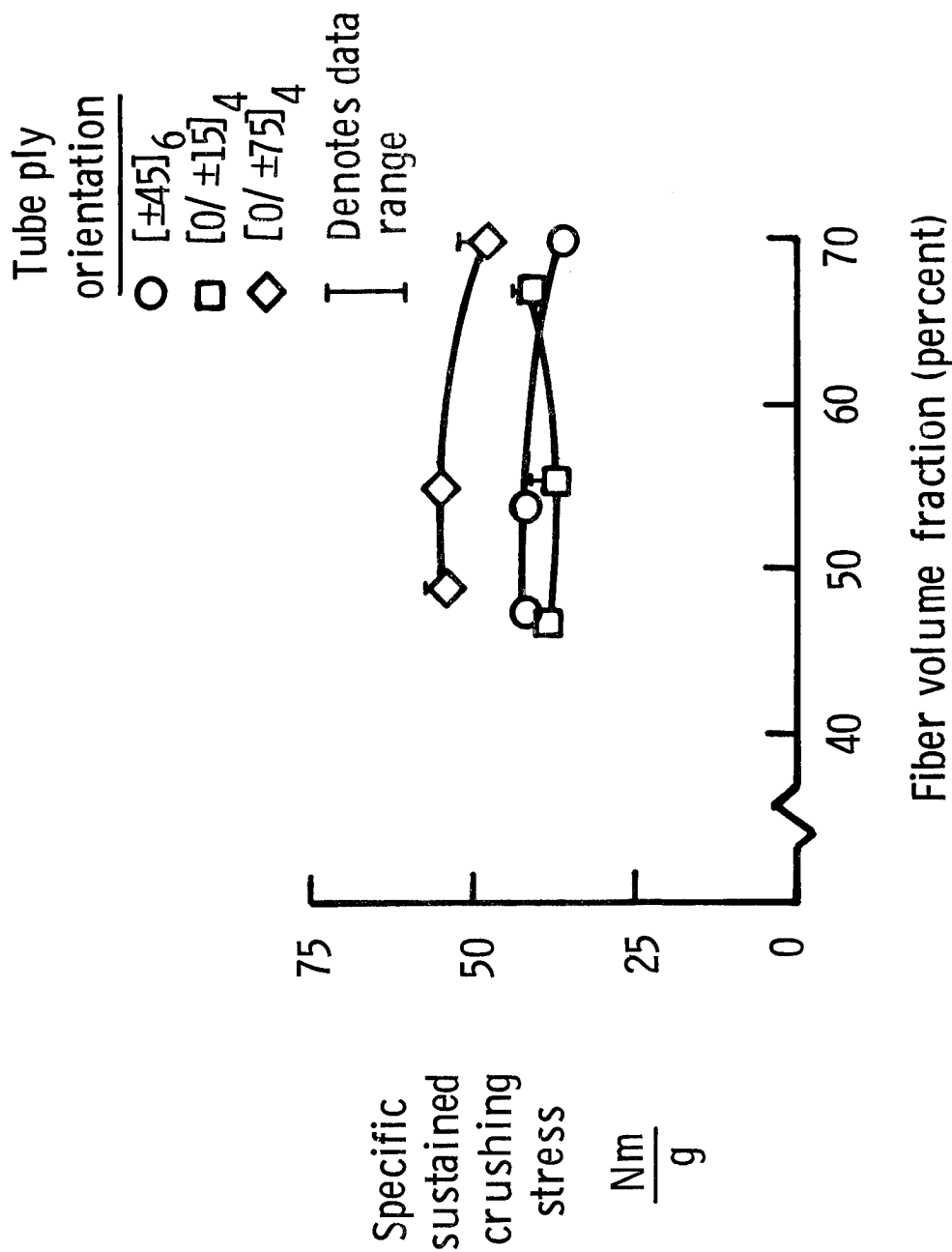


Figure 14

ENERGY ABSORPTION OF GRAPHITE-KEVLAR/EPOXY HYBRID COMPOSITES

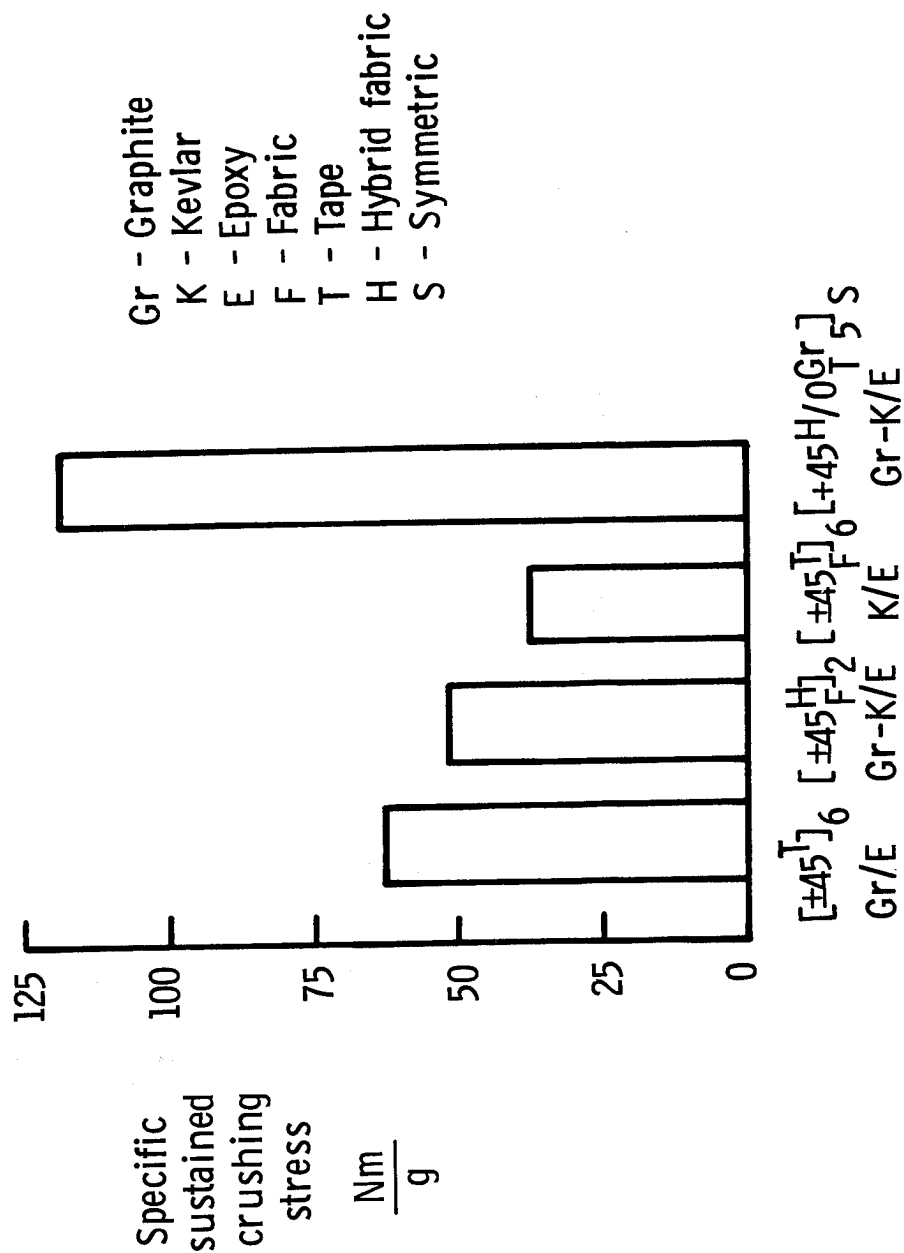


Figure 15

EFFECTS OF D/t RATIO ON THE ENERGY ABSORPTION OF $[\pm 45]_N$ Gr / E TUBES

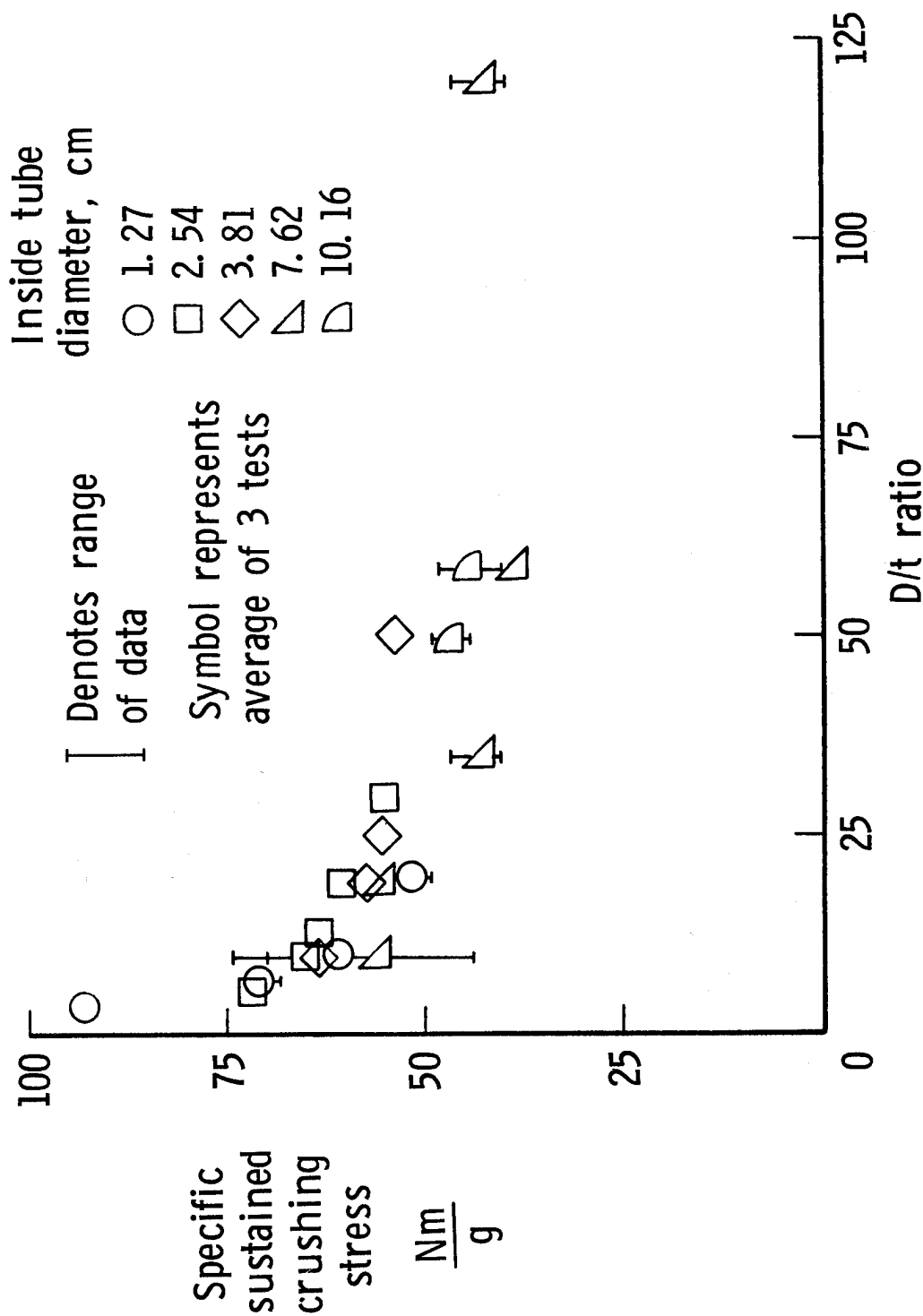


Figure 16

EFFECTS OF D/t RATIO ON THE ENERGY ABSORPTION OF $[\pm 45]_N$ K/E TUBES

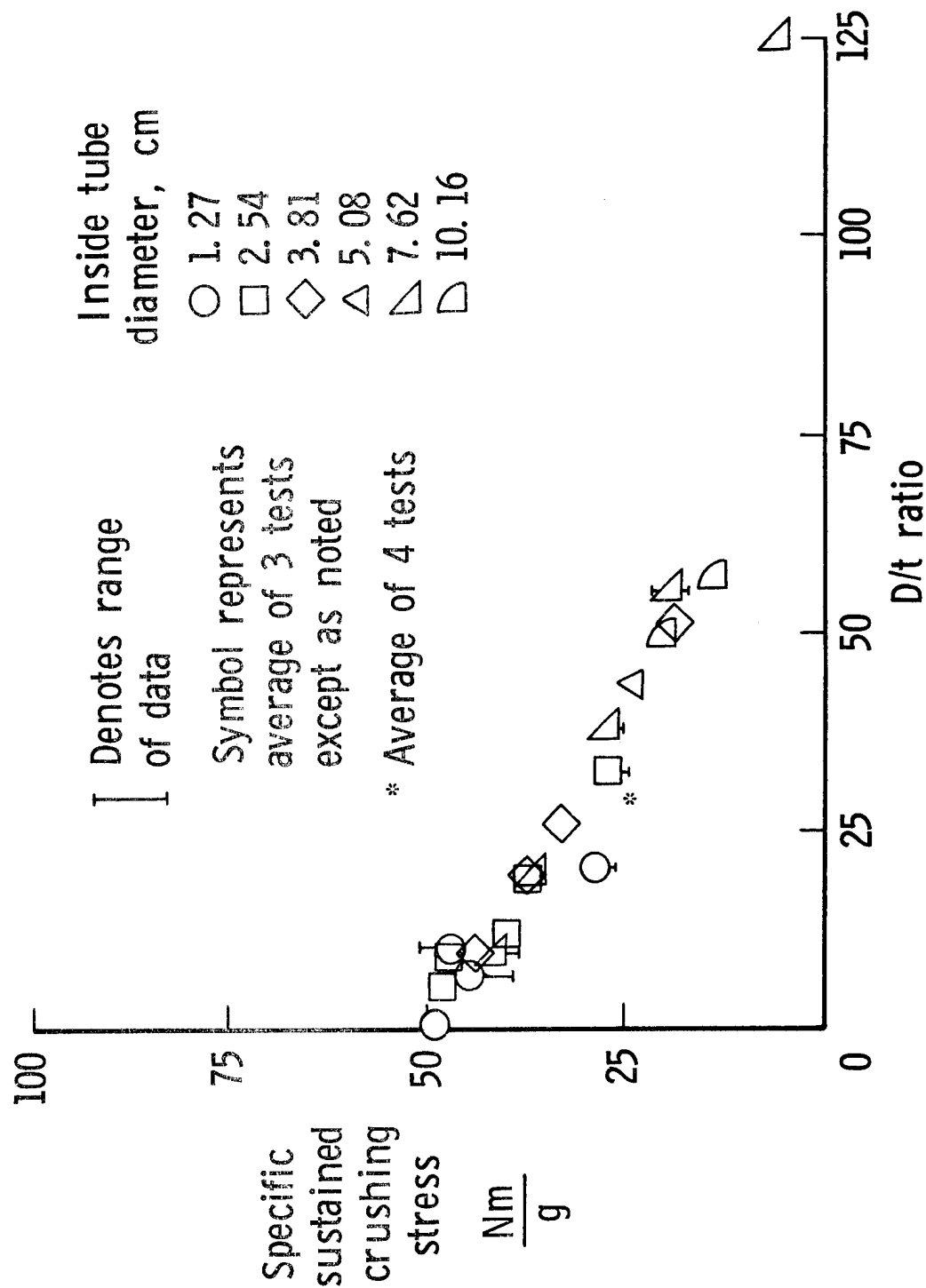


Figure 17

ENERGY ABSORPTION CAPABILITY OF SQUARE GRAPHITE/EPOXY TUBES

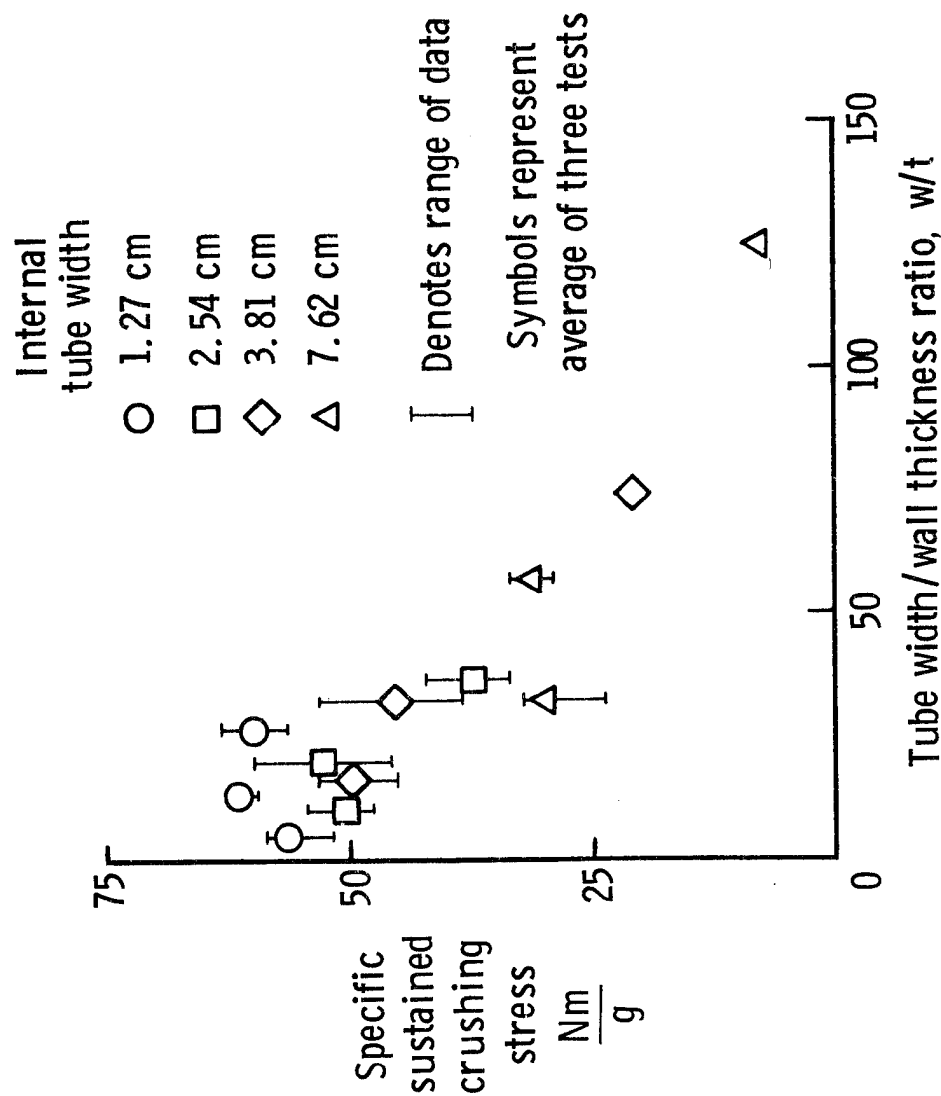


Figure 18

ENERGY ABSORPTION CAPABILITY OF SQUARE KELVAR/EPOXY TUBES

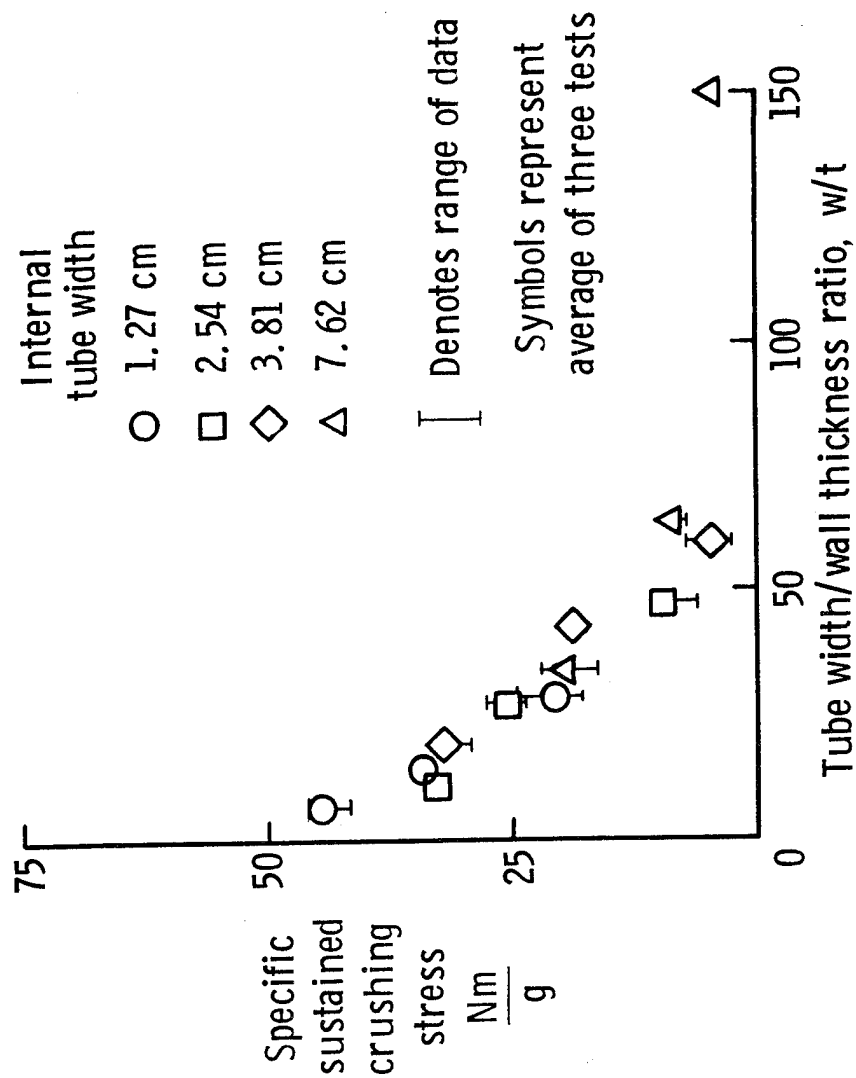


Figure 19

EFFECTS OF CRUSHING SPEED ON Gr/E TUBES

- \circ $[0/\pm 15]_2$ All symbols denote
 \square $[0/\pm 45]_2$ average of three tests
 \diamond $[0/\pm 75]_2$ unless otherwise denoted
 * one test
 ** two tests
 I data range

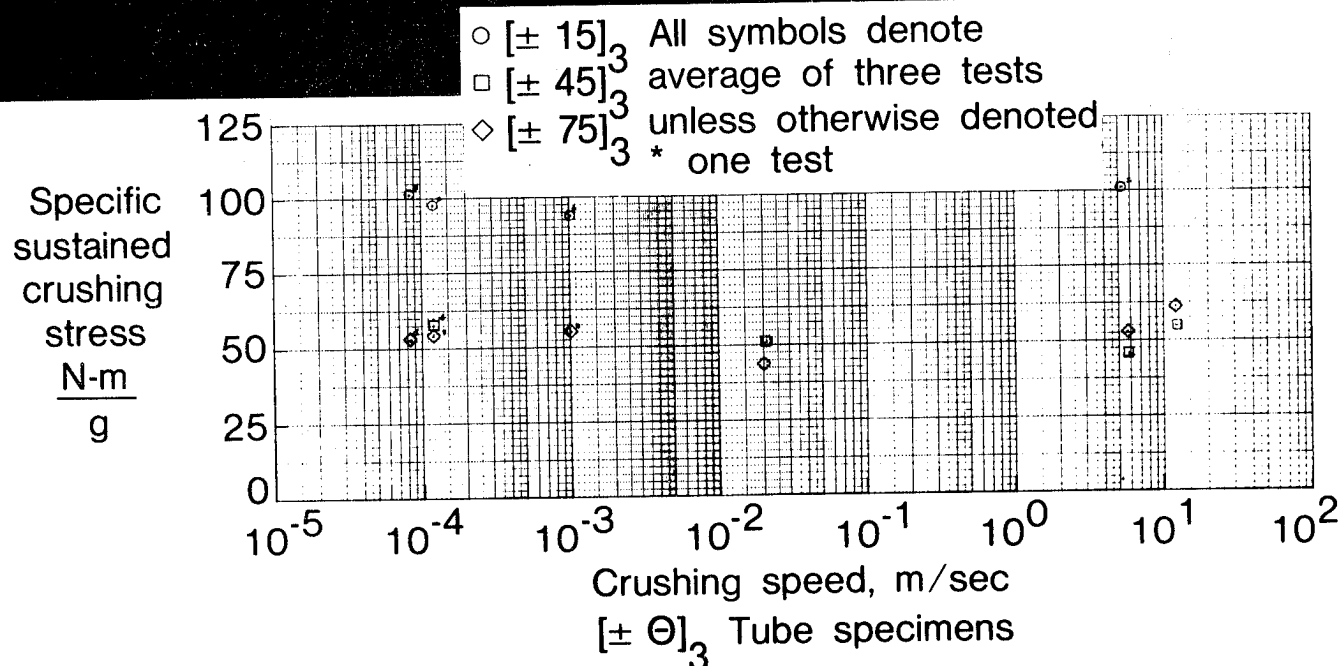
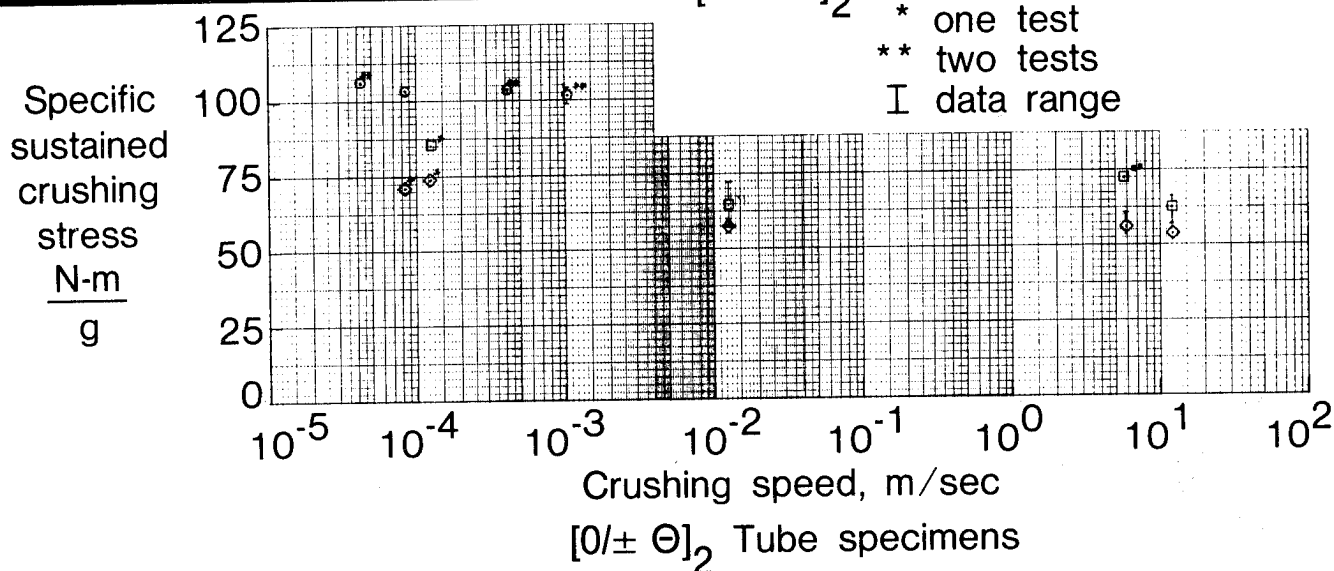


Figure 20

EFFECTS OF CRUSHING SPEED ON K/E TUBES

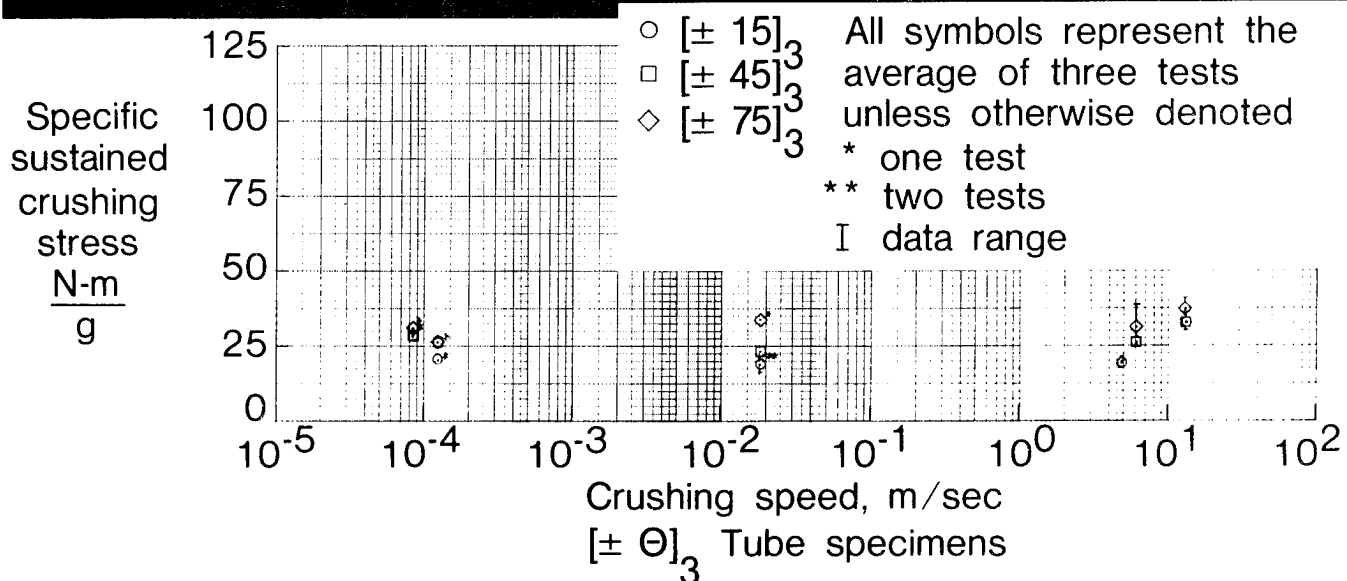
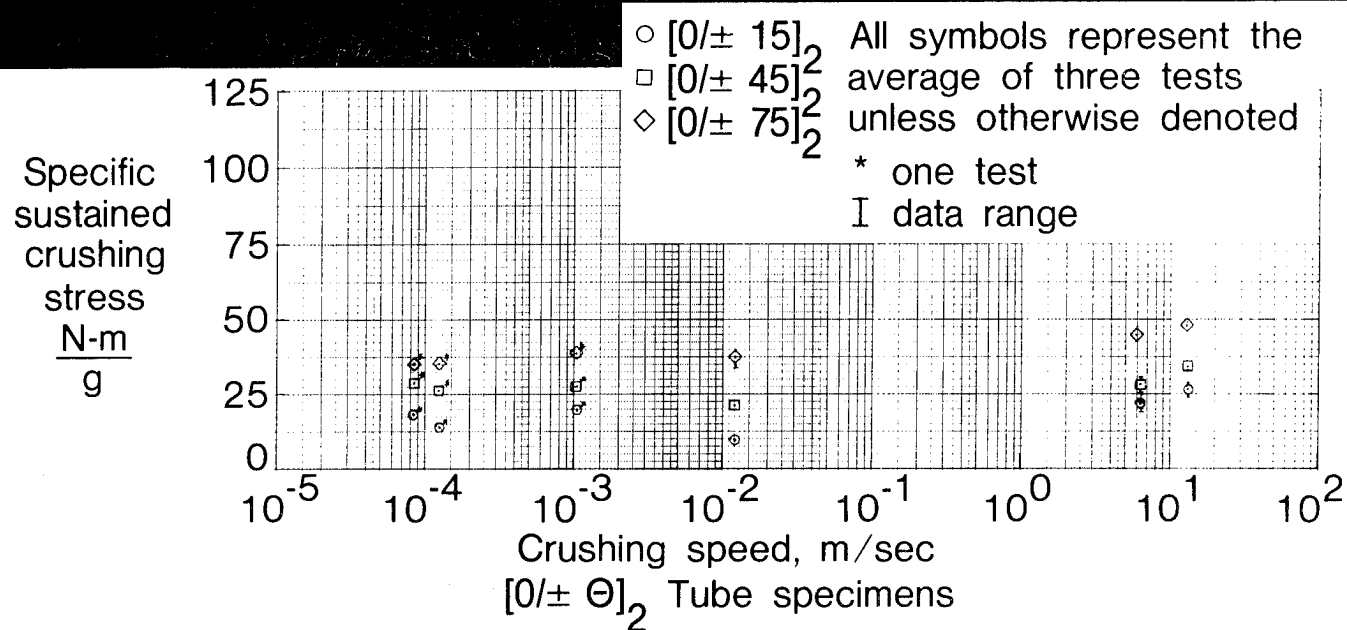
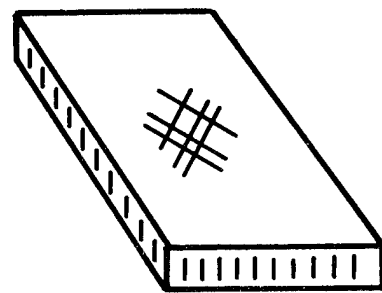
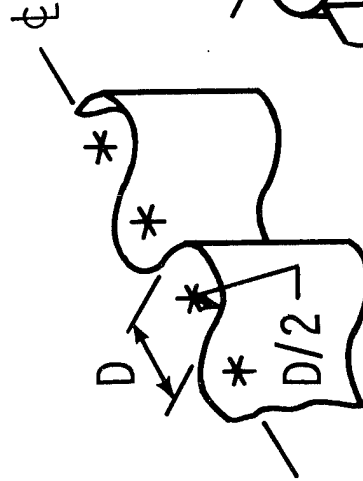


Figure 21

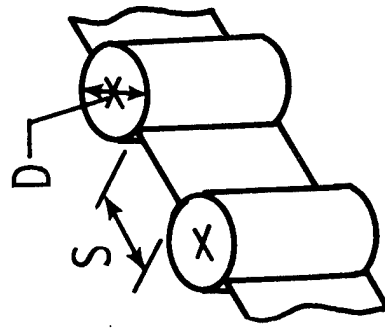
ENERGY ABSORBING BEAM CONCEPTS



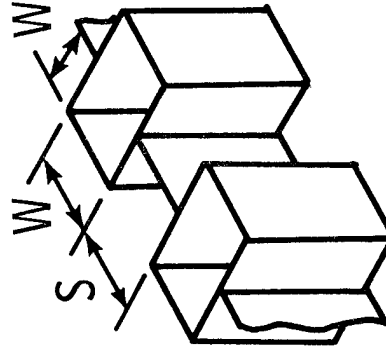
Honeycomb-sandwich beam



Sine-wave beam
(tangent-half circle)



Circular tube stiffened beam



Rectangular tube stiffened beam

ENERGY ABSORPTION OF $[\pm 45^\circ_S / HC]_S$ KEVLAR/EPOXY

SANDWICH BEAM SPECIMENS

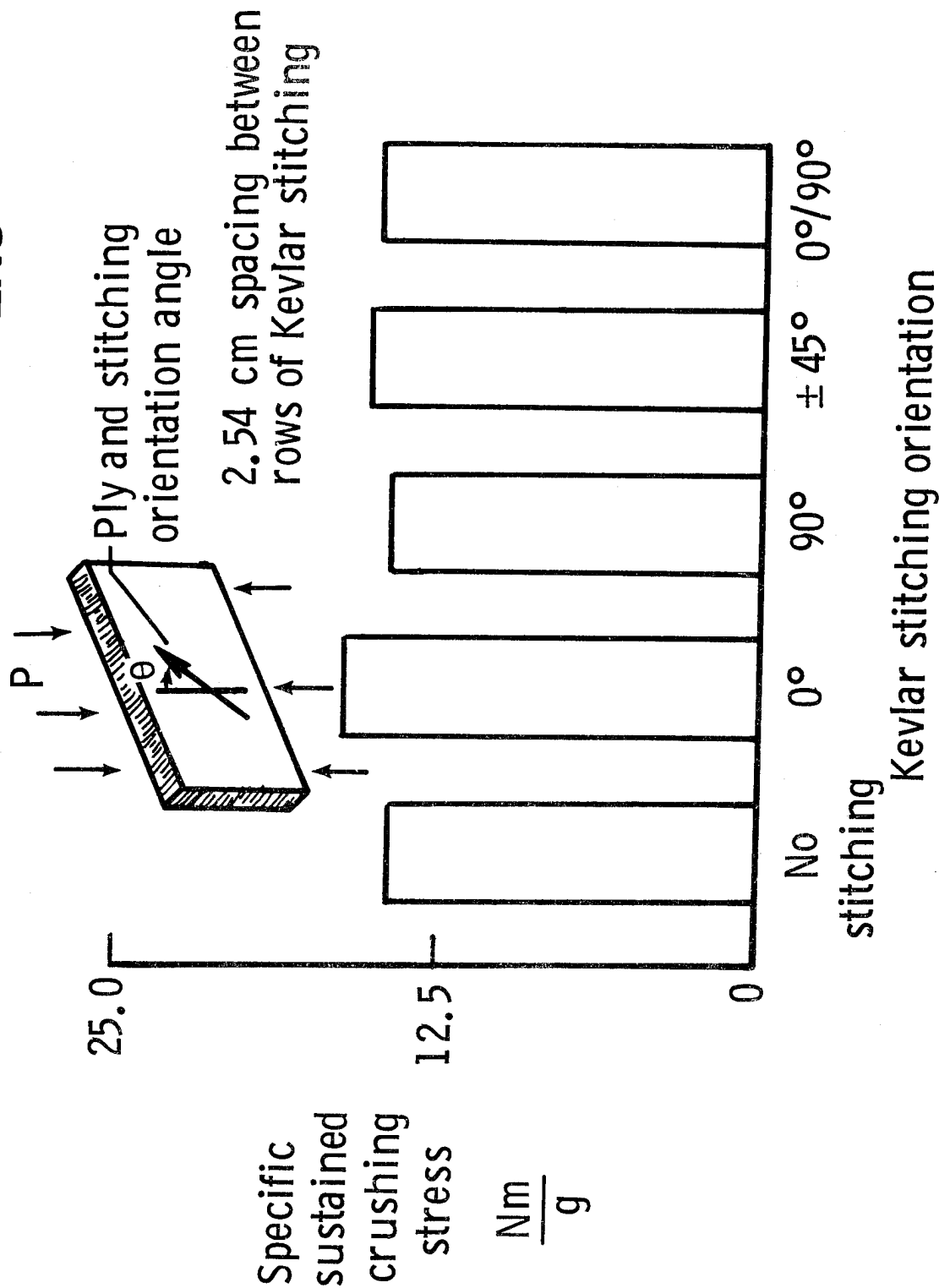


Figure 23

EFFECTS OF D/t RATIO ON THE ENERGY ABSORPTION OF [±45]_N K/E TUBES AND SINE-WAVE BEAMS

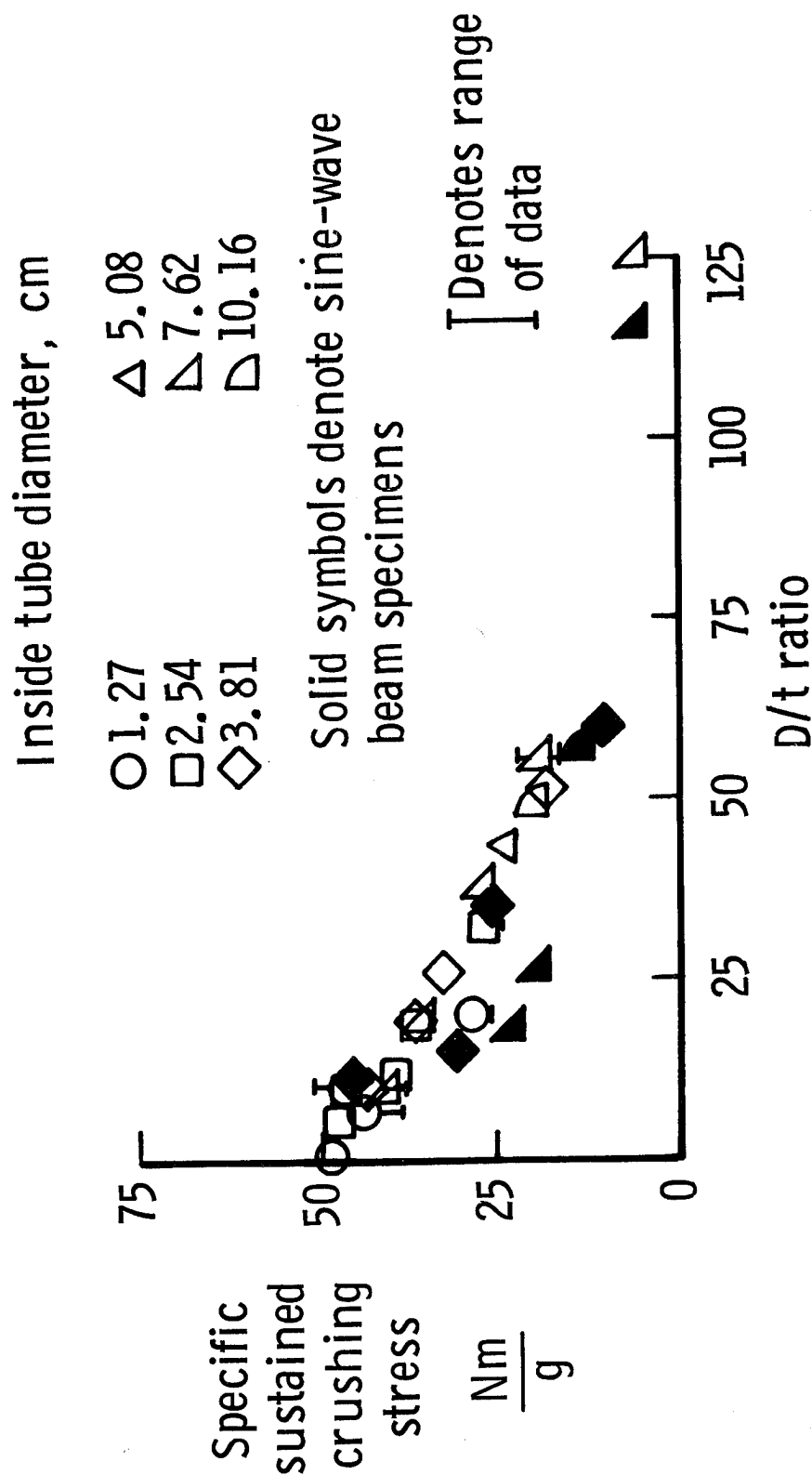


Figure 24

ENERGY ABSORPTION CAPABILITY OF HYBRID COMPOSITE SINE-WAVE BEAMS AND TUBES

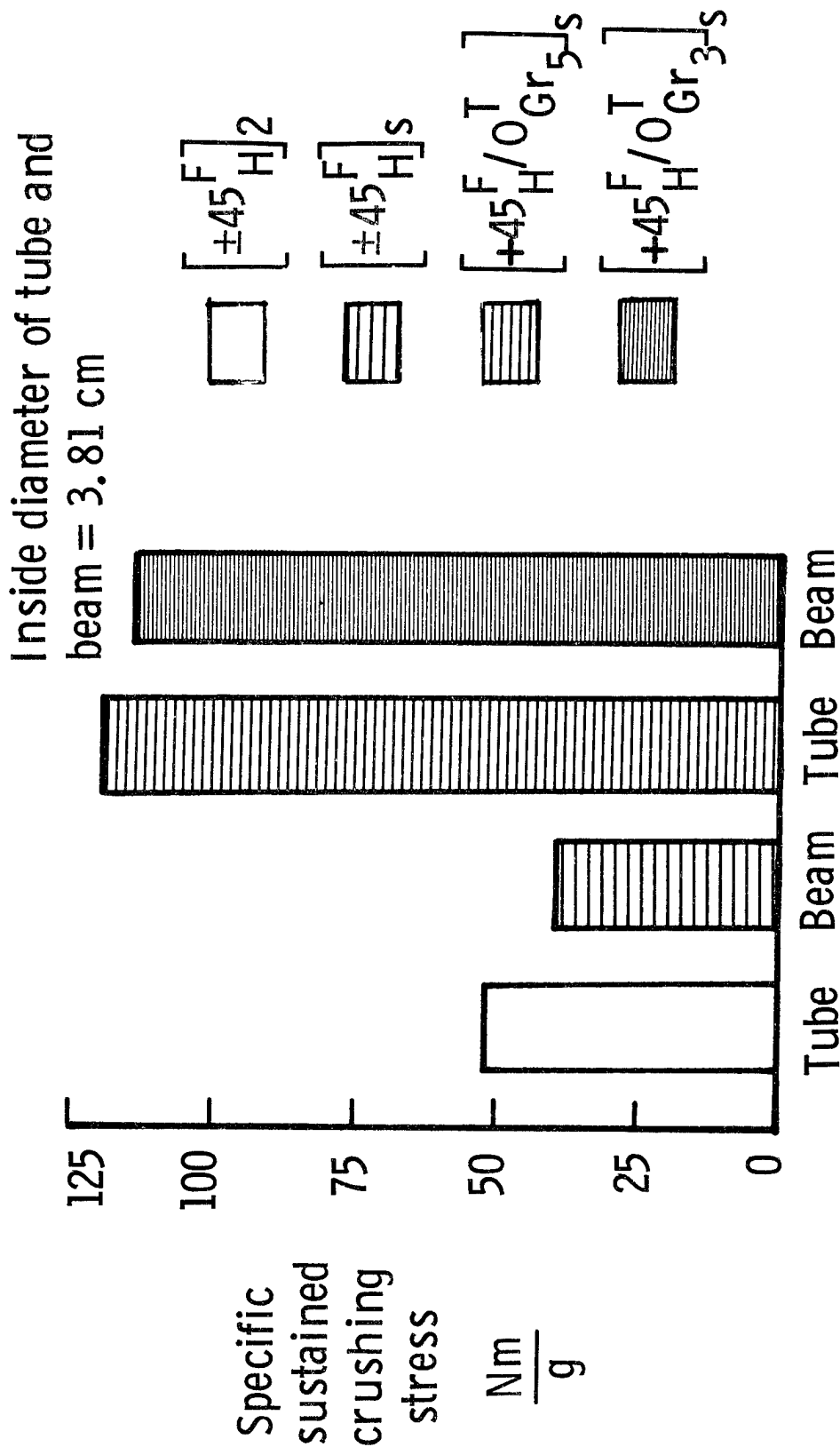
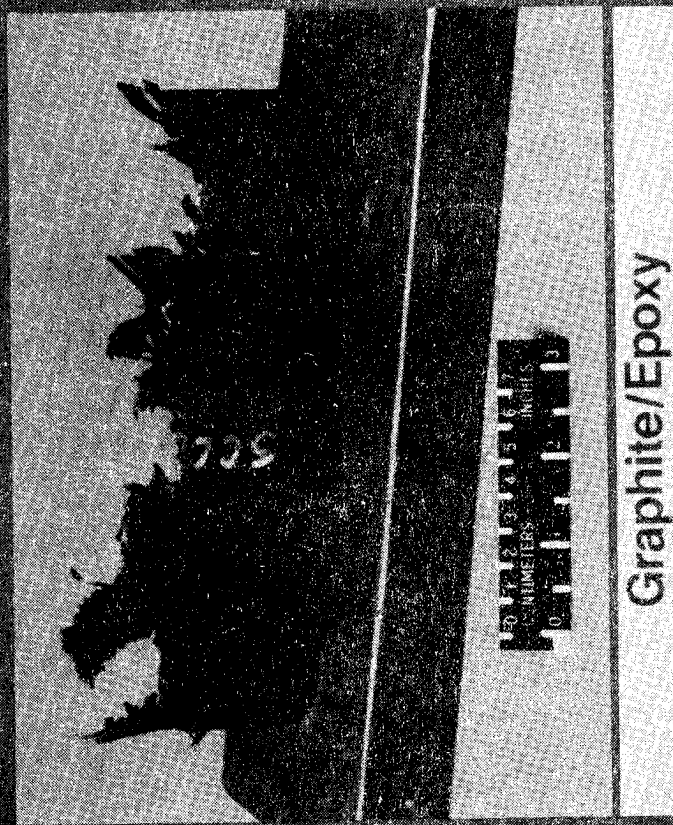


Figure 25

TYPICAL CRUSHING MODE OF COMPOSITE SINE-WAVE BEAMS



Graphite/Epoxy



Kevlar/Epoxy

Figure 26

ENERGY ABSORPTION OF CIRCULAR TUBE STIFFENED BEAMS

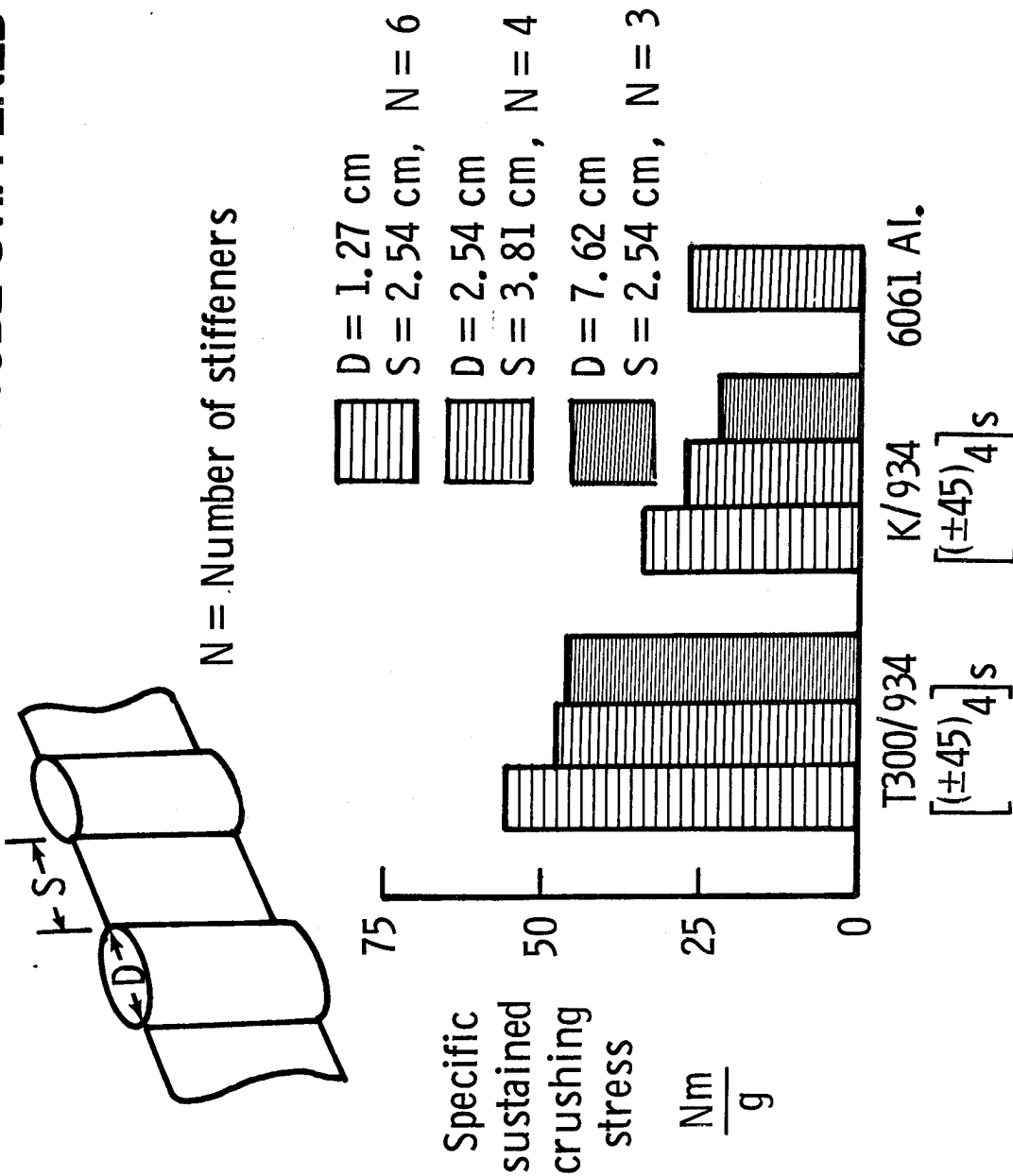


Figure 27

ENERGY ABSORPTION OF RECTANGULAR TUBE STIFFENED BEAMS

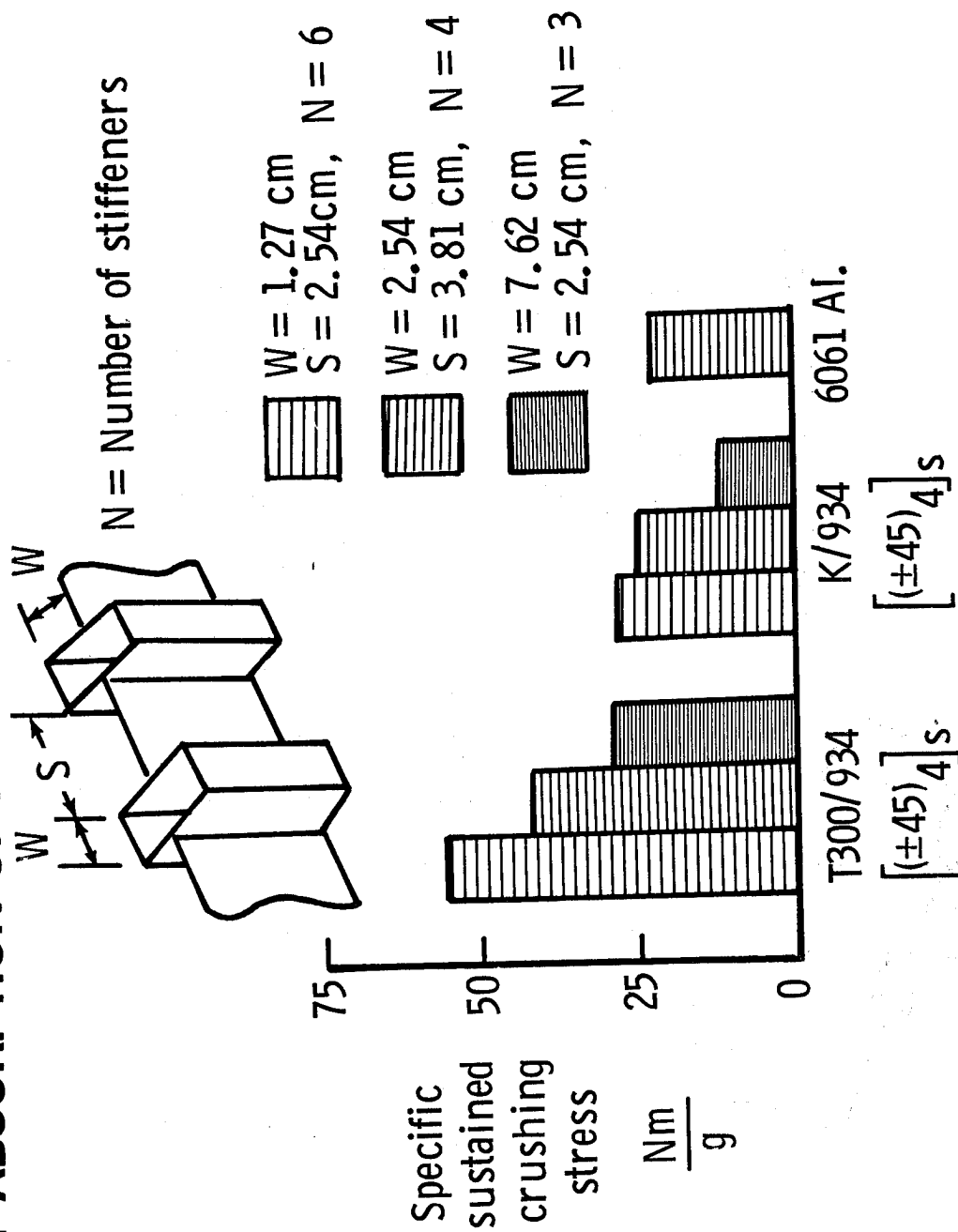


Figure 28

CRUSHED K/934 AND T300/934 $[(\pm 45)_4]_S$ CIRCULAR TUBE STIFFENED BEAMS

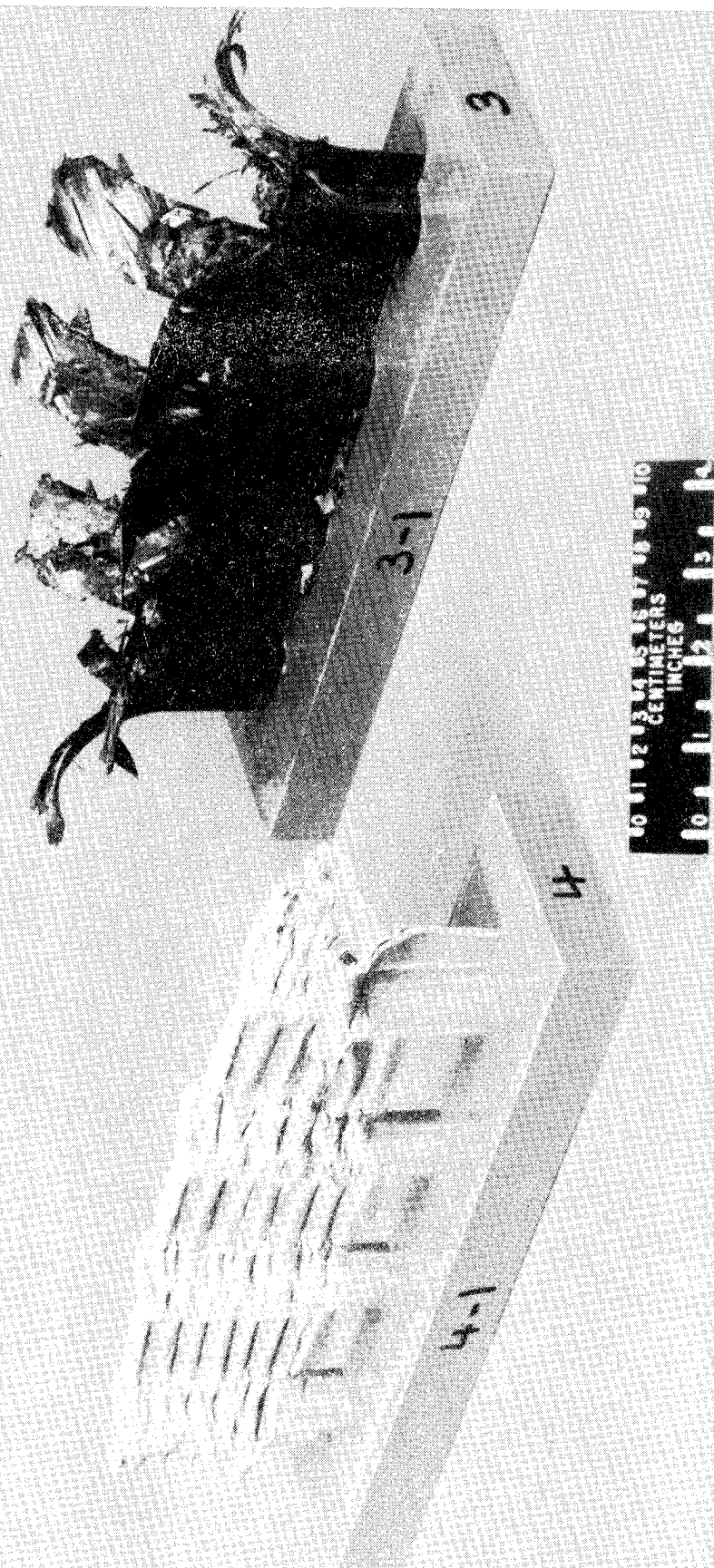


Figure 29

FOUR STIFFENER CIRCULAR CROSS SECTION TUBE STIFFENED BEAM

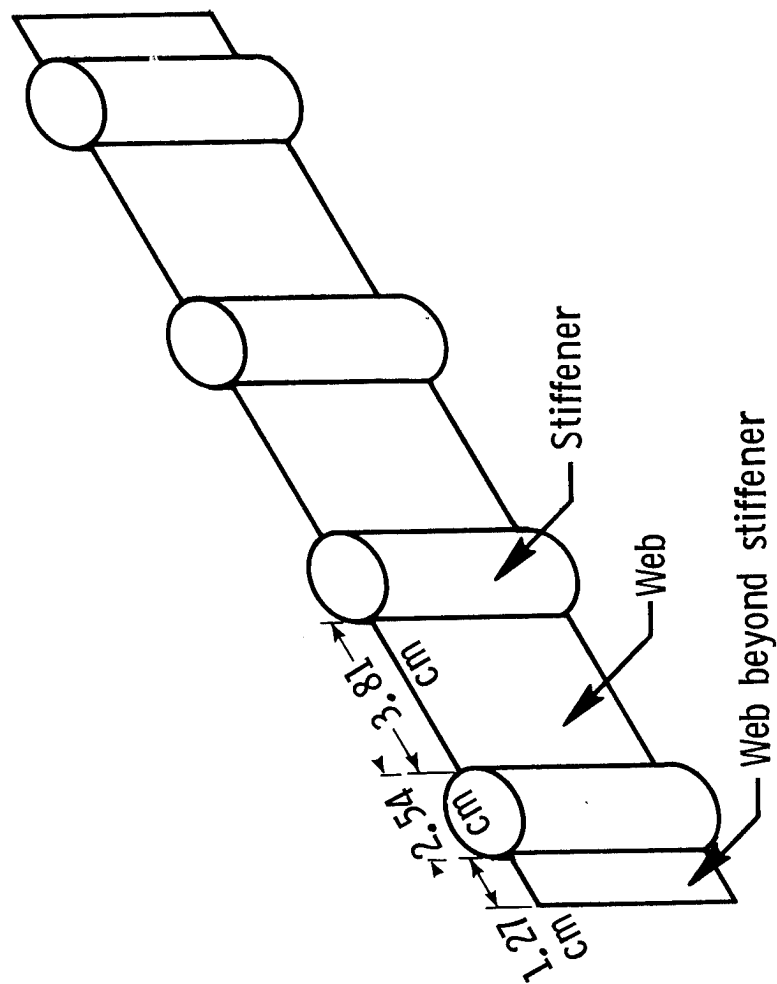
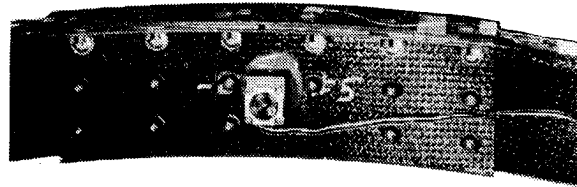
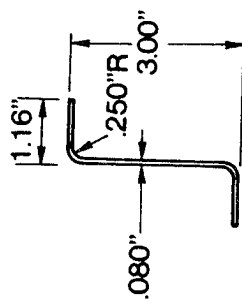


Figure 30

Gr-Ep Frame

GR-EP FRAME CROSS SECTION



FRAME SPLICE PLATE

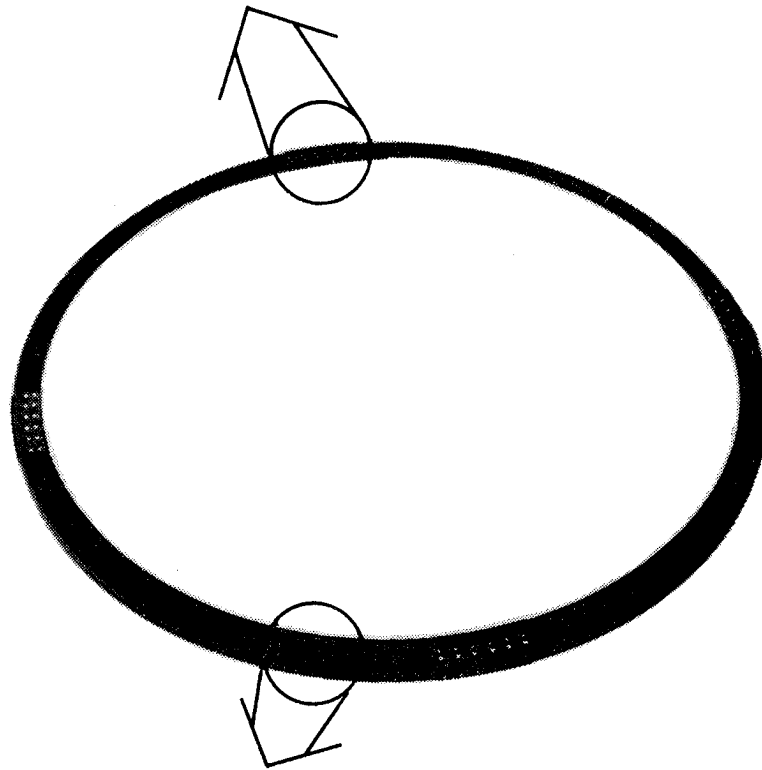


Figure 31

COMPOSITE FRAME STRAIN DISTRIBUTION

TIME = 4.8 MSEC AFTER IMPACT

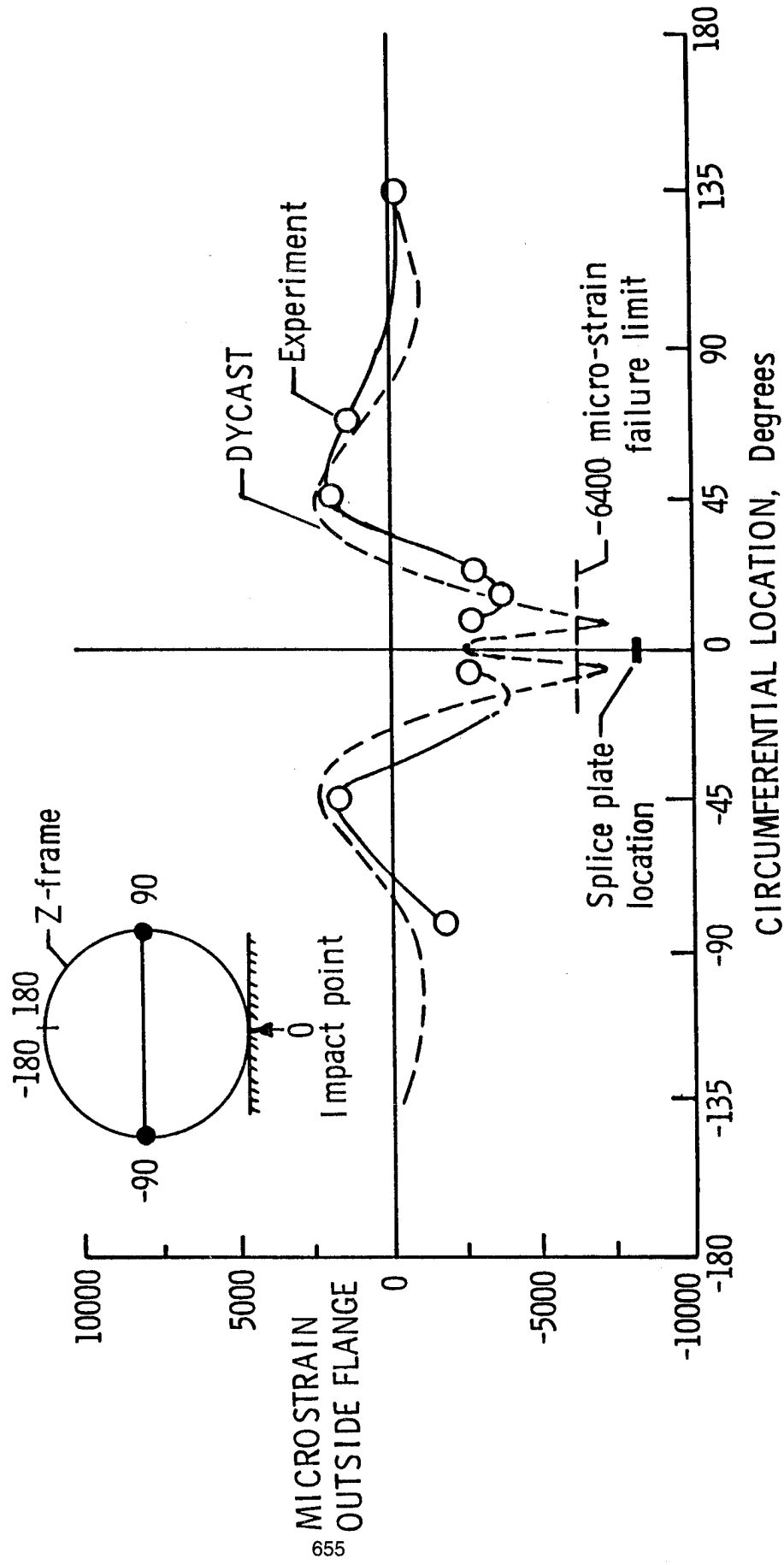


Figure 32

ADVANCED COMPOSITE AIRFRAME PROGRAM -- TODAY'S TECHNOLOGY

DANNY E. GOOD

AND

L. THOMAS MAZZA

AVIATION APPLIED TECHNOLOGY DIRECTORATE
US ARMY AVIATION RESEARCH AND TECHNOLOGY ACTIVITY (AVSCOM)
FT. EUSTIS, VA

1987 NASA/ARMY ROTORCRAFT TECHNOLOGY CONFERENCE

AMES RESEARCH CENTER

MOFFETT FIELD, CA

17-19 MAR 1987

ABSTRACT

The Advanced Composite Airframe Program (ACAP) was undertaken by the Aviation Applied Technology Directorate, US Army Aviation Research and Technology Activity (AVSCOM) to demonstrate the advantages of the application of advanced composite materials and structural design concepts to the airframe structure on helicopters designed to stringent military requirements. The primary goals of the program were the reduction of airframe production cost and airframe weight by 17% and 22% respectively.

The ACAP effort consisted of a preliminary design phase, detail design and design support testing, full-scale fabrication, laboratory testing, and a ground/flight test demonstration. Since the completion of the flight test demonstration programs follow-on efforts have been initiated to more fully evaluate a variety of military characteristics of the composite airframe structures developed under the original ACAP advanced development contracts.

This paper provides an overview of the ACAP program and describes some of the design features, design support testing, manufacturing approaches, and the results of the flight test evaluation, as well as, an overview of Militarization Test and Evaluation efforts.

INTRODUCTION

The ACAP began in 1979 when the US Army awarded contracts to the five major US helicopter manufacturers to conduct a preliminary design of an all composite helicopter airframe for a utility class helicopter with a gross weight under 10,000 lbs. The helicopter was to be designed for a 2.3 hour mission endurance and a 2000 ft - 95⁰ F hover capability. Dynamic systems and subsystem components were to be existing qualified military or commercial components. The results of these five preliminary design studies indicated that the 22% reduction in weight and 17% reduction in production cost could be met or exceeded while at the same time improving military characteristics such as crashworthiness, reliability, maintainability, and survivability.

At the completion of the preliminary design studies the Army proceeded with a two-phased effort to conduct detail design and design support testing and to fabricate, laboratory test and flight test the ACAP helicopter. In March 1981 the Army selected both Bell Helicopter Textron and Sikorsky Aircraft to proceed with the detailed design of their respective ACAP helicopters.

ACAP HELICOPTER DESCRIPTION

The Bell ACAP Helicopter designated, the Model D292, is shown in Fig. 1. The gross weight of the D292 is 7525 lbs. The dynamic systems including the engines, rotors, transmissions and flight controls are taken from the Bell Model 222 commercial helicopter. The Sikorsky S-75 ACAP helicopter shown in Fig. 2. has a gross weight of 8470 lbs. and utilizes the dynamic systems and subsystems of the Sikorsky S-76 commercial helicopter.

AIRFRAME DESIGN

The design of the ACAP airframes was driven to a large extent by requirements other than flight loads. The primary design drivers were the crashworthiness requirements of MIL-STD-1290. As shown in Fig. 3 significant portions of the airframe cockpit, cabin and transition section were designed by crash conditions. The tail sections of the airframes were designed primarily by flight loads in a ballistically damaged condition while the doors, fairings, and portions of the empennage were designed by airloads.

During the design phase numerous trade-offs were made to select the most effective materials and structural configurations for the various airframe components and assemblies in order to provide designs that were structurally and environmentally sound and at the same time light weight, low cost and producible. As the airframe designs evolved a variety of materials and design configurations were used to meet the program goals of reduced airframe production cost and weight and to enhance the military characteristics over those of existing military helicopters. The airframe structural designs make use of a variety of composite materials including graphite, Kevlar,

fiberglass, epoxy, and polyimides and structural configurations including skin/stringer; integrally stiffened panels; solid laminates; and sandwich beams, frames, and longerons. A breakout of the major structural components is shown in Fig. 4. Graphite is utilized in areas where high strength and stiffness are required, such as longerons, frames and beams; Kevlar is used predominantly for both primary and secondary skin panels; and fiberglass is utilized on surfaces subjected to high wear such as floors. In some airframe applications, however, composites were not considered practical. These areas included transparencies, some attachment hardware, door latches, and fasteners. Fig. 5 shows the utilization of materials in the composite airframes of each manufacturer.

Cost effective producible design required that particular attention be given to the airframe breaks and sizing of the major components and subassemblies. The preliminary design studies had shown that, in general, to meet the program cost savings goals, it was essential to minimize the total number of parts and fasteners. However, experience has shown other factors such as tool size, complexity, accessibility and turn around time must be considered, as well.

The basic approach to the design by each manufacturer was significantly different and resulted from many factors including each contractor's background and experience with other composite designs. The Bell ACAP airframe assembly approach utilizes two large half shell fuselage sections which are bonded together to form the basic airframe shell from the nose to bulkhead where the tail boom is attached. Sikorsky Aircraft, on the other hand, elected to use a number of modules or subassemblies, which are mechanically fastened to form the basic airframe shell. In each case the manufacturer reduced the number of parts and fasteners substantially in comparison with their respective metallic baseline airframe.

The ACAP detail design represents the first US military helicopter structural design to be developed using Computer Aided Design. The aircraft lines were developed from CAD terminals as were a major portion of the airframe detail design drawings. The CAD system provided a common data base for the aircraft lines, detail design, and structural analysis. Not only did the CAD system provide the designer with a rapid visualization of his design, it also provided rapid turn around time thus allowing greater flexibility to optimize the part.

The use of CAD did not stop with the designer and analyst, however. The design data base was used by the manufacturing engineers as well to develop tool designs, flat pattern layouts, and tapes for numerically controlled machines such as the Gerber cutter, tape laying machines, and filament winders. From the tool designers viewpoint, a major benefit of the common data base and the CADAM system was the ability to incorporate shrink factors in the tool design to compensate for differential thermal expansion during the cure cycle.

DESIGN SUPPORT TESTING

Prior to committing to full-scale airframe manufacturing each contractor conducted a significant design support test program to verify the structural integrity of the critical components of the airframe. The objectives of these tests were to demonstrate that the structural concepts were properly designed and to compare the results to the design criteria. These tests ranged from coupon and panel tests to substantiate design allowables for specific materials and laminate configurations to static and fatigue tests of major joints, attachments and full-scale components to verify structural integrity. A one-fifth scale model wind tunnel test was conducted to assess the drag and stability characteristics of the ACAP helicopter configurations. Additionally, testing was conducted to assess the crashworthiness, damage tolerance and lightning strike protection of the airframe design.

TOOLING CONCEPTS

The tooling philosophy for the ACAP placed emphasis on controlling dimensional accuracy, stability, and repeatability of the composite components being fabricated. The resulting primary tooling concept used by each of the contractors, however, is quite different. Bell Helicopter elected to fabricate the basic ACAP fuselage shell in two halves, thereby minimizing the number of major assemblies. To minimize the differential thermal expansion between the part and the tool during autoclave curing Bell elected to use graphite tooling. Figure 6 shows the left-hand fuselage shell mold with the initial ply layups in place. The completed fuselage half-shell is shown in Fig. 7.

Sikorsky, on the other hand elected to use metal tooling for their large skin molds. They accounted for the differential thermal expansion in the design of the tool - a task that was greatly simplified by the use of CADAM. The large skin mold tools were made by forming a thin steel shell to the aircraft contour followed by welding studs on the shell mold for attachment to the mold base through the contoured headers. The headers were cut on a numerical control machine utilizing aircraft lines data from the CADAM data base. Figure 8 shows the completed mold with the formed steel shell in place. The posts at the corners of the mold base are used to stack tools for multiple autoclave curing.

Other components with critical dimensions such as ribs, frames, bulkheads, and beams, are fabricated on steel tooling like that shown in Fig 9. Electroplated nickel and fiber reinforced composite tools were also used for some components where dimensional control was less critical.

MANUFACTURING METHODS

Each contractor developed a manufacturing plan considering both existing and developmental manufacturing methods and technologies which could impact favorably on the manufacturing cost of the composite airframe. Autoclave curing was used for fabrication of the large skin sections. Filament winding was used to fabricate the Bell truss tailcone and the Sikorsky tailcone and vertical pylon spar. The graphite windshield post on the Sikorsky ACAP was fabricated using the pultrusion process. Computer generated pattern books (Fig. 10) were used to aid shop layup. Computer controlled rapid ply pattern cutting (Fig. 11) was used to prepare composite laminac for layup kits. Water jet trimming (Figure 12) of precured parts was also utilized.

Various computer aided and robotic manufacturing methods which were under investigation at the time were identified as potentially promising methods for factories-of-the-future. However, where the technology had not matured to the point it could be demonstrated under the ACAP contract it was not included in the manufacturing cost analysis. Each contractor was required to conduct a production cost analysis to compare the direct labor and material cost of the advanced composite airframe to the equivalent metallic baseline airframe. This cost comparison was based on FY 80 dollars and a production run of 1000 aircraft at a rate of 14 aircraft per month. Figure 13 shows a comparison between the ACAP airframe production costs and the metallic baseline in terms of materials and labor. It can be seen that the cost savings achieved is due to the labor cost reduction. The material costs for the airframe are significantly higher than for the metallic airframe despite the reduction in the weight of the airframe. Hopefully, future volume production of composite raw materials will result in lower prices and thus increase the cost savings on future aircraft systems.

Each contractor fabricated three airframes. The first airframe was used for proofing the tooling concept. The Tool Proof Airframes (TPA) shown in Figs. 14 and 15 were ballistically tested at the AATD Ballistics Test Range at Ft. Eustis, VA. The second airframe fabricated was designated the Static Test Article (STA). The STA was used both for static testing and shake testing. The third airframe fabricated was assembled with all the dynamic systems, subsystems and landing gear to produce a complete flightworthy Flight Test Vehicle (FTV).

During the fabrication effort the contractors were required to track the weight of the composite airframe and to compare the weight to that predicted both for the baseline metal and composite airframes. Figure 16 compares the weight of a composite airframe to a metal baseline from the preliminary design to the completion of the fabrication of the three airframes.

STATIC TEST PROGRAM

Static testing was conducted on the STA's to verify the structural integrity of the ACAP airframes for the applied design loads. The contractors selected the design loading conditions based on their NASTRAN model results. In the case of Sikorsky several critical load conditions were tested to insure that the most critical loading conditions were introduced to each section of the airframe. The flight and landing load conditions tested are shown in Table 1. Bell Helicopter also choose critical flight conditions which would introduce critical loading in each section of the airframe. Table 2. summarizes the flight and landing loading conditions applied in the Bell static test program.

AMCP 706-203 states that thermal environmental effects shall be accounted for in static testing by: (1) application of the operational environment, or (2) by accelerating the applied loads to account for the environmental degradation. This requirement was extended in the ACAP static test program to include the effect of moisture on composites as well as temperature. This requirement presented a dilemma for the contractors because conditioning of the entire airframe, particularly, moisture conditioning was considered impractical. On the other hand, full load acceleration to account for environment could impact too severely on environmentally insensitive components. The approach taken, therefore, was to test at elevated temperature with loads accelerated to account for moisture degradation. Figures 17 and 18 show the Sikorsky and Bell airframes in static test, respectively.

FLIGHT TEST PROGRAM

The structural substantiation process was continued throughout the flight test program to verify that the applied design loads were not exceeded during flight. The flight test vehicles were instrumented with strain gages to monitor flight loads during the test program. Safety of flight monitoring of the strain levels was a major concern. Since using design allowables as flight allowables would only guard against "failure under the gage", the flight strain allowables were based on the full scale static test results. In this manner the strain gages are monitored as "load cells" to assure that the loads substantiated in static testing were not exceeded in flight. The "Do Not Exceed" (DNE) flight strains were based on measured static strains reduced to appropriate safe flight levels by:

$$\epsilon_{DNE} = \epsilon_{STATIC} \times 2/3 \times 1/LAF \times K$$

Where:

- ϵ_{STATIC} = Peak Static Test Strain
- 2/3 = Ultimate to Limit Safety Factor
- LAF = Load Acceleration Factor
(eg. Temperature/humidity effects)
- K = Other Appropriate Factors

For those areas of the structure that were statically tested at elevated temperature the LAF was based on the ratio of room temperature dry to room

temperature wet design allowables. When the critical area was not tested at elevated temperature then the LAF was based on the ratio of room temperature dry to elevated temperature wet design allowables. Early in the flight test program a K factor of 0.8 was used as added conservatism.

The Sikorsky S-75 ACAP made its first flight (Fig. 19) in July 1984 at the Sikorsky Aircraft Flight Test Facility in West Palm Beach, Florida. The FTV completed a 43 hour flight test program which included a 5 hour Government Pilot Evaluation in March of 1985. The S-75 flight envelope established, which was limited by the dynamics system installed, is shown in Table 3.

In September 1985 the Bell D-292 made its first Flight (Fig. 20) at the Bell Flight Test Center in Ft. Worth, Texas. The Bell FTV completed 25 hours in July 1986. The D-292 flight envelope established is shown in Table 5.

ACAP MILITARIZATION TEST AND EVALUATION

Although the basic ACAP program included an evaluation of some of the military characteristics of the airframes developed there were some areas that either were not evaluated completely or were not examined at all. In September of 1985 contracts were awarded to both Bell and Sikorsky to conduct additional test and evaluation of the ACAP airframes. These efforts included the following areas of interest: (1) landing gear/airframe crashworthiness, (2) repairability and inspectability, (3) lightning strike protection, and (4) internal acoustic noise.

The landing gear for the ACAP helicopters were designed in concert with the airframe design because the ability of the helicopter to meet the requirements established for crashworthiness is dependent on the ability of the total system to absorb crash energy. The airframe, landing gear and seats all play a role in the safety of the crew and troops in a crash. Drop testing of the main and auxiliary landing gear at sink speeds up to 20 fps was included in the original contract. The original contract also included a full-scale drop test of the complete airframe, landing gear and seat system. In order to preserve the assets for other testing it was decided to delete the full scale drop testing from the original contract. Therefore, the testing was picked up in the follow-on ACAP Militarization Test and Evaluation (MTE) Programs. In addition, to insure that both the main and auxiliary landing gear would function as designed, drop testing at sink speeds up to 42 fps was included in the MTE programs. Drop testing of the landing gear at sink speeds up to 42 fps is in progress now and the full-scale aircraft drop tests are scheduled for mid-1987.

Analyses of the reliability and maintainability characteristics of the ACAP airframes were conducted during the basic ACAP program. In addition, limited repair demonstrations were made. In the MTE program each contractor is further developing field repair techniques and procedures compatible with the personnel skills, materials and equipment expected to be available for field (AVIM level) repairs. These repair techniques and procedures to be demonstrated on the tool-proof and static test airframes will be completed early in 1987.

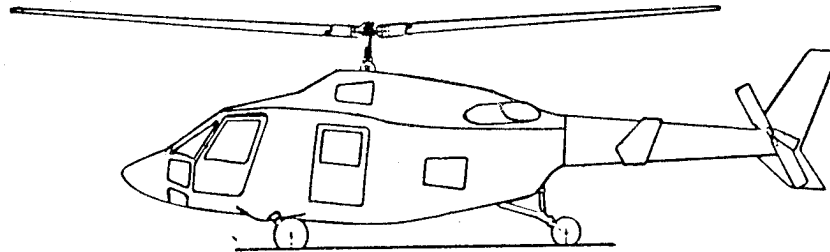
Lightning strike test of composite panels were conducted as a part of the ACAP design support test program to provide comparative test data to aid in the selection of a means for protecting the Kevlar skin from lightning strikes. Although the panel test results were favorable it was desirable to evaluate the performance of the lightning strike protection system on a full scale airframe. The testing included both direct and indirect lightning strikes. Testing of the Sikorsky ACAP was successfully conducted at the McDonnell Douglas Facilities in St. Louis, MO. The Bell ACAP lightning strike testing was conducted by Boeing Aircraft in Seattle, WA. This testing was conducted in cooperation with the Air Force's Atmospheric Electrical Hazards Protection (AEHP) program. In addition to the evaluation of the effects of lightning strike on the airframe structure, a variety of electrical and avionics components were installed onboard the Bell ACAP to enable the evaluation of electromagnetic compatibility and interference characteristics. Shown in Fig. 21 is the Bell tool-proof airframe being subjected to a direct lightning strike.

The transmission of internal acoustic noise in an all composite airframe has been a concern from the standpoint of increased sound pressure levels in both the cockpit and crew compartments. During the initial flight test evaluation of the Sikorsky S-75 ACAP and Bell D292 ACAP the pilots' qualitative reports were that the noise and vibration levels were about the same as in the parent S-76 and Model 222 helicopters. The ACAP MTE program included a 5-hour flight test evaluation to measure sound pressure levels and accelerations in an effort to quantitatively assess the internal acoustic noise. In addition, noise predictions were made using a computer code originally developed by Cambridge Collaborative for a Sikorsky S-76 helicopter under a NASA Langley Research Center contract. The acoustic flight testing of the Sikorsky S-75 ACAP was conducted in April 1986. Figure 22 shows a typical comparison of the acoustic noise data measured on the S-75 ACAP with data measured on the metal S-76. The Bell D292 ACAP is scheduled for acoustic flight testing in early 1987.

Finally, under separate contract competitively awarded to Bell Helicopter in September 1986, a full suite of communications and navigation equipment commensurate with the Army's UH-60 BLACK HAWK helicopter is being installed on the Bell FTV. The Bell ACAP FTV will be used as a flying test bed to evaluate the electromagnetic compatibility and interference characteristics and operational performance levels of a full-up avionics suite on-board an all composite airframe.

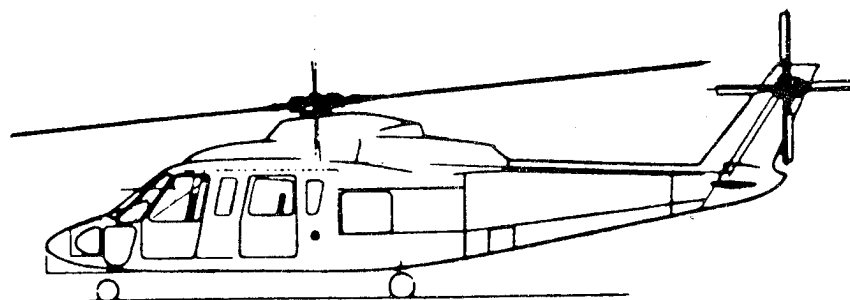
CONCLUSIONS

The Advanced Composite Airframe Program has successfully demonstrated the feasibility of applying advanced composite materials to the airframe of military helicopters. The ACAP has greatly reduced the risk of introducing composites into next generation helicopter full-scale engineering development programs. The primary goals for weight and cost reductions have been achieved and both a cost and weight data base have been established. The benefits of composites technology for enhanced military characteristics have or are being demonstrated through test and evaluation of the ACAP airframes.



DYNAMIC SYSTEMS: MODEL 222
GROSS WEIGHT: 7525 LBS

Figure 1. Bell D292 ACAP Helicopter



DYNAMIC SYSTEMS: S-76
GROSS WEIGHT: 8470 LBS

Figure 2. Sikorsky S-75 ACAP Helicopter

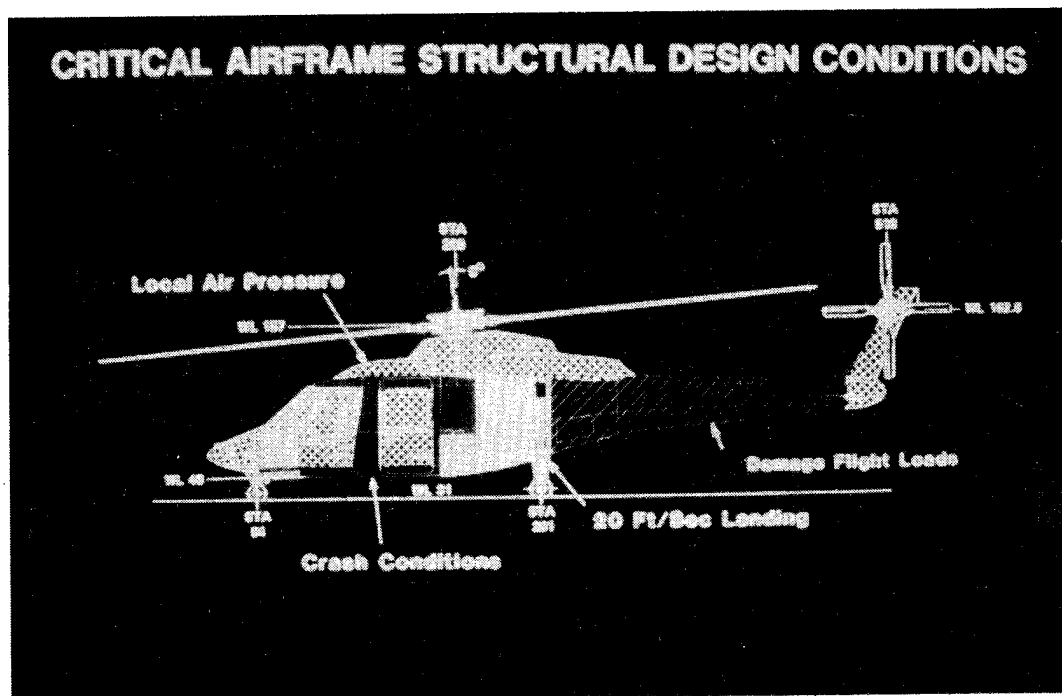


Figure 3. ACAP Helicopter Design Drivers

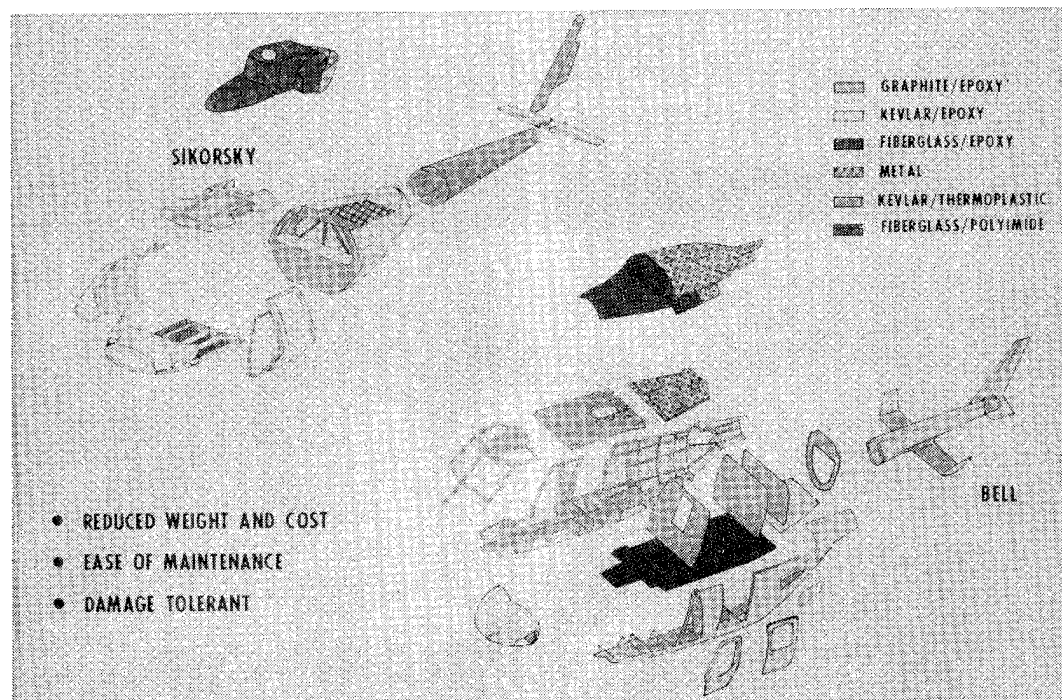


Figure 4. ACAP Helicopter Structural Arrangement

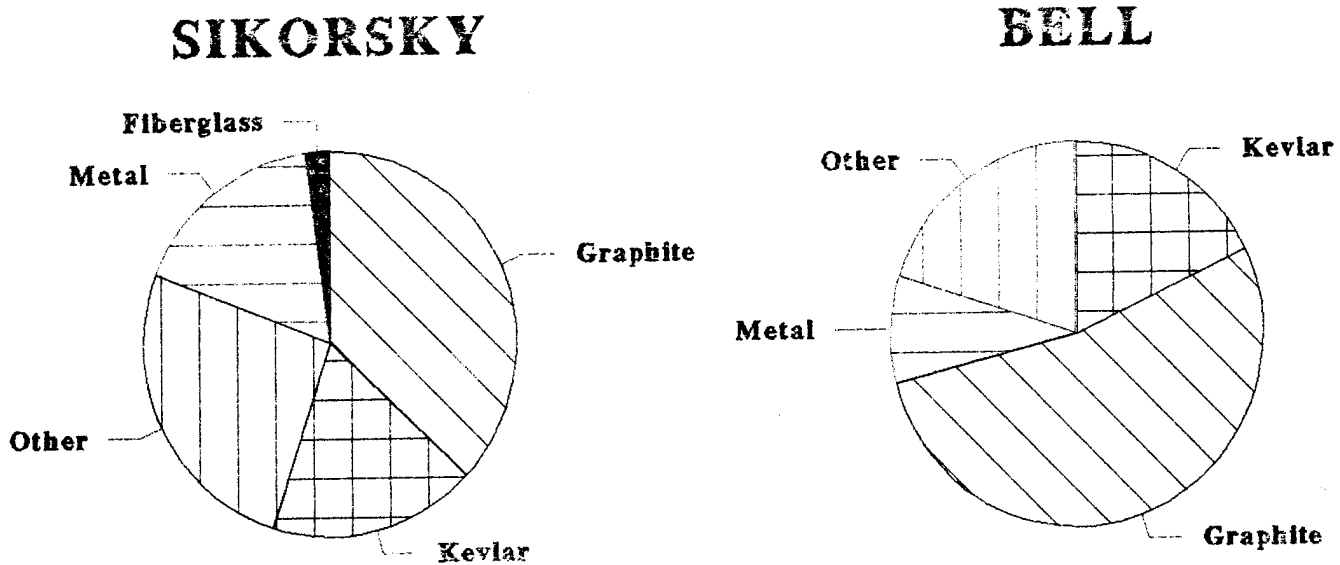


Figure 5. ACAP Material Utilization

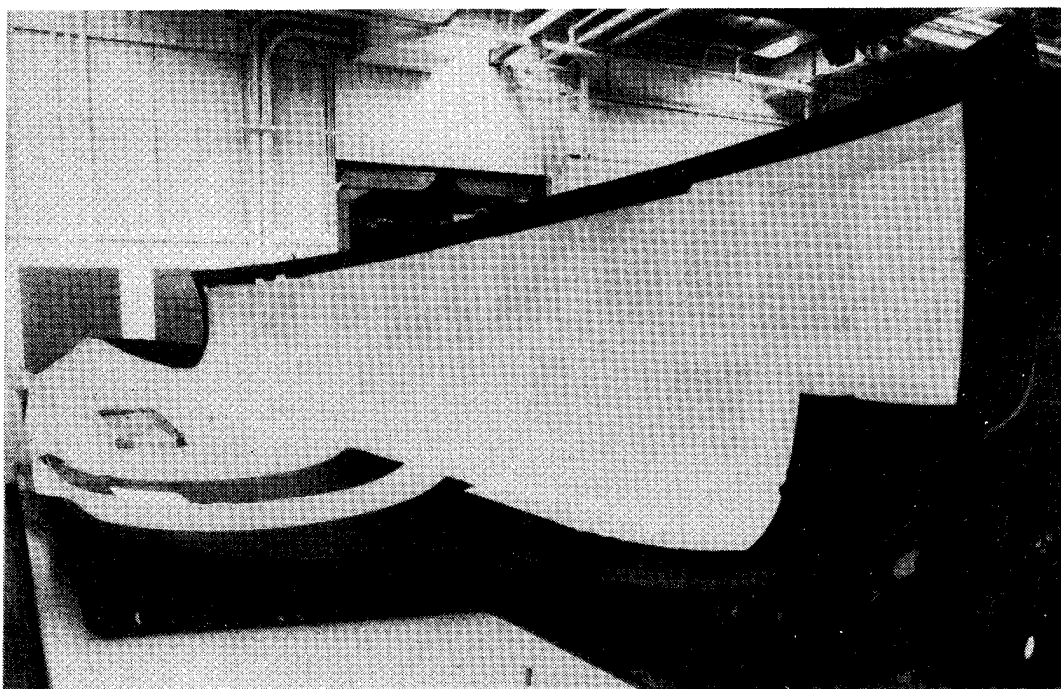


Figure 6. Bell ACAP Half-Shell Tool

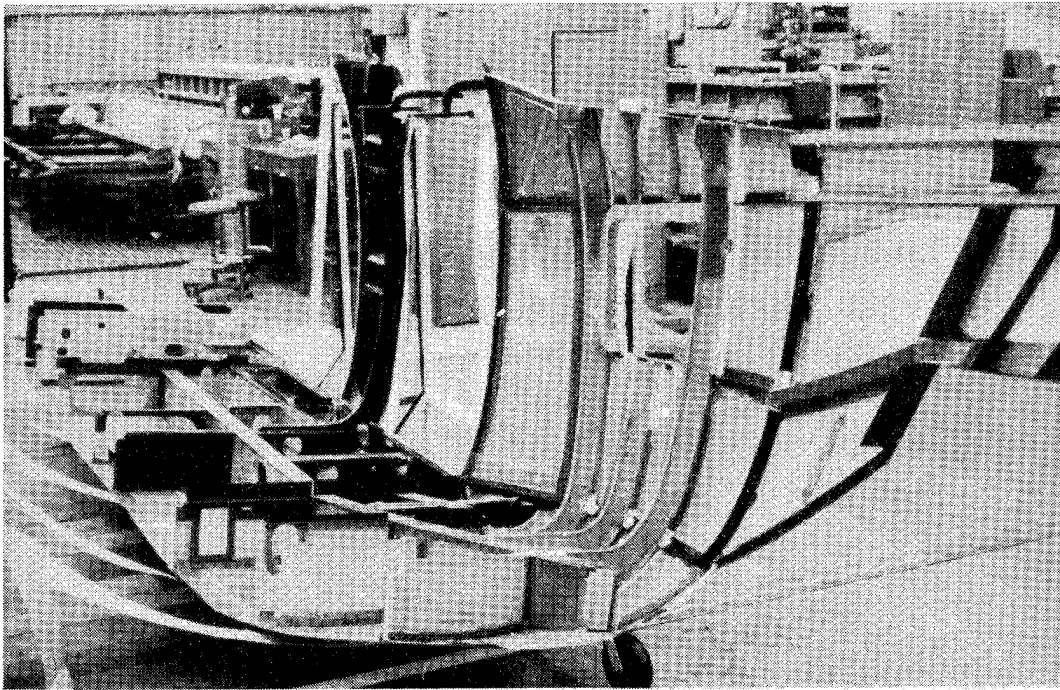


Figure 7. Bell Fuselage Half-Shell

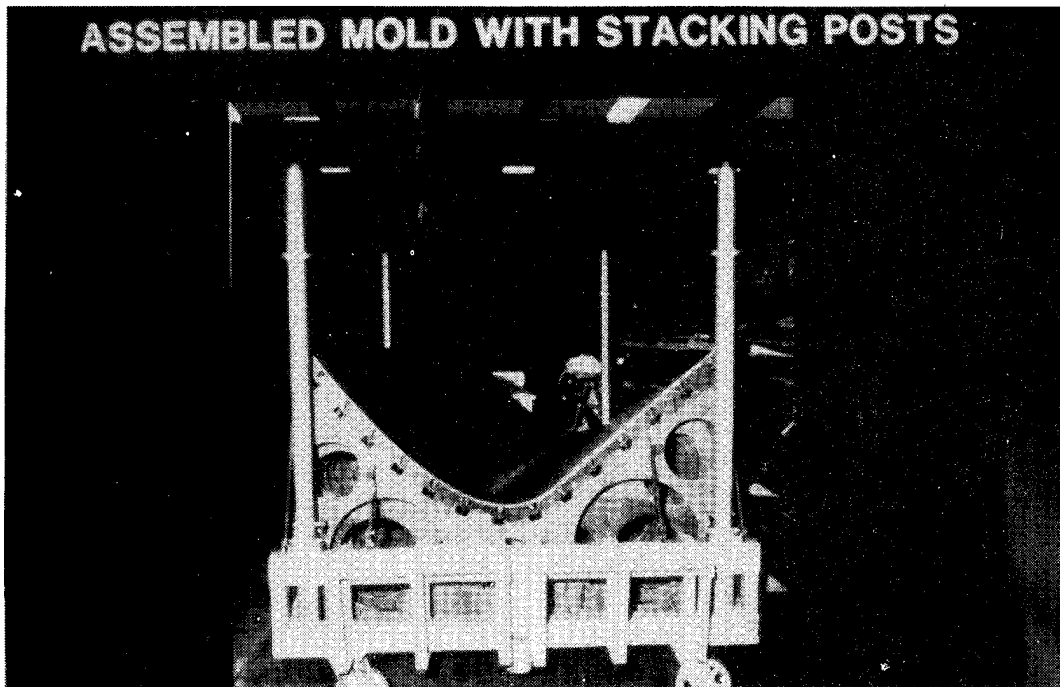


Figure 8. Sikorsky Steel Shell Mold Tool

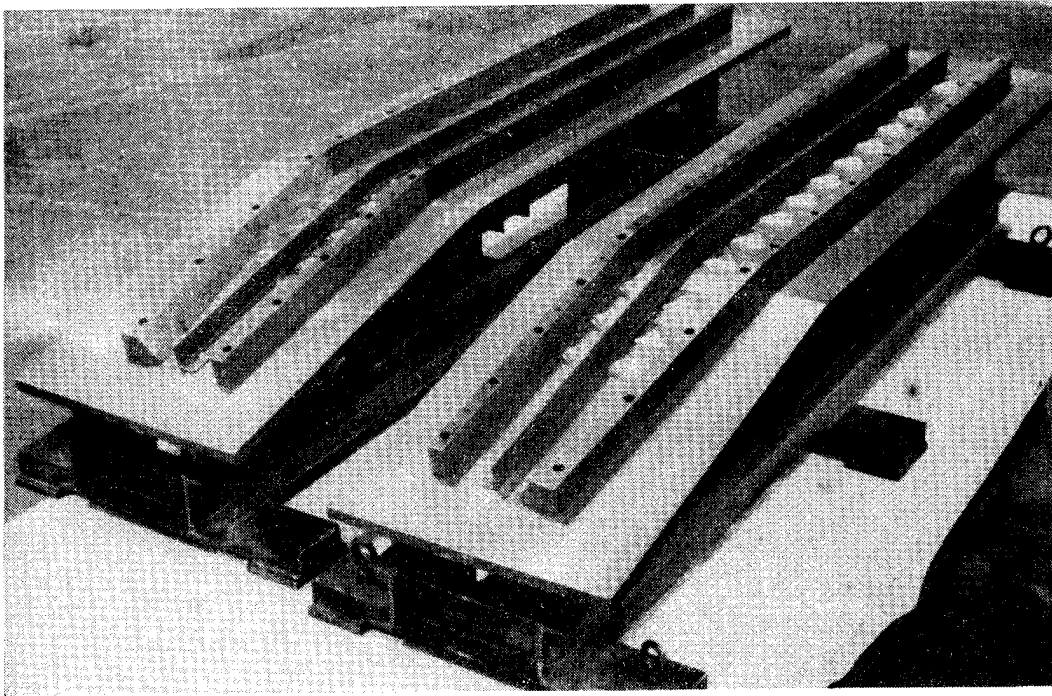


Figure 9. Typical Steel Frame Tool

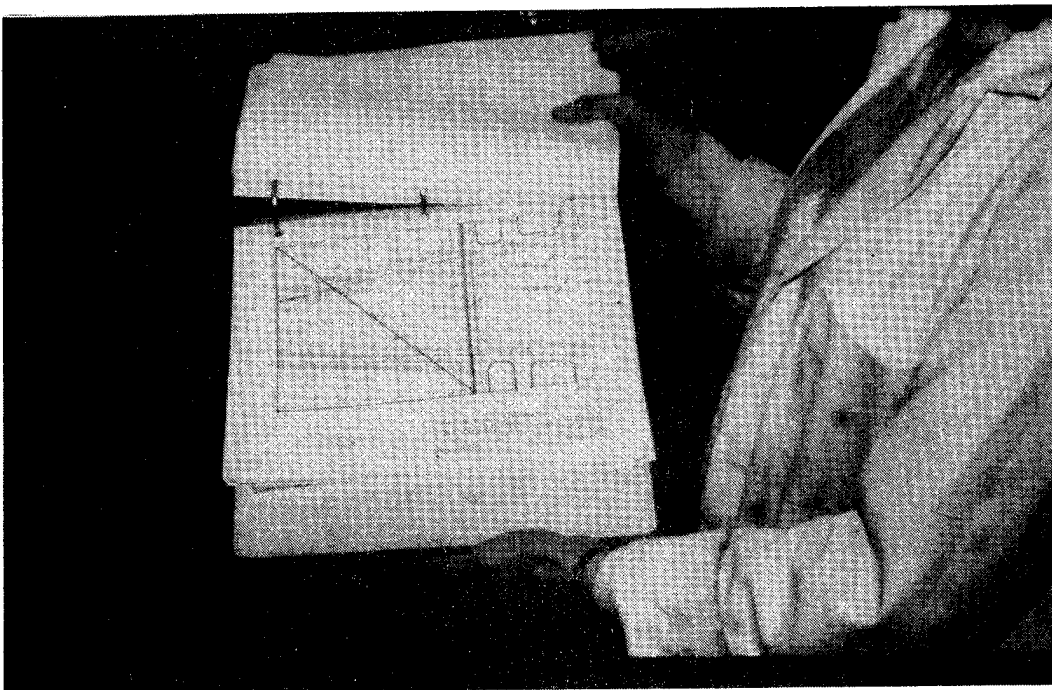


Figure 10. Computer Generated Composite Ply Layup Book

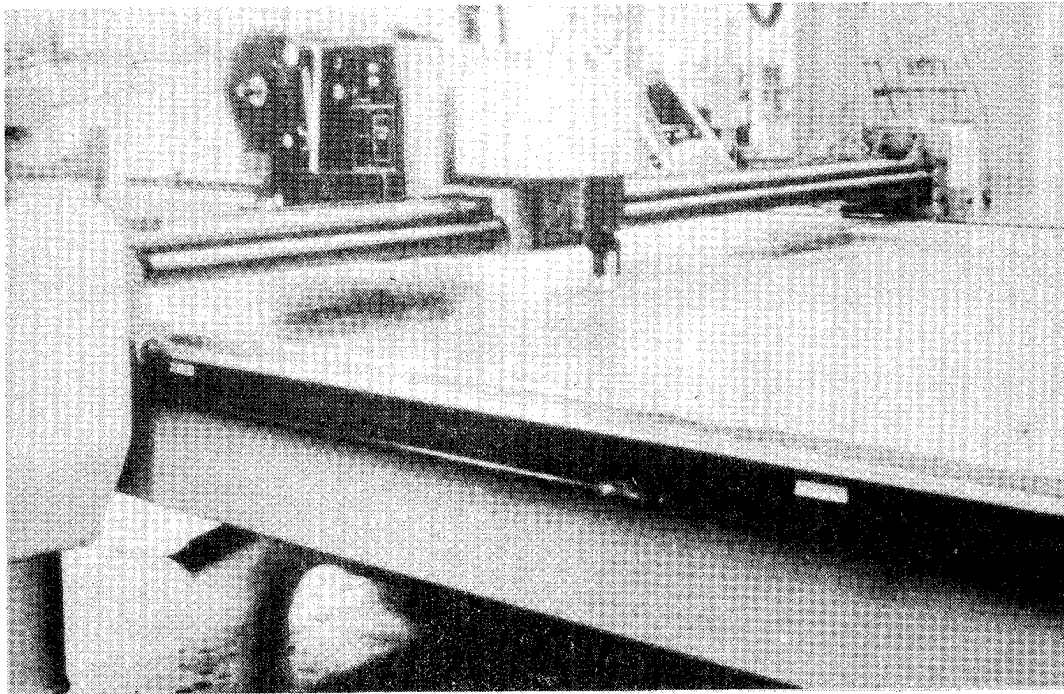


Figure 11. Computer Controlled Rapid Ply Cutting

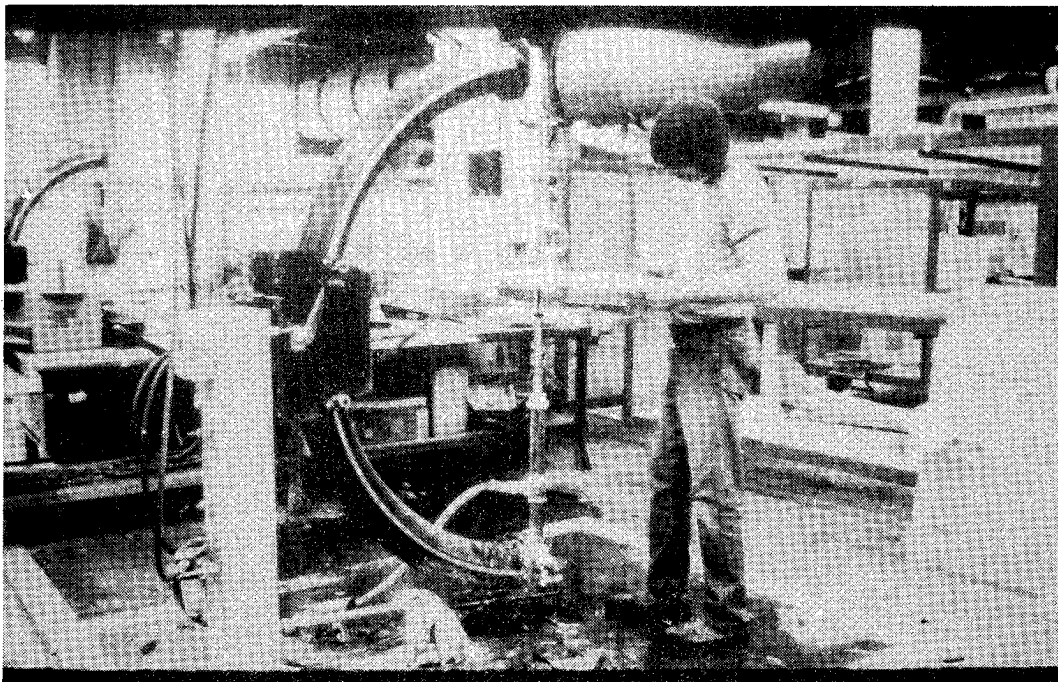


Figure 12. Water Jet Trimming

METAL AIRFRAME
Total Cost \$240,041

COMPOSITE AIRFRAME
Total Cost \$185,458

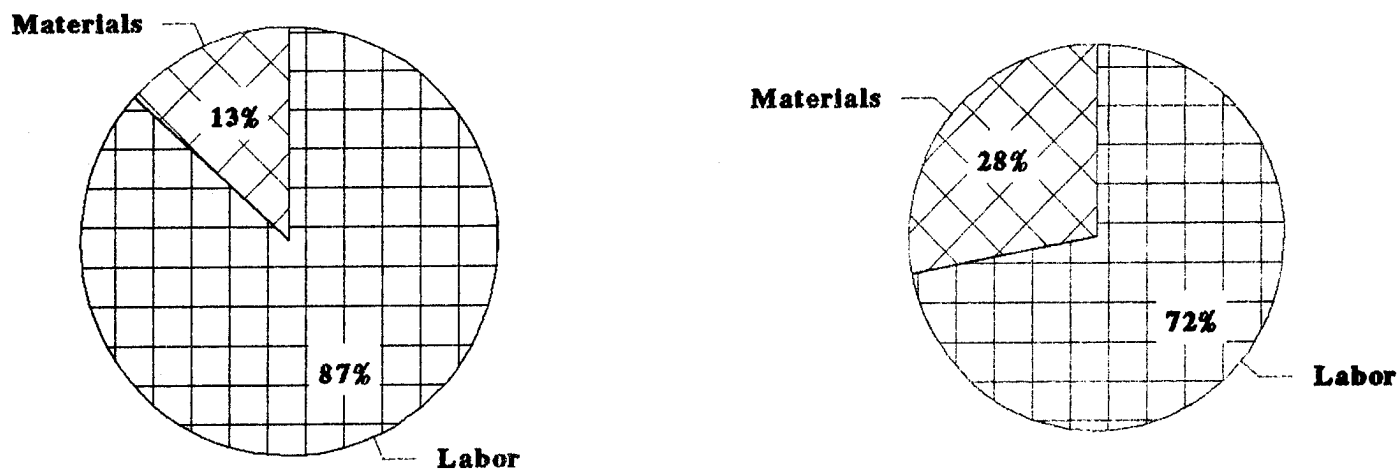


Figure 13. Comparison of Composite and Metal Airframe Cost



Figure 14. Bell ACAP Tool Proof Article

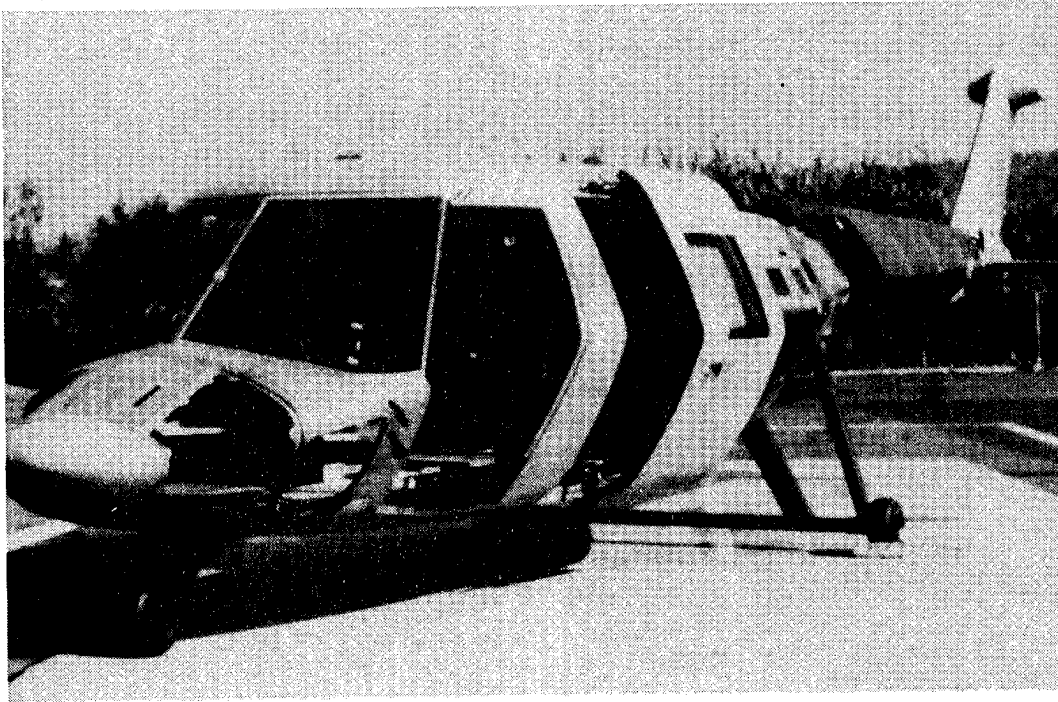


Figure 15. Sikorsky ACAP Tool Proof Article

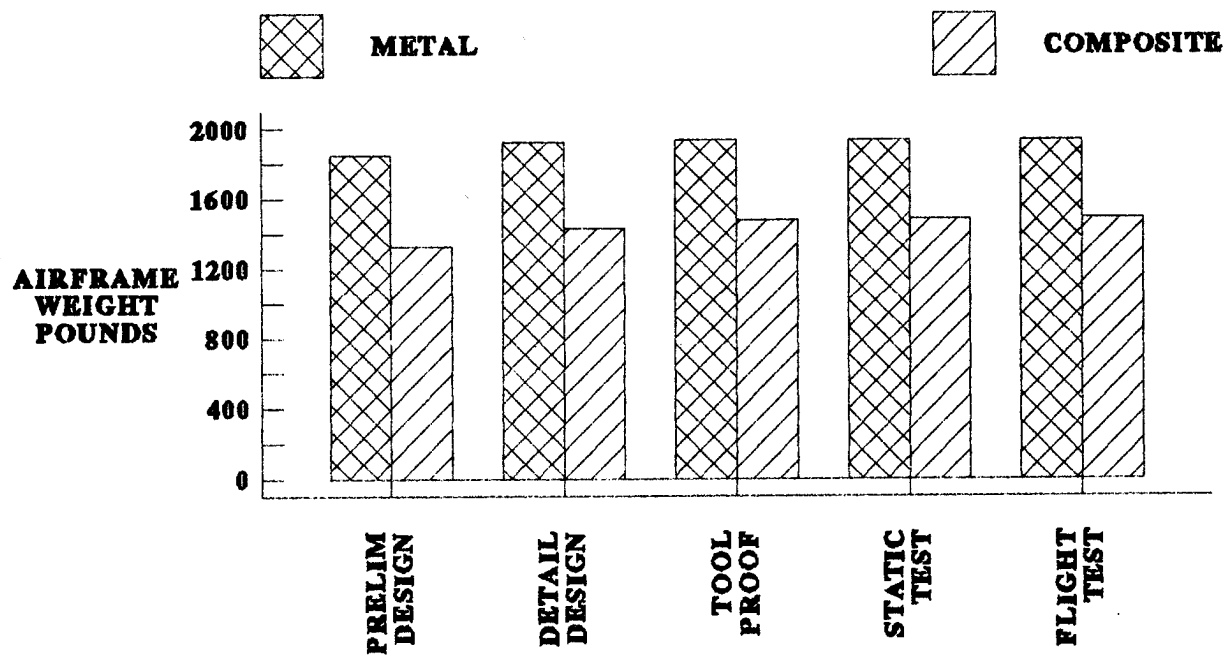


Figure 16. ACAP Airframe Weight Trends

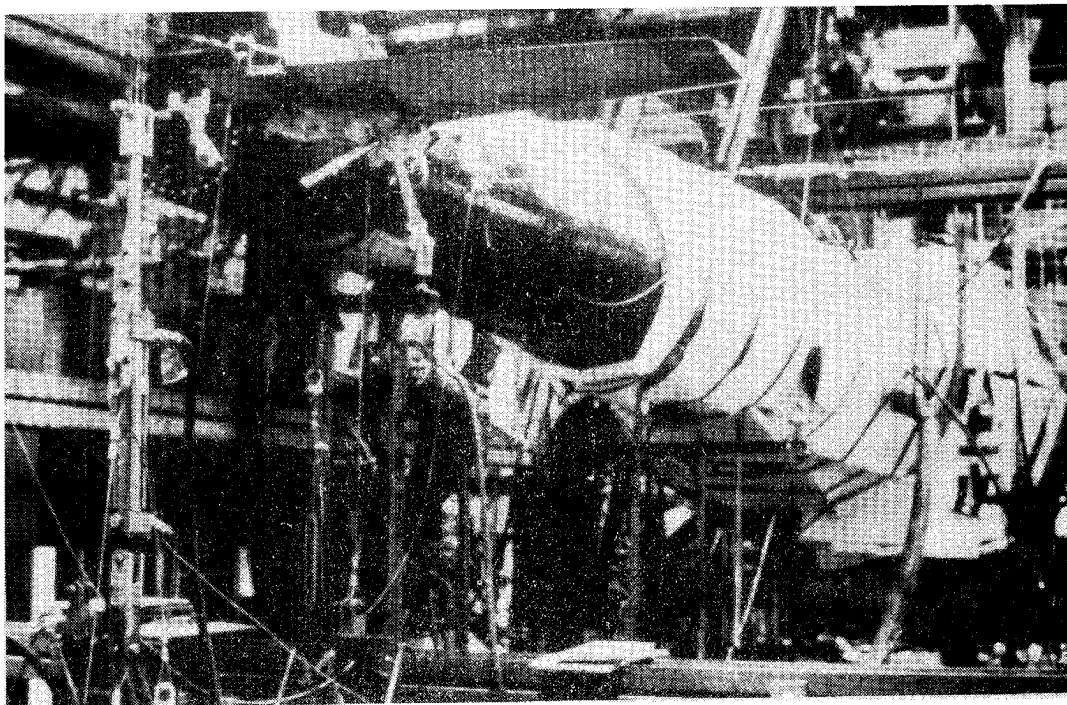


Figure 17. Sikorsky ACAP Airframe in Static Test

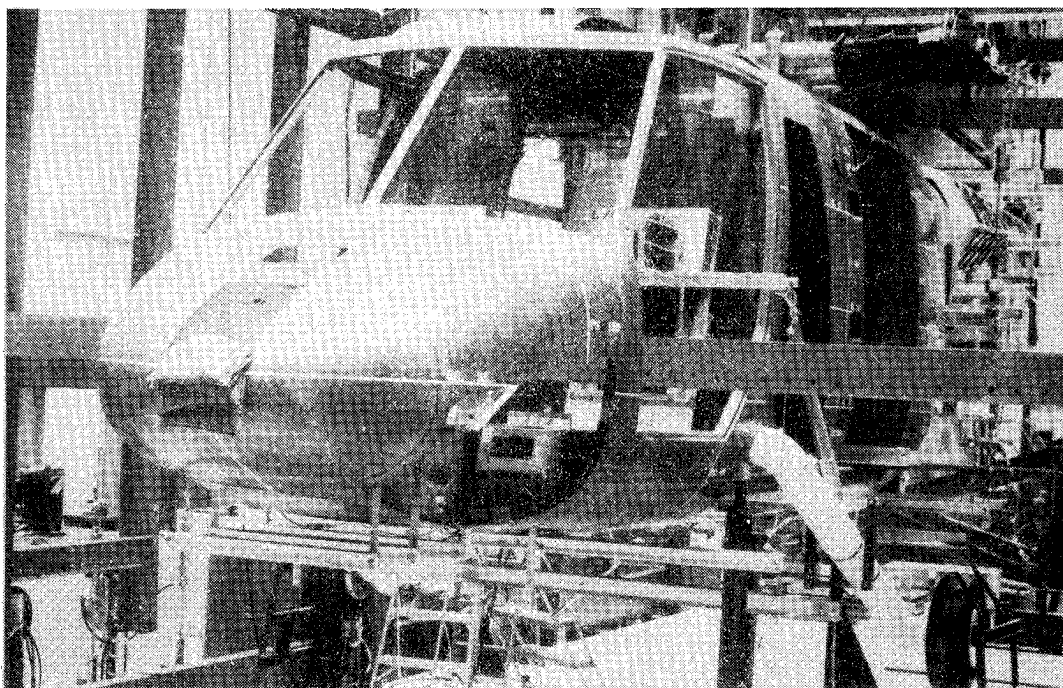


Figure 18. Bell ACAP Airframe in Static Test



Figure 19. Sikorsky Flight Test Vehicle



Figure 20. Bell Flight Test Vehicle

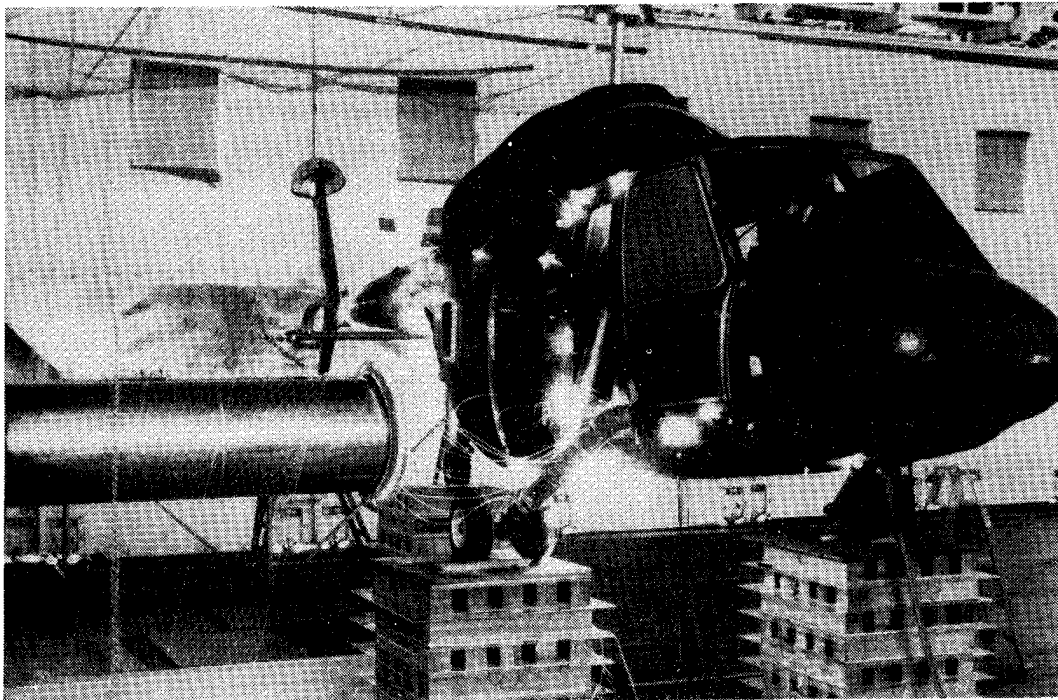


Figure 21. Lightning Strike Test of Bell ACAP Airframe

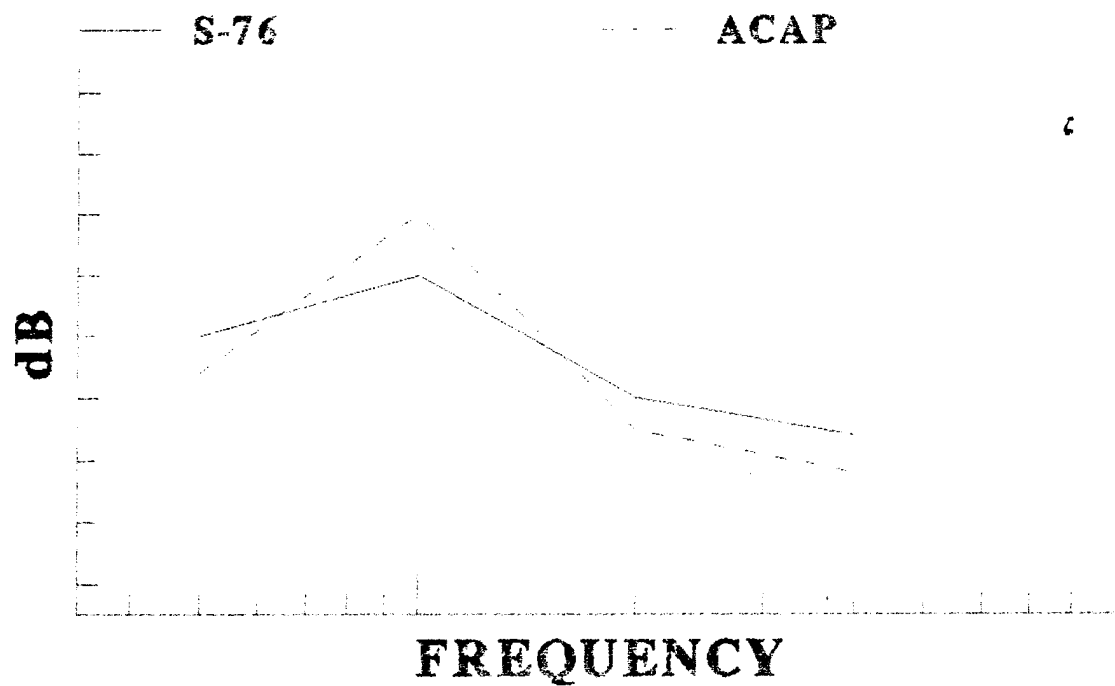


Figure 22. Comparison of ACAP and S-76 Internal Noise Levels

Table 1. Bell Static Test Conditions

<u>Cond. No.</u>	<u>Description</u>
1	Symmetrical Pull Out
2	15 ⁰ Yaw Left Return
3	15 ⁰ Yaw Right Return
4	Vertical Jump Take-Off
5	20 fps, 2 Point Landing
6	Vertical Fin, 15 ⁰ Yaw Trim
7	Horizontal Stabilizer, 15 ⁰ Yaw Trim
8	Horizontal Stabilizer, Sym. Pull Out

Table 2. Sikorsky Static Test Conditions

<u>Cond. No.</u>	<u>Description</u>
1	Horizontal Stabilizer, Asymmetrical Airloads
2	Horizontal Stabilizer, Symmetrical Airloads
3	Empennage, Rolling Pull Out
4	Empennage, Right Yaw Kick
5	Mid Cabin, Rolling Pull Out
6	Mid Cabin, Symmetrical Pull Out
7	Forward Fuselage, 20 fps
8	Rear Fuselage, 20 fps
9	Windshield/Crew Door, Dive, Airloads

Table 3. Bell D292 Flight Test Envelope

<u>Flight Condition</u>	<u>Level Demonstrated</u>
Forward Flight	120 Kts
Rearward Flight	35 Kts
Sideward Flight	15 Kts
Bank Angle	60 ⁰
Load Factor	0.5 to 2.0 g

Table 4. Sikorsky S-75 Flight Test Envelope

<u>Flight Condition</u>	<u>Level Demonstrated</u>
Forward Flight	141 Kts
Rearward Flight	35 Kts
Sideward Flight	35 Kts
Bank Angle	60 ⁰
Load Factor	-0.2 to 2.75 g

PROPULSION AND DRIVE SYSTEMS

Session Cochairmen:

Calvin L. Ball, NASA

Gilbert J. Weden, Department of the Army

PROPULSION AND DRIVE SYSTEMS SESSION

SUMMARY

Session papers addressed a wide spectrum of advanced technologies applicable to rotorcraft. The first two papers highlighted powerplant research aimed at evolving highly advanced, efficient engine systems with potential fuel burned reductions of up to 40 percent. The first paper highlighted Compound Cycle Engine (CCE) research directed toward a helicopter application. The CCE is a highly turbo-charged, power-compounded power plant combining the lightweight pressure rise capability of a gas turbine with the high efficiency of a diesel. Results of recent activities to establish a technology base for development of diesel engine life (friction, wear and lubrication) were reviewed.

The second paper addressed advanced small gas turbine engines. The results of recently completed comprehensive studies conducted by government and industry to identify and quantify high-payoff technology benefits for rotorcraft were summarized. Significant advances were projected in the areas of materials, components and cycles. Advanced non-concentric high pressure and temperature simple cycles and lower pressure, high temperature, heat recovery cycles were applied to both conventional and tiltrotor type rotorcraft. Recent accomplishments in component and materials research, aimed at evolving the technology base for these advanced engines were highlighted.

The third paper described a significant recent accomplishment applicable to a wide range of advanced rotorcraft. This accomplishment embodies the demonstration of a dual mode convertibe engine system which transitions from shaft power for the VTOL mode to the turbofan mode for high speed forward flight. This was the first demonstration of such an engine, and is applicable to x-wing, folding tilt-rotor and other high speed rotorcraft concepts.

The fourth paper discussed results of transmission research for rotorcraft. Advanced transmission concepts (bearingless planetary and split torque) were discussed and technology needs identified for light-weight, quiet and reliable drive systems. Plans for future research in noise reduction, code development and advanced drive systems concepts were addressed.

The last paper presented the rotorcraft icing research program. The objective was to develop technology for all-weather rotorcraft designs. Research programs and recent accomplishments involving ice protection, and icing simulation for rotorcraft were summarized. Results of flight testing a pneumatic boot were reviewed to include handling qualities, hover icing, forward flight icing, and rain and sand erosion. Progress on electromagnetic magnetic impulse (EIDI) systems, which have potential for low weight, low power consumption, high reliability and efficient deicing, was highlighted.

TECHNOLOGY DEVELOPMENTS FOR A COMPOUND CYCLE ENGINE

G.A. Bobula
Propulsion Directorate
U.S. Army Aviation Research and Technology Activity - AVSCOM
Lewis Research Center
Cleveland, Ohio 44135

W.T. Wintucky
National Aeronautics and Space Administration
Lewis Research Center
Cleveland, Ohio 44135

and

J.G. Castor
Garrett Turbine Engine Company
Phoenix, Arizona 85010

SUMMARY

The Compound Cycle Engine (CCE) is a highly turbocharged, power compounded power plant which combines the lightweight pressure rise capability of a gas turbine with the high efficiency of a diesel. When optimized for a rotor-craft, the CCE will reduce fuel burned for a typical 2 hour (plus 30 min reserve) mission by 30 to 40 percent when compared to a conventional advanced technology gas turbine. The CCE can provide a 50 percent increase in range-payload product on this mission.

Results of recent activities in a program to establish the technology base for a Compound Cycle Engine are presented. The objective of this program is to research and develop those critical technologies which are necessary for the demonstration of a multicylinder diesel core in the early 1990's. A major accomplishment has been the initial screening and identification of a lubricant which has potential for meeting the material wear rate limits of the application.

An in-situ wear measurement system has also been developed to provide accurate, readily obtainable, real time measurements of ring and liner wear. Wear data, from early single cylinder engine tests, are presented to show correlation of the in-situ measurements and the system's utility in determining parametric wear trends.

The paper concludes with a plan to demonstrate a compound cycle engine by the mid 1990's.

INTRODUCTION

A program is being conducted to develop those technologies critical to demonstrating a 2000 hour mean time between overhauls, MTBO, high specific power, light weight compound cycle engine (CCE). Recent studies have shown that fuel is 70 percent of the tonnage shipped by the Army for supply and

E-3426

support under battlefield conditions. Another study (ref. 1), showed that a compound cycle engine, with its superior fuel efficiency, when installed in a Blackhawk helicopter and operated over a typical 2-hour mission, could have a specific weight as high as 0.76 pound per horsepower (lb/hp) and still be competitive with a gas turbine engine in terms of range-payload product. This result assumed the same take-off gross weight, and balanced the CCE's increased engine weight against its lower fuel consumed plus tankage weight.

This paper summarizes the activities and results to date under this technology development program. The major part of these activities is being conducted by the Garrett Turbine Engine Company, under the sponsorship of the U.S. Army Aviation Systems Command (AVSCOM). The efforts include an analytical feasibility study of a compound cycle engine for a light helicopter application; a lubricant and material research and development program; and a component technology development program. The paper will conclude with a long range plan to meet a 1990's multicylinder diesel core demonstration date.

BACKGROUND

A comparison of the performance of small to medium size shaft power engines (200 to 6000 hp), shows the potential for reduced fuel consumption with the incorporation of a diesel or compound cycle power plant (fig. 1.). The greatest fuel savings come from the use of a compound cycle, which is also the lighter of these two options.

The compound cycle engine, shown schematically in figure 2, combines the airflow capacity and light-weight pressure rise features of a gas turbine with the highly efficient, although heavier, diesel. The compressor of the turbomachinery module delivers a highly pressurized charge of air to the diesel cylinders. Within the cylinders, further compression, fuel injection, combustion, and expansion takes place, as in any conventional reciprocating engine, but at substantially higher pressures and temperatures. Power is extracted during the expansion stroke and the exhaust gases are then returned to the turbomachinery module. The exhaust energy available is in excess of what is required to drive the compressor, and that excess power is extracted in a free turbine and combined with the diesel output through a gear train. This combined output comprises the total cycle output, hence the name compound cycle engine.

As outlined in reference 2, the 1940's and early 1950's saw considerable interest in compound cycle engines being applied to aircraft. During the early 1950's, the most fuel efficient internal combustion engine ever flown, the Napier Nomad, demonstrated an SFC of less than 0.35 lb/hp-hr in flight (ref. 3). The engine used a highly turbocharged, power compounded cycle to reach this level of performance. It delivered 3050 hp output at a weight of 3580 lb. The advent of the gas turbine, however, coupled with the low cost of fuel at the time and the drive toward faster speeds, brought an end to the Nomad. This technology stagnated while gas turbines flourished in the 30-plus intervening years. As figure 3 indicates, the performance of small simple cycle gas turbines is now at a level where further improvement in specific fuel consumption is very difficult to achieve due to the high pressure ratios that would be required. In addition, to produce a smaller package than presently in production for a given power class of engine, would require higher

turbine-inlet temperatures than either materials, cooling, or manufacturing technologies are ready to deal with.

The Army/NASA Small Engine Technology program (ref. 4), indicated that performance increases of significant magnitude for the year 2000 turbomachine will require improved cycles incorporating the results of intensive research and development efforts in: (1) materials, i.e., ceramics for higher cycle temperatures, and (2) in component aerodynamic design for improved efficiencies. Efforts in other areas will provide payoffs of a smaller magnitude. The reduction in fuel burned predicted for the year 2000 rotorcraft application was dependent on all the key technologies reaching the applications phase (refs. 5 and 6).

Economic and logistic pressures have forced us to reconsider other, more efficient power plants such as the compound cycle. The already mentioned tonnage which the Army must supply and support under battlefield conditions, and the need for a deep penetration capability, are examples of the drivers toward better fuel efficiency. It is estimated that by adapting the Napier Nomad to a helicopter mission and incorporating modern technologies into its 35 year old design, this compound cycle engine could be made to run at an SFC in the range of 0.35 lb/hp-hr and weigh 0.6 lb/hp or less. The weight reduction would be accomplished by removing the reduction gearbox, which had been needed for a propeller drive, and deleting the variable-speed transmission, which had been needed for turbomachinery and diesel speed matching. Instead a free turbine stage would be used for power extraction and the number of turbomachinery stages reduced substantially from the original Nomad design. Modern materials and structural analysis techniques would also be employed

Until recently, few major advances have occurred in reciprocating engines. In 1977, however, a joint Defense Advanced Research Project Agency (DARPA), Air Force program, the Compound Cycle Turbofan Engine (CCTE) of reference 7 at Garrett, investigated a highly turbocharged, power compounded turbofan/diesel engine for a cruise missile application. Power densities greater than seven times that of the best current production diesels were demonstrated in a single cylinder rig. A mission redirection terminated that effort. However, that program formed the basis for the present activity.

COMPOUND CYCLE ENGINE PROGRAM

The goal of the compound cycle engine (CCE) program is a 30 to 40 percent reduction in mission fuel weight with a resultant 50 percent improvement in payload-range product for a light helicopter. The program objective is to demonstrate the low specific fuel consumption and low specific weight potential of a compound cycle turbine-diesel engine for a light helicopter application. The immediate activity is focused on those technologies which are critical to the demonstration of a high specific power, long life (2000 hr mean time between overhauls, MTBO), light weight multicylinder diesel core in the early 1990's. Toward this end, the Garrett Turbine Engine Company has been under contract since 1984 to perform a technology research and technology development program. The contracted activity includes a feasibility study to determine the merit of using a CCE in a dual, 1000 hp engine, light helicopter; lubricant and material research and development; and single cylinder component research.

Light Rotorcraft Feasibility Study

A thorough review of the feasibility study is presented in reference 2. Selected highlights of the results are presented here, to preface the technology development discussion.

The final engine design (fig. 4), is quite similar to a free turbine turboshaft engine, but with the combustor replaced by a power producing six cylinder diesel core operating on a uniflow scavenged, 2-stroke cycle. A two stage centrifugal compressor raises the charge air pressure to 10.6 atmospheres. This air then passes through an air-to-air aftercooler which lowers its temperature (increases density) prior to it being inducted into the cylinders through circumferential ports at the bottom of the piston stroke. The air is compressed to 1/7.5 times its original volume on the upward stroke of the piston and fuel is injected near top dead center, burned, and exhausted through valves in the head on the piston down (power) stroke. The engine exhaust gases then flow through the single-stage, radial-inflow gas generator turbine which drives the compressor. The exhaust then flows through the axial flow free power turbine which puts power back into the diesel crankshaft through gearing. A cutaway of a generic installation is shown in figure 4.

Table I provides a list of selected design point parameters for the CCE and for current production heavy duty diesels. The comparatively low weight of the CCE is achieved, to a large extent, by doing the majority of the cycle pressure rise through compression in the turbomachinery. The CCE's high power density results from a combination of the 2-stroke cycle, high engine speed, high cylinder pressures and small piston displacement.

The study indicated that substantial fuel savings and improvements in range-payload product are potentially available with the CCE. For a representative mission of 2 hours (plus 30 min reserve fuel) during which 80 percent of the time is spent at or below 50 percent power, the CCE propulsion system plus fuel and tankage weight equalled that of a gas turbine in less than one hour. Beyond this time the CCE system became progressively lighter than a gas turbine. This result arises from the lower specific fuel consumption of the CCE; 25 percent better than a current development gas turbine at design power, and improving to 36 percent better at 50 percent power, as shown in figure 5.

The study identified three critical technology development areas: piston ring/liner interface wear life; exhaust valve temperatures; and rapid fuel injection with high heat release combustion. Since the completion of the feasibility study and with identification of the critical technologies, program activity has concentrated on the major challenge to meeting the high power density 2000 hour MTBO goal. This challenge is the low piston ring/liner interface wear at high speed and power densities. The wear is investigated in the lubricant/material screening, and in the single cylinder engine testing. The following sections of this report discuss the screening and engine testing activities and progress to date.

Lubricant/Material Screening

The objectives of this effort are to: identify a lubricant that is compatible with the critical environment and requirements of the diesel and gas turbine engines; and identify potential diesel engine piston ring/cylinder liner material and lubricant combinations. Lubricants and materials are being screened on a modified Hohman friction and wear tester (fig. 6). Two rub blocks wear against a rotating shaft under simulated cylinder pressure, velocity and temperature conditions (P, V, T).

This activity began with the best tribological combination from the DARPA/Air Force program of reference 7 as a baseline. This combination was Koppers K-1008 (Cr_2C_3 -Moly) coated blocks (simulating a piston ring) rubbing on an N-135 (Nitr alloy) Nitrided shaft (simulation a cylinder liner), and lubricated with Stauffer STL + 10 percent TAP. The lubricant approach is to use gas turbine type of lubricant basestocks and modify them to meet diesel requirements. This activity is underway and will be followed by tests of potential piston ring/cylinder liner hard wear resistant material combinations with the most promising lubricant. The best lubricant to date has been Monsanto MCS-2189 (MIL-L-27502 type) which reduced the wear rate to 1/7 of baseline level, and the friction coefficient (0.016 avg.) and frictional temperature rise (205° F avg.) at 800° F to 60 percent of their baseline levels. Additives are also being tested with MCS-2189.

While the systematic approach used in screening lubricant and material combinations has provided promise of approaching the TBO goal, there is a need to extend the qualitative screening activity to a quantitative understanding of the dependence of wear on the cycle parameters of cylinder pressure and temperature and piston velocity, on the tribology of the system, and on the overall engine operation. Figure 7 depicts the interrelationship of in-cylinder operational parameters. Although the parameters are being varied, no attempt is being made to develop a correlation between the parameters.

Single Cylinder Engine Testing

The overall objective of the single cylinder engine testing is to demonstrate single cylinder diesel component life and performance in preparation for the multicylinder diesel core engine demonstrator program. This activity is presently concentrating on in-cylinder piston ring/liner wear and tribology. It began by using hardware from the DARPA-Air Force program in which the single cylinder engines had been run at more than seven times the power density of the best current production diesels, reaching 7.2 hp/cu.in. These engines, although loop scavenged, provided an early opportunity to concentrate on piston ring/liner wear while operating at the specific power levels of the CCE. It should be noted that during the single cylinder engine tests, power densities of nearly 5 hp/cu-in were consistently obtained in over 100 hours of testing.

The present program piston ring/liner wear activity has dealt mainly with the development of a method for making in-situ, real time measurements of wear. These measurements are obtained using a SPIRE-WEAR radionuclides measurement system (ref. 8), which has been developed to a point of relatively

good utility and accuracy. Data using this system were used to establish baseline wear rate measurements.

Figure 8 is a representation of how the radionuclide system works. Hardware, in this example a piston ring, is irradiated by exposing the wear surface to an accelerator particle beam. Careful control over the bombardment parameters results in a desirable distribution and level of activity in the surface of the ring. The ring is then subjected to wear in an engine under controlled conditions of P, V, T. The ring activity is measured through the top of the cylinder by a scintillation counter and is continuously recorded for computer analysis. The activity history is compared against the known radioactivity distribution, corrected to account for normal isotope decay, to provide a history of wear versus time. The wear rate of change is then correlated with the test P, V, T conditions. The discussion in reference 8 provides more detail on this method of wear measurement. Those items that required special attention for use in the single cylinder engine rig are mentioned below.

Development of the wear measurement system required identification of an appropriate material/isotope combination to provide a reasonable energy level and half life to accomplish wear rate test objectives. Location of the radiation detector for optimum data acquisition, and maintenance of a constant detector temperature were key to achieving consistent results. Software modifications included changing the energy integration technique to an area integration scheme over a wider bandwidth than originally proposed. This allowed faster, more accurate acquisition of data. As a result, the SPIRE-WEAR system and test setup was ready to be applied on the next test sequence which will utilize a uniflow scavenged engine, modified to operate as a single cylinder test rig.

Figure 9 shows representative ring wear data recorded over 15 nonconsecutive test hours of operation on the single cylinder, loop scavenged engine test rig. All the running was at a speed of 6000 rpm with a cylinder inlet temperature of 300° F, and with the baseline tribological combination. The data from the first 4 1/2 hours were recorded at an inappropriate sample rate and therefore reliable wear rate calculations were not possible. From 4 1/2 hours on, a more optimum sampling was used, and it can be seen that the wear rate (slope of the line) is quite repeatable for repetitions of the same power level: 0.6 $\mu\text{m/hr}$ at 40 IHP, 0.7 to 1 $\mu\text{m/hr}$ at 60 IHP, and 2.0 $\mu\text{m/hr}$ at 80 IHP. These wear rates when projected onto the composite helicopter mission profile, and allowing a 0.006 inch allowable radial ring wear, indicate a 200 hour TBO (time between overhauls) with the baseline materials and lubricant in a loop scavenged engine. Projecting the improvement of using Monsanto MCS-2189 into the uniflow scavenged single cylinder engine, a 1400 hour TBO life would be anticipated.

The set of data shown in figure 9 also provided one check on the accuracy of the measurement system. The calculated wear over 15 hours of operation was 22.7 μm , while the actual measured wear was 25 μm , indicating an overall difference of about 10 percent. The percentage difference was greater on some of the other tests. A nominal value of uncertainty has not yet been determined.

Figure 10 provides an indication of the capability afforded with the in-cylinder wear measurement. It represents over 20 data points recorded in

slightly less than 31 non-consecutive test hours with a single activated ring, run on one build of the engine. Using standard, intrusive types of measurements would have required at least twenty partial disassembly/assembly operations, introducing substantial doubt about the configuration repeatability. The wear data was acquired on the loop scavenged configuration, and is therefore not quite representative of the uniflow scavenged design. However, it does demonstrate that the radionuclides system provides the capability to perform the type of parametric studies of ring wear rate versus cycle parameters and cylinder tribology that were indicated by figure 7. As the uniflow scavenged single cylinder activity approaches the power levels of the CCE, actual configuration wear rate parametric relationships should begin to emerge.

COMPOUND CYCLE ENGINE PROGRAM PLAN

The CCE program plan is presented in figure 11. As shown, the component technology activities have been ongoing since late 1984, these being mainly the lubricant/wear (tribology) and single cylinder research under contract to the Garrett Turbine Engine Company. The immediate objective of these activities is to demonstrate that we know how to meet the 2000 hour MTBO goal. In addition, it is necessary to develop the critical technologies required for the demonstration of a high specific power, light-weight multicylinder diesel core in the early 1990's. The diesel core engine (gas generator) demonstration would lead into a full CCE demonstrator by the mid 90's. It is anticipated that the component technologies effort would continue through the entire program, with specific tasks changing as requirements arose. To meet the overall program timeframe, progress in the component technologies must continue

SUMMARY OF RESULTS

Studies have shown that a compound cycle turbine diesel engine is an advanced engine concept which has potentially high benefits for the Army light helicopter application. These benefits include a 30 to 40 percent reduction in fuel burned and a 50 percent increase in payload-range product for a dual-1000 hp engine helicopter on a 2 hour (plus 30 minute reserve fuel) mission.

Early tribological screening and single cylinder engine tests indicate that good progress is being made toward obtaining the 2000 hour MTBO life goal. It is expected that continued progress will be made in the development of improved lubricants such as Monsanto MCS 2189, with equal success in material optimization, in order to reach utility in time for use in the CCE program.

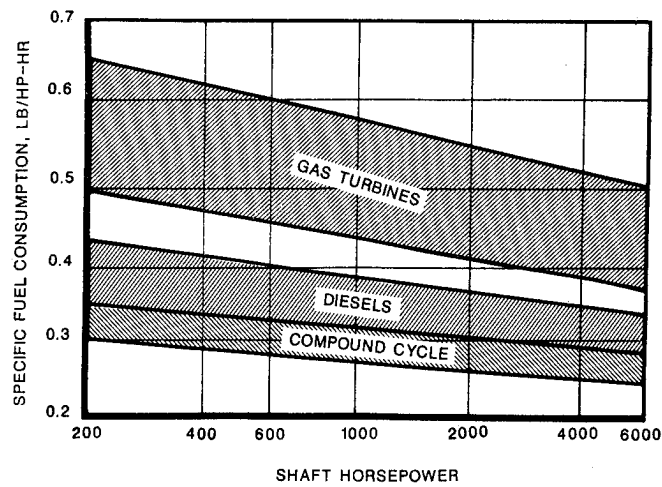
REFERENCES

1. Wilsted, H.D.: Preliminary Survey of Possible Use of the Compound Adiabatic Diesel Engine for Helicopters. SAE Paper 820432, 1982.
2. Castor, J.G.: Compound Cycle Engine for Helicopter Application. NASA CR-175110, 1986.

3. Sammons, H.; and Chatterton, E.: Napier Nomad Aircraft Diesel Engine. SAE Transactions, vol. 63, 1955, pp. 107-131.
4. Vanco, M.R.; Wintucky, W.T.; and Niedzwiecki, R.W.: An Overview of the Small Engine Component Technology (SECT) Studies. AIAA Paper 86-1542, June 1986.
5. Turk, M.; and Zeiner, P.: Advanced Technology Payoffs for Future Rotorcraft, Commuter Aircraft, Cruise Missile, and APU Propulsion Systems. AIAA Paper 86-1545, June 1986.
6. Larkin, T.R.; Staton, D.V.; and Mongie, H.C.: Rotorcraft Propulsion for Year 2000 Plus. AIAA Paper 86-1543, June 1986.
7. Castor, J.G.: Compound Cycle Turbofan Engine. AIAA Paper 83-1338, June 1983.
8. Blatchley, C.C.; and Sioshansi, P.: Surface Layer Activation Technique for Monitoring and In Situ Wear Measurement of Turbine Components. Journal of Propulsion and Power, vol. 2, no. 3, May-June 1986, pp. 248-252.

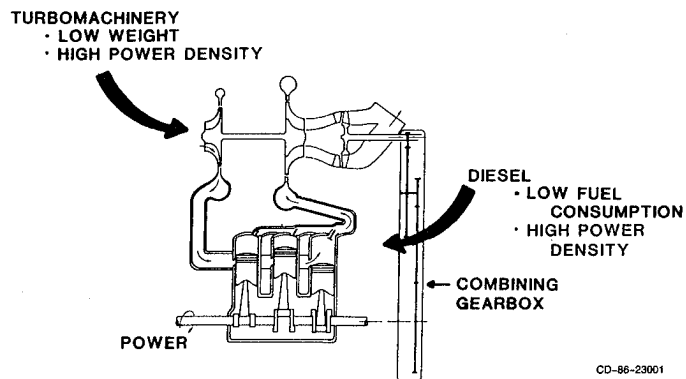
TABLE I. - COMPARISONS OF DESIGN PARAMETERS
FROM 1000 HP HELICOPTER ENGINE STUDY WITH
CURRENT DESIGN PRACTICE

Parameter	Target	Current design practice
P/P _{compressor}	10.6	2 - 3
Comp. ratio	7.5	14 - 17
Diesel speed	6000 rpm	1800 - 2500 rpm
Top ring reversal temperature	800 °F	<450 °F
Brake mean effective pressure	393 psi	150 - 250 psi
Mean piston speed	3000 fpm	<2000 fpm
lbm/hp	0.432	5 - 10
hp/in ³	5.7	0.5 - 1



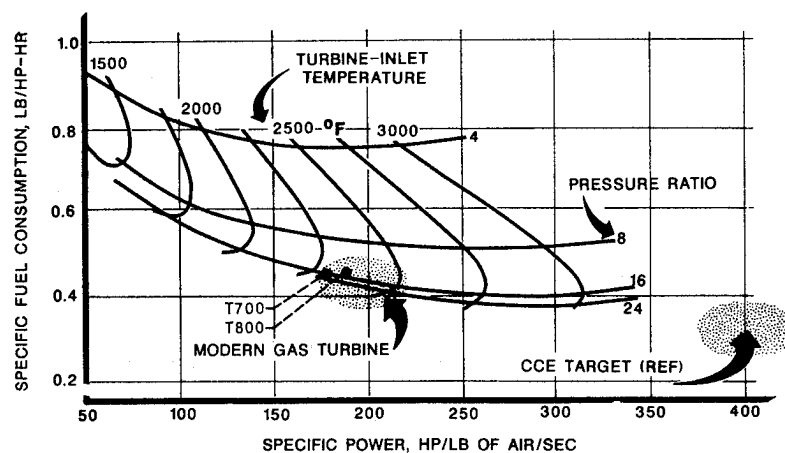
CD-86-20633

FIGURE 1. - GENERAL PERFORMANCE COMPARISON OF SHAFT-POWER ENGINES (200-6000 HP).



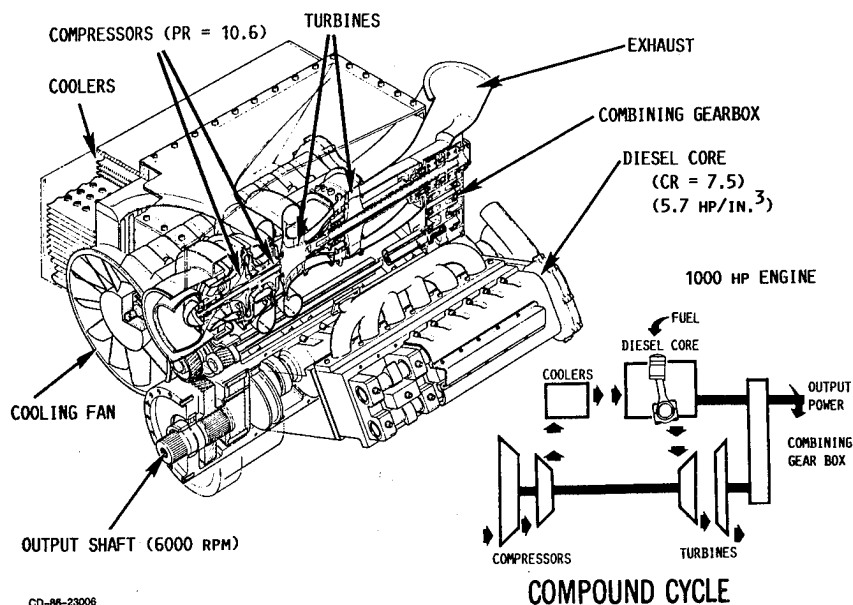
CD-86-23001

FIGURE 2. - SCHEMATIC OF A COMPOUND CYCLE ENGINE.



CD-86-23003

FIGURE 3. - GAS TURBINE ENGINE PERFORMANCE DEPENDANCE ON PRESSURE RATIO AND TURBINE-INLET TEMPERATURE.



CD-86-23006

FIGURE 4. - CONCEPTUAL CONFIGURATION OF 1000 HP COMPOUND CYCLE ENGINE.

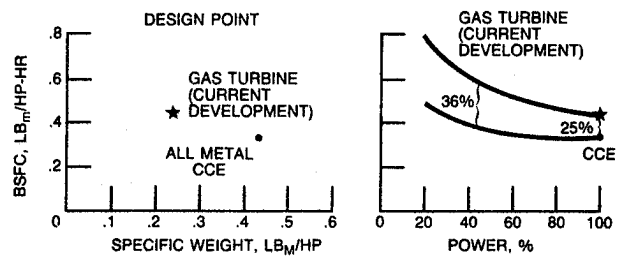
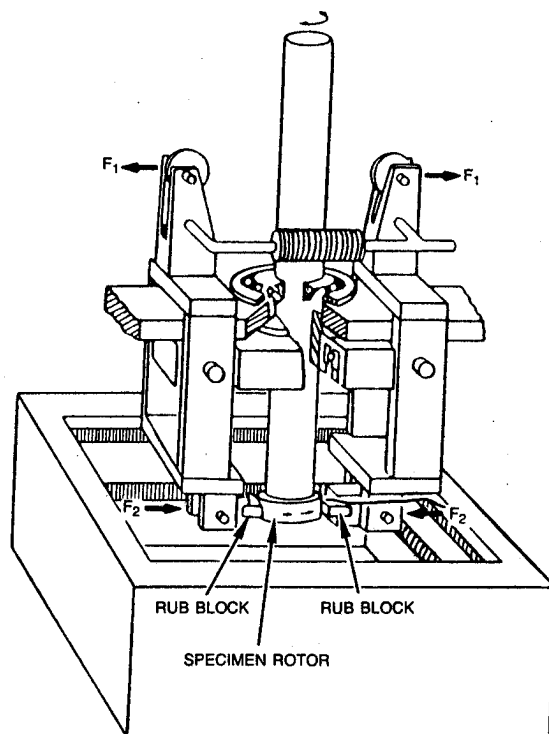


FIGURE 5. - CYCLE PERFORMANCE AND WEIGHT (INCLUDING FUEL AND TANKAGE) COMPARISONS FOR 1000 HP CCE AND GAS TURBINE.



CD-86-23007

FIGURE 6. - MODIFIED HOHMAN FRICTION AND WEAR TESTER.

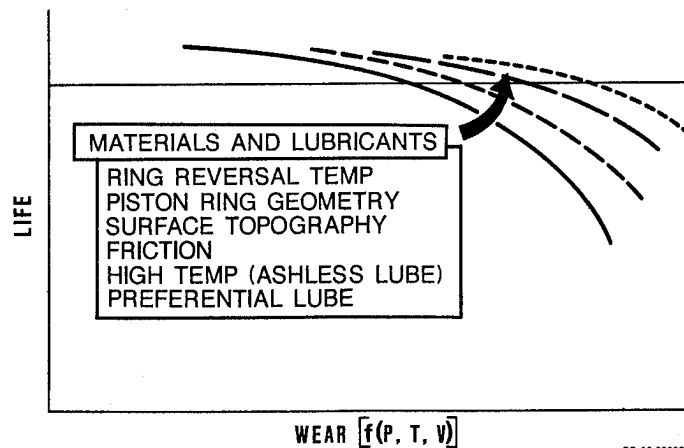


FIGURE 7. - REPRESENTATION OF THE DEPENDENCE OF ENGINE LIFE ON THE CYCLE PARAMETERS (CYLINDER PRESSURE AND TEMPERATURE, AND PISTON VELOCITY) AND TRIBOLOGY.

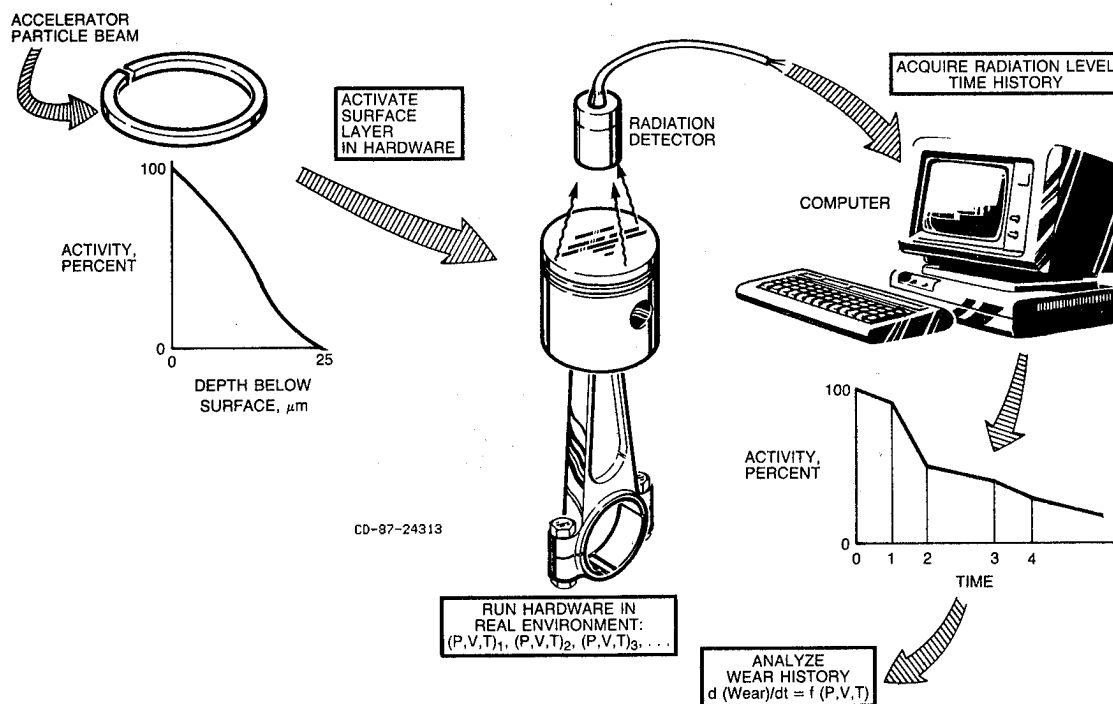


FIGURE 8. - USE OF RADIONUCLIDES DETECTION FOR IN-SITU MEASUREMENT OF COMPONENT WEAR.

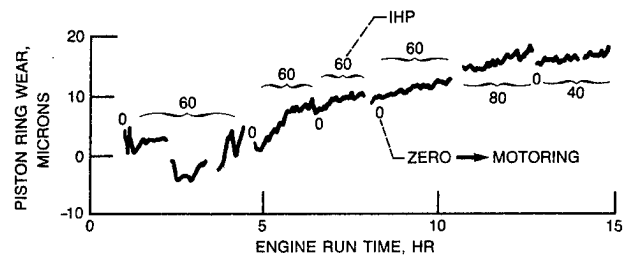


FIGURE 9. - REPRESENTATIVE IN-SITU RING WEAR DATA FROM SINGLE CYLINDER, LOOP SCAVENGED HARDWARE. ENGINE SPEED 6000 RPM, INLET TEMPERATURE 300 °F.

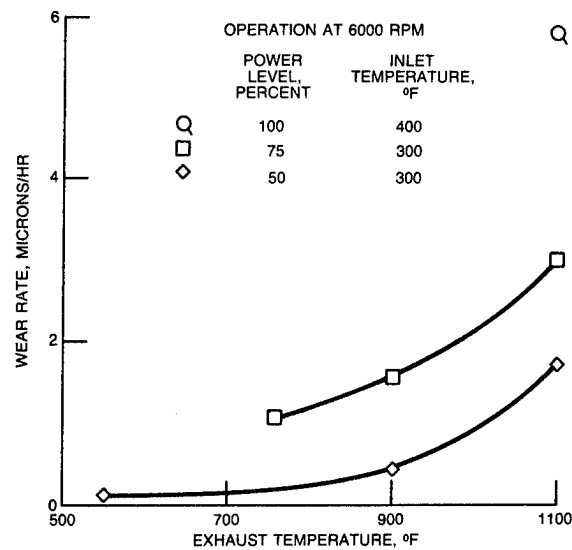


FIGURE 10. - VARIATION OF RING WEAR RATE WITH EXHAUST TEMPERATURE AND POWER LEVEL ON SINGLE CYLINDER, LOOP SCAVENGED HARDWARE. (KOPPERS K1008/K28 PISTON RING ON NITRIDED NITRALLOY LINER.)

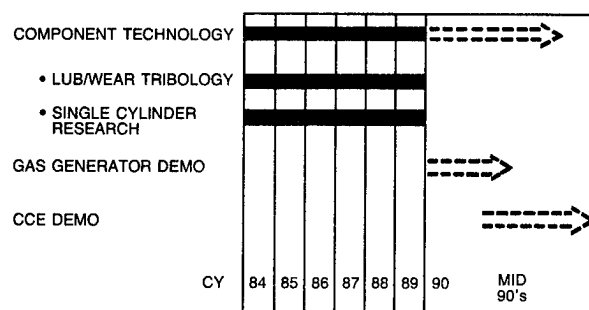


FIGURE 11. - COMPOUND CYCLE ENGINE PROGRAM SCHEDULE.

SMALL GAS TURBINE ENGINE TECHNOLOGY

Richard W. Niedzwiecki
National Aeronautics and Space Administration
Lewis Research Center
Cleveland, Ohio 44135

Peter L. Meitner
Propulsion Directorate
U.S. Army Aviation Research and Technology Activity - AVSCOM
Lewis Research Center
Cleveland, Ohio 44135

ABSTRACT

Performance of small gas turbine engines in the 250 to 1,000 horsepower size range is significantly lower than that of large engines. Engines of this size are typically used in rotorcraft, commutercraft, general aviation and cruise missile applications. Principal reasons for the lower efficiencies of smaller engines are well known: Component efficiencies are lower by as much as 8 to 10 percentage points because of size effects. Small engines are designed for lower cycle pressures and temperatures because of smaller blading and cooling limitations. The highly developed analytical and manufacturing techniques evolved for large engines are not directly transferrable to small engines. Thus, it has been recognized that a focused effort addressing technologies for small engines was needed and could significantly impact their performance. Recently, in-house and contract studies were undertaken at the NASA Lewis Research Center, under joint NASA/Army-AVSCOM sponsorship to identify advanced engine cycle and component requirements for substantial performance improvement of small gas turbines for projected year 2000 applications. This paper presents the results of both in-house research and contract studies, conducted with Allison, AVCO Lycoming, Garrett, Teledyne CAE and Williams International. Rotorcraft results are emphasized. In summary, projected fuel savings of 22-percent to 42-percent could be attained. Accompanying direct operating cost reductions of 11-percent to 17-percent, depending on fuel cost, were also estimated. High payoff technologies are identified for all engine applications, and recent results of experimental research to evolve the high payoff technologies are described.

INTRODUCTION

Small gas turbine engine performance in the 250 to 1,000 horsepower size class is significantly lower than that of large engines. The major reasons for this are generally well known and consist of lower component efficiencies, poorer cycle efficiencies due to lower operating pressures and turbine inlet temperatures, and the difficulty of transferring large engine derived improvements to small engine sizes. The purpose of this paper is to define those

technologies required to significantly improve small engine performance by the year 2000, emphasizing rotorcraft applications. Source materials for defining these technologies were obtained from NASA Lewis Research Center in-house research and contract studies conducted under the Small Engine Technology (SECT) Program under joint NASA/Army-AVSCOM sponsorship.

Small turbine engines are used in a broad spectrum of aeronautical applications including rotorcraft, commuters, general aviation and cruise missiles. Rotorcraft are used extensively by the military to rapidly deploy troops and supplies in ground battles and perform attack, scout, search and rescue missions. Civil helicopter uses include commuters, traffic/police observation, off-shore oil rig transport, airborne rescue and ambulance, agricultural, and other utilitarian roles. These applications require 350 - 1500 SHP turboshaft powerplants.

Turboprop commuters serve to efficiently transport small groups of people over short distances. They frequently interconnect with long-range commercial air transport carriers and thus provide an essential link in our national air transportation system. Commuter engines generally range from about 800 SHP upwards to about 2000 SHP.

General aviation aircraft provide a variety of public services: Flying people and freight; surveying and mapping natural resources; seeding and treating crops; patrolling pipelines, forests and fisheries; mineral prospecting; rescue and ambulance services; flight training and other such business and commercial purposes. These fixed-wing airplanes employ piston and turboprop engines in the 150 to 1000 SHP class.

Cruise missiles deliver a military warhead to a target at supersonic/subsonic speeds over a range of less than a hundred to several thousand miles, depending on the mission. These generally use a single turbofan/turbojet engine in the 200 - 1000 lb thrust class.

These broad ranges of applications and mission requirements lead to a variety of technology needs. However, there is considerable commonality in terms of needs between the various applications: These are:

1. Expanded vehicle capability in terms of range, speed and/or payload.
2. Reduced costs, both initial and operational.
3. Increased logistic flexibility relating to reduced demands for logistic support such as consumables.
4. Improved survivability, primarily a military concern.

Approaches for satisfying these technology needs are described in this paper, with special emphasis on rotorcraft applications.

MULTIPLE MISSION NEEDS

As shown in Figure 1, small turbine engines are used in a broad spectrum of aeronautical applications including rotorcraft, commuters, general aviation and cruise missiles. The broad range of applications and mission requirements has led to a variety of technology needs. However, there is considerable commonality between the various applications. These mission needs are summarized in the following table:

MULTIPLE MISSION NEEDS

<u>ROTORCRAFT</u>	<u>COMMUTER AIRCRAFT</u>
<ul style="list-style-type: none">° EXPAND VEHICLE CAPABILITY° INCREASE LOGISTIC FLEXIBILITY° REDUCE OPERATING COST° IMPROVE SURVIVABILITY	<ul style="list-style-type: none">° EXPAND VEHICLE CAPABILITY° REDUCE OPERATING COST
<u>GENERAL AVIATION</u>	<u>CRUISE MISSILES</u>
<ul style="list-style-type: none">° EXPAND VEHICLE CAPABILITY° REDUCE INITIAL AND OPERATING COSTS	<ul style="list-style-type: none">° EXPAND VEHICLE CAPABILITY° IMPROVE SURVIVABILITY

Expanded Vehicle Capability:

This refers to an extension of vehicle operating limits in terms of range, speed and/or payload. An improvement in the propulsion system can be used to maximize any one of these parameters depending on mission requirements. An important feature of rotorcraft propulsion systems, unlike the other propulsion systems, is that they are required to operate at power levels near 50-percent of rated power for as much as 75-percent of the time for typical missions. Thus, for these systems, it is of major importance that the efficiency at part power be significantly increased to realize large reductions in fuel burned and, therefore, increased range and/or payload. Accomplishing this will depend to a large extent on the application of variable geometry in small size turbomachinery, particularly in the power turbine. Present practice is to minimize the amount of variable geometry required in the compression system by limiting the cycle pressure ratio, and to provide no variability within the turbine. This is a result of trying to keep cost and complexity to a minimum. Highly advanced small turbine engines will require novel and innovative concepts that minimize the cost and complexity of variable geometry if full benefit is to be achieved in the advanced cycles.

Reduced Cost:

This includes both initial and operating cost. While all users are interested in reduced costs, generally system users with high utilization rates tend to be more concerned with operating costs as opposed to users with low utilization rates, who are more concerned about initial cost. Users with high utilization rates may be more willing to absorb higher initial costs with the potential of reduced operating costs.

Increased Logistic Flexibility:

This relates to a reduced demand for logistic support, such as reduced consumables. This is of special significance to military missions. Presented below is a battlefield scenario which reflects on the impact that a 50-percent fuel savings can have on reducing the amount of tonnage shipped across the battlefield and its effect on mission capability and flexibility.

IMPACT OF FUEL ON MILITARY MISSION FLEXIBILITY -FROM BATTLEFIELD SCENARIOS-

- ° FUEL IS 70% OF TONNAGE SHIPPED
 - ° ARMOR/MECH/INF DIVISIONS
 - AVIATION: 100,000 GAL/DAY PER DIV
 - GROUND: 50,000 GAL/DAY PER DIV
 - FOR 15,000 MAN DIVISION, 10 GAL/DAY/MAN PER DIV
- ° AIR ASSAULT DIVISION
 - AVIATION: 320,000 GAL/DAY PER DIV
 - GROUND: 20,000 GAL/DAY PER DIV
- FOR 15,000 MAN DIVISION, 22 GAL/DAY/MAN PER DIV

- ° A 50% SAVINGS IN AVIATION FUEL CAN SIGNIFICANTLY REDUCE TOTAL TONNAGE SHIPPED, THUS INCREASING MISSION CAPABILITY AND FLEXIBILITY.

Improved Survivability:

This is primarily a military concern, although increased safety of operation is always sought for civil aircraft.

Needs, Goals and Approach:

The mission needs identified above can be translated into the goals contained in the following table:

<u>NEEDS</u>	<u>GOALS</u>	<u>APPROACH</u>
° EXPAND VEHICLE CAPABILITY	° DECREASE SFC	° ADVANCED CYCLES
° REDUCE OPERATING COST	° IMPROVE RELIABILITY AND DURABILITY	
° INCREASE LOGISTIC FLEXIBILITY	° SIMPLER, FEWER PARTS	° ADVANCED COMPONENTS (IFM)
° REDUCE INITIAL COST	° SPECIAL CONSIDERATIONS	
° IMPROVE SURVIVABILITY		° ADVANCED MATERIALS

Reduced fuel consumption can directly benefit the first three needs: Vehicle capability, operating costs, and logistic flexibility. Reliability and durability improvements can reduce operating costs, while simpler, fewer parts can cut both initial and operating costs. Special considerations refer to military survivability.

The approach column identifies the major thrusts to be addressed to achieve overall goals - efficient engines. These are further illustrated in Figure 2 as technology opportunities. Advanced cycles offer the potential of large reductions in specific fuel consumption (SFC). This will be further illustrated below. Enhanced computational tools development, verification and application to advanced concepts are required to provide highly advanced, efficient, durable components. Advanced materials such as ceramics and composites are required to achieve the maximum performance and life from the advanced engine concepts.

EFFICIENT ENGINE CYCLES

Small vs. Large:

Previous investments in technology programs by government and industry have led to significant efficiency gains for large engines. These gains have resulted from improved cycles, components and materials. However, much of these technologies have not been transferrable to smaller engines. As engine power size decreases, performance decreases due to the combined effects of increased relative clearances, lower Reynolds number, increased relative surface roughness, etc. The result of these adverse effects, illustrated in Figure 3, are particularly noticeable below 2000 SHP where the benefits of high cycle pressure ratio are unobtainable for small engines due to the severity of adverse scaling penalties. Small engines employ different component configurations such as centrifugal compressors, reverse flow combustors, and radial turbines to minimize these effects.

In the future, problems associated with size effects will no longer be limited to small engines. Future large turbofan engines designed for high bypass ratios and higher cycle pressure ratios (greater than 50:1) will be limited

in performance by some of the same size related problems which presently limit the performance of small engines. This is the result of the inherent reduction in core engine flow size associated with the higher bypass ratio and the higher core pressure ratio, all of which reduces the turbomachinery size and the combustor length and volume. To counter the losses associated with the small turbomachinery blading, such things as replacing the back stages of the typically all axial compressors with a centrifugal stage are now being considered, following the same trends as for small engines.

State-of-the-Art Cycle Performance:

Figure 4 presents one example of the performance of a state-of-the-art 800 SHP uninstalled, simple-cycle gas turbine. It is used as a reference for comparison to advanced cycles. A turbine inlet temperature of 2200°F and a pressure ratio of 14:1 were assumed as being representative. In addition, correct state-of-the-art component efficiencies and combustor/turbine cooling requirements were assumed. The Brake Specific Fuel Consumption (BSFC) for these operating conditions is approximately 0.43 lbs/shp-hr and the specific power is approximately 180 SHP/lb/sec.

Advanced Simple Cycle:

Figure 5 presents the performance of an advanced simple cycle in comparison to the state-of-the-art simple cycle. For the advanced simple cycle, advanced component efficiencies were assumed, along with higher operating pressures to 24:1, higher temperature to 2600°F, and uncooled ceramic hot section components. The advanced simple cycle BSFC of 0.36 lb/hp-hr is 17-percent less than the state-of-the-art engine, and its specific power is 55-percent higher. Of the 17-percent BSFC improvement, 8-percent is attributable to advanced component efficiencies, 4-percent is due to the higher cycle pressure, temperature and reduced coolant penalty, and 5-percent is a result of entirely eliminating the coolant penalty by using uncooled ceramics.

Regenerative Cycle:

Figure 6 presents the performance of an advanced regenerative cycle in comparison to the state-of-the-art simple cycle and the advanced simple cycle. Again, advanced component efficiencies were assumed, along with the high turbine inlet temperature of 2600°F, and uncooled ceramics. In terms of BSFC, the advanced regenerated cycle provides the potential for a very significant 37-percent reduction over the state-of-the-art engine, along with some increases in specific power. In addition, the optimum cycle pressure ratio for the regenerated cycle is much lower than that for the advanced simple cycle, thus resulting in fewer compression states. Regenerative cycles could utilize either a rotary regenerator in a stationary recuperator.

While these potential performance gains are quite large, they must be examined in a representative mission model, taking into consideration projected changes in engine size, weight, cost and other factors before the real benefits of advanced cycles can be assessed. Because of the diversity of small engine applications, representative missions for each application must be individually examined. A typical rotorcraft application is shown in Figure 7. As can be

seen, advanced technology could deliver a potential fuel savings of 30 to 55-percent compared to today's state-of-the-art- technology. The reduction in fuel requirements would result in a 12-percent decrease in airframe weight for a new airframe and could lead to a 21-percent to 25-percent decrease in Direct Operating Cost (DOC), depending on the assumed acquisition and maintenance costs for an advanced new regenerative engine.

Using similar calculations for missions other than rotorcraft, the potential payoffs contained below were calculated:

PAYOFFS

ROTORCRAFT

- 50% FUEL SAVED
- 20% LESS DOC

COMMUTERS

- 35% FUEL SAVED
12-15% LESS DOC

ADVANCED ENGINES

GENERAL AVIATION

20-40% FUEL SAVED
0-15% LESS DOC

CRUISE MISSILES

60% RANGE INCREASE

The mission analyses conducted for the various applications focused on fuel savings and resulting economic benefits. On this basis, fuel savings would be at least 20-percent for advanced simple cycles and as much as 55-percent for advanced regenerative cycles for rotorcraft, assuming a "rubber" aircraft sized to accomplish a fixed mission. However, the higher performance of the advanced engines could alternatively be exploited to expand the range or payload capability of fixed gross weight aircraft.

To achieve these payoffs, the technology challenges listed below would have to be successfully met.

TECHNOLOGY CHALLENGES

SIMPLE CYCLES

- ° IMPROVE TURBOMACHINERY PERFORMANCE SIGNIFICANTLY
- ° ELIMINATE COOLING PENALTY AT HIGH CYCLE TEMP. AND PRESSURE
- ° IMPROVE RELIABILITIES AND COST

REGENERATIVE CYCLES

- ° REDUCE HEAT EXCHANGER WEIGHT, SIZE, AND COST PENALTIES
- ° ESTABLISH HIGH EFFICIENCY/RELIABILITY VARIABLE AREA POWER TURBINE TECHNOLOGY
- ° IDENTIFY USEFUL MULTI-PURPOSE ENGINE

To achieve approximately 20-percent fuel savings and approximately a 10-percent DOC reduction with simple cycles requires: Significant turbomachinery performance improvements; establishing approximately 2600°F uncooled hot section technology; and novel design/manufacturing approaches to improve the economics and reliability without significantly sacrificing performance potential.

Regenerative and recuperative cycles provide the potential for doubling the preceeding fuel and DOC payoffs. However, major reductions in heat exchanger weight, size, and cost penalties are required. Technology for highly efficient, yet reliable variable area power-turbines is also necessary for rotorcraft applications. The DOC and fuel savings gains cited above are merely potential until applied to specific missions. This is done in the next section.

Application of Efficient Engine Technologies to Specific Missions:

Contract studies aimed at identifying high payoff technologies for year 2000 small gas turbine applications were conducted under the Small Engine Component Technology (SECT) Program under joint NASA/Army-AVSCOM sponsorship. A list of contractors and the applications studied follows:

SMALL ENGINE COMPONENT TECHNOLOGY (SECT) STUDIES CONTRACTOR SELECTED APPLICATIONS

CONTRACTOR	ROTORCRAFT 500-1,000 HP	GENERAL AVIATION/ COMMUTER 500-1,000 HP	APU 300-500 HP	CRUISE MISSILE 200-1,000 LB T
ALLISON	X			
AVCO LYCOMING		X		
GARRETT	X	X	X	X
TELEDYNE CAE				X
WILLIAMS INTERNAT'L				X

Details describing the studies, conditions imposed, procedures, etc. are contained in references 1 through 6. Guidelines are essentially the same as those described previously; i.e. year 2000 technology, etc. The discussion below will focus on the rotorcraft missions studied.

Allison:

Allison selected for study the eight passenger tilt rotor executive/commercial aircraft shown in Figure 8. The mission for the twin turboshaft powered tilt rotor aircraft is 350 nautical miles with a cruise speed of 250 knots at an altitude of 20,000 feet. The reference current technology engine has a turbine rotor inlet temperature of 2200°F, a pressure ratio of 14:1 and 1,000 SHP at take-off. The advanced cycles studies and the optimum cycle parameters for each advanced cycle considered follow:

	Concentric	Non-Concentric	Recup.	Regen.	Wave Rotor
Pressure Ratio	25	30	14	10	38
TRIT, °F	2800	2800	2800	2800	2800
Effectiveness P/P			.6 .10	.7 .13	
LP Compressor	Axial	Axi-Centrif.	-	-	Axial/ Centrif.
HP Compressor	Centrif.	Centrif.	Axial/ Centrif.	Axial/ Centrif.	Wave Rotor
HP Turbine	Radial	Radial	Axial	Axial	Wave Rotor
LP Turbine	Axial	Radial	-	-	Axial
Power Turbine	Axial	Axial	Axial	Axial	Axial

Turbine inlet temperatures of 2200° to 2800°F were studied. Uncooled turbines were assumed. The 2800°F temperature was selected on the basis of hot spot temperature capability of ceramic composite material and projected year 2000 combustor pattern factors of less than 0.2. Regenerator and recuperator effectiveness values of 0.6 to 0.8 and pressure drops of 6-percent to 14-percent were used.

During preliminary analysis of the five configurations, two designs were eliminated: The wave rotor cycle because of a lack of analytical capability to evaluate the cycle; and the simple concentric cycle because analysis indicated that the bore stresses in the ceramic HP turbine were prohibitive.

The remaining advanced engine concepts were installed (analytically) in the tilt rotor aircraft and flown over the reference mission. Reductions in fuel burned were 30.5-percent for the regenerative; 30.7-percent for the recuperative; and 16.5-percent for the non-concentric engines. DOC reductions achieved are shown in Figure 9. All configurations achieved the program goal of 10-percent DOC reduction. However, the non-concentric engine produced the greatest reduction and was selected for further study.

The general arrangement of the non-concentric engine is shown in Figure 10. The configuration incorporates the following: Turbine rotor inlet temperature of 2800°F, pressure ratio of 30, axial/centrifugal high pressure compressor, radial high pressure turbine, radial low pressure turbine, and an axial power turbine. Required advanced technologies for bringing this concept to fruition are ceramic/ceramic composites for the combustor and turbine; highly efficient components and three-dimensional codes; and advanced bearings for reliability and durability. Assuming \$1/gal fuel cost, advanced ceramic/ceramic composites provide 58-percent of the DOC reduction, with advanced aerodynamics providing approximately 40-percent.

Garrett:

The utility helicopter shown in Figure 11 was selected for the military/civil mission shown in Figure 12. The mission consists of five segments with four hover periods and total mission length of 130.4 nautical miles. The reference current state-of-the-art engine has a turbine inlet temperature of 2100°F, a pressure ratio of 13.5, and produces 1,000 HP at take-off. An advanced simple cycle and a recuperated cycle were studied. A summary of their characteristics follows:

	<u>Advanced Simple Cycle</u>	<u>Recuperated Cycle</u>
TRIT	2600°F	2600°F
Pressure Ratio	22.1	10:1
Compressor	2-Stage Centrifugal	1-Stage Centrifugal
HP Turbine	Axial, Uncooled	Axial, Uncooled
LP Turbine	Axial, Uncooled	Axial, Variable Geometry, Uncooled
Recuperator Effectiveness	-	.8

Selection of 2600°F temperature was based on hot spot temperature capability of ceramic/ceramic composite material and year 2000 combustor pattern factors of less than 0.2. Regenerator and recuperator effectiveness values of 0.6 to 0.8 and pressure drops of 6 to 14-percent were investigated.

Analysis results, based on DOC and fuel burned, are contained in Figure 13. Reduction in fuel burned is 21.9-percent for the simple cycle and 41.6-percent for the recuperated cycle, compared to the reference engine. At \$1/gal fuel cost, both cycles produce approximately 7-percent reduction in DOC. Recuperator weight and cost offset the additional reduction in fuel burned of the recuperated cycle. However, at \$2/gal, the recuperated cycle has 11.4-percent reduction in DOC - 2.7-percent more than the simple cycle. The increased fuel cost more than offsets the recuperator weight and cost.

Required technologies for bringing these concepts to fruition are primarily: Advanced materials - Ceramic/ceramic composites and Ni₃Al disk; advanced aerodynamics; and system technologies - metal matrix shafts, bearings, and seals.

Technology Rankings:

SECT contractor technology rankings for all of the missions studied are summarized:

CONTRACTOR TECHNOLOGY RANKINGS BASED ON DOC OR LCC

	ROTORCRAFT/COMMUTER						CRUISE MISSILE	
	ALLISON		AVCO LYCOMING		GARRETT		TELE- DYNE	WILLIAMS
	\$1/GAL	\$2/GAL	\$1/GAL	\$2/GAL	\$1/GAL	\$2/GAL		
MATERIALS								
CERAMICS	58%	57%	65%	55%	45%	40%	31%	23%
ADVANCED METALLIC DISK					20%	3%		
ADVANCED AERO- DYNAMICS	40%	42%	29%	25%	30%	34%	22%	24%
3-D CODES AND COMPONENTS								
TURBINE	17%	18%	11%	10%	17%	17%	15%	12%
COMPRESSOR	14%	15%	18%	15%	10%	14%	7%	12%
COMBUSTOR	9%	9%			3%	3%		
RECUPERATOR			6%	20%		22%		
SYSTEMS TECH- NOLOGIES								
BEARINGS	°	°			°	°	°	45%
SHAFTS					°	°	°	
SEALS					°	°	°	
GEARBOX							40%	
SLURRY FUEL COMBUSTOR							°°	°°

- ° NECESSARY TO ACHIEVE GAINS FROM MATERIALS AND AERODYNAMICS
- °° CRUISE MISSILE RANGE BENEFIT

The technologies are ranked on cost benefit based on direct operating cost or life cycle costs. Ranking the technologies by fuel savings instead, would lead to somewhat different conclusions.

For the rotorcraft/commuter applications, materials and advanced aerodynamics provide significant cost benefit irrespective of the fuel cost. The recuperator, however, pays off at \$2/gal for the cycles selected. The system technologies, while not displaying cost benefits, are necessary to achieve the gains from the advanced materials and aerodynamics.

For subsonic strategic cruise missile applications, the high payoff technologies in order of priority are reversed. System technologies provide approximately 40-percent of the cost benefits; advanced materials provide 23 to 31-percent; and advanced aerodynamics provide approximately 23-percent.

SMALL GAS TURBINE TRENDS AND CURRENT RESEARCH ACTIVITIES

Recent trends in small gas turbine design and performance are described in this section. Also described are research activities aimed at improving the efficiency of engine components.

Compressors:

Compressor design trends during the last 5 to 10 years have been towards increasing blade speed and aerodynamic blade loading to reduce the number of stages and to increase the overall compression system pressure ratio; implementing tailored blade shapes for axial machines; and evolving highly swept-back, high tip-speed centrifugal blade designs. The highly swept-back designs have demonstrated higher efficiencies and increased stall margin at peak efficiency point operation. These performance improvements have been achieved through the evolution and extensive use of advanced aerodynamic and structural codes. State-of-the-art efficiencies of current compressors are shown in Figure 14. This figure also shows the fall-off in efficiency with size. The NASA/Army advanced compressor technology goal is also shown on the figure.

Major thrusts of the current NASA/Army-AVSCOM compressor research program are shown in Figure 15. They include higher pressure ratios, increased efficiency and reduced number of stages. A recent major accomplishment was to quantify factors degrading the performance of centrifugal compressors as flow size is reduced. In the near future, the detailed flow measurements within the centrifugal blading will be obtained for use in developing and validating 3-D inviscid and viscous codes. These codes will then be available for designing compressors which minimize the losses associated with flow size.

The program to quantify the degradation in performance as flow size is reduced is depicted in Figure 16. As shown, a 25 lb/sec centrifugal compressor, described in references 7 and 8, was directly scaled-down to a 10 lb/sec size. The design was also scaled-down to a 2 lb/sec compressor. However, in scaling to the 2 lb/sec size, the blade thickness had to be increased in order to maintain a structurally sound design. Thus, to maintain a link to the original compressor, the 2 lb/sec compressor was then directly scaled-up to a 10 lb/sec size, incorporating the thicker blades. The three compressors were then experimentally evaluated. Impellers with two relative blade surface roughnesses were also evaluated for the 2 lb/sec size.

Results are summarized in Figure 17. Defined are effects resulting from Reynolds Number, shroud thickness, blade thickness, tip clearance and surface finish. For reference purposes, the design Reynolds Number for each compressor is indicated along the abscissa.

The data presented in Figure 17(a) reflect that for the directly scaled 2 and 10 lb/sec compressors, essentially the same efficiencies were achieved when operated at the same Reynolds Number. In fact, when factoring in the impact of different relative shroud thicknesses between the two machines, the efficiencies are identical. The effect of shroud thickness is reflected in Figure 17(e) for the 10 lb/sec thin-bladed configuration. Shroud thickness affects the amount of interheating which occurs within the compression process, which is inherently inefficient. Thus, this data indicates that the scaling laws hold for directly scaled machines operated at the same Reynolds Number. The problem is that the Reynolds Number changes with changes in characteristic length such as blade chord; and seldom can the relative surface finish, tip clearance, blade thickness and even shroud thickness be maintained as flow size is reduced. The impact of these parameters on performance is reflected in Figures 17(b) to 17(e), respectively.

Further analysis of the data is currently in process, and reports are being written. In addition to quantifying the scaling effects, the experimental data will provide a basis for validating advanced mathematical codes. These codes will then be used to minimize these losses. It is also assumed that advanced manufacturing technology will minimize the adjustments now required when scaling down to the smaller sizes.

Turbines:

The current performance of small turbines and future goals are shown in figure 18. The turbines are separated into gas generator and power turbines due to their contrasting characteristics. Gas generator turbines are smaller, operate at high temperature and pressure, develop high work per stage, are unshrouded and usually cooled. Power turbines are larger, uncooled, shrouded, and develop less work per stage. The current technology is indicated by dashed curves and include only axial machines, the current in-service type. The solid curve, figure 18(b), represents the goal for future axial power turbines. Axial machines are expected to remain the preferred type because of ease of packaging behind the gas generator turbine. The goal for gas generator turbines, figure 18(a), is represented by a rather broad band and includes both radial and axial machines. The bottom part of the band represents the goal for axial turbines and the upper part the near term performance of radial turbines. The chief obstacles to the use of radial turbines in rotorcraft engines is not their performance level, but rather developing the technology to make them compact, lightweight, and able to operate at much higher temperatures. To accomplish this requires improved high-temperature alloys, cooled radial rotors and, ultimately, ceramic rotors.

Current turbine aerodynamic design methods consist largely of the use of two and three-dimensional inviscid computer codes with empirically determined loss correlations based on stage loading, blading aerodynamic parameters, and

endwall effects. Heat transfer calculations are generally made with two-dimensional boundary layer codes based primarily on flat plate data and empirical correlations. This design approach has provided efficient aerodynamic blade shapes for many large turbines that perform as predicted. However, many advanced designs and small low-aspect ratio turbines have highly three-dimensional blade shapes with strong secondary flows. These flows cannot be predicted accurately with current computer codes and consequently increased aerodynamic losses and inaccurate heat transfer calculations result. At present, there are uncertainties as high as 35/25-percent in gas-side and coolant-side heat transfer coefficients, respectively. This, in turn, can result in life prediction uncertainty factors greater than ten.

Recently, radial turbines have been given renewed emphasis for small engine applications due to several inherent advantages they possess over axial turbines. Among these are: Improved packaging when mated with reverse flow combustors; higher work extraction per stage; greater aerodynamic efficiency; less sensitivity to tip-clearances; and increased ruggedness. Technology challenges for radial turbines are also formidable, and include: Higher rotor inertia; less understanding of the rotor flow-field; and an almost total absence of existing rotor cooling technology, including cooled rotor fabrication techniques.

Major thrusts of the NASA/Army-AVSCOM turbine research program are contained in Figure 19. Both axial and radial turbines are being studied: Major emphasis, however, is being placed on radial turbine research. Emphasis is also placed on high temperature operation. Highly efficient engine cycles require that the turbine operate efficiently up to 2800°F average temperatures with minimal coolant. Achieving these capabilities will come largely from: Application of high temperature materials, especially composites and ceramics; a more thorough understanding of fluid behavior in turbine passages, and the concomitant ability to predict this behavior; rigorous computer codes for hot gas convective coefficient prediction arrived at through fundamental experiments; and experiments in near-engine environments to validate the advanced technology.

An example of turbine research currently underway is the aero and structural design of an advanced mixed-flow ceramic turbine. The mixed-flow configuration allows blading to be used, which increases the aerodynamic efficiency, while maintaining radial blade elements, thus eliminating blade bending stresses. A new, advanced structural analysis code was developed and used to predict fast fracture failure probability of the monolithic ceramic rotor. To date, the aerodynamic and structural analyses of the rotor are complete and indicate high efficiency and a probability of survival of 0.985. The turbine is shown in Figure 20. Future work will focus on verifying the design results.

Other turbine research activities in progress or recently completed include: An experimental program to determine the performance of variable geometry radial turbines; small axial turbine scaling studies; performance and code verification for high-work, high-temperature radial turbines; and a comprehensive investigation of the performance and heat transfer of a cooled radial rotor.

Combustors:

Major combustion concerns of the 1970's and early 1980's aimed at gaseous emissions control and usage of alternative fuels have abated considerably by the mid-1980's. However, many combustion problems remain, especially for small combustors operating at aggressive, fuel-efficient cycles. Problems areas are summarized in Figure 21. An especially serious problem is liner cooling and durability. Small combustor liners require proportionately more coolant due to their increased surface to volume ratios, compared to large combustors. State-of-the-art small combustors, for example, can require up to 30-percent of the combustor airflow for cooling. At advanced cycle conditions of increased temperature and pressure, heat loads to the liners will increase, coolant temperatures will also increase and the amount of coolant available will decrease. More air will be required for combustion and mixing. Recuperative/regenerative cycles impose their own unique combustion problems in that coolant air temperatures are further increased. Another significant size related combustion problem is fuel injection, due to proportionately smaller passages which are subject to clogging. Current trends are to replace pressure atomizing nozzles with air blast designs. These contain larger passages but impose additional problems of poorer spray quality at low power and off-design conditions.

Major thrusts of the NASA/Army-AVSCOM combustion research program are contained in Figure 22. The overall objective of evolving the combustor technology required for advanced, fuel-efficient cycle operation can be realized by: Increasing the temperature and pressure operating capability of the combustor, including achieving higher temperature rises; reducing or eliminating air coolant requirements; and, simultaneously improving combustor durability and reliability.

Small gas turbines incorporate a variety of combustor types. Several of these are shown on Figure 22. Axial flow designs are large combustors scaled down in size. As their name implies, flow is directly through the combustion system. This design minimizes combustor surface area but can produce somewhat higher pressure loss and somewhat less uniform exit temperature distributions than the other designs shown. Reverse flow, or flowback combustors, are unique to small engine designs. They are often selected for application because they package well in small engines. However, they incorporate large combustor surface areas as well as a reverse turn, which must also be cooled. Radial outflow combustors approximate the reverse flow type. These combustors often eliminate the need for fuel injectors by introducing fuel through the engine shaft.

Research activities currently underway are applicable to all three combustor types. An example of combustion research in progress is contained in Figure 23. Advanced ceramic matrix liner concepts were evolved, applied to a full-size combustor and performance evaluated at simulated pressure ratio conditions to 22:1. The liner incorporated a thick yttria-stabilized zirconia coating on a pliable metallic surface. Details are contained in reference 9. Only backside convective cooling was supplied. Direct injection of film/transpiration coolant into the combustor, mandatory for current technology designs, was not required. Good short-term durability was demonstrated to outlet temperatures exceeding 2600°F. This is at least 300°F hotter than current cycle requirements. Measured liner temperatures were less than 1600°F, which is well within design limits. For comparative purposes, liner wall temperature for the ceramic matrix liner, as well as conventional liner design, are included on the figure.

REFERENCES

1. Vanco, M.R., Wintucky, W.T., and Niedzwiecki, R.W., "An Overview of the Small Engine Component Technology (SECT) Studies," AIAA Paper No. 86-1542, Presented at the AIAA/ASME/SAE/ASEE 22nd Joint Propulsion Conference, Huntsville, Alabama, June 16-18, 1986.
2. Larkin, T., Staton, D. and Mongia, H., "Rotorcraft Propulsion for Year 2000 Plus," AIAA Paper No. 86-1543, Presented at the AIAA/ASME/SAE/ASEE 22nd Joint Propulsion Conference, Huntsville, Alabama, June 16-18, 1986.
3. Kaehler, H. and Scheider, W., "Small Engine Technology Payoffs for Future Commuter Aircraft," AIAA Paper No. 86-1544, at the AIAA/ASME/SAE/ASEE 22nd Joint Propulsion Conference, Huntsville, Alabama, June 16-18, 1986.
4. Turk, M. and Zeiner, P., "Advanced Technology Payoffs for Future Rotorcraft, Commuter Aircraft, Cruise Missile and APU Propulsion Systems," AIAA Paper No. 86-1545, Presented at the AIAA/ASME/SAE/ASEE 22nd Joint Propulsion Conference, Huntsville, Alabama, June 16-18, 1986.
5. Singh, B. and Benstein, E., "Year 2000 Small Engine Technology Payoffs in Cruise Missiles," AIAA Paper No. 86-1546, Presented at the AIAA/ASME/SAE/ASEE 22nd Joint Propulsion Conference, Huntsville, Alabama, June 16-18, 1986.
6. Pampreen, R., "Engine Studies for Future Subsonic Cruise Missiles," AIAA Paper No. 86-1547, Presented at the AIAA/ASME/SAE/ASEE 22nd Joint Propulsion Conference, Huntsville, Alabama, June 16-18, 1986.
7. Cargill, G., "Final Report For Scaled Centrifugal Compressor Program", NASA CR-174912, September, 1986.
8. Kennehan, J.G., "Final Report For Scaled Centrifugal Compressor, Collector and Running Gear Program", NASA CR-168167, October, 1983.
9. Acosta, W.A., Small Gas Turbine Combustor Experimental Study-Compliant Metal/Ceramic Liner and Performance Evaluation, "AIAA Paper No. 86-C-6, Presented at the AIAA/ASME/SAE/ASEE 22nd Joint Propulsion Conference, Huntsville, Alabama, June 16-18, 1986.

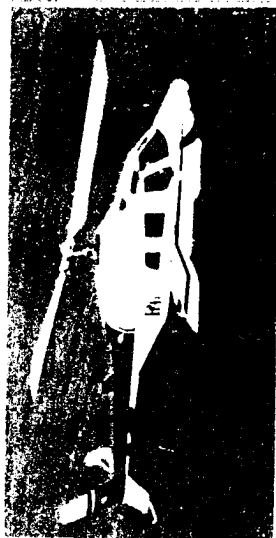
Lewis Research Center

NASA

ADVANCED SMALL ENGINE TECHNOLOGY

BROAD CIVIL/MILITARY APPLICATIONS

HELICOPTER



COMMUTER AIRCRAFT



GENERAL AVIATION



CRUISE MISSILES



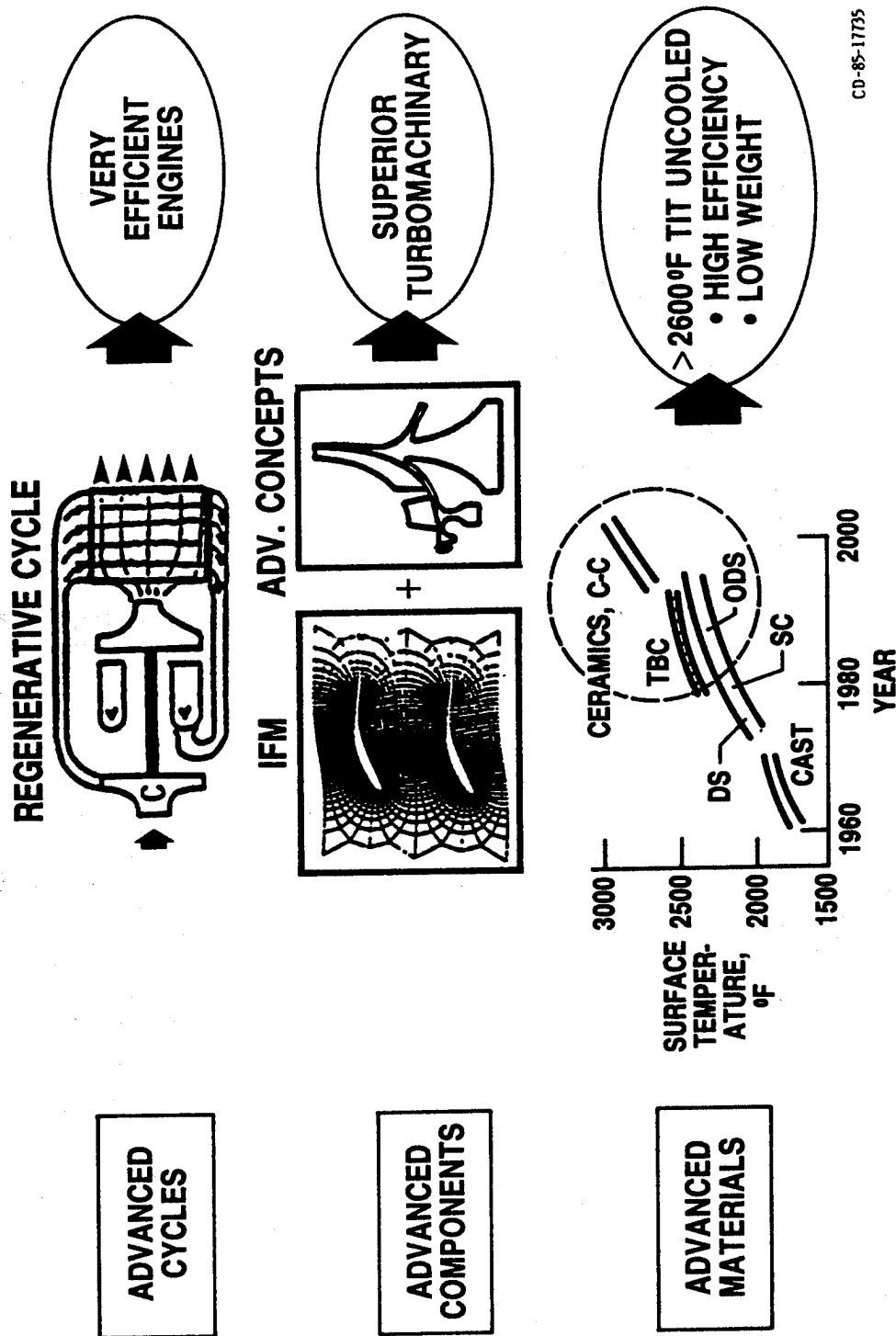
CD-85-17089

FIGURE 1

Lewis Research Center

ADVANCED SMALL ENGINE TECHNOLOGY

SMALL ENGINE TECHNOLOGY OPPORTUNITIES



CD-85-17735

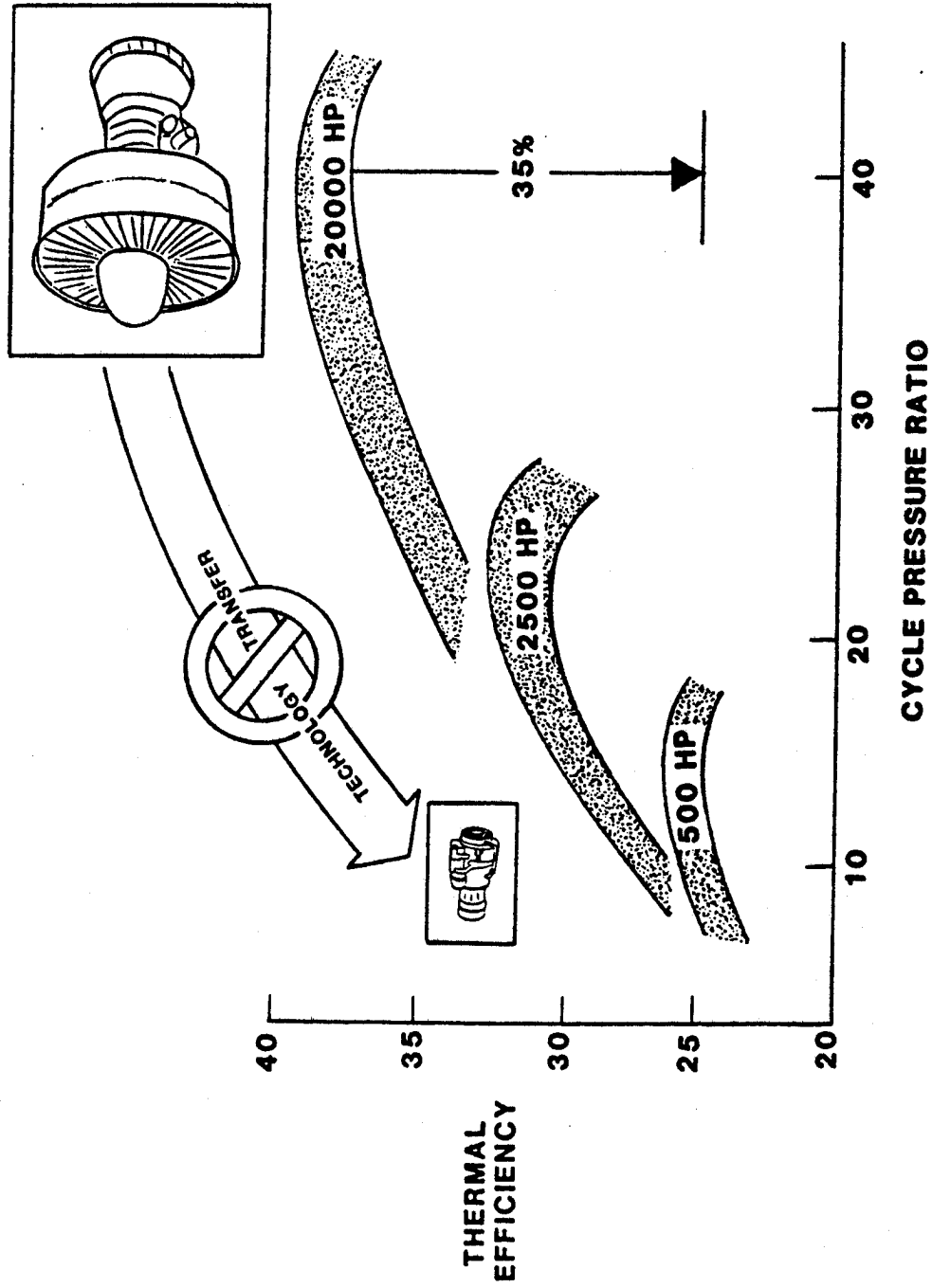
FIGURE 2

Lewis Research Center

NASA

ADVANCED SMALL ENGINE TECHNOLOGY

SMALL ENGINES ARE NOT AS EFFICIENT



CD-85-17094

FIGURE 3

Lewis Research Center ADVANCED SMALL ENGINE TECHNOLOGY

STATE-OF-THE-ART CYCLE PERFORMANCE

800 HP SLS

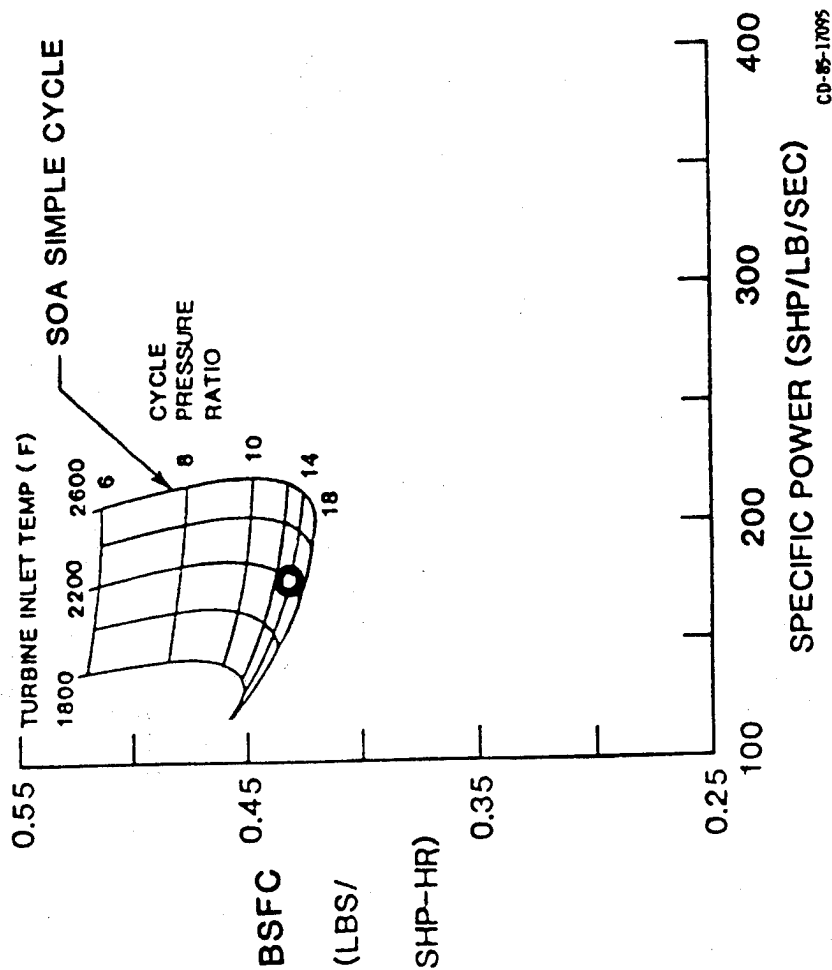


FIGURE 4

Lewis Research Center
ADVANCED SMALL ENGINE TECHNOLOGY

NASA

IMPACT OF ADVANCED TECHNOLOGY ON CYCLE PERFORMANCE

800 HP SLS

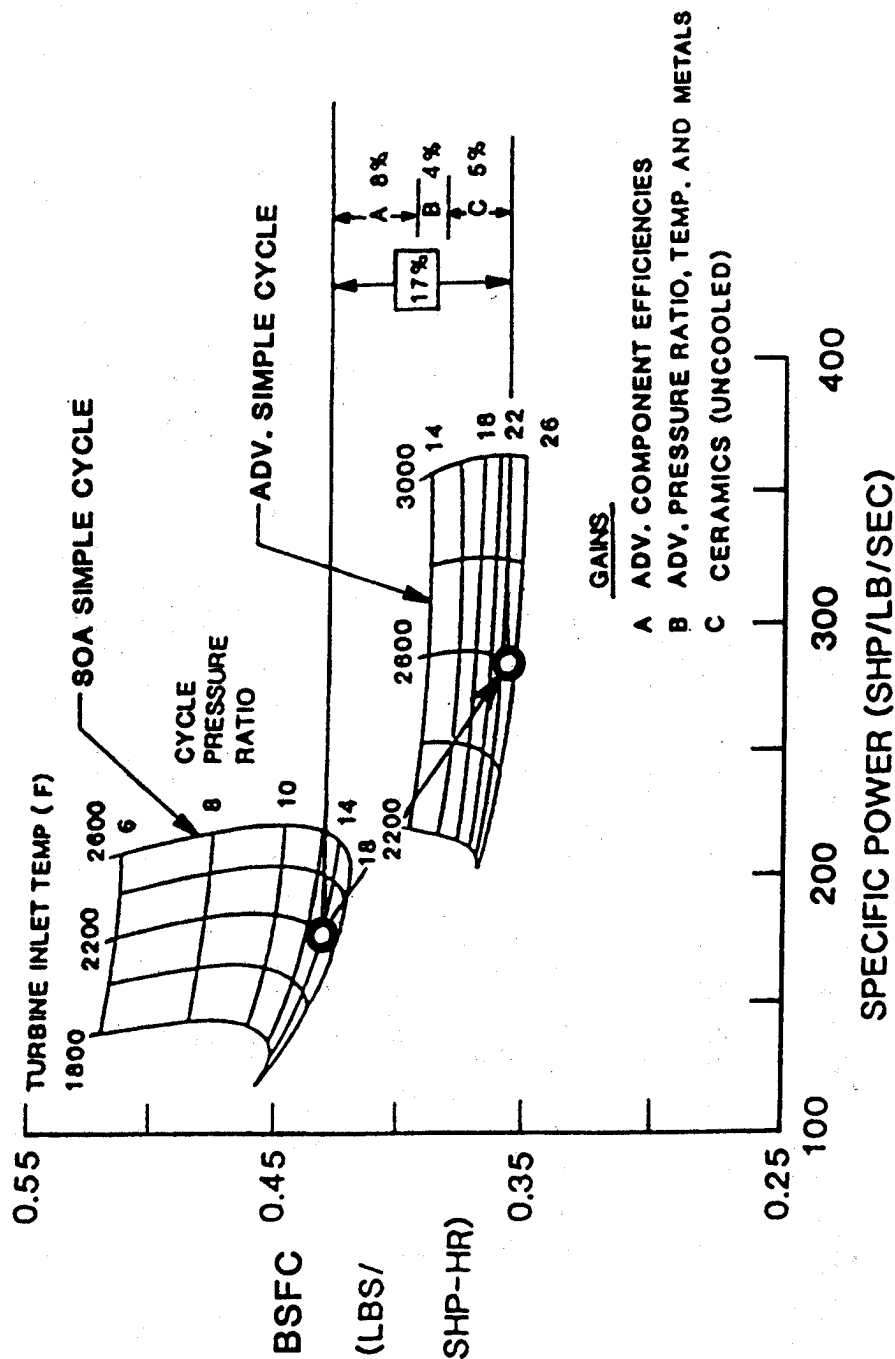


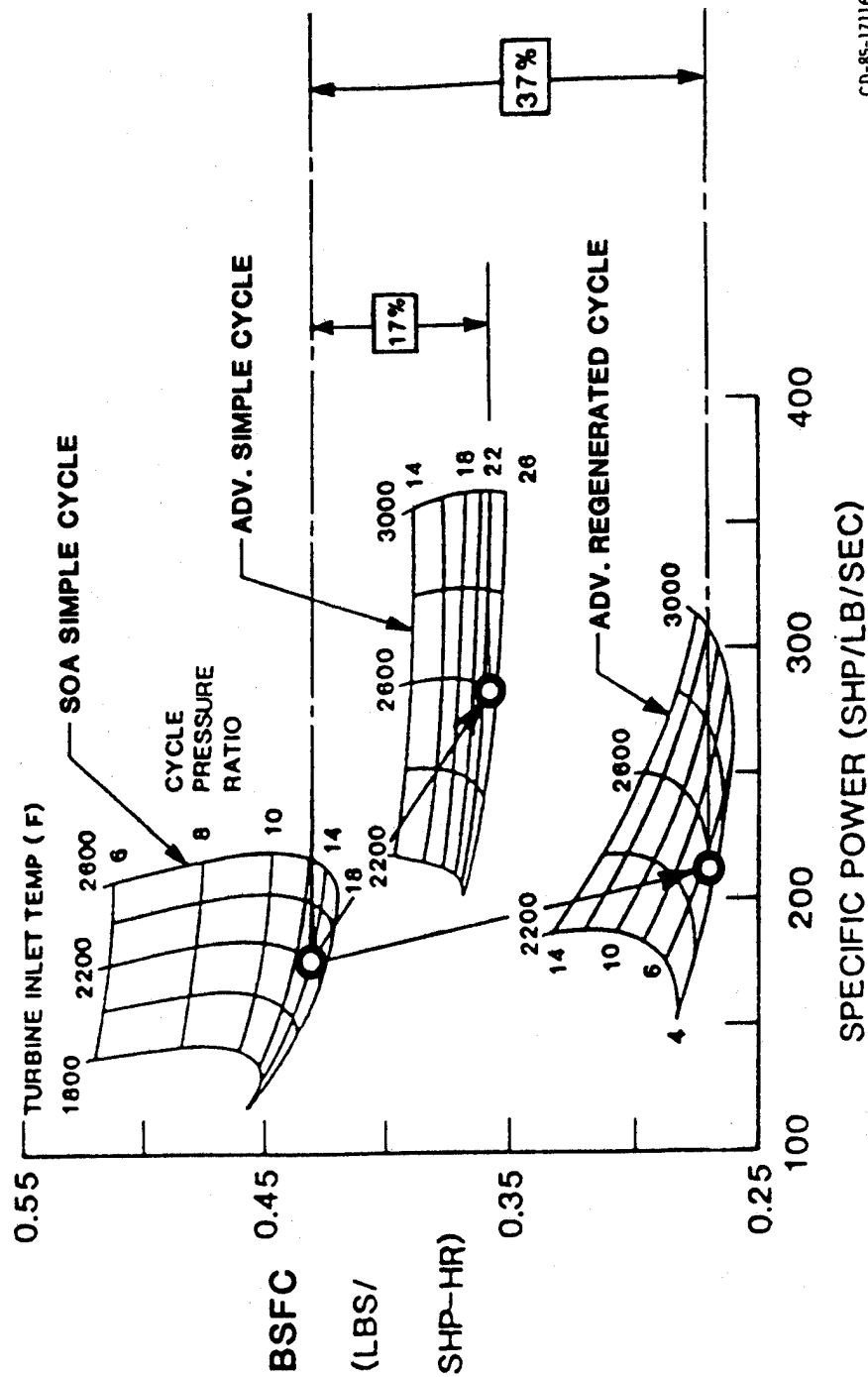
FIGURE 5

Lewis Research Center

ADVANCED SMALL ENGINE TECHNOLOGY

NASA

IMPACT OF ADVANCED TECHNOLOGY ON CYCLE PERFORMANCE 800 HP SLS



CD-85-17116

FIGURE 6

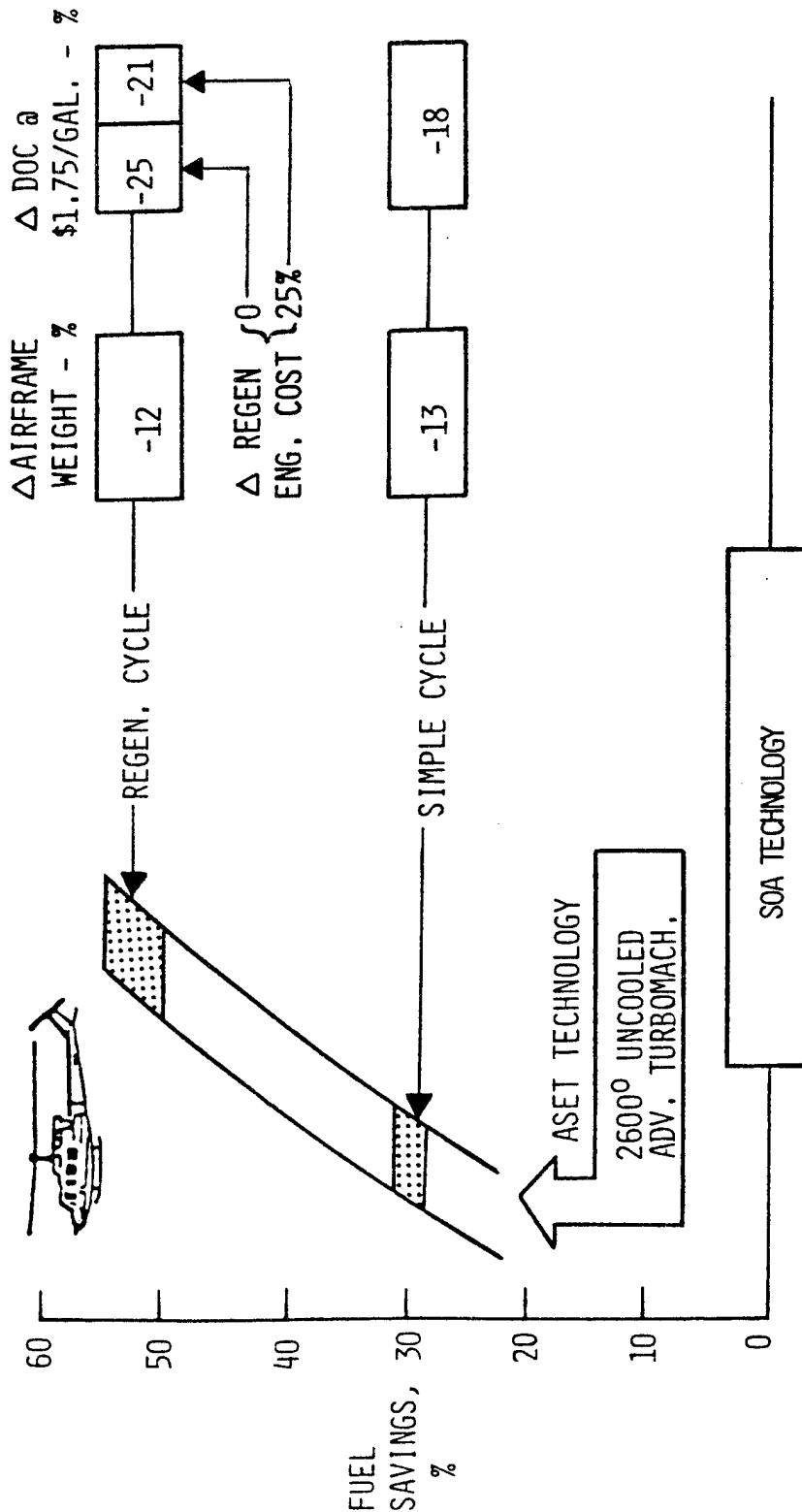
Lewis Research Center
ADVANCED SMALL ENGINE TECHNOLOGY

NASA

ASET TECHNOLOGY BENEFITS--HELICOPTER APPLICATION

4 PASSENGER, 0.15 MACH, 4000 FT. ALT., 300 N.M. DES. RANGE, 400 SHP/ENG.

REGENERATOR PENALTY: 50% ENGINE WEIGHT



CD-85-18106

FIGURE 7

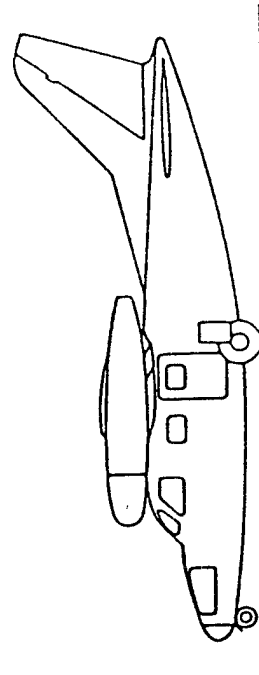
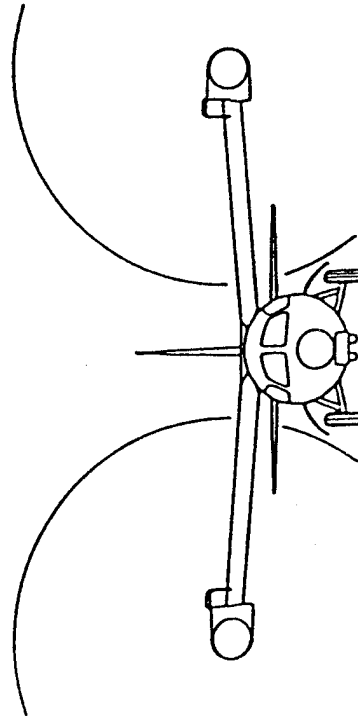
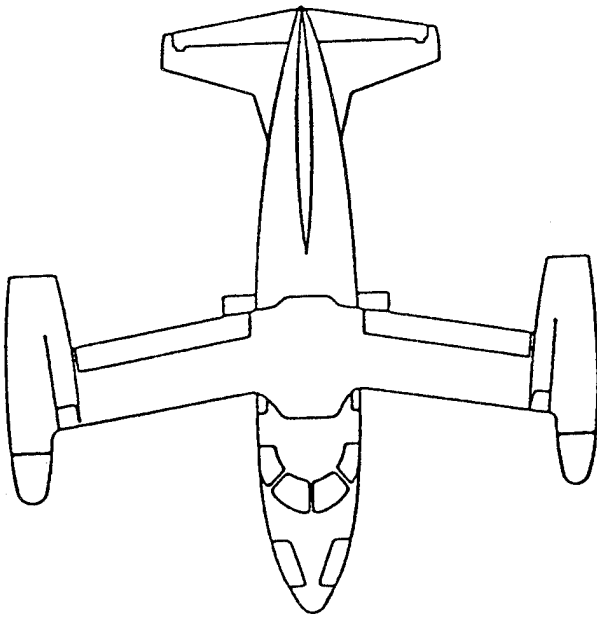


FIGURE 8: ALLISON TILT ROTOR AIRCRAFT

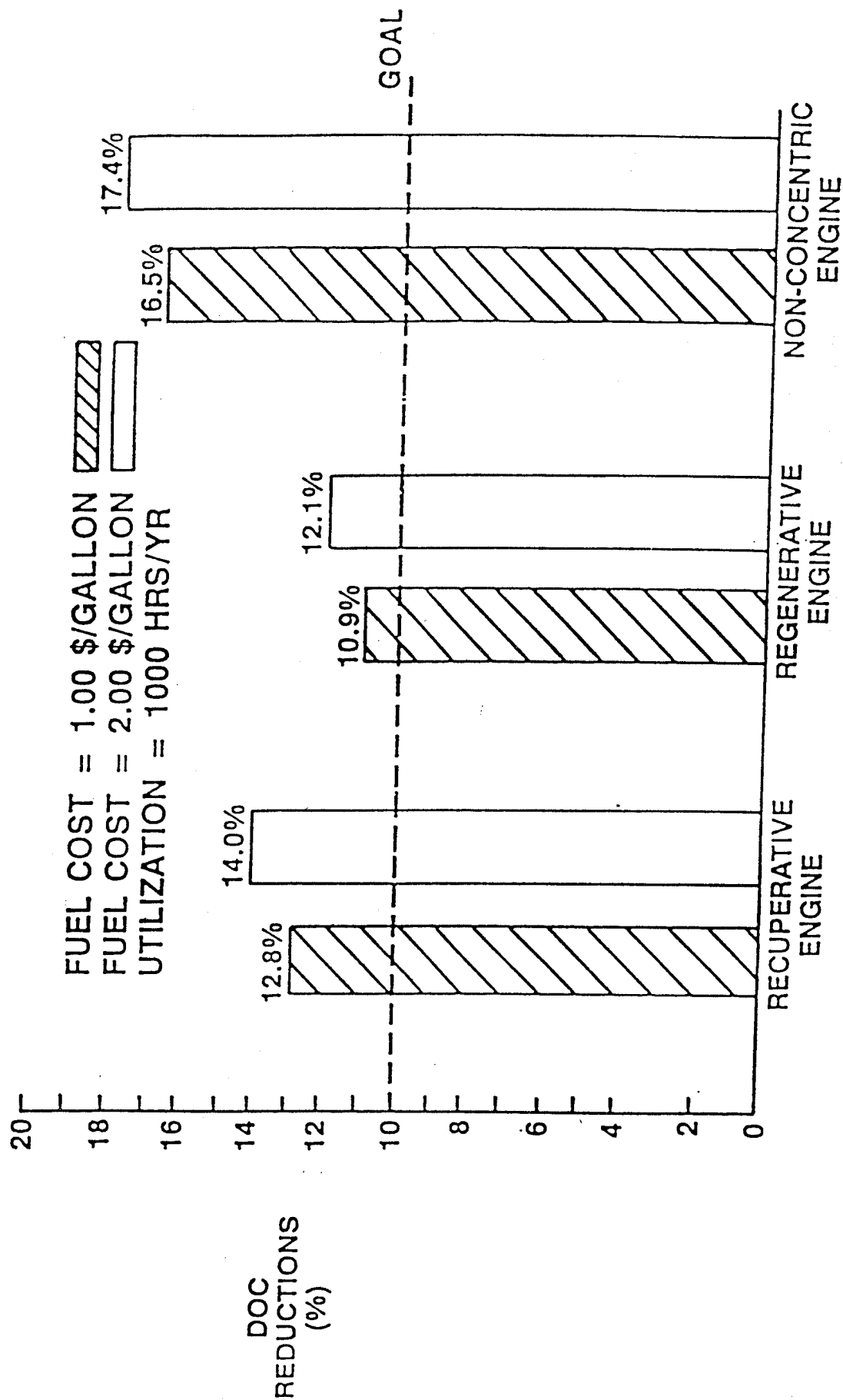
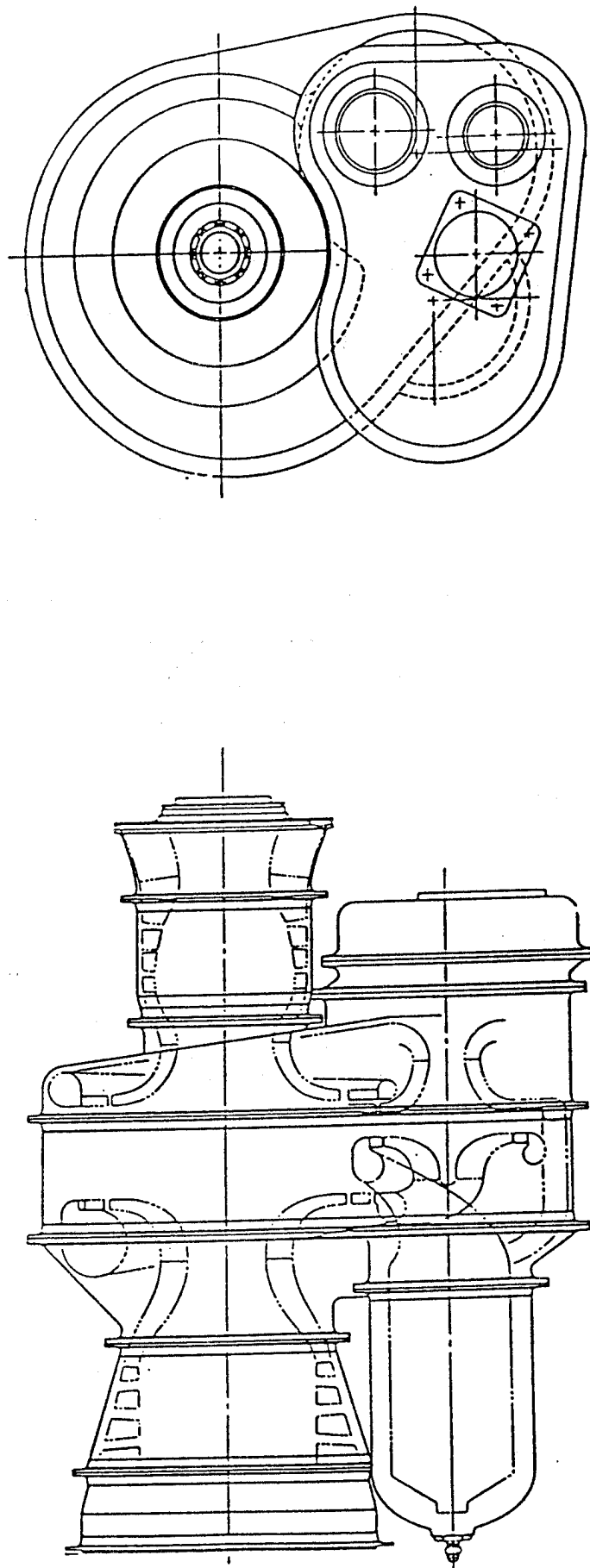
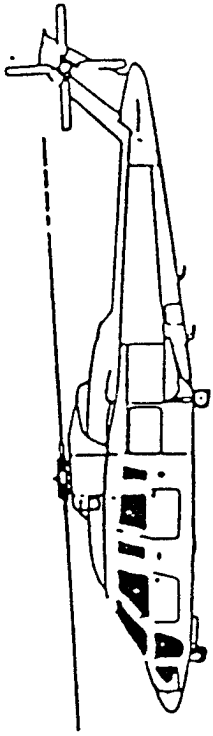


FIGURE 9: ALLISON MISSION ANALYSIS RESULTS

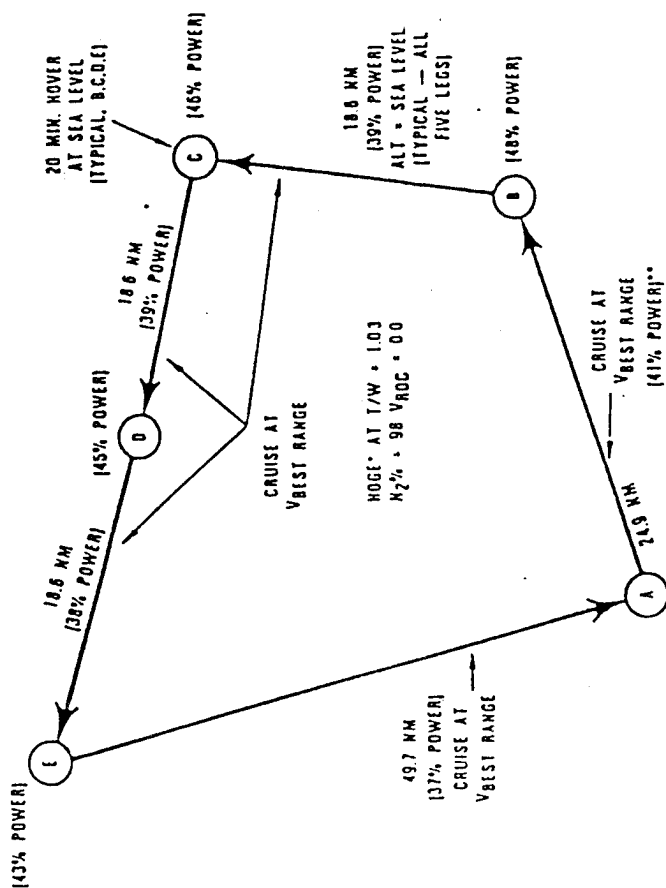
FIGURE 10: ALLISON NON-CONCENTRIC ENGINE





- TWIN ENGINE (1000 SHP EACH)
- WEIGHTS
 - EMPTY - 4375 LB
 - FUEL - 1303 LB
 - PAYLOAD - 3676 LB
 - TOGW (INCLUDES PILOT WEIGHT OF 210 LB) - 9564 LB

FIGURE 11: GARRETT REFERENCE ROTORCRAFT

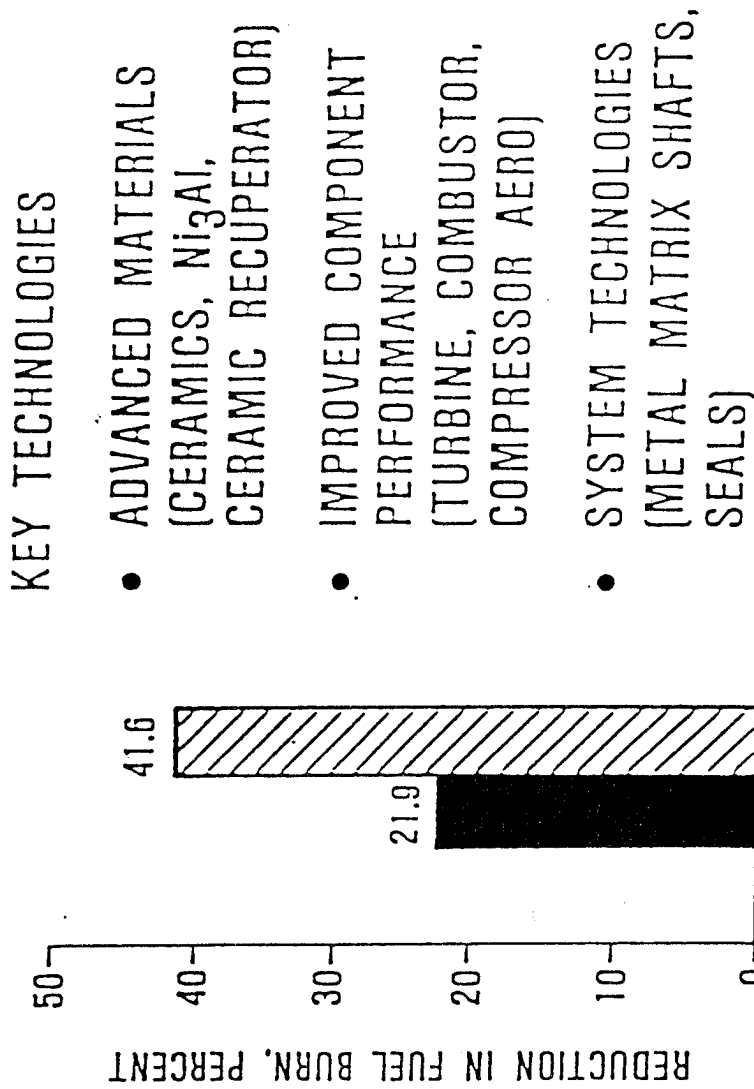
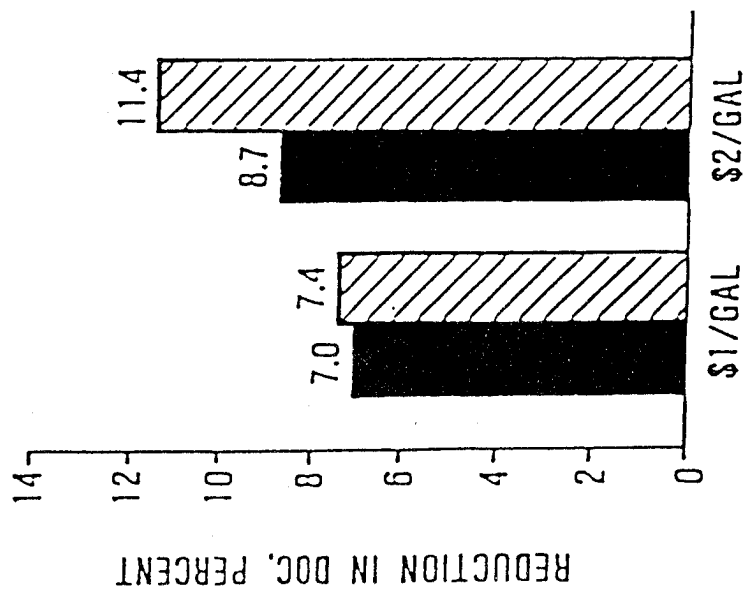


*HOVER OUT OF GROUND EFFECT

**PERCENTAGE OF SLS T/O RATING (1000 SHP)

FIGURE 12: GARRETT ROTORCRAFT MISSION

 SIMPLE CYCLE
 RECUPERATED

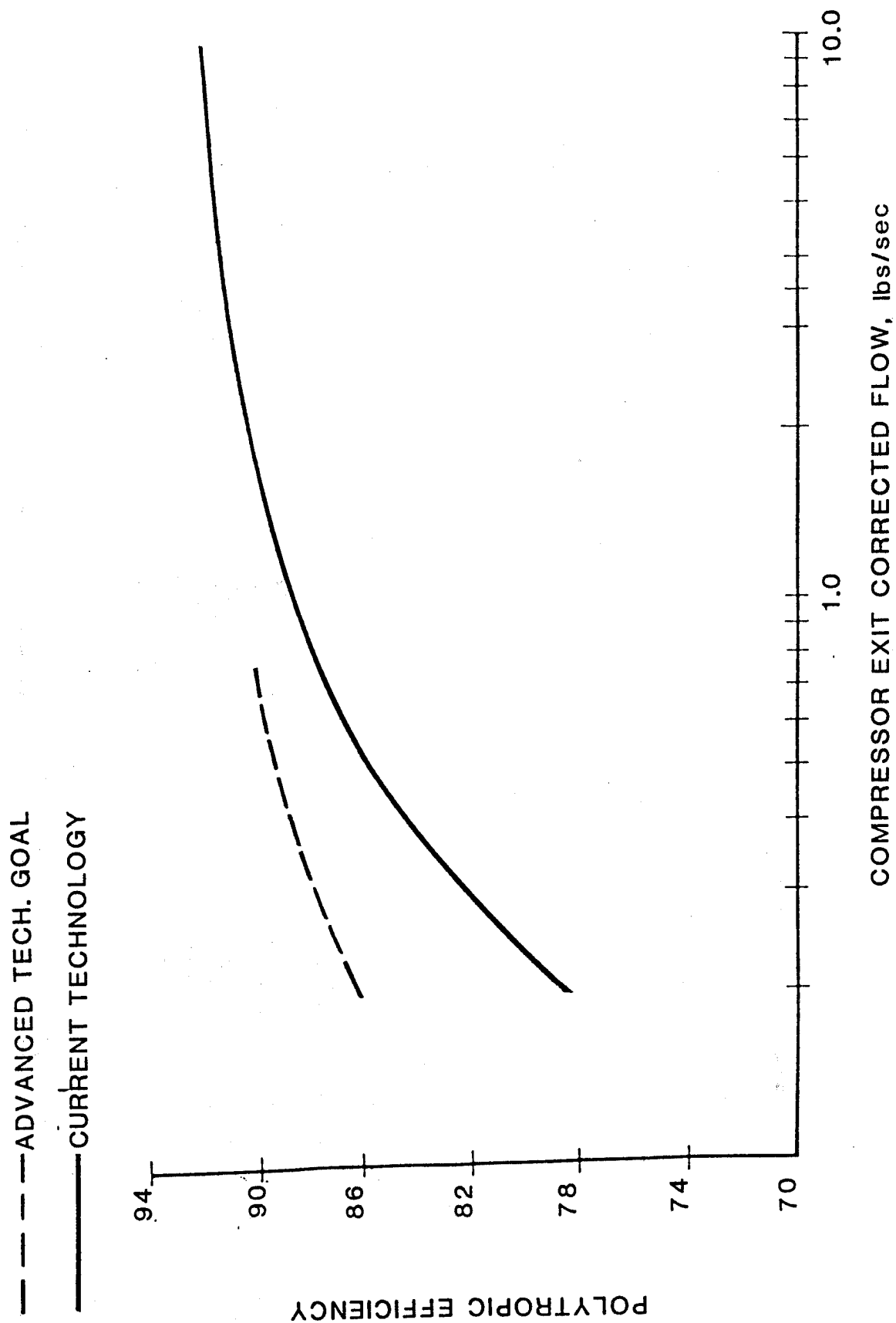


KEY TECHNOLOGIES

- ADVANCED MATERIALS (CERAMICS, Ni_3Al , CERAMIC RECUPERATOR)
- IMPROVED COMPONENT PERFORMANCE (TURBINE, COMBUSTOR, COMPRESSOR AERO)
- SYSTEM TECHNOLOGIES (METAL MATRIX SHAFTS, SEALS)

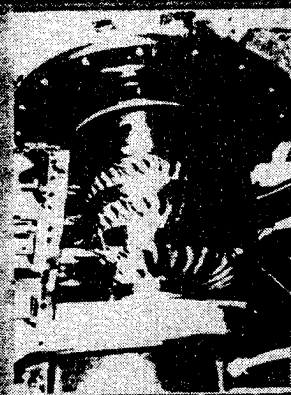
FIGURE 13: GARRETT MISSION ANALYSIS RESULTS

FIGURE 14: COMPRESSOR EFFICIENCY

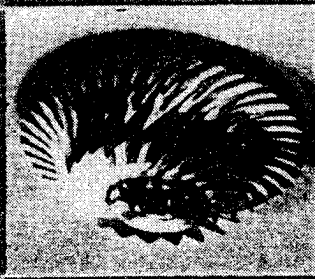


COMPRESSOR TECHNOLOGY

AXIAL



CENTRIFUGAL



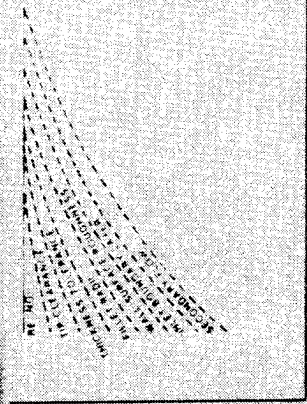
- HIGHER PRESSURE RATIOS
- INCREASED EFFICIENCY
- REDUCE NUMBER OF STAGES

COMPUTER-AIDED ANALYSIS



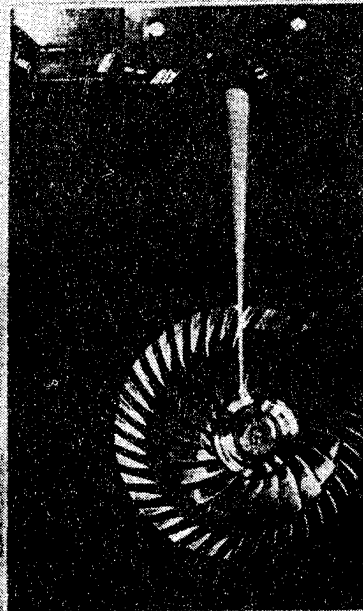
DEVELOP ANALYTICAL
MODELS AND CODES

PERFORMANCE DEGRADATION
FACTORS



QUANTIFY/MINIMIZE EFFECT
WITH FLOW SIZE

LASER ANEMOMETRY



OBTAIN DETAILED INTERNAL
FLOW MEASUREMENT

V-2517

FIGURE 15

FIGURE 16

SCALED CENTRIFUGAL COMPRESSOR PROGRAM

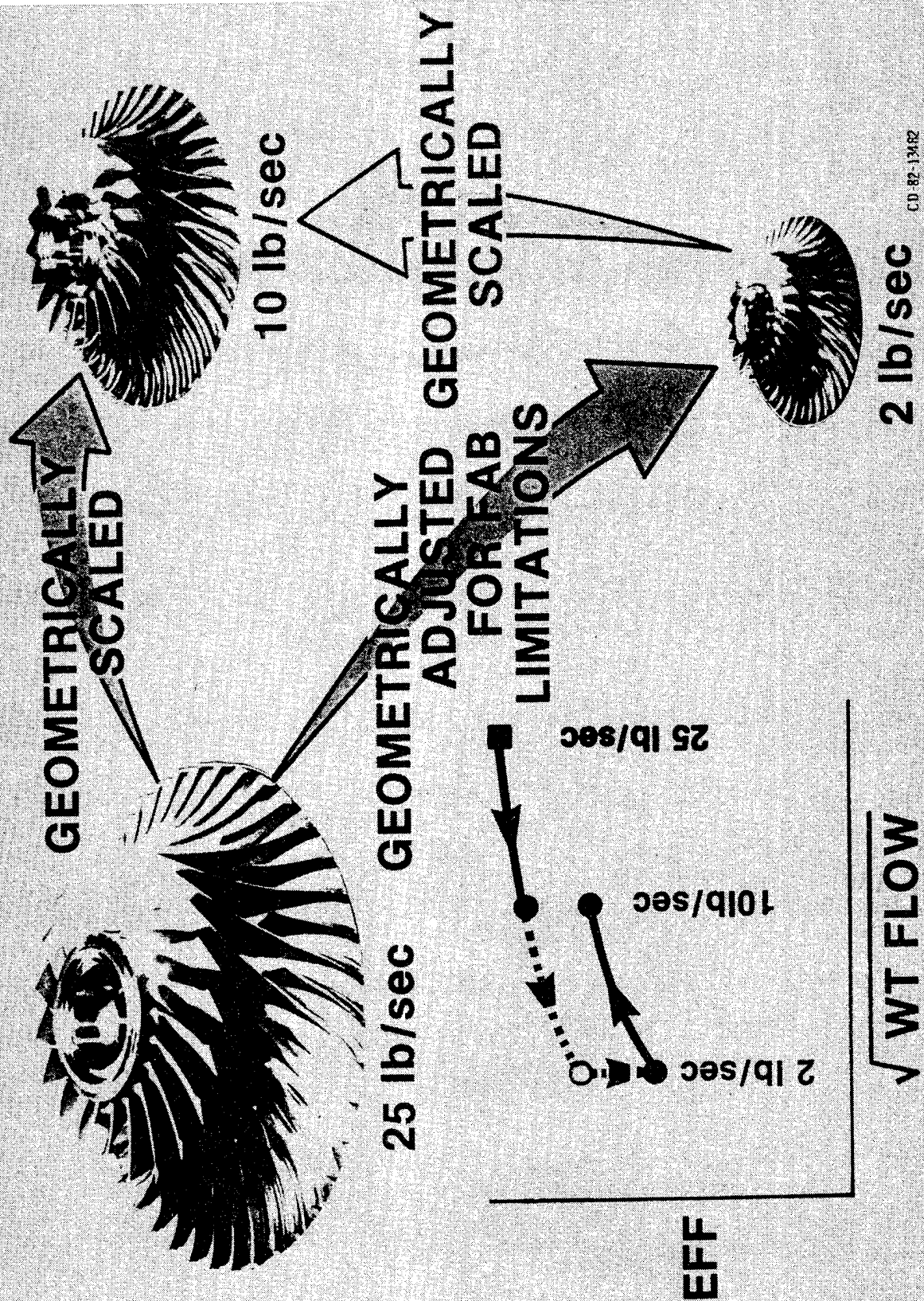


FIGURE 17 SCALED CENTRIFUGAL COMPRESSOR PROGRAM RESULTS

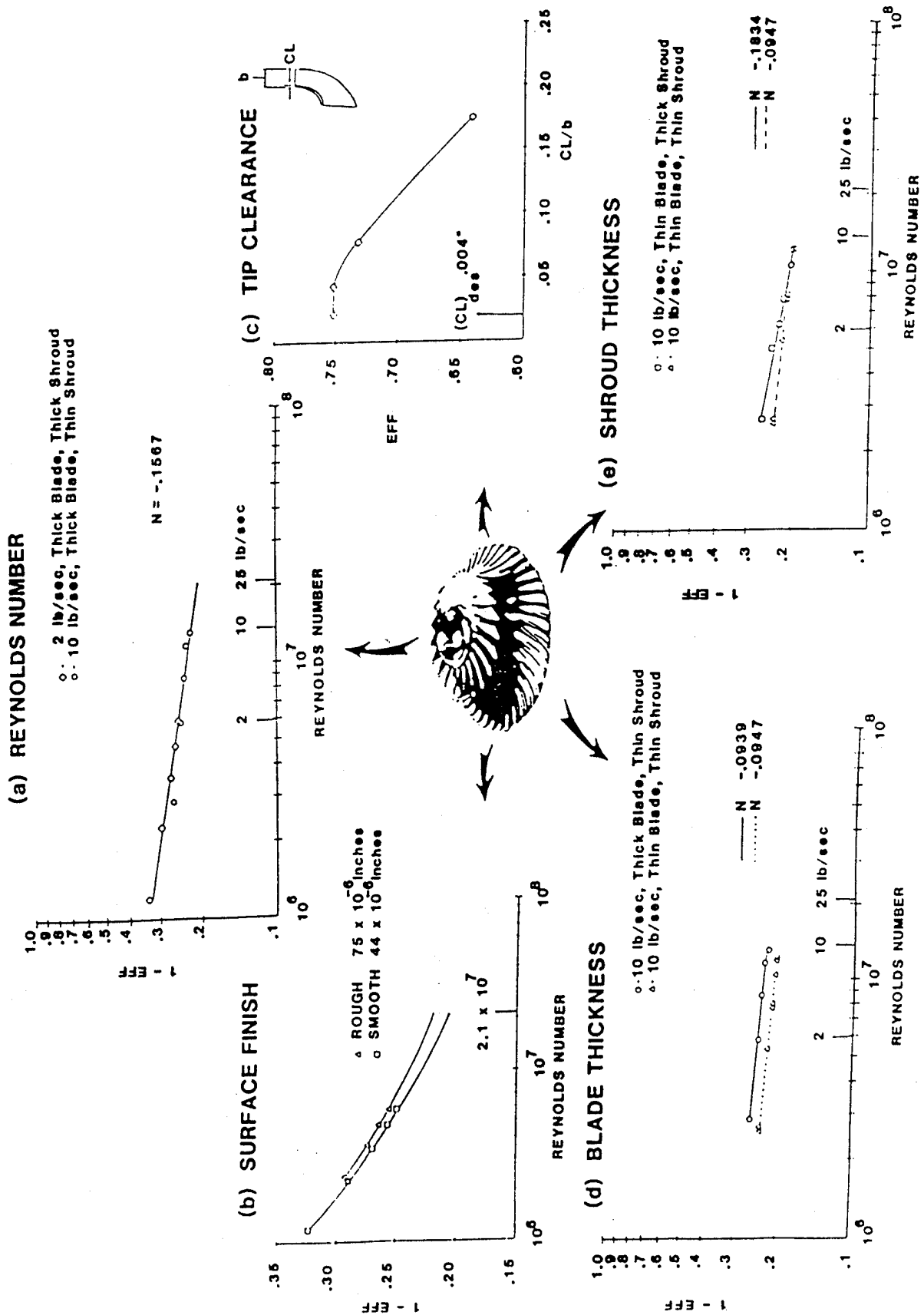


FIGURE 18: TURBINE EFFICIENCY

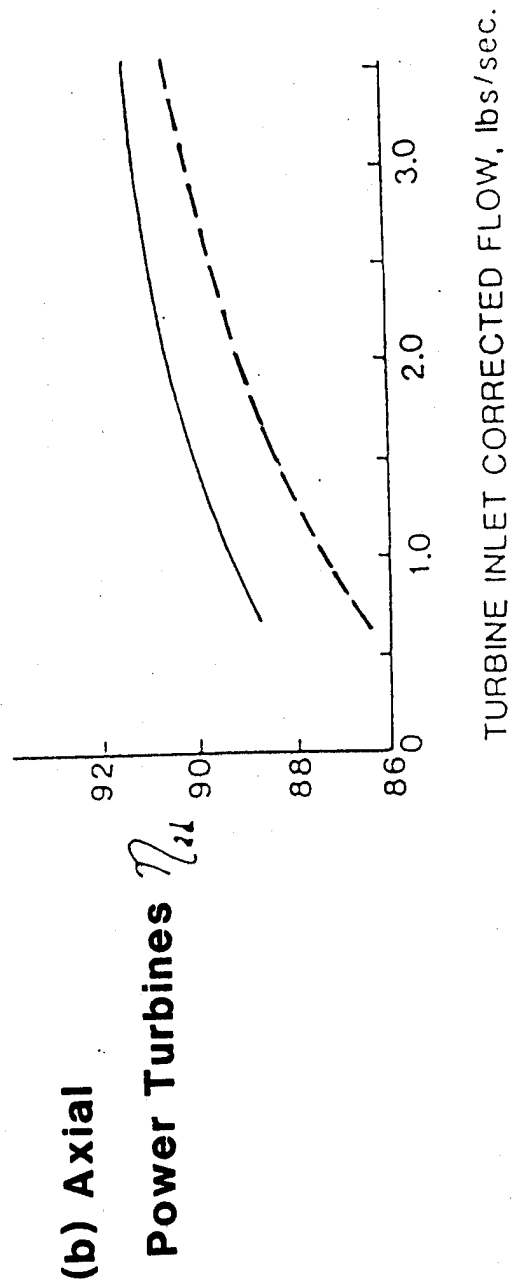
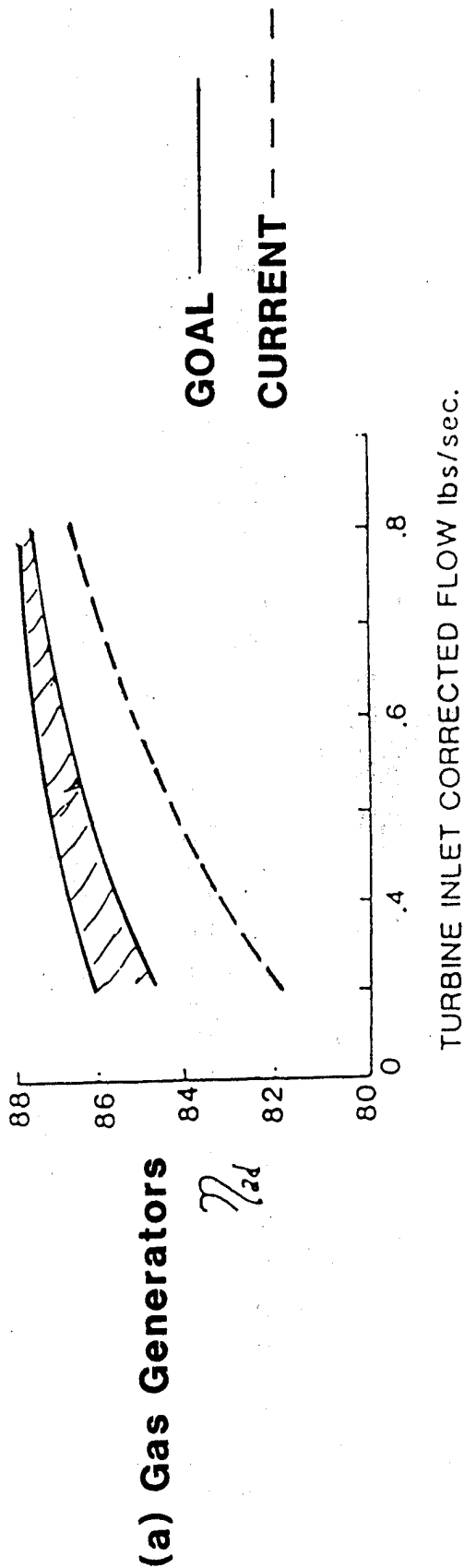
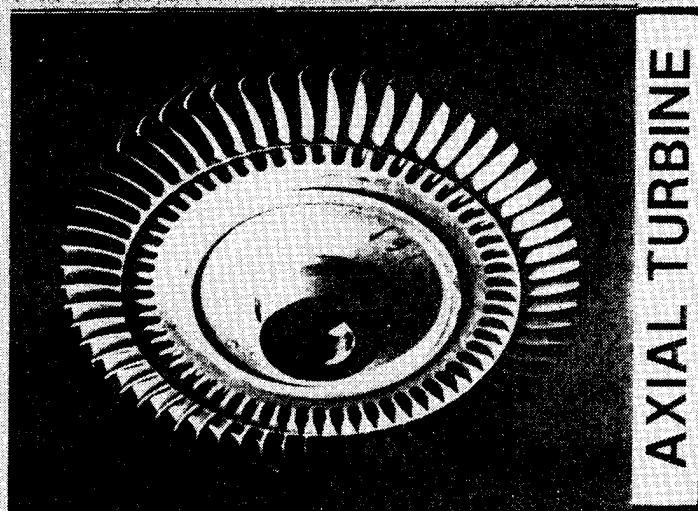
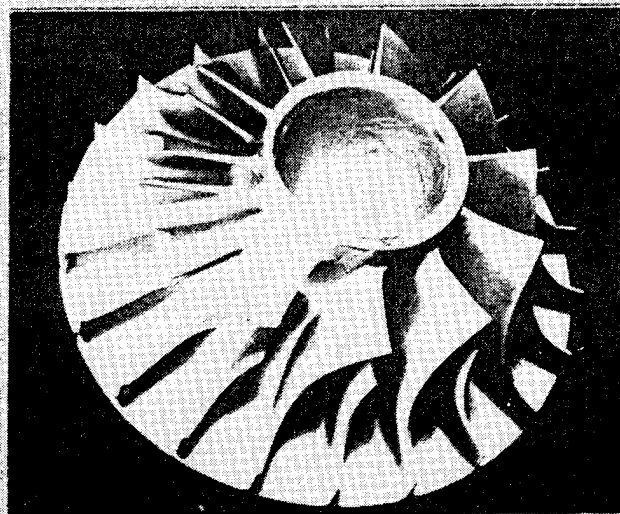


FIGURE 19 SMALL TURBINE AERODYNAMICS



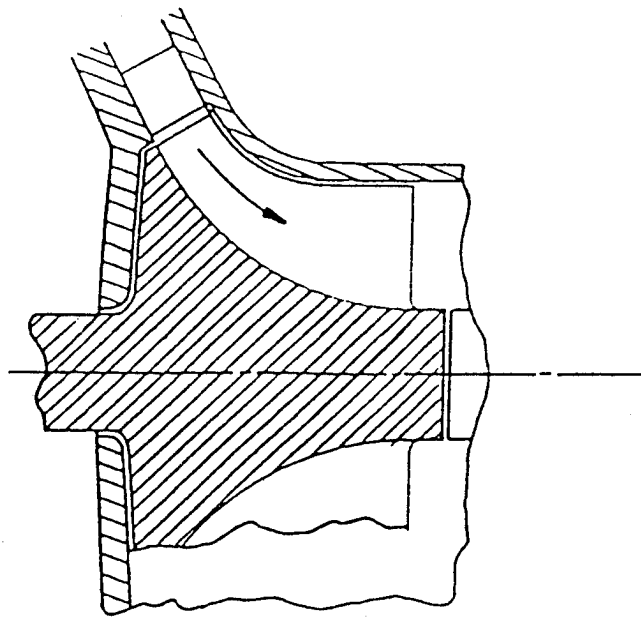
AXIAL TURBINE



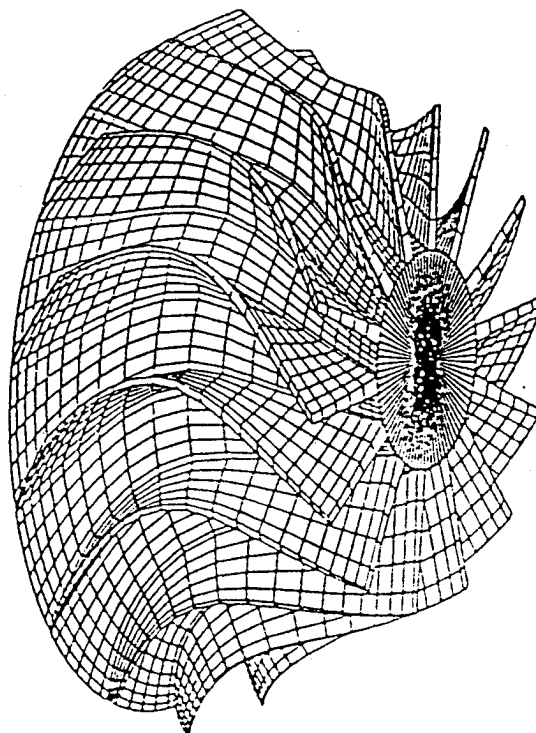
RADIAL TURBINE

- ENDWALL EFFICIENCY IMPROVEMENT
- LOW ASPECT RATIO AERODYNAMICS
- ENGINE ENVIRONMENT EFFECTS
- SMALL SIZE PENALTIES
- HIGHLY LOADED STAGES
- VARIABLE GEOMETRY
- MANIFOLDS & DUCTS
- COOLING AERODYNAMICS
- VALIDATION OF COMPUTATIONAL METHODS

FIGURE 20: MIXED-FLOW TURBINE



(a) Flow Path

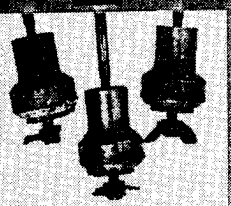


(b) Structural Analysis

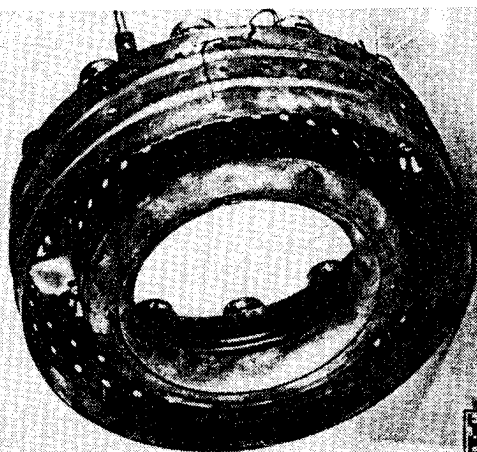
FIGURE 21

SMALL COMBUSTOR TECHNOLOGY PROBLEM AREAS

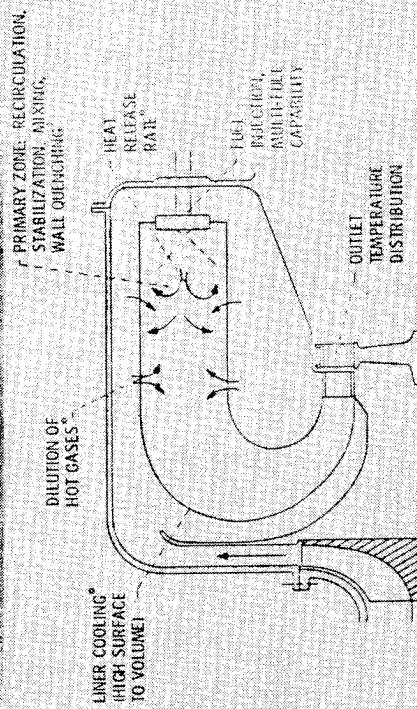
CARBON DEPOSITION AND SMOKE



PRIMARY ZONE DESIGN METHODS



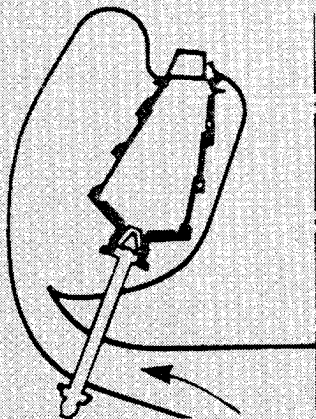
ADVANCED FUEL INJECTORS



ADVANCE LINER COOLING



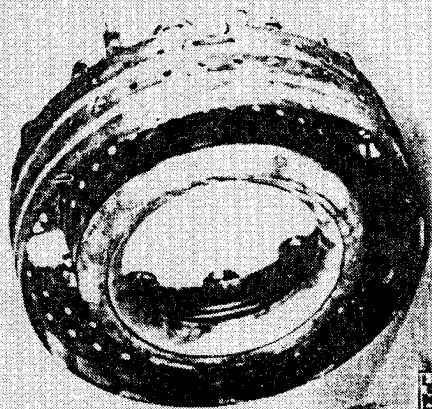
SMALL COMBUSTOR TECHNOLOGY



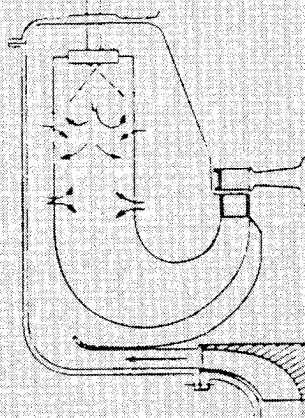
AXIAL FLOW

TECHNOLOGY NEEDS

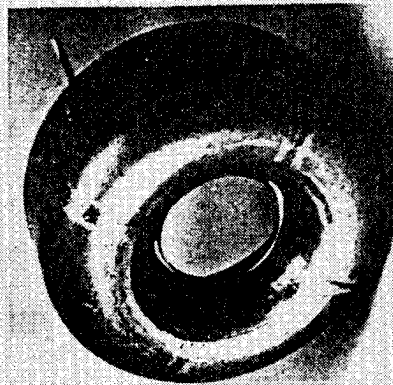
- INCREASED TEMP/PRESSURE CAPABILITY
- REDUCED AIR COOLANT REQUIREMENTS
- INCREASED DURABILITY/RELIABILITY



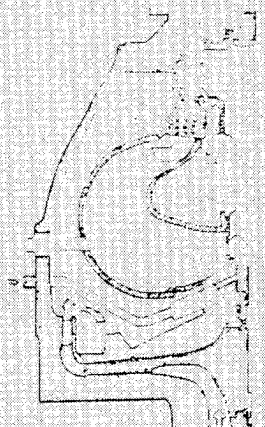
PRIMARY ZONE DESIGN
METHODS



REVERSE FLOW



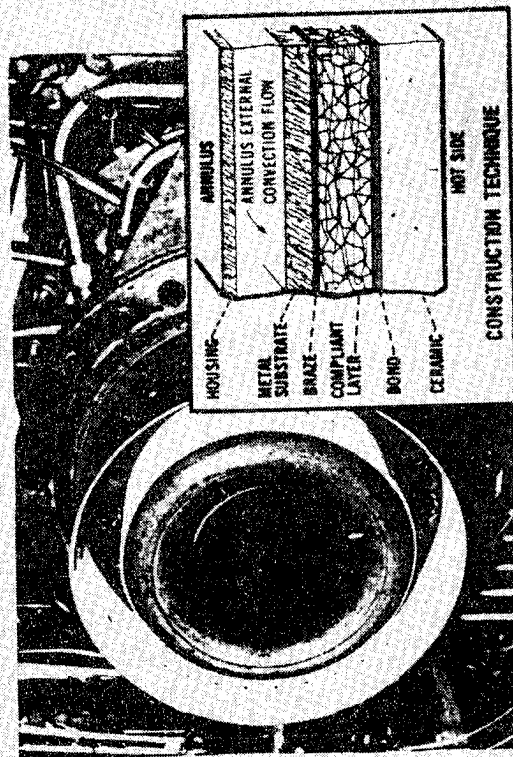
ADVANCED LINER
COOLING



RADIAL OUTFLOW

FIGURE 22

HIGH TEMPERATURE EVALUATION OF CERAMIC MATRIX LINER



CERAMIC MATRIX LINER RESULTS

- OPERATION TO 2630 °F DEMONSTRATED
- 300° HIGHER THAN CURRENT
- FILM/TRANSPIRATION COOLING
NEED ELIMINATED
- NON-STRATEGIC MATERIALS USED

SIGNIFICANT SFC REDUCTIONS REQUIRE

- APPLICATION OF ADVANCED CYCLES TO
 - SIMPLE CYCLES
 - REGENERATIVE CYCLES
- APPLICATION OF UNCOOLED CERAMICS
- EVOLUTION OF ADVANCED COMPONENTS

COMPARISON OF COMBUSTOR LINER CONCEPTS

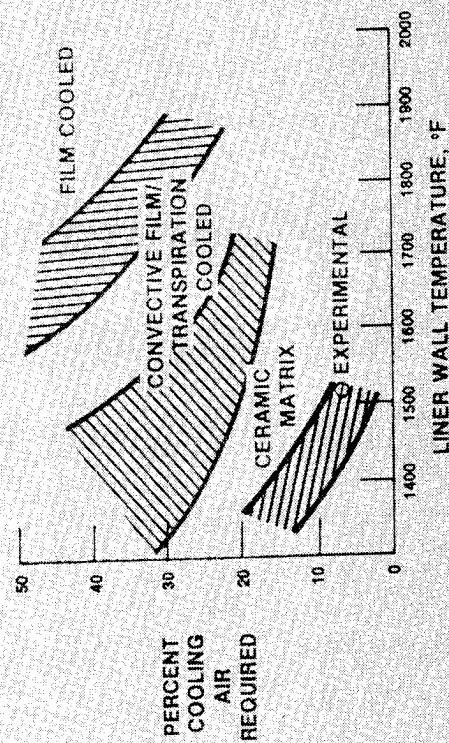


FIGURE 23

CD-85-16478

THE CONVERTIBLE ENGINE: A DUAL-MODE PROPULSION SYSTEM
FOR ADVANCED ROTORCRAFT

Jack G. McArdle
National Aeronautics and Space Administration
Lewis Research Center
Cleveland, Ohio 44135

SUMMARY

A variable inlet guide vane (VIGV) convertible engine that could be used to power future high-speed rotorcraft was tested on an outdoor stand. The engine ran stably and smoothly in the turbofan, turboshaft, and dual (combined fan and shaft) power modes. In the turbofan mode with the VIGV open, fuel consumption was comparable to that of a conventional turbofan engine. In the turboshaft mode with the VIGV closed, fuel consumption was higher than that of present turboshaft engines because power was wasted in churning fan-tip airflow. In dynamic performance tests with a specially built digital engine control and using a waterbrake dynamometer for shaft load, the engine responded effectively to large steps in thrust command and shaft torque. Previous mission analyses of a conceptual X-wing rotorcraft capable of 400-knot cruise speed were revised to account for more fan-tip churning power loss than was originally estimated. The new calculations confirm that using convertible engines rather than separate lift and cruise engines would result in a smaller, lighter craft with lower fuel use and direct operating cost.

INTRODUCTION

A convertible engine can produce turbofan thrust, turboshaft power, or any combined thrust and shaft power continuously while operating up to full speed. Convertible engines could be used to power vertical/short-takeoff-and-landing (V/STOL) airplanes and advanced high-speed rotorcraft such as those shown in figures 1 and 2. Studies of conceptual high-speed rotorcraft (fig. 3) have shown that using convertible engines rather than separate engines for rotor power and forward thrust affords installation advantages and can save as much as 16 percent in fuel and 20 percent in direct operating cost (refs. 1 and 2). For rotorcraft a convertible engine would operate as a turboshaft engine to drive a lifting rotor for vertical and low-speed horizontal flight, and as a turbofan engine to produce thrust for high-speed horizontal flight. For a jet-powered V/STOL airplane the convertible feature could be used to cross-couple the fans in a two-engine configuration for safety in case one engine should fail.

In a convertible engine the power turbine drives both the fan and an output shaft connected to some other load. Total turbine power is just the sum of the powers absorbed by all the loads; therefore any turbine power over that needed by the fan is available at the power output shaft. Maximum turbine power is limited by cycle temperature (fuel flow) and speed. For high thrust the shaft load is reduced or decoupled, as by releasing a clutch. When shaft power is required, the fan is unloaded aerodynamically. Two general methods have been devised to unload the fan (ref. 3). One method is based on variable-pitch fan blades - fan power is reduced as the pitch is made "flatter." This

method has been demonstrated in tests of engines such as QCSEE (ref. 4), Q-fan (ref. 5), and Astafan (tested successfully as a convertible engine in a U.S. Army Research and Technology Laboratories test program). The other method is based on variable inlet guide vanes (VIGV) that can be deflected to change fan airflow and inflow swirl - fan power is reduced as the vanes are closed. This method has been demonstrated in fan research tests (ref. 6) and in tests of a high-bypass-ratio turbofan engine with no output shaft power (ref. 7).

Recognizing the potential installation and performance advantages of convertible engines, the Defense Advanced Research Project Agency (DARPA) and the National Aeronautics and Space Administration (NASA) have joined in a Convertible Engine System Technology (CEST) Program to establish the feasibility of the convertible engine concept. This program is intended to expand basic technology, to generate design criteria, and to provide data and experience applicable to engines and controls for future convertible propulsion systems. The program includes defining requirements for convertible engine systems and evaluating an engine type that could be used on advanced rotorcraft such as the X-wing (refs. 8 and 9), the Advancing Blade Concept (ABC), and the folding tilt rotor (refs. 10 and 11, in which use of a new torque converter was proposed to uncouple the fan for shaft-only power). The experimental work described in this report was done at NASA Lewis. The engine was a TF34-400B (8000-lb-thrust class) turbofan modified to a VIGV convertible engine. The tests were performed on an outdoor test stand with a waterbrake dynamometer used for the shaft load. For some tests a new digital electronic system was used to control engine speed and variable-geometry actuators. The test objectives were to demonstrate operation of this type of convertible engine in the turbofan, turboshaft, and dual (combined fan and shaft) power modes and to evaluate the effects of the new and modified components on performance through internal flow path measurements.

The tests included steady-state and dynamic performance tests plus engine response to simulated aircraft maneuvers such as takeoff and X-wing conversion between fixed- and rotary-wing flight. The engine tests are summarized in this paper by showing typical results at selected operating conditions. (Detailed results and a more thorough discussion of the steady-state tests are given in ref. 12.) In addition, some of the conclusions of a previous mission analysis study are reviewed on the basis of calculations made with measured convertible engine performance instead of the original analytically predicted performance.

APPARATUS AND PROCEDURE

Engine

The test engine was a previously used TF34-400B especially modified by the manufacturer as sketched in figure 4. The standard TF34 is a 6:1 bypass ratio turbofan that can produce 9100 lb of sea-level-static thrust. The single-stage fan is driven by a four-stage low-pressure turbine. The core has a 14-stage axial compressor, an annular combustor, and a two-stage high-pressure turbine.

The engine modifications, shown in more detail in figure 5, were made by using as many existing parts as feasible. The resulting configuration, called the CEST TF34, was not meant to be a production engine. The fan was unloaded aerodynamically by deflecting part-span VIGV to change the rate and swirl angle of the flow entering the fan tip. The vanes are "part span" because they reach

only from the outer wall to the core/bypass flow splitter and thus have little effect on core flow. When the vanes are deflected, the fan air load is reduced and the power turbine can drive an external load through the power output shaft.

Each of the major modifications is described in the following paragraphs. For additional detail, consult references 12 and 13.

Variable inlet guide vanes. - A set of 30 vanes was installed just ahead of the fan rotor to unload the fan in the turboshaft power mode. Each vane consisted of a fixed forward strut and a movable rear flap. The flaps were deflected together by a hydraulic actuator system.

Flow splitter. - The core/bypass flow splitter was extended forward to the VIGV to minimize core inlet flow distortion from the deflected VIGV.

Fan blades. - Full-chord shrouds, continuing the core/bypass flow splitter, were added to the standard TF34 fan blades. The shrouds were hollow to reduce weight, and contained seals to minimize leakage between the hub and tip flows. In addition, the hub airfoil shape was changed to improve pumping performance in the low-aspect-ratio passage formed by the hub/splitter annulus.

Variable exit guide vanes. - A set of 44 variable exit guide vanes (VEGV) replaced the same number of standard TF34 exit stator vanes in the fan-tip (bypass) flow. Deflection of the new vanes by hydraulic actuators was scheduled to VIGV deflection to prevent stall buffetting at high VIGV closure such as was encountered in previous tests of a similar configuration (ref. 7).

Bleed valve. - A core/bypass bleed valve was installed in the flow splitter behind the VEGV to improve the fan-hub/core-engine flow match at low-power operation. The valve was a sliding-ring valve moved by three actuators evenly spaced around the core engine.

Shaft extension. - The power output shaft extended forward from the fan disk. The extension included a flexible coupling and bearings supported by spider struts built into the inlet ducting.

Control Systems

For the CEST TF34, fan speed and thrust were controlled by the engine control system, and shaft torque (power) was controlled by the waterbrake torque control.

Engine control system. - A new digital control system (described in ref. 14) was supplied with the engine. The system worked together with the standard TF34 fuel control in two operating modes.

(1) In the "shaft" mode the digital system varied the VIGV (open loop) to match the thrust command input and adjusted the fuel to hold the fan speed steady (closed loop) as the output shaft torque changed.

(2) In the "thrust" mode the digital system locked the VIGV in the fully open position and controlled the fan speed to a preprogrammed schedule (open loop) to match the thrust command input.

In both modes the control also adjusted the VEGV and the bleed valve to positions determined from internally programmed schedules.

Waterbrake torque control. - The waterbrake torque control system adjusted the power output shaft torque (closed loop) to match the torque command input. Control was accomplished by positioning the exit flow valve to vary the water annulus level in the waterbrake. The water throughflow rate, and thus the water temperature rise, was set by sizing the inlet flow valve.

The excellent performance of the waterbrake and its control is indicated by its response to a large torque command step (fig. 6). The exit flow valve, driven by a large hydraulic actuator and a high-response electrohydraulic servovalve, moved fast enough to change torque at a rate of more than 12 000 ft-lb/sec. For the test shown the engine fuel flow was fixed (nominally constant engine power) and the water inlet valve was of maximum size. For smaller inlet valve openings the torque changed at a lower rate because the water annulus filled more slowly. The initial dead time in torque response may have been caused by an unexplained flow effect within the waterbrake; its presence caused no problems in the tests reported herein but might limit other types of control transient testing that can be done successfully with this type of power absorber.

Test Facility and Engine Installation

The engine was tested on an outdoor static test stand at the NASA Lewis Research Center (fig. 7). The separate-flow exhaust nozzles were standard TF34 nonadjustable nozzles. The power output shaft was supported by a pedestal just in front of the bellmouth and then connected to the waterbrake. A honeycomb screen flow straightener was located at the bellmouth. The honeycomb caused up to 2-percent total-pressure loss but reduced inlet distortion that might have been caused by the shaft support pedestal. The residual distortion near the fan face, indicated by the conventional gradient parameter (Maximum total pressure - Minimum total pressure)/Average total pressure, was only about 0.5 percent.

Total-pressure rakes, wall-pressure orifices, thermocouples, load cells, fuel flowmeters (both turbine and beam types), and other conventional instrumentation transducers were used to measure steady-state engine operation and internal flow path performance. Because transient engine changes were slow enough that the necessary transducers could follow the changes satisfactorily, no special dynamic performance instrumentation was required. A photoelectric scanner (ref. 15) was used to monitor fan-blade-tip motions for possible aeromechanical instability.

Procedure and Data Recording

Steady-state tests. - The steady-state tests were performed with the engine running at constant referred speed. The engine VIGV, VEGV, and bleed valve positions, plus the waterbrake torque, were adjusted manually as desired. Performance data were averaged from several (usually 20) scans through the instrumentation list. Computed results are referred to the engine inlet plane just ahead of the VIGV.

Dynamic tests. - Some of the dynamic tests were performed with the engine control in the thrust mode, but most were performed in the shaft mode because that mode is more typical of rotorcraft operation. After steady-state data were taken to define the transient end points, the transient was performed with thrust command to the engine control and torque command to the waterbrake torque control. Both commands were generated by programmable facility controllers. The commands and selected performance data were recorded on magnetic tape and later digitized or played back on strip charts for analysis.

CEST TF34 TEST RESULTS AND DISCUSSION

The test results presented in this report were obtained on an outdoor static test stand and are referred (corrected) to sea-level-static, standard-day conditions at the engine inlet. Symbols used in this report are defined in an appendix.

Steady-State Tests

Data are shown for a referred fan speed N_{FR} of 90 percent, and are representative of performance for speeds of 70 to 100 percent. Complete test results are contained in reference 12.

Thrust and shaft power. - When the engine is running with no output shaft power, it is said to be operating in the turbofan mode; when it is running at limiting power-turbine inlet temperature $T_{4.5R,L}$, in the turboshaft mode; when it is running with both thrust and shaft power, in the dual power mode.

As shown in figure 8, at constant referred fan speed the shaft power in the turboshaft mode was greatest with the VIGV closed. As the limiting power-turbine inlet temperature $T_{4.5R,L}$ was reduced by decreasing fuel flow at any fixed VIGV position, the engine produced less shaft power when running in the dual power mode, but the thrust was reduced only slightly because the fan-tip flow and the speed were the same. In the turbofan mode the thrust was highest with the VIGV open. Although the thrust decreased as the VIGV closed, thrust never went to zero. Residual thrust was mainly from the core engine. The engine was stable as speed, output shaft power, and any of the variable engine hardware settings were changed. It ran smoothly in all modes, except for a small region of fan-tip aeromechanical instability at high VIGV closure and high fan speed. The instability is not considered to be a problem in a new VIGV type of convertible engine. Instability could be avoided by designs which either reduce the blade-tip aspect ratio or include part-span shrouds or dampers.

The success of these tests, the first for a VIGV convertible engine running in the dual power mode, demonstrated that this type of engine is suitable for applications needing both thrust and shaft power.

Power balance. - When the VIGV were closed, the fan was unloaded by changing the tip airflow and the inflow swirl. In the turboshaft mode as the VIGV were closed, airflow fell off until at full closure it was reduced by 90 percent (fig. 9). By design, some throughflow remained with the VIGV closed in order to cool fan-stage parts heated by churning. The fan-hub power was essentially constant as the airflow changed (fig. 10) because the speed was

steady and because the bleed valve was opened to keep hub flow constant at low power. The tip power fell off as the VIGV were closed to about 60 percent and then remained the same for further closure. The constant tip power, in view of the decreasing tip airflow, indicates worsening compression efficiency and more power lost in churning the tip airflow. With fully closed VIGV the tip wasted 23 percent of the turbine power in churning. Reduction in the churning loss would add to available shaft power. However, churning losses as large as those measured on the CEST TF34 may not be detrimental for high-speed rotorcraft applications in which engine size is determined by the thrust needed for cruise flight. As an example the power requirement for a conceptual X-wing is shown in figure 11. In rotary-wing flight this aircraft would use only 30 percent of the power that it needs for high-speed, horizontal, fixed-wing flight. An engine having performance like the CEST TF34 could easily meet this requirement.

Another way to view engine behavior is to consider a power balance for the engine running at constant fan speed in the dual power mode with partially closed VIGV. A typical power balance for this type of operation is shown in figure 12. Both the fan-hub and fan-tip powers were nearly constant as shaft power was raised (fig. 12) because both of those powers depend on speed and VIGV closure. Turbine power went up with shaft power, and $T_{4.5R,L}$ rose as fuel was added to provide this power. The turbine and hub powers are easily computed from component maps and cycle computer programs. When the tip power is computed (using known methods at open VIGV) or estimated (closed VIGV), the power balance is complete and engine performance is defined.

As discussed previously, the tip churning power loss is dependent on airflow and compression efficiency. Because of instrumentation limitations the efficiency reported in figure 13 is based on fan-inlet and fan-nozzle measurements and thus includes the pressure loss in the bypass ducting. With open VIGV the efficiency was good and was close to the value predicted analytically by the engine manufacturer. As the VIGV were closed, efficiency fell to nearly zero. The poor efficiency at high closure seems to be related to unusual fan airflow behavior. During testing it was observed that the fan pumped air radially outward when the VIGV were closed past about 75 percent, resulting in flow concentration along the fan-case wall and leading to high turbulence and recirculation in the duct behind the fan stage (ref. 12). The poor efficiency produced high tip outflow temperatures - values as high as 1.5 times the inlet temperature (as much as a 250 deg F rise) were measured.

Fan research tests reported in reference 6 were done with a VIGV/fan rotor/VEGV different from the CEST TF34 design. Several differences from the CEST performance were measured, including significantly lower churning power loss with closed VIGV. The lower loss was obtained with the VEGV closed also (not done with CEST), but the rotor-exit temperature reached almost 500 °F. Better understanding of fan flow behavior with closed VIGV might lead to designs that successfully reduce flow and churning loss without thermal or mechanical problems.

Specific fuel consumption. - For high-speed rotorcraft cruise flight a convertible engine would be run in the turbofan mode at low VIGV closure to produce high thrust, and thrust specific fuel consumption (SFC) would be most important. The test results (fig. 14) show that for this type of operation the thrust SFC was very nearly the same as that for the unmodified engine. The reason was that the only significant change in fuel use came from the inlet

pressure loss across the VIGV, which was small. The large rise in SFC at high VIGV closure was due to low thrust rather than to a sudden increase in fuel flow.

In the turboshaft mode only the output shaft power is used to compute power SFC. Because most of the fuel is used to produce thrust at low VIGV closure, the power SFC is very high. A convertible engine probably would not be operated in this way just to produce power; therefore the poor power SFC is of no real interest. As the VIGV were closed, more of the turbine power went to the shaft load, and the power SFC improved. The best power SFC was obtained with fully closed VIGV, but it was still not as good as that of modern shaft engines mainly because of tip churning loss. These characteristics probably would be acceptable for a high-speed rotorcraft in which high shaft power normally is needed only during takeoff and landing. For aircraft in which hover is a large portion of the mission, the convertible engine would use significantly more fuel than a conventional shaft engine.

In the dual power mode the definition of SFC is complicated because there is no general way to apportion total fuel between thrust and shaft power. Describing engine performance in terms of power-turbine SFC or block fuel used during a particular maneuver or mission would be satisfactory.

Noise. - Far-field noise was measured with conventional microphones. The noise spectra were dominated by tones at the fan-blade passing frequency (BPF) and its harmonics. The tone noise generally decreased as the VIGV were closed, as shown in figure 15 for the front hemisphere. The tone power was reduced 8 db for 77-percent VIGV closure (reduced to one-sixth its open-VIGV level). The overall power (OASPL) was reduced also, but not as much as the tone power. Similar results were obtained for the noise in the rear hemisphere. To an observer, the noise changed from a loud whining tone with the VIGV open (high-speed cruise operation) to a jet-like sound with much less discernible tones when the VIGV were closed.

The dominant tones at open VIGV were caused by the design of the CEST TF34 engine. It was a mature turbofan modified for research, and did not include features commonly used now to reduce noise. In a new convertible engine the tone noise could be lessened by increasing the spacings between the fan blades and the VIGV and VEGV vanes, and by choosing the numbers of vanes and blades to cut off spinning acoustic modes inside the engine.

Dynamic Tests

The dynamic tests were performed using the digital engine control system to control the VIGV, the VEGV, and the bleed valve and to hold fan speed constant when the engine was run in the shaft control mode.

Simulated rotorcraft maneuvers. - The engine was commanded to provide the estimated thrust and shaft power requirements at constant fan speed for several rotorcraft maneuvers (fig. 16). The requirements came from the X-wing study of reference 8 and included a takeoff with sufficient "thrust" for vector control. The X-wing conversion requirements were based on the same study but modified to account for loss of engine thrust due to inlet momentum at conversion speed. The resulting transient exercised the engine over the same core engine changes as conversion at 5000-ft altitude and 250 knots. All the tests, except gust

response, were done with control anticipation. The engine responded stably and effectively in every test (table I).

Thrust-step response. - Engine response (fig. 17) to a large thrust-command step was much quicker in the shaft control mode (speed constant; VIGV changing) than in the thrust control mode (VIGV locked; speed changing) because the fan did not have to accelerate. The data suggest that the response was limited only by the VIGV slewing rate. This attribute would be useful for thrust vector control but might require large actuators.

The dead time (~50 msec) between command input and VIGV action can be partially explained by hysteresis from mechanical wear in the VIGV actuation system and by digital data synchronization in the engine control system. Further investigation of this dead time was not possible within the scheduled test period.

Torque-step response. - The engine responded effectively to a large torque change (fig. 18). The waterbrake fulfilled the torque command in 1.5 seconds. Anticipation circuits in the engine control gave an initial fuel surge that caused overtorque in the power turbine and a consequent increase in speed. Then the speed control reacted to reduce fuel, resulting in speed droop. The speed overshoot was 2.6 percent, and the droop was 5.8 percent. These variations are within a range comparable to that of modern production shaft engines. The overshoot could be reduced by optimizing the anticipation circuitry gain, and the droop could be minimized by optimizing the fuel/speed loop gain.

MISSION ANALYSIS UPDATE

Previous mission analyses (e.g., refs. 1, 2, 10, and 11) have shown that convertible engines have installation and cost advantages over separate engines for lift and cruise in high-speed rotorcraft. Because these studies were done before convertible-engine test data were available, performance was based on analytical predictions. In this section some of the comparisons in the X-wing studies of reference 2 are updated with appropriate CEST TF34 test data. The new results confirm that convertible engines are better than separate engines but that the improvement in some areas is not as great as originally predicted.

Mission and aircraft. - The X-wing aircraft envisioned in reference 2 was a 48-passenger offshore oil rig crew transport. The baseline design and the economic missions analyzed are shown in figure 19. Propulsion was provided by two turboshaft engines for rotary-wing flight plus two turbofan engines for climb and cruise or by two VIGV convertible engines. All engines contained advanced technology features and were sized for sea-level hover with one lift engine inoperative. This amount of power enabled 400-knot cruise speed at 30 000-ft altitude. (The combined ability of one-engine hover and high-speed, high-altitude cruise is characteristic of X-wing and other low-disk-loading rotorcraft, as illustrated in fig. 11.)

Characteristics of the aircraft and the separate and convertible engines considered in the study are given in table II. With the convertible engines the craft is smaller and lighter because all the engines are about the same size, and only two engines are needed in contrast to four separate engines. The predicted churning loss shown in the middle row was only about half the

power estimated by scaling CEST TF34 data on the basis of open-VIGV fan-tip power at the same fan speed. The last row in table II shows the performance of convertible engines enlarged to account for the revised churning loss. To provide the same hover capability as the study engines, the revised engines have about 12 percent more turbine power and are scaled to be 10 percent heavier. The additional engine weight and fuel were counteracted by reducing the payload by four passengers. Thus the aircraft with revised engines has the same takeoff gross weight and fuel reserve capability as the study aircraft. This approach simplified the calculations and enabled better comparison with the study results. Also, it was assumed that the fans in the revised engines were larger to take advantage of the extra power available with open VIGV, giving a proportional thrust increase and higher cruise speed.

Fuel use. - For one-engine-inoperative (OEI) hover the convertible engine with VIGV closed uses less fuel than the separate engines (fig. 20) because the gross weight is less, even though the SFC is higher. For normal takeoff the advantage disappears because the SFC for the convertible engines is increased further as churning losses are doubled (same rotor speed and both engines now operating with closed VIGV with each having the same churning loss as the working engine in the OEI case), but total shaft power is about the same. In cruise the SFC is practically the same for each propulsion system (fig. 14(a)), but as described previously the smaller craft with convertible engines cruises at higher speed. The block fuel used for the whole economic mission (fig. 19) is about 11 percent less with the revised convertible engines. This is not as good as the 16 percent result in reference 2 for the convertible engines with lower churning losses.

Direct operating cost. - Comparison of direct operating cost (DOC) (fig. 21) is based on data from reference 2, but fuel costs were reduced to be more representative of expected 1990's costs and total DOC was increased for inflation since the study was made several years ago. As mentioned previously, the X-wing with revised convertible engines was assumed to carry 37 instead of 41 passengers in order to keep the same aircraft weight and reserve capability. Even with the lower payload the revised convertible-engine case showed 12 percent improvement over separate engines due to lower block fuel, less expensive airframe, fewer engines, and reduced maintenance.

CONCLUDING REMARKS

A convertible engine using variable inlet guide vanes (VIGV) to unload the fan aerodynamically was successfully tested on an outdoor test stand at the NASA Lewis Research Center. The tests demonstrated that this type of engine could be used for propulsion of new high-speed rotorcraft needing both thrust and shaft power. The engine might also be used to cross-couple the fans of a two-engine V/STOL aircraft, but the controls and dynamics for that application were not tested.

In the steady-state tests the engine was operated in the turboshaft, turbofan, and dual (combined fan and shaft) power modes. The engine ran smoothly except for a small region at high VIGV closure and high fan speed where fan-tip aeromechanical instability was found; otherwise, it was stable as speed, shaft power, and any of the variable hardware settings were changed. This instability is not considered to be a big problem for a new engine and could be avoided by changes in blade design.

For rotorcraft propulsion the engine would be used in the turboshaft or the dual power mode to drive a rotor for takeoff and low-speed flight. If thrust during takeoff is low, the VIGV would be closed and the engine fuel consumption would be about 25 percent more than that of a turbofan engine running at the same core power level. The additional fuel is needed because power is wasted in churning and heating the tip airflow with the VIGV closed. The wasted power is not detrimental to rotorcraft having engines sized for high-speed cruise, such as the X-wing, because the installed power would be great enough to permit one-engine inoperative (OEI) hover at sea level.

In high-speed cruise flight the engine would be operated in the turbofan mode with the VIGV open (or nearly open) to produce thrust or in dual power mode if shaft power is also needed for auxiliary equipment such as a compressor for X-wing blowing. The engine fuel consumption would be comparable to that of a conventional turbofan engine because the only change in fuel use comes from the inlet pressure loss across the VIGV. The loss is small when the VIGV are nearly open.

In dynamic performance tests with a specially built digital engine control system and using a waterbrake dynamometer for shaft load, the engine easily handled large torque and thrust command steps, as well as simulated flight maneuvers. The fastest thrust step was made by changing the VIGV closure at constant fan speed; in this control mode the response seems to be limited only by the VIGV slewing rate and would be useful for thrust vector control. During a large torque step the speed droop was 5.8 percent, which is comparable to the droop shown by production turboshaft engines. Simulated takeoff, X-wing conversion, and collective pitch change maneuvers were performed successfully with control anticipation, and response to a simulated gust load was performed successfully without anticipation.

When the analysis of an X-wing capable of OEI sea-level hover and 400-knot cruise at 30 000-ft altitude was revised to account for higher churning power loss, the required engine power increased by about 12 percent. With the larger engines the improvement in block fuel use and direct operating cost over that for separate lift and thrust engines was 11 and 12 percent, respectively. These results were calculated for a mission requiring engine operation with closed VIGV mainly during takeoff and landing; improvement would be less if the mission included additional hover time, and more if the fan-tip churning power loss was reduced.

Engine performance was predictable with conventional analytical techniques and computer cycle programs, except for the fan-tip churning power loss with the VIGV closed. The experimental data showed about twice the power loss expected in a previous study, probably because of unusual fan-stage flow behavior at high VIGV closure. Other reported test results measured less churning loss with a VIGV/fan rotor/VEGV different from the CEST design; however, rotor-exit temperature was very high. Better understanding of fan flow behavior with closed VIGV might lead to reduction of churning loss without other problems.

APPENDIX - SYMBOLS

F	engine gross thrust, ¹ lb
F _R	referred engine gross thrust, ¹ F/δ
NF	fan, power-output-shaft, and power-turbine speed, percent of rated speed
NF _R	referred fan, power-output-shaft, and power-turbine speed, NF/ θ, percent of rated speed
PWSD	output shaft power, hp
PWSD _R	referred output shaft power, PWSD/δ θ
T	temperature, °R
T4.5	power-turbine inlet total temperature, °R
T4.5 _R	referred power-turbine inlet total temperature, T4.5/(θ) ^{0.84}
T4.5 _{R,L}	upper limit of power-turbine inlet total temperature for standard TF34 engine, °R
WA12	fan-tip airflow, lb/sec
WA12 _R	referred fan-tip airflow, WA12 θ/δ
WF	fuel flow rate, lb/hr
WF _R	referred fuel flow rate, WF/δθ
δ	ratio of pressure to 14.696 psi
θ	ratio of temperature to 518.7 °R

¹Called "gross thrust" because, by convention with the TF34 engine, the reported thrust is net (measured in test stand) thrust plus calculated core cowl scrubbing drag.

REFERENCES

1. Eisenberg, J.D.: Rotorcraft Convertible Engines for the 1980's. NASA TM-83008, 1982.
2. Goldstein, D.N.; Hirschcron, R.; and Smith, C.E.: Rotorcraft Convertible Engine Study. (R83AEB047, General Electric Company; NASA Contract NAS3-22743.) NASA CR-168241, 1983.
3. Abdalla, K.L.; and Brooks, A.: TF34 Convertible Engine System Technology Program. American Helicopter Society. 38th Annual Forum, AHS, 1982, pp. 163-169.
4. Quiet Clean Short-Haul Experimental Engine (QCSEE) Under-the-Wing (UTW) Engine Composite Nacelle Test Report. Vol. 1, (R78AEG573-Vol. 1, General Electric Company; NASA Contract NAS3-18021.) NASA CR-159471, 1979.
5. Schaefer, J.W.; Sagerser, D.A.; and Stakolich, E.G.: Dynamics of High-Bypass-Engine Thrust Reversal Using a Variable-Pitch Fan. NASA TM X-3524, 1977.
6. Wright, D.L.; and Jones, B.A.: Convertible Fan/Shaft Engine Variable Fan Geometry Investigation. USAAVLABS-TR-70-28, PWA-FR-3567, Pratt & Whitney Aircraft, 1970.
7. Bobula, G.A.; Soeder, R.H.; and Burkardt, L.A.: Effect of a Part-Span Variable Inlet Guide Vane on the Performance of a High-Bypass Turbofan Engine. AIAA Paper 81-1362, July 1981.
8. Williams R.M.; and Boyd, T.H.: Preliminary X-Wing Characteristics and Propulsion Interface Document. DTNSRDC/TM-16-81/06, David W. Taylor Naval Ship Research and Development Center, May 1981.
9. Biggers, J.C.; and Linden, A.W.: X-Wing - A Low-Disc-Loading V/STOL for the Navy. SAE Paper 851772, Oct. 1985.
10. Gill, J.C. Earle, R.V.; and Mar, H.M.: Rotorcraft Convertible Engine Study. (DDA-EDR-10978, Detroit Diesel Allison; NASA Contract NAS3-22742.) NASA CR-168161, 1982.
11. Eisenberg, J.D.; and Bowles, J.W.: Folding Tilt Rotor Demonstrator Feasibility Study. American Helicopter Society, 42nd Annual Forum, Vol. 2, AHS, 1986.
12. McArdle, J.G.; Barth, R.L., and Burkardt, L.A.: Steady-State Performance of a Turbofan/Turboshaft Convertible Engine with Variable Inlet Guide Vanes. NASA TP-2673, 1987.
13. Lindsay, H.: TF34 Convertible Engine System Technology Program. NASA CR-179453, 1986.
14. Gilmore, D.D., Jr.: TF34 Convertible Engine Control System Design. American Helicopter Society, 40th Annual Forum, AHS, 1984, pp. 609-620.
15. Nieberding, W.C.; and Pollack, J.L.: Optical Detection of Blade Flutter ASME Paper 77-GT-66, Mar. 1977.

TABLE I. - CEST TF34 ENGINE RESPONSE TO SIMULATED ROTORCRAFT
MANEUVERS SHOWN IN FIGURE 15

Maneuver	Command time, sec	Shaft power	Thrust	Speed overshoot, percent	Speed droop, percent
		Time from start to reach 95 percent of level, sec			
Takeoff	1.8	2.2	---	3.6	5.1
Takeoff with maximum vector control	1.8	2.1	2.6	1.4	5.2
Collective pitch	1.0	1.0	1.0	3.5	2.7
Unanticipated gust	.15	.5	.5	1.3	0
X-wing conversion	18.0	(a)	(a)	0	0

^aFollowed commands.

TABLE II. - CONCEPTUAL 48-PASSENGER X-WING OIL CREW TRANSPORT (REFERENCE 2)

[Aircraft sized for 600-n mi still-air range and cruise at 30 000-ft altitude; engines sized for sea-level hover, ISA + 27 °F ambient temperature, and one lift engine inoperative; rotary-wing disk loading, 15 lb/ft² at sea level.]

	Aircraft gross weight, lb	Fan-tip churning power loss at sea level with closed VIGV, hp	Sea-level hover, ISA + 27 °F, OEI		Sea-level takeoff, ISA day	Cruise at 30 000 ft, ISA day	Cruise airspeed, kn	Passenger load for economic mission study (see fig. 18)
			Engine output, shaft hp plus 1b thrust					
Separate lift and cruise engines (two of each; from ref. 2)	51 869	----	11 960 + 1d1e TF	5610 + 1d1e TF		340 + 2600 TF	400	41
VIGV convertible engines (two, from ref. 2)	43 950	1075	a9945 + 1630	a4670 + 960		b300 + 2280	400	41
VIGV convertible engines (two, from ref. 2, but with tip loss increased per CEST TF34 data	43 950	2460	a9945 + 1830	a4670 + 1150		b300 + 2550	c420	37

aVIGV closed.

bVIGV closure, ~8 percent.

cEstimated.

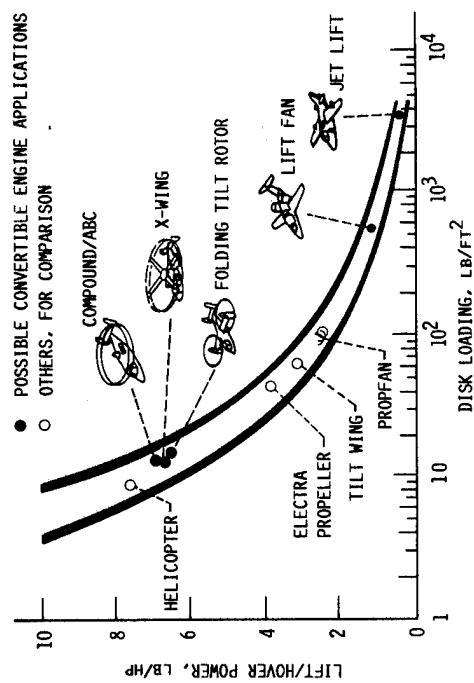


FIGURE 1.- AIRCRAFT THAT COULD USE CONVERTIBLE ENGINES. (DATA FROM REFS. 10 AND 12.)

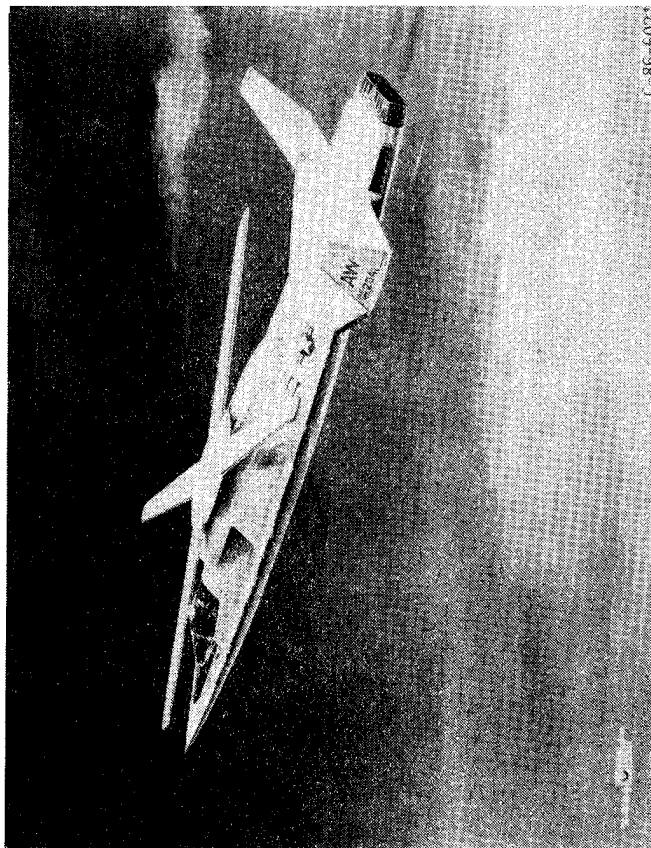


FIGURE 2.- CONCEPTUAL X-WING ROTORCRAFT WITH CONVERTIBLE ENGINES.

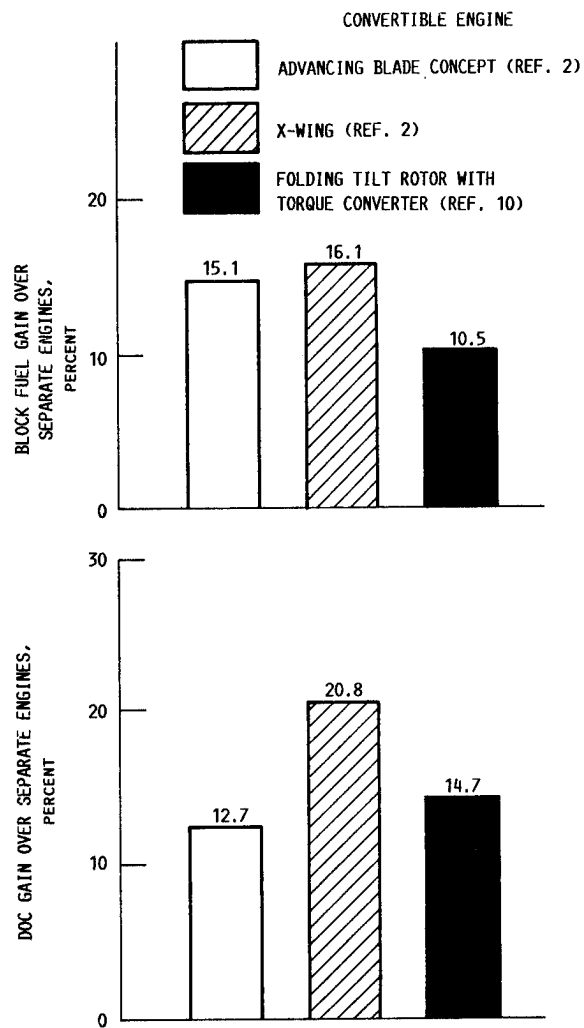


FIGURE 3. - DIRECT OPERATING COST (DOC) AND BLOCK FUEL GAINS WITH CONVERTIBLE ENGINES.

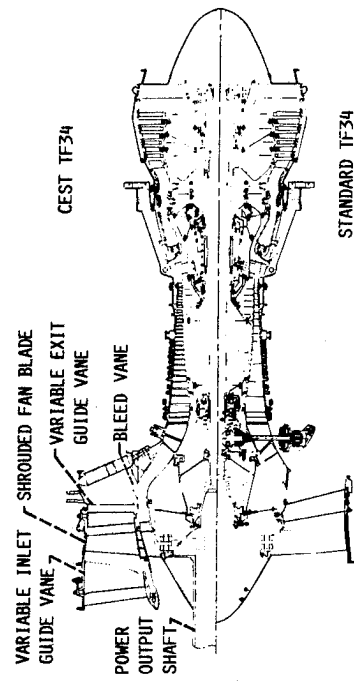


FIGURE 4.- TF34 CONVERTIBLE ENGINE COMPARED WITH STANDARD TF34 ENGINE.

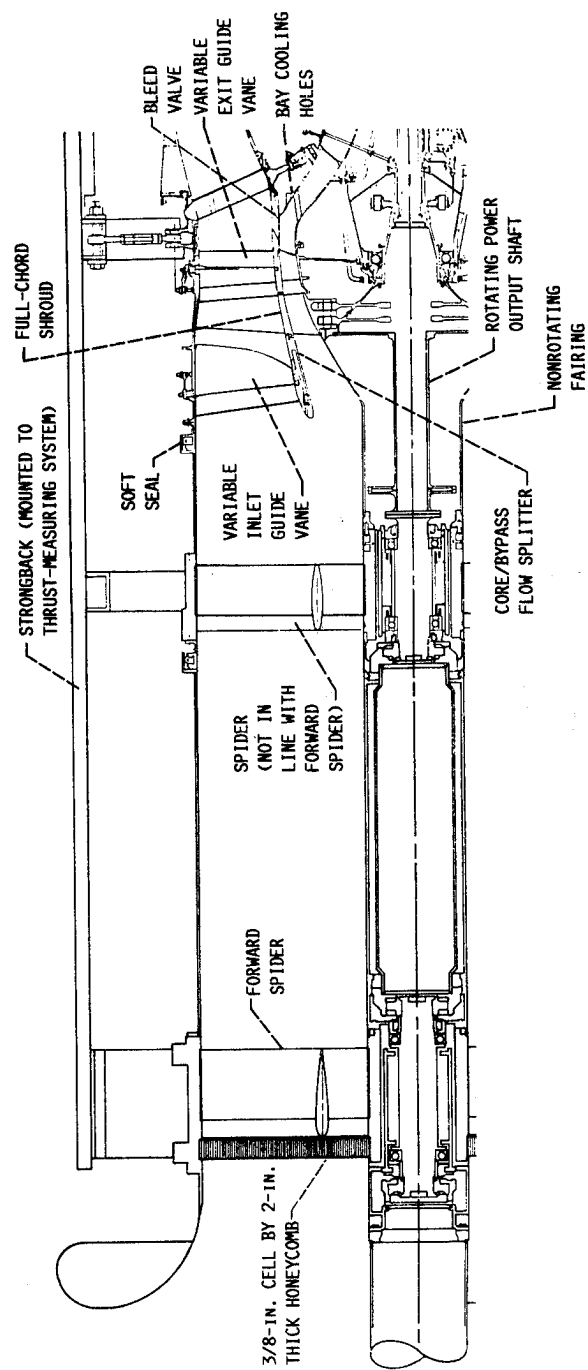


FIGURE 5.- CEST TF34 DESIGN FEATURES.

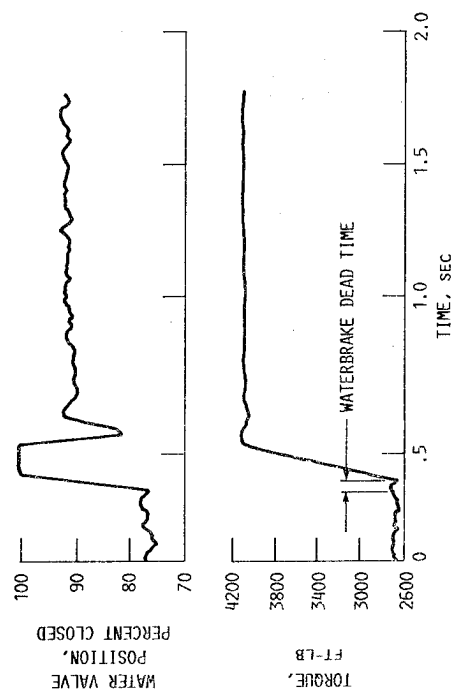


FIGURE 6.- CLOSED-LOOP RESPONSE OF WATERBRAKE TORQUE CONTROL SYSTEM TO STEP CHANGE. INITIAL FAN SPEED, NF, 85 PERCENT; CONSTANT ENGINE FUEL FLOW.

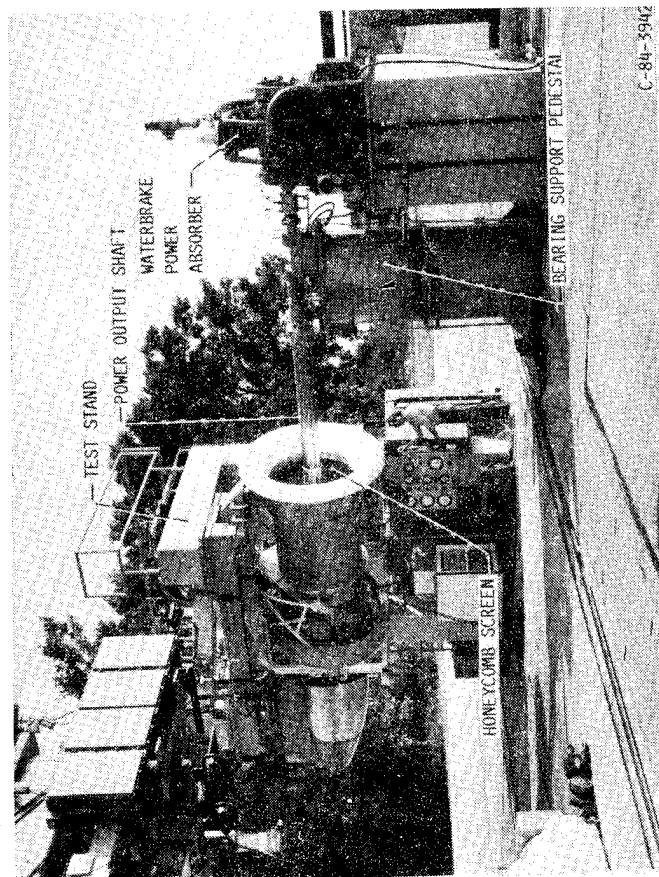


FIGURE 7.- CEST TF34 CONVERTIBLE ENGINE ON TEST STAND

C-84-3942

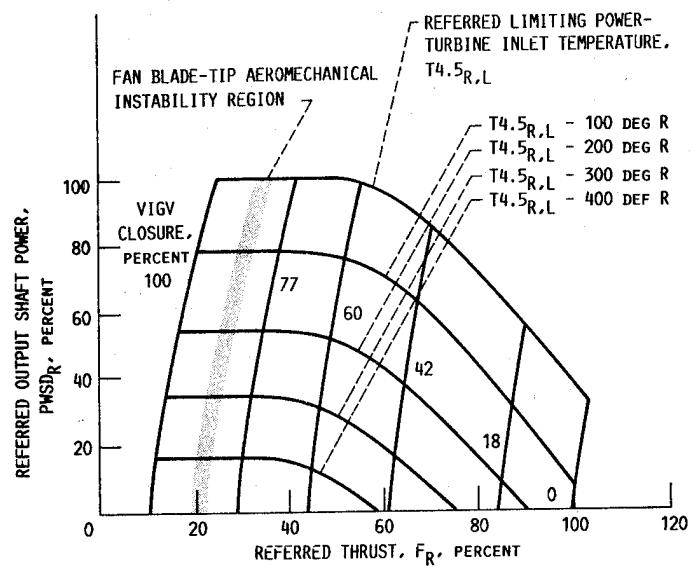


FIGURE 8. - SEA-LEVEL-STATIC PERFORMANCE OF CEST TF34 ENGINE.
REFERRED FAN SPEED, N_{FR} , 90 PERCENT.

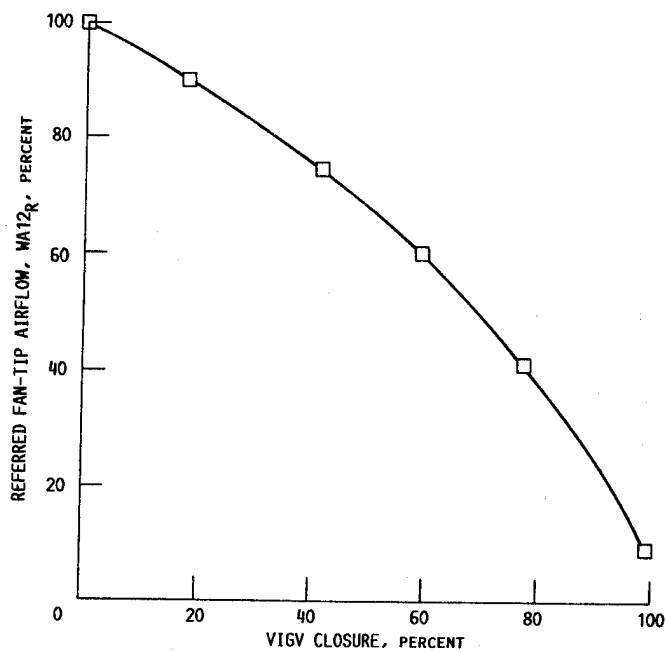


FIGURE 9. - FAN-TIP AIRFLOW IN TURBOSHAFT MODE. REFERRED FAN
SPEED, N_{FR} , 90 PERCENT.

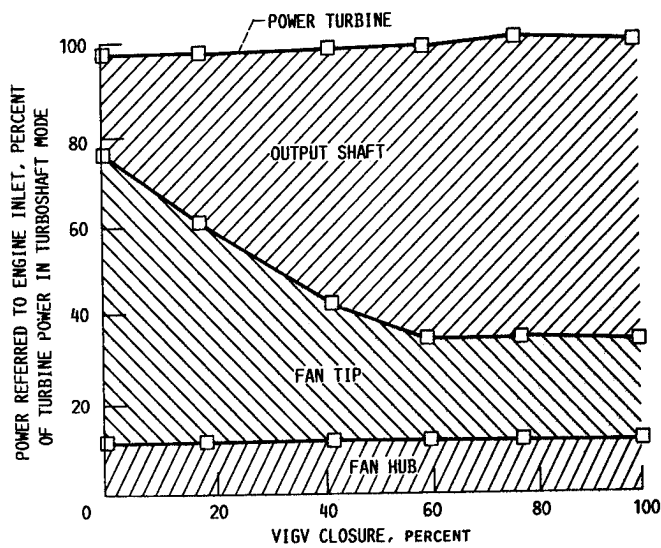


FIGURE 10.- POWER BALANCE IN TURBOSHAFT MODE. REFERRED FAN SPEED, N_{FR} , 90 PERCENT.

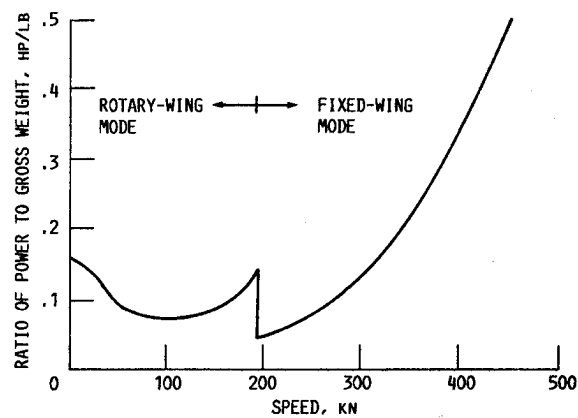


FIGURE 11.- POWER REQUIRED FOR CONCEPTUAL X-WING AIRCRAFT. (FROM REF. 9.) SEA-LEVEL STANDARD CONDITIONS.

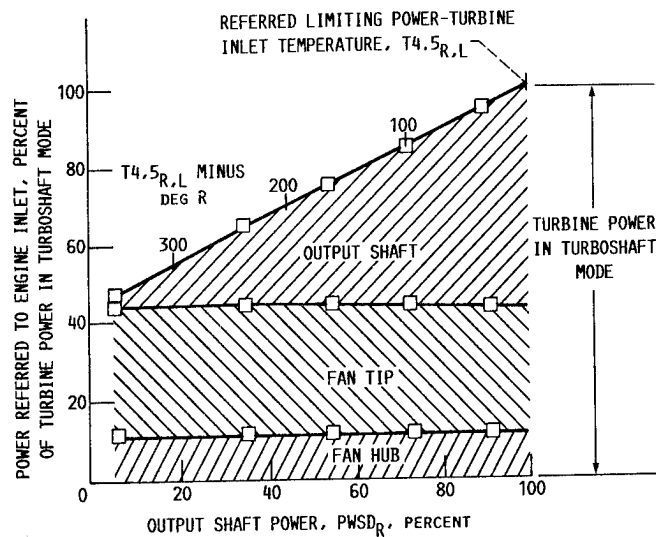


FIGURE 12.- TYPICAL POWER BALANCE IN DUAL POWER MODE. REFERRED FAN SPEED, N_{FR} , 90 PERCENT; VIGV CLOSURE, 42 PERCENT.

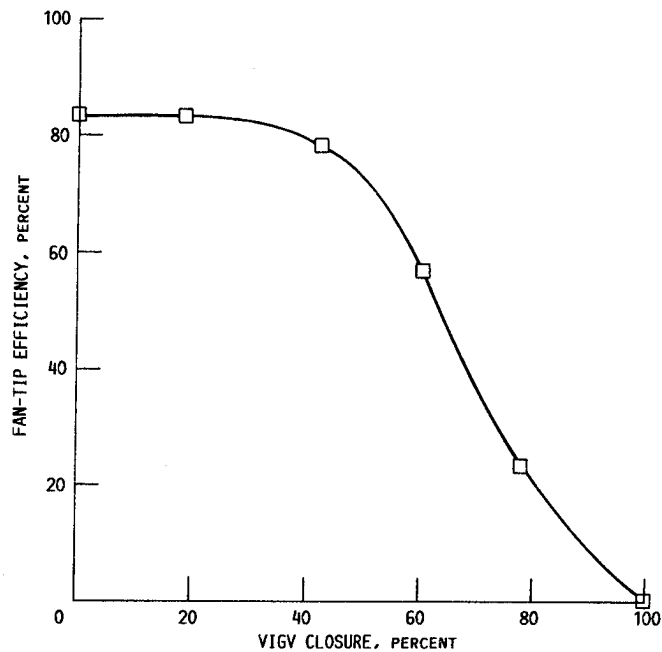


FIGURE 13.- FAN-TIP ADIABATIC COMPRESSION EFFICIENCY BASED ON FAN-INLET AND FAN-EXHAUST NOZZLE MEASUREMENTS. REFERRED FAN SPEED, N_{FR} , 90 PERCENT.

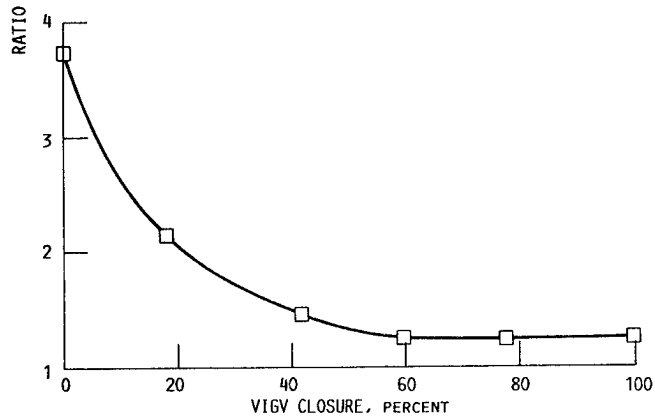
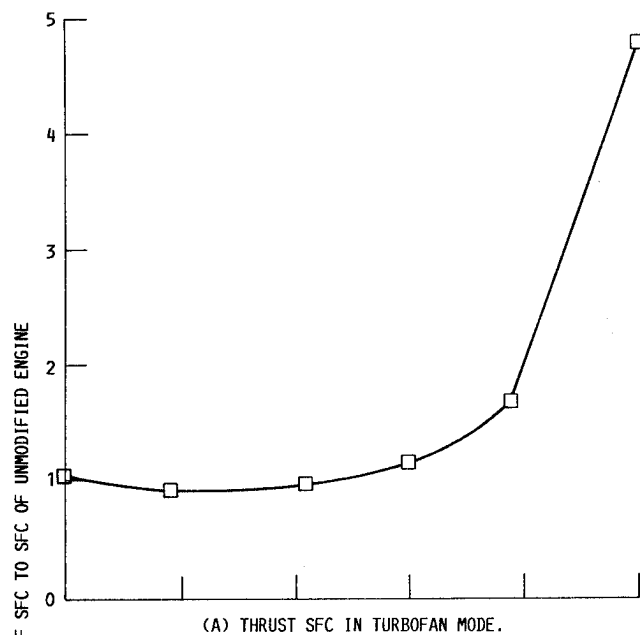


FIGURE 14.- SEA-LEVEL STATIC SPECIFIC FUEL CONSUMPTION (SFC). REFERRED FAN SPEED, N_{FR} , 90 PERCENT.

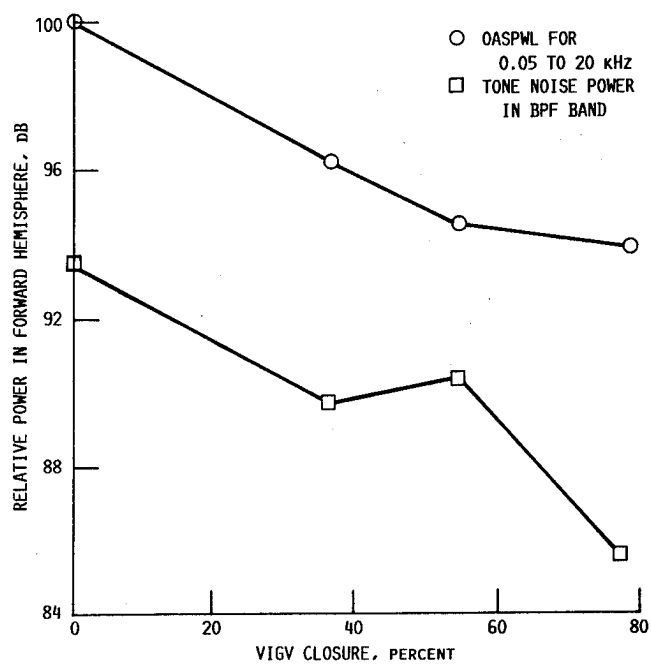


FIGURE 15. - STANDARD-DAY, FREE-FIELD, 100-FT-RADIUS NOISE POWER IN FORWARD HEMISPHERE. REFERRED FAN SPEED, N_{FR} , 94 PERCENT.

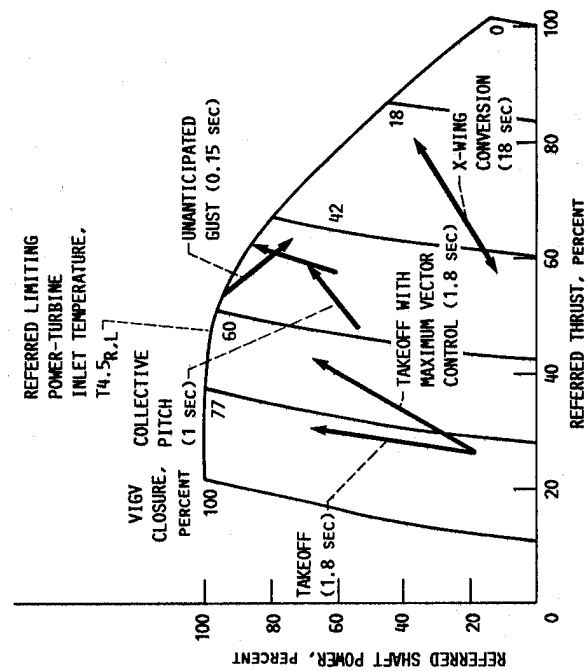


FIGURE 16.- SIMULATED ROTORCRAFT MANEUVERS TESTED WITH CEST TF34 ENGINE AND CONTROL SYSTEM. REFERRED FAN SPEED, M_R , 95 PERCENT; TIMES SHOWN ARE COMMANDED TIMES.

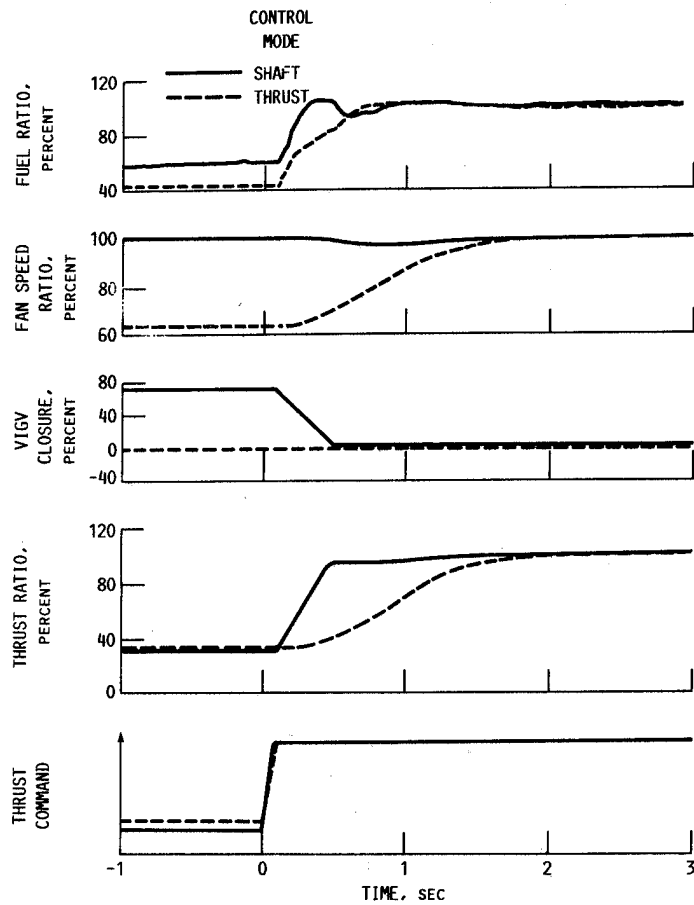


FIGURE 17. - ENGINE RESPONSE TO LARGE THRUST COMMAND STEPS IN SHAFT AND THRUST CONTROL MODES. CONSTANT POWER OUTPUT SHAFT TORQUE; FINAL REFERRED SHAFT POWER, P_{WSDR} , 21 PERCENT; FINAL REFERRED FAN SPEED, N_{FR} , ~95 PERCENT. RATIOS SHOWN AS PERCENT OF FINAL VALUES.

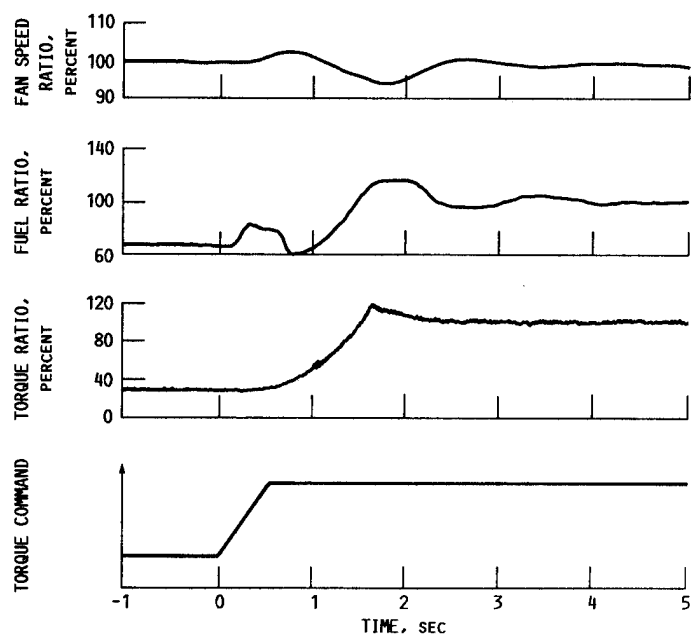
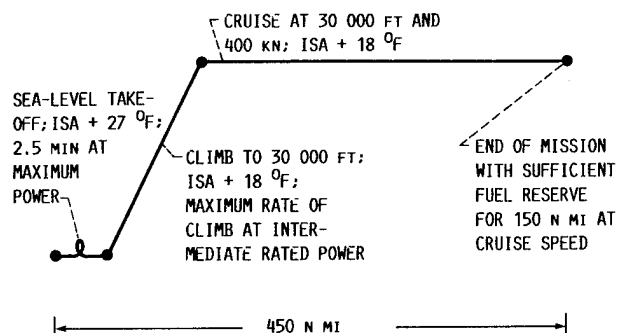
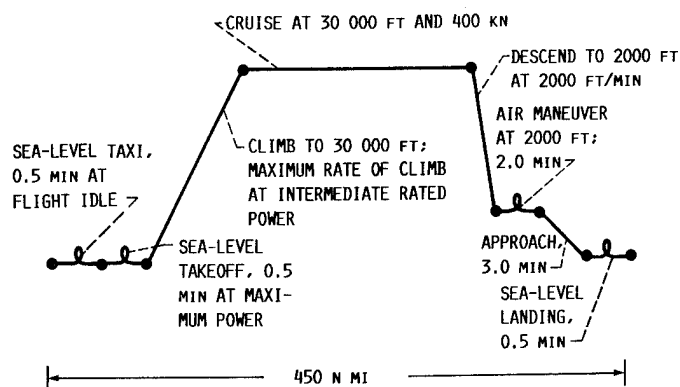


FIGURE 18.- ENGINE RESPONSE TO LARGE POWER OUTPUT SHAFT TORQUE CHANGE. ENGINE CONTROL IN SHAFT MODE; VIGV CLOSURE, 77 PERCENT; REFERRED FAN SPEED, W_{F_R} , AT END OF TRANSIENT, 95 PERCENT. RATIOS SHOWN AS PERCENT OF FINAL VALUE.



(A) BASELINE DESIGN MISSION PROFILE FOR AIRCRAFT SIZING.



(B) MISSION PROFILE FOR ECONOMIC ANALYSIS. LOAD FACTOR, 85 PERCENT (41 PASSENGERS IN 48-SEAT AIRCRAFT). ISA AMBIENT CONDITIONS.

FIGURE 19.- MISSION PROFILES FOR CONCEPTUAL X-WING AIRCRAFT ANALYZED IN REFERENCE 2.

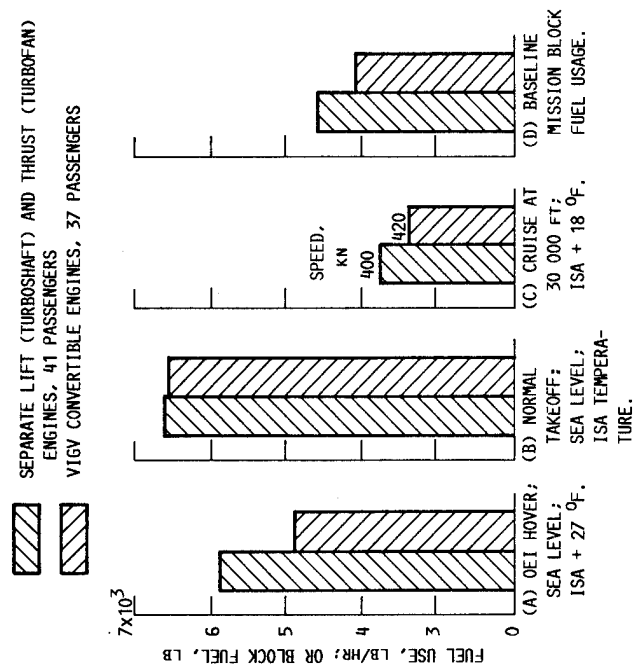
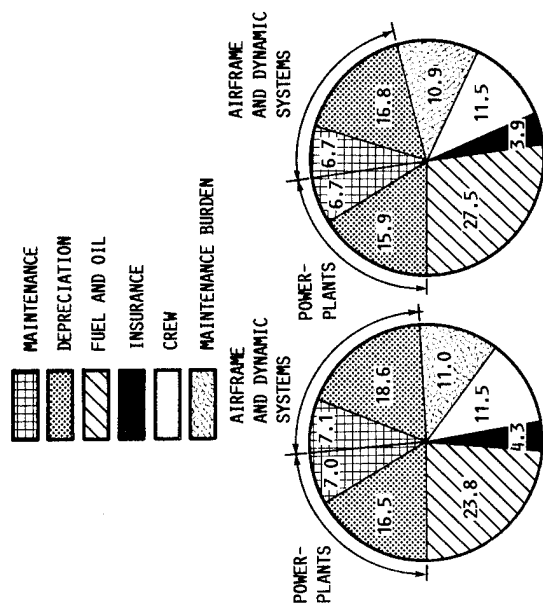


FIGURE 20.- FUEL USAGE FOR 48-SEAT X-WING OIL CREW TRANSPORT. (FROM REF. 2, BUT TIP POWER LOSS FOR CONVERTIBLE ENGINES INCREASED PER CEST TF34 TEST DATA.)



(A) SEPARATE LIFT AND THRUST (B) VIGV CONVERTIBLE ENGINES;
 ENGINES; DOC, 17.58¢/SEAT - DOC, 15.46¢/SEAT - N MI
 N MI (41 PASSENGERS). (37 PASSENGERS).

FIGURE 21.- DIRECT OPERATING COST (DOC) FOR 48-SEAT X-WING OIL
 CREW TRANSPORT. 450-N MI ECONOMIC MISSION; ISA STANDARD DAY;
 \$1.30/GAL FUEL COST; 1986 DOLLARS. (FROM REF. 2; VALUES IN
 PERCENT.)

RESULTS OF NASA/ARMY TRANSMISSION RESEARCH

John J. Coy
Propulsion Directorate
U.S. Army Research and Technology Activity - AVSCOM
Lewis Research Center
Cleveland, Ohio 44135

and

Dennis P. Townsend and Harold H. Coe
National Aeronautics and Space Administration
Lewis Research Center
Cleveland, Ohio 44135

SUMMARY

Since 1970 the NASA Lewis Research Center and the U.S. Army Aviation Systems Command have shared an interest in advancing the technology for helicopter propulsion systems. In particular, this paper outlines that portion of the program that applies to the drive train and its various mechanical components. The major goals of the program were (and continue to be) to increase the life, reliability, and maintainability, reduce the weight, noise, and vibration, and maintain the relatively high mechanical efficiency of the gear train. Major historical milestones are reviewed, significant advances in technology for bearings, gears, and transmissions are discussed, and the outlook for the future is presented. The reference list is comprehensive.

INTRODUCTION

Since 1970 the NASA Lewis Research Center and the U.S. Army Aviation Systems Command have shared an interest in advancing the technology for helicopter propulsion systems. In particular, this paper outlines the aspect of that program that applies to the drive train and its various mechanical components.

The NASA Lewis Research Center has had a strong research program for aircraft mechanical components since the early 1940's. A program for rolling element bearing technology for turbine engine application was built up during the 1950's and 1960's. Since many high-bypass turbine engines have a geared fan, in 1969 Lewis began a technology program for gear materials endurance. Meanwhile, during the period from the late 1940's to the late 1960's, the helicopter came into wide use as an Army air mobile vehicle. In 1970 the common interest of the Army and Lewis was recognized. The Army had a wide spectrum of helicopters in its inventory along with the requirement to increase their performance and NASA Lewis had established a capability in mechanical component research that could be applied to helicopter transmissions. A joint program was undertaken in 1970.

The major goals of the program were (and continue to be) to increase the life, reliability, and maintainability, reduce the weight, noise, and vibration, and maintain the relatively high mechanical efficiency of the gear train.

The purpose of this paper is to review and summarize the most significant results of the NASA/Army work on helicopter transmission technology. The major historical milestones are reviewed; significant advances in technology for bearings, gears, and transmissions are discussed; and the outlook for the future is presented. The reference list does not include every publication from the research that was completed, but it is comprehensive in that several of the cited references are themselves overview summary reports, and sources of complete listings of references at the time of their publication (refs. 1 to 5).

PROGRAM OVERVIEW

Mechanical Components Research

During the 1950's and 1960's NASA Lewis conducted research programs in mechanical components. Special attention was directed to bearings, seals, shafting, and lubricants for gas turbine engines, and space applications such as generators and launch vehicle components. Gear research began at NASA Lewis late in the 1960's and the Gear Fatigue Test Rigs were constructed. The work on gearing concentrated on materials and lubricants investigations and established a unique data base to be used for life prediction in aviation applications. In 1970 the Army Aviation Propulsion Laboratory of the Aviation Systems Command (AVSCOM) was established at NASA Lewis, and a joint NASA/Army program in mechanical components was initiated.

NASA Helicopter Transmission Program

In 1977 NASA began a 6-yr, 7 million dollar program for helicopter transmission research for civilian and military helicopters. The program was coordinated with the Army and supported goals for major advances for transmissions in the following categories (fig. 1): (1) Life, Reliability, and Maintainability, (2) Weight, and (3) Noise and Vibration.

Significant achievements were made in advancing mechanical component and transmission system technology in the ensuing 6 yr. Advanced gear materials and lubricants were identified, unique test facilities for mechanical components and transmissions were constructed, a baseline of current technology was established, and existing designs were studied to determine power densities. Advanced technology for materials, lubricants, and components were integrated into an upgraded design for the OH-58 transmission to demonstrate the benefits inherent in such an approach. In addition, advanced transmission concepts were explored including traction drive, self-aligning bearingless planetary, and split torque. Several of those transmissions were built for test and evaluation using the NASA Lewis test stands.

During the 6-yr program on transmissions, an effort was begun in developing computer programs for component and system analysis for transmissions. The technical advances are discussed later in this paper.

Current and Future Direction

Presently, the NASA program in helicopter transmission is emphasizing noise reduction technology. There is a small base effort in gearing

technology, consisting mainly of in-house research projects in lubrication, cooling, and materials. The noise reduction program is discussed in a companion paper presented in the session on helicopter noise.

An in-house and university grant effort continues to develop computer programs for analysis and design of transmission systems. The unique facilities and hardware resulting from the 6-yr program are being used to collect data to validate existing computer codes and subroutines for transmission system analysis is being assembled. The goal is to develop a comprehensive computer program library for transmission system modeling (fig. 2).

An important new initiative in transmissions by the Army will be conducted through the Propulsion Directorate, Aviation Research and Technology Activity (ARTA). A 5-yr program will begin in 1987 to develop advanced concept demonstrator transmissions for two categories of helicopters, the Advanced Cargo Helicopter (ACA), and the Future Attack Rotorcraft (FAX). The program will parallel the concept offered by engine demonstrator programs, and provide a way for the industry to develop advanced concepts and designs well in advance of critical needs. This is the first demonstrator program for transmissions. By request of the Assistant Secretary of the Army for Research, Development, and Acquisition, the program will address the issues of weight, noise, and reliability. The goals are to reduce weight by 25 percent, noise by 10 dB, and increase the meantime between removals (MTBR) to 5000 hr. The transmission program will build on the strong technology base from the joint NASA/Army programs as well as NASA's noise reduction research.

SIGNIFICANT TECHNICAL ADVANCES

Transmission Data Base Established

An extensive data base has been established for two sizes of helicopter transmissions (refs. 6 to 10). The Army's UH-60 Blackhawk transmission (fig. 3) has been run in the NASA Lewis test stand to determine thermal, vibration, stress, and efficiency information for a matrix of operating conditions. Figure 4 shows the measured efficiency as a function of input power, rotor speed, and oil inlet temperature. This information is being used to compare with computer code predictions for code validation and to provide a baseline from which to assess the promised advantages of future designs and concepts. Information of a similar nature and purpose was collected for the OH-58 transmission. The NASA Lewis test stands are currently operational and available for use in experimental transmission work.

Gear Materials Technology

The heavy load and speed condition of helicopters and turboprop gearing require materials that have high strength and improved fatigue life at elevated temperatures. Several advanced gear materials and processes have been evaluated and they show promise for improved transmission (refs. 11 to 13).

Figure 5 shows the fatigue life obtained with four advanced materials or processes in comparison with baseline AISI 9310 gear steel. In each case a life improvement resulted.

The standard AISI 9310 gear fatigue life was improved by 60 percent (fig. 5) through shot peening of the gear flanks (ref. 11). The shot peening increased the subsurface residual compressive stress resulting in increased surface fatigue life.

Three high temperature materials have been evaluated for surface life and endurance at heavy test load and moderate speed conditions. The CBS 600 material maintains its hot hardness to 500 °F and has shown an improved fatigue life over that for AISI 9310 (ref. 12). The CBS 600 has good fracture toughness and is a good gear material for aircraft use.

The Vasco X-2 material retains its hardness to 600 °F and has shown improved fatigue life over AISI 9310 when it has been heat treated under very closely controlled conditions (ref. 12). Because the Vasco X-2 has a high chromium content it is very difficult to carburize and harden which means that high standards of quality control are required for aircraft applications. It also has a modest fracture toughness and can be subject to tooth breakage, precipitated at a fatigue spall.

The EX-53 gear material has shown the largest improvement in fatigue life (ref. 13). It has a fatigue life more than twice that of AISI 9310 and has very good fracture toughness. The EX-53 material has a temperature limit of 450 °F which limits its use for some high temperature applications.

Gear Lubricant Evaluation

Spur gear surface fatigue tests were conducted with five lubricants using a single lot of consumable-electrode vacuum melted (CVM) AISI 9310 spur gears. The gear were case carburized and hardened to Rockwell C 60. The gear pitch diameter was 8.89 cm (3.5 in.). The lot of gears was divided into five groups, each of which was tested with a different lubricant. The test lubricants can be classified as either a synthetic hydrocarbon, mineral oil, or ester-based synthetic lubricant. All five lubricants have similar viscosity and pressure-viscosity coefficients. Test conditions included a bulk gear temperature of 350 K (170 °F), a maximum Hertz stress of 1.71 GPA (248 000 psi) at the pitch line, and a speed of 10 000 rpm. A pentaerythritol base-stock without sufficient antiwear additives (lubricant C) produced a 10-percent surface fatigue life that was approximately 22 percent that of a pentaerythritol base stock of the same viscosity with chlorine and phosphorus type additives (fig. 4), (refs. 14 and 15). The presence of a sulfur type antiwear additive in the lubricant did not appear to affect the surface fatigue life of spur gears at the conditions tested. No statistical difference in the 10-percent surface fatigue life was produced, with four of the five lubricants having similar viscosity and pressure-viscosity coefficients and various antiwear additives.

These same lubricants and seven additional ones were run in an OH-58 transmission to determine the effect of lubricant type on mechanical efficiency. The efficiency varied between 98.3 and 98.8 percent (ref. 8). In a separate study, the chemical and physical properties were determined for the 11 lubricants used (ref. 16).

Gear Thermal Behavior

Experimental testing and theoretical analysis have been conducted to determine optimum methods for gear lubrication and cooling. High-speed photography was used to study oil jet impingement depths for into-mesh, out-of-mesh, and radial oil jets (fig. 7). These were compared with analytical predictions of oil jet impingement depths. The analysis and tests show that there is limited impingement depth for into-mesh and out-of-mesh lubrication while radial jet lubrication with adequate oil jet pressure can provide maximum cooling and lubrication for gears (refs. 17 to 20). A thermal analysis was also performed and experimental verifications made which show the superior effect of radial oil jet lubrication and cooling.

Gear Geometry

Gear geometry has been investigated (refs. 21 to 31). High contact ratio gears were examined as a means to improve the surface fatigue life, scoring load capacity, and power-to-weight ratio of transmissions. High contact ratio gears (HCRG) have at least two pairs of teeth in contact at all times, whereas standard (low) contact ratio gears (LCRG) have between one and two pairs in contact. Because the transmitted load is shared by at least two pairs of teeth, the individual tooth loading is less for HCRG than for LCRG designs, thereby enabling a higher power-to-weight ratio. HCRG, however requires finer pitches, or increased working depths; all of which tend to increase the tooth bending stress. In addition, it is expected that HCRG is more sensitive to tooth spacing errors and profile modifications because of the simultaneous tooth contacts. The basic problem to be resolved was whether the lower tooth loads occurring in the high contact ratio design more than offset the effects of the weakened tooth form, especially when run under dynamic load conditions. The investigation revealed that HCRG designs have twice the fatigue life of LCRG designs and slightly better scoring resistance. Therefore HCR gears can significantly increase life, reliability, and power-to-weight ratio for helicopter transmission (ref. 22).

Special attention has been directed to understanding the nature of the contact zone between gear teeth (fig. 8) (refs. 23 to 29). The contact between spiral bevel gears has been especially difficult to model because there are no equations with which one may represent the contact geometry; it must be developed numerically with a computer, based on the settings of the machine used to manufacture the gears. The contact geometry is essential to predicting the life, lubrication effects, and stress for spiral bevel gears. Kinematic errors have been identified as a contributor to gear mesh vibration (ref. 23). Kinematic errors are the time varying deviations from a constant gear ratio during gear rotation (fig. 9). A method for eliminating these errors has been developed (ref. 28) but the method still needs to be verified by experimental testing. These zero kinematical error gears have potential for reducing gear noise.

Straight and involute tooth shapes have been examined to determine the effect of speed on the stress and deflection of the teeth (ref. 30). The results of this analysis provide a criterion for defining the high-speed regime of operation for gears, where special analysis must be employed to predict dynamic loads. In reference 31, a procedure is given for designing minimum noise gears (spur gears), using a novel frequency domain approach.

Bearing Technology

Progress in bearing technology is reported in references 32 to 41. Advances in materials and lubrication techniques have increased speed capacity, load capacity, and fatigue life.

The development of fracture tough bearing steels has increased the fatigue life of bearings (refs. 36 and 37). Without fracture tough steel, the hardened races of the bearings are too sensitive to crack propagation from fatigue nucleation sites. The M 50 NiL steel (ref. 37) is fracture tough but there is a continuing need for more corrosion resistance.

Lubrication techniques have been improved so that the bearing contacts are not starved and the bearing is properly cooled. This has lengthened the fatigue life and decreased wear as well as increased cooling of the bearing to enable high-speed operation (refs. 33 and 38 to 41).

The design and lubrication of large bore tapered-roller bearings for operation at speeds up to 2.4 million DN under combined radial and thrust loads has been demonstrated (ref. 41). (DN is a speed parameter equal to the product of shaft speed in rpm and diameter in millimeters.) The advanced bearing ran with less heat generation and ran cooler than the baseline bearing to which it was compared (fig. 10). It was also capable of higher speed operation--20 000 rpm compared to 15 000 rpm for the baseline bearing. In fatigue tests, four advanced bearings ran to 24 times rated catalog life without failure.

Tapered roller bearings offer advantages in reducing the total number of parts in a transmission. Often, several ball bearings and roller bearings can be replaced with tapered roller bearings (fig. 11). The reduction in parts count translates into increased reliability, but tapered roller bearings are sensitive to lack of adequate lubrication, especially at the roller ends that contact the ribs on the races. Research continues on tapered roller bearings to meet vulnerability resistance tests requiring 30 min of operation after loss of lubricant.

Traction Drive Technology

During the years of the NASA Helicopter Transmission Technology program, there was significant progress in traction drives (refs. 3 and 42). A modern approach to life analysis was developed and applied to test models at NASA Lewis (fig. 12). Advanced materials and lubricants, combined with accurate analysis and prediction methods for life, efficiency, and traction coefficients made it possible to achieve high power transfer for experimental models. Traction drives are now capable of transmitting many horsepower, quietly and efficiently. Investigations showed that multiple, load-sharing contacts significantly benefit torque capacity and drive life. Torque capacity and drive life are proportional to size to the 2.8 and 8.4 power, respectively. Figure 12(b) shows the parametric variation of life with speed, torque, and power, where the life adjustment factors that come from lubricant film thickness as a function of speed have been factored in.

The drive shown in figure 12(a) was attached between a gas-turbine engine and a power absorption dynamometer and parametrically tested (ref. 42). Good

performance was achieved at speeds to 73 000 rpm and power to 180 kW. The peak efficiency was 94 to 96 percent, and there was only a 3.5 percent speed loss due to creep (microslip) of the rollers.

ANALYTICAL DESIGN CODES

Bearing Codes

The NASA/Army program has produced some very useful computer programs for designing and analyzing rolling element bearings (refs. 43 to 46). Generally, the computer programs can predict performance characteristics including Hertz stress, load distribution, lubrication film thickness, component kinematics, fatigue life, heat generation, operating temperature, and power loss as a function of input parameters such as bearing geometry, speed, and load. The programs permit better designs and eliminate much trial and error testing prior to selection of a final design. The various computer programs are for particular types of bearings as follows:

- (1) SHABERTH - Shaft bearing program, shaft load, and deflection with up to five bearings (ball, cylindrical roller, tapered roller) on shaft.
- (2) CYBEAN - Cylindrical roller.
- (3) PHERBEAN - Spherical roller.
- (4) PLANETSYS - Cylindrical or spherical roller in planetary system.

All of these programs are in the public domain and available through COSMIC (ref. 47).

A few examples will illustrate some of the capabilities of the bearing computer programs. In reference 48 the computer program SHABERTH was used to calculate the thermal performance of ball bearings for which sufficient test data were available to make a comparison over a range of test conditions. Three angular-contact ball bearings of differing sizes were selected. The variables used for comparison of experimental and calculated data were bearing temperatures, oil outlet temperatures, and bearing heat generation. The predicted bearing heat generation, inner and outer race temperatures, and oil outlet temperatures agreed very well with the experimental data obtained from three sizes of ball bearings (35, 120, and 167 mm bores) over a speed range from 1 to 3 million DN.

Figure 13 shows the comparisons as a function of shaft speed for the 120 mm bore bearing. The solid and dashed lines refer to two different assumptions for the amount of lubricant that enters the bearing cavity. Lubricant was supplied to the bearing cavity by feed holes at the split line of the inner race and to the running lands of the inner-race-riding cage. It was assumed that the minimum volume of oil in the cavity would result if none of the lubricant directed to the lands ever entered the bearing cavity, leaving the oil entering at the split line as the only source feeding the bearing cavity. At most it was assumed that only half of the lubricant supplied to the cage lands could enter the cavity. Hence the dashed lines and solid lines are an estimated maximum and minimum condition with respect to volume of oil in the bearing cavity.

In figure 13(d), the solid symbols represent power loss that was determined from a heat balance calculation on the oil flowing through the bearing. The open symbols represent power loss calculated by measuring the power used by the drive motor and subtracting a small amount of estimated tare loss. It is reported in reference 48 that the first method is the most accurate experimental method. Therefore, the solid symbols represent the better experimental measurements of power loss and the calculated power losses agrees well with the experimental data.

The good agreement of experimental and calculated data verifies the capability of computer program SHABERTH to calculate the thermal performance for ball bearings.

Computer program CYBEAN was used to calculate the thermal performance of a 118 mm bore cylindrical roller bearing with shaft speeds to 3 million DN (25 000 rpm), radial loads to 8900 N (2000 lb), and total lubricant flow rates to 0.0102 m³/min (2.7 gal/min). The calculations compared to the experimental data are shown in figure 14 (ref. 49).

Computer program PLANETSYS can simulate the thermo-mechanical performance of a multistage planetary transmission, including spherical roller bearings. SPHERBEAN can make calculations for outer-ring rotation and misalignment such as found in planetary transmission applications. These programs are useful for helicopter transmission applications where severe performance demands are placed on bearings that require analysis for outer ring rotation, for nonlubricated operation (dry friction) and for transient thermal performance. SPHERBEAN and PLANETSYS calculations were compared to data from parametric tests and loss-of-lubricant tests for an OH-58 transmission (ref. 50). Using both programs, calculations of temperatures at the output shaft and transmission case agreed with the data within 1-percent difference for steady-state operating conditions. Calculations to simulate the loss of lubricant compared well with data from an actual loss-of lubricant test on an OH-58 transmission (fig. 15).

Gear Codes

Analyses and/or computer codes have also been developed for gears to provide the following types of calculations (refs. 51 to 65): (1) power loss and efficiency, (2) bevel gear contact geometry, (3) gear dynamic analysis, (4) weight minimization, (5) life prediction, (6) lubrication, and (7) temperatures.

Figure 16 shows results of power loss calculations for high contact ratio gears compared to low contact ratio gears for two different sizes. The analytical method was developed from many existing methods and empirical data. It includes effects of sliding friction, elastohydrodynamic lubricant film thickness, windage, and rolling resistance. Using this method, the power loss and efficiency of spur gears and aircraft gear boxes may be predicted (refs. 51 and 52).

Computer program TELSGE (ref. 53) calculates dynamic loads, lubrication film thickness, stress, and temperature for spur gears. A similar program was developed for spiral bevel gears (ref. 54). Figure 17 (ref. 65) shows a sample calculation produced by TELSGE. The dynamic load is caused by the

interaction of the tooth stiffness and the mass of the gear. The figure compares the calculated dynamic load with the static load which is the load for very slow rotation of the gears.

Gear dynamic analysis computer programs have been developed for epicyclic gear systems (refs. 55 to 57).

Program PGT (ref. 55) calculates dynamic loads in a simple planetary assembly with three planet gears. A special feature of PGT is the determination of orbit motion for a floating sun gear.

The epicyclic gear program (refs. 56 and 57) is a multiple mesh/single stage, gear dynamics program. It is a versatile gear tooth dynamic analysis computer program which determines detailed geometry, dynamic loads, stresses and surface damage factors. The program can analyze a variety of both epicyclic and single mesh systems with spur and helical gear teeth including internal, external, and buttress tooth forms. The program includes options for flexible carrier or flexible ring gear, a floating sun gear, a natural frequencies option, and a finite element compliance formulation for helical gear teeth. The program can also determine maximum tooth loads as a function of speed which is useful for critical speed analysis. Figure 18 is a typical output of the program showing the sun planet dynamic loads for nine teeth passing through the contact zone.

At high speed, an important effect is the interaction of the gear tooth load with the mass and stiffness of the tooth itself. A computer code was developed to predict these effects (ref. 58). A computer code was also developed to consider the effect on dynamic load of the drive shaft stiffness and inertia of the connected loads (ref. 59).

Figure 19 shows the result of analysis for weight minimization (ref. 60). The problem was to determine the effect on weight of design parameters such as numbers and pitch of gear teeth. The weight of a spur gear pair is related to the center distance (fig. 19(a)); the smaller the center distance, the lighter the weight and for military applications, the smaller the size, the smaller is the vulnerability. The study produced a design chart (fig. 19(b)) which gives the allowable number of teeth on the pinion as a function of diametral pitch. Diametral pitch is the number of teeth per inch of diameter and is a measure of size. Smaller teeth have a large pitch number. The two design parameters cannot be selected without examining the limitations which are the criterion for pitting fatigue failure, bending failure and scoring. There is a geometry limitation also--involute interference, which is when the pinion teeth are badly undercut and involute action is lost. The figure shows that there is an allowed region for design (shaded area). The line C is the locus of designs which all have the same center distance, arrived at by different combinations of teeth number and pitch. The slope of the line is equal to the center distance. The minimum center distance design is on the lowest sloped line that has at least one point inside the shaded region.

Figure 20 shows results for life analysis of a planetary gear transmission. The analysis is based on rigorous statistical methods and is implemented in an interactive computer program (refs. 61 to 64). The program can analyze a variety of configurations composed of spiral bevel gear meshes

and planetary gear meshes. Spiral bevel reductions may have single or dual input pinions and gear shafts can be straddle mounted or overhung on the support bearings. The planetary reduction has the sun gear as input, the planet carrier as output, and the ring gear fixed. The planet gears may be plain or stepped and the number of planets may vary. The program determines the forces on each bearing and gear for a given transmission configuration and loading. The life of each bearing and gear is determined using the fatigue life model appropriate to that component. The transmission system life is determined from the component lives using Weibull statistical methods. The transmission life at a given reliability can then be found as shown in figure 20.

The life analysis has been integrated with a dynamic analysis (using computer program TELSGE), to determine the effect of speed on gear life (ref. 65). Figure 21 shows the result of the analysis, where the dynamic factor, C_v , represents the relative change in life due to dynamic loads. The static load, when applied in a quasi-static load cycle to the gear, will give a certain life which should be multiplied by C_v to get the life under dynamic load. There is a significant increase in life at speeds above the torsional natural frequency of the gear drive, ω_n . Reference 65 gives design charts that may be used to calculate gear life for dynamic load conditions.

ADVANCED TRANSMISSION DESIGN CONCEPTS

Based on the experimental, analytical, and design studies conducted under the transmission technology program, some advanced transmission concepts were evolved: The advanced 500 HP transmission (fig. 22), the bearingless planetary (fig. 23), the traction/gear hybrid transmission, (fig. 24), and the split torque transmission (fig. 25).

Advanced 500 HP Transmission

The design emphasis for the NASA/Bell Helicopter Textron (BHT) 500 HP advanced technology demonstrator transmission (fig. 22) was placed on designing a 500 HP version of the OH-58C, 317 HP, transmission that would have a long, quiet life with a minimum increase in the cost, weight, and space that usually increases along with power increases. This was accomplished by implementing advanced technology that has been developed during the last decade and making improvements dictated by field experience (ref. 66).

These advanced technology components, concepts, and improvements, and their effect on the 500 HP transmission are:

(1) High contact ratio planetary gear teeth reduce the noise level and increase life.

(2) Improved spiral bevel gears made of vacuum carburized gear steels, shot peened for increased gear tooth pitting fatigue life, as well as gear tooth bending fatigue strength, and lubricated with Aeroshell 555 oil save weight and space and increase transmission life.

(3) Improved bearings made of cleaner steels, and designed with improved analytical tools to save weight and space and increase the reliability.

(4) Improved design of the planet carrier made of two piece construction with straddle mounting of the planet gears for improved gear alignment and power capacity.

(5) The cantilever-mounted planetary ring gear has no working spline to generate wear debris; it isolates the meshing teeth from the housing to reduce noise; and it provides a flexible mount for a more uniform load distribution among the planets.

(6) The sun gear now has an improved spline (crown hobbed and hardened) running submerged in a bath of flowthrough oil which prevents the spline from wearing.

(7) The straddle-mounted bevel gear allows higher torque to be transmitted without detrimental shifting of the tooth contact pattern.

In summary, the improved 500 HP design has a weight/HP ration of 0.26 lb/HP compared to 0.37 lb/HP for the 317 HP OH-58C transmission. This transmission is the basis for the transmission in the Army's improved OH-58D model helicopter.

Bearingless Planetary Transmission

One recent development in the area of high performance power transmissions is the self-aligning, bearingless planetary (SABP) (fig. 23). This transmission arrangement can be generically classified as a quasi-compound planetary which utilizes a sun gear, planet spindle assemblies, ring gears, and rolling rings.

The design study projects a weight savings of 17 to 30 percent and a reliability improvement factor of 2:1 over the standard transmission (ref. 67). The benefits of using a SABP transmission are most effective when one uses reduction ratios between 16:1 and 26:1. It permits high reduction in two compound stages of high efficiency, providing sufficient flexibility and self-centering to give good load distribution between planet pinions, while effectively isolating the planetary elements from housing deflections.

This new transmission concept offers advantages over transmissions that use conventional planetary gear: higher reduction ratio, lighter weight, increased reliability, and decreased vulnerability. Since it has no planet bearings, there is a weight savings and power losses and bearing failures commonly associated with conventional-design transmission are nonexistent.

In conventional-design transmissions, planet bearings are heavily loaded and are the weak link when the lubricant is interrupted. The SABP transmission has decreased vulnerability because of increased operating time after loss of lubricant since there are no planet bearings.

One SABP transmission with a 17.44:1 ratio is currently being tested in the 500 HP transmission facility at NASA Lewis, and another variant with a ratio of 101:1 is being fabricated for testing.

Traction/Gear Hybrid Transmission

Two variants of this type of transmission have been fabricated as test models. The benefits of traction are combined with the benefits of gears in these novel transmission designs. In the version which simulates the OH-58 transmission (fig. 24), the hybrid transmission is only 22 percent heavier but transmits 58 percent more power. The transmission has advantages of increased power-to-weight ratio (0.27 lb/HP) and an estimated 300 percent increase in reliability. A high ratio variant, which eliminates a 40-lb gearbox on the engine offers an even higher advantage of 68 percent increase in power-to-weight ratio to 0.20 lb/HP.

Split Torque Transmission

Advancements in transmissions can come from either improved components or improved designs of the transmission system. The split torque arrangement is in the second category. Figure 25 shows a split torque design which is compatible with the Black Hawk (UH-60A) helicopter. The fundamental concept of the split torque design is that the power from the engine is divided into two parallel paths prior to recombination on a single gear that drives the output shaft. Studies have shown that replacement of the planetary gear reduction stage with a split torque results in weight savings and increased reliability. There can be many pinions driving the output gear, but in the case of the UH-60A application it was found that four pinions gave the optimum design on the basis of least overall weight, reduced power losses, comparable total parts count compared to the existing UH-60 design, and least number (one) of nonredundant gears. The advantage of split torque over planetary is greatest for the larger sized helicopters.

The engineering analysis (ref. 68) showed that the following performance benefits can be achieved for a 3600 HP split torque transmission compared to the conventional transmission with a planetary gear stage:

- (1) Weight is reduced 15 percent.
- (2) Drive train power losses are reduced by 9 percent.
- (3) Reliability is improved and vulnerability is reduced because of redundant power paths.
- (4) The number of noise generation points (gear meshes) is reduced.

The transmission has potential for installation in the Black Hawk helicopter. The design study has carried the transmission to the detail design stage for a test model to be used for validation studies in the NASA Lewis 3000 HP helicopter transmission facility, but a test model has not been built. For the transmission to be used in the Black Hawk, a separate detail design and installation study would be required first.

CONCLUDING REMARKS

The purpose of this paper has been to review significant developments in helicopter transmission technology as a result of the NASA/Army Transmission

Research Program of the last two decades. The helicopter demands an extremely light, long-lived and quiet drive system. The NASA/Army research, along with the helicopter builders' careful designs, has provided reliable and strong drive systems for civilian and Army helicopters. This paper has reviewed significant research in drive systems and their components.

The critical issues that were identified are: (1) to achieve significant advances in power-to-weight ratio, (2) to increase reliability, and (3) to reduce the transmission noise. New concepts to achieve these goals have been investigated. The advanced 500 HP transmission has explored an increased power-to-weight ratio using advanced design techniques, component improvements, and advanced materials. The value of this kind of research activity was realized during the upgrading of the Army's OH-58 helicopter, when the research on the advanced 500 HP transmission laid the groundwork for the transmission used in the D model. The split torque concept offers significant weight savings for large size helicopters. The bearingless planetary transmission with helical gears offers advantages in reliability and reduced noise. The traction/gear hybrid transmission has explored the advantage of noise reduction and reduced cost.

It is reasonable to expect that helicopters will continue to evolve in the future. To achieve the necessary advances in rotary wing flight capability, drive train technology must keep pace with advances in engines, controls, structures, and rotors. The current plan for NASA/Army Transmission Research calls for increased emphasis on noise reduction, an aggressive development of computer aided design codes for transmissions, and the design and construction of demonstrator transmissions in large and small size categories.

REFERENCES

1. Zaretsky, E.V.; Townsend, D.P.; and Coy, J.J.: NASA Gear Research and Its Probable Effect on Rotorcraft Transmission Design. NASA TM-79292, 1979.
2. Zaretsky, E.V.; Coy, J.J.; and Townsend, D.P.: NASA Transmission Research and Its Probable Effects on Helicopter Transmission Design. NASA TM-83389, AVRADCOM TR 83-C-3, 1983.
3. Advanced Power Transmission Technology. G.K. Fischer, ed. NASA CP-2210, AVRADCOM TR 82-C-16, 1983.
4. Weden, G.J.; and Coy, J.J.: Summary of Drive-Train Component Technology in Helicopters. NASA TM-83726, USAAVSCOM TR-84-C-10, 1984.
5. Coy, J.J.; Townsend, D.P.; and Zaretsky, E.V.: Gearing. NASA RP-1152, AVSCOM TR 84-C-15, 1985.
6. Townsend, D.P.; Coy, J.J.; and Hatvani, B.R.: OH 58 Helicopter Failure Analysis. NASA TM X-71867, 1976.
7. Lewicki, D.G.; and Coy, J.J.: Vibration Characteristics of the OH 58A Helicopter Main Rotor Transmission. NASA TP (in process), 1987.
8. Coy, J.J.; Mitchell, A.M.; and Hamrock, B.J.: Transmission Efficiency Measurements and Correlations with Physical Characteristics of the Lubricant, NASA TM-83740, USA AVSCOM TR 84-C-11, 1984.
9. Mitchell, A.M.; Oswald, F.B.; and Schuller, F.T.: Testing of YUH-61A Helicopter Transmission in NASA Lewis 2240-kW (3000 hp) Facility. NASA TP-2538, 1986.

10. Mitchell, A.M.; Oswald, F.B.; and Coe, H.H.: Testing of UH-60A Helicopter Transmission in NASA Lewis 2240-kW (3000 hp) Facility. NASA TP-2626, 1986.
11. Townsend, D.P.; and Zaretsky, E.V.: Effect of Shot Peening on Surface Fatigue Life of Carburized and Hardened AISI 9310 Spur Gears. NASA TP-2047, 1982.
12. Townsend, D.P.; and Zaretsky, E.V.: Endurance and Failure Characteristics of Modified VASCO X-2, CBS 600 and AISI 9310 Spur Gears. J. Mech. Des., vol. 103, no. 2, Apr. 1981, pp. 506-515.
13. Townsend, D.P.: Surface Fatigue Life and Failure Characteristics of EX-53, CBS 1000M, and AISI 9310 Gear Materials. NASA TP-2513, 1985.
14. Scibbe, H.W.; Townsend, D.P.; and Aron, P.R.: Effect of Lubricant Extreme-Pressure Additives on Surface Fatigue Life of AISI 9310 Spur Gears. NASA TP-2408, 1984.
15. Townsend, D.P.; and Zaretsky, E.V.: Effect of Five Lubricants on Life of AISI 9310 Spur Gears. NASA TP-2419, 1985.
16. Present, D.L., et al.: Advanced Chemical Characterization and Physical Properties of Eleven Lubricants. (AFLRL-166, Army Fuels and Lubricants Research Lab.; NASA Order C-67295-D), NASA CR-168187, 1983. (Avail. NTIS, AD-A131945.)
17. El-Bayoumy, L.E.; Akin, L.S.; and Townsend, D.P.: An Investigation of the Transient Thermal Analysis of Spur Gears. Journal of Mechanisms, Transmissions, and Automation in Design, vol. 107, no. 4, Dec. 1985, pp. 541-548.
18. Akin, L.S.; and Townsend, D.P.: Lubricant Jet Flow Phenomena in Spur and Helical Gears with Modified Center Distances and/or Addendums - for Out-of-Mesh Conditions. Journal of Mechanisms, Transmissions, and Automation in Design, vol. 107, no. 1, Mar. 1985, pp. 24-30.
19. Akin, L.S.; and Townsend, D.P.: Into Mesh Lubrication of Spur Gears with Arbitrary Offset Oil Jet. Part 1; For Jet Velocity Less than or Equal to Gear Velocity. Journal of Mechanisms, Transmissions, and Automation in Design, vol. 105, no. 4, Dec., 1983, pp. 713-718.
20. Akin, L.S.; and Townsend, D.P.: Into Mesh Lubrication of Spur Gears with Arbitrary Offset Oil Jet. Part 2; For Jet Velocities Equal to or Greater than Gear Velocity. Journal of Mechanisms, Transmissions, and Automation in Design, vol. 105, no. 4, Dec. 1983, pp. 719-724.
21. Townsend, D.P.; Baber, B.B.; and Nagy, A.: Evaluation of High-Contact-Ratio Spur Gears with Profile Modification. NASA TP-1458, 1979.
22. Frint, H. K.: Design and Evaluation of High Contact Ratio Gearing. NASA CR-174958, 1986.
23. Litvin, F.L.; and Coy, J.J.: Spiral Bevel Geometry and Gear Train Precision. Advanced Power Transmission Technology, G.K. Fischer, ed. NASA CP-2210, AVRADCOM-TR-82-C-16, 1983, pp. 335-344.
24. Litvin, F.L.; Rahman, P.; and Goldrich, R.N.: Mathematical Models for the Synthesis and Optimization of Spiral Bevel Gear Tooth Surfaces. NASA CR-3553, 1982.
25. Litvin, F.L., et al.: Synthesis and Analysis of Spiral Bevel Gears. Design and Synthesis, H. Yoshikawa, ed., North Holland, New York, 1985, pp. 302-305.
26. Litvin, F.L.; Tsung, W.-J.; and Coy, J.J.: Generation of Spiral Bevel Gears with Zero Kinematical Errors and Computer Aided Simulation of their Meshing and Contact. Computers in Engineering 1985, R. Raghavan and S.M. Rohde, eds., vol. 1, ASME, New York, 1985, pp. 335-339.

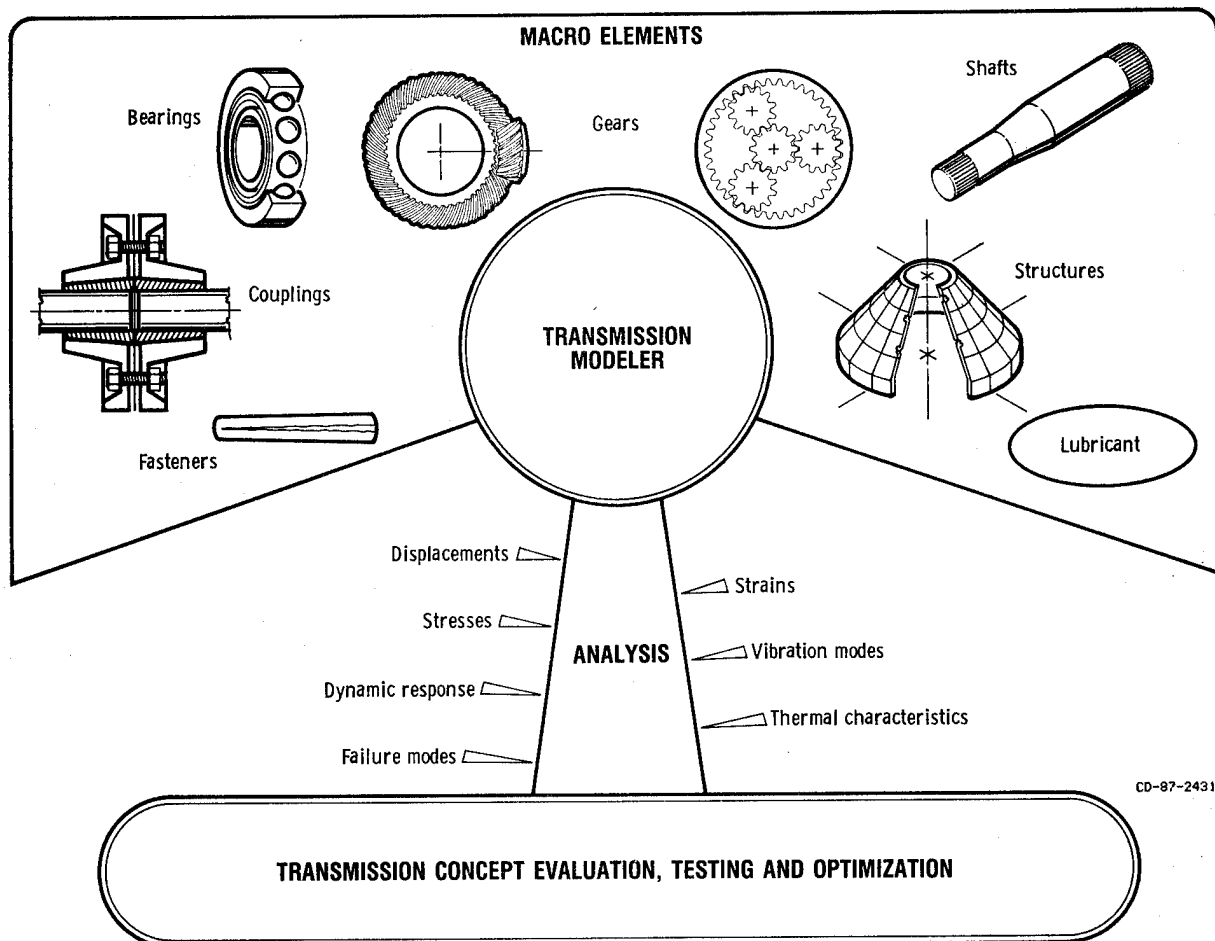
27. Litvin, F.L., et al.: Method for Generation of Spiral Bevel Gears with Conjugate Gear Tooth Surfaces. ASME Paper 86-DET-3, 1986.
28. Litvin, F.L., et al.: Generation of Spiral Bevel Gears with Zero Kinematical Errors and Computer Aided Tooth Contact Analysis. NASA TM-87273, USAAVSCOM TR 86-C-2, 1986.
29. Litvin, F.L., et al.: New Generation Methods for Spur, Helical, and Spiral-Bevel Gears. USAAVSCOM TR-86-C-27, NASA TM-88862, 1986.
30. Lin, H.H.; Huston, R.L.; and Coy, J.J.: Dynamic Analysis of Straight and Involute Tooth Forms. ASME Paper 84-DET-226, Oct. 1984.
31. Mark, W.D.: The Transfer Function Method for Gear System Dynamics Applied to Conventional and Minimum Excitation Gearing Designs. NASA CR-3626, 1982.
32. Parker, R.J.: Present Technology of Rolling-Element Bearings. Advanced Power Transmission Technology, G.K. Fischer, ed., NASA CP-2210, AVRADCOM TR 82-C-16, 1983, pp. 35-48.
33. Hamrock, B.J.; and Anderson, W.J.: Rolling Element Bearings. NASA RP-1105, 1983.
34. Zaretsky, E.V.; and Anderson, W.J.: Effect of Materials - General Background. Interdisciplinary Approach to the Lubrication of Concentrated Contacts, P.M. Ku, ed., NASA SP-237, 1970, pp. 379-408.
35. Nahm, A.H.: Impact of NASA-Sponsored Research on Aircraft Turbine Engine Bearing Specifications. Advanced Power Transmission Technology, G.K. Fischer, ed., NASA CP-2210, AVRADCOM TR 82-C-16, 1983, pp. 173-184.
36. Bamberger, E.N.; and Kroeger, D.J.: Rolling Element Fatigue Life of a Carburized Modified M50 Bearing Steel. NASA CR-168295, 1984.
37. Bamberger, E.N.; and Nahn, A.H.: Improved Fracture Toughness Corrosion - Resistant Bearing Material. NASA CR-174990, 1986.
38. Zaretsky, E.V.; Schuller, F.T.; and Coe, H.H.: Lubrication and Performance of High-Speed Rolling-Element Bearings. Lubr. Eng., vol. 41, no. 12, Dec. 1985, pp. 725-732.
39. Schuller, F.T.: Lubrication of 35-mm - bore Ball Bearings of Several Designs to 2.5 Million DN. Advanced Power Transmission Technology, G.K. Fischer, ed., NASA CP-2210, AVRADCOM TR 82-C-16, 1983, pp. 221-238.
40. Morrison, F.R.; Gassel, S.S.; and Borenkerk, R.L.: Development of Small Bore, High-Speed Tapered Roller Bearing. NASA CR-165375, 1981.
41. Parker, R.J.: Large Bore Tapered Roller Bearing Performance and Endurance to 2.4 Million DN. Advanced Power Transmission Technology, G.K. Fischer, ed., NASA CP-2210, AVRADCOM TR 82-C-16, 1983, pp. 253-270.
42. Loewenthal, S.H.; Rohn, D.A.; and Anderson, N.E.: Advances in Traction Drive Technology. SAE Paper 831304, 1983.
43. Haddon, G.B., et al.: User's Manual for Computer Program SHABERTH. (SKF-AT81D040, SKF Technology Services; NASA Contract NAS3-22690.) NASA CR-165365, 1981.
44. Dyba, G.J.; and Kleckner, R.J.: User's Manual for SKF Computer Program CYBEAN. (SKF-AT81D049-vol-2, SKF Technology Services; NASA Contract NAS3-22690.) NASA CR-165364, 1981.
45. Kleckner, R.J.; Dyba, G.J.; and Ragen, M.A.: User's Manual for SKF Computer Program SPHERBEAN. (SKF-AT81D007, SKF Technology Services; NASA Contract NAS3-22807.) NASA CR-167859, 1982.
46. Haden, G.B., et al.: User's Manual for SKF Computer Program PLANETSYS. (SKF-AT81D044, SKF Technology Services; NASA Contract NAS3-22690.) NASA CR-165366, 1981.
47. COSMIC Software Catalog. NASA CR-176274, 1986.
48. Parker, R.J.: Comparison of Predicted and Experimental Thermal Performance of Angular-Contact Ball Bearings. NASA TP-2275, 1984.

49. Coe, H.H.; and Schuller, F.T.: Calculated and Experimental Data for a 118-mm Bore Roller Bearing to 3 Million DN. *J. Lubr. Technol.*, vol. 103, no. 2, Apr. 1981, pp. 274-283.
50. Coe, H.H.: Thermal Analysis of a Planetary Transmission with Spherical Roller Bearings Operating after Complete Loss of Oil. NASA TP-2367, 1984.
51. Anderson, N.E.; and Loewenthal, S.H.: Spur-Gear-System Efficiency at Part and Full Load. NASA TP-1622, AVRADCOM TR 79-46, 1980.
52. Anderson, N.E.; Loewenthal, S.H.; and Black, J.D.: An Analytical Method to Predict Efficiency of Aircraft Gearboxes. NASA TM-83716, USAAVSCOM TR 84-C-8, 1984.
53. Wang, K.L.; and Cheng, H.S.: Thermal Elastohydrodynamic Lubrication of Spur Gears. NASA CR-3241, 1980.
54. Chao, C. H.-C.: A Computer Solution for the Dynamic Load, Lubricant Film Thickness and Surface Temperatures in Spiral Bevel Gears. PhD Dissertation, Northwestern University, 1982.
55. August, R., et al.: Dynamics of Early Planetary Gear Trains. NASA CR-3793, 1984.
56. Boyd, L.S.; and Pike, J.: Multi-Mesh Gear Dynamics Program Evaluation and Enhancements. NASA CR-174747, 1985.
57. Pike, J.A.: Interactive Multiple Spur Gear Mesh Dynamic Load Program. NASA CR-165514, 1982.
58. Shuey, L.W.: An Investigation of the Dynamic Response of Spur Gear Teeth with Moving Loads. M.S. Thesis, Michigan Technological University, 1983.
59. Lin, H.-H.; and Huston, R.L.: Dynamic Loading on Parallel Shaft Gears. (UC-MIE-051586-19, Cincinnati University; NASA Grant NSG-3188.) NASA CR-179473, 1986.
60. Savage, M.; Coy, J.J.; and Townsend, D.P.: Optimal Tooth Numbers for Compact Standard Spur Gear Sets. *J. Mech. Des.*, vol. 104, no. 4, Oct. 1982, pp. 749-758.
61. Savage, M., et al.: Life and Reliability Modeling of Bevel Gear Reductions. ASME Paper 85-DE-7, Mar. 1985.
62. Lewicki, D.G., et al.: Fatigue Life Analysis of a Turboprop Reduction Gearbox. *Journal of Mechanisms, Transmissions, and Automation in Design*, vol. 108, no. 2, June 1986, pp. 255-262.
63. Savage, M.; and Brikmanis, C.K.: System Life and Reliability Modeling for Helicopter Transmissions. NASA CR-3967, 1986.
64. Savage, M.; Caldwell, R.J.; and Lewicki, D.G.: Gear Mesh Compliance Modeling. NASA TM-88843, USAAVSCOM TR 86-C-28, 1986.
65. Lewicki, D.G.: Predicted Effect of Dynamic Load on Pitting Fatigue Life for Low-Contact-Ratio Spur Gears. NASA TP-2610, AVSCOM TR 86-C-21, 1986.
66. Braddock, C.E.; and Battles, R.A.: Design of an Advanced 500 HP Helicopter Transmission. *Advanced Power Transmission Technology*, G.K., Fischer, ed., NASA CP-2210, AVRADCOM TR 82-C-16, 1983, pp. 123-140.
67. Folenta, D.J.: Design Study of Self-Aligning Bearingless Planetary (SABP). (TTC-80-01R, Transmission Technology Co.; NASA Contract NAS3-21604.) NASA CR-159808, 1980.
68. White, G.: 3600 HP Split Torque Helicopter Transmission, NASA CR-174932, 1985.

REQUIREMENT	GOAL	BENEFIT
LIGHTER STRONGER	DRIVE TRAIN SPECIFIC WEIGHT .3 TO .5 LB/HP (CURRENTLY .4 TO .6 LB/HP)	INCREASED RANGE AND PAYLOAD
MORE RELIABLE	5000 HR MTBO (CURRENTLY 500-2000 HRS)	LOWER OPERATING COST AND SAFER OPERATION
QUIETER	70-80 db IN CABIN (CURRENTLY 100-110 db)	GREATER USE FOR COMMERCIAL COMMUTER SERVICE INCREASED PASSENGER AND PILOT COMFORT

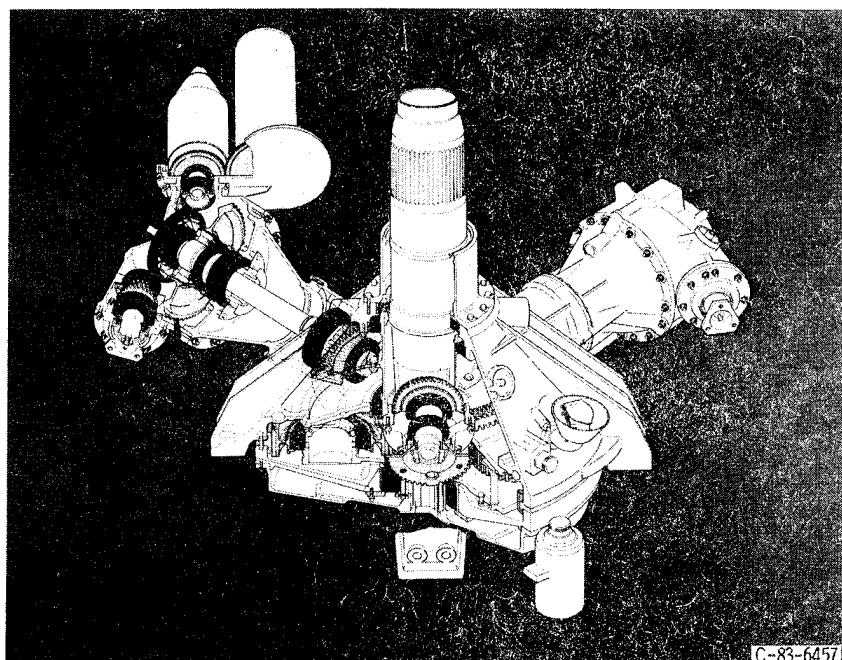
CD-84-15112

Figure 1. - Required technological advancements for helicopter transmissions in the 1990's.



CD-87-24315

Figure 2. - Concept for a comprehensive computer program library for modelling and analysis of transmissions.



C-83-6457

Figure 3. - Isometric section view of UH-60A helicopter transmission.

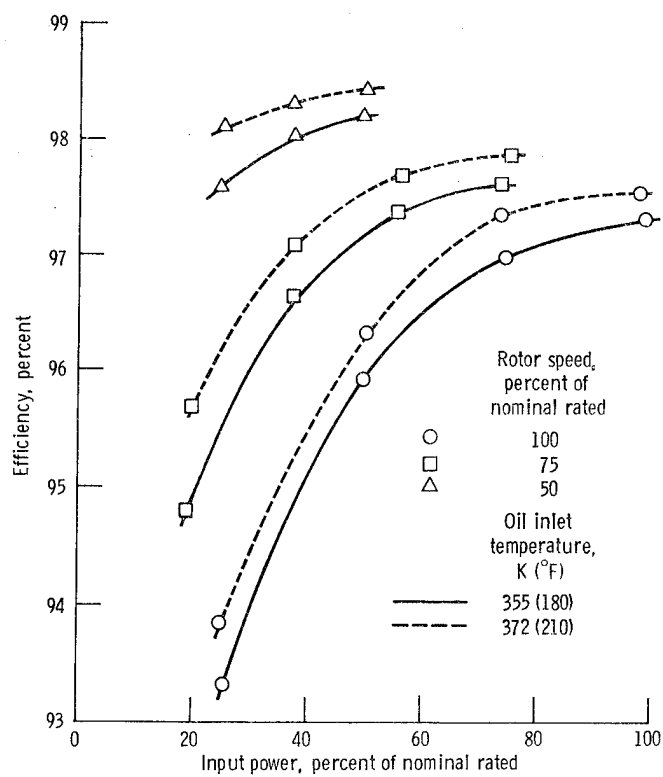


Figure 4. - Measured mechanical efficiency of UH-60A helicopter transmission plotted against input power, as a function of rotor speed and oil temperature.

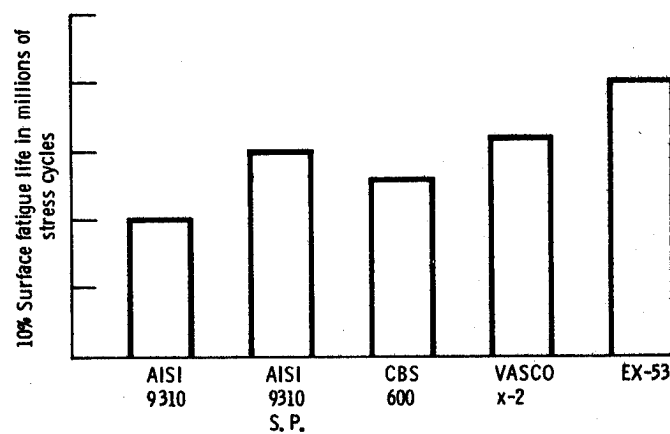


Figure 5. - Fatigue life for four gear materials compared to baseline AISI 9310 material. (S, P. = Shot Peened). Tests conducted on NASA Spur Gear Rig.

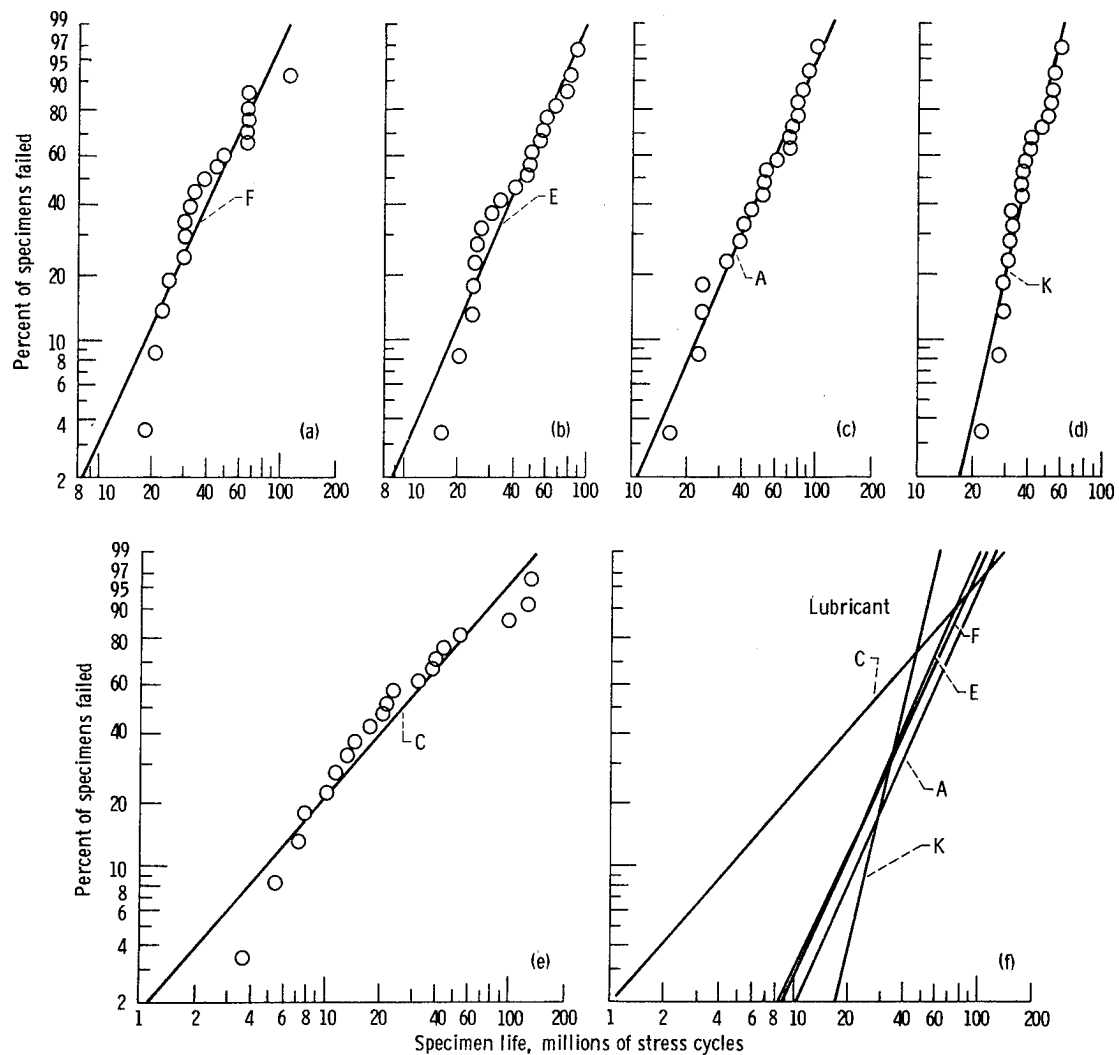
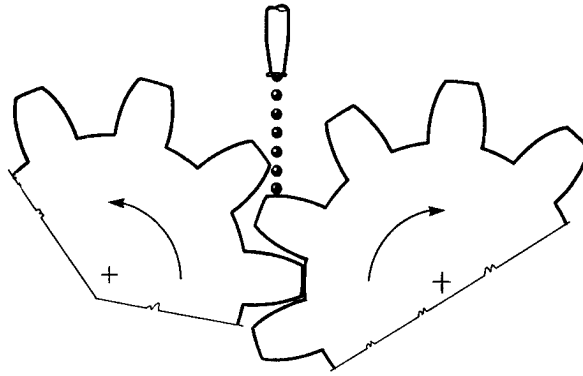


Figure 6. - Surface pitting fatigue life as affected by type of lubricant. Tests conducted on NASA Spur Gear Rig. Gear material - CVM AISI 9310, speed - 10 000 rpm, temperature - 350 K (170 °F), maximum Hertz stress - 1.7 MPa (248 000 psi). Lubricant types: A - Mobil ATF 220, C - Aeroshell 500, E - Syn Tech NS677, F - Mobil RL714, K - Aeroshell 555.

Out-of-mesh jet lubrication



Radial jet lubrication

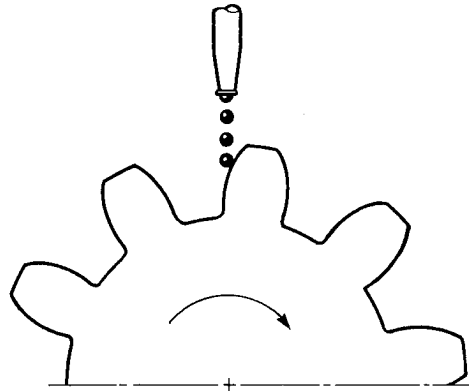


Figure 7. - Two ways of aiming the oil jets to lubricate gear teeth. Radially aimed jet penetrates further to better cool gear tooth. Out-of-mesh aimed jet has less power loss compared to into-mesh directed flow.

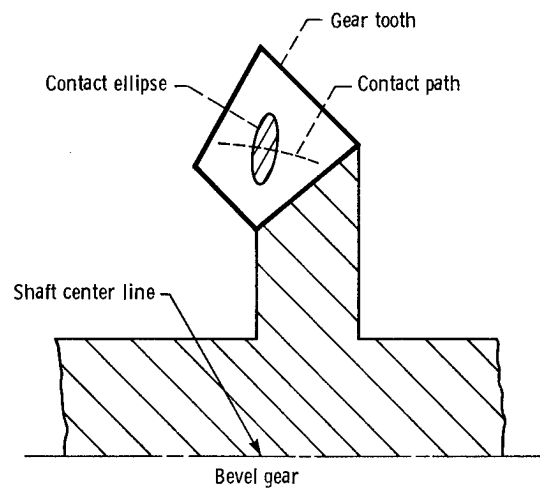


Figure 8. - Contact ellipse moves across the face of the gear tooth as the gear meshes with its mating gear (not shown).

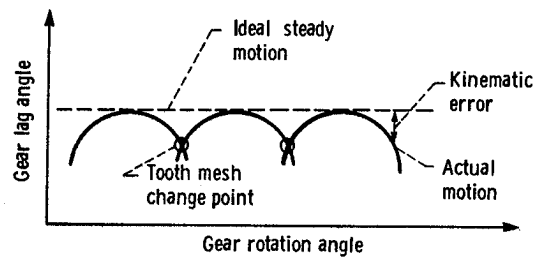


Figure 9. - Kinematic error function for the mesh of several gear teeth.

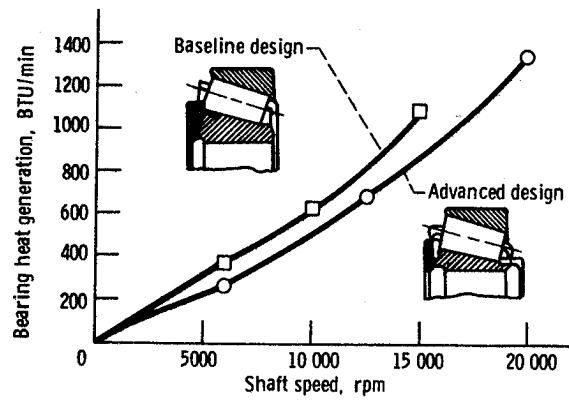
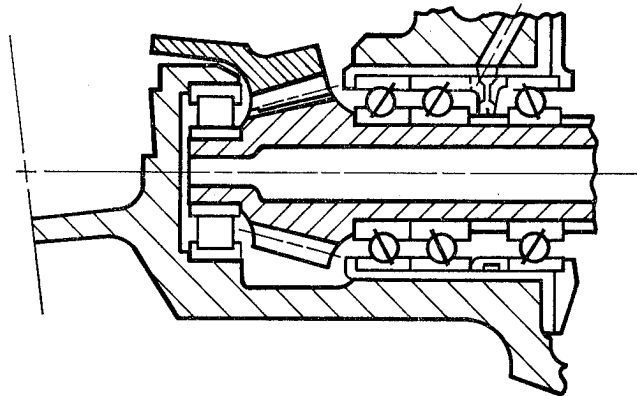
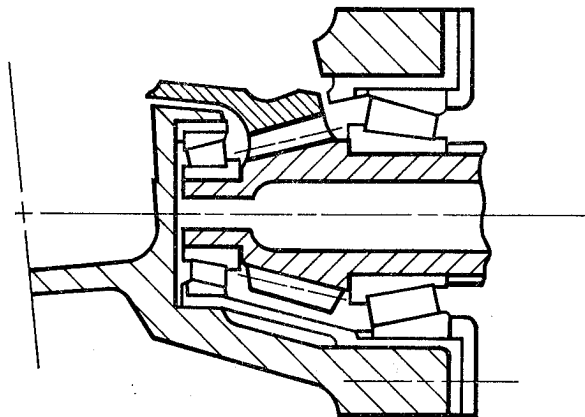


Figure 10. - Advanced design for tapered roller bearings provides cooler operation at high speed.

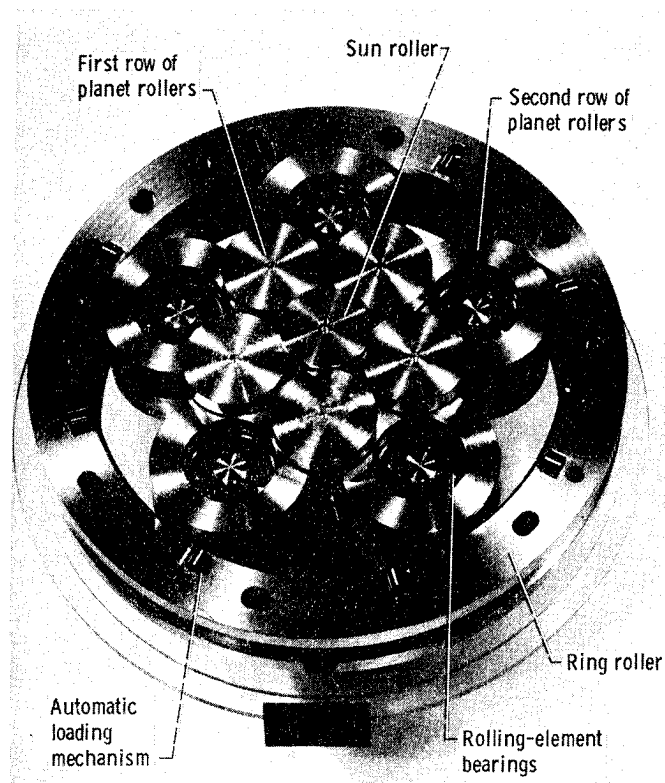


(a) Ball and roller bearings.

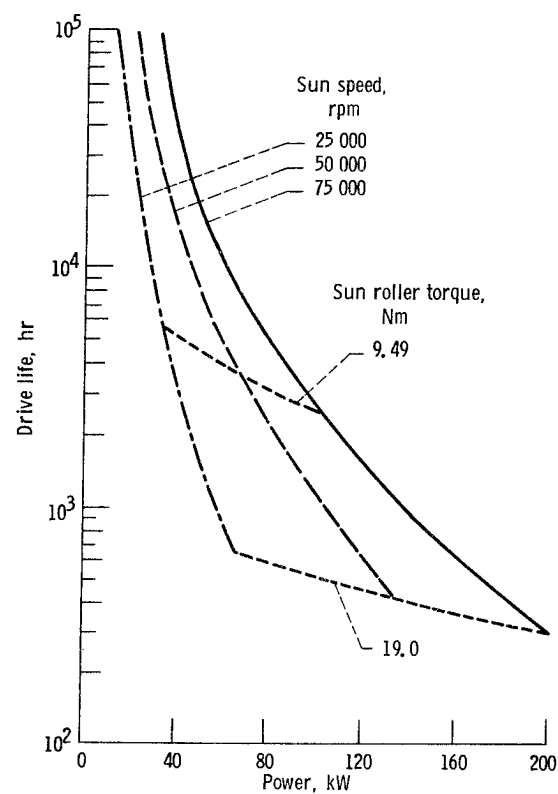


(b) Tapered-roller bearings.

Figure 11. - Tapered roller bearings replace ball and cylindrical roller bearings on input shaft for helicopter transmission.



(a) Experimental traction drive transmission.



(b) Analytical results for drive life as a function of power, torque, and speed.

Figure 12. - Results of traction drive research.

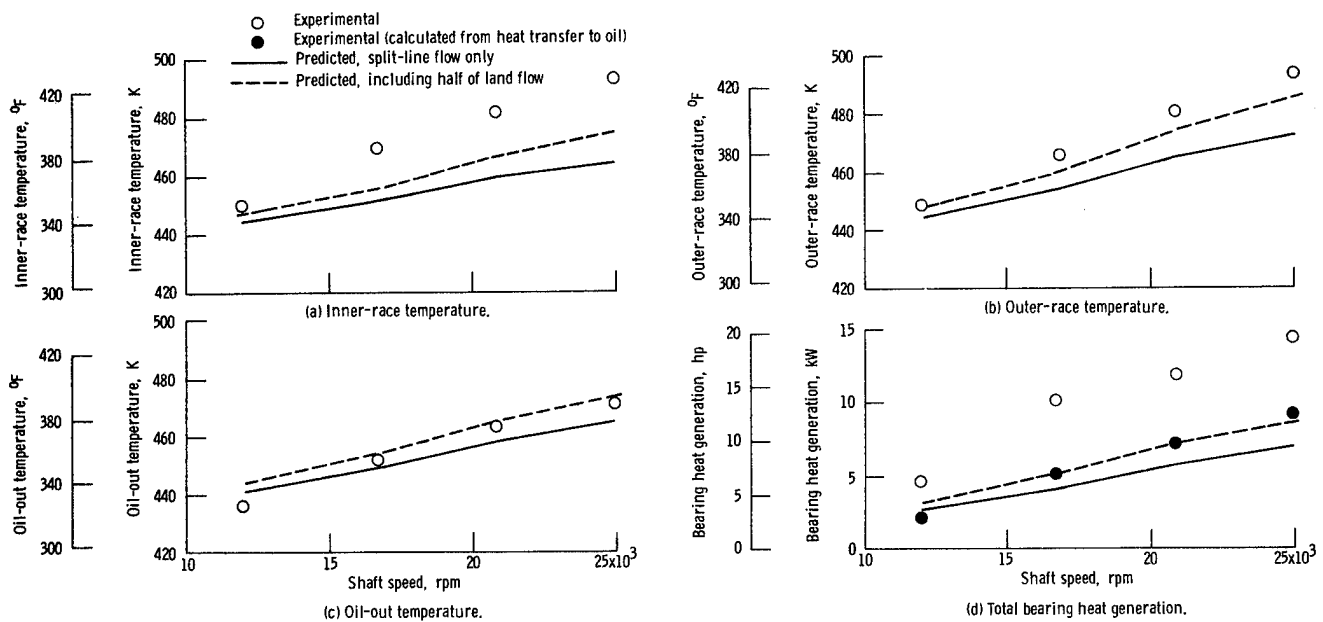


Figure 13. - Predicted and experimental thermal performance of 120 mm bore ball bearing as function of shaft speed. Thrust load, 22 240 N (5000 lb); oil-in temperature, 427 K (310 °F); total lubricant flow rate, 4740 cm³/min (1.253 gpm).

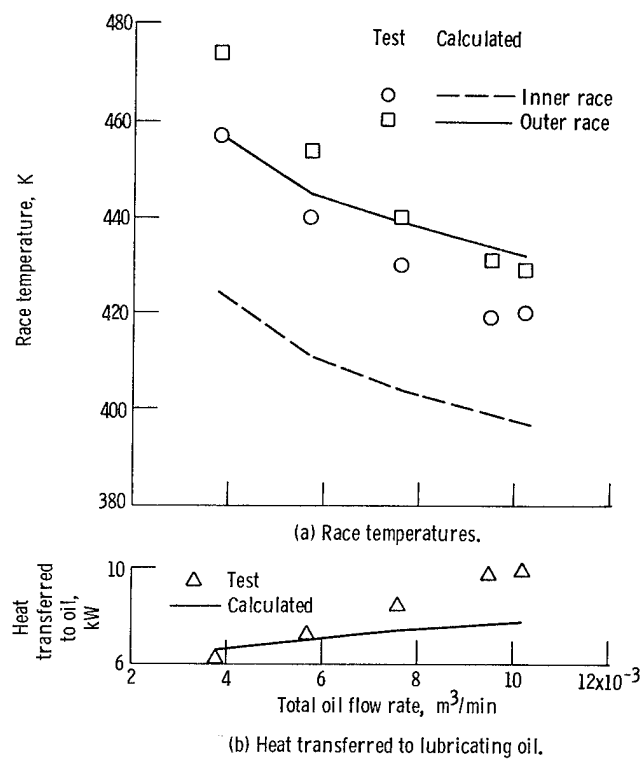


Figure 14. - Comparison of calculated and experimental bearing data using a cold diametral clearance of 0.09 mm in the computer program. Shaft speed, 20 000 rpm; radial load, 8900 N (2000 lb); lubricant volume, 2 percent.

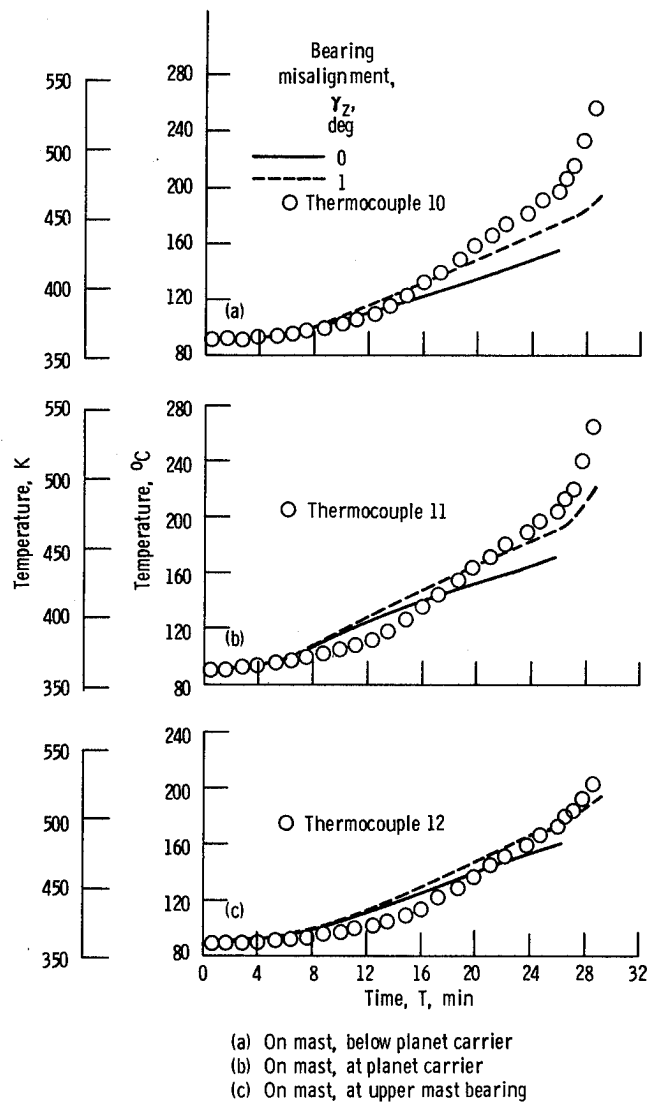


Figure 15. - Computer simulation of loss of lubricant in the OH-58 transmission. Predicted transient temperatures compared to experimental data, output shaft area. Drain plug removed at $T = 0$; oil pressure to zero at $t = 1.5$ minutes.

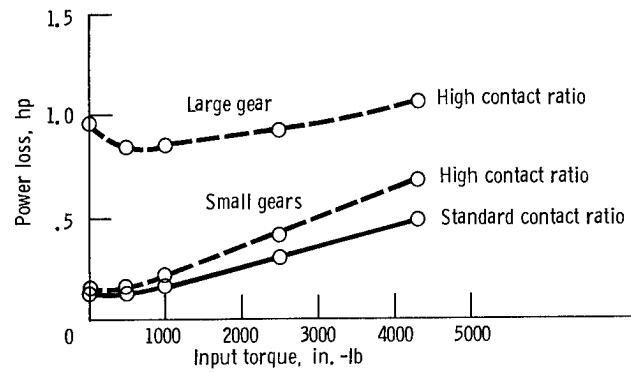


Figure 16. - Power loss predictions as a function of speed for gears, showing effect of size and contact ratio.

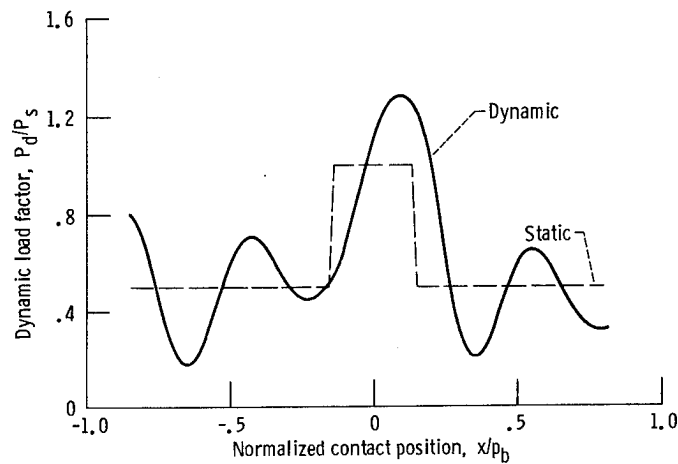


Figure 17. - Gear tooth dynamic load factor compared to static load as a function of position of the contact point.

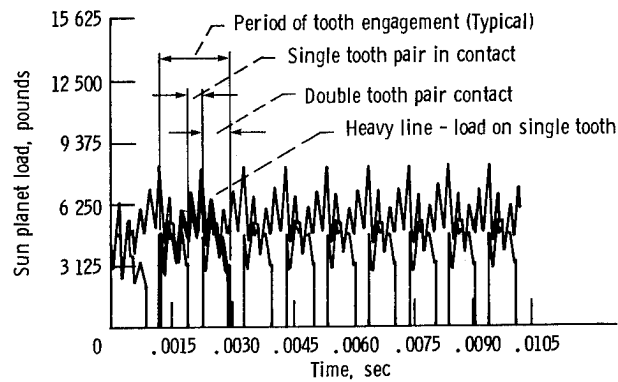
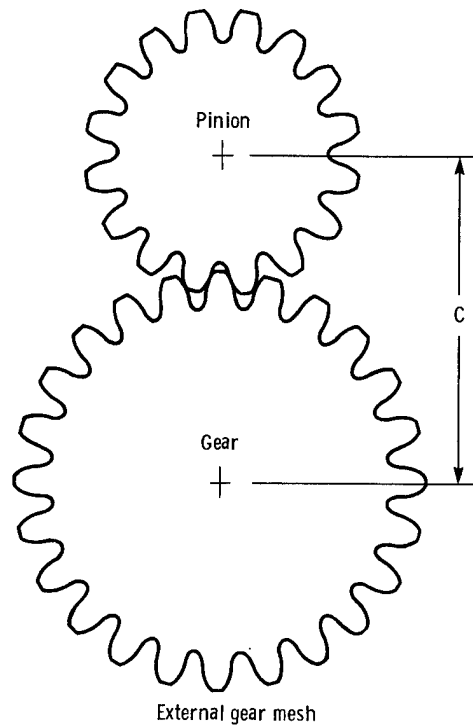
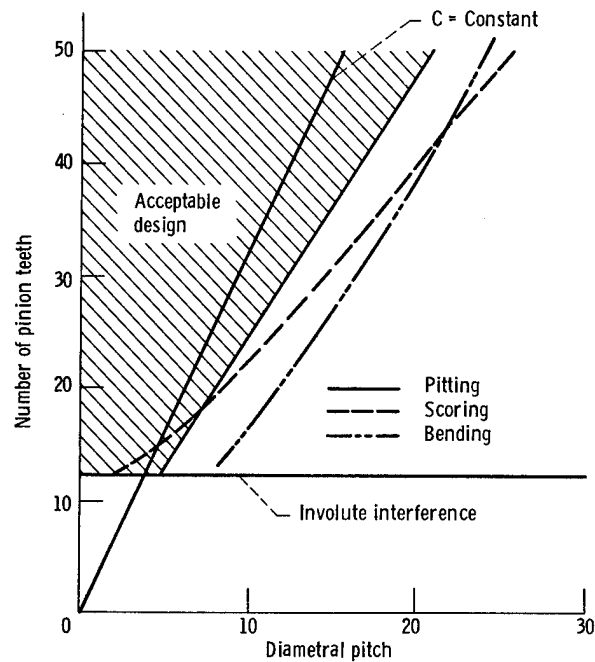


Figure 18. - Sun-planet dynamic load for 9 teeth engagements on 3000 hp helicopter transmission. Speed - 1200 rpm, Torque - 4500 in.-lb.



(a) Minimization of center distance reduces size and weight.



(b) In design space of number of pinion teeth versus diametral pitch, there is an allowable region of design. Line labeled "C = Constant" is locus of constant center distance designs. Minimum weight designs lie on the right hand edge of the shaded region.

Figure 19. - Results of weight minimization study for spur gears.

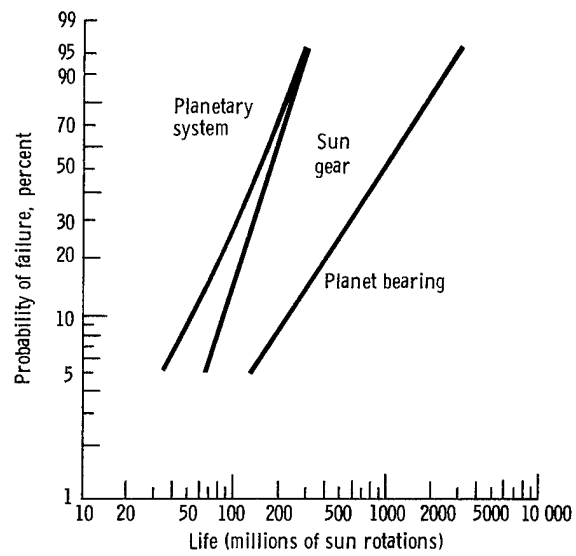


Figure 20. - Calculated Weibull distributions for sun gear, planet bearing, and complete planetary assembly of sun, bearings, planets, and gear.

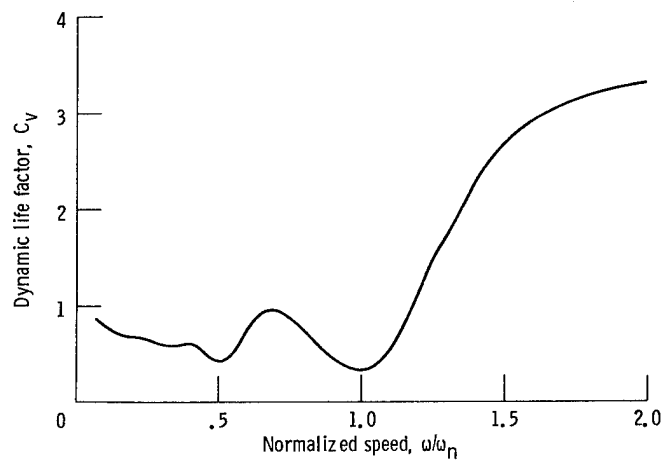


Figure 21. - Gear mesh life plotted against speed.

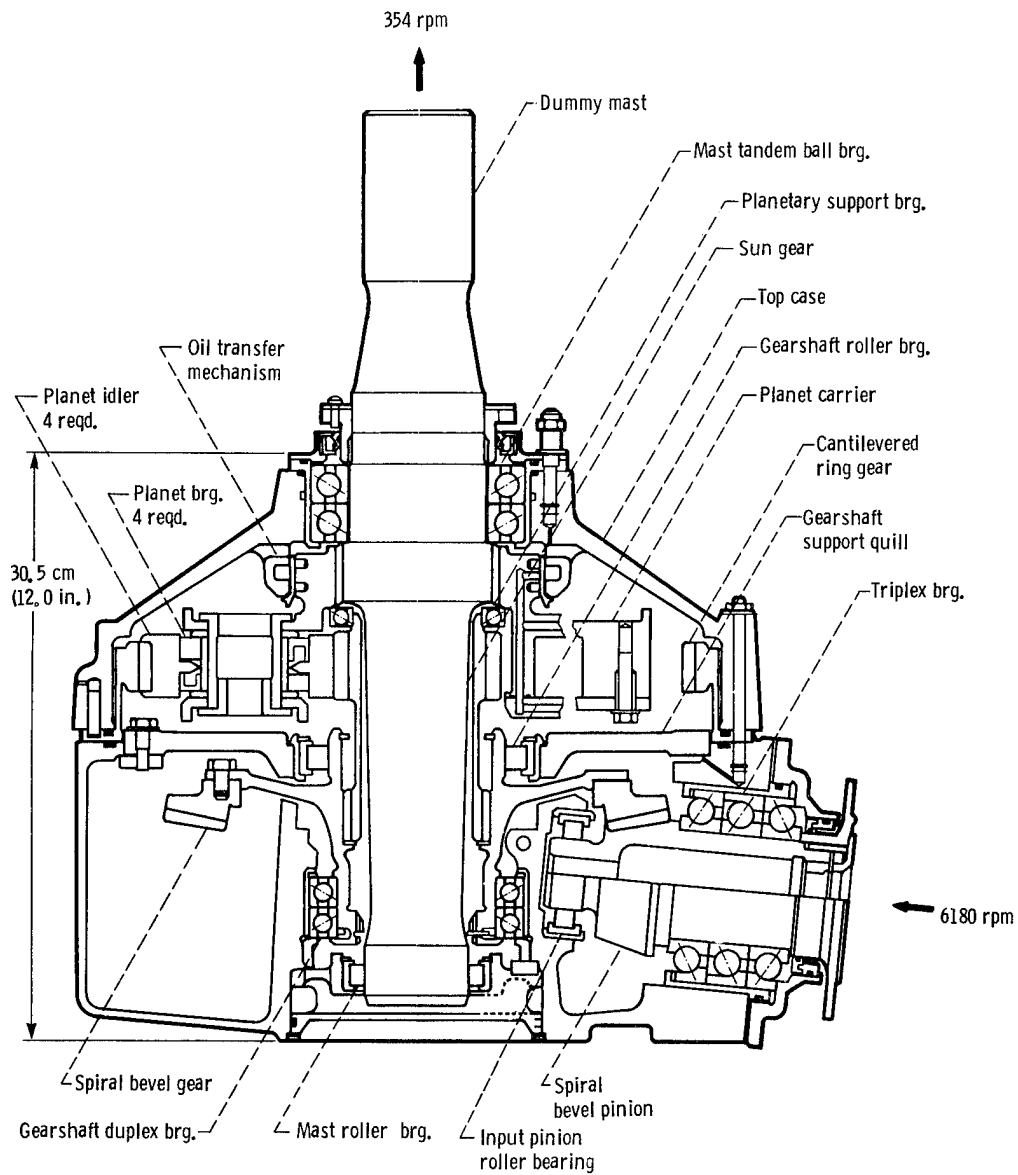
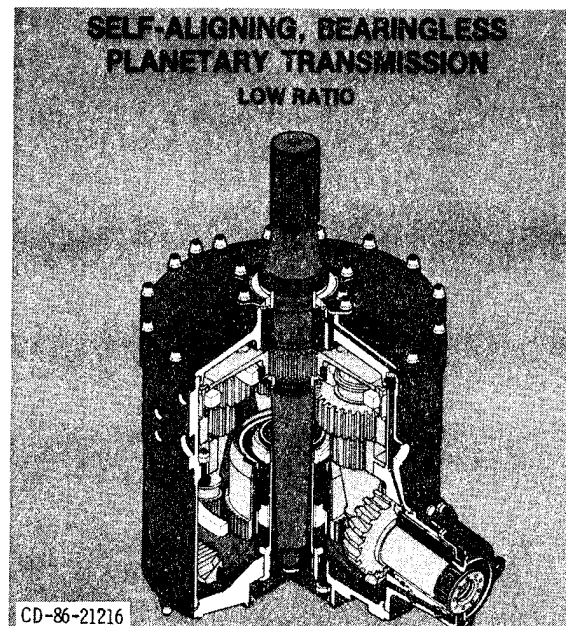
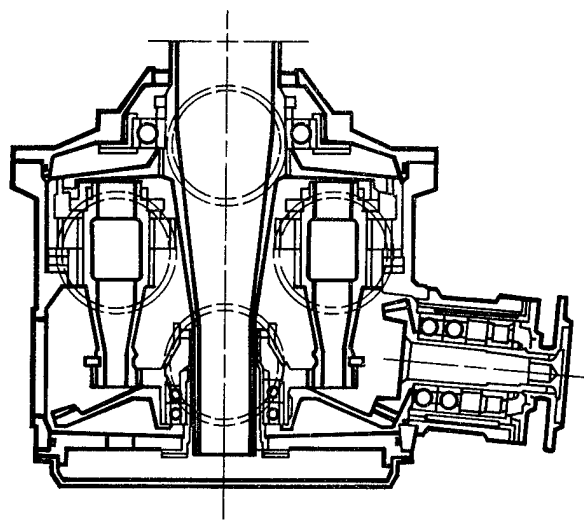


Figure 22, - Advanced 500 hp transmission.



(a) Isometric view.



(b) Cross section view.

Figure 23. - Self-aligning bearingless planetary transmission.

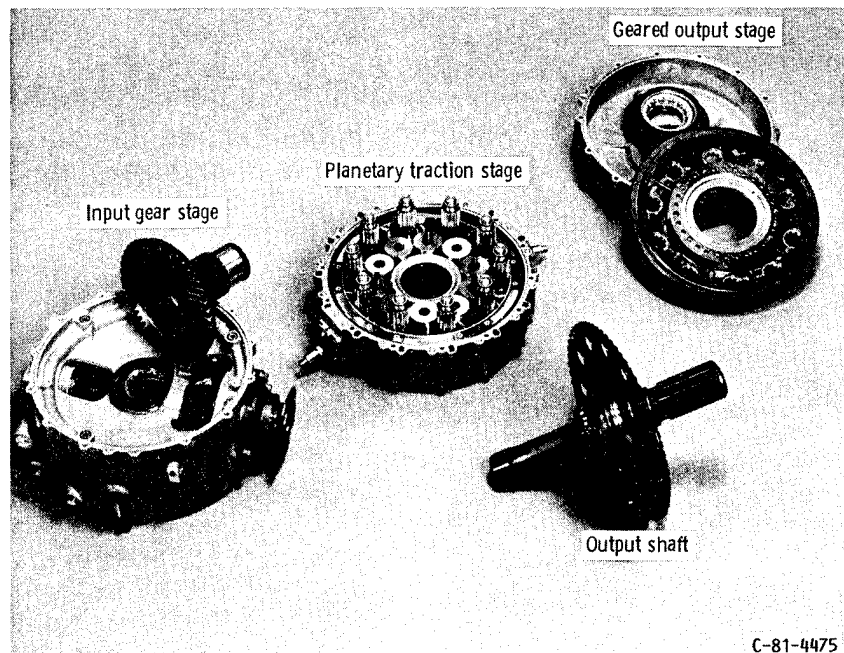


Figure 24. - Traction hybrid transmission.

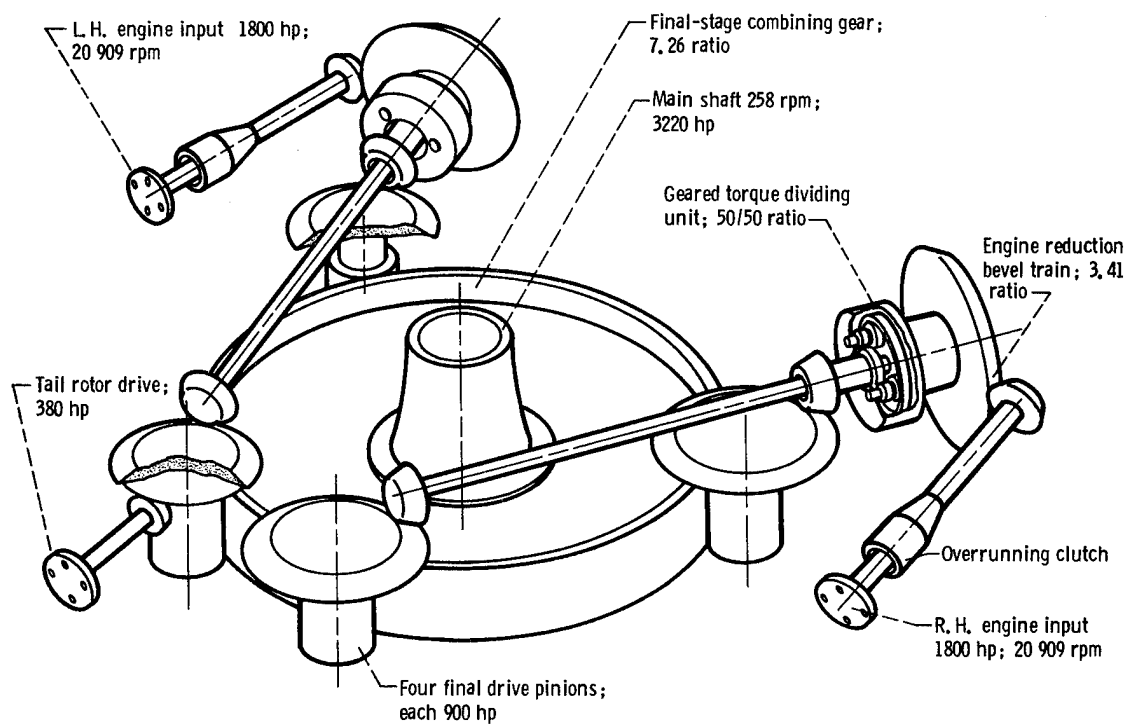


Figure 25. - Split-torque transmission generally configured for UH-60 Blackhawk helicopter.

NASA's ROTORCRAFT ICING RESEARCH PROGRAM

Robert J. Shaw and John J. Reinmann
National Aeronautics and Space Administration
Lewis Research Center

Thomas L. Miller
Sverdrup Technology, Incorporated
NASA Lewis Research Center

SUMMARY

The objective of the NASA aircraft icing research program is to develop and make available icing technology to support the needs and requirements of industry for all weather aircraft designs. While a majority of the technology being developed is viewed to be generic (i.e. appropriate to all vehicle classes), vehicle specific emphasis is being placed on the helicopter due to its unique icing problems. In particular, some of the considerations for rotorcraft icing are indicated in figure 1. The NASA icing research program emphasizes technology development in two key areas: ice protection concepts and icing simulation (analytical and experimental). The NASA research efforts related to rotorcraft icing in these two technology areas will be reviewed in this paper.

ICE PROTECTION CONCEPTS

Currently, the only rotor ice protection system being employed on operational military and civilian helicopters is the electrothermal deicing system. While the electrothermal concept has been shown to be capable of effectively deicing rotors, the weight and power requirements have caused the industry to seek other concepts. NASA research efforts have focused on two concepts: pneumatic boot and electro-impulse deicers.

PNEUMATIC BOOT

The pneumatic boot is probably one of the oldest of all ice protection concepts with its use on fixed wing aircraft dating back to at least the 1930's. The application of the pneumatic boot concept to the helicopter rotor was studied by Lockheed under an Army contract in the 1970's (ref. 1) and rejected, primarily on materials concerns. Specifically, it was felt that the pneumatic boot would not withstand the service dynamic environment of the helicopter rotor. It was feared that the boots might be damaged or completely torn off by the high levels of centrifugal forces. Also, it was felt that the rain/erosion characteristics of the neoprene rubber, from which the boots would be constructed, would be unacceptable. Concern was also expressed about the possible aerodynamic performance degradation of the rotor due to the presence of the boots especially when the tubes were inflated. These concerns were sufficient to eliminate the pneumatic boot from further consideration at that time.

However, the B.F. Goodrich Company, the only company marketing pneumatic boots in this country, subsequently investigated other candidate materials for boot construction and became convinced that a polyurethane material (trade name Estane) would solve several of the aforementioned problems. Furthermore, the possible simplicity, light weight, low power consumption and low cost of a rotor pneumatic boot deicing system justified pursuing a technology development program. Based on these considerations, NASA and B.F. Goodrich conducted a joint program in 1979 to investigate the deicing capability and aerodynamic performance of candidate pneumatic boot designs. The results of that test program conducted in the NASA Icing Research Tunnel (IRT) are given in reference 2.

The wind tunnel model used in the test (fig. 2) was a 6 ft span segment of a full scale UH1H rotor blade. Of the three pneumatic boot configurations tested, the one judged to be the most effective at removing ice is shown in figure 3. This configuration had two spanwise tubes surrounding the leading edge and chordwise tubes aft of the leading edge tubes on both the suction and pressure surfaces.

Deicing performance of this configuration for representative rime and glaze icing conditions is shown in figure 4. The drag levels as measured by a translating wake survey probe indicated large drag increases relative to clean model levels due to the ice accretions (80 to 171 percent) and drag increases of 21 to 52 percent due to the residual ice left after one boot inflation.

The results of this preliminary, proof-of-concept test were encouraging enough that a joint NASA/Army/Bell/B.F. Goodrich program was established to conduct the required flight tests to further evaluate the feasibility of the pneumatic boot concept for rotor deicing. This flight testing effort has been conducted in several phases: flight loads survey performance and handling qualities tests, hover icing (artificial), forward flight icing (artificial and natural), and rain and sand erosion testing.

Clear air and icing flight tests were conducted by the Army Engineering Flight Activity (Edwards Air Force Base) while Bell Helicopter Textron instrumented the set of rotor blades to which had been affixed the pneumatic boot deicers provided by B.F. Goodrich. The system as installed on the JUH-1H weighed only 30 lb and consisted of only six major components: pneumatic deicer, regulator-reliever shut-off valve, timer, rotary union, hose and flap assembly, and ejector flow control valve to keep the deicers deflated. Figure 5 shows a schematic of the JUH-1H helicopter with the key pneumatic deicer components indicated.

Hover icing tests were conducted in the Canadian National Research Council's Ottawa Spray Rig (fig. 6) while the forward flight icing tests were conducted behind the Army's Helicopter Icing Spray System (HISS) tanker (fig. 7). Natural icing flight tests were conducted in the general vicinity of Duluth, MN. Sand and rain erosion tests were conducted at Fort Rucker, Alabama by the Army Aviation Development Test Activity (USAAVNDTA). Limited artificial rain erosion flight tests were conducted at Edwards Air Force Base, CA by the Army Aviation Engineering Flight Activity (USAAEFA).

The deicing capability of the deicer configurations tested on the JUH-1H was judged to be satisfactory for the range of light thru moderate icing conditions tested. Structural loads measured during flight tests were all within acceptable endurance limits except the main rotor pitch link axial load which exceeded the limit by 20 percent. This was not judged to be critical. No unusual dynamic responses were noted and handling qualities of the JUH-1H were essentially unchanged by installation of the pneumatic boots. However, significant hover and level flight performance degradation due to pneumatic boot installation effects of the JUH-1H was measured. A summary of the flight test efforts is given in reference 3.

As already indicated, the ability of the Estane material to withstand the sand and rain erosion environment of the rotor was a key issue regarding feasibility of the pneumatic boot deicer. Ten hours of sand erosion testing at Fort Rucker and 6 hours of artificial rain erosion testing behind the HISS tanker failed to result in any detectable erosion. However, 10 hours of flying in natural rain of varying intensity required four separate blade repairs due to pitting and chunking of the Estane material. These repairs were required in the outer span region of the blades. This region was covered by a layer of Estane and was not protected by an active pneumatic deicer, but rather relied on self shedding for deicing.

The preliminary results from the NASA/Army/Industry program suggest that the pneumatic boot deicer is a feasible alternate rotor ice protection system. However, additional field testing appears to be needed to gain more experience with the erosion problems including the practicality of making repairs in the field before final conclusions can be drawn.

ELECTROMAGNETIC IMPULSE DEICER

The electromagnetic impulse deicer (EIDI) is a potentially attractive system for low weight, low power consumption, highly reliable and efficient deicing of aircraft components. The EIDI concept, while first suggested as early as 1937, had not been adequately developed to allow industry to consider incorporation in current or future aircraft designs. However, NASA sponsored an intensive 4 year joint effort with industrial and university partners to develop the required technology base for the EIDI concept. This activity was completed in 1986. Reference 4 summarizes the NASA industry university program for EIDI technology development.

The basic principles behind the operation of the EIDI system are shown in figure 8. Flat-wound coils made of copper ribbon wire are placed just inside the leading edge of a wing's skin with a small gap separating skin and coil. Either one or two coils are placed at a given spanwise station, depending on the size of the leading edge. Two methods of supporting coils are shown: support by the front spar or from a beam attached to the ribs. Also, mounting to the skin itself is sometimes used.

The coils are connected by low resistance, low inductance cables to a high voltage capacitor bank, and energy is discharged through the coil by a remote signal to a silicon-controlled-rectifier ("thyristor"). Discharge of the capacitor through the coils creates a rapidly forming and collapsing electromagnetic field which induces eddy currents in the metal skin. The

fields resulting from current flow in the coil and skin create a repulsive force of several hundred pounds magnitude, but for a duration of only a fraction of a millisecond. A resulting small amplitude, high acceleration movement of the skin acts to shatter, debond and expel the ice. Two or three such "hits" are performed sequentially, separated by the time required to recharge the capacitors, then ice is permitted to accumulate until it again approaches an undesirable thickness.

The EIDI system is lightweight and uses a small amount of electrical energy (about 200 J per foot). For fixed-wing aircraft, system weights are comparable to those for pneumatic deicers, and the power used is about equal to the landing light power. The power required is about one percent of that used by a hot gas anti-icing system, or about 10 percent of an electrothermal system.

The ability of the EIDI system to efficiently deice the many fixed wing icing components which were tested in the IRT suggested that the system might also be used to deice helicopter rotors. In order to provide a preliminary evaluation of this hypothesis, a midspan section of an AH1 Cobra rotor blade was reworked to include EIDI coils and the resulting model was tested in the IRT (fig. 9). The Cobra blade section was of all composite design and had a chord of 31 in., but for these tests the leading edge was made of sheet metal, and attached only at its upper and lower surface extremities.

Acceptable deicing characteristics (as shown in fig. 10) were observed for a configuration which had mini-coils located every 8 inches on the pressure surface. Coils placed adjacent to the upper or suction surface did not yield such satisfactory deicing results either when tested alone or in conjunction with selected lower surface coils.

While these initial fixed position airfoil de-icing tests gave satisfactory deicing results, several design related problems became apparent. In particular, the rotor leading edge abrasion shield must be free to move in a normal direction in order to expel ice so bonding of the shield to the composite nose would have to be restricted to well downstream of the nose on the upper and lower surfaces. Space must also be found forward of the rotor main spar to run the required number of insulated wires to the coils as well as for the coils themselves. Also, the delicate aeroelastic balance of the rotor must not be upset by inclusion of the EIDI system.

These concerns strongly suggest that the incorporation of EIDI into a helicopter rotor must be done as either part of a redesign of an existing rotor or design of a new system. That is, the EIDI is not an add-on system for helicopter rotor blades. Thus the development of the required technology cannot be accomplished so readily as it was for fixed wing aircraft where retrofitting of EIDI was an acceptable approach.

In the future, it is hoped that a joint NASA/Army/industry/university consortium can be established which will develop the required technology base. It is envisioned that a series of IRT tests will be initially required followed by hover icing tests at the Ottawa Spray Rig and forward flight icing tests, in both artificial and natural conditions.

ICING SIMULATION

The rotorcraft icing community is severely lacking in available validated simulation techniques (both experimental and analytical) to investigate icing problems for research and development, design, or certification/qualification purposes. A major goal of the NASA rotorcraft icing research effort is to develop and validate the required simulation techniques. The following section describes the various research efforts, the results of which will contribute to this goal.

AIRFOIL PERFORMANCE IN ICING

Prior to the NASA icing research program, the vast majority of the airfoil performance-in-icing data was acquired in the IRT by NACA researchers in the 1944 to 55 time period. The IRT has a maximum test section velocity of 300 mph ($M \approx 0.4$) which does not allow the high speed icing studies needed by the rotorcraft community to be conducted. It is well known that the outer span regions of helicopter rotors contribute significantly to the overall lift and drag and thus a knowledge of rotor outer span icing characteristics is essential. A first step to gaining this understanding is to understand the high speed icing characteristics of airfoil sections which are representative of outer span sections. Also, it should be noted that the airfoil geometries tested by NACA researchers in the IRT were primarily for fixed wing applications.

In order to begin to acquire the required airfoil high speed icing data base, NASA sponsored an extensive research program in the Canadian National Research Council's (NRC) 12 by 12 in. high speed icing wind tunnel. At the time of this program, the NRC wind tunnel was the only operational high speed icing wind tunnel in North America.

This program, which was conducted by Sikorsky Aircraft and The Ohio State University and is discussed in reference 5, involved testing several different subscale airfoil geometries over a wide range of aerodynamic and environmental conditions. Figure 11 shows the main airfoil geometries tested. The NACA0012 airfoil represented a first generation rotor airfoil while the VR-7 SC1095, SC1094 R8, and SC1012 R8 represented second generation airfoil contours. The SSC-A09 and circulation control sections were chosen to represent advanced airfoil designs.

A large amount of airfoil icing performance and ice accretion shape data was acquired for Mach numbers from 0.3 to as high as 0.7. In addition to airfoil force and moment levels, measurements were also made of surface pressure distributions for some of the models.

Figure 12 shows some typical data gathered during the test program. Changes in airfoil lift and moment coefficients are shown as a function of icing time. For all airfoil configurations, increases in drag coefficient were large while the changes in lift and pitching moment coefficients were smaller (but certainly not insignificant).

Data such as that shown in figure 12 was used to formulate correlation equations for changes in airfoil lift and moment coefficients as functions

of aerodynamic, environmental, and airfoil geometric variables. These correlation equations gave predictions which agreed with the experimental data to within about 30 percent.

These two-dimensional airfoil icing correlation equations were then used along with appropriate rotor performance analysis codes to predict rotor performance in icing for the S-76, UH-1H, and UH-60A aircraft and to compare the predictions with available icing flight data. Predictions were made for torque rise levels for both hover and forward flight conditions. The results are shown in figure 13. Appreciable scatter existed in the results, although the general agreement was judged to be better for the hover condition. Generally, the predicted torque rise levels for forward flight conditions were less than the observed values.

It is difficult to evaluate the shortcomings of the analysis from these limited comparisons since the quality of the flight data can be questioned. The data was gathered during programs for which the main goal was to evaluate ice protection system performance rather than to acquire rotor performance-in-icing data. It is felt that dedicated flight test programs must be conducted to acquire quality code validation data. Also, shedding of ice, especially from the outer span region of the rotor, is felt to be a key aspect of rotor icing. The prediction methodology had only a very simple treatment of this complex phenomenon, and no information about shedding was contained as part of the reported experimental results. Again, future flight test programs must adequately document the shedding characteristics.

In 1985, Fluidyne Engineering Corporation (Minneapolis, MN) began operation of a 22 by 22 in. transonic icing wind tunnel (fig. 14). This is an atmospheric total pressure facility which relies on ambient conditions to provide proper air temperature. NASA has initiated a series of tests in this facility to acquire larger chord rotorcraft airfoil icing data. First phase of testing involved acquiring ice accretion shapes for a NACA0012 section for Mach numbers up to 0.6 while follow on testing will involve acquisition of ice shapes and resulting section drag levels. Eventually, tests will be conducted with other representative airfoil sections.

Lower speed icing studies of the NACA0012 airfoil (21 in. chord) have been conducted in the NASA IRT (ref 6). These studies are also aimed at acquiring airfoil ice accretion and resultant drag increase levels.

An oscillating rig mechanism for the IRT has been fabricated and will be used in future tests to assess the importance of pitch oscillation on ice accretion and resultant aero degradation levels.

MODEL ROTOR ICING

While two-dimensional airfoil icing data is a required part of a comprehensive rotor icing data base, data is also required for actual rotors operating in the icing environment. This data would include ice accretion shapes, ice shedding characteristics, and resultant rotor loads. Natural and artificial icing flight tests of full scale helicopters is the most obvious way to acquire such data, but flight testing is an expensive, man-

power intensive effort and it is not realistically possible to be able to acquire data for "worst" icing conditions.

A more desirable approach to acquiring such rotor icing data would be through icing wind tunnel tests of properly scaled model rotors. This approach would allow systematic exploration within the icing envelopes of liquid water content, droplet size, and ambient temperature to determine areas of increased rotor sensitivity to icing. To date the only model rotor icing tests conducted have been done by the French (ref 7). The French claimed their results, when compared with natural icing flight test data, showed that meaningful ice accretion and aero performance data could be acquired but the value of electrothermal deicer data was questioned.

Model rotor icing tests could be a valuable test technique not only for icing R&D purposes but also for icing certification purposes. However, for either application, the simulation approach must be validated by comparison with full scale flight data.

In order to develop this model rotor icing test technique, NASA, the four major helicopter companies, and Texas A&M University have formed a consortium to plan and carry out model rotor icing tests in the IRT. The first model to be tested will be a fully instrumented Powered Force Model (PFM) provided by Sikorsky (fig. 15). The rotor diameter will be 6 ft and the airfoil section will be NACA0012. The initial tests of the PFM are tentatively scheduled for late 1987. Follow on tests would involve a properly scaled model rotor to allow direct comparisons to be made with data acquired from a complementary flight test program. It is envisioned that this proposed flight test program would likely be a joint NASA/Army venture.

One issue which must be addressed as part of the model rotor icing effort is what icing scaling relations to apply between full scale and model scale tests. The issue of icing scaling is a key one within the entire icing community since icing research facilities do not exist which allow testing of either full scale components or complete aircraft (model or full-scale) over the complete range of desired conditions. Current NASA efforts with regard to scaling are to concentrate on improving the understanding of the fundamental physics of ice accretion and to conduct comparison tests of the several scaling laws that have been published in the literature. Improvement in the formulation of ice accretion modeling should allow improved scaling relations to be developed.

Another desirable approach to acquiring rotor aero performance-in-icing data is to conduct dry wind tunnel tests of model rotors to which have been affixed to the leading edge representative artificial ice shapes. Initial attempts to explore this simulation approach have involved model helicopter tests in the Texas A&M 7 by 10 low speed wind tunnel (fig. 10). A two-dimensional glaze like ice accretion was affixed to the rotors and resulting rotor loads measured for a variety of hover and forward flight conditions. Typical forward flight test results shown in figure 17 indicate large increases in required torque were experienced relative to the clean rotor levels. The results also indicate that the ice shape covering the final 15 percent span of the rotor makes a large contribution to overall performance degradation.

Supporting two-dimensional airfoil tests were conducted in the Texas A&M 7 by 10 wind tunnel to measure local section performance degradation due to the ice shape. Overall results of both the two-dimensional airfoil and model rotor tests are reviewed in reference 8.

Follow on testing of this model helicopter is currently underway to investigate the importance of using more detailed artificial ice shapes. Simulated asymmetric ice shedding cases are also being studied.

The artificial ice shape testing approach offers another potentially attractive simulation testing technique if it can be properly validated. The ice shapes could be determined by analytical predictions, available experimental data and/or personal judgement. Data acquired could be useful for validating analytical prediction methodologies and for providing data to support qualification/certification programs.

FULL SCALE HELICOPTER ICING

As previously indicated, icing flight testing is a very expensive and time consuming test technique, and validated simulation approaches are preferable. However, some icing flight testing is required to develop the necessary validation data base. These test programs must be dedicated to acquiring such data rather than the data being acquired as a by product of a program aimed at some other goal, such as, development of an ice protection system.

NASA and the Army have completed the first such flight program called the Helicopter Icing Flight Test (HIFT) program (refs. 9 and 10). The overall HIFT program has been a multi year effort which has involved several other organizations Bell Helicopter Textron, Fluidyne Engineering Corporation, Hovey and Associates, and The Ohio State University.

The major elements of the HIFT program and how they are related are shown in figure 18. Phase I flight tests were conducted in the Canadian NRC'S Ottawa Spray Rig while Phase II flight tests were conducted behind the Army's HISS tanker. For each Phase of the flight testing, ice was allowed to accrete on the unprotected rotors of the test aircraft, a UH-1H, and resultant aero performance degradation was measured. The test aircraft was then landed with care so as to minimize the ice shed from the rotors during shut down. Rotor ice accretions were then measured along the span primarily using two techniques - ice shape tracings and silicone molds.

Ice shape tracings recorded along the span of the rotor for flight E of the Phase I hover tests are shown in figure 19 while figure 20 shows one of the silicone molds acquired for the same flight. The increase in horsepower required to sustain hover flight for the icing of flight E was 96-HP which was about a 17 percent increase over the clean rotor value. Summaries of the ice shape documentation efforts for the two phases of flight testing are given in references 11 and 12.

The silicone molds acquired from Flight E were then used to make detailed epoxy castings of the ice accretions such as the one shown in figure 21. Full scale UH1H rotor sections, with these castings affixed to the leading

edge were tested in the Fluidyne dry transonic wind tunnel to measure rotor sections drag increases due to the artificial ice shapes. The results of these tests are shown in figure 22. These results were then used along with Bell rotor performance codes to predict the rotor degradation. The comparisons for Flight E shown in figure 23 indicated good agreement existed between measured and predicted performance degradation.

For the forward flight tests (phase II), one flight test point has been chosen for follow-on testing and analysis. The wind tunnel tests have been completed and the rotor performance degradation predictions will soon be made.

The HIFT program has demonstrated that it is possible to acquire rotor ice accretion/aero-performance data for hover and forward flight icing. Future test programs should incorporate in-flight ice shape documentation in addition to the ground documentation techniques employed in the HIFT program. One such flight system might be the hub mounted video camera system developed by the Army as part of the rotor pneumatic boot program already discussed. Such a system could document when and where ice shedding occurred during the test flights.

ROTOR ICING ANALYSIS

The major efforts in rotor icing analysis are in the areas of rotor aero performance degradation and electrothermal de-icing performance.

Initial aero performance predictions were accomplished through joint NASA/Boeing-Vertol/Texas A&M studies to predict Boeing Chinook front rotor degradation due to rime icing (refs. 13 and 14). The intent of this initial study was to determine whether it was feasible to predict rotor performance in icing using a purely theoretical approach. In particular, a droplet trajectory code, an airfoil performance degradation correlation expression, and a rotor performance code were coupled to form an analysis methodology. Initial studies were done for hover icing (ref. 13) and then extended to forward flight conditions (ref. 14). The droplet trajectory code used was that developed by Bragg (ref. 15).

Figure 24 shows the predictions for horsepower required to maintain a constant value of rotor thrust coefficient for two different assumed radial extents of icing (85 and 100 percent). The figure shows the important contribution of the rotor outer span to overall rotor degradation. These results clearly show that a comprehensive rotor icing performance methodology must be able to predict radial extent of icing. Also these results suggest the importance of being able to handle rotor ice shedding, especially in the outer span region.

The hover icing predictions were encouraging enough to extend the predictions to forward flight conditions. This conclusion was primarily on the basis that the performance degradation levels predicted were reasonable, especially when compared to reported values for other helicopters. Unfortunately, no data was available at the time for Chinook performance in icing.

For the hover icing analysis, it was possible to take advantage of the rotor axial symmetry so that droplet trajectory and airfoil performance analyses had to be performed only as a function of radial position and not also as a function of azimuthal position. However, for the forward flight analysis it was necessary to account for the azimuthal dependence.

Initially, trajectory and airfoil performance calculations were performed for 13 radial locations for each 15° increment of rotor disk (24 total azimuthal locations). This matrix of information was then input into the forward flight performance code and rotor degradation predicted. A simplified approach was also investigated which involved calculating average section Mach number and angle-of-attack for each radial location on the rotor. These average conditions were then used as inputs into the trajectory and airfoil performance analyses. The resultant array of airfoil degradation levels were then input into the rotor performance code to make the final prediction. While the number of calculations required for this simplified approach was far less than for the detailed analyses, the results differed by no more than 5 percent in predictions of horsepower required to sustain level flight.

Figure 25 shows the predictions of horsepower required (referenced to the no ice value) using the detailed analytical approach. Four different assumed radial extents of icing are shown, and again the importance of the outer span icing is evident. Sikorsky employed this same basic analytical approach in the studies already mentioned. Improvements on the initial NASA/Boeing-Vertol/Texas A&M methodology were in the areas of predictions of spanwise extent of icing, prediction of ice shedding, and use of general airfoil correlations rather than just a rime icing correlation.

The major conclusion to be reached from the rotor icing analysis efforts completed is that it appears to be possible to develop a comprehensive rotor icing analysis methodology which will predict with reasonable accuracy the rotor degradation levels to be expected from ice accretions. Current NASA efforts are aimed at developing such a comprehensive methodology, the main elements of which are shown in figure 26. In the near term, correlations will be used to predict airfoil degradation due to icing while in the longer term it is envisioned that these correlations will be replaced by codes which predict the actual ice accretion distribution on the rotor and the resultant section changes in lift, drag, and moment coefficients. These codes are currently being developed and validated by NASA as part of the aircraft icing research program. Also, ongoing fundamental research (both analytical and experimental) in the area of ice structural properties should provide some guidance in the development of the ice shedding module.

While this rotor icing analysis methodology will certainly require significant computational resources, it is felt that it will be a fundamentally correct methodology which will not be based on extensive use of correlations which can always be questioned when "new" or different rotor configurations are investigated.

Again, it must be emphasized that additional high quality icing flight test data must be acquired to validate this rotor icing analysis methodology. Currently, the data being used is that provided through the HIFT program as well as unprotected British RAF Chinook data provided by the British Royal

Aircraft Establishment (RAE) through the joint NASA/RAE studies on helicopter icing.

The other analysis effort has been the development and validation of a series of transient heat conduction codes which model the electrothermal deicer. Figure 27 gives the important characteristics of the six different codes developed to date and how they differ from one another. As the table suggests, the codes vary greatly in complexity and therefore, in the size of computer required. Codes 1 and 2 which model the electrothermal deicer on a one-dimensional, time varying basis can be run on a personal computer. Code 6 which analyzes the complete two-dimensional geometry, including the variable thickness ice layer and the many layers of the airfoil geometry requires a supercomputer (i.e. a Cray 1S or XMP) to achieve reasonable run times. A unique feature of all codes is that they treat the melting of the ice through a phase change routine.

Currently, the code predictions are being compared with electrothermal deicer data from icing wind tunnel and helicopter natural icing flight tests. These comparisons are aimed at providing a better understanding of how accurately the various codes can predict electrothermal deicer performance for the various levels of modeling complexity.

References 16 to 20 give detailed descriptions of the individual electrothermal deicer codes.

CONCLUDING REMARKS

This paper has reviewed the accomplishments to date of NASA research efforts related to helicopter icing. Some suggestion has also been given as to future planned efforts. The two major areas of concentration will continue to be developing advanced rotor ice protection concepts and developing/validating rotor icing analytical and experimental simulation methodologies. The development of advanced ice protection concepts will provide the helicopter industry with alternatives to the electrothermal system which is viewed by many to be too expensive and too heavy and to require too much power. Validated analytical and experimental simulation methodologies are tools needed by the industry to increase their understanding of the rotor icing problem and to reduce time and cost associated with icing certification/qualification. In order to accomplish a timely transfer of this icing technology, most of the research efforts are performed jointly with industry through either formal contracts or co-operative programs.

REFERENCES

1. Werner, J.B.: Ice Protection Investigation for Advanced Rotary-Wing Aircraft. LR-25327-10. Lockheed-California Co., 1973. (USAAMRDL-TR-73-38, AD-771182)
2. Blaha, B.J.; and Evanich, P.L.: Pneumatic Boot for Helicopter Rotor Deicing. NASA CP-2170, 1980.

3. Haworth, L.A.; and Graham, M.S.: Flight Tests of the Helicopter Pneumatic Deicing System. American Helicopter Society. National Specialists Meeting, Helicopter Testing Technology, October 29 - November 1, 1984.
4. Zumwalt, G.W.; Schrag, R.L.; Bernhart, W.D.; and Friedburg, R.A.: Analysis and Tests for Design of an Electro-Impulse Deicing System. NASA CR-174919, May 1985.
5. Flemming, R.J.; and Lednicer, D.A.: High Speed Ice Accretion on Rotorcraft Airfoils. NASA CR-3910, August 1983.
6. Olsen, W.; Shaw, R.; and Newton, J.: Ice Shapes and the Resulting Drag Increase for a NACA0012 Airfoil. NASA TM-83556, 1984.
7. Guffond, d.P.: Icing and Deicing Test on a 1/4 Scale Rotor in the ONERA SIMA Wind Tunnel. AIAA Paper 86-XXX, January 1986.
8. Korkan, K.D.; Cross, E.J.; and Cornell, C.C.: Experimental Study of Performance Degradation of Performance Degradation of a Model Helicopter Main Rotor with Simulated Ice Shapes. AIAA Paper 84-0184, January 1984.
9. Abbott, W.Y.; Belte, D.; Williams, R.A.; and Stellar, F.W.: Evaluation of UH-1H Hover Performance Degradation Caused by Rotor Icing. USAAEFA Report 82-12, August 1983.
10. Abbott, W.Y.; Linehan, J.L.; Lockwood, R.A.; and Todd, L.L.: Evaluation of UH-1H Level Flight Performance Degradation Caused by Rotor Icing. USAAEFA Report 83-23.
11. Lee, J.D.; Harding, R.; and Palko, R.: Documentation of Ice Shapes on the Main Rotor of a UH-1H Helicopter in Hover. NASA CR-168332.
12. Hanson, M.K.; and Lee, J.D.: Documentation of Ice Shapes on the Main Rotor of a UH-1H Helicopter in Level Flight. NASA CR-175088, March 1986.
13. Korkan, K.D.; Dadone, L.; and Shaw, R.J.: Helicopter Rotor Performance Degradation on a National Icing Encounter. AIAA Journal of Aircraft, Vol. 21, 1984, p.84.
14. Korkan, K.D.; Dadone, L.; and Shaw, R.J.: Performance Degradation of Helicopter Rotor Systems in Forward Flight Due to Rime Ice Accretion. AIAA Paper 83-0029, 1983.
15. Bragg, M.B.: Rime Ice Accretion and Its Effect on Airfoil Performance. NASA CR-165599, 1982.
16. DeWitt, K.J.; and Baliga, G.: Numerical Simulation of One-Dimensional Heat Transfer in Composite Bodies with Phase Change. NASA CR-165607, 1982.
17. Marano, J.J.: Numerical Simulation of an Electrothermal Deicer Pad. NASA CR-168097, 1983.

18. Chou, D.F.K.: Numerical Simulation of Two-Dimensional Heat Transfer in Composite Bodies with Application to Deicing of Aircraft Components. NASA CR-168283, 1983.
19. Masiulaniec, K.K., et al.: Full Two-Dimensional Transient Solutions of Electrothermal Aircraft Blade Deicing. AIAA Paper 85-0413, January 1985.
20. Leffel, K.L.: A Numerical and Experimental Investigation of Electrothermal Aircraft Deicing. NASA CR-175024, 1986.

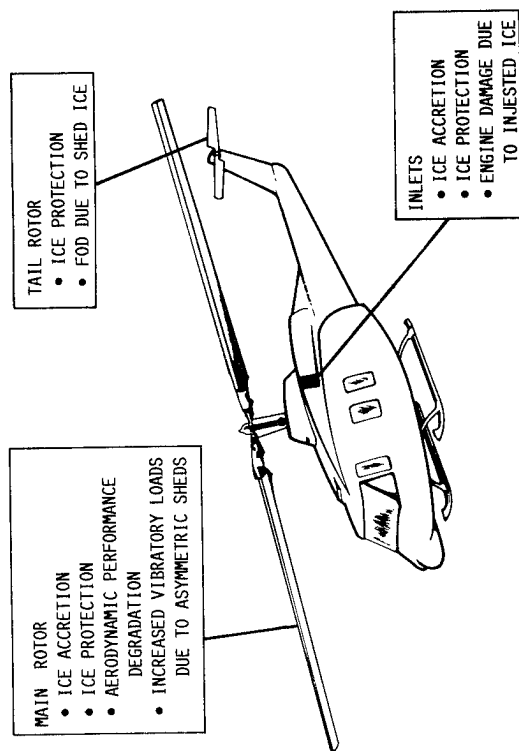


FIGURE 1. - MAJOR ROTORCRAFT ICING CONSIDERATIONS.



FIGURE 2. - PNEUMATIC BOOT ON ROTOR SECTION MODEL INSTALLED IN
6x9 FT NASA LEWIS ICING RESEARCH TUNNEL.

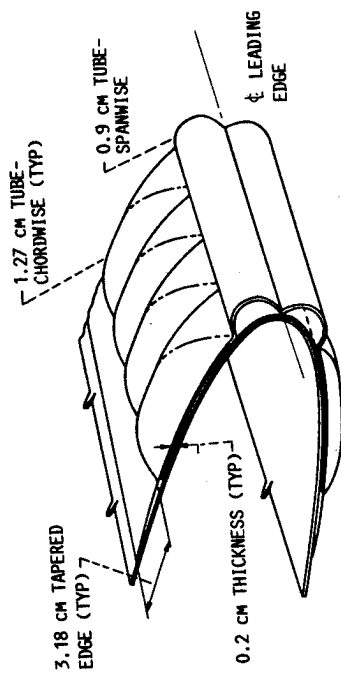


FIGURE 3.- TYPICAL CROSS SECTION OF INSTALLED DEICER (INFLATED).

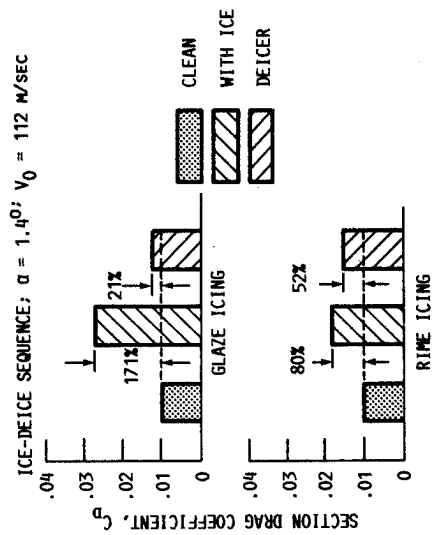


FIGURE 4.- SECTION DRAG OF HELICOPTER ROTOR MODEL WITH PNEUMATIC BOOT.

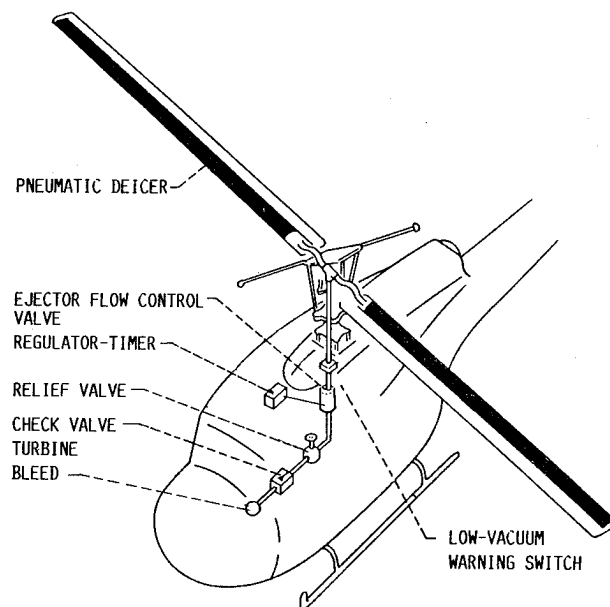


FIGURE 5. - MAIN ROTOR APPLICATION OF PNEUMATIC DEICER.



FIGURE 6.- CANADIAN NATIONAL RESEARCH COUNCIL'S OTTAWA SPRAY RIG.

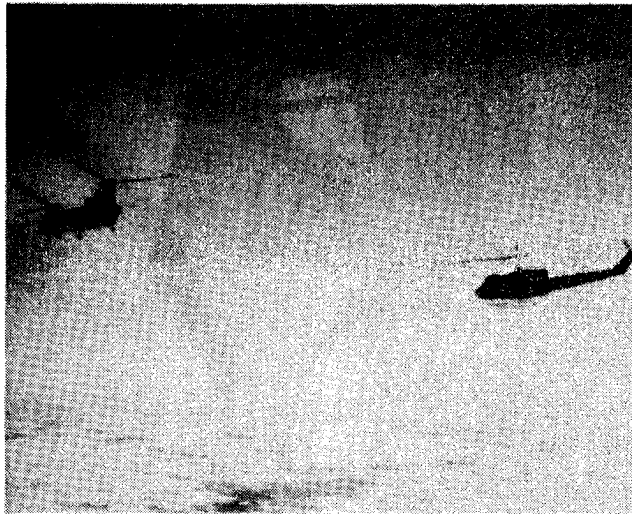


FIGURE 7.- ARMY'S HELICOPTER ICING SPRAY SYSTEM (HISS) TANKER.

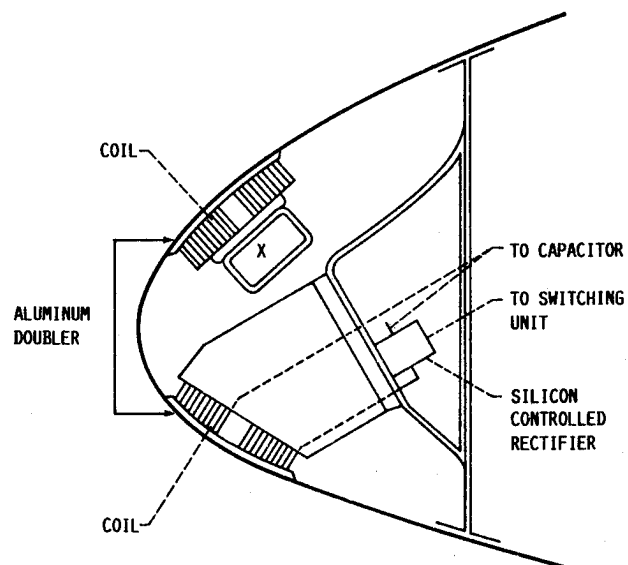


FIGURE 8.- EIDI IMPULSE COILS IN A LEADING EDGE.

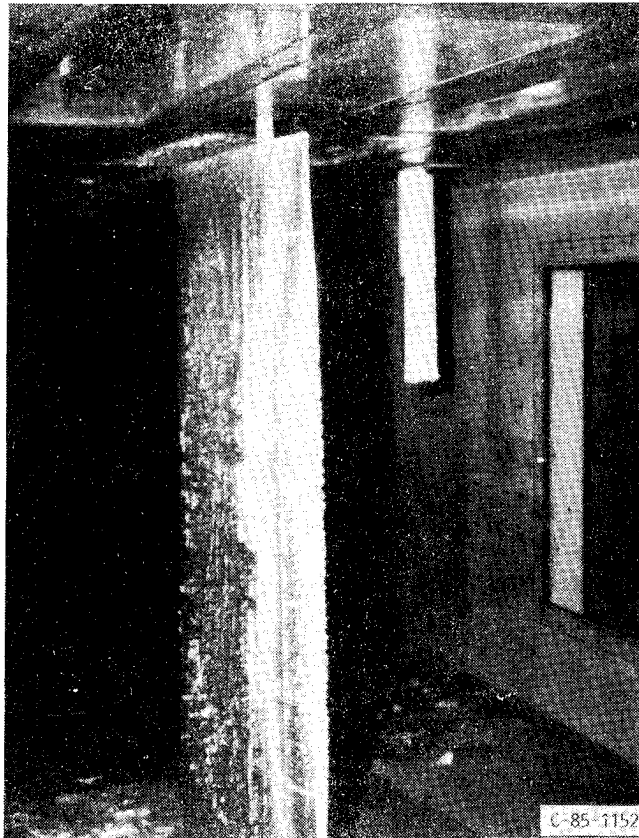


FIGURE 9.- AH1 CORBA ROTOR SECTION IN NASA IRT WITH LEADING EDGE
ICE ACCRETION.



FIGURE 10.- AH1 COBRA ROTOR SECTION AFTER ACTIVATION OF EIDI SYSTEM.

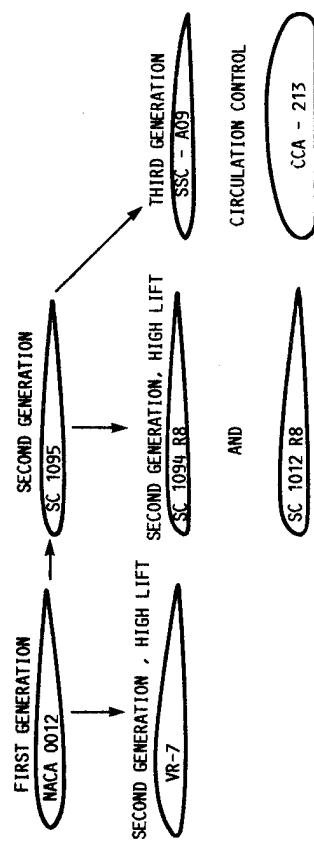


FIGURE 11.- ROTOR AIRFOIL GEOMETRIES TESTED IN CANADIAN NATIONAL RESEARCH COUNCIL'S HIGH SPEED ICING WIND TUNNEL.

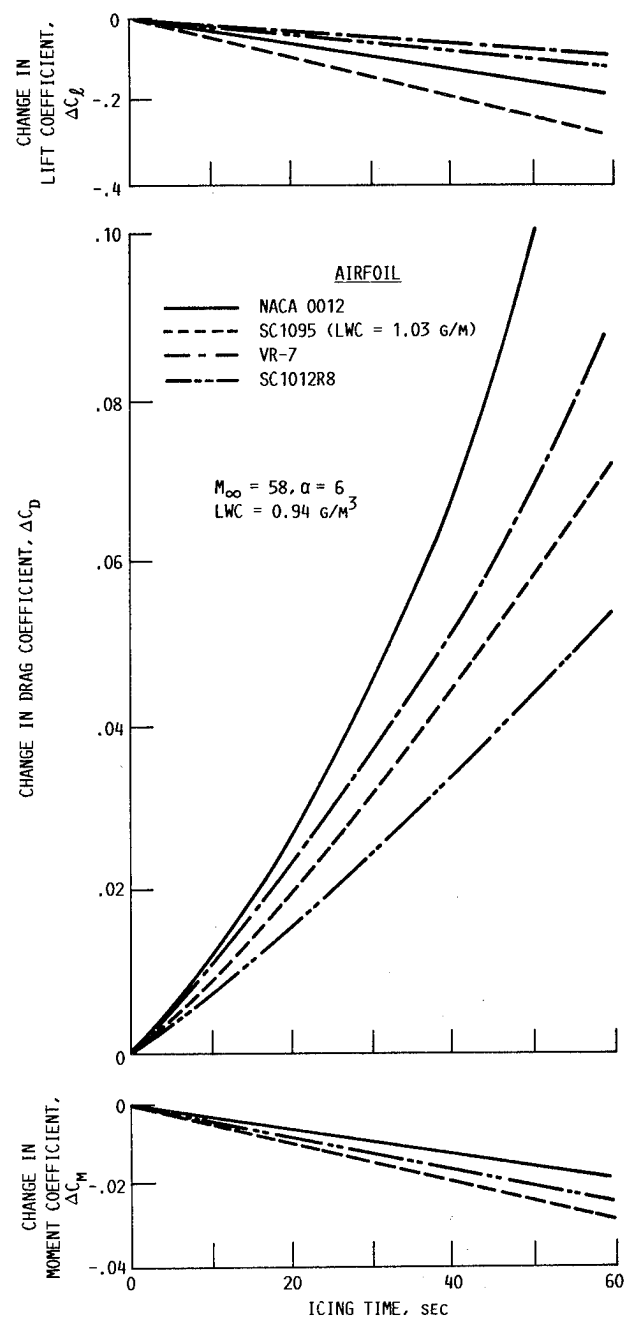


FIGURE 12.- EFFECT OF ICING TIME AT AN ANGLE OF ATTACK OF 6 DEGREES AT HIGH MACH NUMBERS.

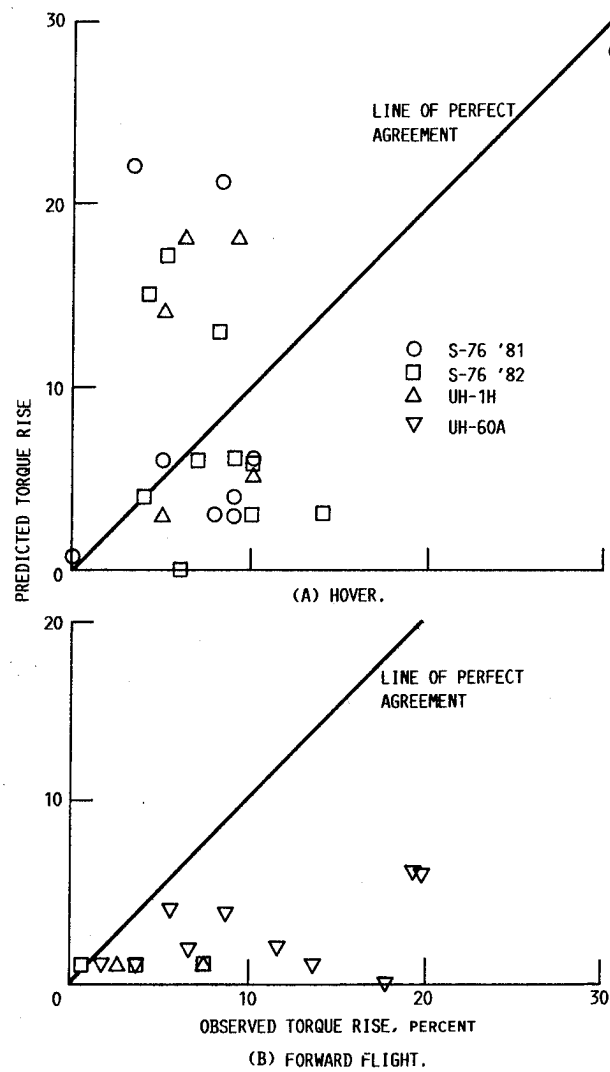


FIGURE 13.- COMPARISON OF PREDICTED AND MEASURED TORQUE RISES FOR HOVER AND FORWARD FLIGHT ICING CONDITIONS.

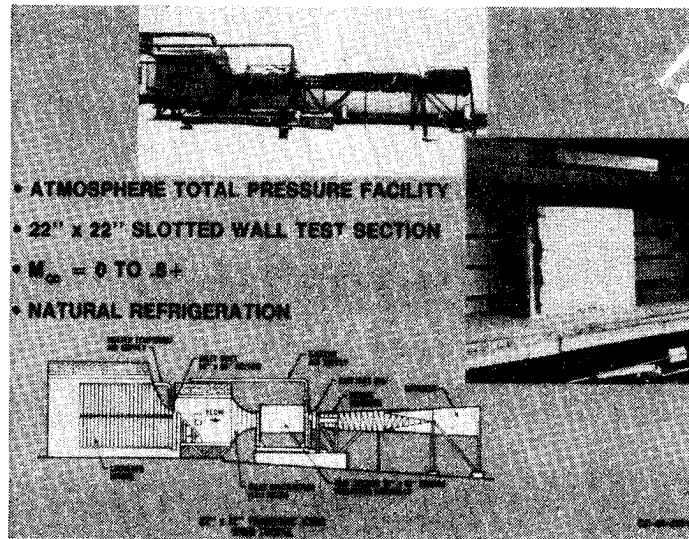


FIGURE 14.- FLUIDYNE HIGH SPEED ICING WIND TUNNEL.

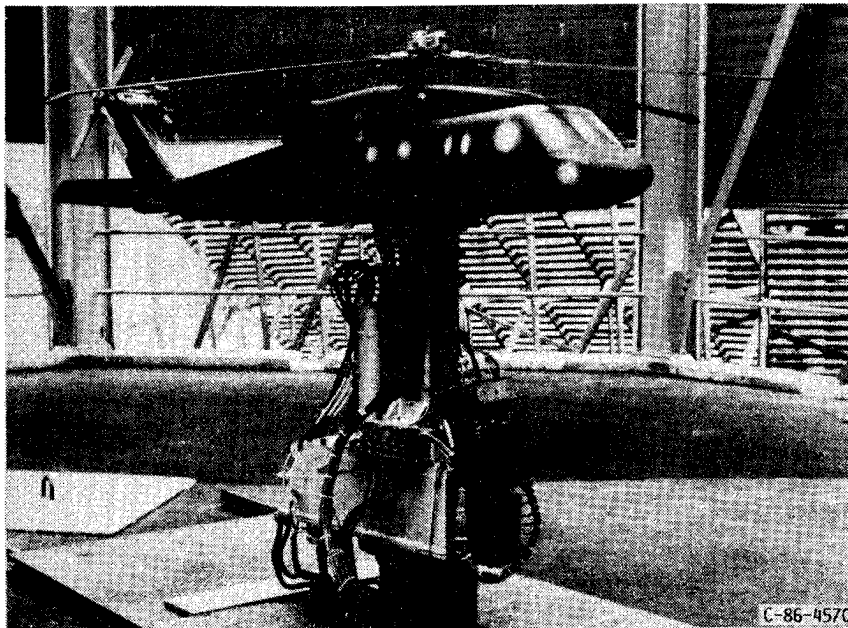


FIGURE 15.- SIKORSKY POWERED FORCE MODEL TO BE TESTED IN NASA IRT.

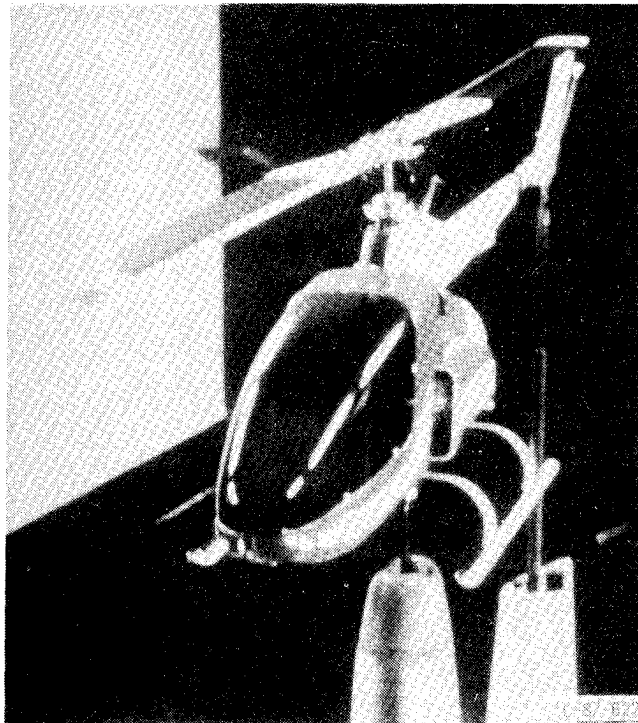


FIGURE 16.- MODEL HELICOPTER INSTALLED IN TEXAS A & M 7x10 LOW SPEED WIND TUNNEL.

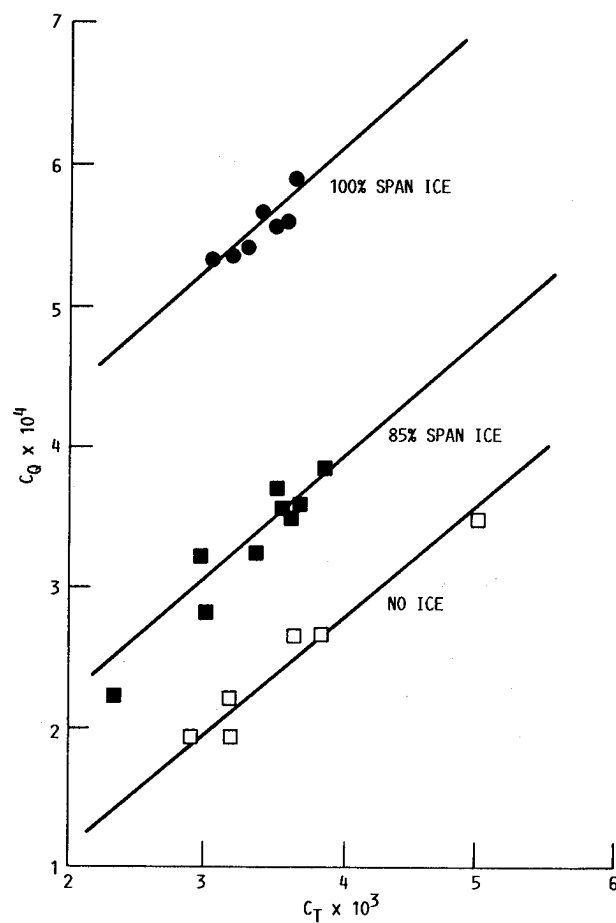


FIGURE 17.- VARIATION OF TORQUE COEFFICIENT VERSUS THRUST COEFFICIENT FOR VARIOUS SPANWISE ADDITIONS OF GENERIC ICE: FORWARD-FLIGHT CONDITION.

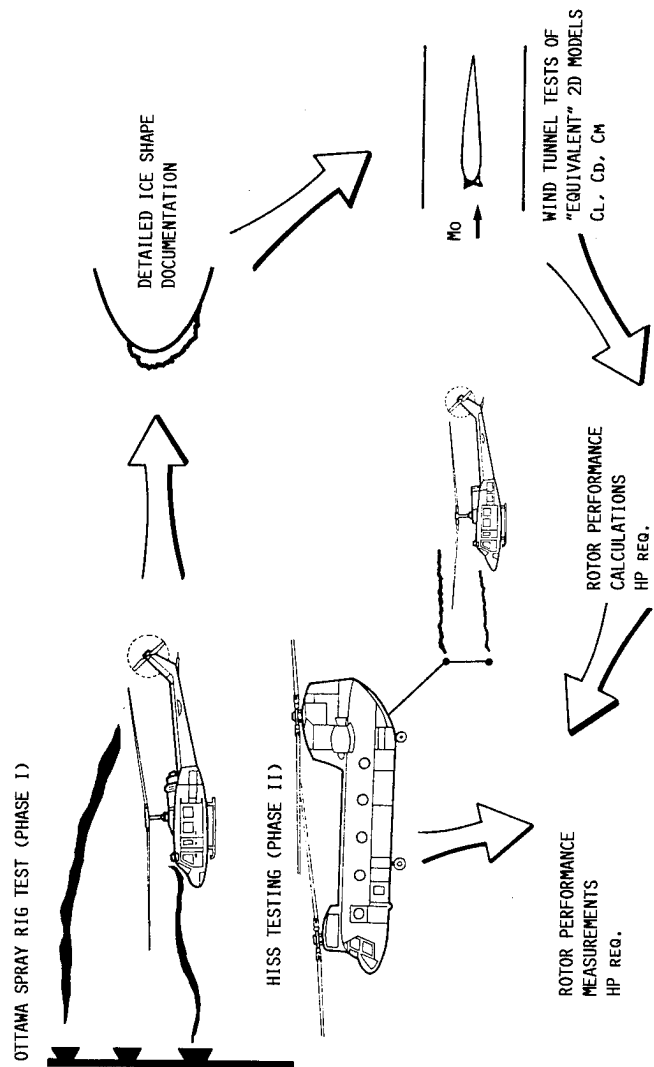


FIGURE 18.- ELEMENTS OF HELICOPTER ICING FLIGHT TEST PROGRAM.

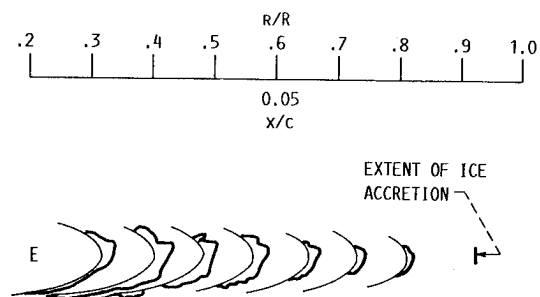


FIGURE 19.- SPANWISE VARIATION IN ROTOR ICE SHAPES FOR FLIGHT E OF PHASE I TESTING.

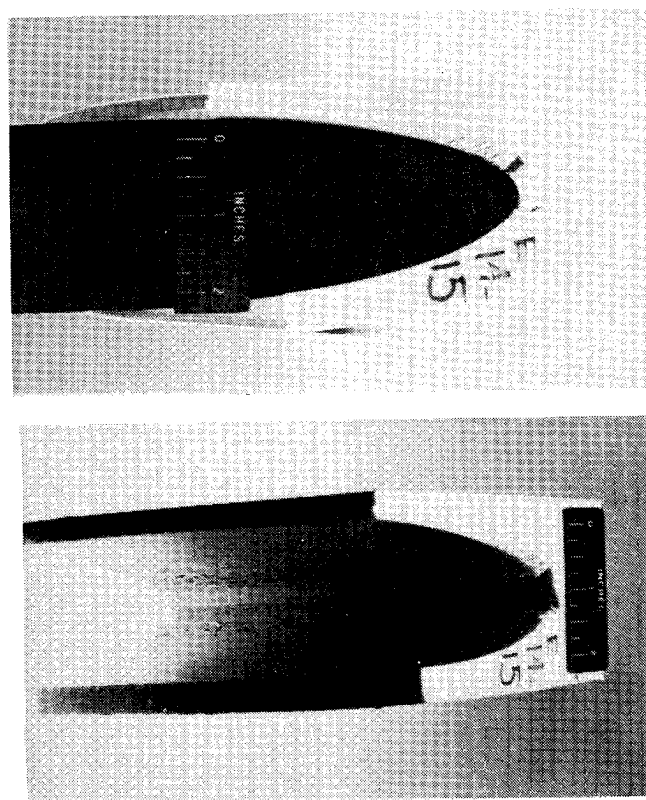


FIGURE 20.- TYPICAL MOLDS OBTAINED OF ICE FORMATION FOR FLIGHT E.

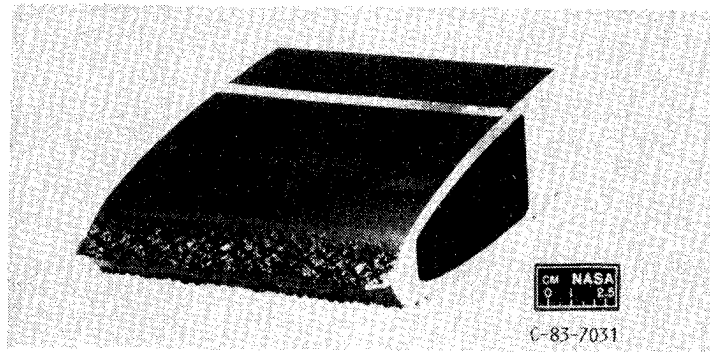


FIGURE 21.- EPOXY CASTING AFFIXED TO UH-1H ROTOR SECTION.

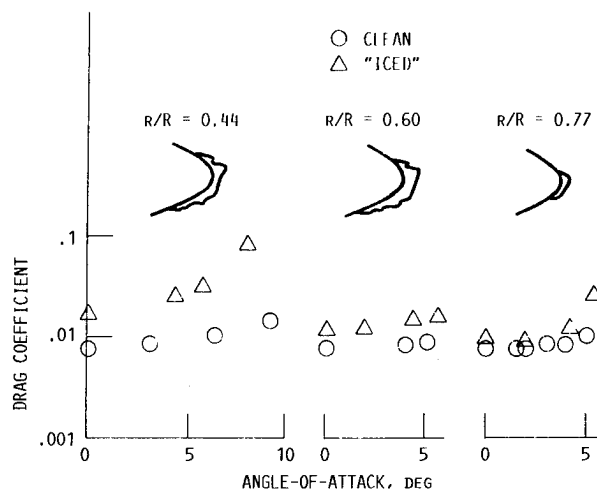


FIGURE 22.- DRY WIND TUNNEL RESULT FOR "ICED" AIRFOIL PERFORMANCE.

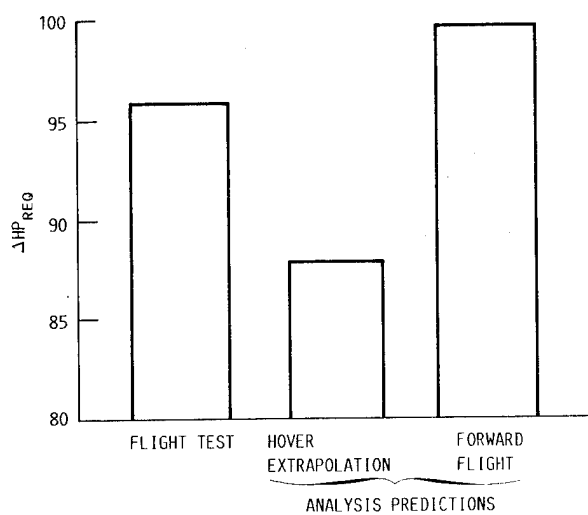


FIGURE 23.- UH-1H ROTOR PERFORMANCE DEGRADATION DUE TO ICING FOR FLIGHT E - EXPERIMENTAL AND PREDICTED.

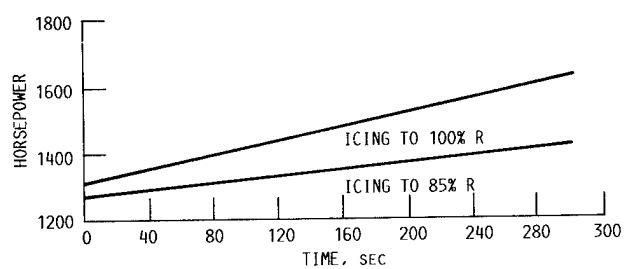


FIGURE 24.- HORSEPOWER REQUIRED TO MAINTAIN A C_T OF 0.004 AS A FUNCTION OF ICING TIME - CH47D HELICOPTER ROTOR BLADE, HOVER CONDITION.

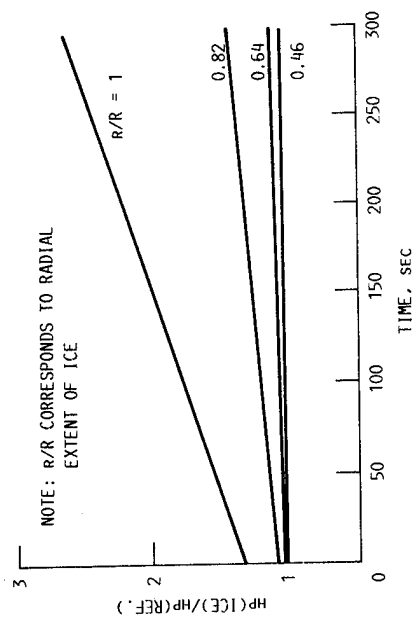


FIGURE 25.- HORSEPOWER REQUIRED WITH RIME ICE ACCRETION TO MAINTAIN A PROPULSIVE FORCE OF 1460 LB AND THRUST OF 20 750 LB (HP (REF.) = 1990, FRONT ROTOR) (360° AVERAGE - 15° SEGMENT).

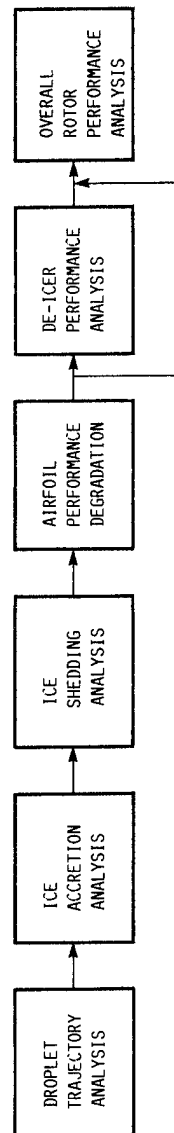


FIGURE 26.- ELEMENTS OF COMPREHENSIVE ROTOR ICING ANALYSIS METHODOLOGY.

GEOMETRY	ICE THICKNESS	NUMBER OF HEATERS	PHASE CHANGE
1. ONE DIMENSIONAL	CONSTANT	ONE	APPROXIMATE
2. ONE DIMENSIONAL	CONSTANT	ONE	WEAK ENTHALPY
3. TWO DIMENSIONAL (RECTILINEAR)	CONSTANT	ONE	WEAK ENTHALPY
4. TWO DIMENSIONAL (RECTILINEAR)	CONSTANT	VARIABLE	WEAK ENTHALPY
5. TWO DIMENSIONAL (RECTILINEAR)	VARIABLE	ONE	WEAK ENTHALPY
6. TWO DIMENSIONAL (EXACT)	VARIABLE	MULTIPLE	WEAK ENTHALPY

FIGURE 27.- ELECTROTHERMAL DEICER CODES.

FLIGHT DYNAMICS AND CONTROL

Session Cochairmen:

J. Victor Lebacqz, NASA

David L. Key, Department of the Army

FLIGHT DYNAMICS AND CONTROLS SESSION

SUMMARY

The Flight Dynamics and Controls session consisted of four papers describing progress made in the disciplines concerned with piloted control of rotorcraft. These disciplines are centered on the pilot's ability to control the dynamic environment of a rotorcraft, and including modelling these dynamics over the frequency range of concern to the pilot, developing flight control methodologies to improve those dynamics, determining the pilot-centered requirements for the dynamics, and evaluating mission effectiveness of the combined pilot-vehicle system. To varying degrees, all of the papers are concerned with aspects of these problems and progress that has been made through NASA/Army research in the past decade.

The first paper, by Chen, Lebacqz, Aiken, and Tischler, reviews the development and validation of flight dynamics models for use in real-time simulations and highlights several of the control system design methodologies that have been examined in the rotorcraft context. A key point from the paper is that, as rotorcraft are required to perform ever more demanding missions, the required model complexity increases, and the control design must be carefully integrated with an appropriate level of understanding of the relevant dynamics. The second paper, by Mihalow, Ballin, and Rutledge, concentrates on one aspect of this required integration, which is integrated flight-propulsion control, and demonstrates that successful solutions to these complex problems really require a "global" or integrated modelling and design approach. The third paper, by Nagel and Hart, describes the pilot-centered, or human factors, part of the problem. An important result reviewed here is the development of consistent workload measures that can help to form the basis for the pilot-centered requirements. Finally, the fourth paper, by Aiken, Lebacqz, Chen, and Key, is concerned with integrated pilot-vehicle analyses and experiments and reviews the progress made in simulation capabilities and evaluations of rotorcraft flying qualities. A key point made here is that ground simulation capabilities have improved dramatically in the past decade, providing the basis for a wealth of experimental handling qualities data, but that this research requires an integrated approach which

includes not only analysis and ground simulation but also in-flight simulation, with the last element being of fundamental importance to the validation of the technology.

Taken together, the papers illustrate the tremendous progress made in rotorcraft flight dynamics and control in the past decade. Real-time models have gone from rudimentary six-degree-of-freedom versions to blade element representations that are sufficiently accurate to permit valid examination of specific vehicle problems. Ground simulation hardware has improved from limited or no-motion platforms with a single window terrain board visual scene to an extensive motion capability with broad field-of-view potential. The handling qualities data base for near-earth operations has gone from nil to extensive, and new handling qualities requirements for military and civil operations have been developed. Finally, flight validated rotorcraft dynamics and handling qualities information has been obtained to provide anchor points for the progress made in the modelling, controls, and flying qualities areas.

The lessons for the future are also clear. A variety of interactive elements concerning dynamics, controls, and human factors must be considered during the rotorcraft design process. Because of increasingly demanding missions for rotorcraft, such as air-to-air combat or automated nap-of-the-earth, the degree of interaction of these elements has increased markedly. The review of the past decade presented in these papers shows that these interactive elements must be considered in an integrated fashion to provide a successful mission capability, but the increased complexity caused by the increased interaction cannot be adequately addressed with current knowledge and techniques. A considerable extension is therefore required to perform the integration of these elements for these new design situations, and the goal for the next decade must be to provide these integration technologies and to validate them through ground and in-flight simulation.

HELICOPTER MATHEMATICAL MODELS AND CONTROL LAW DEVELOPMENT FOR HANDLING QUALITIES RESEARCH

Robert T. N. Chen, J. Victor Lebacqz, and Edwin W. Aiken
NASA Ames Research Center, Moffett Field, CA 94035

Mark B. Tischler
U.S. Army Aeroflightdynamics Directorate
NASA Ames Research Center, Moffett Field, CA 94035

SUMMARY

Progress made in joint NASA/Army research concerning rotorcraft flight-dynamics modeling, design methodologies for rotorcraft flight-control laws, and rotorcraft parameter identification is reviewed in this paper. Research into these interactive disciplines is needed to develop the analytical tools necessary to conduct flying qualities investigations using both the ground-based and in-flight simulators, and to permit an efficient means of performing flight test evaluation of rotorcraft flying qualities for specification compliance. The need for the research is particularly acute for rotorcraft because of their mathematical complexity, high order dynamic characteristics, and demanding mission requirements. The research in rotorcraft flight-dynamics modeling is pursued along two general directions: generic nonlinear models and nonlinear models for specific rotorcraft. In addition, linear models are generated that extend their utilization from 1-g flight to high-g maneuvers and expand their frequency range of validity for the design analysis of high-gain flight control systems. A variety of methods ranging from classical frequency-domain approaches to modern time-domain control methodology that are used in the design of rotorcraft flight control laws is reviewed. Also reviewed is a study conducted to investigate the design details associated with high-gain, digital flight control systems for combat rotorcraft. Parameter identification techniques, both frequency- and time-domain approaches, developed for rotorcraft applications are reviewed. The paper describes the results of both the in-house research and other related efforts via contracts to industry, grants to universities, and international collaborative programs.

INTRODUCTION

This paper summarizes the results of the joint NASA/Army efforts in the development of the helicopter math models and the flight control laws for handling-qualities research using both the ground-based and in-flight simulators at Ames Research Center (ARC). The paper also discusses the development of state estimation and parameter identification techniques using flight test data. These techniques provide a capability to improve the fidelity of the math models and permit an

efficient means of conducting flight test evaluation of helicopter flying qualities for specification compliance.

Efforts began in 1975 to develop a generic flight-dynamics model suitable for real-time simulation motivated primarily by the need to conduct piloted ground-based simulation to determine the helicopter handling qualities requirements for the Army's new doctrine of nap-of-the-Earth (NOE) operations and for airworthiness standards for civil operations in the terminal area. Efforts were also directed at developing simpler math models expressly for use in the investigation of control and display laws to enhance the capability of military helicopters to perform NOE missions under night/adverse weather conditions or to conduct aerial combat. In addition, simulation models for the UH-1H VSTOLAND and the variable-stability CH-47B research helicopter were developed to support the in-flight research programs using the two aircraft.

Until 1981, these analytical flight-dynamics math models were developed mainly for use on the Ames ground simulators which at that time had only a moderate level of computational speed and capacity, typical of the Xerox Sigma class of digital computers. To stay within a reasonable computational cycle time, the frequency range of applicability of these simple models was somewhat limited. They included at most the flapping-dynamics and the main rotor rotational-speed degrees of freedom (DOF), in addition to the basic 6 DOF of the rigid-body dynamics. With the introduction of a CDC 7600 machine dedicated to the Vertical Motion Simulator (VMS) in 1982, the level of sophistication of the helicopter flight-dynamics models was expanded both in the calculation of the aerodynamic forces and moments and in the number of degrees of freedom in the model. Details in the simulation for the engine and its fuel control system were also expanded to be compatible with the level of sophistication of the simulation for the airframe and its flight control system. These high-frequency, full-flight-envelope real-time simulation models for the aircraft/engine system were validated with flight test data and were used to examine helicopter flight characteristics near the boundaries of the operational flight envelopes. They were also used as a basis for an investigation of potential benefits of integrating flight and propulsion controls.

To provide for design analyses of control and display laws, linear models were generated from the nonlinear simulation models. In particular, a new procedure was developed to permit linearization from a nonlinear model that simulates a coordinated or uncoordinated, steep, high-g turn. This new analytical procedure was used to systematically examine the rotorcraft coupling characteristics in high-g turns, the significance of the direction of turns for single-rotor helicopters, and the impact of high-g maneuvers on the performance of the stability-and-control-augmentation systems. In addition to extending the linear model from 1-g flight to high-g maneuvers, the frequency range of validity of the linear model was also expanded by including high-order effects such as rotor and inflow dynamics. These high-order models were used in the analytical and flight investigation of the influence of rotor and other high-order dynamics on helicopter flight-control-system bandwidth.

Several methods have been used to design helicopter flight control laws for handling-qualities investigations. Early on, classical frequency-domain methods were used in the design of control laws to provide a variety of control response characteristics for experimental determination of their suitability for various mission tasks. Time-domain, linear quadratic regulator theory was subsequently applied to the design of a high performance stability-and-control-augmentation system for a hingeless rotor helicopter to be used for piloted evaluation on a ground-based simulator. The linear quadratic regulator (LQR)-based, low-order compensation method developed at Stanford University was applied to the design of a hover hold system for the CH-47 research helicopter and was evaluated in flight on that aircraft. An optimal cooperative-control synthesis method developed originally for fixed-wing aircraft at Purdue University which includes an optimal pilot model in the design procedure, was extended and applied to a CH-47 helicopter and was evaluated in a piloted ground-based simulation. In collaboration with industry, advanced control laws were developed for the Advanced Digital/Optical Control System (ADOCS) demonstrator helicopter based on single-axis model-following control concepts. A multivariable model-following control system was developed for the variable-stability CH-47B to enhance its in-flight simulation capability. In addition, problems associated with the design and implementation of high-bandwidth digital control systems for combat rotorcraft were investigated in order to reduce the cost and time involved in control system modifications or redesigns often required during the flight test phase of a development program.

It is essential that the mathematical models for real time simulations or for analyses and syntheses of flight control laws be evaluated based on comparison with flight test data. To determine how well a simulation model represents the real rotorcraft, the trim characteristics and the response-time histories from flight tests must be compared with those predicted from the model. If the comparison between the test and the calculated data is clearly unacceptable, the correlation must be improved. This can be achieved through the use of parameter identification techniques. The development of parameter identification techniques suitable for rotorcraft application has also been an active area of research at ARC; these techniques have used both time- and frequency-domain approaches.

In the following sections, the results of both the in-house research and the related efforts via contracts to industry, grants to universities, and international collaborative programs are described.

REAL-TIME FLIGHT DYNAMICS MATHEMATICAL MODELS FOR ROTORCRAFT

The development of rotorcraft flight dynamics math models at ARC has been prompted primarily by the need for real-time, piloted ground-based simulation. The complexity of a rotorcraft math model for real-time, pilot-in-the-loop simulation depends on the purpose for which the model is to be used. The math model complexity may be conveniently classified using the two major factors: (1) levels of detail in representing the dynamics of the rotorcraft and (2) levels of sophistication in

calculating the rotorcraft forces and moments, especially for the rotor systems. The first factor determines the validity of the model in terms of the frequency range of applicability. For digital computation in a real-time simulation, the frequency range of interest sets the maximum permissible cycle time. The second factor determines the domain of validity in the flight envelope of the rotorcraft. These two factors together dictate the requirements for simulation computer hardware, software, and programming techniques.

Table 1 shows a list of rotorcraft math models for pilot-in-the-loop simulations. Depending on specific applications, these models reflect differing levels of completeness in representing the aerodynamics and rotor dynamics. The term linear aerodynamics implies simplifications such as small angles of flapping and inflow, and use of simple strip theory with no consideration of compressibility or stall. Models with such simplifications can be used for exploratory investigations of handling qualities of a generic nature within limited regions of the flight envelope. However, for investigations involving exploration to the edges of the flight envelope, then even in generic studies the effects of compressibility, stall, and other nonlinearities must be included. Also, nonlinear effects must be included in the simulations whenever the characteristics of specific rotorcraft are investigated. The rotor dynamic modes include flap, lag, rpm, and inflow degrees of freedom. These rotor dynamic modes are generally of much higher frequency than those of the rigid-body modes. The most important rotor dynamic mode with regard of the interaction with the rigid-body modes is the flapping-regressing mode; therefore, it is generally included in flight dynamics simulation studies. However, for simulation investigations involving the use of high-gain feedback control, the inclusion of lag and other degrees of freedom may also be required.

The math model development has been pursued along the two general directions: generic models and models for specific rotorcraft.

Generic Models

Efforts began in 1975 to develop a simplified generic flight-dynamic model for exploratory pilot-in-the-loop simulation investigations on ground-based simulators that at that time had only moderate computational speed and capacity, typical of the Xerox Sigma class of digital computers. To stay within a reasonable computational cycle time (on the order of 40 ms), the frequency range of applicability of the model was necessarily limited. It included only the flapping dynamics and the main rotor rotational degrees of freedom, in addition to the basic 6 DOF of the rigid-body dynamics. The overall arrangement of the simulation model, which is called "ARMCOP" (refs. 1-3) is shown in figure 1. The model elements are: (1) main rotor, (2) tail rotor, (3) empennage, (4) fuselage, (5) engine-dynamics-and-rpm governor, and (6) control systems. The model elements denoted T_i in figure 1 are required to achieve transfer of velocities, forces, and moments from one axis system to another.

The main rotor model assumes rigid blades with rotor forces and moments radially integrated and summed about the azimuth, using essentially linear aerodynamics

as discussed earlier. The flapping equations of motion explicitly contain the primary design parameters, namely: flapping-hinge restraint, hinge offset, blade Lock number, and pitch-flap coupling. The tail rotor is assumed to be a teetering rotor without cyclic pitch and without including the tip-path plane dynamics. The empennage aerodynamics are modeled with a lift-curve slope between stall limits and a general curve fit for large angles of attack. The fuselage aerodynamic model uses a detailed representation over a nominal angle of attack and sideslip range of $\pm 15^\circ$, and it uses a simplified curve fit at large angle of attack or sideslip. The helicopter model has a generalized control system, as shown in figure 2, which accepts inputs from the pilot, facilitates control augmentation and stability augmentation, and provides for mechanical control mixing or phasing of the cyclic inputs. In addition, a simplified engine/governor model, atmospheric turbulence, and a linearized six-degree-of-freedom dynamic model for stability and control analysis are included.

Some improvements have been made to this model to permit piloted simulator investigations of the engine-out operations (refs. 4, 5). The model has been expanded to include representation of some of the aerodynamic effects of low speed, low altitude, and steeply descending flight (refs. 6, 7). The effect of low-speed, low-altitude flight on main rotor downwash was obtained by assuming a uniform-plus-first-harmonic inflow model and then by using wind tunnel data in the form of hub loads to solve for the inflow coefficients. The results are given as a set of tables for the inflow coefficients as functions of ground proximity, angle of attack, and airspeed. For steep descending flight in the vortex-ring state, the aerodynamic effects were modeled by replacing the steady induced downwash derived from momentum theory with an experimentally derived value and by including a thrust-fluctuation effect caused by vortex shedding. The induced downwash and magnitude of the thrust fluctuations were represented as functions of angle of attack and airspeed.

This model has been used extensively in experimental design analyses and ground-simulator investigations of helicopter handling qualities for NOE operations (ref. 8), for helicopter air combat (refs. 9, 10), and for civil operations in the terminal area (refs. 11-13). The model has also been modified and/or configured to simulate other specific helicopters for handling qualities and flight control research within government agencies, in industry, and in the university. Continuing improvements of the model have been sought through grants in the areas of aerodynamic representation in ground proximity (refs. 14-16) for research in NOE mission tasks and of dynamics details to expand the frequency range of applicability of the model.

A simpler generic model (called "TMAN") was developed for use as the simulation model for the opponent (red) helicopter in the first helicopter-air-combat simulation at ARC (ref. 9). Because of computer capacity limits, the model was required to be relatively simple. Even so, it is capable of realistic maneuvers at hover, of low speeds, and in forward flight, and is easy to fly with a simple set of controllers. The model uses quasi-static linear stability and control derivatives for its aerodynamic representation, but it also uses the complete nonlinear kinematic and

gravitational terms. When configured for the simulation of the red helicopter, it had the following specific characteristics: an attitude command system for pitch and roll at hover and for low-speed flight; and an altitude-rate command and a yaw-rate command system in the vertical and directional axes, respectively. In forward flight, the pitch and roll axes were transformed into angular rate command systems while the directional axis provided an automatic-turn-coordination feature. The model is very easy to modify to achieve other desired stability-and-control response characteristics, and as such it was used extensively as both the blue and red helicopters in the subsequent helicopter air-combat simulations (ref. 17). In addition, it is currently being used in helicopter human-factors laboratory experiments and simulations.

Specific Rotorcraft Math Models

Several flight-dynamics models for specific rotorcraft have also been developed in-house or jointly with the manufacturers. Some of these were developed by modifying the generic ARMCOP model described earlier. Other models such as UH-1H, CH-47B, UH-60, AH-64A, and XV-15 were developed separately. These math models are briefly described below.

UH-60 ARMCOP- The ARMCOP model was modified to allow the simulation of the UH-60 Black Hawk helicopter (ref. 18). This model has been used for piloted simulator investigations of advanced flight control systems for Army helicopters (ref. 19) and a Navy-sponsored piloted simulation of shipboard landings using the SH-60 Sea Hawk (ref. 20). The modifications included the effects of a canted tail rotor, a variable-incidence horizontal stabilator, and the UH-60 pitch-bias actuator. In addition, the ARMCOP fuselage model was significantly modified to incorporate UH-60 fuselage aerodynamics, based upon extensive wind-tunnel test data, and a representation of the UH-60 engine and governor dynamics implemented using the generic model available in ARMCOP.

UH-1H/VSTOLAND and BO-105 S3 ARMCOP- As part of a joint research program of the U.S. Army and the German Aerospace Research Establishment (DFVLR), under the Helicopter Flight Controls Memorandum of Understanding (MOU), a multivariable model-following control system (MFCS) has been developed for use in flight research. In the process of developing the MFCS, the performance of the system was first evaluated on a ground-based simulator at Ames using two helicopter models which have large differences in flight dynamics and control characteristics as well as in control system actuators. One of these is the NASA/Army UH-1H V/STOLAND helicopter and the other the DFVLR BO-105 S3 helicopter. Figures 3 through 6 from reference 21 show the typical control systems and the actuating systems of the two helicopters. The generic ARMCOP model was configured to simulate the flight dynamic characteristics of these two aircraft and the specifics of their control and actuator systems. In addition, the generic simple-engine dynamic model resident in the ARMCOP (fig. 7a) was configured to simulate the BO-105's engine and governor dynamics (fig. 7b), since its rotor rpm dynamics and limits have a strong impact on the collective rate limit allowable for the BO-105 S3 helicopter (ref. 21).

A109 ARMCOP- Under the MOU between the U.S. Army and Italy, the ARMCOP model is being configured to simulate the flight dynamics of an Agusta A109 helicopter. Efforts have been made to correlate the A109 ARMCOP model with the flight test data from the A109K tests conducted during the spring of 1986 in Italy. Current efforts include the development of the A109 digital SCAS for inclusion in the A109 ARMCOP model and the preparation for a piloted simulation on the VMS at ARC.

AH-64A/OH-58D- A model of the AH-64 Apache helicopter (ref. 22) was developed as part of an investigation of its control system and display requirements (ref. 23). The model initially consisted of six degree-of-freedom equations of motion with a full set of nonlinear gravitational and inertial terms. The aerodynamic forces and moments are expressed as the reference values and first-order terms of a Taylor series expansion about a reference trajectory defined as a function of longitudinal airspeed. This particular model allowed a simulation valid for small perturbations from level flight conditions for an airspeed range of -40 to 160 knots. Aerodynamic force and moment data in the form of trim conditions as well as stability and control derivatives were supplied by the manufacturer. Subsequently, the same model was used as the basis for a piloted simulator investigation of certain characteristics of the AH-64 Back-Up Control System (ref. 24).

A similar technique was employed to generate a simulation model of the OH-58D helicopter for a simulator investigation of directional control problems and requirements (ref. 25). In this case, the required aerodynamic force and moment data were generated using an off-line ARMCOP representation of that aircraft based upon input data supplied by the Army and the manufacturer. The model was further modified to include rotor RPM degree-of-freedom and certain nonlinear yaw-damping and control-sensitivity effects which were modeled as functions of relative wind magnitude and direction.

UH-1H ("UNCLE") Model- A model of a Bell UH-1H helicopter was developed specifically for use in flight dynamics investigations and for simulation of terminal-area guidance and navigation tasks (ref. 26). It has been used in simulations for the development of software for the navigation and guidance programs associated with an avionics system known as V/STOLAND (ref. 27) and for a simulator investigation of the effects of failures of the stability augmentation system (ref. 28). The model uses a quasi-static, main-rotor forces and moments representation similar to that of the classical Bailey-Wheatley type, and uses simple expressions for the contributions of the tail rotor, fuselage, and empennage.

CH-47B Model- Similar to the UNCLE model, this model was developed for use in real-time piloted ground-based simulations to support the in-flight research programs using the variable-stability CH-47B research helicopter. This nonlinear simulation model developed by the Boeing Vertol company (ref. 29) has been adapted for use in the ARC simulation facility (ref. 30). It is implemented in the ARC Sigma IX computer where it is operated with a digital cycle time of about 30 msec. The model uses a total-force approach in six rigid-body DOF; steady-state tip-path plane solutions for rotor flapping dynamics form the basis for the simulation of the rotors in this model. The model also includes an option for simulation of externally suspended slung-load equations of motion. This model option, along with

detailed slung-load equations of motion developed in-house (ref. 31), will expedite research in areas related to sling-load operations. The CH-47B model has been used in conjunction with flight research conducted on the CH-47B research helicopter to develop a multivariable model-following control system (ref. 32) and to verify, in-flight, a control-system-design method using modern control theory (ref. 33). These research activities related to the control laws development are further discussed later in the paper.

UH-60 (GENHEL)- As part of a joint Army/NASA program for ground-based simulator validation, a blade-element simulation model for the UH-60 Black Hawk was acquired from Sikorsky Aircraft (ref. 34). Unlike all the other models discussed previously, which were developed expressly for use on ground simulators which had only a moderate level of computational speed and capability (such as the Xerox Sigma class of digital computers), the Black Hawk model was intended for implementation on a CDC 7600 computer, which is a much more powerful machine than a Sigma computer. The UH-60 GENHEL model acquired from Sikorsky includes six rigid-body DOF as well as the main rotor flapping, lagging, air mass, and hub-rotational-speed DOF. It is a blade element model, rather than a total force-and-moment model, and as such, it covers the full range of angles of attack, sideslip, and inflow, without using small-angle assumptions. From this model, the computer code was written to execute in real time on the CDC 7600 computer (dedicated to the VMS). In addition, fidelity of the model has been improved considerably by NASA (ref. 35), notably in the area of engine and drive train modeling. Figure 8 taken from ref. 35 shows a block diagram representation of the simulation elements and their interactions. This improved high-frequency, full flight-envelope, real-time simulation model has been used to conduct the Black Hawk accident simulation investigations on the VMS. It also serves as a basis to investigate potential benefits of integrating flight and propulsion controls (refs. 36, 70).

Other Rotorcraft Mathematical Models- Also available at ARC are several specific rotorcraft math models developed for real-time simulation in a variety of projects. They include a math model for SH-2F (ref. 37), one for SH-3G (ref. 38), one for RSRA (ref. 39), and a math model for the XV-15 (ref. 40). The XV-15 simulation model, in addition to extensive use during the development phase of the aircraft, has been utilized in the ground simulator investigation of VTOL instrument flight rules airworthiness criteria (ref. 41). The model, along with some other models described previously has also been used in the investigations of high-g flight dynamics and high-order dynamic effects to be discussed next.

SMALL PERTURBATION FLIGHT DYNAMICS

Traditionally, the standard equations of airplane motion for small-disturbances from steady, symmetrical, rectilinear 1-g flight as the reference flight condition (refs. 42, 43) have been the basis for stability and control analyses, handling-qualities specifications (refs. 44-47), and design analyses of the stability-and-control-augmentation system (SCAS) for rotorcraft. However, modern military

rotorcraft are now being designed with a view toward expanding their roles in tactical missions such as combat rescue, antitank, and air-to-air operations that require high-g maneuvers that make frequent excursions to the limits of their maneuvering flight envelopes. Therefore, a new analytical framework is needed to permit a systematic examination of the flight dynamics and control characteristics of the basic aircraft and its SCAS to ensure that the overall aircraft-SCAS system will perform satisfactorily, not only in operations near 1-g flight but also in high-g maneuvers.

A fundamental characteristic associated with a rotorcraft with increasing load factor in high-g maneuvers is an increase in control effectiveness and damping, particularly in the pitch and roll axes. The extent of the increase depends, to a large measure, on the main rotor hub design. For a teetering-rotor helicopter, the control in pitch and roll is almost entirely through tilting the thrust vector of the main rotor; therefore, the increase in control effectiveness in these two axes is directly proportional to the load factor. At the other extreme, for a hingeless rotor the increase is much less because the direct hub moment, which produces most of the control power, is independent of the thrust level of the rotor system. The increase in the control effectiveness with the load factor has an obvious effect on the selection of the SCAS. Further, interaxis cross-coupling, such as pitch, roll, and yaw, that results from collective inputs and pitch-roll coupling which results from aircraft angular rates, also changes with load factor. The ramifications of these variations in stability-and-control characteristics for the handling qualities and the design of SCAS needed to be considered.

In addition to this extension of the linear model to high-g maneuvers, the frequency range of validity of the linear model must also be expanded for the design analysis of high-gain FCSs for rotorcraft to meet the requirements for demanding mission tasks such as NOE flight and aerial combat. In the design analysis of such high-gain control systems, it is now essential that high-order dynamics of the system components be adequately modeled, in contrast to past practice in which only the lower-frequency, quasi-static, rigid-body flight dynamics were used in the design of low-gain FCSs. Recent flight investigations that used a variable-stability CH-47B research helicopter at ARC showed that not only high-order elements such as rotor dynamics are required (refs. 48, 49, 32), but also other high-order effects such as dynamics of sensor filters, servo actuators, and data processing delays of the airborne computer must also be adequately modeled.

Inclusion of the air-mass dynamics associated with a lifting rotor has also been shown in recent studies (refs. 49, 51) to be important in the design of high-gain FCSs. The frequencies of the inflow dynamic modes are the same order of magnitude as those of the rotor blade flapping and lead-lag modes; therefore, the dynamic inflow has a significant influence on the aeromechanic stability of the rotor system. In the following sections, we will first discuss the linearization of the rotorcraft motion about a curved flightpath as a reference flight conditions, followed by a discussion of the high-order dynamics.

Linearization of Rotorcraft Motion About Steady High-g Turns

Small-perturbation equations of motion about a generic curved flightpath will result in a set of linear time-varying differential equations which generally is difficult to operate and to interpret. However, if the reference flightpath is chosen to be a steady turn, then the resultant small-perturbation equations of motion will be a set of linear time-invariant differential equations, similar to those obtained from steady rectilinear 1-g flight as the reference flight condition most commonly employed (e.g., refs. 42, 43). Before perturbation operations are applied, the steady reference flight conditions must be established first.

Algorithms have been developed (refs. 52-54) that permit efficient computations of 1) aircraft states and control positions in coordinated steady, steep turns and 2) the associated small-perturbation equations of motion. In developing these algorithms, special attention was given to the influence of sideslip which normally exists in asymmetrical rotorcraft in coordinated turns as discussed previously. Using these algorithms, a study was conducted to investigate the static and dynamic characteristics of several rotorcraft in coordinated, steep, high-g turns (ref. 55). The results indicate 1) that strong coupling in longitudinal and lateral-directional motions exists for rotorcraft in coordinated, high-g turns, 2) that for single-rotor helicopters, the direction of turn has a significant influence on flight dynamics, and 3) that an SCAS that is designed on the basis of standard small-disturbance equations of motion from steady, straight, and level flight and that otherwise performs satisfactorily in operations near 1 g becomes significantly degraded in steep, turning flight.

For some operations, such as in aerial combat, turns may intentionally be flown uncoordinated to reduce the turn radius. To investigate the extent to which the static and dynamic characteristics of asymmetric and symmetric rotorcraft in steep turns are influenced by the levels and direction of uncoordination, the algorithm developed expressly for coordinated turns was extended (ref. 56) to permit an efficient computation of the trim states and control positions in a general, uncoordinated turning maneuver. Table 2 gives the set of trim algorithms for general uncoordinated flight including both uncoordinated steep turns and uncoordinated rectilinear flight. The level and direction of uncoordination are represented by the magnitude and sign of the lateral accelerometer signal n_y (side force) at the aircraft center of gravity. The closed-form kinematic relationships shown in the table decouple the governing equations for a general, steady, uncoordinated turn and thereby greatly simplify the trim computation (to the extent comparable to the normal 1-g flight).

Once the steady, reference flight conditions are determined, the small-perturbation equations of motion are obtained in two steps: 1) by applying the perturbation operation on the Euler equations and on the kinematic equations that relate the time rate of change of pitch- and roll-attitudes to the angular rates about the body-axis system, and 2) by then imposing the constraints that the perturbations are from a steady turn. This development accounts for complete kinematic, inertial, and aerodynamic coupling. Also, the aerodynamic terms include a complete set of acceleration derivatives. Table 3 shows a simpler form of the stability and

control matrices in which the acceleration derivatives are neglected. The equations are given with respect to the general body-axis system and they are cast in the first-order, vector matrix format to which many efficient software packages can be readily adapted.

These equations were implemented in conjunction with the trim algorithms for generic uncoordinated, steep high-g turns in a variety of nonlinear simulation models (refs. 1, 34, 40) to investigate a tilt-rotor aircraft and two single-rotor helicopters in various levels of uncoordinated, high-g turning maneuvers at low speeds. The results show 1) that the aircraft trim attitudes in uncoordinated, high-g turns can be grossly altered from those for coordinated turns; and 2) that within the moderate range of uncoordinated flight (side-force n_y up to ± 0.1 g), the dynamic stability of the rotorcraft is relatively insensitive. However, the coupling between the longitudinal- and lateral-directional motions is strong, and it becomes somewhat stronger as the sideslip increases (ref. 57).

The results of a recent study conducted in a European laboratory (ref. 58) generally confirmed those of ARC. In particular, their results also indicate that in high-g turns, the coupling between the longitudinal and lateral-directional motions is strong. Consequently, the conventional short-period approximation and other approximations (ref. 59) suitable for rectilinear cruise flight become inadequate for predicting stability and response characteristics of the helicopter in high-g turns. As in the Ames studies (refs. 55, 57), their results for turns also show that all the helicopter stability and control derivatives change with load factor (or bank angle). The variations in these derivatives are caused by aerodynamic, inertial, kinematic, and gravitational terms, but it is primarily the increased aerodynamic terms that have the most influence on the short-term dynamic modes.

Considerations for High-Order Dynamics

The increasing use of highly augmented digital FCSs in modern military helicopters has prompted a recent examination at Ames of the influence of rotor dynamics and other high-order dynamics on control-system performance. In the past, industry has predicted stability augmentation gains that could not be achieved in flight (ref. 60, fig. 9). The operators of variable-stability research helicopters have also been aware of severe limitations in feedback gain settings when attempting to increase the bandwidth of FCSs needed to assure good fidelity during in-flight simulations. Now, with an increasing emphasis on high-bandwidth mission tasks, such as NOE flight and aerial combat for military helicopters, coupled with the development of new rotor systems and the trend toward using superaugmented, high-gain, digital FCSs (refs. 19, 61, 62), there is a widespread need for improved understanding of these limitations.

Therefore, a study was conducted at ARC to correlate theoretical predictions of feedback gain limits in the roll axis with experimental test data obtained from the variable-stability CH-47B research helicopter. The feedback gains, the break frequency of the presampling sensor filter, and the computational frame time of the

flight computer were systematically varied. The results, which showed excellent theoretical and experimental correlation (fig. 10), indicate that the rotor flapping dynamics, sensor filter, and digital-data processing delays can severely limit the usable values of the roll-rate and roll-attitude feedback gains.

In addition to rotor flapping dynamics, inflow dynamics can be also significant in the design of high-gain FCSs for rotorcraft. Recent research (refs. 63-67) on dynamic inflow has shown that the frequencies of the inflow dynamic modes are of the same order of magnitude as those of the rotor blade flapping and lead-lag modes; therefore, dynamic inflow can produce significant changes in the modes of rotorcraft motion. A study was therefore conducted at Ames to investigate the effects of dynamic inflow on rotor-blade flapping and vertical motion of the helicopter in hover. Linearized versions of two dynamic inflow models, one developed by Carpenter and Fridovich (ref. 68) and the other by Pitt and Peters (ref. 67), were incorporated in simplified rotor-body models and were compared for variations in thrust coefficient and the blade Lock number (ref. 49). In addition, a good correlation was obtained between the results of linear analysis, and the transient and frequency responses measured in-flight on the CH-47B variable-stability helicopter. The linear analysis also shows that dynamic inflow plays a key role in destabilizing the flapping mode. the destabilized flapping mode, along with the inflow mode introduced by the dynamic inflow, results in a large initial overshoot in the vertical acceleration response to an abrupt input in the collective pitch. This overshoot becomes more pronounced as either the thrust coefficient or the blade Lock number is reduced.

The influence of the lead-lag degrees of freedom on the automatic-control-system design for a helicopter has recently been investigated analytically by Curtiss (ref. 69) under a NASA-ARC grant for near hover flight. He showed that attitude feedback gain is limited primarily by body-flap coupling, but the rate feedback gain is limited by the lag degrees of freedom. An experimental verification is needed.

Beyond the high-order effects caused by rotor and inflow dynamics, the propulsion system dynamics can also have a profound effect on the helicopter flight dynamics and handling qualities. The helicopter rotor and drive train systems have lightly damped torsional dynamic modes which are within the bandwidth of the engine fuel-control system. Traditionally, engine manufacturers use a sophisticated engine dynamic model in conjunction with a rather rudimentary model for the helicopter rotor/airframe dynamics when designing the control system. Helicopter flight dynamicists have used the opposite approach. As a result, the dynamic interface problems that are not anticipated in the design stage can surface later in the ground- or flight-test phases of a helicopter development program, requiring costly add-on modifications to rectify the problems. Therefore, it is important to model the propulsion system dynamics at the levels of sophistication compatible with those of the airframe dynamics in the design of both the fuel control system and the FCS (see ref. 70).

FLIGHT CONTROL LAWS DEVELOPMENT

A variety of methods have been used to design rotorcraft flight control laws for handling qualities investigations. They range from classical frequency-domain design methods to modern time-domain control methodology. Classical frequency-domain methods were first used in the design of control laws to provide a wide spectrum of control response characteristics for experimental determination of their suitability for various mission tasks. These designs were performed mostly in the continuous (or analog) s-domain. To expose potential problems associated with digital implementation, especially for high bandwidth digital control systems, an extensive case study based on the ADOCS was conducted in a discrete z-domain and w-domain.

Modern methods for time-domain control law design were subsequently employed in several case studies. Lienar quadratic regulator theory was applied to the design of a high-performance SCAS for a hingeless rotor helicopter for piloted evaluation on a ground-based simulator. An LQR-based, low-order compensator method was applied to the design of a hover hold system for the CH-47 research helicopter as part of the collaborative efforts with Stanford University. An optimal cooperative control-law-synthesis method, which includes an optimal pilot model in the design procedure, was modified and applied to a tandem-rotor helicopter and was evaluated in a piloted ground-based simulation. A multivariable MFCS was developed for the variable-stability CH-47B research helicopter to enhance its in-flight simulation capability.

Generic Control Laws for Various Types of Response Characteristics

Generic FCSs which can be configured to provide a variety of helicopter response characteristics including rate and attitude were implemented in the basic ARMCOP model (ref. 1) and the ARMCOP/UH-60 model (ref. 18) for handling qualities research. The general form of the SCAS that was incorporated in the ARMCOP model employs a complete state feedback as well as a control mixing structure that facilitates implementation of control crossfeed, with control quickening from each of the four cockpit control inputs. Also, the augmentation-system gains may be programmed as functions of flight parameters, such as airspeed (fig. 2). This constant-gain configuration was subsequently modified (ref. 20) to include dynamic compensation elements in order to represent the SH-60B for the handling qualities investigation of its shipboard operations.

A more complicated implementation of the generic FCS was incorporated in the ARMCOP/UH-60 for the development of the Army's ADOCS. As part of the ADOCS program, control laws suitable for an attack helicopter mission were synthesized, evaluated in piloted simulations of both visual (ref. 71) and instrument flights (ref. 72) under various meteorological conditions, and implemented in a UH-60 demonstrator helicopter. Figure 11 presents a block diagram of the FCS design for the ADOCS program. The primary flight control system (PFCS) shown in the figure was designed to yield satisfactory unaugmented flight by providing feed-forward command

augmentation and shaping. The advanced flight control system (AFCS) included both stabilization feedback loops and a feed-forward control-response model. Stabilization feedback loops were designed solely for maximum gust and upset rejection; no compromise for control response was necessary. The use of a control-response model allowed the shaping of the short- and long-term response to the pilot's control inputs independent of the stabilization level. Various control response and stabilization schemes were developed using this approach to control system design and were evaluated for the attack helicopter mission in conjunction with a range of integrated side-stick controller configurations. These generic configurations are identified in figure 12 in a matrix format.

A generic SCAS configuration was also incorporated in the XV-15 model to provide SCAS features such as rate command, attitude command, rate command/attitude hold, and the translational rate command, to be used for a ground simulation investigation of control actuator authority requirements (ref. 73) and of instrument-flight-rules airworthiness criteria for the tilt-rotor class of Vertical Takeoff and Landing (VTOL) aircraft (ref. 41). The mechanizations were kept as simple as possible so that the results could be easily understood. Consequently, the feed-forward and feedback loops in the generic SCAS configurations employ primarily constant gains with little dynamic shaping required.

Implementation Considerations for High-Gain Digital Control Systems

Proposed concepts for the Light Family Helicopter (LHX) and Joint Services Operational Tilt-Rotor Aircraft (JVX) are embodied in a complex, highly maneuverable, versatile vehicle with avionics systems which are as important to mission success as the airframe itself. Single-pilot and NOE operations require handling qualities which minimize the involvement of the pilot in basic stabilization tasks. These requirements will demand a full-authority, high-gain, multimode DFCS. The gap between these requirements and current low-authority, low-bandwidth rotorcraft flight control technology is considerable. Ongoing research aims at smoothing the transition between current technology and advanced concept requirements.

A study was conducted (ref. 74) to

1. extensively review the state-of-the-art of high-bandwidth digital control systems,
2. expose areas of specific concern for FCSs of modern combat rotorcraft, and
3. illustrate the important concepts in design and analysis of high-gain, digital systems with a detailed case study involving a current rotorcraft system.

A comprehensive case study based on the ADOCS Black Hawk was conducted. Methods for analyzing and designing high-bandwidth digital control systems were discussed and illustrated. Figure 13 (from ref. 74) diagrams a typical attitude control system, including the many elements needed for a practical digital system

implementation. The response of the actuator rate ($\dot{\delta}_A$) to a step command input at δ_c is shown in figure 14 (30 Hz system). The solid curve is the result obtained using approximate (continuous system) methods. The digital-system exact response is shown as open and closed dots, the latter being the response at the even sampling instants. This figure shows that the even-sample instants are a very poor reflection of the complete digital system response. The approximate analysis gives a fairly good estimate for the intersample behavior, although the level of "roughness" is underestimated.

Modern Control Methodology

Certain modern multivariable design methods have been applied to helicopter flight control. These methods include (1) a linear quadratic method, (2) a method that produces robust, low order compensators, (3) a multivariable model-following control technique, and (4) a quadratic optimal control synthesis method. These techniques are generally better than the classical methods in reducing the number of design iterations, especially for multivariable control problems such as helicopter flight control. All four design applications have been carried through piloted evaluations on ground-based simulators, and two have been carried all the way to in-flight evaluation on the variable-stability CH-47 research helicopter. Each of the four case studies is discussed briefly in the following.

Linear Quadratic Regular-Least Squares Design Method- This method consists of a two-stage design process: LQR theory is applied to determine appropriate feedback gains for the stability augmentation system (SAS), followed by the design of the control augmentation system (CAS) using a least-squares design method (ref. 75). This method was employed to design a stability-and-control-augmentation system for a hingeless rotor helicopter to meet a set of 10 performance criteria (ref. 76) derived from handling quality requirements. For the SAS design using the LQR methodology, constant weighting factors were used for state and control variables. The ratio of these factors was employed as a parameter in the selection of feedback gains to satisfy three of the 10 performance criteria for full and partial state feedback systems. For the design of the CAS, which consists of a matrix of cross-feed gains, a least-squares method was used to satisfy the remaining seven performance criteria. The design was performed at three flight conditions (hover, 70, and 130 knots) using a 6-DOF linear model that represents the hingeless rotor helicopter. The designed SCAS was then evaluated using nine degree-of-freedom equations, which include flapping motion, to determine the influence of rotor dynamics. The results indicate that the flapping/regressing mode does couple with fuselage motions and produces roll/regressing and pitch/regressing oscillatory modes (fig. 15) at frequencies below 2 Hz. These oscillatory modes are not present in rigid body equations; therefore, the SCAS gains determined by analysis of rigid body equations of motion should be evaluated using a model which includes at least the blade-flapping motion.

A piloted ground-based simulation was conducted on the Ames Flight Simulator for Advanced Aircraft (FSAA), which is a 6-DOF moving-base simulator, to evaluate

the merit of the designed SCAS. The experiment was performed using a combined longitudinal and lateral-directional task--flying a course of barriers combined with trees placed down the centerline of the barriers (ref. 50). The results of the experiment indicated that satisfactory handling qualities (level I) were achieved with the designed SCAS operational, in contrast to marginally acceptable handling qualities (near the borderline of level II and level III) that were obtained for the basic aircraft.

Robust, Low-Order Compensator Design Method- An LQG-based control design methodology was developed at Stanford University which produces robust, low-order control laws for multiinput, multioutput dynamic systems (ref. 33). The design method is illustrated by a flow diagram in figure 16. After proper model scaling to facilitate the choice of weighting matrices in the standard LQG method, an initial, stable full-order dynamic compensator (regulator/Kalman-filter pair) is obtained which provides the desired control characteristics. The order of the initial compensator is then reduced using two measures of mode sharing of the compensator as criteria for deciding which modes of the compensator can be eliminated. These two measures are the singular value of the residue matrix associated with that mode and the singular value weighted by the real part of the mode. The order reduction is then followed by reoptimization and implementation of a robust design for the simplified compensator. This step uses a gradient-search algorithm based on a finite-time quadratic performance index (ref. 77), which produces a design that is stable and has adequate performance at specified normal and off-normal operating conditions. The final design step involves the design of the feed-forward gains to generate the command outputs. A command output matrix is calculated from the steady-state controls for the desired outputs, in a manner similar to the least squares approach discussed in the preceding method (LQG-LS). These command outputs are then summed with outputs produced from the compensator.

The methodology was applied to the design of a velocity-command system and a hover-hold system for a tandem rotor helicopter. These two control systems were implemented on the variable-stability CH-47B research helicopter and were flight-tested during 1984. The results of the flight tests and a detailed description of the design methodology are presented in reference 33.

Multivariable Model-Following Control System- An explicit MFCS consists of three basic elements: (1) the "model," (2) the "plant" (the rotorcraft), and (3) the model-following control law as shown schematically in figure 17. The purpose of the control law is to ensure that the rotorcraft follows the model, whose equations of motion represent the desired or ideal dynamic characteristics for rotorcraft. An MFCS is an attractive scheme for achieving variable-stability characteristics for in-flight simulation because, in principle, model characteristics can be varied over wide ranges without requiring corresponding changes in the model-following control law. This method is particularly useful in a situation in which a model that is used in a ground-based simulation investigation can be duplicated for use in an airborne simulator to provide a direct comparison of the two studies. In addition to in-flight simulation, a wider application of the model-following concept may lie in the design of advanced augmentation systems for future generations of

rotorcraft. By incorporating the desired characteristics in the model, satisfactory handling qualities may be assured for the augmented rotorcraft. An example of using the concept is the automatic FCS of the ADOCS discussed in the preceding section where a set of single-input, single-output MFCSs is utilized.

The development of the multivariable model-following control system began on the ground simulator as part of a joint research program of the U.S. Army and the German Aerospace Research Establishment (DFVLR). The results of the ground-based investigations (refs. 21, 78) indicate that the performance of the MFCS is dependent on the dynamics of the explicit model and on the limitations of the actuating system. Increases in the model bandwidth placed higher demands on the control system and resulted in degraded model-following performance. Significant improvements in model-following performance were achieved when a control-law switching feature, which was designed to account for position- or rate-limited actuators, was included in the control system.

When the model-following control laws that were initially developed on the ground-based simulator were implemented and evaluated on the variable-stability CH-47 research helicopter (fig. 18), it became clear that improvements to the initial design were needed to compensate for large time delays caused by the high-order effects such as rotor dynamics, sensor filter dynamics, and computational time delays (ref. 48) as discussed in the preceding section. An analysis that used a high-order dynamic model exposed the basic limitations of the original design and resulted in the development of a final four-axes multivariable MFCS (fig. 19, ref. 32). The final system, which features a feed-forward control and a "pseudo-complementary" feedback-compensation scheme, achieves high-bandwidth control and excellent model-following performance. Figure 20 shows an example of the model-following performance in the roll axis. The model characteristics that were implemented were second-order attitude-command systems with natural frequencies of 1.4 rad/sec and damping ratios of 0.707. Details of the design, implementation, and flight-test development of the system are reported in reference 32.

Quadratic Optimal Cooperative-Control Synthesis- Similar to the LQR-LS design method discussed previously, the quadratic optimal cooperative control synthesis (CCS) method also uses LQR theory. However, the CCS method offers two distinct features. (1) The CCS method uses output feedback rather than full state feedback as the case of LQR-LS method, thereby making it simpler for implementation. (2) In contrast to the three preceding design methods, the CCS method requires, in principle, no detailed a priori design criteria, because an assumed analytic pilot-model structure is an inherent feature of the approach (fig. 21). This can be a great advantage in cases where no existing design criteria exist because of either the nature of aircraft being controlled or of the task being performed. The need for explicit a priori design criteria is eliminated through the use of an explicit optimal pilot model (depicted schematically in fig. 22); the pilot model is based only on the task to be performed. The SCAS is then designed to minimize the "work-load" of the assumed pilot model while limiting the SCAS control inputs.

The CCS method was developed for and previously applied to the longitudinal SCAS design for a fixed-wing aircraft and was found, on a fixed-based ground

simulation evaluation, to compare favorably with the augmentation system currently being used on that aircraft. This design method was modified for application to the helicopter, which has more complex flight dynamics. Two CCS designs were obtained (using the original and modified methods) for a CH-47 helicopter and compared with two other designs based on classical frequency-domain method and LQR theory. Results from a fixed-base piloted simulation indicate that the modified CCS design compares favorably with the classical frequency-domain design (which was obtained using detailed a priori design criteria), and was superior to LQR design (ref. 79).

PARAMETER IDENTIFICATION

Parameter identification is a process of determining the coefficients or parameters in the set of equations of motion of the aircraft, called the model, by disturbing the aircraft with known test inputs. The general form of the model is assumed a priori or is derived from knowledge of the aircraft. Thus, parameter identification is a subfield of system identification, which is concerned with the more difficult problem of determining the model itself without assuming the form of the model. Parameter identification methodology may therefore be used to improve rotorcraft simulation models, to assess their handling-qualities characteristics, and to help develop better models for FCS design.

While significant progress has been made in the last two decades in the field of parameter identification for fixed-wing aircraft (refs. 80-82), progress has been relatively slow in its rotary-wing counterpart. Several important issues in rotorcraft parameter identification need to be resolved.

Unlike the flight dynamics of fixed-wing aircraft, the dynamics of rotary-wing aircraft are characteristically those of a high-order system, as discussed earlier. Significant interaxis coupling exists for single main-rotor helicopters; dynamic interactions exist between the engine and drive train/rotor system; and high-order effects such as rotor dynamics and inflow dynamics exist inherently in the system. The large number of degrees of freedom associated with the coupled high-order dynamics leads to a large number of unknown parameters that have to be identified, making it extremely difficult to achieve a successful application of system or parameter-identification techniques. Vibration levels of rotorcraft are high, a fact which causes high noise contamination in response measurements and makes it even more difficult to achieve accurate state estimation and parameter identification. Further, the basic rotorcraft are generally unstable, so only short flight records can be used for direct identification of the basic aircraft parameters or indirect identification of them with SCASs operational. Either case can cause difficulty for parameter identification: for the short-flight record, the information contents are likely to be inadequate for all the dynamic modes, and with SCAS operational, inputs can be highly correlated with output responses, if the design of test inputs is ignored.

Early efforts were made by the Army and NASA in the development of advanced time-domain techniques for rotorcraft state estimation and parameter identification (refs. 83, 84), in attempts to overcome some of the difficulties described previously. Considerable efforts were subsequently devoted to the development of frequency-domain techniques (refs. 85-87), thereby providing a better perspective from which to assess the two approaches, and leading toward the development of a unified time- and frequency-domain parameter identification methodology for rotorcraft in the future.

Time-Domain Parameter Identification

First applications of time-domain (digital) parameter identification techniques to rotorcraft by NASA and the Army at Langley and elsewhere employed a measurement error method--Newton Raphson (ref. 88) and a simpler advanced method using the Extended Kalman Filter algorithm (refs. 89, 90). Typical procedures of using these two parameter identification methods are shown schematically in figure 23 (ref. 91). Both methods include the initial step of using a digital filter to process the raw flight data to reduce the data noise content. Applications have been made to the identification of quasi-static, rigid-body stability-and-control derivatives of single-rotor helicopters and a tandem-rotor helicopter. Both methods give a gross underestimation of primary derivatives such as roll, pitch, and yaw damping; it is not uncommon for positive values of the damping derivatives to be identified using the quasi-static rigid-body model. If the lower-order model is used, large fitting errors in some response variables (e.g., vertical acceleration) are also apparent (fig. 24). The then-available identification software and the lack of measurements of the rotor blade motion have limited those applications to the identification of only the rigid-body quasi-static stability-and-control derivatives without considering the effects of rotor dynamics and other high-order effects discussed in the earlier sections.

In addition to adequate modeling of the vehicle/rotor system, two other areas must be addressed to accurately identify the stability-and-control parameters: (1) instrumentation and measurement data analysis and (2) test input design. A joint Army/NASA program involving both Ames and Langley was therefore initiated in 1976 with the aim of developing a comprehensive advanced technique for rotorcraft state estimation and parameter identification, which addressed all aspects of problems peculiar to rotorcraft. The techniques developed by a contractor (ref. 84) are illustrated in figure 25. Applications of some of these techniques have been made to the Rotor System Research Aircraft (refs. 92, 93) and to the Puma helicopter (ref. 94) under a NASA/UK (Royal Aircraft Establish) collaboration.

As part of an ongoing US/German MOU on helicopter flight control, an extensive joint study is being conducted to analyze the XV-15 database using both time domain and frequency domain techniques. The objectives of this study are to gain a better appreciation for the relative strengths and weaknesses of those two different approaches and to develop improved methods of identification for rotorcraft. The time domain approach used by the DFVLR of the Federal Republic of Germany (FRG)

(refs. 95, 96) is shown in figure 26. The data compatibility analysis and data analysis blocks shown in the figure are similar to the state estimation and parameter identification described in figure 25, although different in detailed computational algorithms. The frequency domain approach employed by the U.S. Army in conjunction with this MOU effort is discussed next.

Frequency-Domain Parameter Identification

The frequency-domain-identification approach developed at ARC (refs. 85, 86) is shown in figure 27. Flight data are generated using frequency-sweep inputs for model extraction and step inputs for model verification. Two typical, concatenated, lateral-stick frequency sweeps completed during the hover flight tests of the XV-15 are shown in figure 28(a) with the corresponding roll rate response shown in figure 28(c). Pilot-generated, rather than computer-generated, inputs are used. The frequency-sweep input is especially well suited to the frequency-domain identification procedure because: (1) the wave form is roughly symmetric about the trim condition so that the aircraft motions are not excessive and the aircraft dynamics are likely to stay within the linear range; (2) the input and output wave forms are smooth and regular, so the resulting spectral functions are well behaved; and (3) the input autospectrum is generally constant over the desired frequency range.

For the spectral analysis, the ARC approach employs methods based on the Chirp z-transform to extract high-resolution frequency responses between selected input and output pairs. The identification results are presented in Bode-plot format: magnitude and phase of the output to the input vs. frequency (fig. 27). These results are nonparametric since no model structure has been assumed. As such, they can be used directly for FCS design or handling-qualities-compliance testing. These nonparametric identification results can also be compared directly with those obtained from real-time and nonreal-time simulations to expose limitations and discrepancies in the simulator models. Approximate transfer functions and modal characteristics may also be obtained by fitting the identified frequency-response plots with assumed analytical models of transfer function. The results are parametric models that are useful for transfer-function-based control-system-design studies and for handling qualities specifications given in lower-order equivalent-system terms. Since this fitting procedure is completed after the frequency response is extracted, the order of the transfer function can be carefully selected to avoid an overparameterized model. Multiinput/multioutput frequency-response methods are suitable for extracting a transfer matrix which includes the important coupling effects. Finally, the extracted models are driven with the flight-test-control inputs to verify the time-domain response characteristics.

The frequency-domain identification procedure has been applied to an XV-15 tilt-rotor aircraft, a Bell-214-ST single-rotor helicopter, and the NASA/Army CH-47B tandem-rotor research helicopter. The results are briefly described below.

Frequency-Domain Identification of the XV-15- The frequency-domain identification was initiated in 1983 and completed in 1986. The objectives were to identify and document the open-loop dynamics of the XV-15 from flight tests for several

operating conditions including hover, to compare the aircraft and simulation response characteristics for identifying problem areas in the math modeling, and to develop a validated transfer-function model description for future use in control-system studies. The results for hovering flight and cruise flight are reported in detail in references 86 and 85.

Figure 29 shows an example of a comparison of the frequency responses, extracted from flight and simulator data, of the open-loop roll rate response to lateral control input in hovering flight. The correlation of the VMS simulation and the flight data is quite good for the frequency range from 1.0 to 10.0 rad/sec, which indicates that the roll-response control effectiveness is accurately modeled. However, considerable discrepancies are apparent in the math model for the low-frequency-magnitude response. The low-frequency phase comparison suggests that the damping ratio of the unstable roll mode is slightly overestimated by the simulation model (i.e., more unstable), whereas the natural frequency is accurate. Incidentally, these low-frequency errors in the simulation model were also reported during the pilot's qualitative evaluation on the simulator.

Subsequent analysis of the real-time math model indicated problems in the representation of rotor flapping for large lateral-velocity changes (such as the case of the low frequency range of the roll response). There is also strong sensitivity of the numerically linearized transfer functions to the size of perturbation. Corrections to the math modeling in these two areas were included later in the nonreal-time XV-15 simulation. The comparison between the current nonreal-time model, real-time model, and the flight data is shown in figure 29, and indicates the significant improvements achieved during the last 3 years.

Having completed the extraction of the frequency responses, the next step is to fit the frequency response with a transfer-function model. A standard fourth-order model with an effective time-delay term was chosen (ref. 86) as the structure of the model for identification of its attendant parameters. Figure 30 shows a fit of the magnitude and phase of the identified transfer function. The predictive capability of the transfer-function model is illustrated in figure 31, which shows the roll-rate response of the open-loop aircraft to a step aileron input. When the identified transfer function is driven with the same input, the response coplotted in the dashed curve is obtained, which shows the model and flight data responses generally compare very well, and thus provides a validation for the identified model.

Demonstration of Frequency-Sweep Testing Technique Using a Bell 214-ST Helicopter- Research supporting the development of the LHX-handling-qualities specification ADS-33 (ref. 97), which is an updated version of MIL-H-8501A, indicates the need for frequency-domain descriptions to adequately characterize the transient angular-response dynamics of highly augmented combat rotorcraft. The proposed LHX criteria for short-term angular response are given in terms of two frequency-domain parameters--bandwidth (ω_{BW}) and phase delay (τ_p). These quantities are determined directly from frequency response plots of the on-axis angular responses to control inputs, such as was generated from the XV-15 (fig. 29). A key concern in incorporating such descriptions in a specification is the practical problem of extracting frequency responses from flight data for compliance testing.

To address this and other concerns associated with the practicality of using frequency-sweep testing technique, a flight-test demonstration program (6 flight hours) was conducted in October 1985 using an instrumented Bell-214-ST helicopter (fig. 32). Frequency-sweep and step-input tests were performed in hover and cruise (90 knots) for each control axis. The data were then analyzed using the frequency-domain identification procedure described previously. Excellent identification of the frequency responses was achieved for all axes at both flight conditions. As an example, the extracted response of pitch attitude to longitudinal cyclic stick is shown for the hover flight condition in figure 33. An accurate spectral estimate is achieved over a broad frequency range (0.2-10.0 rad/sec), and the required specification compliance parameters are readily obtained. Additional analyses were conducted to identify transfer function models for each axis. These models accurately predict the large-amplitude step response behavior and validate the linearized frequency-response concept for single-rotor helicopters.

Identification of CH-47B Vertical Dynamics Model in Hover- The same frequency-domain procedure that was used in the identification of the two aircraft was also applied to the identification of the vertical dynamics of the CH-47B research aircraft in hover. The objective of this work was to identify the helicopter vertical dynamics for correlation with those developed from the analytical modeling efforts (ref. 50).

Frequency-sweep inputs in collective pitch were employed to identify the frequency response of the vertical acceleration to collective input. The extracted frequency response (fig. 34) indicates that there is a resonant peak at around 17 rad/sec and a substantial phase lead as previously predicted in the analytical study (ref. 49). Based on the analytical modeling efforts, a series of parametric transfer-function models, ranging from first to fifth order was fit to the identified frequency plots. The first-order model corresponds to the classical quasi-static model, and the fourth-order model includes the effects of flapping and inflow dynamics (the fifth-order was used to account for possible effects caused by variation in rotor rpm). The frequency-response fits for a first- and a fourth-order model are shown in figure 34. For the first-order quasi-static model, it proved to be difficult to fit the model accurately over the entire frequency range; the fit was therefore limited to the range of 0.1 to 3 rad/sec instead of 0.1 to 20 rad/sec as applied to all of the other models. This causes the first-order model to match the flight data better at low frequency than the higher-order models (fig. 34). All of the higher-order models exhibit a nonminimum phase characteristic as predicted in the analytical modeling efforts (ref. 49).

As a means for testing the predictive capability of the identified models, the vertical responses to a step input in collective input were generated from the models. These responses compare favorably with those of the analytical model. Some of the responses of the identified models are plotted together with flight data as shown in figure 35. As expected, the first-order models, because of the limited frequency range of applicability, fails completely to predict the overshoot of the vertical acceleration owing to the high-order effects of inflow and flapping

dynamics. The fourth-order model provides a much better predictive capability than does the first-order model for the initial transient.

CONCLUDING REMARKS

This paper has reviewed the progress made in joint NASA/Army research concerning rotorcraft flight-dynamics modeling, flight control design methodologies, and parameter identification. These interactive research disciplines all require attention in order to provide a basis for exploring analytically and experimentally the handling qualities implications of a variety of dynamic concepts aimed at assisting the pilot in performing a required mission. Although this integrated approach to the research is probably required for all classes of aircraft, the need is particularly acute for rotorcraft because of their mathematical complexity, high-order dynamic characteristics, and demanding mission requirements. Accordingly, the results that have been reviewed here form the basis for combined research efforts which are currently under way to integrate dynamics, controls, and identification methodologies.

The need for this integration is apparent from most of the work reviewed here. As was reviewed in the paper, the research on real-time simulation models has led to a capability of including rigid blade flapping modes, initially for the rotor disk and more recently using blade element models. These models have been appropriate for the types of missions considered to date, but must be extended for missions which require more pilot-aircraft performance to include the important effects of additional degrees of freedom such as lag or elastic modes while retaining adequate simplicity for design and simulation purposes. Further, the models must be accurate over greater regions of the flight envelope; the work described in the paper for high-g maneuvering forms the basis for more accurate full-flight-envelope design tools. To ascertain the importance of the higher-order terms, parameter identification techniques must be integrated into the modeling process, using flight data as the verification standard. In particular, the frequency-domain procedures developed at NASA and discussed in this paper are excellently suited to assessing the influence of these dynamics and providing a rational basis for the selection of lower-order models.

It is also clear from the joint work reviewed here that these higher order dynamics must be accounted for explicitly early in the design process, regardless of their origin. The flight experiments demonstrated the importance for modern control applications of rotor dynamics and also aerodynamic (inflow) dynamics; the high-gain, model-following system that has been developed and demonstrated has utilized models that are accurate to higher frequencies to achieve improved control system performance. Equally important, the control system implementation itself adds dynamics that have historically been overlooked in rotorcraft control designs; the review of an existing rotorcraft digital-control-system design and implementation showed that current practices do not account sufficiently for the digital design details and that the achievable control system performance remains far less than was

predicted. Therefore, in general, the work conducted in the past 10 yr has inevitably pointed to the need for models and methodologies accurate over higher frequency ranges and capable of dealing explicitly with a variety of interactive effects, and, as demonstrated in this paper, the research has become increasingly oriented in this direction.

The current NASA/Army research for rotorcraft flight dynamics and controls is oriented to examining concepts that require even higher gains and more interaction among the controls and the various dynamics of the rotorcraft systems, and hence may be said to be becoming more closely coupled to the actual details of the rotorcraft. The need for this closer coupling to the details of the rotorcraft stems from the increasing emphasis on demanding rotorcraft missions such as air-to-air combat and automated nap-of-the-Earth flight. To achieve the requisite improvements in agility and maneuverability, a variety of interactive elements must be considered in the modeling and control design process; such elements include integrated flight/propulsion control, rotor state control, high bandwidth stability/control augmentation, rotor-rpm energy transfer, higher harmonic control, and envelope limiting and cueing. As the review of previous work presented in this paper has shown, a considerable extension of existing knowledge and techniques is required to perform the integration of all of these elements. The goal is to provide systematic modeling and design procedures capable of dealing with these new problems, and to integrate the technologies that have been initiated in the joint research of the past 10 years.

REFERENCES

1. Talbot, P. D.; Tinling, B. E.; Decker, W. A.; and Chen, R. T. N.: A Mathematical Model of a Single Main Rotor Helicopter for Piloted Simulation. NASA TM-84281, Sept. 1982.
2. Chen, R. T. N.: A Simplified Rotor System Mathematical Model for Piloted Flight Dynamics Simulation. NASA TM-78575, 1979.
3. Chen, R. T. N.: Effects of Primary Rotor Parameters on Flapping Dynamics. NASA TP-1431, Jan. 1980.
4. Decker, W. A.; Adam, C. F.; and Gerdes, R. M.: Model Development and Use of Simulators for Investigating Autorotation. Paper FAA Conf. on Helicopter Simulation, Atlanta, GA, Apr. 1984.
5. Decker, W. A.; Adam, C. F.; and Gerdes, R. M.: Pilot Use of Simulator Cues for Autorotation Landing. 1986 AHS Forum, Washington, DC, June 1986.
6. Sheridan, P. F.; Robinson, C.; Shaw, J.; and White, F.: Mathematical Modeling for Helicopter Simulation of Low speed, Low Altitude, and Steeply Descending flight. NASA CR-166385, 1982.
7. Chen, R. T. N.: Selection of Some Rotor Parameters to Reduce Pitch-Roll Coupling of Helicopter Flight Dynamics. Preprint no. I-6, National Specialists' Meeting, Rotor System Design, AHS Mideast Region, Philadelphia, Oct. 1980.
8. Chen, R. T. N.; and Talbot, P. D.: An Exploratory Investigation of the Effects of Large Variations in Rotor System Dynamics Design Parameters on Helicopter Handling Qualities in NOE Flight. J. AHS, July 1978, pp. 23-36.
9. Lewis, M. S.; and Aiken, E. W.: Piloted Simulation of One-on-One Helicopter Air Combat at NOE Flight Levels. NASA TM-86686, Apr. 1985.
10. Lewis, M. S.: A Piloted Simulation of One-on-One Helicopter Air Combat in Low Level Flight. J. AHS, vol. 31, no. 2, Apr. 1986, pp. 19-26.
11. Lebacqz, J. V.; and Forrest, R. D.: Control Position Gradient and Stability/Control Augmentation Effects on Helicopter Handling Qualities for Instrument Approach. J. AHS, Jan. 1982, pp. 35-41.
12. Lebacqz, J. V.; Chen, R. T. N.; Gerdes, R. M.; and Weber, J. M.: A summary of NASA/FAA Experiments Concerning Helicopter IFR Airworthiness Criteria. J. AHS, July 1983, pp. 63-70.

13. Lebacqz, J. V.: Ground Simulation Investigation of Helicopter Decelerating Instrument Approaches. J. Guidance, Control, and Dynamics, vol. 6, no. 5, Sept./Oct. 1983, pp. 330-338.
14. Curtiss, H. C., Jr.; Sun, M.; and Putman, W. F.: Rotor Aerodynamics in Ground Effect at Low Advance Ratios. Paper 81-5, 37th Annual Forum of the AHS, New Orleans, LA, May 1981.
15. Curtiss, H. C., Jr.; Sun, M.; and Hanker, E. J.: dynamic Phenomena in Ground Effect. Paper A-83-39-76-000, 39th Annual Forum of the AHS, May 1983.
16. Curtiss, H. C., Jr.; Erdman, W.; and Sun, M.: Ground Effect Aerodynamics. Paper presented at the International Conf. on Rotorcraft Basic Research, Triangle Part, NC, Feb. 19-21, 1985.
17. Lewis, M. S.; Mansur, M. H.; and Chen, R. T. N.: A simulator Investigation of Parameter Affecting Helicopter Handling Qualities in Air Combat. AHS National Forum, St. Louis, MO, May 1987.
18. Hilbert, K. B.: A Mathematical Model of the UH-60A Helicopter. NASA TM-85890, Apr. 1984.
19. Landis, K. H.; and Glusman, S. I.: Development of ADOCS Controllers and Control Laws. NASA CR-177339, March 1985.
20. Jewell, W. F.; Clement, F. W.; and Johns, J. B.: Real Time Piloted Simulation Investigation of Helicopter Flying Qualities During Approach and Landing on Nonaviation Ships. AIAA Paper 86-0490, Jan. 1986.
21. Bouwer, G.; and Hilbert, K. B.: A Piloted Simulator Investigation of Decoupling Helicopters Using a Model-Following Control System. AHS Annual Forum, May 1984.
22. Aiken, E. W.: A Mathematical Representation of an Advanced Helicopter for Piloted Simulator Investigations of Control-System and Display Variations. NASA TM-81203, July 1980.
23. Aiken, E. W.; and Merrill, R. K.: Results of a Simulator Investigation of Control System and Display Variations for an Attack Helicopter Mission. 36th Annual AHS Forum, Washington, DC, May 1980.
24. Aiken, E. W.; and Blanken, C. L.: Piloted Simulation of the YAH-64 Backup Control System Engagement. NASA TM-81293 (USAAVRADCOM TR-81-A-11), July 1981.
25. Bivens, C. C.: Directional Handling Qualities Requirements for Nap-of-the-Earth Tasks. J. AHS, vol. 31, no. 1, Jan. 1986, pp. 37-42.

26. Talbot, P. D.; and Corliss, L. D.: A Mathematical Force and Moment Model of a UH-1H Helicopter for Flight Dynamics Simulations. NASA TM-73254, June 1977.
27. Baker, F. A.; Janes, D. N.; Corliss, L. D.; Liden, S.; Merrick, B.; and Dugan, D. C.: V/STOLAND Avionics System Flight Test Data on a UH-1H Helicopter. NASA TM-78591, Feb. 1980.
28. Corliss, L. C.; and Talbot, P. D.: A Failure Effects Simulation of a Low Authority Flight Control Augmentation System on a UH-1H Helicopter. NASA TM-73258, 1977.
29. Hackett, W. E., Jr.; Gernett, T. S., Jr.; and Borek, B. V.: Mathematical Model fo the CH-47B Helicopter Capable of Real-Time Simulation of the Full Flight Envelope. NASA CR-166458, July 1983.
30. Weber, J. M.; Liu, T. Y.; and Chung, W.: A Mathematical Simulation Model of a CH-47B Helicopter. NASA TM-84351, Aug. 1984.
31. Weber, J. M.; et al.: A Lagrange-D'Alembert Formulation of the Equations of Motion of a Helicopter Carrying an Externally Suspended Load. NASA TM-85864, Feb. 1985.
32. Hilbert, K. B.; Lebacqz, J. V.; and Hindson, W. S.: Flight Investigation of a Multivariable Model-Following Control System for Rotorcraft. AIAA Paper 86-9779, AIAA 3rd Flight Test Conf., Las Vegas, April 1986.
33. Holdridge, R. D.; Hindson, W. S.; and Bryson, A. E.: LQG-Design and Flight-Test of a Velocity-Commands System for a Helicopter. Paper presented at AIAA Conf. on Guidance and Control, Snowmass, CO, Aug. 19-21, 1985.
34. Howlett, J. J.: UH-60A Black Hawk Engineering Simulation Program. NASA CR-166309, 1981.
35. Ballin, M. G.: Validation of a Real-Time Engineering Simulation of the UH-60A Helicopter. NASA TM-88359, Feb. 1987.
36. Miheloew, J. R.; and Chen, R. T. N.: Rotorcraft Flight-Propulsion Control Integration. Vertiflite, vol. 30, no. 6, Sept./Oct. 1984, pp. 45-47.
37. Paulk, C. H., Jr.; Astill, D. L.; and Donley, S. T.: Simulation and Evaluation of the 54-2F Helicopter in a Shipboard Environment Using the Interchangeable Cab System. NASA TM-84387, Aug. 1983.
38. Phillips, J. D.: Mathematical Model of the 34-3G Helicopter. NASA TM-84316, Dec. 1982.

39. Howlett, J. J.: RSRA Simulation Model--Vol. I. Mathematical Model Equations. Sikorsky Aircraft, SER-72009 (under contract NAS1-13000), Oct. 1974).
40. Harendra, P. B.; et al.: V/STOL Tilt Rotor Study. Vol. V. A Mathematical Model for Real Time Flight Simulation of the Bell Model 301 Tilt Rotor Research Aircraft. NASA CR-114614, 1973.
41. Lebacqz, J. V.; and Scott, B. C.: Ground Simulation Investigation of VTOL Airworthiness Criteria for Terminal Area Operations. AIAA J. GCD, vol. 8, no. 6, Nov./Dec. 1985, pp. 761-767.
42. Etkin, B.: Dynamics of Atmospheric Flight. John Wiley & Sons, Inc., 1972.
43. Seckel, E.: Stability and Control of Airplanes and Helicopters. Academic Press (New York), 1964.
44. General Requirements for Helicopter Flying and Ground Handling Qualities. Specification MIL-H-8501A, Sept. 1961.
45. V/STOL Handling. Part I. Criteria and Discussion. AGARD Report 577, June 1973.
46. Flying Qualities of Piloted V/STOL Aircraft. Specification MIL-F-83300, Dec. 31, 1970.
47. Flying Qualities of Piloted Airplanes. Specification MIL-F-8785B(ASG), 7 Aug. 1969.
48. Chen, R. T. N.; and Hindson, W. S.: Influence of High-Order Dynamics on Helicopter Flight-Control System Bandwidth. AIAA J. Guidance, Control, and Dynamics, vol. 9, no. 2, March/April 1986, pp. 190-197.
49. Chen, R. T. N.; and Hindson, W. S.: Influence of Dynamic Inflow on the Helicopter Vertical Response. NASA TM-88327, June 1986.
50. Chen, R. T. N.: Unified Results of Several Analytical and Experimental Studies of Helicopter Handling Qualities in Visual Terrain Flight. NASA CP-2219, April 1982, pp. 59-74.
51. Chen, R. T. N.; and Tischler, M. B.: The Role of Modeling and Flight Testing in Rotorcraft Parameter Identification. Presented at the 1986 AHS Forum, Washington, DC, June 1986.
52. Chen, R. T. N.: Kinematic Properties of Rotary-Wing and Fixed-Wing Aircraft in Steady Coordinated High-g Turns. AIAA Paper 81-1855, Aug. 1981.

53. Chen, R. T. N.: Kinematic Properties of Rotary-Wing and Fixed-wing Aircraft in Steady Coordinated High-g Turns. AIAa Paper 81-1855, Aug. 1981.
54. Chen, R. T. N.; and Jeske, J. A.: Influence of Sideslip on the Helicopter in Steady Coordinated Turns. J. AHS, Oct. 1982, pp. 84-92.
55. Chen, R. T. N.: Flight Dynamics of Rotorcraft in Steep High-g Turns. J. Aircraft, vol. 21, no. 1, Jan. 1984, pp. 14-22.
56. Chen, R. T. N.: Efficient Algorithms for Computing Trim and Small-Disturbance Equations of Motion of Aircraft in Coordinated and Uncoordinated, Steady, Steep Turns. NASA TM-84324, Feb. 1983.
57. Chen, R. T. N.; Jeske, J. A.; and Steinberger, R. H.: Influence of Sideslip on the Flight Dynamics of Rotorcraft in Steep Turns at Low Speeds. AHS 39th Annual Forum, St. Louis, MO, May 1983.
58. Houston, S. S.: On the Analysis of Helicopter Flight Dynamics During Maneuvers. Paper 80, 11th European Rotorcraft Forum, 10-13 Sept. 1985, London.
59. Padfield, G. D.: On the Use of Approximate Models in Helicopter Flight Mechanics. Vertica, vol. 5, 1981, pp. 243-259.
60. Briczinski, S. J.; and Cooper, D. E.: Flight Investigation of Rotor/Vehicle State Feedback. NASA CR-132546, Jan. 1975.
61. Landis, K. H.; and Aiken, E. W.: Simulator Investigations of Side-Stick Controller/Stability and Control Augmentation Systems for Night Nap-of-the-Earth Flight. J. AHS, Jan. 1984, pp. 56-65.
62. McRuer, D.; Johnson, D.; and Meyers, T.: A Perspective on Superaugmented Flight Control Advantages and Problems. AGARD Conference on Active Control, Ontario, Canada, 1984.
63. Ormiston, R. A.: Application of Simplified Inflow Models to Rotorcraft Dynamic Analysis. J. Am. Helicopter Sci., July 1976, pp. 34-37.
64. Johnson, W.: Influence of Unsteady Aerodynamics on Hingeless Rotor Ground Resonance. J. Aircraft, vol. 19, 1982, pp. 668-673.
65. Friedmann, P. P.; and Venkatesan, C.: Influence of Various Unsteady Aerodynamic Models on the Aeromechanical Stability of a Helicopter in Ground Resonance. NASA CP-2400, 1985, pp. 207-218.
66. Gaonkar, G. H.; and Peters, D.: A Review of Dynamic Inflow and Its Effect on Experimental Correlations. NASA CP-2400, 1985, pp. 187-203.

67. Pitt, D. M.; and Peters, D. A.: Theoretical Prediction of Dynamic-Inflow Derivatives. J. Vertica, vol. 5, 1981, pp. 21-34.
68. Carpenter, P. J.; and Fridovich, B.: Effect of a Rapid-Pitch Increase on the Thrust and Induced-Velocity Response of a Full-Scale Helicopter Rotor. NACA TN-3044, 1953.
69. Curtiss, H. C., Jr.: Stability and Control Modelling. Paper 41, 12th European Rotorcraft Forum, Sept. 1986, Garmisch-Partenkirchen, Germany.
70. Mihalow, J.; Ballin, M. G.; and Rutledge, D. C. G.: Rotorcraft Flight-Propulsion Control Integration. Paper 1987 NASA/Army Rotorcraft Technology Conference, 1987.
71. Landis, K. H.; Dunford, P. J.; Aiken, E. W.; and Hilbert, K. B.: Simulator Investigation of Side-Stick Controller/Stability and Control Augmentation Systems for Helicopter Visual Flight. J. AHS, vol. 30, no. 2, April 1985, pp. 3-13.
72. Aiken, E. W.; Hilbert, K. B.; Landis, K. H.; and Glusman, S. I.: An Investigation of Side-Stick Controller/Stability and Control Augmentation System Requirements for Helicopter Terrain Flight Under Reduced Visibility Conditions. AIAA Paper 84-0235, Jan. 1984.
73. Brigadier, W. L.: Analysis of Control Actuator Authority Requirements for Attitude and Translational Rate Command Augmentation Systems for the XV-15 Tilt Rotor Research A/C. NASA TM-81243, Dec. 1980.
74. Tischler, M. B.: Pigtail Control of Highly Augmented Combat Rotorcraft. NASA TM-88346, 1987.
75. Lebacqz, J. V.; and Chen, R. T. N.: Design and Flight Test of a Decoupled Velocity Control System for VTOL Landing Approach. AIAA/AFM Conf., Aug. 1977.
76. Miyajima, K.: An Analytical Design of a High Performance Stability and Control Augmentation System for a Hingeless Rotor Helicopter. J. AHS, July 1979, pp. 29-35.
77. Ly, U. L.: A Design Algorithm for Robust Low-Order Controllers. Report 536, Stanford Univ., Stanford, CA, Nov. 1982.
78. Hilbert, K. B.; and Bouwer, G.: The Design of a Model-following Control System for Helicopters. AIAA G. and C. Conf., Seattle, WA, 1984.
79. Townsend, B. K.: The Application of Quadratic Optimal Cooperative Control Synthesis to a CH-47 Helicopter. 1986 AHS Lichten Award Paper, NASA TM-88353, Sept. 1986.

80. Parameter Estimation Techniques for Applications in Aircraft Flight Testing. NASA TN D-7647, April 1974.
81. Methods for Aircraft State and Parameter Identification. AGARD-CP-172, Nov. 1974.
82. Parameter Identification. AGARD-LS-104, Nov. 1979.
83. Tomaine, R. L.: Flight Data Identification of Six Degree-of-Freedom Stability and Control Derivatives of a Large "Crane" Type Helicopter. NASA TM X-73958, Sept. 1976.
84. Hall, W. W., Jr.; Bohn, J. G.; and Vincent, J. H.: Development of Advanced Techniques for Rotorcraft State Estimation and Parameter Identification. NASA CR-159297, Aug. 1980.
85. Tischler, M. B.: Frequency Response Identification of XV-15 Tilt-Rotor Aircraft Dynamics. Ph.D. Dissertation, Stanford Univ., Stanford, CA, 1987.
86. Tischler, M. B.; Leung, J. G. M.; and Dugan, D. C.: Frequency-Domain Identification of XV-15 Tilt-Rotor Aircraft Dynamics in Hovering Flight. AIAA Paper 83-2695 (also in condensed version in J. Amer. Helicopter Soc., vol. 30, no. 2, Apr. 1985, pp. 38-48).
87. Tischler, M. B.; and Kaletka, J.: Modeling XV-15 Tilt-Rotor Aircraft Dynamics by Frequency and Time-Domain Identification Techniques. AGARD Paper 9, Oct. 1986.
88. Gould, D. G.; and Hindson, W. S.: Estimates of the Stability Derivatives of a Helicopter and a V/STOL Aircraft from Flight Data. AGARD-CP-172, Nov. 1974.
89. Molusis, J. A.: Helicopter Stability Derivative Extraction from Flight Data Using a Bayesian Approach to Estimation. J. Amer. Helicopter Soc., July 1973.
90. Molusis, J. A.: Rotorcraft Derivative Identification from Analytical Models and Flight Test Data. AGARD-CP-172, Nov. 1974.
91. Tomaine, R. L.; Bryant, W. H.; and Hodge, W. F.: VALT Parameter Identification Flight Test. European Rotorcraft Paper 73, Sept. 1978.
92. DuVal, R. W.; and Mackie, D. B.: Identification of a Linear Model at Rotor-Fuselage Dynamics from Nonlinear Simulation Data. Proceedings of the 6th European Rotorcraft and Powered Lift Aircraft Forum, Bristol, England, 1980.
93. DuVal, R. W.; Wang, J. C.; and Demiroz, M.: A Practical Approach to Rotorcraft System Identification. Proceeding of 39th American Helicopter Society Forum, 1983.

94. Padfield, G. D.; and DuVal, R. W.: Application of Parameter Estimation Methods to the Prediction of Helicopter Stability, Control, and Handling Characteristics. Proceedings of the NASA/American Helicopter Society Specialists Meeting on Helicopter Handling Qualities, NASA CP-2219, 1982.
95. Kaletka, J.: Rotorcraft Identification Experience. AGARD-LS-104, Nov. 1979, pp. 7-1 to 7-32.
96. Kaletka, J.: Practical Aspects of Helicopter Parameter Identification. AIAA CP849, AIAA Paper 84-2081, 1984, pp. 112-122.
97. Hoh, R. H.; Mitchell, D. G.; Ashkenas, I. L.; Aponso, B. L.; Ferguson, S. W.; Rosenthal, T. J.; Key, D. L.; and Blanken, C. L.: Proposed Airworthiness Design Standard: Handling Qualities Requirements for Military Rotorcraft. System Technology, Inc. TR-1194-2, 20 Dec. 1985.

TABLE 1.- ROTORCRAFT MATH MODELS FOR PILOT-IN-THE-LOOP SIMULATION

Applications	Model complexity				
	Linear aerodynamics with simplifications			Nonlinear aerodynamics	
	Fuselage and quasi-static rotor 6 DOF	Fuselage and rotor flap 9 DOF	Fuselage and rotor flap/rpm 10 DOF	Fuselage and rotor flap/lag 12 DOF	Fuselage and rotor flap/lag/rpm 16 DOF
General handling qualities--well within flight envelope					
Basic aircraft					
Low frequency maneuvers	X				
High frequency maneuvers		X			
SCAS research					
Fuselage feedback	X	X			
Fuselage/rotor feedback		X	X	X	
General handling qualities--full flight envelope					
Basic aircraft					
Envelope					
exploration and maneuvering					
performance					
Boundary					
limiting and expanding SCAS					
Specific aircraft handling qualities					

TABLE 2.- ALGORITHMS FOR COMPUTING TRIM CONDITIONS FOR A ROTORCRAFT IN A STEADY, UNCOORDINATED FLIGHT

A. Steady Uncoordinated Turns

Steady-state Euler equations

$$n_x - \sin \theta - \tan \phi_1 (\sin \alpha \cos \beta \cos \theta \sin \phi - \sin \beta \cos \theta \cos \phi) = 0$$

$$n_y + \cos \theta \sin \phi - \tan \phi_1 \cos \beta (\cos \alpha \cos \theta \cos \phi + \sin \alpha \sin \theta) = 0$$

$$n_z + \cos \theta \cos \phi + \tan \phi_1 (\sin \beta \sin \theta + \cos \alpha \cos \beta \cos \theta \sin \phi) = 0$$

$$L + I_{yz}(q^2 - r^2) + I_{xz}pq - I_{xy}rp + (I_y - I_z)qr = 0$$

$$M + I_{xz}(r^2 - p^2) + I_{xy}qr - I_{yz}pq + (I_z - I_x)rp = 0$$

$$N + I_{xy}(p^2 - q^2) + I_{yz}rp - I_{xz}qr + (I_x - I_y)pq = 0$$

$$\begin{aligned} \phi_1 &= \tan^{-1} \left(\frac{\dot{\psi}V}{g} \right) \\ &= \pm \tan^{-1} \left[\frac{(n^2 - 1)^{1/2}}{\cos \gamma} \right], \quad + \text{right turn; } - \text{left turn} \\ n^2 &= n_x^2 + n_y^2 + n_z^2 \end{aligned}$$

Kinematic relationships

$$\begin{aligned} q &= \dot{\psi} \sin^2 \phi_1 \left\{ -(\sin \gamma \sin \beta + n_y \cotan^2 \phi_1) \right. \\ &\quad \left. \pm \left[(\sin \gamma \sin \beta + n_y \cotan^2 \phi_1)^2 - \frac{1}{\sin^2 \phi_1} (\sin^2 \gamma - \cos^2 \beta + n_y^2 \cotan^2 \phi_1) \right]^{1/2} \right\} \\ q &\geq 0 \end{aligned}$$

$$r' = \frac{q + \dot{\psi} n_y}{\tan \phi_1 \cos \beta}$$

$$p' = -\frac{\dot{\psi} \sin \gamma}{\cos \beta} - q \tan \beta$$

$$p = p' \cos \alpha - r' \sin \alpha$$

$$r = p' \sin \alpha + r' \cos \alpha$$

$$\theta = \sin^{-1} (-p/\dot{\psi})$$

$$\phi = \tan^{-1}(q/r)$$

B. Steady Uncoordinated Straight Flight

$$\text{Steady-state Euler equations} \quad n_x - \sin \theta = 0 \quad n_z + \cos \theta \cos \phi = 0$$

$$n_y + \cos \theta \sin \phi = 0 \quad L = M = N = 0$$

Kinematic relationships

$$p = q = r = 0$$

$$\theta = \sin^{-1} \left\{ \frac{\cos \alpha (\sin \gamma - n_y \sin \beta) + \sin \alpha [\cos^2 \beta - \sin^2 \gamma + n_y (2 \sin \beta \sin \gamma - n_y)]^{1/2}}{\cos \beta} \right\}$$

$$\phi = \sin^{-1} \left(\frac{-n_y}{\cos \theta} \right)$$

TABLE 3.- SMALL-PERTURBATION EQUATIONS OF MOTION OF AIRCRAFT FROM STEADY TURNING FLIGHT (ACCELERATION DERIVATIVES NEGLECTED)

$$\dot{\mathbf{x}} = \mathbf{F}\mathbf{x} + \mathbf{G}\mathbf{u}$$

$$\mathbf{x} \triangleq (\delta u, \delta w, \delta q, \delta \theta; \delta v, \delta p, \delta \phi, \delta r)^T$$

$$\mathbf{u} \triangleq (\Delta \delta_e, \Delta \delta_c, \Delta \delta_a, \Delta \delta_p)^T$$

x_u	$x_w - q_0$	$x_q - w_0$	$-g \cos \theta_0$	$x_v + r_0$	x_p	0	$x_r + v_0$
$z_u + q_0$	z_w	$z_q + u_0$	$-g \cos \phi_0 \sin \theta_0$	$z_v - p_0$	$z_p - v_0$	$-g \sin \phi_0 \cos \theta_0$	z_r
m_u	m_w	m_q	0	m_v	$m_p - 2p_0 \frac{I_{xz}}{I_y}$	0	$m_r + 2r_0 \frac{I_{xz}}{I_y}$
0	0	$\cos \phi_0$	0	0	$-r_0 \frac{(I_x - I_z)}{I_y}$	0	$-p_0 \frac{(I_x - I_z)}{I_y}$
$y_u - r_0$	$y_w + p_0$	y_q	$-g \sin \phi_0 \sin \theta_0$	y_v	$y_p + w_0$	$g \cos \phi_0 \cos \theta_0$	$y_r - u_0$
l'_u	l'_w	$l'_q + t_1 p_0 - t_2 r_0$	0	l'_v	$l'_p + t_1 q_0$	0	$l'_r - t_2 q_0$
0	0	$\sin \phi_0 \tan \theta_0$	$\dot{\psi}_0 \sec \theta_0$	0	1	0	$\cos \phi_0 \tan \theta_0$
n'_u	n'_w	$n'_q - t_3 p_0 - t_1 r_0$	0	n'_v	$n'_p - t_3 q_0$	0	$n'_r - t_1 q_0$

$$\mathbf{G} = \begin{bmatrix} x_{\delta_e} & x_{\delta_c} & x_{\delta_a} & x_{\delta_p} \\ z_{\delta_e} & z_{\delta_c} & z_{\delta_a} & z_{\delta_p} \\ m_{\delta_e} & m_{\delta_c} & m_{\delta_a} & m_{\delta_p} \\ 0 & 0 & 0 & 0 \\ y_{\delta_e} & y_{\delta_c} & y_{\delta_a} & y_{\delta_p} \\ l'_{\delta_e} & l'_{\delta_c} & l'_{\delta_a} & l'_{\delta_p} \\ 0 & 0 & 0 & 0 \\ n'_{\delta_e} & n'_{\delta_c} & n'_{\delta_a} & n'_{\delta_p} \end{bmatrix}$$

where

$$\left. \begin{aligned} x_i &= \frac{X_i}{m}; y_i = \frac{Y_i}{m}; z_i = \frac{Z_i}{m} \\ m_i &= \frac{M_i}{I_y} \end{aligned} \right\} \quad i = u, v, w; p, q, r; \delta_e, \delta_c, \delta_a, \delta_p$$

$$l'_i = \frac{I_z}{I_x I_z - I_{xz}^2} L_i + \frac{I_{xz}}{I_x I_z - I_{xz}^2} N_i$$

$$n'_i = \frac{I_{xz}}{I_x I_z - I_{xz}^2} L_i + \frac{I_x}{I_x I_z - I_{xz}^2} N_i$$

$$t_1 = \frac{I_{xz}(I_z + I_x - I_y)}{I_x I_z - I_{xz}^2}; \quad t_2 = \frac{I_z(I_z - I_y) + I_{xz}^2}{I_x I_z - I_{xz}^2}; \quad t_3 = \frac{I_x(I_y - I_x) - I_{xz}^2}{I_x I_z - I_{xz}^2}$$

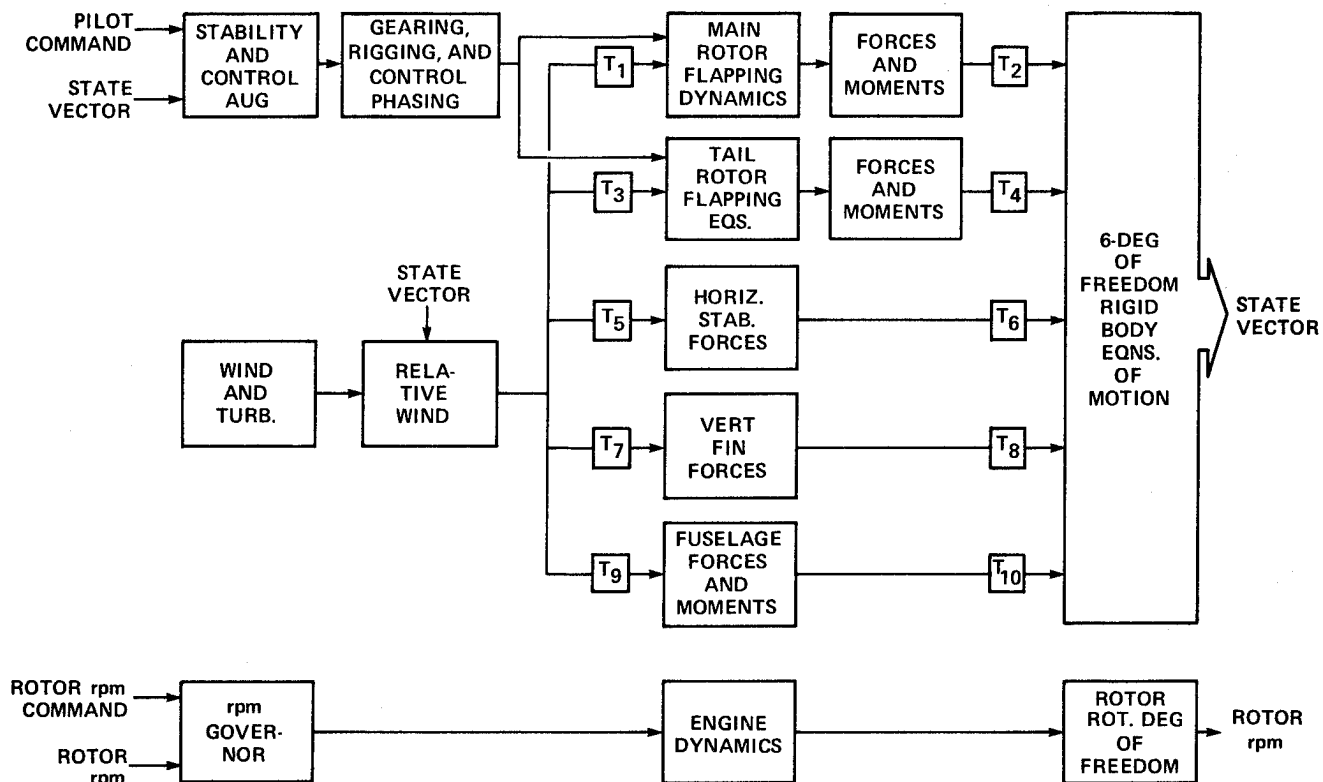


Figure 1.- Block diagram showing principal elements of single rotor helicopter model.

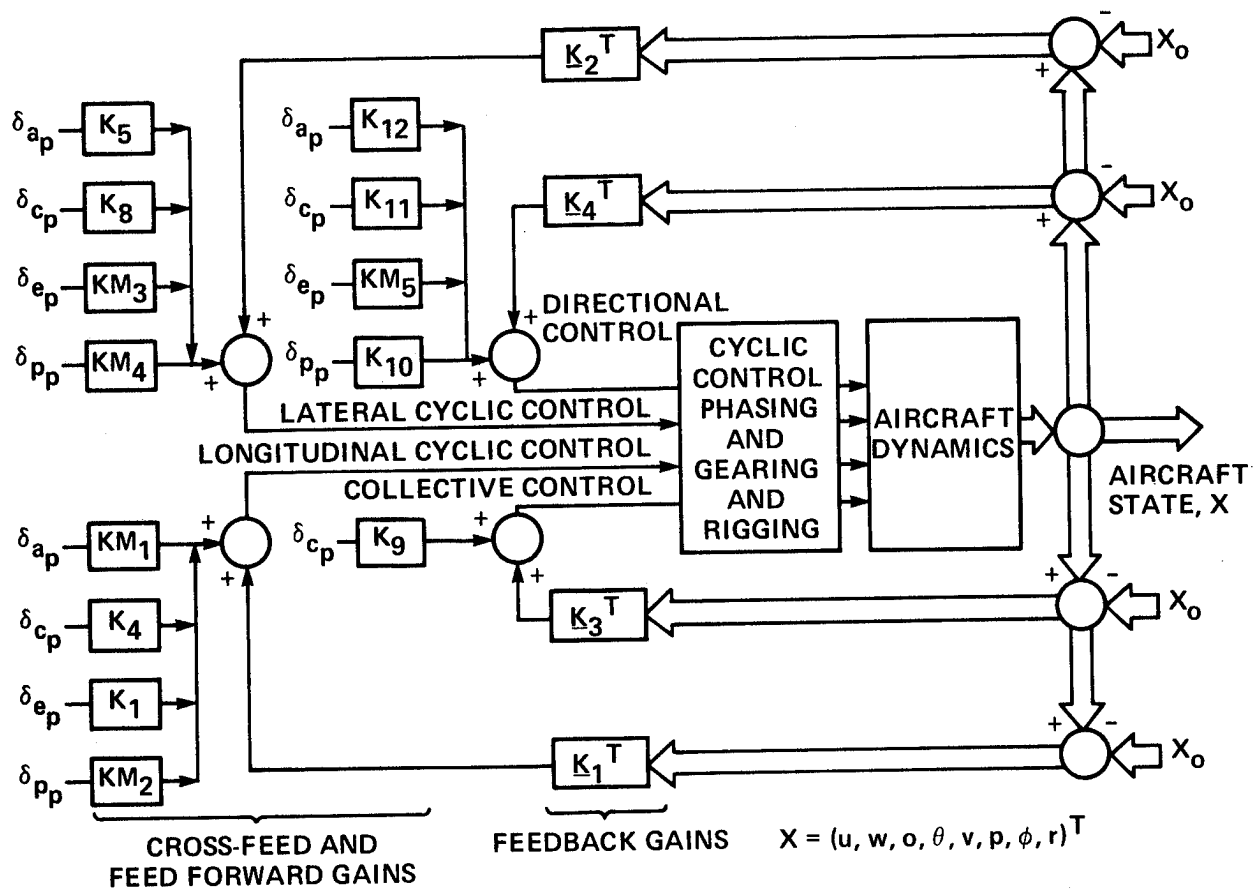


Figure 2.- Structure of control system model.

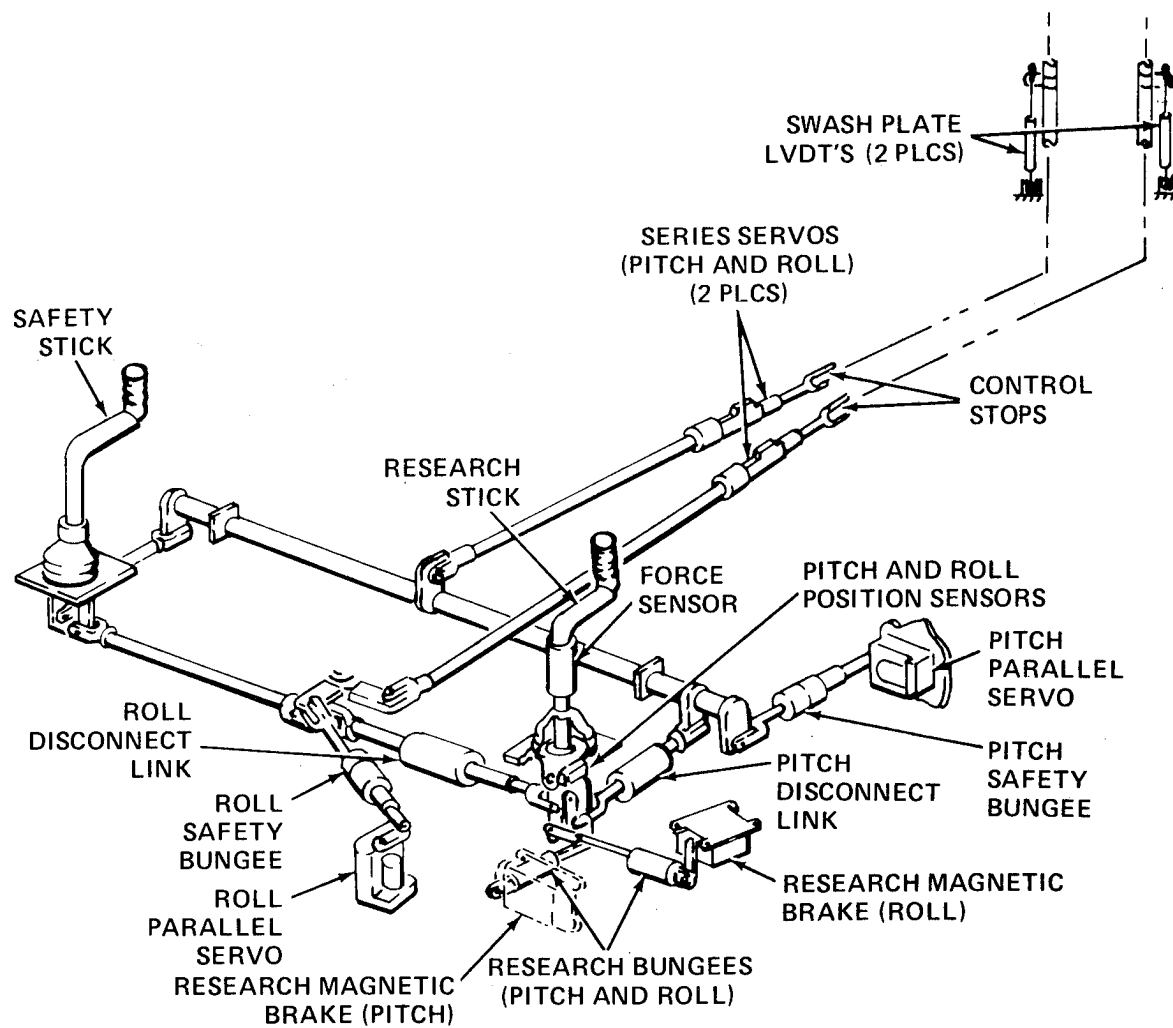


Figure 3.- UH-1H V/STOLAND control system longitudinal and lateral cyclic controls.

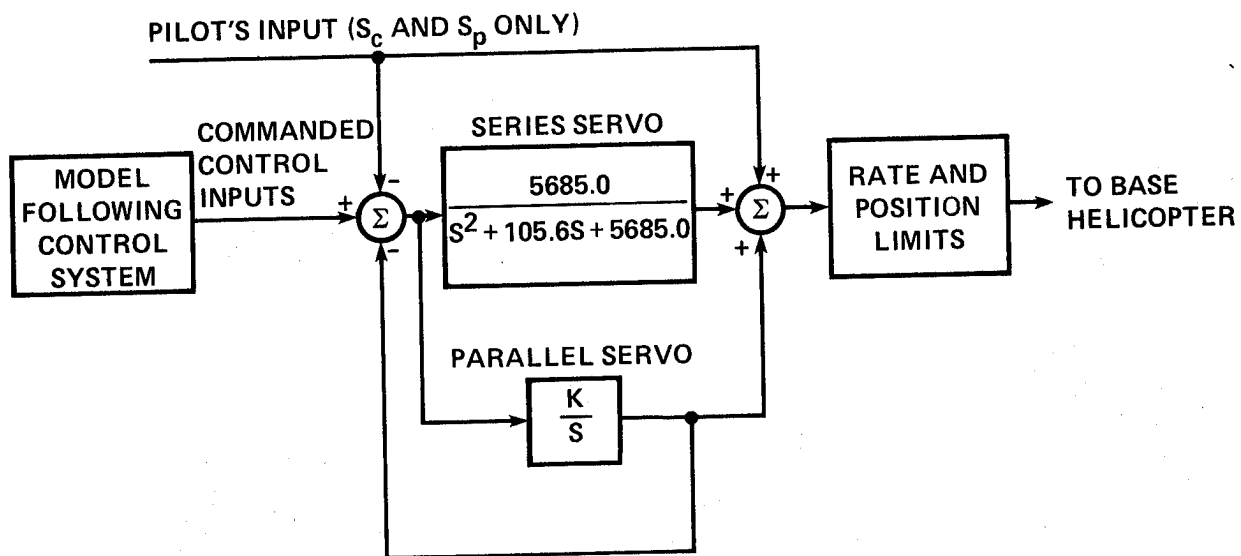


Figure 4.- Simulated UH-1H V/STOLAND actuating system.

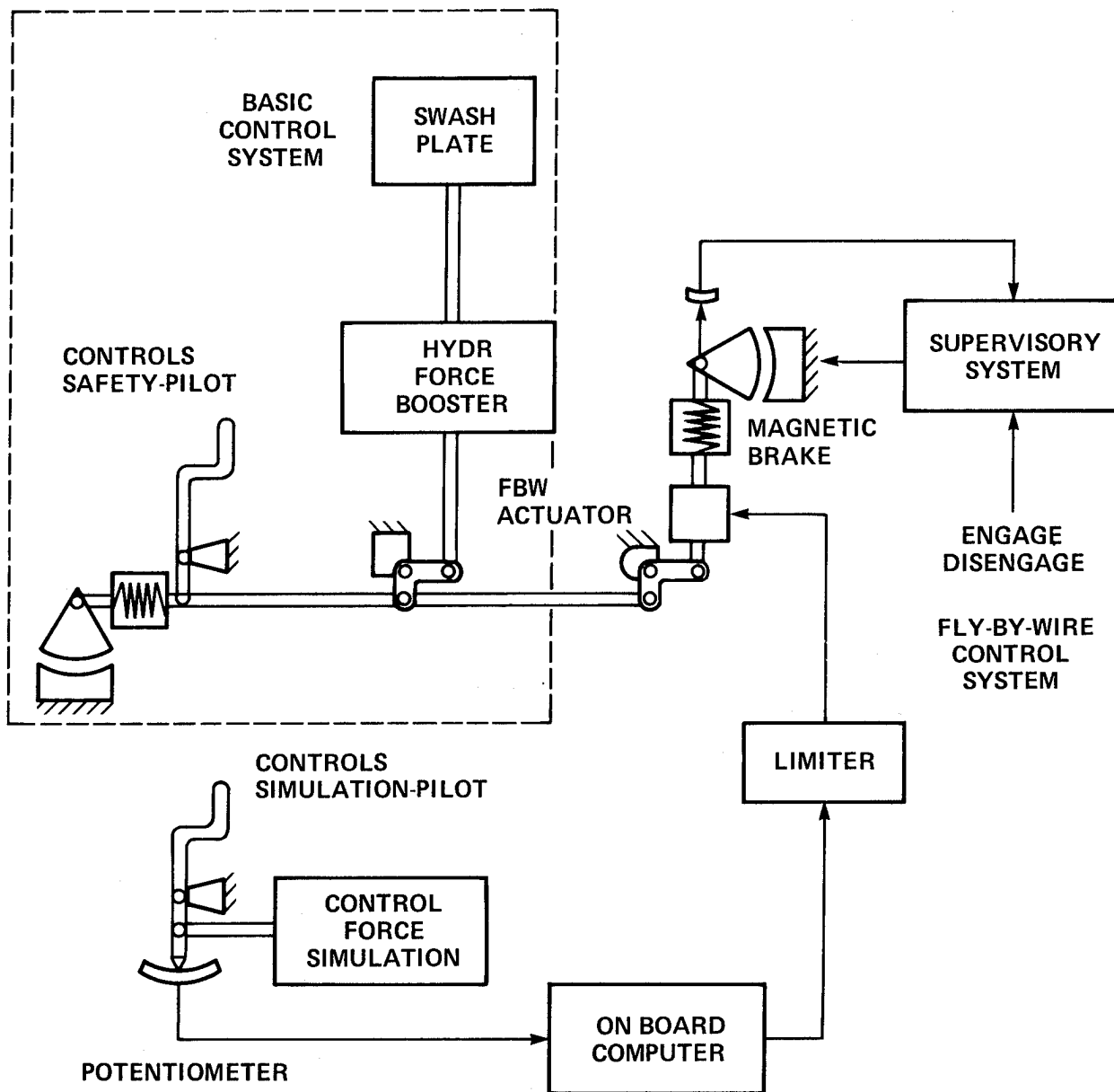


Figure 5.- B0-105 S3 control system.

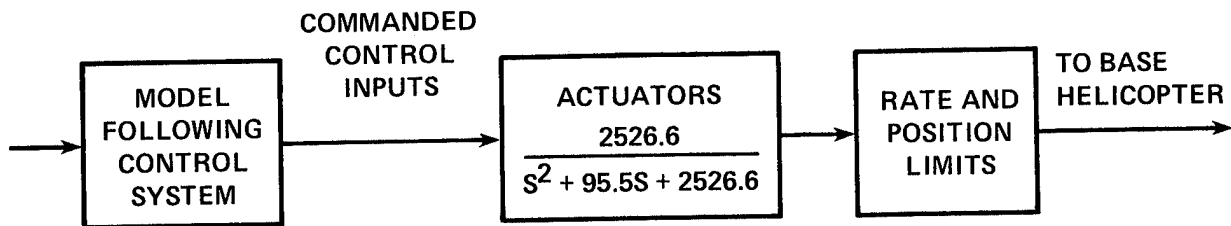


Figure 6.- Simulated BO-105 S3 actuator dynamics.

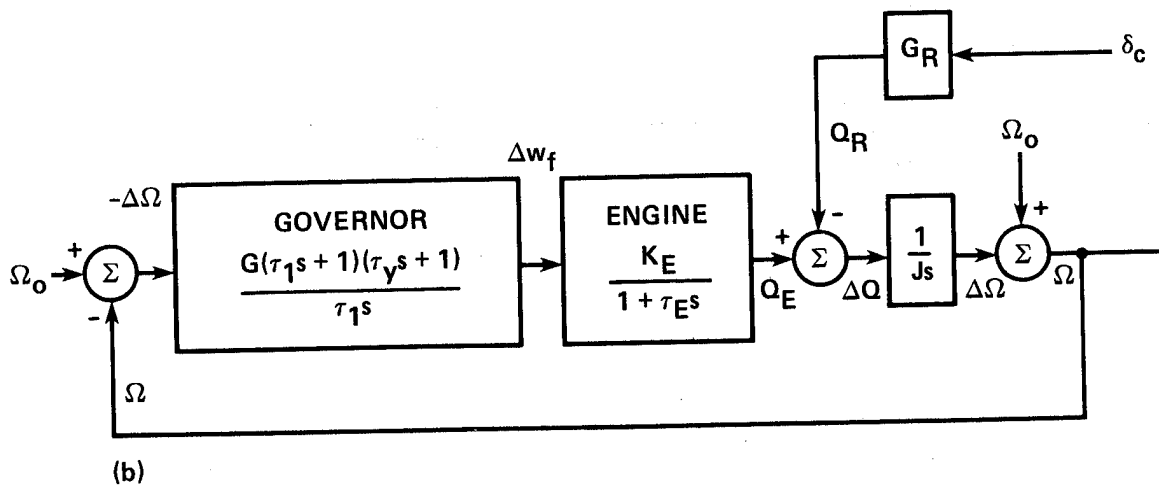
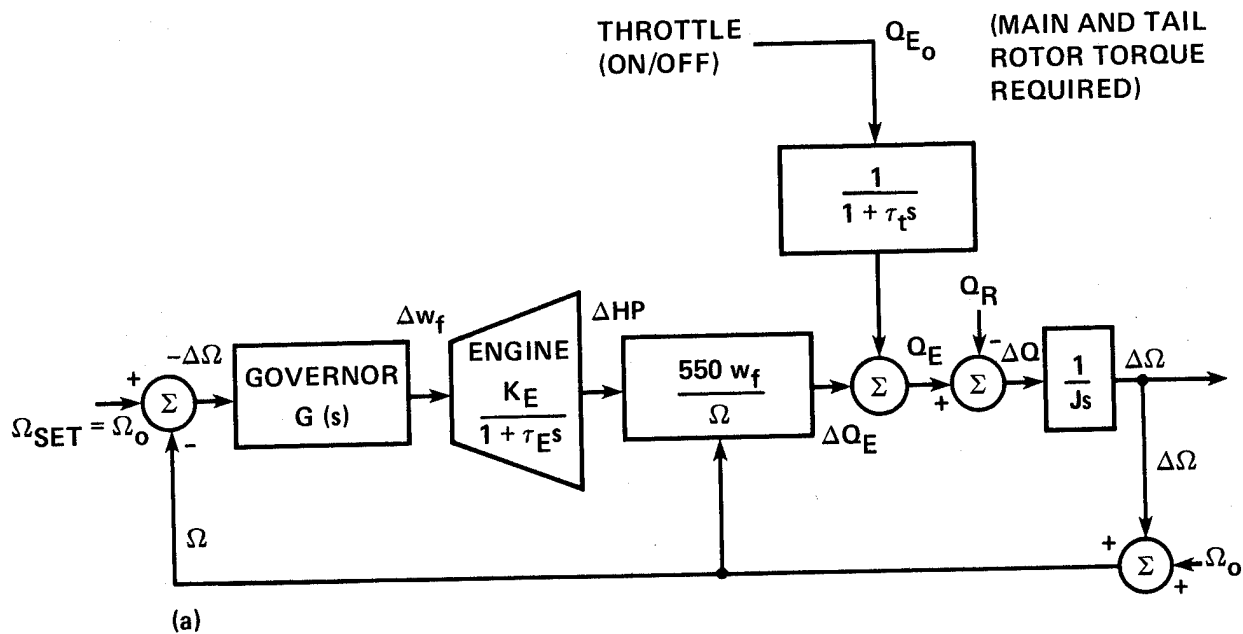


Figure 7.- RPM governor. (a) Generic. (b) Simulated.

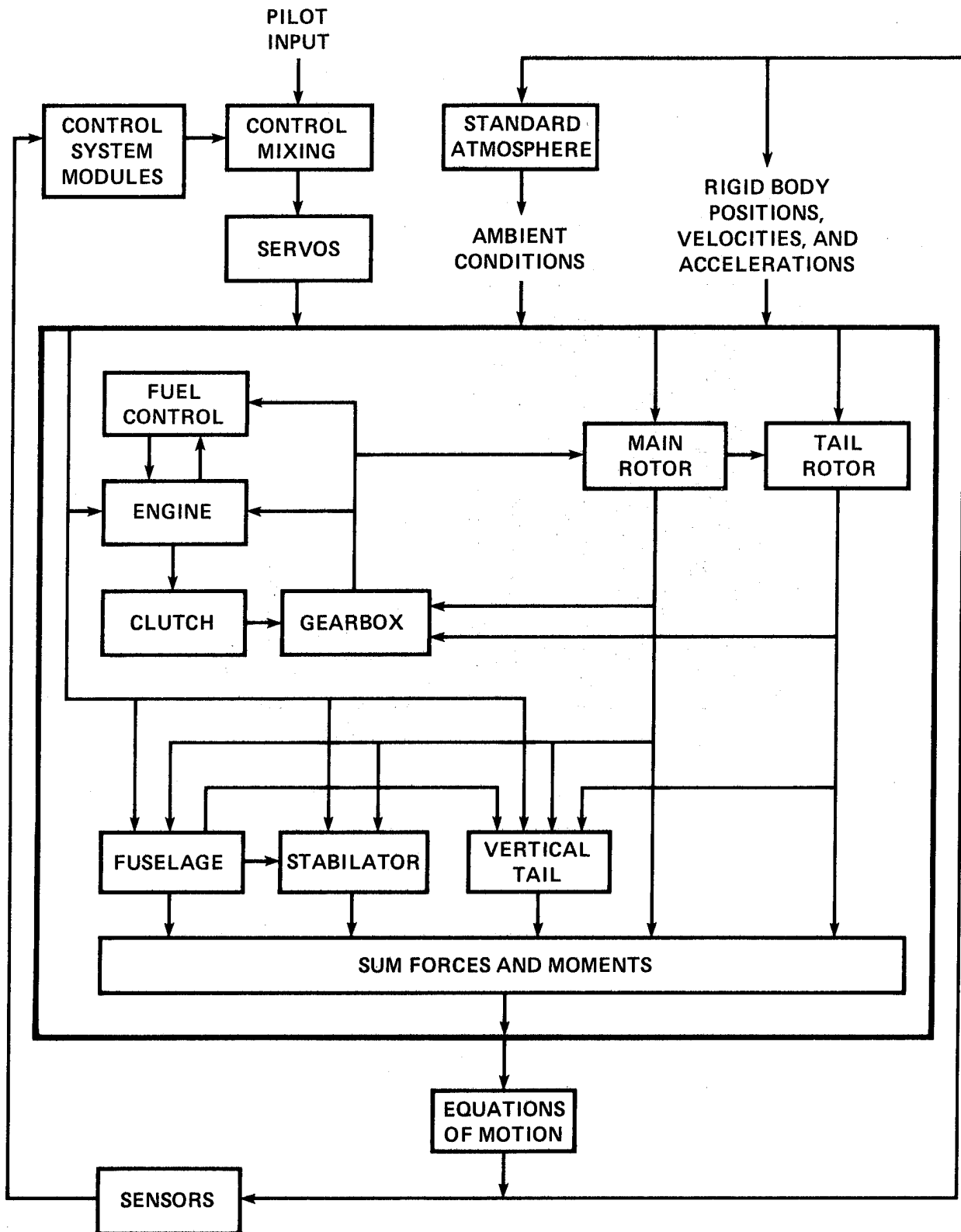


Figure 8.- GenHel simulation elements.

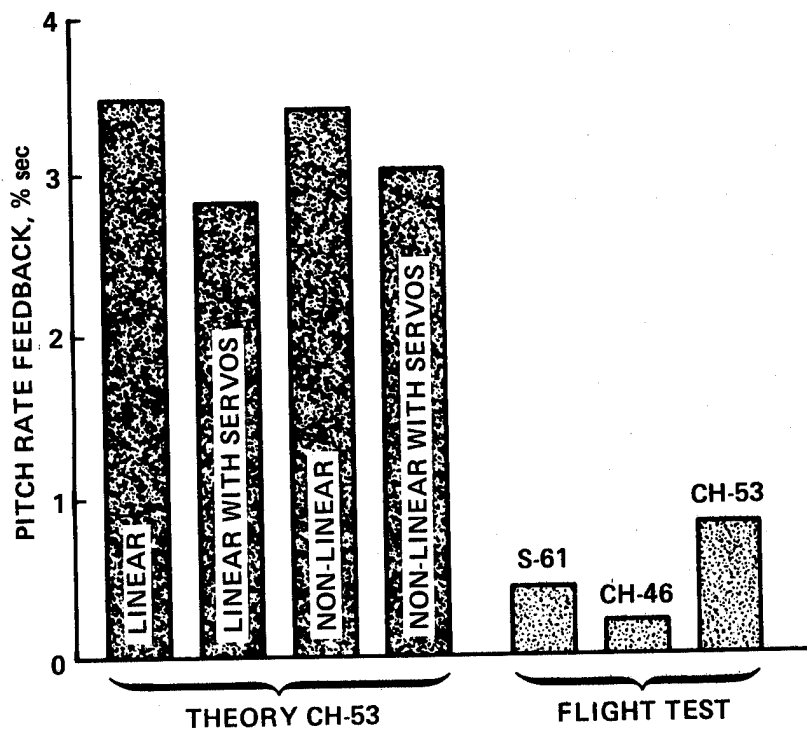


Figure 9.- Analytical and flight test gain limits for pitch rate feedback (from ref. 60).

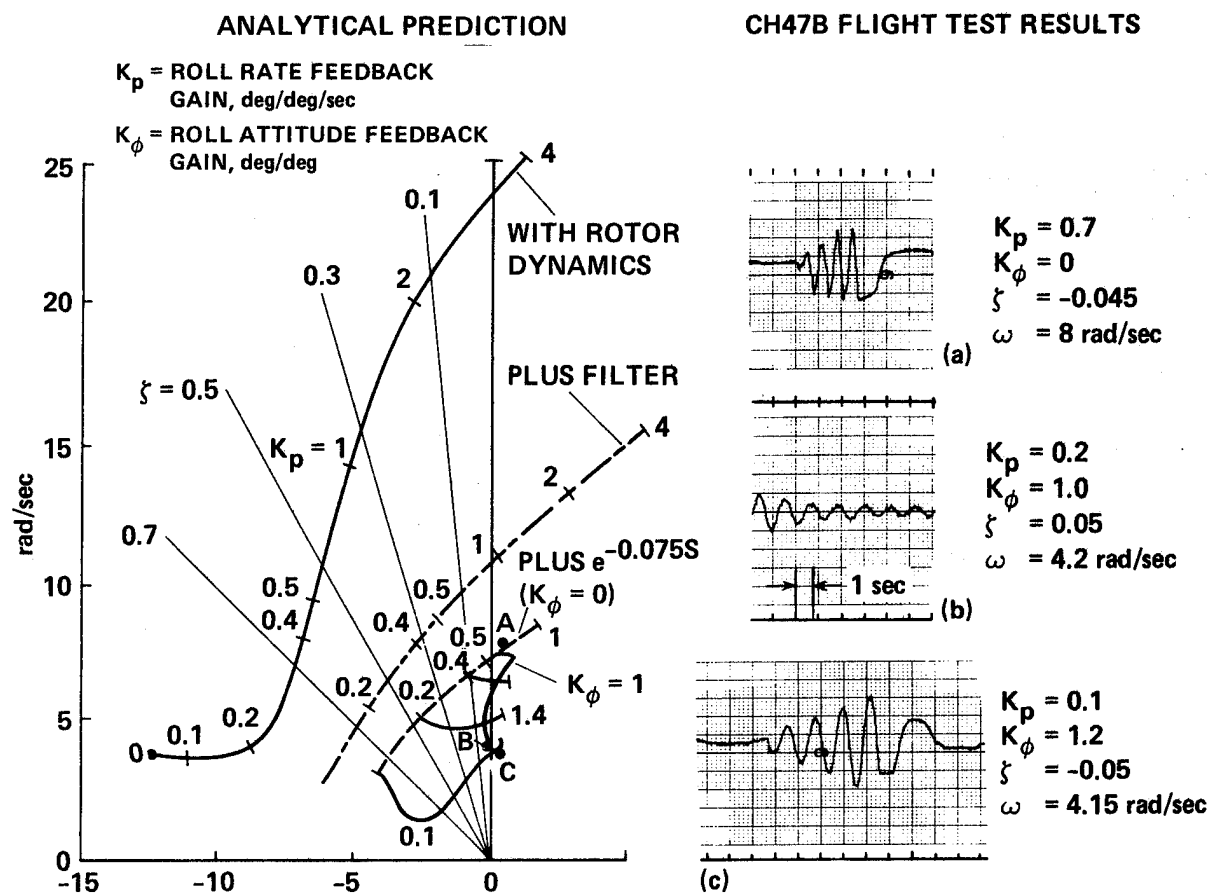


Figure 10.- Comparison of calculated and CH-47B flight test results concerning gain limits.

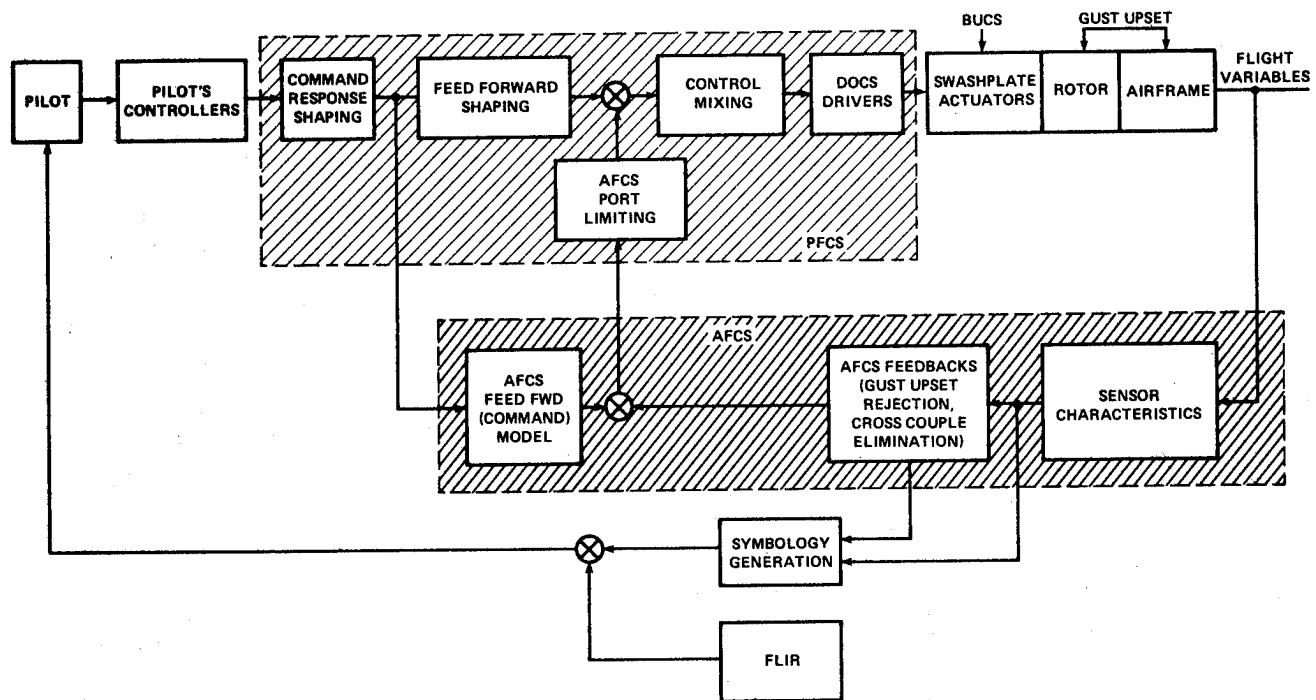


Figure 11.- ADOCS flight control system concept (from ref. 19).

		STABILIZATION LEVEL							
		LONGITUDINAL/LATERAL				DIRECTIONAL		VERTICAL	
		RA	AT	LV	LP	RA	AT	LV	LP
RESPONSE COMMAND MODEL	AC	●				●	●	NA	
	RA	●	●	●			●		
	AT		●	●					
	LA					NA		●	●
	LV			●	●				●

IDENTIFICATION CODE

		PITCH/ ROLL	YAW	VERTICAL
ANGULAR ACCELERATION	AC	$\ddot{\psi}$	—	—
ANGULAR RATE	RA	$\dot{\psi}$	—	—
ANGULAR ATTITUDE	AT	ψ_H	—	—
LINEAR ACCELERATION	LA	—	\ddot{h}	—
LINEAR VELOCITY	LV	—	\dot{h}	—
LINEAR POSITION	LP	—	h_H	—

EXAMPLE: RA/AT

ANGULAR RATE COMMAND/ATTITUDE STABILIZATION

$\dot{\psi}/\psi_H$

YAW RATE COMMAND/HEADING HOLD

Figure 12.- Generic SCAS configurations (from ref. 19).

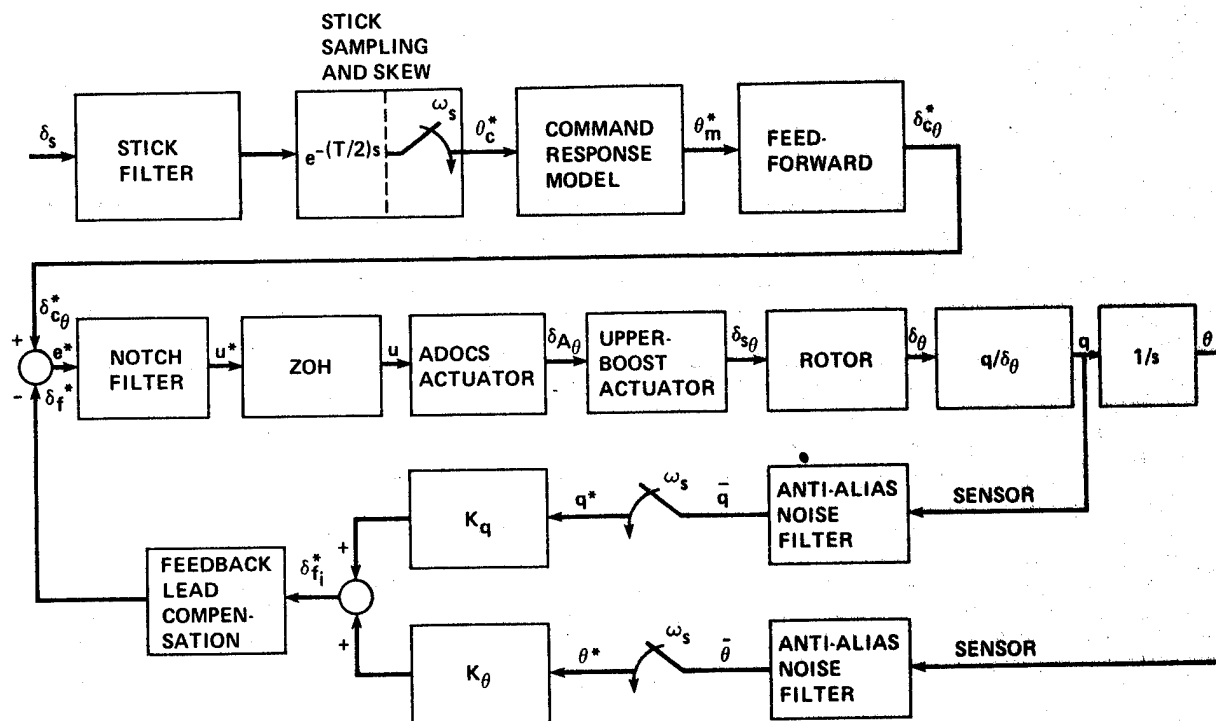


Figure 13.- Pitch axis, digital control system.

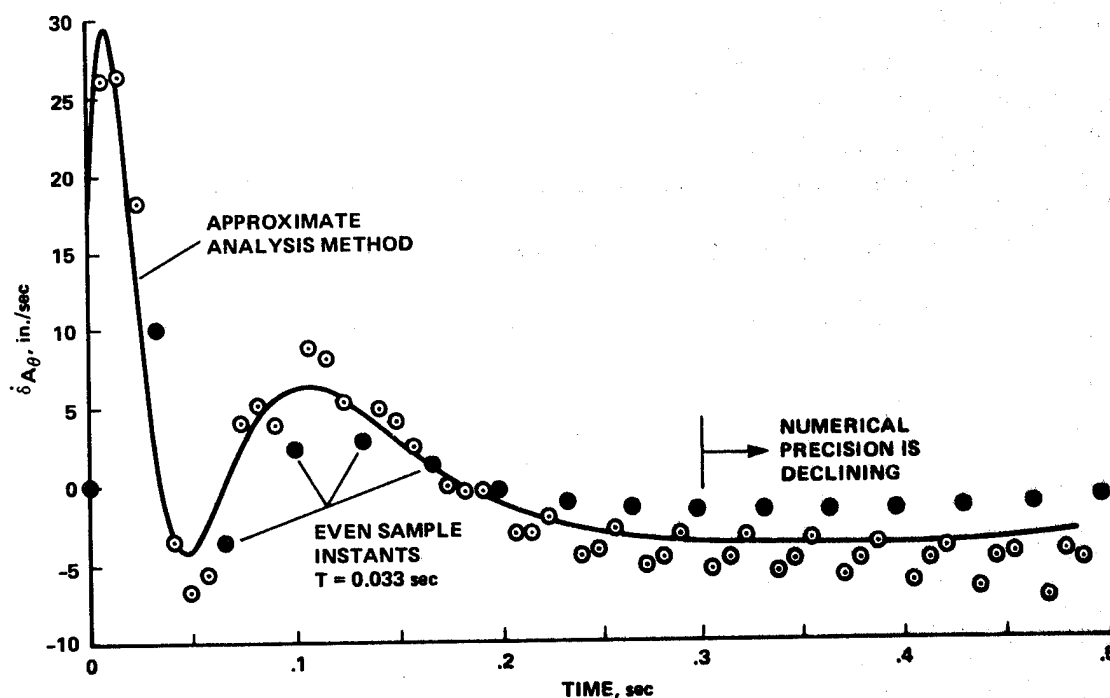
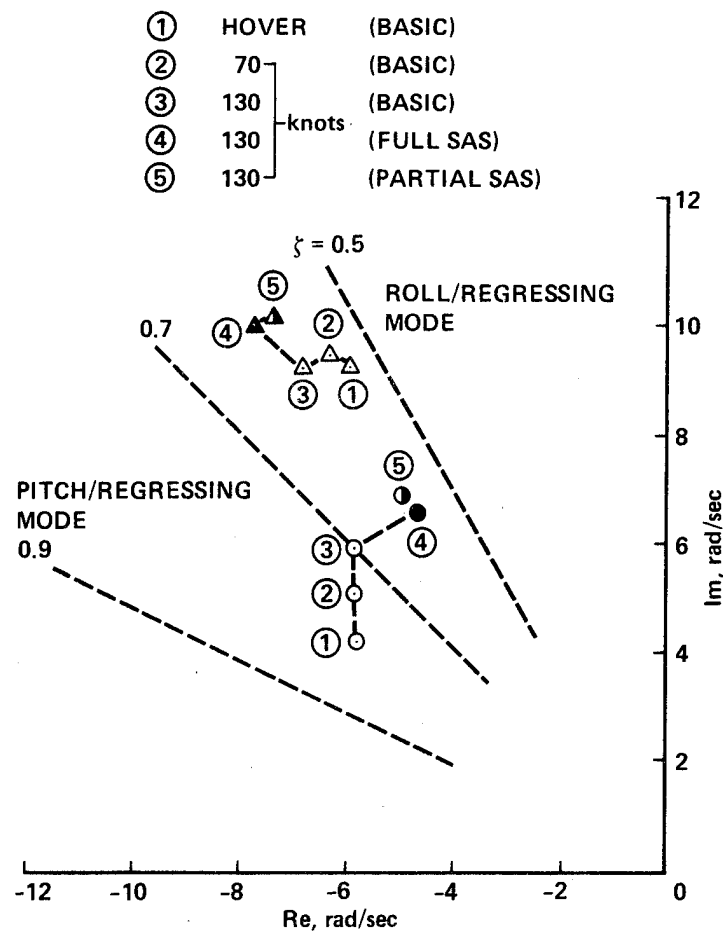
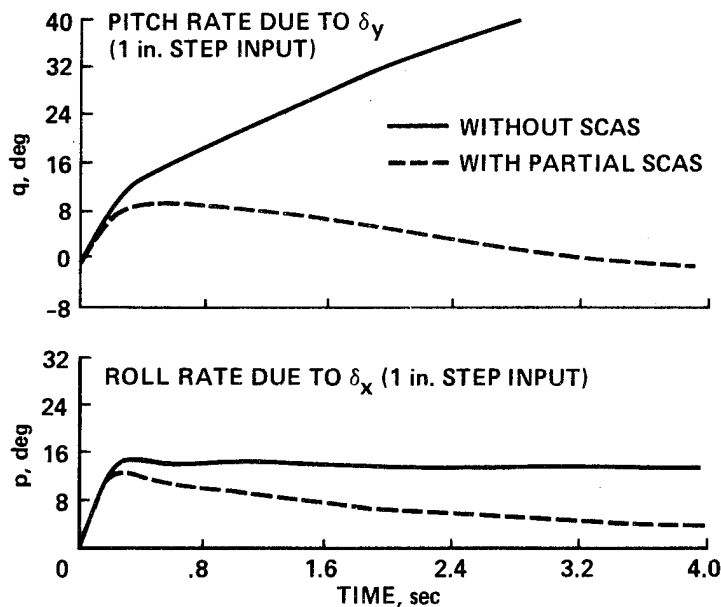


Figure 14.- Actuator rate ($\dot{\delta}_{A\theta}$) response to a step input, $\delta_{c\theta} = 1$ in.



(a) PITCH/REGRESSING AND ROLL/REGRESSING MODES



(b) TIME HISTORIES OF THE 9X9 EQUATIONS (130 knots)

Figure 15.- Influence of flapping dynamics on SCAS performance. (a) Pitch/regressing and roll/regressing modes. (b) Time histories generated from coupled body-flapping model.

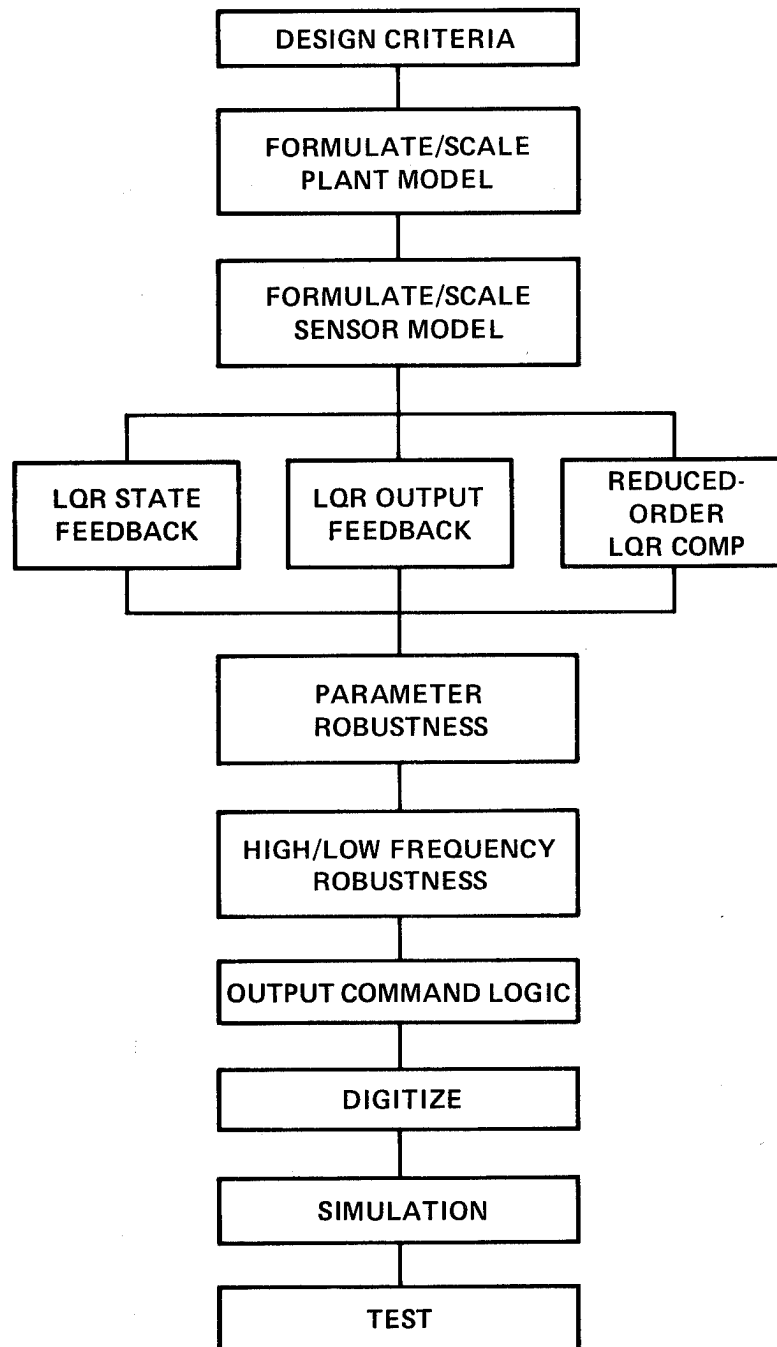


Figure 16.- The refined design methodology (from ref. 33).

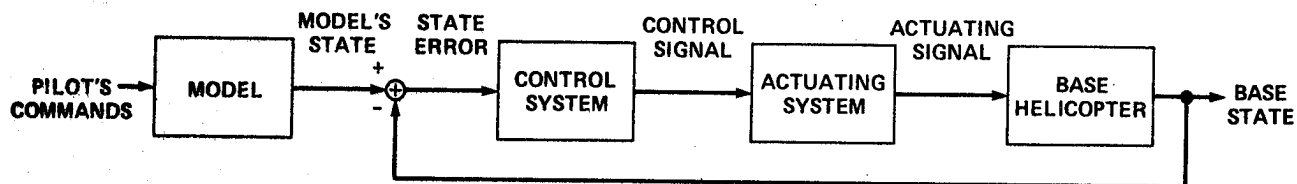


Figure 17.- Basic model-following control system concept.

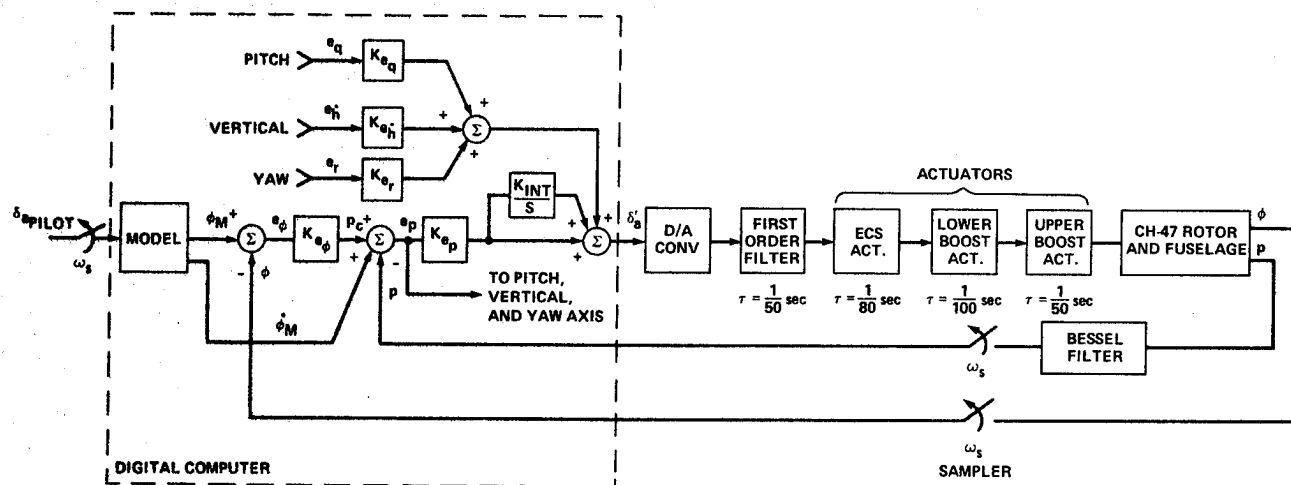


Figure 18.- Lateral model-following control system: CH-47B Implementation.

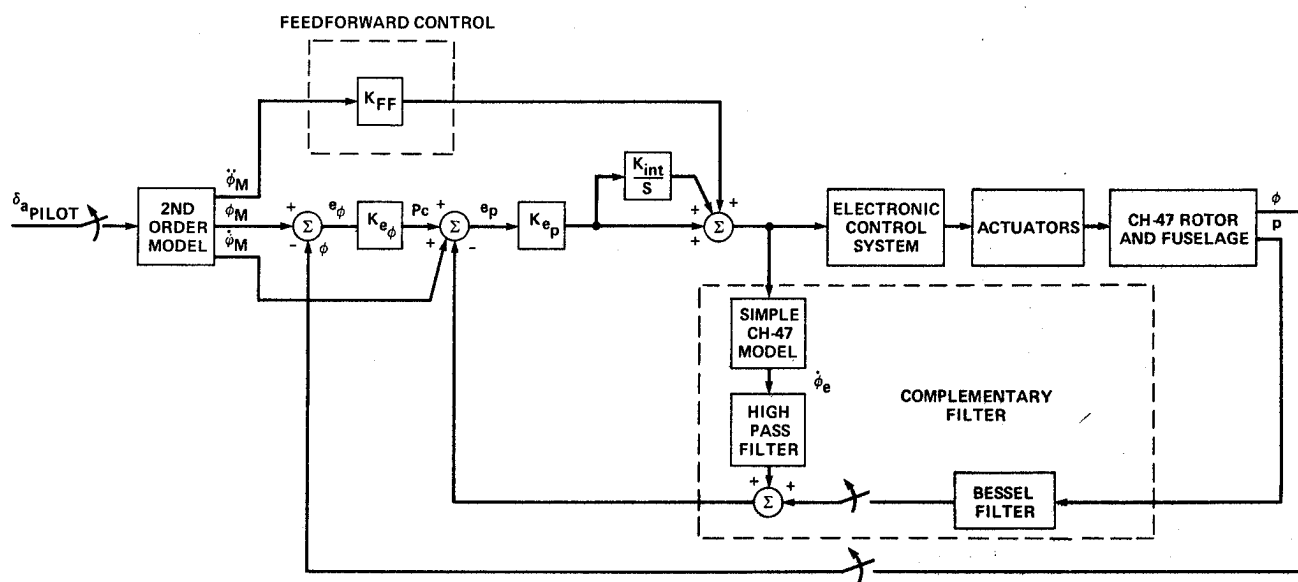


Figure 19.- Revised lateral model-following control system.

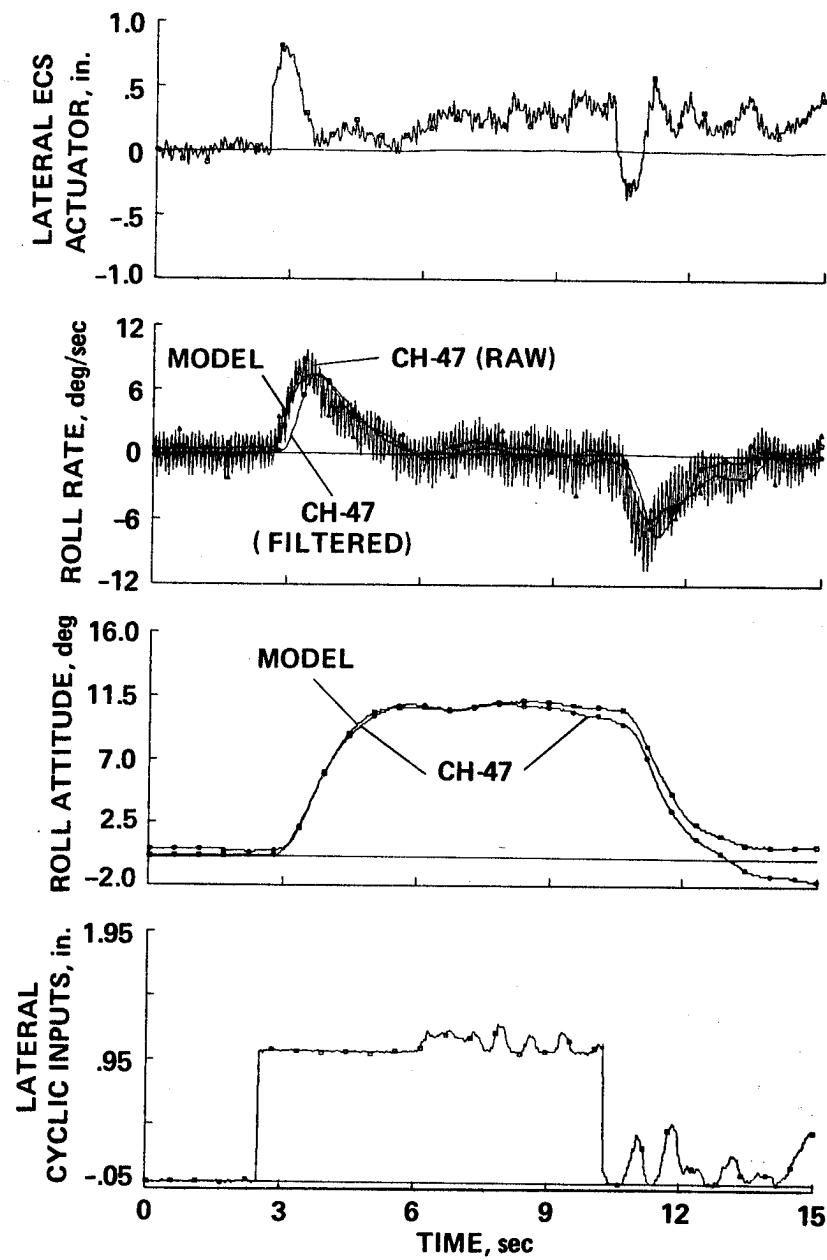
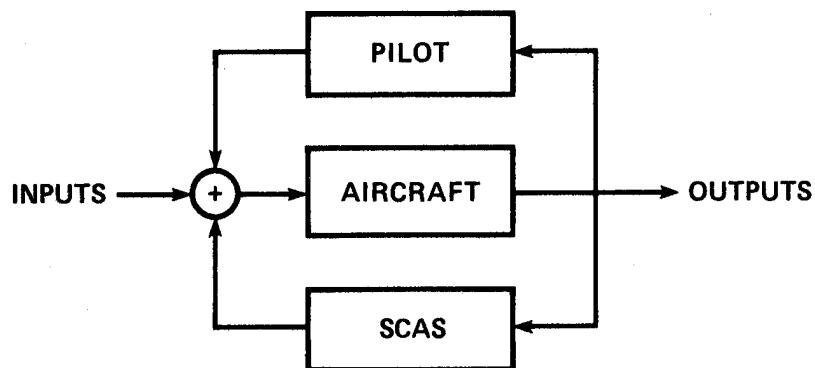


Figure 20.- CH-47B flight-test results: roll axis step response in hover.



- STEP 1: SET SCAS TO ZERO, SOLVE FOR OPTIMAL PILOT
- STEP 2: SOLVE FOR OUTPUT FEEDBACK SCAS FOR AIRCRAFT + PILOT SYSTEM
- STEP 3: SOLVE FOR OPTIMAL PILOT FOR SCAS + AIRCRAFT SYSTEM
- STEP 4: REPEAT STEPS 1-3 UNTIL A STATIONARY SOLUTION IS FOUND

Figure 21.- CCS design structure.

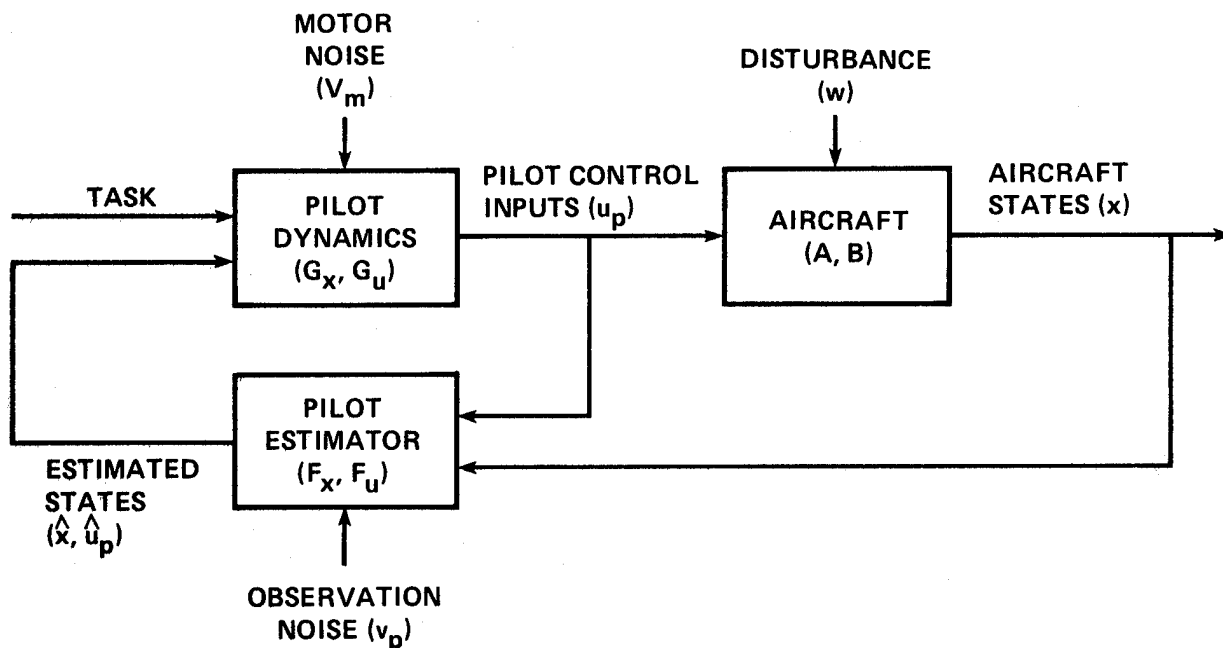
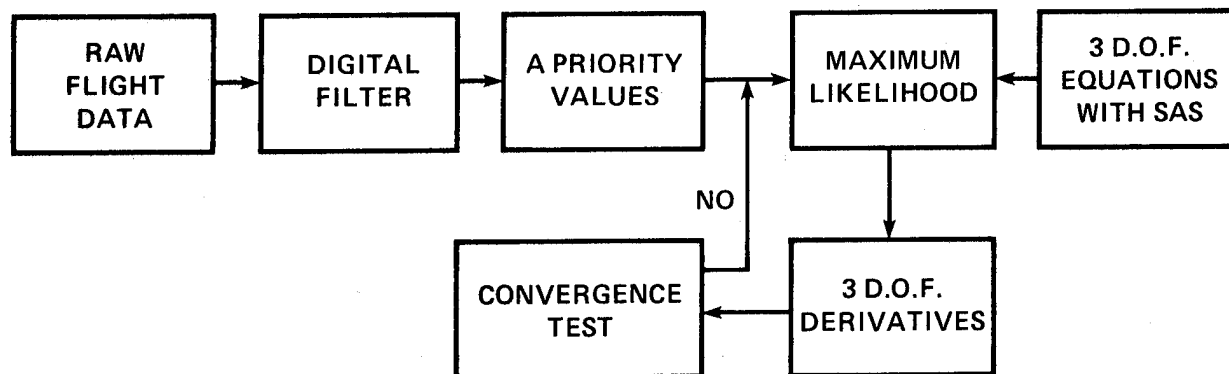
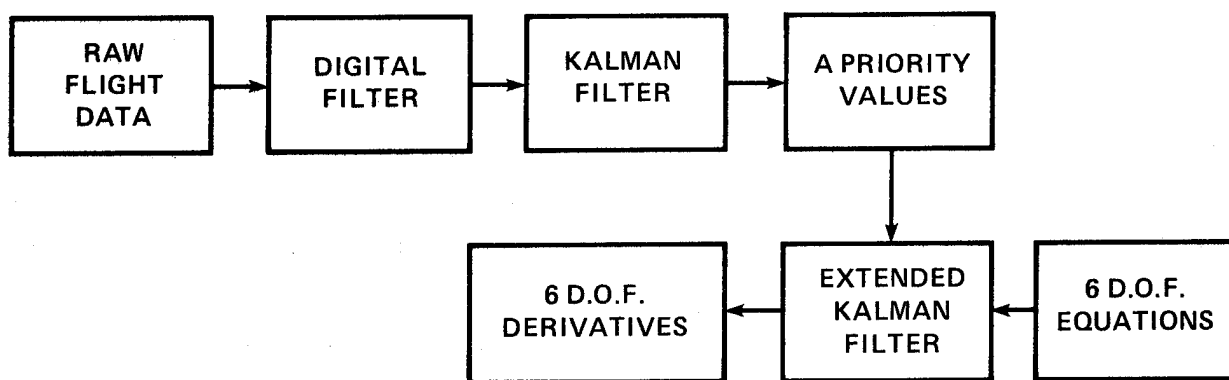


Figure 22.- Optimal pilot-model.



(a) MODIFIED NEWTON-RAPHSON



(b) EXTENDED KALMAN FILTER METHOD

Figure 23.- Parameter identification methods (from ref. 91). (a) Modified Newton-Raphson. (b) Extended Kalman filter method.

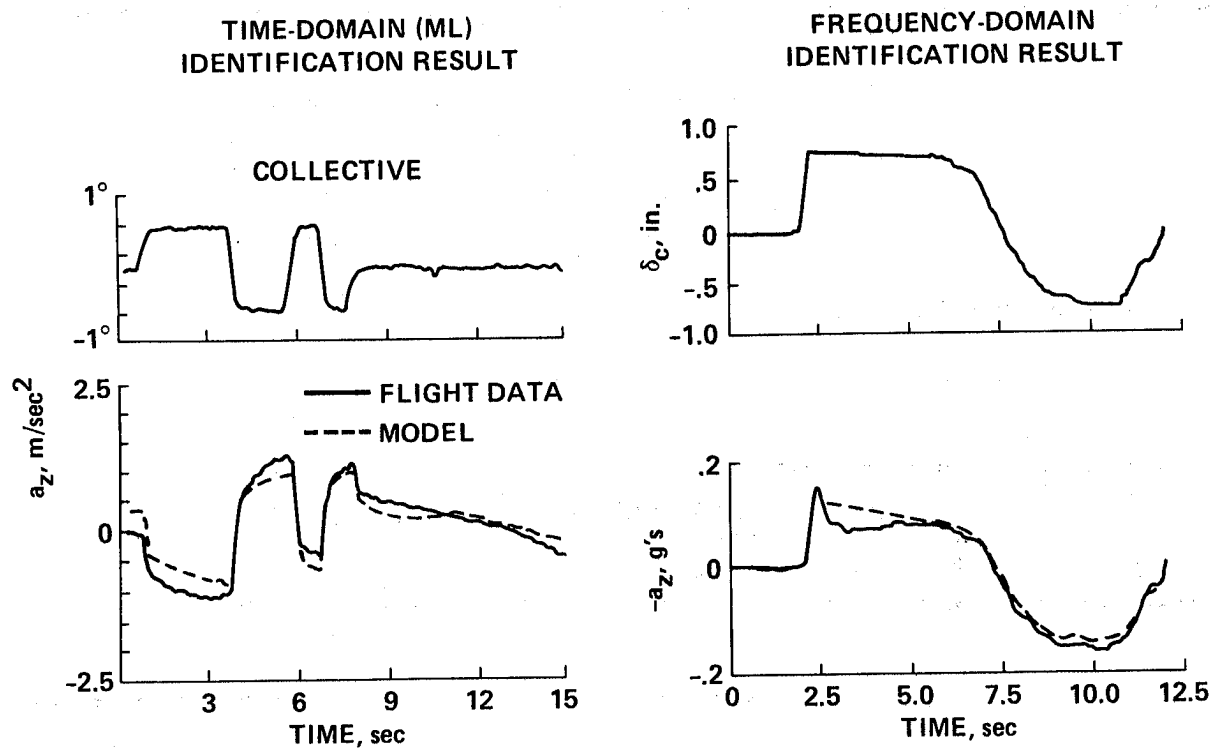


Figure 24.- Examples of time-history mismatch using good identification algorithms.

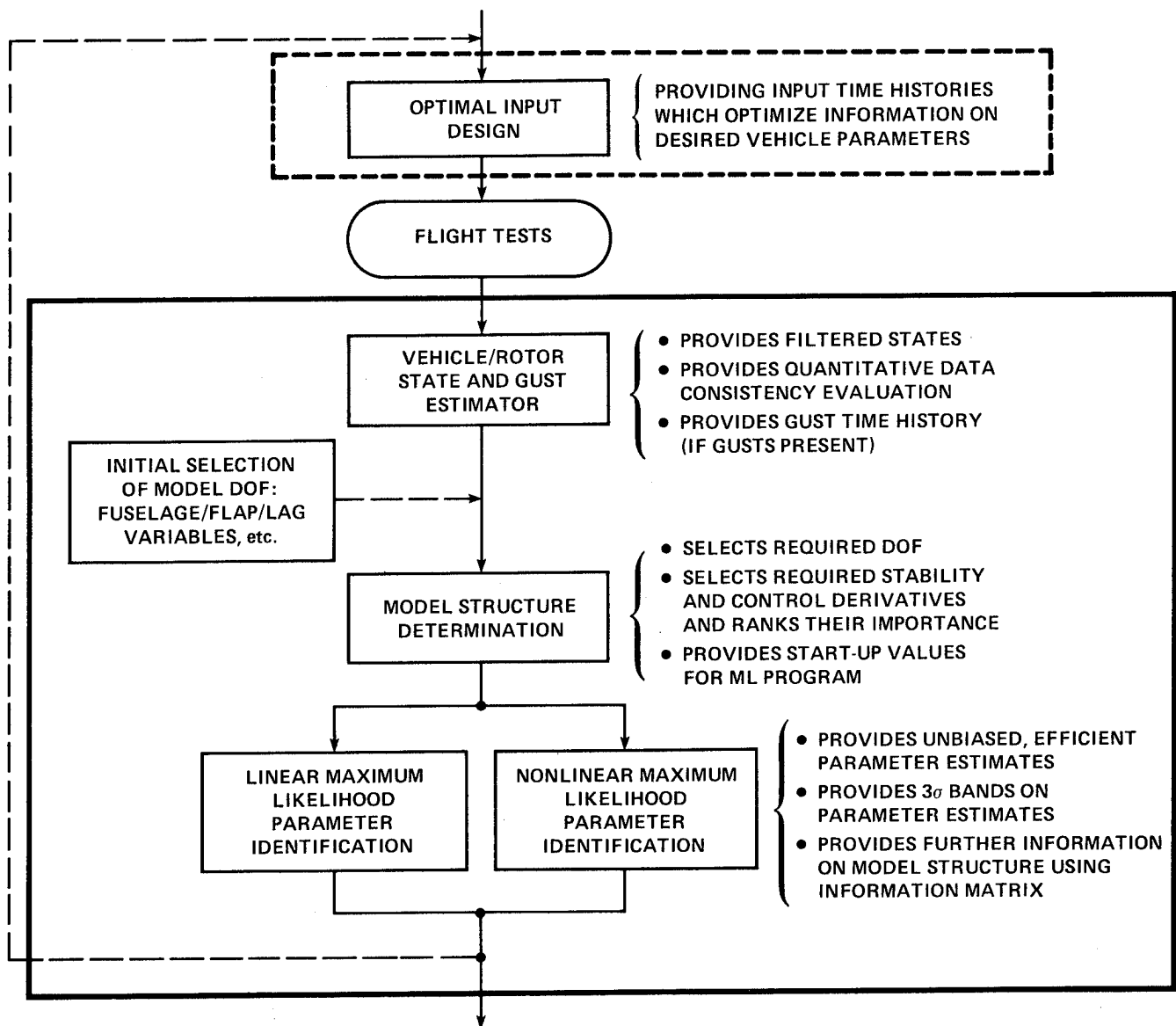


Figure 25.- Integrated rotorcraft system identification procedure (from ref. 84).

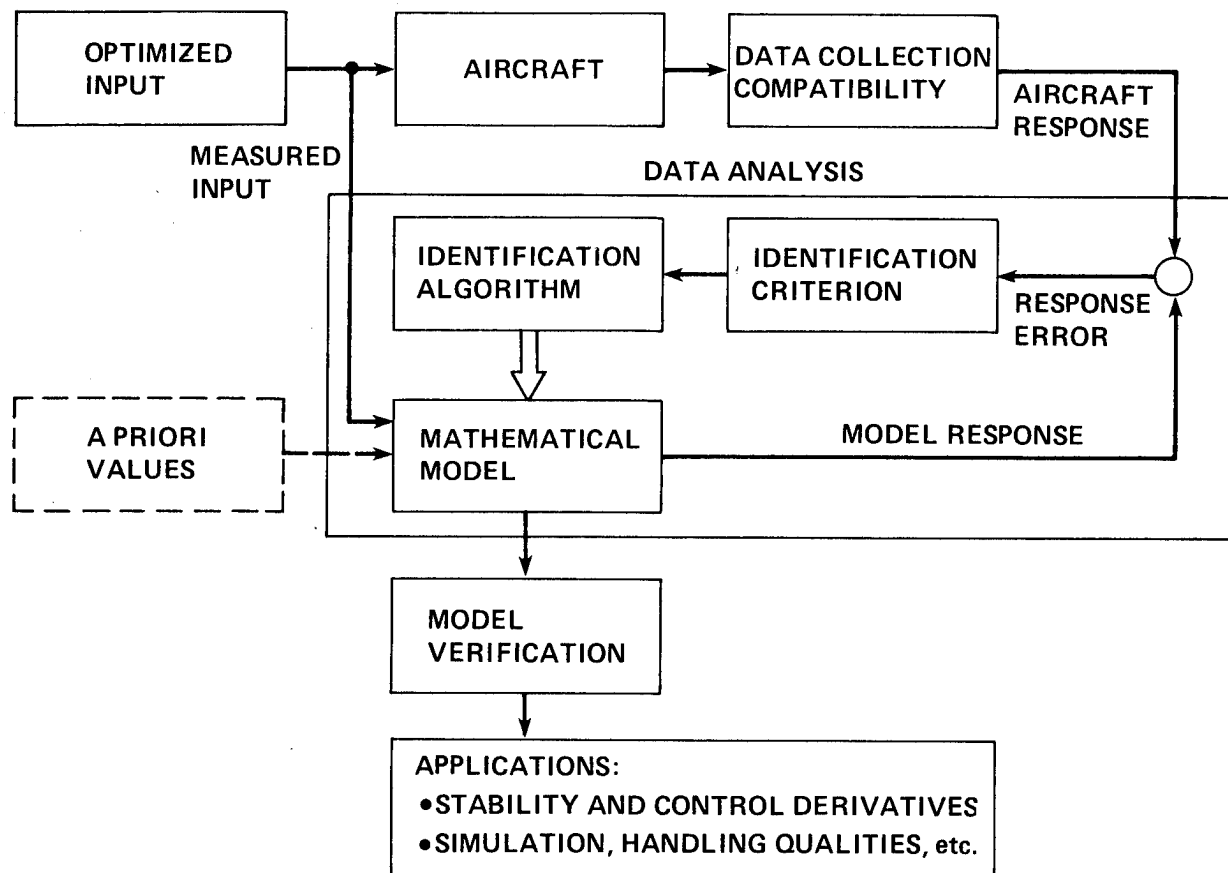


Figure 26.- Time-domain identification method.

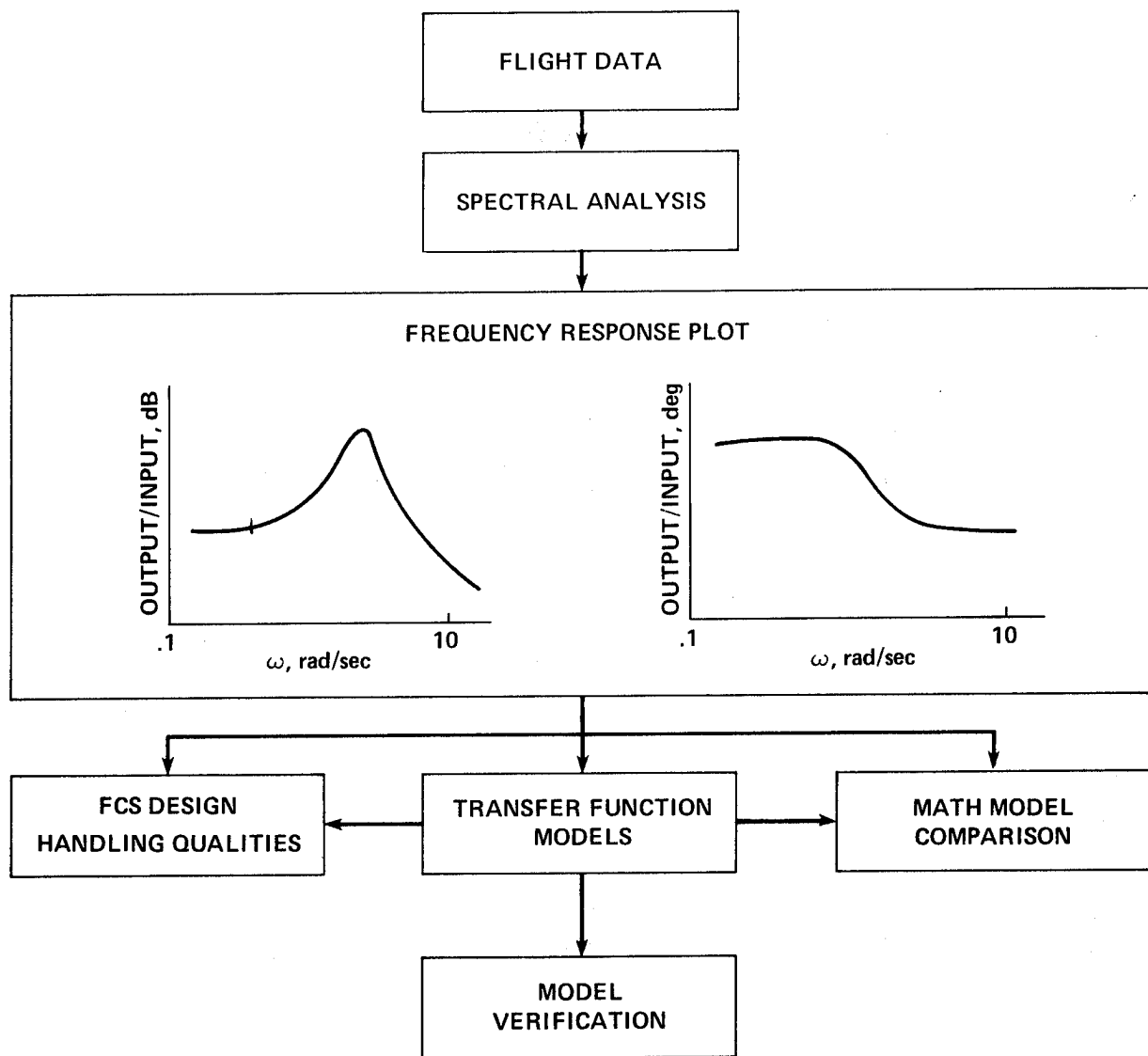


Figure 27.- Frequency-domain identification method.

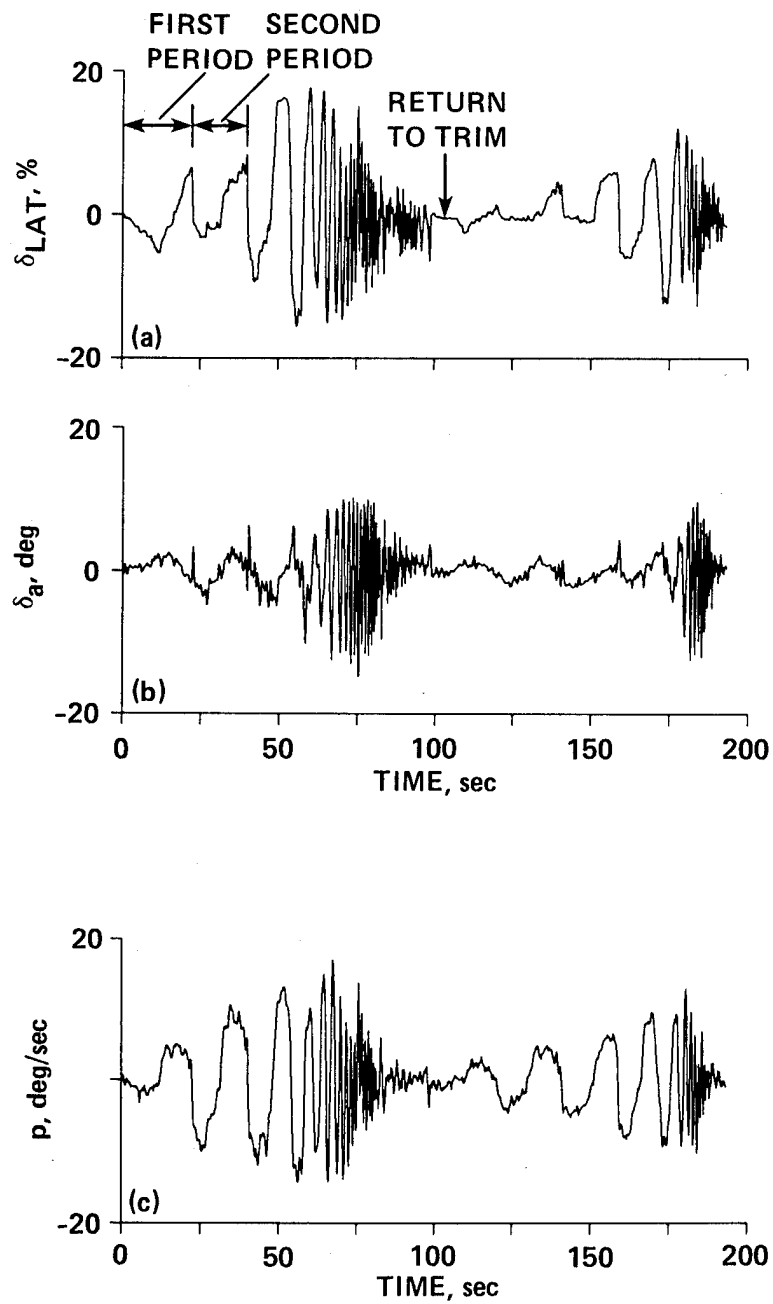


Figure 28.- Sample input and output time histories. (a) Lateral stick inputs. (b) Aileron surface deflections. (c) Roll rate response.

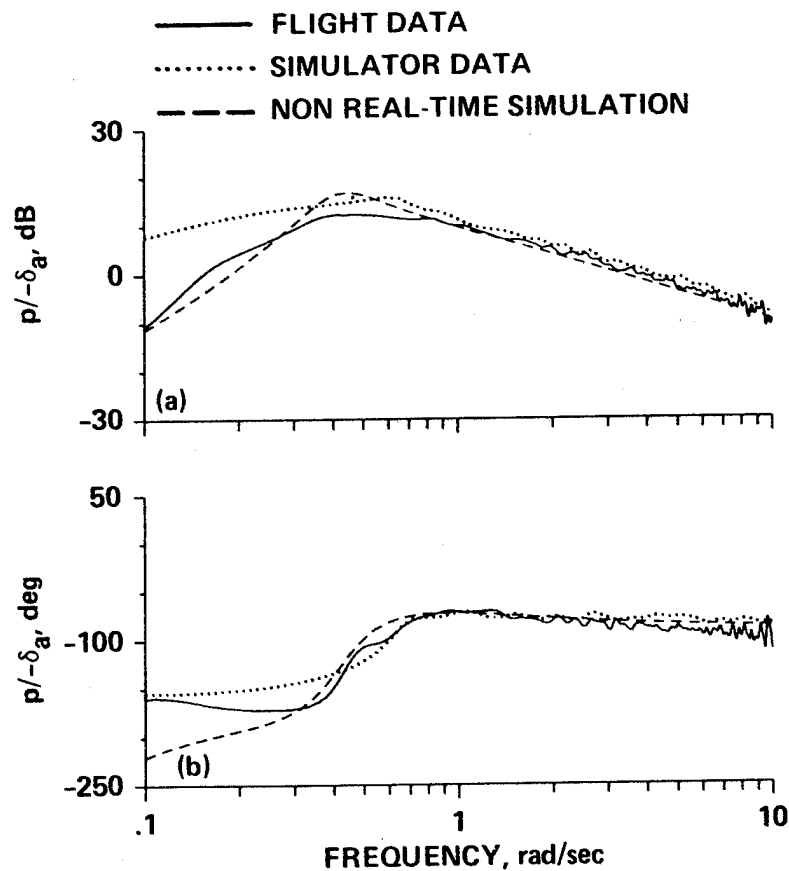


Figure 29.- Comparison of frequency response of roll rate to lateral control in hover, extracted from flight and simulation models for the XV-15.

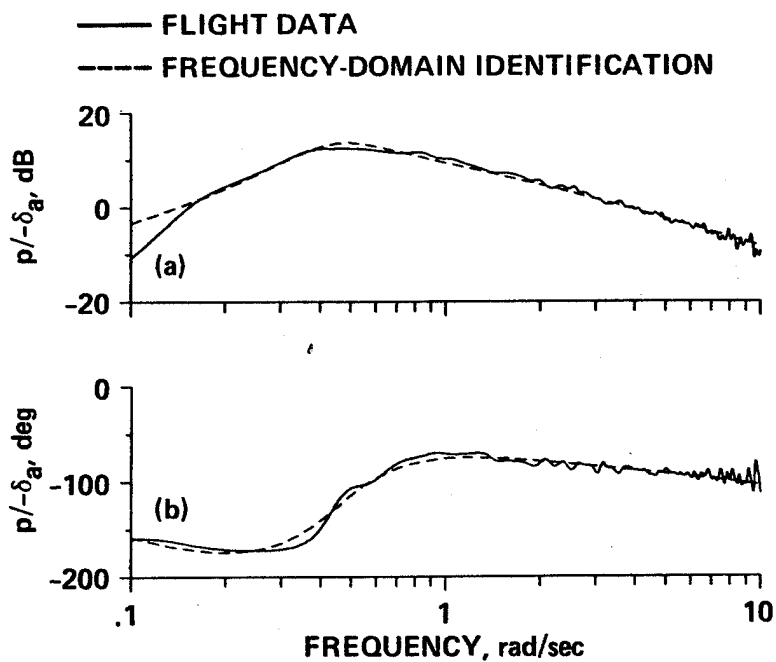


Figure 30.- Comparison of frequency responses extracted from flight with those generated from identified model.

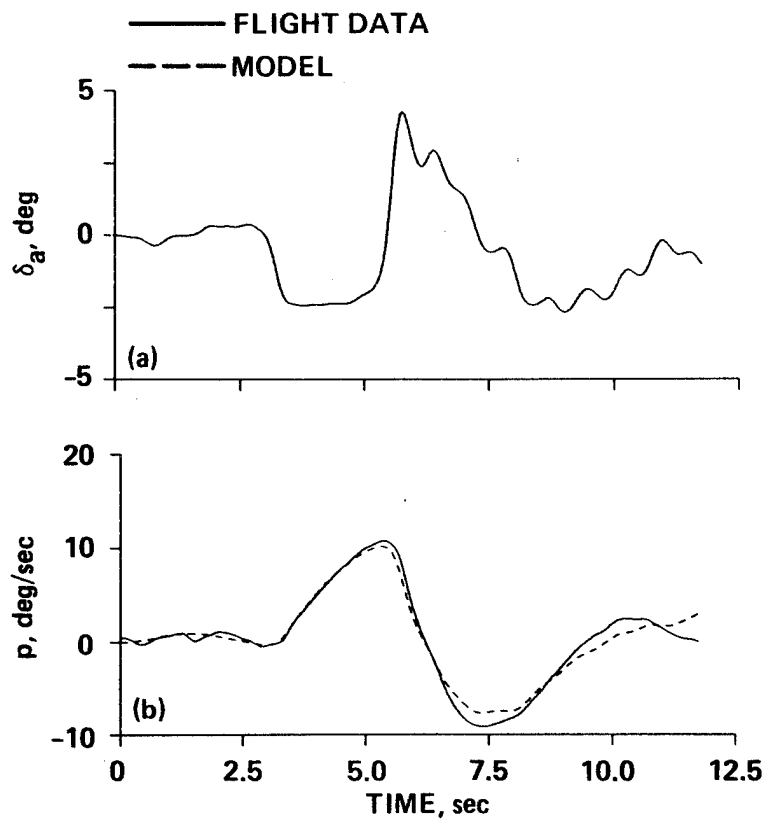


Figure 31.- Comparison of roll rate response predicted from identified model with flight data.

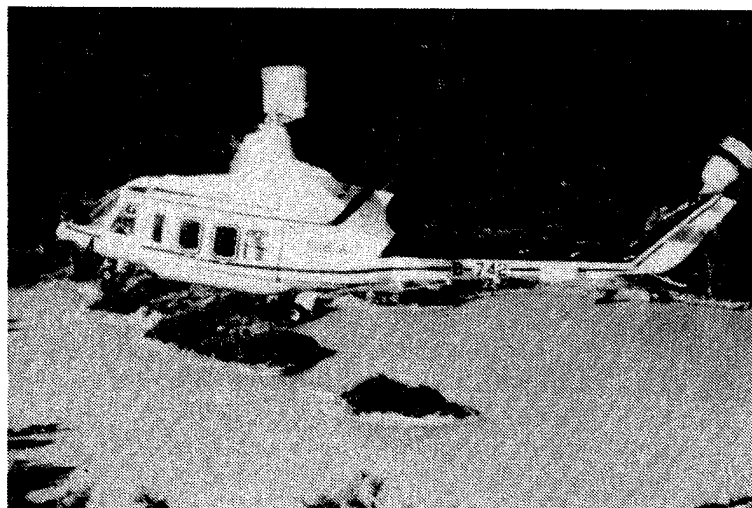


Figure 32. Bell 214-ST helicopter.

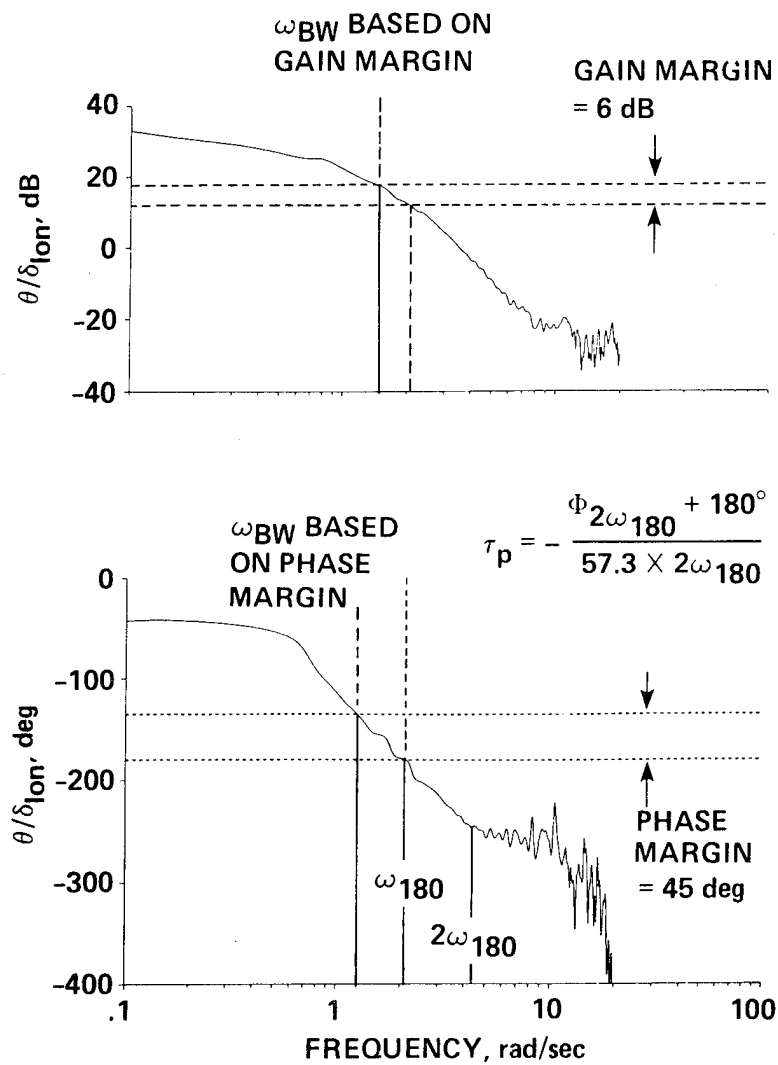


Figure 33.- Identified pitch response, θ/δ_{LON} .

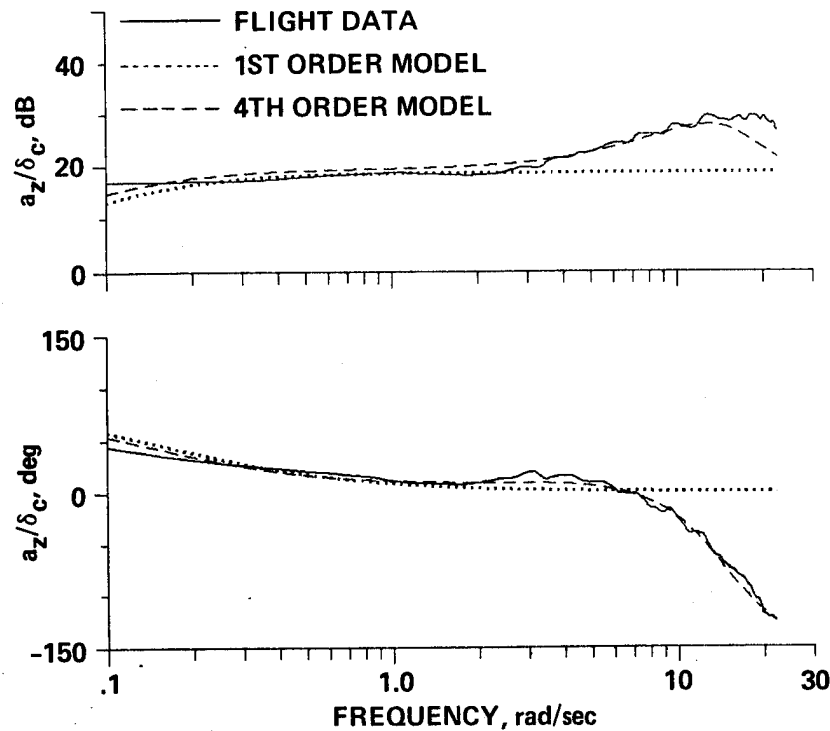


Figure 34.- Transfer-function models fit to flight-extracted Bode plots of the CH-47B.

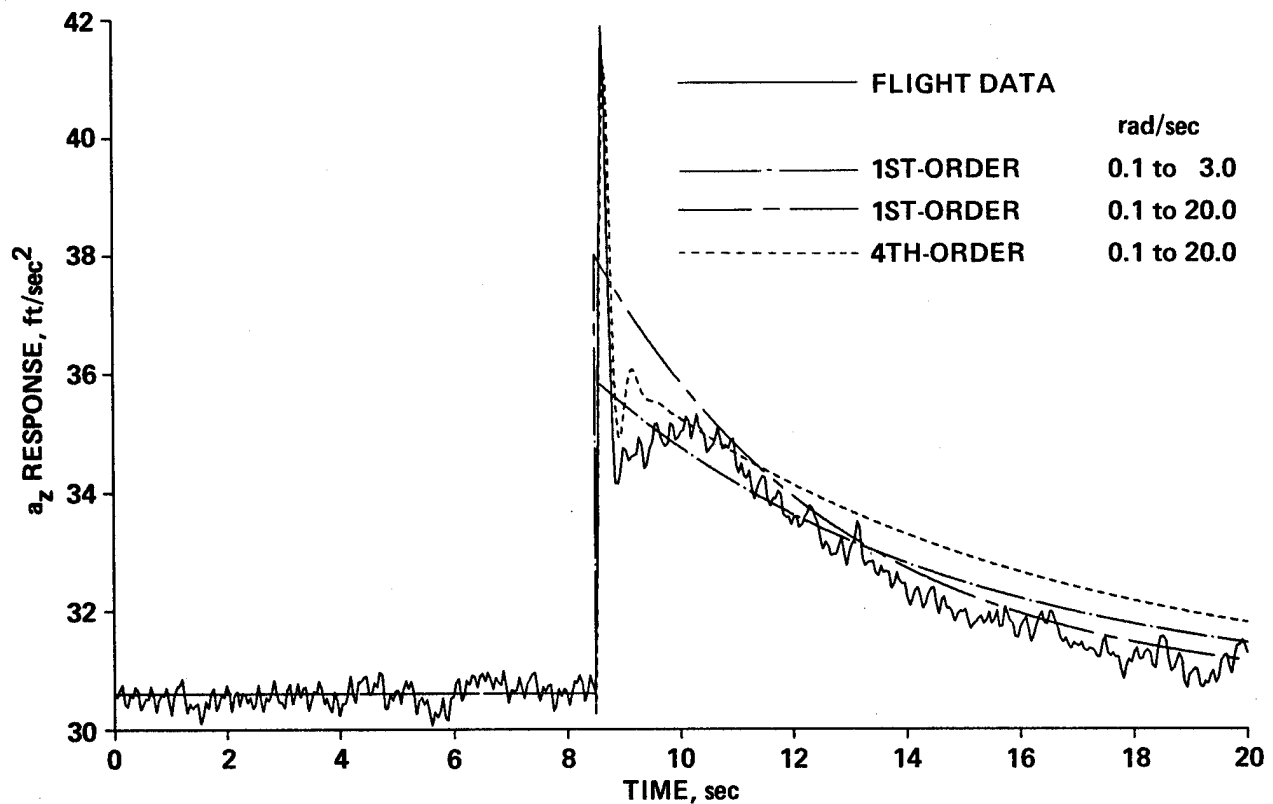


Figure 35.- Comparison of predicted responses of identified models with flight data.

ROTORCRAFT FLIGHT-PROPULSION CONTROL INTEGRATION

James R. Mihalow
National Aeronautics and Space Administration
Lewis Research Center
Cleveland, Ohio

Mark G. Ballin
National Aeronautics and Space Administration
Ames Research Center
Moffett Field, California

and

D. G. C. Rutledge
Sikorsky Aircraft Division
United Technologies Corporation
Stratford, Connecticut

SUMMARY

The NASA Ames and Lewis Research Centers, in conjunction with the Army Research and Technology Laboratories have initiated and completed, in part, a joint research program focused on improving the performance, maneuverability and operating characteristics of rotorcraft by integrating the flight and propulsion controls. The background of the program, its supporting programs, its goals and objectives, and an approach to accomplish them are discussed in this paper. Results of the modern control governor design of the T700 and the Rotorcraft Integrated Flight-Propulsion Control Study, which were key elements of the program, are also presented.

BACKGROUND

Dynamics interface problems involving the engine/fuel control and the helicopter rotor/airframe have been around for a long time. They include engine torque and fuel control system oscillations, multi-engine load-sharing, undesirable rotor speed variations during maneuvers, and excessive helicopter vibration. The helicopter rotor and drive train system have lightly damped torsional dynamic modes which are within the bandwidth of the engine fuel control system as shown in figure 1. This figure is a bar chart of frequencies at which various dynamic modes commonly occur in rotorcraft. It also shows the frequency ranges involved in rotorcraft design and analysis tasks and that the majority of these tasks require models that are accurate in a frequency range up to 10 hertz. In addition, the trend towards using lower inertia rotor systems in modern helicopters reduces the level of kinetic energy stored in the system and makes the rotor even more susceptible to large variations in its rotational speed during rapid maneuvers. These rotor and speed transients can increase pilot workload and can eventually lead to under-utilization of the aircraft's maneuvering capability because of pilot apprehension.

Toward the end of the 1970's the U.S. Army Applied Technology Laboratory instituted a contractual program designed to provide a complete report of past and present engine/airframe/drive-train dynamic interface problems. The result of this effort was a series of reports from several helicopter airframe manufacturers who documented their specific problems with vehicles developed over the last several years (refs. 1 to 5). The ultimate benefit was to be the accumulation of data that would eventually lead to a solution of these generic dynamic interaction-type problems. Although much of the documentation dwelt upon vibration and oscillatory loading problems related to rotor harmonics excitations, stability and response problems associated with the combining of two or more components or systems were universally stated. Dynamic interface problems of this type are among the last to be seen in the design of a subsystem such as an engine since they involve the presence of another subsystem such as a drive train and rotor.

The dynamic interface problems that are not anticipated in the design stage can surface later in the ground or flight test phases of a helicopter development program, requiring costly add-on modifications to "fix" the problems. The prediction of, and solution of, these problems require complementary interaction between manufacturers and the several technical disciplines. In future years, the satisfactory design of fully integrated systems will require more coordination among the airframe, engine, and control manufacturers.

PROGRAM GOALS AND OBJECTIVES

To examine potential benefits that might accrue from integrating the flight and propulsion controls, NASA Lewis and NASA Ames initiated a joint program to investigate advanced concepts in digital active flight-propulsion controls aimed at (1) improving precision flight path control, (2) expanding the operational flight envelope, and (3) reducing pilot workload. These goals are accomplished by applying a systems approach to the design of an integrated flight-propulsion control system to improve performance and handling qualities of the helicopter and evaluating the system through piloted simulation and actual flight.

APPROACH

The program originally conceived consisted of three phases as shown on figure 2. Phase I included modeling and analysis and Phase II concerned itself with piloted ground-based simulation with integrated flight-propulsion controls. Phase III was a proposed flight hardware and software development program leading to a flight evaluation which has since been canceled. Phases I and II were part of an on-going NASA research and technology base program, and Phase III was a planned future activity. In executing this program, a coordinated effort was made which, in addition to NASA Ames and Lewis Research Centers, involved the participation of university, industry, and elements of the Army Aeromechanics and Propulsion Laboratories.

In Phase I, effort focused on the development and use of a comprehensive mathematical model for the combined helicopter/engine system for nonreal-time simulation of flight dynamics and parametric studies. A specific helicopter/

engine system, namely an Army/Sikorsky Black Hawk UH-60A with its GE T700-701 engines is used as the baseline. NASA Lewis Research Center developed the baseline T700 engine/fuel control system model for integration into the Black Hawk mathematical model. This engine model was correlated and validated by T700 ground tests conducted at NASA Lewis. NASA Ames correlated and validated the total system model with Black Hawk flight test data. The primary research emphasis of this phase of the program was to determine and quantify the key parameters that significantly influence the engine/helicopter rotor/airframe coupling and overall systems performance. Piloted simulations using both the vehicle and propulsion models developed by the respective flight and propulsion centers were conducted on the Vertical Motion Simulator (VMS) as depicted in figure 3 to assess the influences of those key system parameters on the handling qualities for important missions such as NOE flight, helicopter air combat, and search and rescue operations.

Coordinated contract effort and in-house research was pursued in Phase II of the program to develop integrated flight-propulsion control concepts. The contract effort involved a team of engine fuel control specialists and engine and airframe manufacturers. Promising concepts were evaluated on the non-linear helicopter-engine model over a wide range of flight conditions and then further assessed using ground-based simulations and engine test. The merits were evaluated with respect to handling qualities, pilot workload, maneuver performance, engine performance, and mission capability using representative military and civil mission tasks.

SUPPORTING PROGRAMS

A number of supporting programs sponsored or conducted by NASA and the Army over the last several years are summarized here to provide background on previous work that led to and related to the current program.

Engine Governor Response Study

At NASA Ames, under a collaborative program with the Army Aeromechanics Laboratory, a sequence of piloted simulation experiments were conducted on the VMS to investigate, in a generic sense, the effects of engine response, rotor inertia, rotor speed control, excess power, and vertical sensitivity and damping on helicopter handling qualities in hover and representative low-speed NOE operations (refs. 6 to 8). It was found that variations in the engine governor response time can have significant effect on helicopter handling qualities as shown in figure 4. Satisfactory (Cooper-Harper pilot rating) handling qualities and rotor speed control were achieved only with a highly responsive governor. An effective engine governor time constant of no more than 0.25 seconds was required to achieve a satisfactory level of handling qualities over a wide range of aircraft vertical damping. Increases in the effective engine governor time constant resulted in poor rotor overspeed and underspeed control.

In addition to requiring rapid engine response time, an appropriate level of excess power, or thrust-to-weight ratio, is required to achieve satisfactory handling qualities for many maneuvers. The excess power requirements for the NOE tasks were investigated with various levels of vehicle vertical

damping. In addition to the required engine response time mentioned earlier, an appropriate level of excess power as shown in figure 5 was found to be required to achieve satisfactory handling qualities for the bob-up task evaluated. Results indicated that the required level of excess power is a strong function of the vertical damping and is minimized at a vertical damping of around -0.8 radians per second.

The thrust response of a helicopter is influenced not only by engine governor dynamics and vertical damping, but also by the energy stored in the rotor which is a function of its inertia. The experimental results indicated, however, that increase in rotor inertia had only a minor but desirable effect on handling qualities. The effect of handling qualities on requirements for pilot monitoring and control of rotor speed was found to be significant. Thus, techniques to relieve the pilot of the task of monitoring and control of rotor speed warrant serious consideration.

Small Turbojet Engine Program

NASA Lewis and the Army RTL Propulsion Laboratory have participated in a cooperative program to conduct digital controls research for small turboshaft engines (ref. 9). The emphasis of the program is on engine test evaluation of advanced modern control logic using a flexible microprocessor-based digital control system. The digital control system used is designed specifically for research on advanced control logic. Control software is stored in programable memory. New control algorithms may be stored in a floppy disk and loaded into memory to facilitate comparative evaluation of different advanced control modes. Software checkout is accomplished prior to engine test by connecting the digital control to a real-time hybrid simulation of the engine.

The engine used in the facility was a General Electric YT700. The hydro-mechanical control was modified to allow electrohydraulic fuel metering and variable guide vane actuation by the research digital control. The research objective was to demonstrate improved power turbine speed governing using modern control theory as compared to the baseline governor control.

Modern Control Governor Design Study

Under the program described above, General Electric recently completed a study under contract to NASA Lewis for the design of a turboshaft speed governor using modern control techniques (ref. 10). Among the objectives of this research program was a requirement to design a high performance power turbine speed governor using modern control methods. A power turbine governor was designed using the linear quadratic regulator (LQR) method of full state feedback control. A Kalman filter observer was used to estimate helicopter main rotor blade velocity. Simulation results, as shown in figure 6, show that the modern control provides better rotor speed governing than the baseline control. Shown is the power turbine speed response to an acceleration caused by a 40 to 70 percent collective pitch increase in 0.1 second. The transients were made with the Black Hawk rotor using the nonlinear DISCUS model, the manufacturer's reference performance standard transient model model of the T700 engine, without load demand spindle compensation. Overall, compared to the baseline T700 power turbine speed governor, the LQR governor in

this study reduced droop up to 25 percent for a 490 shaft horsepower transient in 0.1 second simulating a wind gust, and up to 85 percent for a 700 shaft horsepower transient in 0.5 second simulating a large collective pitch angle transient. Unfortunately, the control design was never evaluated experimentally since the program was terminated at NASA Lewis. More detail on the modern control technique used in this study follow later in this paper.

Adaptive Fuel Control Program

The Adaptive Fuel Control program, sponsored by the Army ATL Research and Technology Laboratories, is an outgrowth of the full authority digital electronic control used on the ATDE (refs. 11 to 13). The objective of Phase I, the feasibility investigation, was to determine the feasibility of designing an electronic control with the capability of adapting its control characteristics while in operation to optimize engine performance. The first step was to identify the prospective adaptive concepts to be investigated and then analyze them using a flight dynamics simulation. The concepts which proved feasible were incorporated into a preliminary design. Phase II of the program was to use the results of Phase I to fabricate an electronic control and conduct bench and engine tests. Phase III is a current activity of the program which brings the adaptive controller into a flight test program. The objective here is to verify the performance of the adaptive control during flight for expected improvements in maneuverability, engine control, torsional stability and pilot workload. In addition, the modern control concept discussed in the previous section will also be flight evaluated.

The Adaptive Fuel Control program has identified significant benefits in agility and reduced pilot workload through the use of several digital fuel control elements for improved rotor speed governing. References 11 to 13 present the results of the program to date. Using combined aircraft and propulsion control simulations, improvements in handling qualities and vehicle performance were noted. For example, significantly reduced rotor speed droop following power recovery from autorotation was shown. Conventional fuel controls in rotorcraft have particular trouble with flight profiles that generate high g fields. A typical example of such a maneuver is the quick-turn evasive maneuver. Figure 7 illustrates the performance of the adaptive control in comparison to the conventional baseline control for such a maneuver. The maneuver was performed from level flight at 120 knots. A bank angle of 60° and 2.5 g's were achieved. The critical issue here is the engine torque recovery when the pilot rolls out of the turn at the 6 second mark. Since collective pitch is not being modulated and the rotor is decoupled from the power turbine, the baseline control has no information with which to arrest the decay rate of the rotor. A subsequent rotor speed droop occurs to the detriment of aircraft flying qualities. The adaptive control, however, sensing rotor speed decay, invokes its rotor decay anticipation feature to spool up the engine and provide for a smooth engine torque recovery. Power recovery time delays are eliminated, rotor speed droop and subsequent overspeed are minimized, and engine torque applications are smooth. When compared to the baseline case, a significant improvement in flying quality has been achieved with the adaptive control.

The Adaptive Fuel Control study also identified a significant benefit from variable rotor speed during cruise. Rotor speed optimization was found to

reduce fuel consumption by 5 to 10 percent for some cruise conditions. Although the focus of the program is on improved propulsion controls, it provides a strong basis further work on integrated flight-propulsion controls.

ROTORCRAFT INTEGRATED FLIGHT-PROPULSION CONTROL STUDY

On the basis of the program described above, the next logical step in the progression of the programs described above was to consider vehicles which will have both digital flight and propulsion controls and to identify the benefits in mission performance for a fully integrated digital flight-propulsion control system. As a part of satisfying that need, NASA Lewis contracted with Sikorsky Aircraft Division of United Technologies Corporation to investigate the benefits of integrating the flight and propulsion control systems in helicopters. The Sikorsky UH-60A Black Hawk helicopter with General Electric T700 engines was used as a typical modern rotorcraft for this effort because state-of-the-art vehicle and propulsion simulations were available for domestic dissemination.

Sikorsky Aircraft conducted a study whose primary objective was the identification of the benefits associated with an integrated flight-propulsion control system for rotorcraft. This was accomplished by designing such a system, following appropriate concept screening, then incorporating and evaluating the integrated control in a NASA supplied Black Hawk/T700 simulation and further recommending experiments to be conducted by NASA using the VMS at NASA Ames with their modified Black Hawk simulation. The work was performed at Sikorsky Aircraft and was supported by General Electric and the Chandler Evans Division of Colt Industries. A detailed report will be available in the near future (ref. 14).

Study Summary

An eclectic approach, taking the best features of past flight and propulsion control concepts, as opposed to a global approach, an approach which considers the system without prior control system knowledge, was taken in a study of the integration of digital flight and propulsion controls for helicopters. The basis of the evaluation was a current simulation of the UH-60A Black Hawk helicopter with a model of the GE T700-GE-701 engine developed by NASA.

A list of segments of flight maneuvers to be used to evaluate the effectiveness of the resulting integrated control system was composed based on past experience and an extensive survey of the recently acquired U.S. Army Air-to-Air Combat Test (AACT) data.

A number of possible features of an integrated system were examined. Those chosen were combined into a design that replaced the T700 fuel control and part of the Black Hawk control system. This design consisted of portions of an existing pragmatic adaptive fuel control design by Chandler Evans and an LQR-based power turbine speed governor design by General Electric. These design features were integrated with changes in the baseline Sikorsky flight control system.

A cursory assessment of the design is presented here with a summary provided for each of the major elements of the study.

Aircraft Modeling

Aircraft simulation model. - The mathematical model of the Black Hawk is a generalized and modularized analytical representation of a total helicopter system developed under Sikorsky's Master Generic Helicopter (MGH) system (ref. 15). It normally operates in the time domain and allows the simulation of any steady or maneuvering condition which can be experienced by a pilot.

The basic model is a total force, nonlinear, large angle representation in six rigid degrees of freedom. In addition, rotor rigid blade flapping, lagging and hub rotational degrees of freedom are represented. The latter degree of freedom is coupled to the engine and fuel control. Motion in the blade lag degree of freedom is resisted by a nonlinear lag damper model.

The total rotor forces and moments are developed from a combination of the aerodynamic, mass and inertia loads acting on each simulated blade. The rotor aerodynamics are developed using a blade element approach. The fuselage is defined by six component aerodynamic characteristics which are obtained from wind tunnel data which have been extended analytically to large angles.

The baseline flight control system for the Black Hawk presented in this model covers the primary mechanical flight control system and the Automatic Flight Control System (AFCS). The latter incorporates the Stability Augmentation System (SAS), the Pitch Bias Actuator (PBA), the Flight Path Stabilization (FPS) and the stabilator mechanization. The analytical definition of the control system incorporates the sensors, shaping networks, logic switching, authority limits and actuators.

Model correlation. - The present MGH representation of the Black Hawk has been correlated with flight test data (ref. 16). In trim, the small number of rotor blade segments and lack of detailed corrections prevent its use for predicting aircraft performance to within performance guarantee levels. However, trim attitudes and control positions are adequately forecast. Dynamically, MGH shows good correlation with aircraft motion taken from flight test data. The simulation system is routinely used for the successful prediction of design values for primary control systems, SAS, first torsional engine/rotor oscillations and aircraft coupled and uncoupled motions.

Propulsion System Modeling

High-fidelity propulsion system modeling is necessary in the investigation of integrated flight and propulsion controls for rotorcraft. Because advanced propulsion control strategies may involve monitoring or estimation of internal engine states, an accurate internal representation of the engine is required. The present generation of real-time blade-element rotor helicopter simulations such as GEN HEL, a derivative of MGH models, are able to accurately model individual blade dynamics at such a bandwidth necessary for propulsion system modeling. Because rotorcraft propulsion system load demand typically varies from zero power to full power, the model must be valid over the full power

range of the actual engine. It must also be valid over a complete range of ambient operating conditions. Engine parameters of primary importance to real-time handling qualities investigations include output torque and dynamics of the gas turbines which are necessary for pilot sound cueing as well as for modeling of power output. Also important are parameters used by the fuel control system, such as compressor discharge static pressure and internal engine temperatures. Of somewhat less importance are the internal mass flows, which may be used to determine proximity to limits such as compressor stall.

Available real-time models are based on simple power versus fuel flow relationships. In more sophisticated models, engine dynamics are based on experimentally determined partial derivatives of changes of output torque to changes in turbine speed and fuel flow. Such models are unsatisfactory because needed internal engine states may not be modeled. In addition, dynamic characteristics of existing models have shown poor results in validation with experimental data (ref. 16). Partial derivative models tend to be valid only for a limited range of operating conditions. Because they are not based on the physical phenomena which they represent, their validity is always in question when used under conditions at which they are not optimized.

A relatively high level of fidelity is achievable by using an engine model made up of individual engine components, each of which is modeled based on physical laws relating the dynamics of mass flow and transfer of energy. Such component-type simulations are used by engine manufacturers to study the transient behavior of engines, but they are usually far too complex for use in real-time digital simulation. A component engine model which is simplified for real-time use is the most promising alternative to partial derivative engine representations. It was therefore chosen in this study to be appropriate for the study of flight and propulsion controls integration.

In addition to a sophisticated engine model, accurate physical models of the fuel control system, mechanical actuators and linkages, and the engine sensors are necessary for a correct representation of closed-loop propulsion system dynamics, engine protection control, and the effects of modification of the propulsion system control. Similarly, the vehicle drive train and accessory loads must be modeled so that an acceptable representation of the power requirements of the vehicle is obtained.

Engine description. - The engine modeled, shown in figure 8, is a General Electric T700-GE-701, a small turboshaft engine of the 1500 horsepower class which is used in the UH-60A Black Hawk and the AH-64 Apache helicopters. It consists of a five stage axial and a single stage centrifugal flow compressor, a low-fuel-pressure through-flow annular combustion chamber, a two stage axial gas generator turbine, and a two-stage independent power turbine (ref. 17). The first two stages of the compressor use variable geometry inlet guide vanes and stator vanes, and air is bled from the compressor exit to cool the gas generator turbine. The power turbine has a coaxial driveshaft which extends forward through the front of the engine where it is connected to the output shaft assembly.

The T700 baseline, or bill-of-material, fuel control system provides power modulation for speed control, overtemperature protection, and load sharing between engines for multiple-engine installations. It consists of a hydro-mechanical control unit (HMU) for fuel metering as a function of schedules of

gas generator speed and power demand, and an electrical control unit (ECU) which performs power turbine speed governing and overtemperature protection (ref. 18). A feed-forward compensation of load demand is achieved by adjusting the set point as a function of collective control. The compressor variable geometry is also controlled as a function of inlet temperature and gas generator speed. The ECU provides output shaft speed control by driving a torque motor in the HMU based on a power turbine speed error signal. The torque motor, which is controlled by the ECU, adjusts the HMU fuel demand downward so that an electrical system failure results in a higher power. Power turbine inlet temperature is also monitored and fuel flow is reduced when it exceeds limits. Power may also be increased if torque is determined to be lower than that of another engine operating in parallel.

Engine model. - As a part of ongoing research in turboshaft engine technology, a component-type mathematical model was developed by NASA Lewis for real-time hybrid computer simulation (ref. 19). It is a greatly simplified version of the component version of the component-type analysis program developed by the manufacturer and, although it is inappropriate for engine development purposes, it is at a level of sophistication necessary to model the operating condition of the engine as well as engine transient behavior. It was chosen to serve as the basis for development of a digital simulation which is adequate for use with real-time blade-element rotorcraft simulations.

A diagram of the major components separated by mixing volumes is shown in figure 9. The four major components are separated by fluid mixing volumes. Each of the fluid mixing volumes is associated with flow passages within the engine where thermodynamic states are quantifiable. States of the gas in each control volume are expressed in terms of pressure, temperature and mass flow. They are determined as functions of energy transfer across each component. Equations describe each component in terms of the component state, thermodynamic states upstream and downstream of the component, energy applied to or from the component, and efficiencies of energy transfer. Dynamics of the rotating components are modeled by relating changes of angular rotation of a given component to its moment of inertia and the applied torque. A load from an external source is required to determine power turbine and output shaft speed. Losses associated with fluid dynamic or mechanical processes are represented by single or multivariable functions based on previously derived or empirical data. Inputs to the simulation consist of ambient temperature and pressure at the inlet, pressure at the exhaust, and fuel flow.

Modeling simplifications made in the development of the NASA Lewis hybrid simulation model were based on a general simulation technique developed at NASA Lewis (ref. 20) as well as experience with small turboshaft engines. Power turbine efficiency as a function of its speed was neglected because, for the designed use of the model, the power turbine deviates only a few percent from its design speed. No modeling of compressor surge, heat soak losses or exhaust pressure losses was attempted. Linear relationships were used to describe secondary effects such as bleed flows. Dynamics of the variable geometry guide vanes were assumed to be instantaneous. A digital program was then produced using the Continuous System Modeling Program (CSMP) which accurately reproduced steady-state operation of an experimental test article operated at NASA Lewis.

In the development of a real-time model, the CSMP model was used as a basis to develop a program in FORTRAN using real-time digital programming methods. During the validation, it was discovered that the original model contained too much simplification to correctly model engine dynamics. Consultation with the engine manufacturer resulted in the addition of models for losses caused by heat dissipation within the gas generator and exhaust flow downstream of the power turbine. A model of power turbine efficiency as a function of its speed was also found to be necessary to model the low power closed-loop dynamic response properly. The HMU required the addition of metering valve and collective anticipation lags, fuel transport delay and combustor lag, and models of sensor hysteresis. The ECU also required a more sophisticated model of torque motor dynamics.

Real-time implementation of engine model. - Each of the control volumes within the engine is associated with a temperature, pressure and change of mass of the air and fuel. During steady-state operation of the engine, a state of equilibrium exists between the control volumes for each of these parameters. A change in the state of any control volume creates pressure and mass flow changes in the other control volumes until a new equilibrium is achieved. The dynamics associated with this change are very rapid and therefore have a negligible effect on the lower frequency engine and vehicle dynamics. Discrete modeling of such high frequency dynamics necessitates stepping forward in time with extremely small increments resulting in a high computation overhead which is unacceptable for real-time simulation. A quasi-static approximation of the volume dynamics of the engine was therefore made. High-speed dynamics were eliminated by approximating pressures and mass flows within the mixing volumes to be in equilibrium at all times.

Several existing real-time and nonreal-time computer models of turbojet engines use the quasi-static volume dynamics approximation (refs. 21 to 23). Methods differ in the application of a numerical scheme which allows an iterative convergence to equilibrium with a minimum use of computation time. An opened iteration scheme is normally used, sometimes in conjunction with a set of predetermined partial derivatives of engine states. However, an opened iteration does not allow control of convergence or of the amount of error produced. A fixed-point iteration method was found to meet the requirements of computational efficiency and small error. A successive overrelaxation technique was used to control the speed of convergence.

Engine model validation. - Steady-state engine performance was verified to be within normal limits of operation by comparison with the experimental engine operated by NASA Lewis and with DISCUS. Loading conditions were duplicated by using a model of the NASA Lewis test engine dynamometer described in reference 9. The load is variable based on a simulated collective pitch control input. This input is used to trim the engine at the design shaft speed for a specified fuel flow. Excellent agreement was obtained with the manufacturer's model. Gas generator speed was found to have a maximum error of 1 percent while output torque error is less than 4 percent. Hot section temperatures also correlated well with a maximum error in gas generator turbine inlet temperature of less than 1 percent with a corresponding error in power turbine inlet temperature of slightly over 1 percent. Comparison of the real-time model with NASA experimental engine test resulted in fair agreement. The experimental engine is a prototype model which does not reproduce specification performance. Real-time model turbine speeds were within 3

percent of the test engine speeds. However, temperatures at the power turbine inlet were 6 to 7 percent lower than those of the test engine.

Transient operation was validated by comparison to DISCUS-generated time histories. The control system was disconnected so that transients resulting from direct fuel flow inputs could be compared. Under these conditions, large changes of fuel flow result in large changes of power turbine speed. Power turbine efficiency is modeled as a function of its speed in the real-time model only for small speed excursions about the design point. Transient data were therefore received from executions of the manufacturer's program with the power turbine dynamics suppressed, allowing power turbine speed to be constant. Output torque was then used as a measure of engine power. Fuel inputs were applied as instantaneous steps.

Results are illustrated in figures 10 and 11. As shown in figure 10, the two simulations are in close agreement for a step increase from mid-power to high power. Gas generator speed is overestimated by approximately 2 percent, due mainly to performance map approximations, whereas the output torque responses correlate well. Power turbine inlet temperature is underestimated by the real-time program. This discrepancy is a characteristic of the model which was experienced under all validation conditions. Because the error is small and dynamic characteristics are retained, the modeling of power turbine temperature is considered adequate. Low power engine performance is shown in figure 11, which represents a step decrease in fuel flow to below idle power. The real-time model torque again shows close agreement with DISCUS. Gas generator dynamics are also accurately modeled.

An example of the closed-loop engine performance with the blade-element helicopter simulation is shown in figure 12. Flight test data obtained from reference 16 were used as inputs to the real-time program and test results are included for comparison. Turbine speeds and torque output are reproduced correctly. Discrepancies seen in fuel flow are attributed to the location of the sensor used on the test vehicle. This sensor was mounted upstream of the HMU's sensor and therefore did not correctly reproduce the fuel flow transients.

Integrated Flight-Propulsion Control Design

The following sections highlight each element of the integrated control design concept and explain its purpose and the techniques used to integrate the feature into the overall system. Because the design is presently a computer simulation, no attempt was made to determine which part of the control software belongs on which processor or the optimal routing of signals between sensors, actuators, and processors that might be applied to a practical flight vehicle implementation. Memory requirements and execution speeds were not considered.

The core of the controller is a modern control power turbine speed governor whose reference speed may be modulated by various combinations of variables representing present or anticipated airframe-engine states. The power turbine governor itself consists of a linear quadratic regulator state feedback algorithm in which rotor tip speed is estimated by a Kalman filter. Additional adaptive logic is used to anticipate rotor decay and help recovery

from the declutched state. The traditional collective pitch-to-load demand spindle input to the fuel control is retained but in digital form. The equally traditional collective pitch-to-tail rotor collective link is replaced by a measured engine torque-to-tail rotor collective link. An indication of power available to hover is provided for the pilot. A cue for inhibiting the application of collective input while the fuel control is on its acceleration schedule is provided by a logic signal. A variety of collective movements following engine failure, depending on height and velocity, are available. A switchable fuel consumption minimizer operating in conjunction with added loops in the AFCS is also available.

Linear quadratic regulator power turbine speed governor. - The purpose of a power turbine governor for helicopter applications is to maintain constant power turbine governor speed in the presence of torque load changes in the helicopter rotor system. Such governors in the past have used feedback of the speed error from some reference value to regulate fuel flow to the engines with an integrator added to the error loop so that the steady-state error could be removed. This results in a governor that maintains speed at the reference value (isochronous) under all steady loads, transients loads not withstanding.

A limitation on this form of governor is caused by the existence of two torsional resonances in the drive train system. The resonances are caused physically by the engine and drive-train rotational freedom working against the blade lag freedom. The torsional resonances of the UH-60A articulated rotor blade/drive system occurs at a frequency of the order of 2.7 hertz with the torsional resonance of the tail rotor/drive-train at about 7 hertz.

The advent of all-digital controls has made the proportional-plus-integral governor easier to implement and has opened the door to more sophisticated mathematical techniques for overcoming the torsional mode problem. Use of higher order notch filters to attenuate response at the first torsional frequency have been implemented successfully (ref. 24). General Electric's approach in the integrated control study presented here is to employ a linear quadratic regulator (LQR) design which allows the bandwidth to be increased and thus improve the response time of the system.

The LQR technique was used to design the power turbine speed governor and a Kalman filter was included in the control system to estimate the helicopter main rotor blade velocity as one of the states in the design (ref. 10). The effect of the LQR governor in the frequency domain is to attenuate the resonant first torsional mode peak.

The LQR governor was analyzed in the frequency domain using standard Bode plot techniques to determine the system stability margins, speed of response, and disturbance rejection characteristics. The frequency response of the closed-loop LQR and T700 baseline systems was calculated for a main rotor torque disturbance and a tail rotor torque disturbance to analyze the effects on power turbine speed and helicopter main rotor speed. The simulated disturbance was a sine-wave frequency sweep. Each disturbance was input separately. The response of power turbine speed to a main rotor disturbance is shown for the LQR governor and for the T700 baseline governor in figure 13. The figure shows that disturbances are rejected better by the LQR power turbine speed governor than by the T700 baseline governor. The LQR governor

provides adequate phase and gain margin for good stability and robustness. The resonant peak attenuation combined with large phase margin allows the system gain to be higher and results in the increased bandwidth.

The higher bandwidth also translates directly into better performance in the time domain. Shown in figure 14 is a load disturbance in the rotor system caused by a simulated wind gust of 40 feet per second over a distance of 200 feet. The LQR power turbine speed governor reduced the speed droop from 3.25 percent to 1.3 percent. The baseline control has several small oscillations before the system stabilizes. The LQR governor virtually eliminates these oscillations demonstrating its better phase margin.

Pragmatic adaptive control elements. - The adaptive fuel control as designed and currently under development by Chandler Evans is fully described in references 11 and 25.

Figure 15 shows a block diagram of the integrated control system which includes the LQR power turbine speed governor, the gas generator acceleration governor (NDOT) and the adaptive elements. The fuel flow features of the control, other than the LQR governor, derive from the pragmatic adaptive system.

The adaptive features which affect the power turbine set speed in the integrated control system are applied to the LQR power turbine speed set-point. These features include rotor decay anticipation, rotor droop recovery, load factor enhancement, torque sharing, and minimum fuel optimization. Collective rate anticipation was not included since the LQR governor had its own collective pitch maps.

For the autorotational rotor decay anticipation, the adaptive control provides a flag which signals when the system goes into autorotation. This flag is used by the LQR governor to temporarily convert it into a proportional-plus-integral controller with a low gain since the LQR feedback paths add no information to the LQR control during autorotation. The autorotational rotor decay anticipator, acting upon the autorotation flag, generates an incremental power turbine speed reference to the LQR controller to keep the power turbine at a higher acceleration potential so that engagement of the engine and rotor will occur at a higher engine speed and thereby reduce droop. The effect of this control element was discussed earlier in the Adaptive Fuel Control Program section.

The logic of the droop compensator subsystem is to detect that a droop has occurred and to inhibit the likely torque and subsequent speed overshoot that will follow. This is accomplished by deliberately delaying the governor demanded fuel flow. As the droop starts to diminish, a signal is generated that reduces the power turbine speed reference, thus, reducing torque load and speed overshoot.

Three further subsystems can influence the fuel flow by changing the power turbine speed reference signal in the LQR power turbine speed governor. The first is a dual installation torque sharing device which is the digital equivalent of the baseline T700 controller. This controller indirectly speeds up the gas generator of the low torque engine to match the output of the non-

degraded engine by applying an incremental power turbine speed reference signal proportional to the torque error to the lower engine.

The second subsystem is the minimum fuel consumption optimizer. This is an extremely simple algorithm which, when switched on in cruise, samples the fuel flow at intervals and perturbs the power turbine speed reference signal to change the rotor speed. Figure 16 shows the results achieved by the simulated MGH Black Hawk system.

The third subsystem is the load factor enhancement feature. In general, it is possible to increase the aerodynamic load factor capability of a helicopter by increasing the rotor speed. Figure 17 shows the order of magnitude of the effect as predicted by the MGH simulation. The form of this subsystem involved ramping an increment in rotor speed reference proportional to pitch rate and keeping it on for a set time after the load factor is removed. This tends to keep the engine spooled up for a longer time and thus able to better deal with large torque increases should the rotor pop in and out of an autorotative state.

The integrated control nominally operates on the LQR power turbine governor. In extreme maneuvers, it will be limited on the top end by the NDOT governor and on the low end by the bottom governor and NDOT deceleration limiter. On each cycle of the control computer these limits determine the upper and lower extremes of the allowable fuel flow.

The acceleration schedule is the usual control which seeks to inhibit compressor surge by allowing the gas generator to accelerate in a pre-programmed fashion with maximum acceleration as a function of gas generator speed. Chandler Evans has also incorporated their adaptive surge margin compensation feature which also uses a lagged compressor discharge pressure to further stabilize surge recovery.

The gas generator topping speed action simulates the action of the power available spindle in acting as an upper limit throttle on gas generator speed and thus maximum engine power output. The intent of this limiter on the baseline T700 fuel control is to give the pilot some control if the electronic function should fail. Its retention in the integrated control gives similar control action.

The temperature limiting section is a straight-forward digital implementation of a power turbine inlet temperature limiter. A logic switch, which is triggered by the engine-failed status flag of the other engine in a twin engine installation, can boost the allowable temperature for emergency power situations.

The lowest output of the above three governor sections is passed to the gas generator acceleration governor (NDOT) section which produces an error signal from the difference between its integrated value and the sampled gas generator speed value and then calculates a weighted proportional-plus-integral type gain which it multiplies by lagged compressor discharge pressure. The resulting fuel flow is the gas generator fuel flow which is compared with the LQR power turbine speed governor flow on a lowest-wins basis. The three components of the gas generator speed governor thus serve as alternate top limits to the fuel flow.

A prescribed deceleration schedule is provided to ensure sufficient margin from flame-out. This path has an integrator in it which is controlled by back-calculation in an exactly similar way to the NDOT governor while it is not actually governing the fuel flow. A bottoming governor, which prevents the gas generator speed from falling below a prescribed self-sustaining lower limit, is also supplied.

The last two flow limits are compared on a highest-wins basis with the LQR power turbine speed governor demand. The resulting fuel flow is the demanded fuel flow value that is passed to the stepper motor which regulates very precisely the pumping of fuel into the engine. A power turbine speed actuated overspeed switch cut-off value is present on the engine side of the stepper motor to deal with runaways such as shaft failures.

Other pragmatic adaptive features. - The flame-out detector relies on the accuracy and constancy of the relationships between a gas generator deceleration and the gas generator speed at which flame-out occurs and the range of gas generator decelerations at given gas generator speeds which are part of normal operations. Figure 18 shows the relationships of the normal decelerations at various gas generator speeds. The detection boundary is the line that appears to give adequate clearance to avoid false signals at legitimate gas generator decels while giving as much warning as possible.

The power available to hover computation uses nominal maps of corrected engine torque and power turbine inlet temperature to calculate the maximum torque available from the engine. These maps are continually updated to include any engine degradation. The torque required to hover is calculated from a map of the ratio of hover-torque-required to current cruise torque versus airspeed as shown graphically in figure 19. While cruising at constant airspeed, the current cruise torque is used to determine the torque required to hover for the current conditions. Maximum torque available is then compared against torque required to hover. A positive difference indicates a surfeit of torque and a hover is therefore feasible.

Airframe originated features. - The collective pitch-to-tail rotor collective link has been removed in the integrated control in favor of a sum of engine output torques-to-tail rotor collective link. The ideal link would be one which produces a yawing moment proportional to the main shaft torque load. The shaft torque is very difficult to measure and the production of yawing moment via manipulation of a tail rotor collective pitch mechanism is not truly linear. The integrated control solution is to use the sum of the engine output torques as an approximation to the main rotor shaft torque and live with the nonlinearities inherent in the tail rotor collective yaw controls. Another alternate approach, which was outside the scope of this study, is to consider model-following type control laws wherein rotor torque is modeled in a nonlinear mode and included in the control system in closed-loop fashion.

Another feature programmed into the control is the use of the fuel control status flag, which indicates that the engine is on its acceleration schedule, to inhibit the pilot from applying increasing torque loads via the collective pitch input faster than the engine can absorb these loads without allowing droop to occur. In the mechanization proposed here, the status flag signals an electric clutch mechanism on the collective lever which adds retardant

stick force when the lever is moved in the upward or torque increasing direction. In use, a pilot would pull collective until he felt the force increase and then maintain a steady pressure which would allow the stick to step upward in very small increments as the controller switched rapidly on and off the acceleration schedule. The collective pitch control thus increases at an optimal rate constrained by constant rotor shaft speed. Figure 20 shows the response obtained in an autorotative recovery by simulating the pilot's collective lever pull limiter with a simple integrator switched on and off by the status flag as it indicates being on the acceleration schedule. The response to the same input without the inhibitor control is also shown.

The last feature to be considered in airframe originated integrated control items is that of automatic control action required under single or dual engine failures. Figure 21 illustrates the response from flight test of a modern helicopter to a dual engine failure at high speed simulated by a dual throttle chop. The Black Hawk does not respond anywhere nearly similar since the relatively heavy rotor tends to keep the shaft speed higher and the large fin area, coupled with the more effective speed of the tail rotor, make the directional stability much greater. Hence, sideslip never develops and the roll response due to the dihedral effect is very mild. Since no problem existed on the Black Hawk and a change in rotor mass to provoke the effect would have a large impact throughout the integrated control design, no further studies were conducted. It seems quite possible, if needed, the engine flame-out warning flag could be used at higher airspeeds to impress a tail rotor pitch input early enough to prevent the yaw and consequent roll response.

At low speeds, a large part of the prohibited area is created by the requirement to allow the pilot time to recognize the engine failure and react to it. The automatic control envisioned would recognize the height-velocity area in which failures occurred and take appropriate action immediately on perceiving the failure flag. The application of cyclic and collective would depend on the area of the altitude-velocity diagram where failure occurred. It would be preprogrammed or possibly use the power-to-hover and performance mapping information of the pragmatic fuel controller to make logical decisions. The stick would be moved by clutch mechanisms which could be overridden by a pilot using stick force alone. The movement-causing forces would be faded out after several seconds.

Control System Evaluation

The evaluation of the integrated flight-propulsion control was conducted in two phases. The first evaluation, presented here, was accomplished using the MGH simulation facilities at Sikorsky. The second part was to be a pilot-in-the-loop study on the NASA Ames VMS. At this writing, the VMS evaluation has not yet been accomplished.

Generic mission tasks. - A selection was made of simple segments of maneuvers that could be reasonably and simply simulated on Sikorsky's MGH simulation of the T700 powered UH-60A Black Hawk, and that would highlight the advantages of an integrated flight-propulsion control system. The first maneuver segments were the results of gathering comments from pilots and designers at Sikorsky on the type of maneuvering mentioned above.

The search of the AACT data for the integrated control study concentrated on maneuvers that exhibited a rotor speed excursion of more than 5 percent on any aircraft which implies a 10 percent change in stick sensitivity with consequent difficulties in pilot control. In this manner, the search and classification reaffirmed the significance of the first selections and added the side acceleration maneuver and the roll reversal maneuver. The final selections included classic autorotative recovery, bob-up and remask, quick-stop, quick-turn deceleration, engine failures, side accelerations, and roll reversals. Most of the results were taken from the AACT data and all of the data were on aircraft other than the Black Hawk. Details of these maneuvers are given in reference 14.

Evaluation using MGH Black Hawk simulation. - The evaluation was performed by flying the simulation through the series of maneuvers listed above. In general, the Black Hawk simulation was flown with the SAS on and FPS off. Both sub-systems could be expected to be incorporated in a total integrated control design. With the SAS active, this is a way of acknowledging that incorporation. The FPS functions of the Black Hawk were largely inappropriate for this study. The coordinated turn feature was provided by the input maneuver controller. Leaving the FPS feature on caused interference with the controller so it was turned off for all flights. The attitude hold feature was the opposite of what was required for the fuel minimization scheme.

Reference 14 contains the time history comparisons of the maneuver segments simulated, using the base control and the integrated control.

Table I is a summary of the autorotational recoveries in terms of rotor droop and overshoot speed peaks during the maneuvers.

In summary, the integrated control is superior only during large split autorotational recoveries when moderate to slow collective pulls are used in the maneuver. Small split recoveries from fast to slow pulls do not show any significant advantage for either control version. However, rotor speed overshoot is controlled in a vastly superior manner by the integrated control. This is due primarily to the LQR power turbine speed governor. Details of the results of the other maneuver flights are also given in reference 14.

CONCLUDING REMARKS

The emergence of digital engine controls in such programs as the Army ATDE and the parallel development of digital flight controls in the Army ADOCS program, makes possible the future application of a fully integrated digital flight-propulsion control system. Although the microelectronics technology required for integrated control is now available, additional research is needed to understand the full implications of the technology. The NASA/Army research program described in this paper is a comprehensive attempt to develop an approach. The payoff will be a generation of rotorcraft with the maneuverability and agility required for military missions and the superior handling qualities and low pilot workload needed for all-weather civil missions.

The real-time component-type digital simulation of a turboshaft engine fills a need in the pilot-in-the-loop investigations involving non-constant rotor speeds and widely varying rotor loads especially in integrated flight-

propulsion control applications. Performance-related questions can also be addressed in real-time. The model reproduces dynamics associated with gas generator spool-up or spool-down caused by large changes of power. Engine degradation is also easily modeled by modifying compressor or turbine flow and energy functions. The engine control system is separate and may be modified or replaced depending on user requirements. This capability allows effective pilot evaluations of new control implementations or of special modes of fuel control system operation.

The integrated flight-propulsion control scheme evaluated in this study was found to be superior to the basic control in most areas. This was in spite of the fact that the baseline control is already a harmonious match of engine and airframe which exhibits few of the problems of other aircraft or, at worst, on a diminished scale as seen in the AACT data.

While fixed-base simulation is a useful tool for the preliminary investigations of control studies such as this, the essence of the evaluation has to be a motion simulation because the critical factor is the extent to which rotor speed droop affects control power and how a pilot copes with the subsequent control problem. To this end, a simulation experiment on a motion simulator in real-time is necessary.

The eclectic approach of selecting versions of elements already existing results in many design compromises that should not have to be made. It is strongly recommended that airframe, engine and controls teams establish a small integrated design team at the start of a program to deal with all aspects of the required integration concepts using modern integrated control design methodologies that have emerged in recent times. Variable rotor speed control, which will require integrated control to be implemented effectively, should also be the object of further study.

REFERENCES

1. Richardson, D.A.; and Alwang, J.R.: Engine/Airframe/Drive Train Dynamic Interface Documentation. USARTL-TR-78-11, Apr. 1978. (Avail NTIS, AD-A055766.)
2. Needham, J.F.; and Banerjee, D.: Engine/Airframe/Drive Train Dynamic Interface Documentation. USARTL-TR-78-12, May 1978. (Avail NTIS, AD-A056956.)
3. Twomey, W.J.; and Ham, E.H.: Review of Engine/Airframe/Drive Train Dynamic Interface Development Problems. USARTL TR-78-13, June 1978. (Avail NTIS, AD-A057932.)
4. Bowes, M.A.: Engine/Airframe/Drive Train Dynamic Interface Documentation. USARTL TR-78-14, June 1978. (Avail NTIS, AD-A063237.)
5. Hanson, H.W., et al: Engine/Airframe Drive Train Dynamic Interface Documentation. USARTL-TR-78-15, Oct. 1978. (Avail NTIS, AD-A063237.)
6. Corliss, L.D.: A Helicopter Handling-Qualities Study of the Effects of Engine Response Characteristics, Height-Control Dynamics, and Excess Power On Nap-Of-The-Earth Operations. Helicopter Handling Qualities, NASA CP-2219, 1983, pp. 47-57.
7. Corliss, L.D.: The Effects of Engine and Height-Control Characteristics On Helicopter Handling Qualities. AHS Journal, vol. 28, no. 3, July 1983, pp.56-62.

8. Corliss, L.D.; Blanken, C.L.; and Nelson, K.: Effects of Rotor Inertia and RPM Control on Helicopter Handling Qualities. AIAA Paper 83-2070, Aug. 1983.
9. Sellers, J.F.; Baez, A.N.; and Bobula, G.A.: Army/NASA Small Turboshaft Engine Digital Controls Research Program. NASA TM-82979, 1981.
10. De Los Reyes, G.; and Gouchoe, D.R.: The Design of a Turboshaft Speed Governor Using Modern Control Techniques. NASA CR-175046, 1986.
11. Morrison, T.; Zagranski, R.D.; and White, A.H.: Adaptive Fuel Control Feasibility Investigation. USAAVRADCOM-TR-83-D-1, July 1983. (Avail NTIS, AD-B076297L.)
12. Yates, T.: Adaptive Fuel Control Feasibility Investigation. USAAVRADCOM-TR-82-D-39, July 1983. (Avail NTIS, AD-B075819L.)
13. Steininger, S.A.; Zagranski, R.D.; and Morrison, T.: Adaptive Electronic Fuel Control for Helicopters. USAAVSCOM-TR-86-D-14, Dec. 1986.
14. Rutledge, D.G.C.: A Rotorcraft Flight/Propulsion Control Integration Study. NASA CR-to be published, 1986.
15. Howlett, J.J.: UH-60A Black Hawk Engineering Simulation Program: Volume I - Mathematical Model. (SER-70452, Sikorsky Aircraft; NASA Contract NAS2-10626.) NASA CR-166309, December 1981.
16. Kaplita, T.T.: UH-60 Black Hawk Engineering Simulation Model Validations and Proposed Modifications. (SER-70982, Sikorsky Aircraft; NASA Contract NAS2-11570.) NASA CR-177360, 1985.
17. Model Specification for T700-GE-701 Turboshaft Engine, Part I. DARCOM-CP-2222-02701, General Electric Aircraft Engine Business Group, Feb., 1983.
18. Prescott, W.E.; and Mabee, R.L.: T700-GE-701 Training Guide. General Electric Aircraft Engine Business Group, Lynn, MA, 1984.
19. Hart, C.E.; and Wenzel, L.M.: Real-Time Hybrid Computer Simulation of a Small Turboshaft Engine and Control System. NASA TM-83579, 1984.
20. Seldner, K.; Mihalow, J.R.; and Blaha, R.J.: Generalized Simulation Technique for Turbojet Engine System Analysis. NASA TN D-6610, 1972.
21. Mihalow, J.R.; and Hart, C.E.: Real Time Digital Propulsion System Simulation for Manned Flight Simulators. AIAA Paper 78-927, July 1978.
22. Mihalow, J.R.: A Nonlinear Propulsion System Simulation Technique for Piloted Simulators. NASA TM-82600, 1981.
23. French, M.W.: Development of a Compact Real-Time Turbofan Engine Dynamic Simulation. SAE Paper 821401, 1982.
24. Alwang, J.R.; and Skarvan, C.A.: Engine Control Stabilizing Compensation-Testing and Optimization. AHS Journal, vol. 23, no. 3, July 1977, pp. 13-18.
25. Howlett, J.J.; Morrison, T.; and Zagranski, R.D.: Adaptive Fuel Control for Helicopter Applications. AHS Journal, vol. 29, no. 4, Oct. 1984, pp. 43-54.

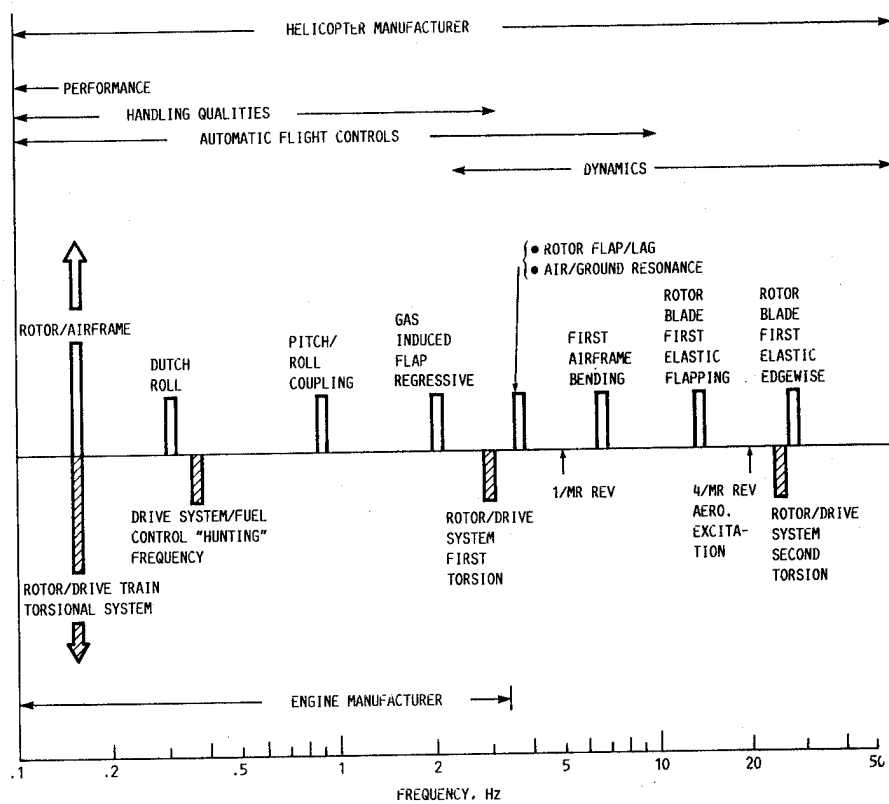


FIGURE 1. - MODAL FREQUENCIES OF INTEREST IN ENGINE-FUEL CONTROL DESIGN AND MODELING.

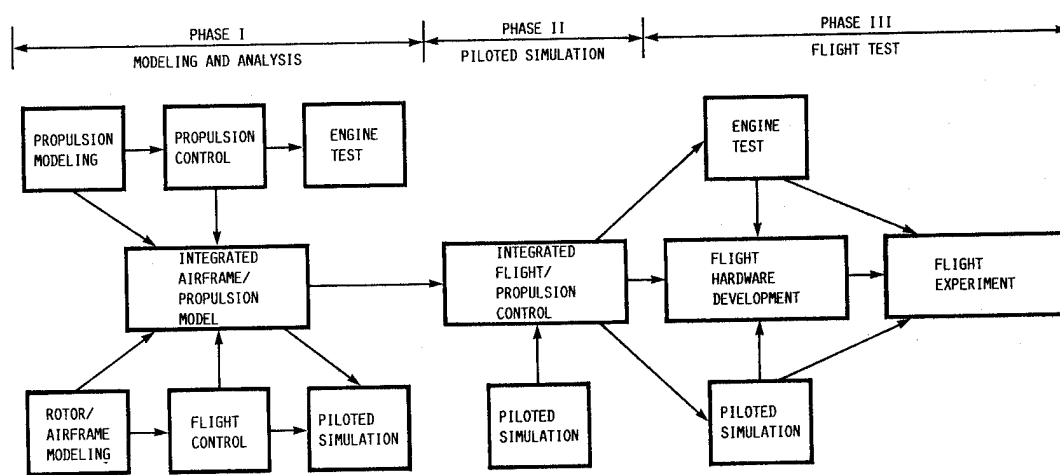


FIGURE 2. - ROTORCRAFT FLIGHT-PROPULSION CONTROL INTEGRATION PROGRAM.

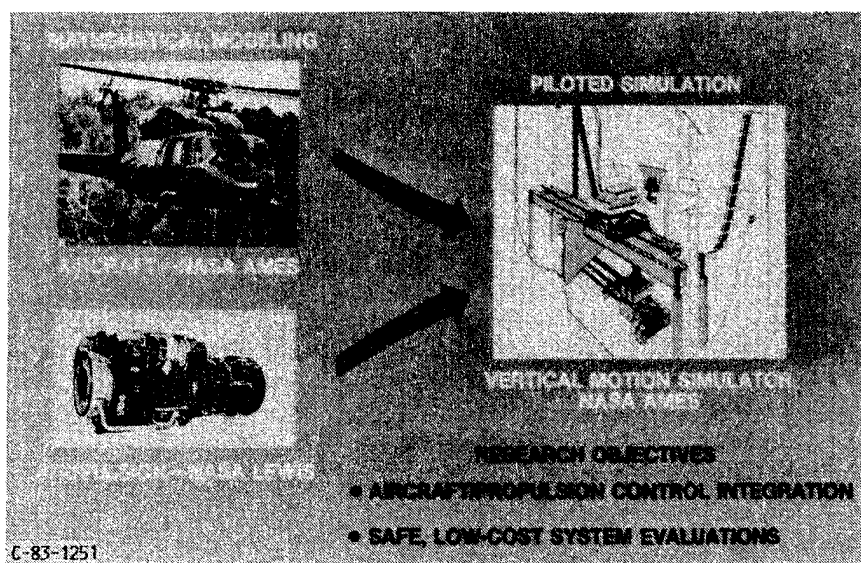


FIGURE 3. - ROTORCRAFT FLIGHT/PROPULSION CONTROLS RESEARCH AMES RESEARCH CENTER/LEWIS RESEARCH CENTER.

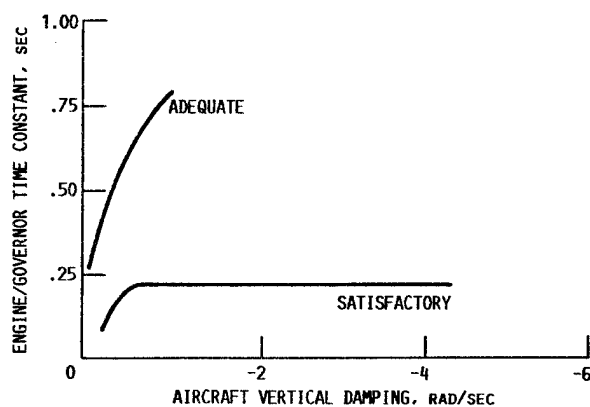
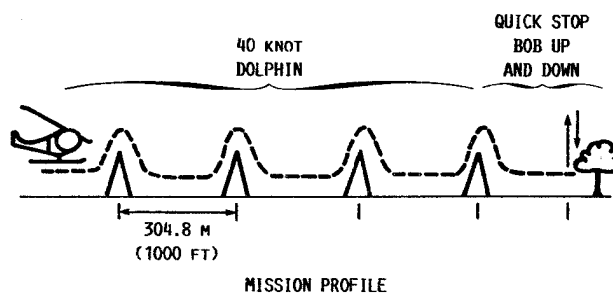


FIGURE 4. - EFFECT OF ENGINE RESPONSE ON HANDLING QUALITIES.

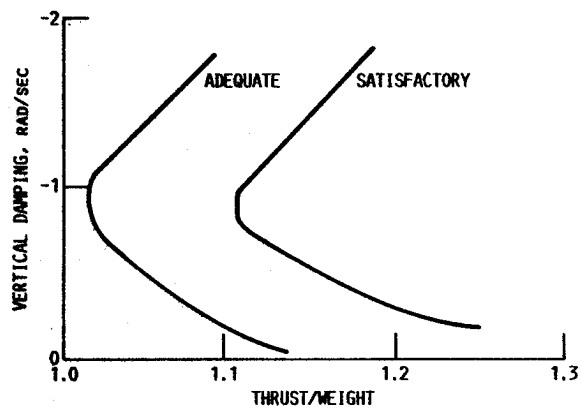


FIGURE 5. - EFFECT OF EXCESS THRUST AND VERTICAL DAMPING ON HANDLING QUALITIES.

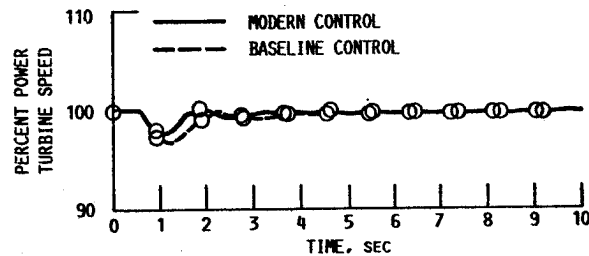


FIGURE 6. - UNCOMPENSATED ENGINE ACCELERATION TRANSIENT CAUSED BY A 40 TO 70 PERCENT COLLECTIVE PITCH BURST.

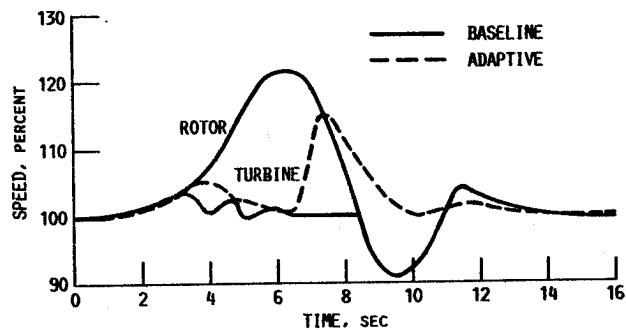


FIGURE 7. - QUICK-TURN MANEUVER FROM 120 KNOTS IN LEVEL FLIGHT WITH TWIN ENGINE CONFIGURATION.

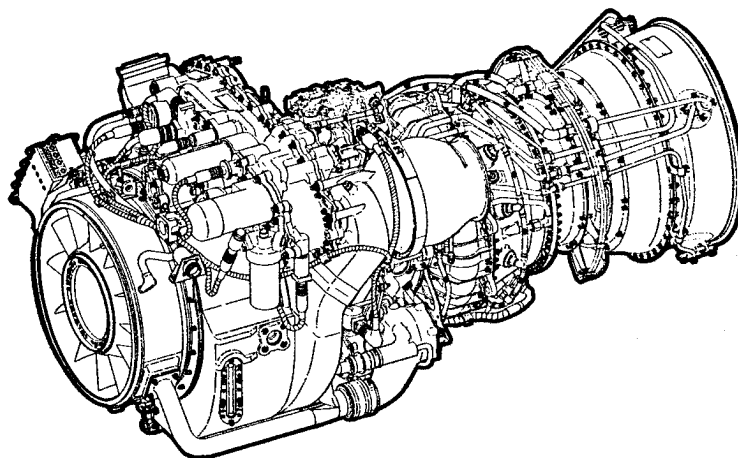


FIGURE 8. - GENERAL ELECTRIC T700-GE-701 TURBOSHAFT ENGINE.

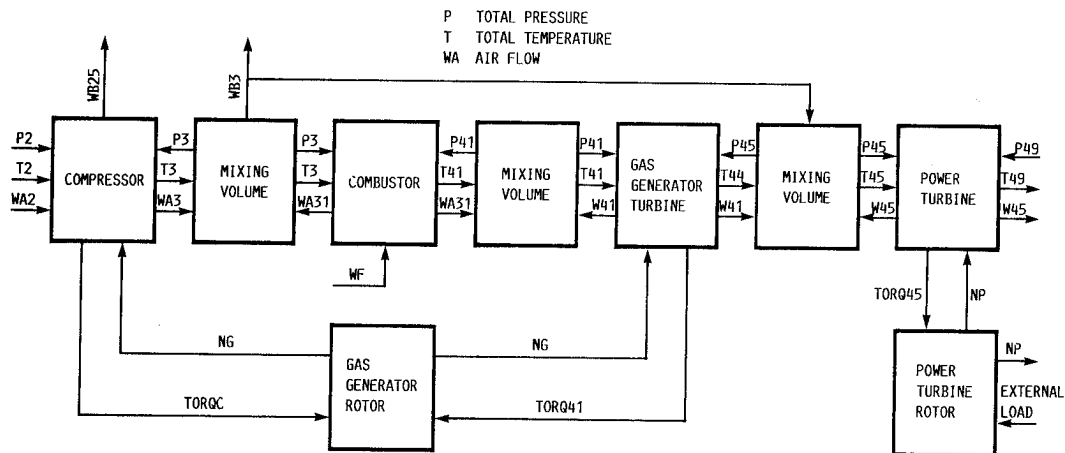


FIGURE 9. - BLOCK DIAGRAM OF SMALL TURBOSHAFT ENGINE MODEL.

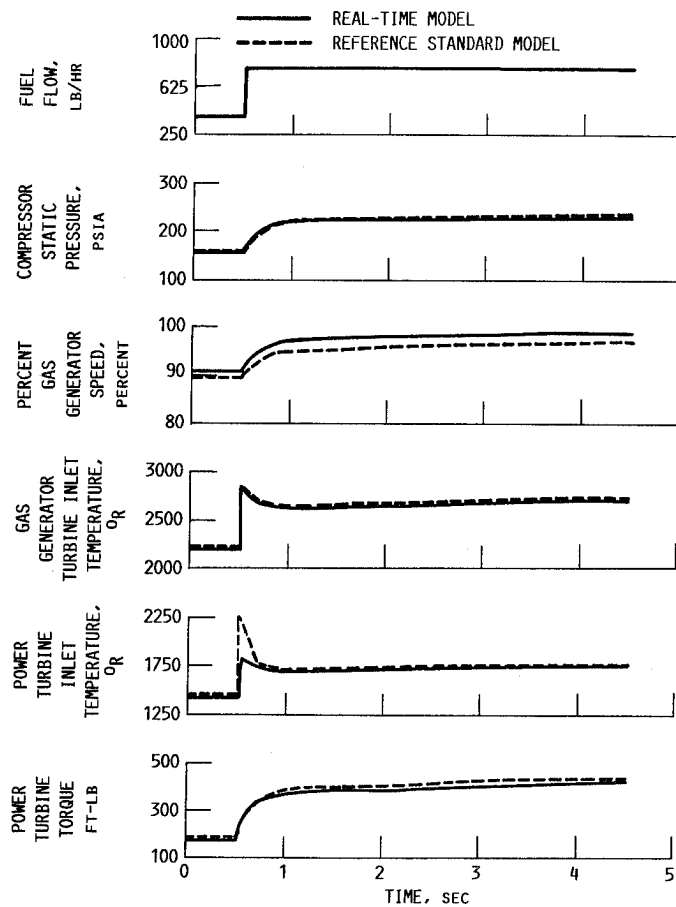


FIGURE 10. - STEP FUEL FLOW INCREASE FROM MID TO HIGH POWER.

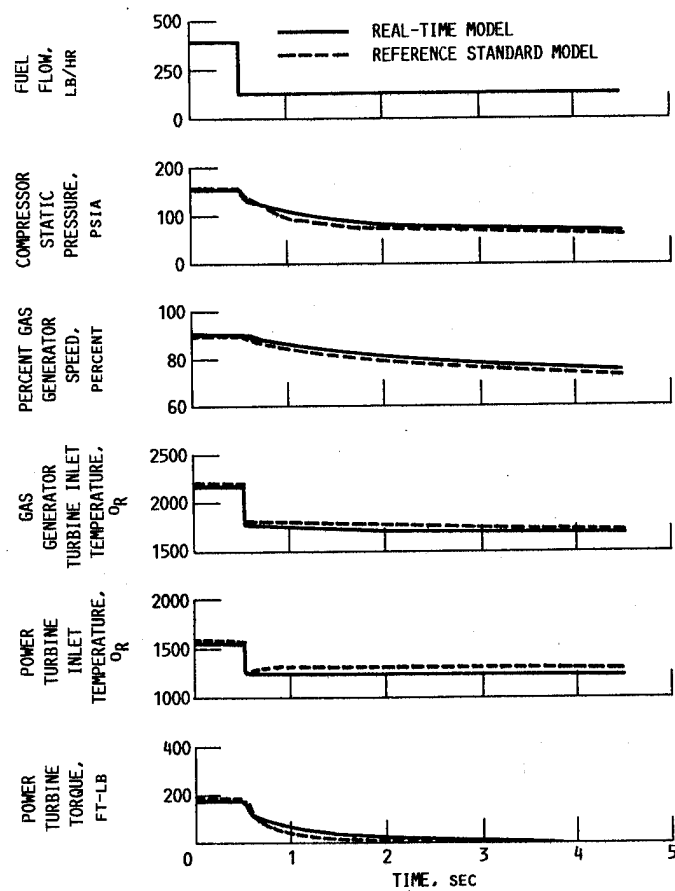


FIGURE 11. - STEP FUEL FLOW DECREASE FROM MID TO LOW POWER.

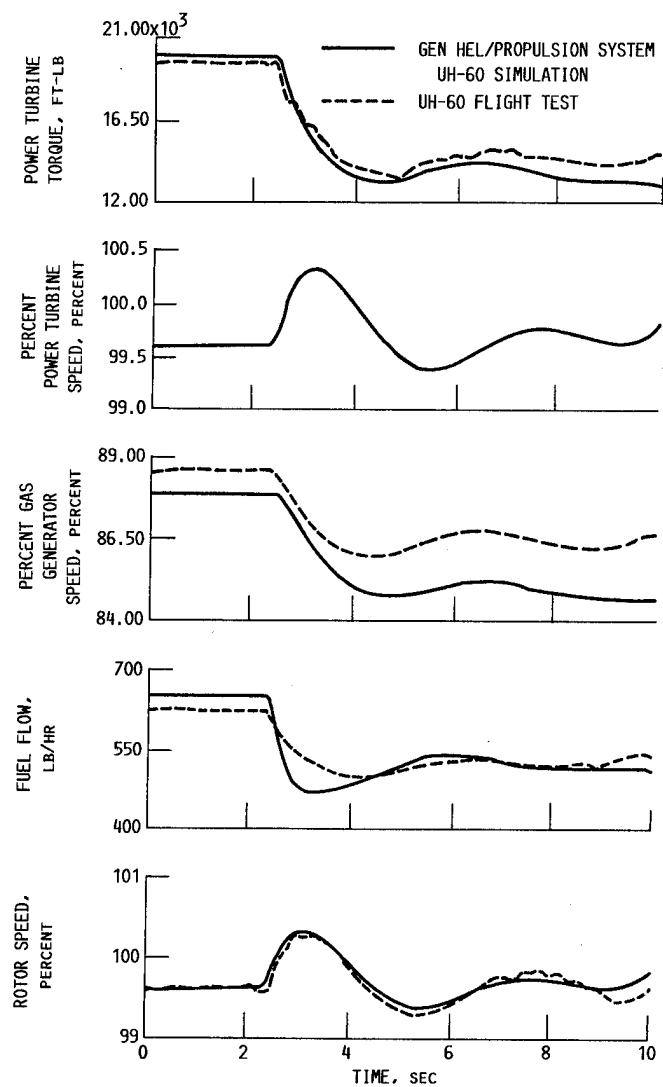


FIGURE 12. - PROPULSION SYSTEM RESPONSE WHEN USED IN CONJUNCTION WITH REAL-TIME ROTORCRAFT SIMULATION. (10 % DOWN COLLECTIVE INPUT, 60 KIAS.)

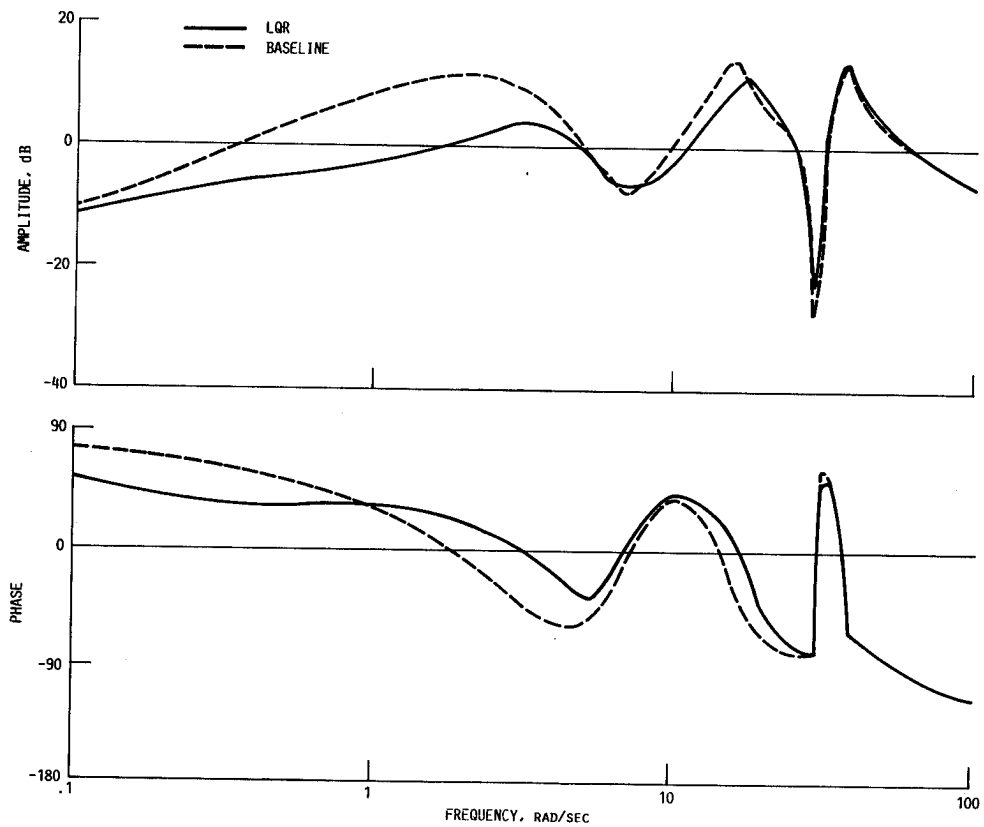


FIGURE 13. - BODE PLOT OF BASELINE AND LQR POWER TURBINE SPEED RESPONSE TO MAIN ROTOR TORQUE.

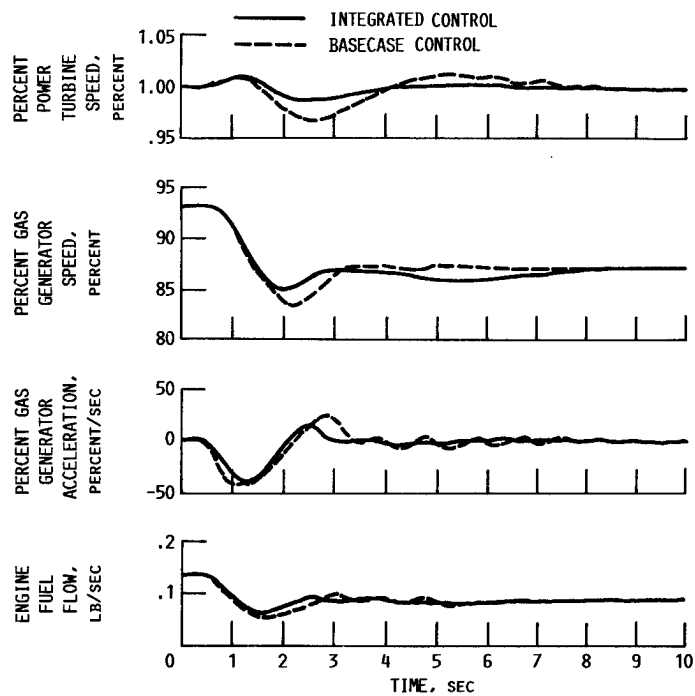


FIGURE 14. - SIMULATED DISCRETE GUST RESPONSE USING LQR CONTROLLER.

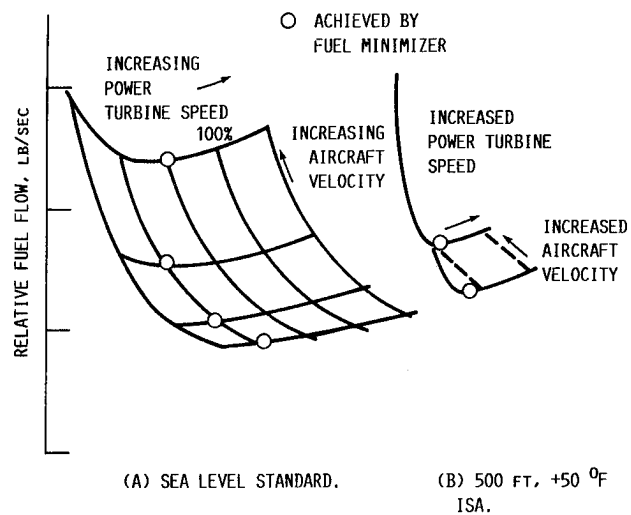


FIGURE 16. - RESULTS OF MINIMUM FUEL CONSUMPTION OPTIMIZER FOR VARIOUS STEADY CRUISE AIRCRAFT OPERATING CONDITIONS OF THE MGH BLACK HAWK SIMULATION.

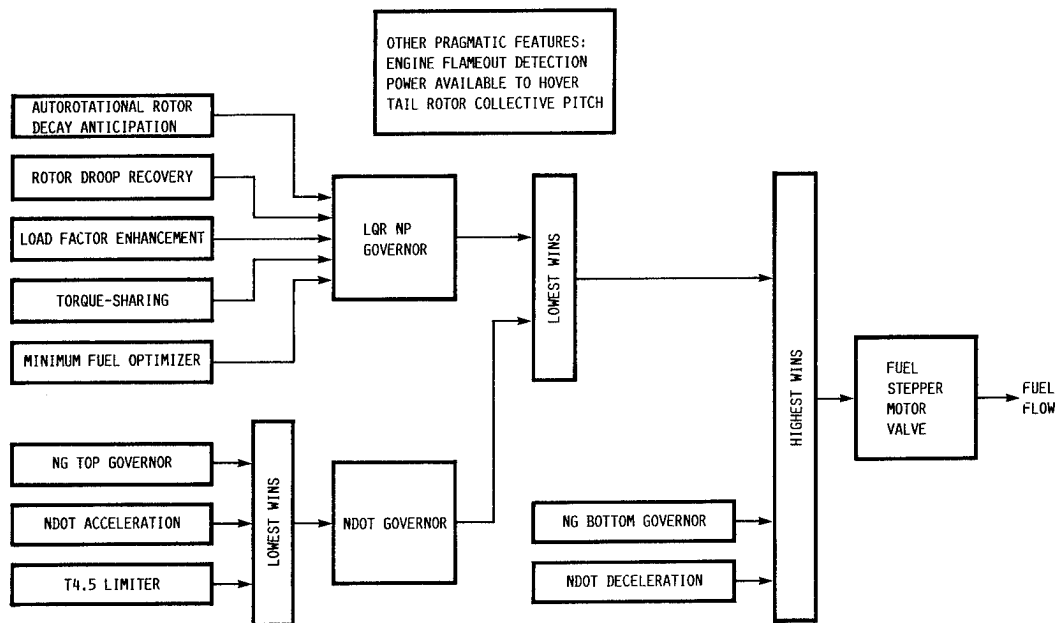


FIGURE 15. - BLOCK DIAGRAM OF INTEGRATED CONTROL.

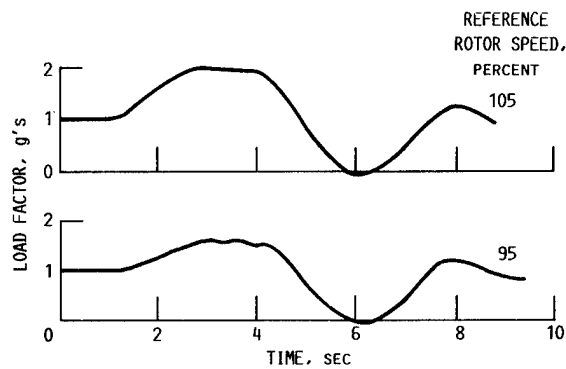


FIGURE 17. - EFFECT OF LOAD FACTOR ENHANCEMENT FEATURE DURING PULL-UP MANEUVER.

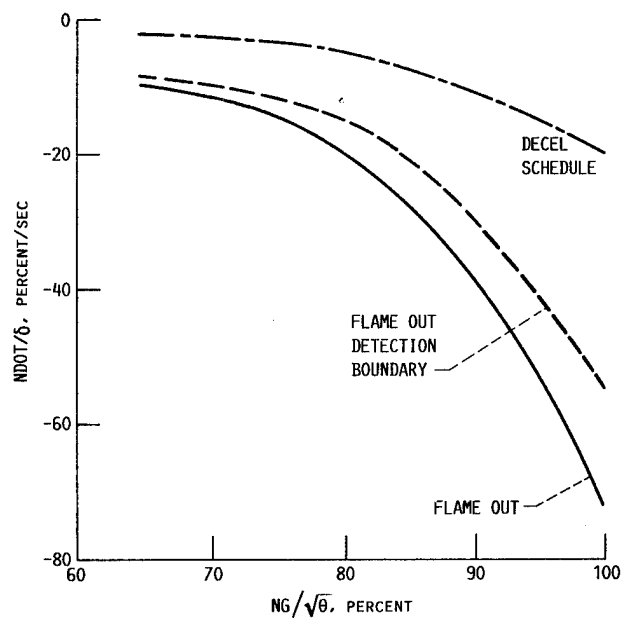


FIGURE 18. - FLAME OUT AND NORMAL ENGINE DECELERATION RATES.

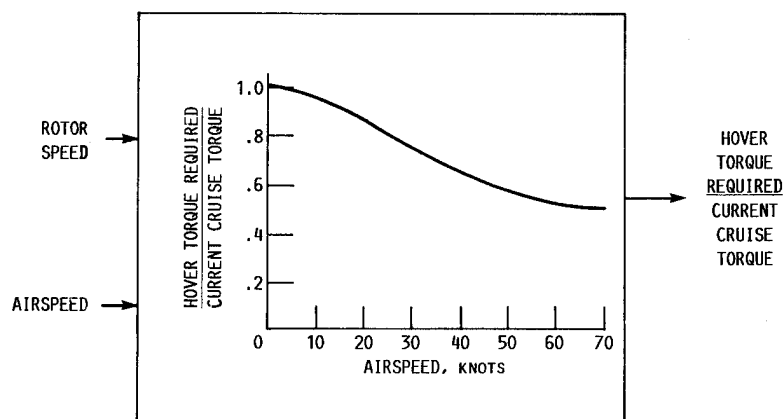


FIGURE 19. - PREDICTED TORQUE REQUIRED TO HOVER RATIOED TO CRUISE OPERATING TORQUE.

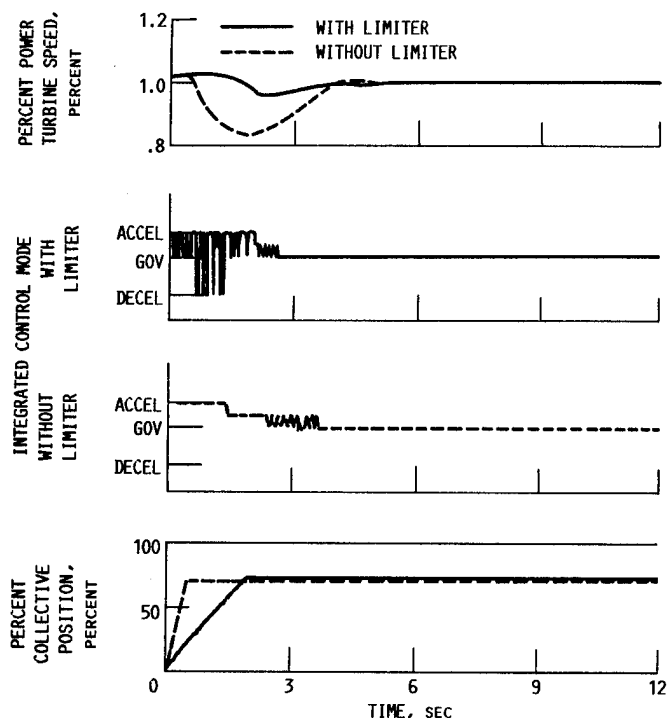


FIGURE 20. - SIMULATED AUTOROTATIONAL RECOVERY USING COLLECTIVE PITCH LEVER PULL LIMITER ON ACCELERATION SCHEDULE.

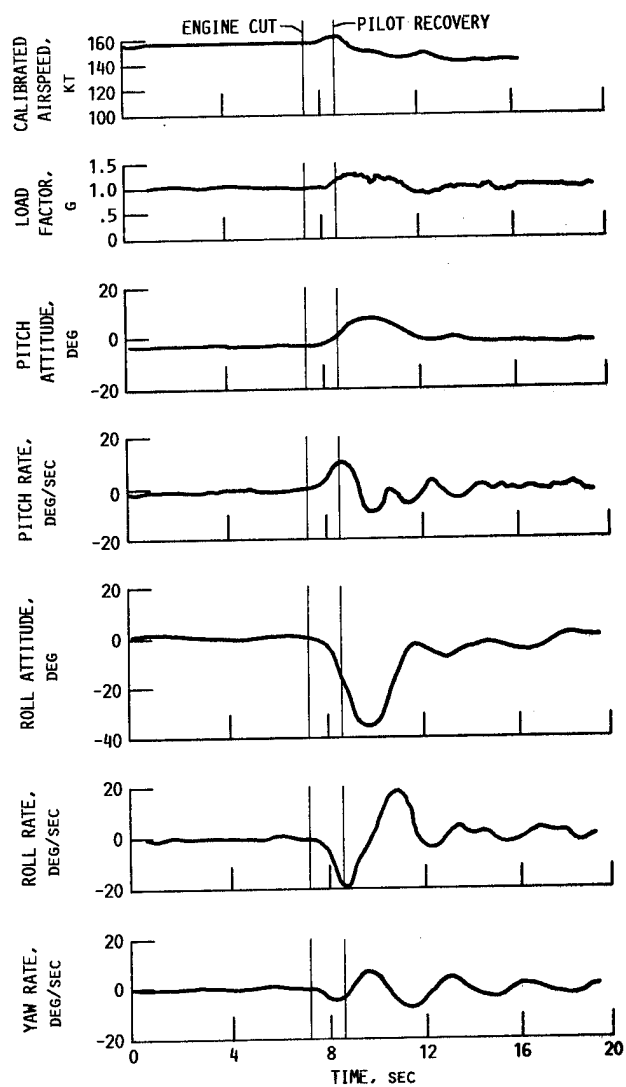


FIGURE 21. - RESPONSE OF A MODERN HELICOPTER TO A DUAL ENGINE FAILURE AT HIGH SPEED.

HELICOPTER HUMAN FACTORS RESEARCH

David C. Nagel

Sandra G. Hart

Aerospace Human Factors Research Division
NASA-Ames Research Center
Moffett Field, CA

ABSTRACT

Helicopter flight is among the most demanding of all human-machine interactions. The inherent manual control complexities of rotorcraft are made even more challenging by the small margin for error created in certain operations, such as nap-of-the-earth (NOE) flight, by the proximity of terrain. Accident data recount numerous examples of unintended conflict between helicopters and terrain and attest to the perceptual and control difficulties associated with low altitude flight tasks.

Ames Research Center, in cooperation with the U.S. Army Aeroflightdynamics Directorate, has initiated an ambitious research program aimed at increasing safety margins for both civilian and military rotorcraft operations. The program is broad, fundamental, and focused on the development of scientific understandings and technological countermeasures. This paper reviews research being conducted in several areas: (1) workload assessment, prediction, and measure validation, (2) development of advanced displays and effective pilot/automation interfaces, (3) identification of visual cues necessary for low-level, low-visibility flight and modeling of visual flight-path control, and (4) pilot training.

INTRODUCTION

Helicopter flight is among the most demanding of all human-machine interactions. The inherent manual control complexities of rotorcraft may be made even more challenging by the small margin for error created in certain operations, such as nap-of-the-earth (NOE) flight, by the proximity of the terrain. Accident data recount numerous examples of unintended conflict between helicopters and the terrain or man-made obstacles and attest to the perceptual and control difficulties associated with low-altitude flight.

This paper reviews research being conducted in several areas. First, studies of workload are described that focus on the development and validation of various approaches to assessment and prediction. Next, we discuss the topics of displays and the development of effective pilot/automation interfaces. Since the visual sense is significantly involved in helicopter flight, particularly in the NOE environment, we describe studies that are being conducted to understand what visual cues are important and the ways in which sensor imagery and other visual aids affect pilots' perception and use of such information. Finally we review research focused on understanding flight-task decomposition and the relationship between workload and training. A companion paper in this volume by Hart, Hartzell, Voorhees, Bucher, and Shively integrates the information, understanding and technology described here into specific requirements for advanced rotorcraft development programs.

Ames Research Center, in cooperation with the U.S. Army Aeroflightdynamics Directorate, has initiated an ambitious research program aimed at increasing the margins of safety for both military and civilian helicopter operations. The program is broad, fundamental, and focused on the development of scientific understandings and technological countermeasures. The overall goal is to provide design principles, guidelines, and computational

models. Specific objectives include: (1) the design of integrated flight management displays and error-tolerant flight management systems, (2) the enhancement of visual and auditory information displays, (3) the development of valid measures and a computer-based predictive model of pilot workload for use in the design of advanced helicopters, (4) specification of human visual requirements and capabilities (in the form of a computational vision model) to serve as the basis for a machine vision system for automated NOE, and (5) guidelines for the development of training systems for advanced rotorcraft.

The primary research areas include workload assessment and prediction, pilot/automation interfaces, pilot vision research (including out-the-window visual cues, panel- and helmet-mounted displays, and biodynamic factors) and training. Figure 1 depicts a schematic overview of the program. The research efforts differ in methodology (e.g., computational modeling, empirical research, simulation and inflight testing), focus (e.g., basic or applied, vehicle-specific or relatively generic), and level of effort. An expanded Rotorcraft Human Factors Program is being formulated in response to an increasing level of interest at NASA Headquarters and urgent

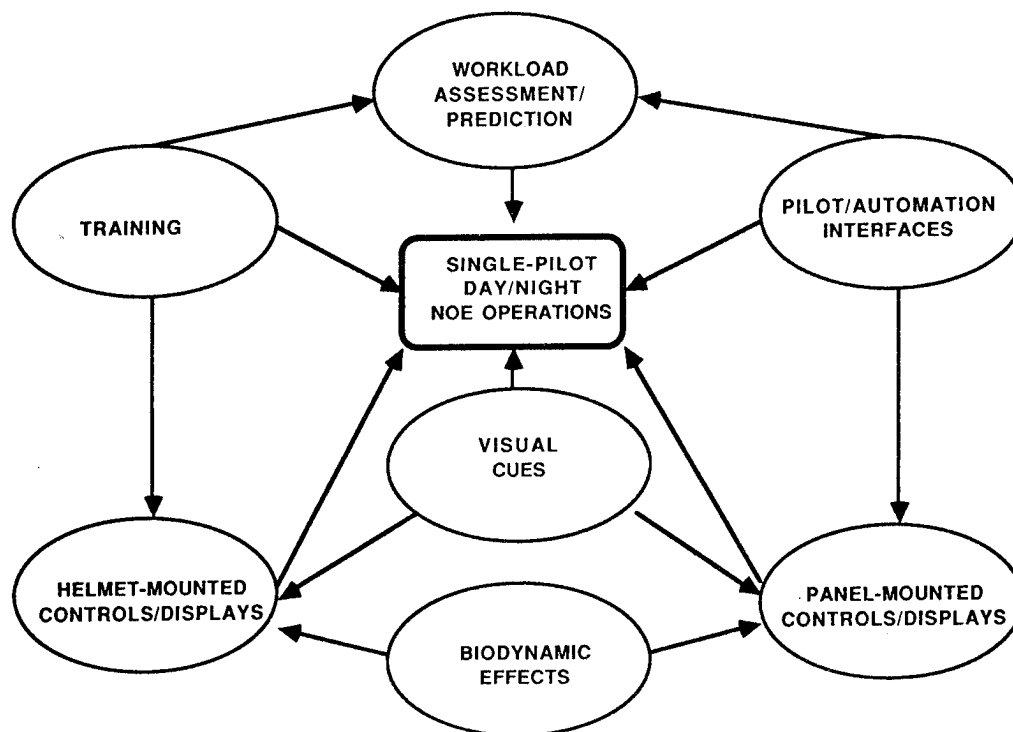


Figure 1: Helicopter Human Factors Program elements

Army research requirements prompted by the LHX program. The major challenges that will be faced by pilots flying advanced technology helicopters will be the requirement for a single pilot to conduct military and civilian missions at night and in adverse weather.

The research is conducted in-house or collaboratively with universities, industry, and government agencies. Results are transferred to user groups by establishing close ties with manufacturers, civil operators, and the military, publishing scientific research papers, participating in and sponsoring workshops and symposia, providing information, guidelines, and computer models, and contributing to the formulation of standards. In addition, the methods and theories developed by members of the scientific staff are applied to specific operational and design problems. We will summarize the accomplishments and future plans for several areas of research.

WORKLOAD RESEARCH

Introduction

The concept of workload has received increasing attention during the past decade, prompted by the realization that the human operators of advanced aircraft represent a limiting factor at the same time that their unique skills and capabilities remain an essential component. Automation has been offered as a solution to an increasing number of workload-related problems found in existing systems or that are predicted for systems under development. However, automation often simply replaces one source of workload for another, rather than accomplishing a significant reduction. In addition, there has been an ever-increasing tendency to reduce the number of crewmembers -- single-pilot operations were specified as an important goal in the early specifications for the Army's most advanced helicopter, the LHX. To achieve single-pilot capabilities, automatic subsystems must be provided to moderate the demands thus placed on the remaining crewmember. Attempts to completely replace humans by automatic systems have failed, however, because human capabilities, adaptability, and flexibility continue to surpass those of the most advanced and sophisticated systems.

If pilots could perform all of the tasks that are required of them accurately and within the allowable time constraints using available equipment, workload would be of little practical importance. Because they often cannot, accurate predictions and assessments of workload must be made during all design stages to develop optimal vehicle configurations, determine the minimum crew complement, establish mission requirements and procedures, and specify the operational envelope for specific missions and vehicles. Thus, interest in workload from an applied perspective has stemmed from the assumption that workload has a direct impact on performance and the workload imposed on the pilots is one of the final tests against which the adequacy and feasibility of operational requirements, system design, and training procedures must be tested.

It was not until ten years ago that well-controlled, theoretically-motivated research in the field of workload began to be conducted, funded by the government and industrial in-house research and development. Until very recently, however, the results of this research were not readily available to the designers and users of advanced systems because individual reports were microscopic in focus and phrased in psychological rather than engineering or aeronautical terms. Nevertheless, this research forms a scientific data base upon which meaningful, valid and reliable workload assessment tools and predictive models should be based.

In 1982, NASA formed a Workload Assessment Program to address many of the issues raised above. The goal was to merge the theoretical information about workload available from academia with the practical requirements of industrial and government organizations to develop a comprehensive definition, practically useful measures and predictors, and workload standards. Throughout the program, basic research provided answers to theoretical questions in the well-controlled environment of the laboratory while simulation and inflight research provided verification that the results were valid and meaningful in the "real world".

A Theoretical Framework

The first phase of the program was devoted to understanding the factors that influence pilot workload, evaluating existing assessment techniques, and developing new techniques. Because the workload experienced by pilots flying complex missions reflects many factors, developing a generally accepted conceptual framework within which to attack the problems of definition, measurement, and prediction has proved to be difficult; different investigators emphasize different dimensions, yet each use the same term (workload) to describe whatever it was they measured.

We defined pilot workload as the cost incurred by human operators of complex airborne systems in accomplishing the operational requirements imposed on them. It reflects the combined effects of the demands imposed by mission requirements, the information and equipment provided, the flight environment, pilots' skills and experience, the strategies they adopt, the effort they exert, and their emotional responses to the situation.

The relationships among these and other factors are depicted in Figure 2. To achieve the desired levels of overall system effectiveness, aircraft must be designed that take advantage of the capabilities of the remaining crewmembers and impose acceptable levels of workload.

The demands imposed on pilots are created by what they are asked to achieve (e.g., the objective goals of a flight and requirements for speed and precision) and the time in which they must achieve it (e.g., schedules, pro-

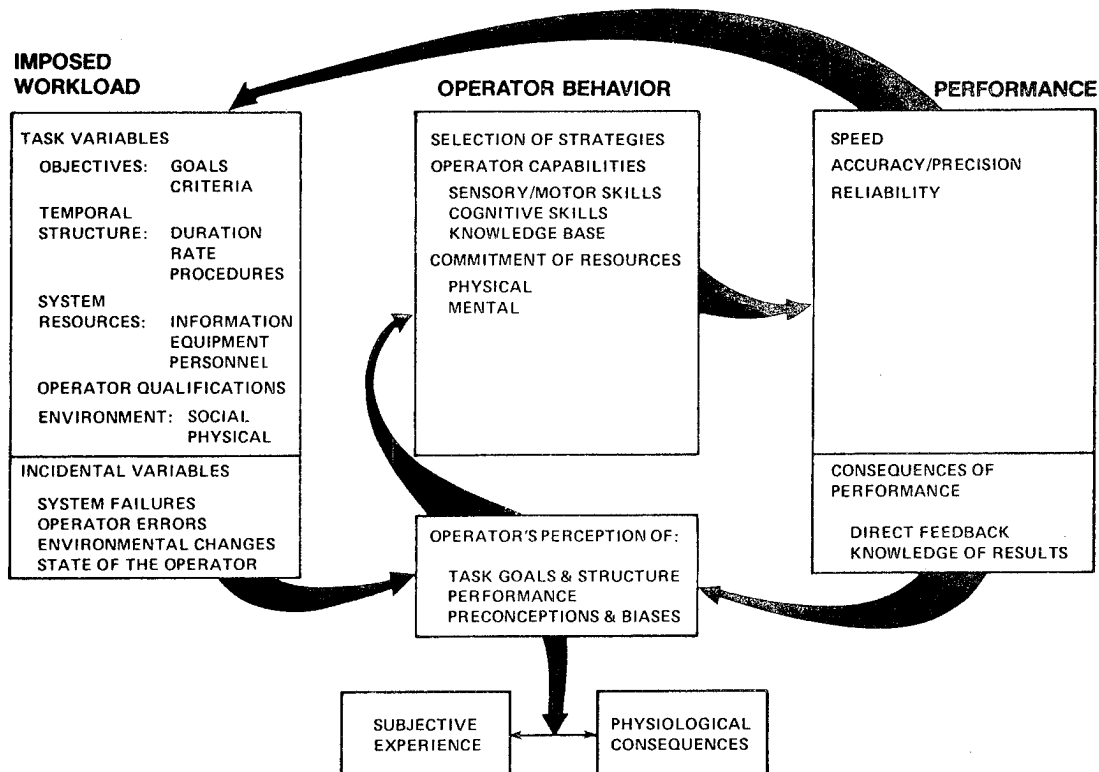


Figure 2: Conceptual framework for the analysis and prediction of workload

cedures, and deadlines). Some flight tasks are intrinsically more demanding than others, and the difficulty of almost any task can be altered by a requirement for additional speed or accuracy. System resources (e.g., controls, displays, automatic subsystems, other crewmembers, and ground support) define how pilots accomplish task demands. Poor display design, inaccessible controls, poor handling qualities, and too much or too little information can increase workload substantially. Finally, the conditions under which a task is performed (e.g., geographical location, altitude, time of day, weather) may also affect workload. For example, visual workload may be increased by low visibility, physical workload may be increased by turbulence, and threats from natural or man-made sources increase stress-related components. These elements may act independently or they may interact, enhancing or mitigating each others' effects.

Finally, the actual level of workload experienced by a particular pilot is determined by his basic skills, knowledge, and training; unskilled or inexperienced pilots experience greater workload than more skilled or experienced pilots. In addition, incorrect strategies, insufficient effort, or pilot errors can increase workload, due to the need for detecting, resolving and recovering from the problems created by the pilots themselves. Finally, pilots' expectations, previous experiences, and physical and emotional states affect their subjective experiences as well as their performance. Thus, although the "work" that is "loaded" on pilots is an important component of the workload they experience, workload may reflect a number of other factors as well.

Measures of Workload

Despite its complexity, workload is assumed to be an important and practically relevant entity and a number of valid, sensitive, and reliable measurement techniques have been developed. Given its complex nature, different measures are needed to evaluate specific components. Workload measures are usually organized into four categories: (1) objective measures of primary or secondary task performance, (2) subjective ratings, (3) physiological recordings, and (4) analytic techniques. Each type of measure has advantages and disadvantages and limitations in the range of activities and questions to which it applies; the evidence they provide may or may not be useful, depending on the situation.

Subjective Measures. Subjective ratings have been used throughout the history of workload measurement. They have face validity and are widely used and practically feasible in most environments. Furthermore, they may come closest to tapping the essence of workload because they provide a direct indication of the impact of flight-related activities on pilots that integrates the effects of many workload contributors.

One of the earliest rating techniques used in the aerospace industry was developed by pilots and engineers: the Cooper-Harper Handling Qualities Rating Scale. This scale addressed workload only indirectly, however. Other scales developed explicitly for evaluating workload were not standardized or validated and never achieved general acceptance. Furthermore, the ratings were characterized by substantial variations of opinion among raters. One of the causes of this variability was the fact that pilots responded to and considered different aspects of complex tasks when they provided ratings. In addition, the factors that contribute to workload vary between tasks. Thus, a multi-dimensional approach is better able to capture all potentially relevant factors. Research on this issue, coupled with the emerging interest in developing tools for expert elicitation by decision theorists and expert system developers, prompted the development of a rating scale that could deal with differences in the sources of workload among tasks and differences in workload definition among raters.

The NASA Task Load Index (NASA-TLX) was developed to provide an estimate of overall workload based on a weighted average of six subscales: physical demands, mental demands, time pressure, own performance, effort, and frustration. These factors represent task-related, pilot-related, and environmental factors, and are the minimum number of dimensions required to describe pilot workload experiences across different activities. The weight given to each rating reflects the importance of the factor to each rater for a specific task. This technique reflects the facts that workload experiences are created by different factors in different activities, the magnitudes of these demands vary within and between tasks, and individuals faced with apparently identical task demands experience different levels of workload. The NASA-TLX is being used extensively by government, industry, and university researchers and has been accepted as an industry standard following a recent evaluation of available measures sponsored by the FAA.

Performance Measures. Performance is the driving force behind workload evaluation in operational or manufacturing environments. It has been assumed, without empirical support, that high levels of workload will result in: (1) an increase in errors and (2) an abrupt and catastrophic decrement in performance. Instead, the typical finding is that errors occur as often when workload is too low (due to inattention) as when it is too high and that increased task demands result in strategy shifts as often as performance breakdowns.

However, measuring performance directly often provides little indication of the effort that pilots exert to achieve the obtained level of performance; as demands are increased, pilots generally put forth additional effort (to the limits of their capabilities) in order to maintain a consistent level of performance. In addition, many measures of performance reflect the characteristics of the system rather than the activities of operators directly. Finally, a common set of performance measures do not exist that can serve as workload indices across different tasks. Thus, acceptable performance-based measures of workload must reflect behavior directly and vary in response to changes in imposed task demands.

Control measures provide an objective summary of how well pilots manage an aircraft to achieve smooth and precise flight-path control. Deviations often indicate periods of time when the pilot is sufficiently overloaded by other actions that primary flight-path control suffers. In addition, the rate, content, and consequences of communications can provide an objective index of the workload imposed on pilots; a standardized taxonomy of communications has been developed in which *a priori* estimates of the workload imposed by communications tasks have been quantified. Errors and delays in response often indicate the presence of excessive workload, and the occurrence of errors is often followed by an increase in workload as the pilot attempts to resolve the consequences of the error.

Secondary Task Measures. Because performance measures do not always reflect the cost of task performance to the pilots, it has been suggested that additional tasks could be imposed that would provide an indirect indication of the resources required from a pilot to perform a primary flying task; as flight-related demands are increased, secondary task performance will degrade in direct proportion to primary task demands. The intent was to discover a secondary task "yardstick" that could be used to compare the workload of different tasks. The fact that specific secondary tasks were found to be differentially sensitive to particular types of primary tasks prompted a remarkable increase in interest in the field of workload assessment from the academic community. Competing models of attention and performance were applied to discover the structure and allocation of human resources, and a more scientific approach to the field of workload assessment evolved.

However, most secondary task measures of pilot workload are inappropriate inflight because they are difficult to implement and might compromise safety. Nevertheless, some measures, such as time estimation, can be included in the primary flight task as a natural component -- an embedded secondary task -- with minimal instrumentation and intrusion on primary task performance. This and other embedded measures have been shown to be sensitive to the workload levels encountered in different segments of flight in simulated and inflight experiments.

Physiological Measures. The earliest conceptualizations of workload focused on the physical effort required to accomplish tasks. Workload was defined in terms of physiological exertion and measures of physical effort, such as oxygen uptake and heart rate, were used to quantify this component of workload. This conceptualization of workload ignored the cognitive demands that have become an important requirement in flying advanced helicopters. Thus, measures of other physiological responses that do reflect cognitive processes (such as evoked cortical brain potentials and heart rate variability) have been investigated.

Physiological measures generally have the advantage of being unobtrusive. That is, they can be obtained without requiring attention from the pilot or interfering with a flight. In addition, since they can be recorded relatively continuously, they can reflect momentary fluctuations in workload. Finally, they provide an objective indication of involuntary physiological changes that often accompany variations in workload. The disadvantages include a lack of diagnosticity. That is, most physiological measures reflect non-specific responses to many sources of stress. These responses may reflect the demands imposed by the flight, the environment, or the pilot directly or other factors that are less directly related to workload. Cardiovascular responses do, however, provide an integrated indication of the total impact of the flight on the pilots that does not also reflect the characteristics of the system (as many performance measures do) or the pilot's biases and misconceptions (as subjective ratings do).

Heart rate reflects the stress associated with specific flight-related activities; it increases as some aspects of workload are increased. For example, heart rates are typically elevated during take-off and landing and return to baseline levels at altitude. In addition, substantially greater increases are found for the pilot-flying during take-off and landing than for the pilot-not-flying. It is possible that the feeling of responsibility and level of preparedness that must be maintained by the pilot-flying could result in their elevated levels of arousal.

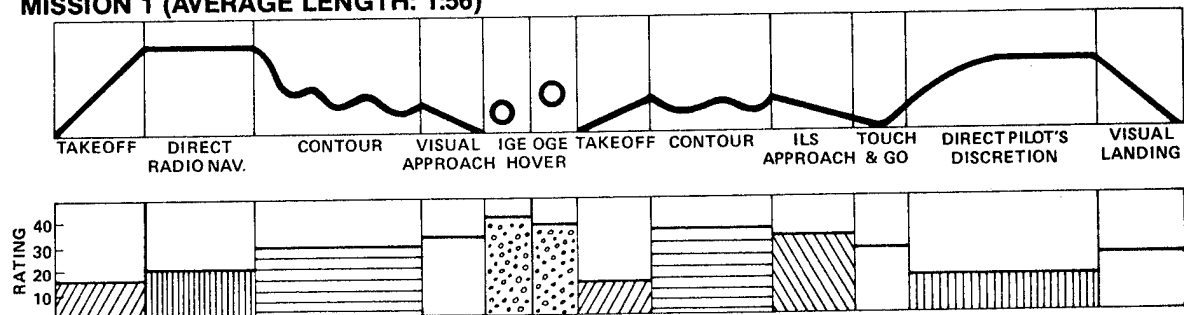
Heart-rate variability is particularly sensitive to even subtle variations in mental workload; heart rate irregularity decreases as the difficulty of a task is increased. A method of obtaining an estimate of heart-rate variability on-line has been developed that provides a sensitive real-time indication of workload variations.

Inflight Verification

The final step in developing and testing these measures was inflight verification. Although simulations provide an analog of an operational environment, important elements are missing that cannot be replicated. A number of the measures developed in laboratory and simulation research were evaluated inflight in the NASA Kuiper Airborne Observatory (KAO) and in the NASA SH-3G helicopter.

In the experiment conducted in the SH-3G aircraft, evaluating the utility of different workload measures was the primary focus of the experiment. Specific missions were defined in advance and flown by each crew. The workload measures obtained for each segment were compared to predictions provided by earlier studies. In addition, portions of the flight were conducted on an instrumented flight-test range so that objective measures of performance, often unavailable inflight, could be obtained. The flight scenarios include straight and level flight above 3000 ft and contour flight, visual landings at an auxiliary site, instrument landings at airfields, hover in and out of ground effect, visual search patterns, and visual and instrument navigation conducted between Moffett Field and Crows Landing. The workload measures included pilot ratings, secondary tasks, heart rate, and selected performance indices.

MISSION 1 (AVERAGE LENGTH: 1:56)



MISSION 2 (AVERAGE LENGTH: 2:11)

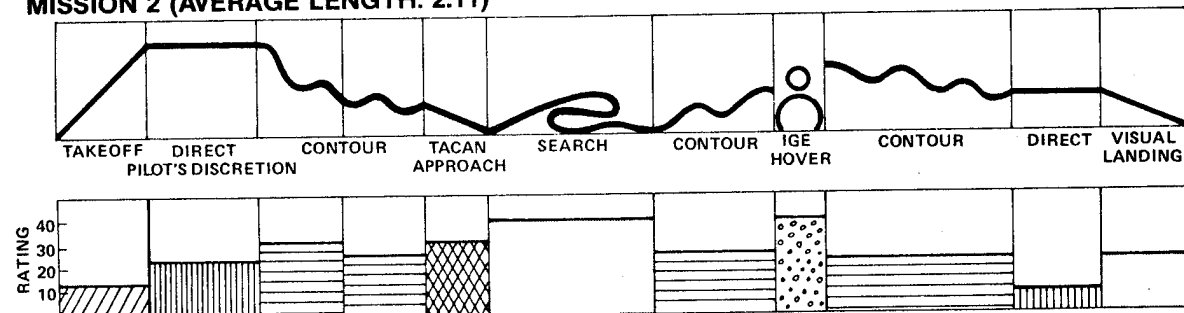
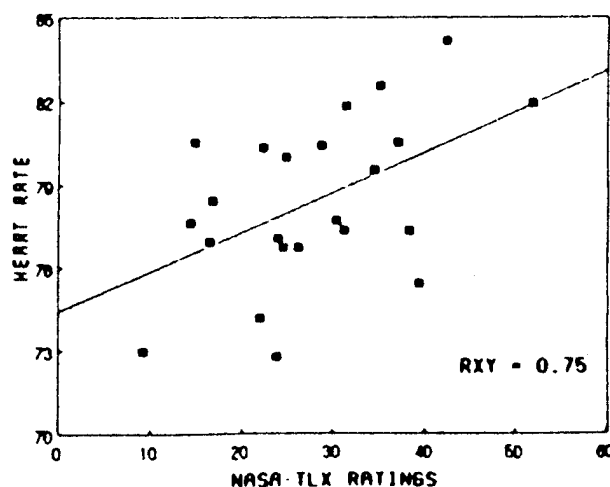


Figure 3: Flight-task segments and pilot workload ratings.

In this experiment, similar estimates of workload were obtained when the same tasks were performed at different times in the flights (Figure 3). For example, all of the visual landings were given the same, low, workload ratings. Subtle variations in tasks, however, prompted differences in workload measures that were in the predicted direction. For example, both primary and secondary performance measures and subjective ratings differed for hover tasks performed in and out of ground effect. As the environmental constraints imposed for different contour flight segments were increased, so did the measured levels of workload. As predicted, there was a high correlation between heart rate and pilot workload ratings (Figure 4). These workload-related task groupings will help in developing a taxonomy of rotorcraft tasks for a predictive workload model, and provide a

Figure 4: Relationship between heart rate and pilot ratings



data base that can be taken into the laboratory for further analysis, and can be incorporated into the Army/NASA Aircrew-Aircraft Integration (A³I) Program designers workstation.

Future Plans

The first phase of the program has been completed: the factors that contribute to pilot workload have been identified and a set of valid and practical measures have been developed. These measures are now being used to solve operational problems posed by the Army, civil operators, and industry. A micro-processor-based expert system for selecting and applying workload assessment techniques has been developed for public distribution.

The primary goals of the second phase of the workload programs are to: (1) complete and apply a computer model for workload prediction in advanced helicopters, (2) develop and publish criteria for workload (e.g., How much workload is "too much" or "too little"?), and (3) continue support for FAA, Army, civil, and industry workload efforts.

Workload Prediction

After several years of research on the structure of pilot workload and developing and applying workload assessment techniques, a computer model to predict pilot workload for current and advanced rotorcraft is being developed. In a research environment, workload predictions are essential so that known levels of workload can be imposed to evaluate candidate measures. In an applied environment, such predictions are needed to estimate the potential impact of design decisions on pilot performance early in the design process. Again, laboratory research provided the initial equations with which the workload of task elements was combined to derive predictions for complex tasks. Here, it was found that the workload of subtasks performed individually, but concurrently, could be added together to predict the performance of the combined task. Subtasks that were functionally related or shared common information, processing, or response requirements, created lower levels of workload in the combined task than would be predicted by adding the values for task components.

Experienced workload is the integrated product of many factors in addition to the objective demands that are placed on a pilot. Although workload predictions, particularly those made during the design of a new system, must necessarily focus on the objective demands that are imposed on a pilot, there are other types of information that might be included as well to enhance the predictive power of such a model. Our approach has been to start with nominal or typical flight segments or mission elements. Information about their duration, intensity, overall workload, and visual, auditory, information processing, and manual control requirements are obtained. A data base of additional tasks or events that might occur during any flight segment are identified and the same information that is obtained for the nominal segments is obtained for them. The functional relationships among specific segments and additional tasks are defined so the model can select the appropriate combination algorithms with which information about tasks and segments performed concurrently can be combined to estimate the workload of the complex task.

A preliminary model was developed based on this structure. The predictions of the model were tested in simulation research, and were highly correlated with objective and subjective measures of workload obtained in simulated flight. (Figure 5) The full model is under development. The predictions of workload made by this model will be incorporated into the A³I Human Factors Engineering Computer-Aided Designers Workstation model under development at Ames. These predictions will allow the designer of system, subsystem, or mission element for an advanced helicopter to test the effects of the design element on the potential pilot-population with a computer graphics workstation which contains many other analytic models as well. With this workstation, potential problems can be identified during the conceptual stage, thereby avoiding expensive and time-consuming cut-and-try methods.

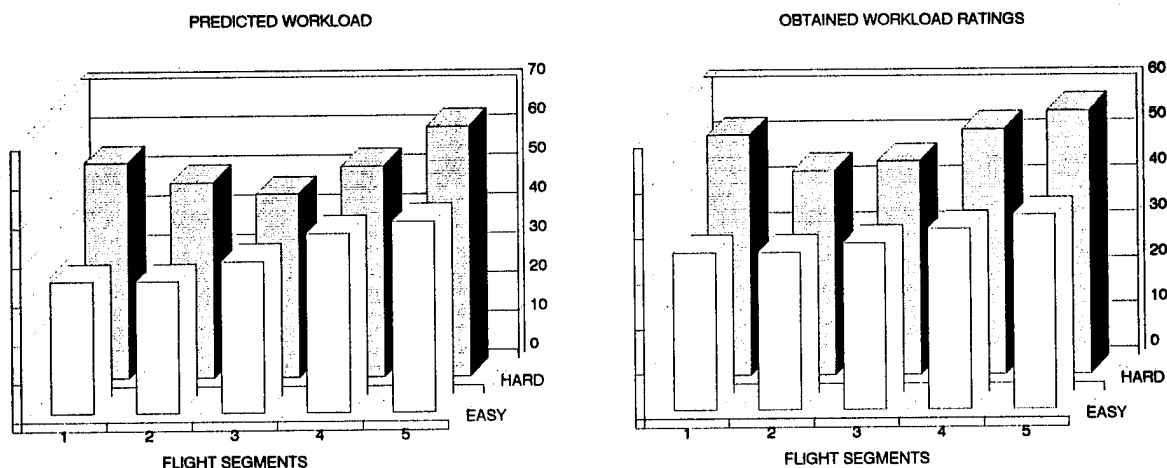


Figure 5: Obtained vs predicted workload ratings for two flight scenarios.

PILOT/VEHICLE INTERFACE

Introduction

The safest and most efficient cockpit is one in which technological advances are integrated with other cockpit systems and the pilot/vehicle interface is designed with the needs of the human user in mind so as to maintain optimal levels of pilot workload. Guidelines for implementing integrated information management, decision-aiding, and control systems are being developed. The goal is to provide specifications for systems that are tolerant of human errors and work with the pilot to accomplish mission objectives. In addition, principles based on theories of human attention, performance, communications, and learning have been used to determine the optimal interfaces for and allocation of functions between pilots and automated systems. Currently, this work is being conducted as part the Automated NOE Program, jointly with the Guidance and Control Branch. NASA researchers have tested the efficacy of some of the features that have been proposed for the next-generation of Army scout/attack helicopters (such as the LHX) to reduce the workload of a single pilot. In particular, the effects of different levels of automation and voice-interactive versus all manual input alternatives have been examined in a simulated military NOE environment.

Human-Centered Cockpit Automation

The primary goal of this program element is to integrate valid psychological principles, rules-of-thumb used in applied design, and operational training procedures to provide guidelines for the design of automation in advanced helicopters.

Rather than automating whatever functions are technically feasible, and leaving the rest to be accomplished by a pilot, cockpit automation decisions should be human-centered. Automation levels should be flexible, pilot-

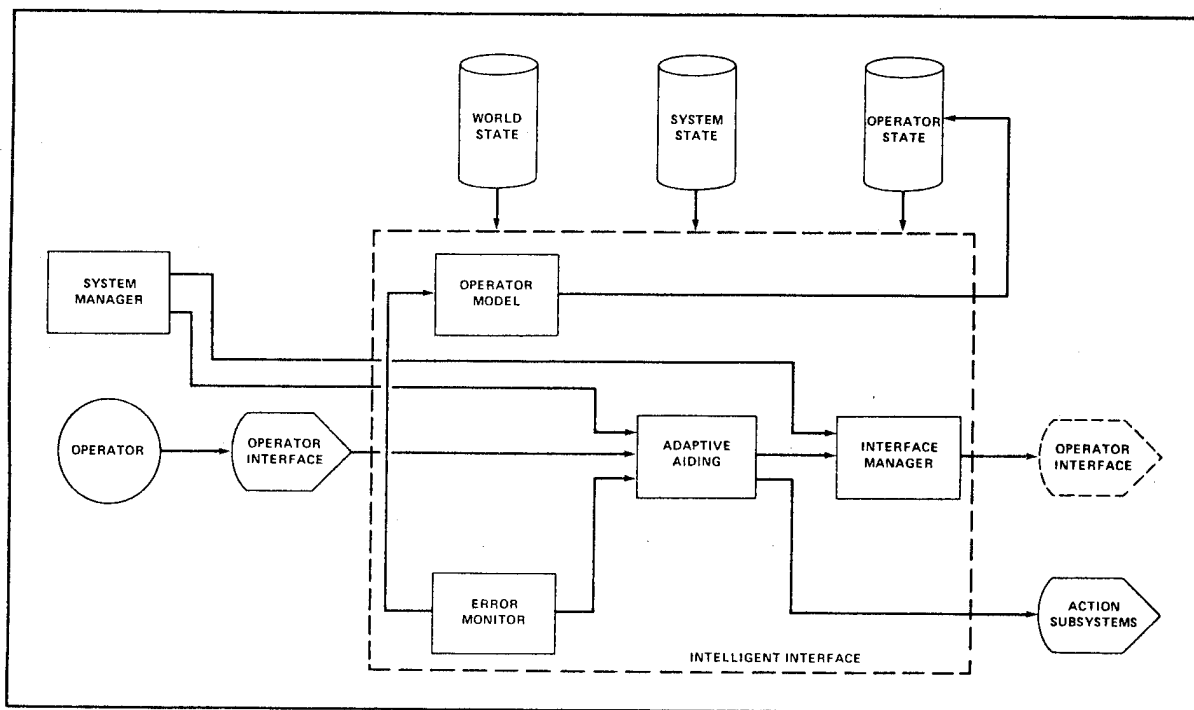


Figure 6: Architecture of an intelligent interface for a goal-directed flight management system.

selectable and driven by the intents and goals of the pilot, rather than by technology. The optimal system would be one that mimics an "ideal" copilot, providing the right level of information at the right time and assuming the level of control previously specified by the pilot at appropriate times in flight. The philosophy and conceptual design for an intelligent, goal-directed flight management system, originally developed for transport aircraft, is being investigated as the basis for the design of automated subsystems in advanced rotorcraft. (Figure 6) System objectives and pilot functions were determined in order to specify what a goal-directed flight management system should accomplish in helicopter operations and the qualitative and quantitative criteria for doing so. Refinement of this model can be obtained through basic research on human attention and performance as well as through applied research on various types of cockpit automation.

A major research effort is underway to determine the applicability of six theoretical models of human attention and performance to the design of automation for advanced rotorcraft. A complex helicopter flight simulation has been developed that mimics the information processing complexity of helicopter flight under combat conditions. Mission segments may include ingress, navigation through familiar and unfamiliar terrain, rescue, egress, and targeting. The task components include manual control, target acquisition, communications, threat response, mission management, monitoring automated subsystems, and resolution of failures. Optimal and non-optimal system configurations will be identified, based on theories of human attention, learning and performance. Model predictions are being verified with simulation research.

Two Single-Pilot Advanced Cockpit Engineering Simulations were conducted in the Ames Vertical Motion Simulator to evaluate the effectiveness of different forms of cockpit automation in reducing single-pilot workload levels to the same levels experienced by pilots in conventional two-crew configurations. Several stability and control augmentation systems, coupled with different levels of automation (e.g., hover hold, position hold, airspeed hold, altitude hold, and turn coordination) provided alone or in combination were evaluated to compare single and dual-pilot performance and workload during low-level military operations in the NOE environment. Two forms of subjective workload ratings (the Subjective Workload Assessment Technique - SWAT, and the NASA-

Task Load Index - NASA-TLX), Cooper-Harper Handling Quality ratings (HQRs), and heart rate measures were obtained to evaluate the effects of the experimental manipulations on the pilots.

A clear difference was evident between the single- and dual-pilot configurations. For example, only one configuration of the twenty tested in the first simulation was judged to be satisfactory for flying NOE with a single pilot. The workload ratings confirmed the results of the HQRs in both single- and dual-pilot configurations. In the second simulation, as in the first, it was found that different automation options were particularly beneficial for specific flight segments. For example, Figure 7 compares the results of the "best" and "worst" of the six configurations included in the second simulation. The "best" configuration (labeled 1 in Figure 7) was the basic Advanced Digital/Optical Control System (ADOCS) system with rate command, attitude stabilization, turn coordination, and heading, altitude, position, and hover hold. The "worst" system (labeled 2 in Figure 7) was an attitude command/attitude stabilization system with heading and attitude hold and turn coordination. Pilot workload and handling quality ratings were similar during the NOE segment for all configurations, while Configuration 1 was superior for the remaining flight segments. These results, as have others, emphasize the points that automation *per se* does not necessarily have the same beneficial effects under all circumstances and that currently available forms of cockpit automation cannot reduce single-pilot workload to dual-pilot levels.

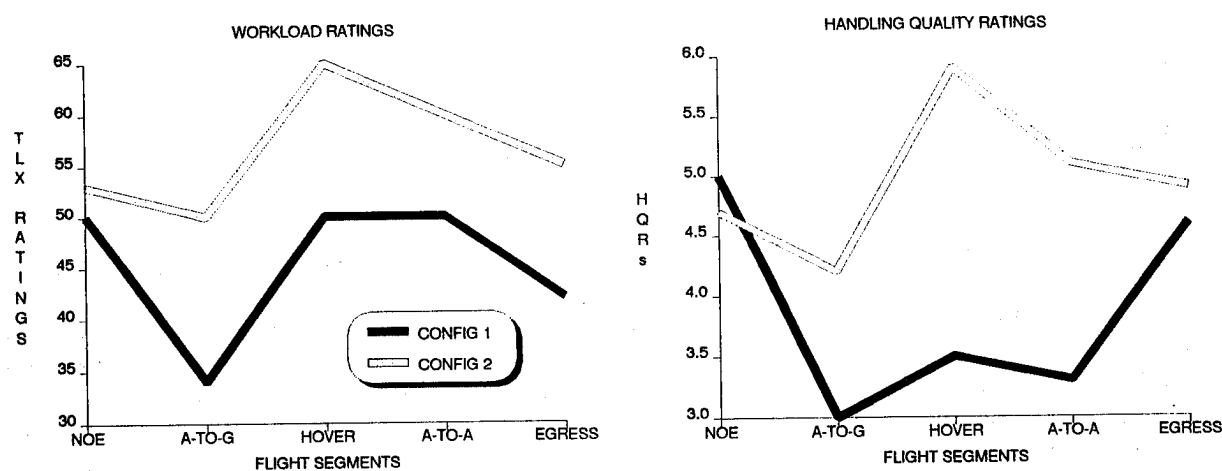


Figure 7: Comparison of workload and handling quality ratings for two stability and control augmentation systems.

Automatic Speech Recognition

Low-level rotorcraft operations are visually demanding, thus, aural displays (e.g., human, digitized, and synthesized speech messages and warning tones) have been proposed as alternative means of providing information to enhance pilots' situational awareness without further overloading their visual systems. And, since flight path control continues to impose demanding manual control requirements in rotorcraft, alternative methods for pilots to enter commands and effect subsystem selections have been investigated. For example, it has been suggested that computer-recognized vocal commands should compete less for pilots' limited resources than would manually-entered commands during activities that impose high manual control demands.

The feasibility of automatic speech recognition as a method of entering commands and information to control helicopter flight systems has been studied for many years. In general, our approach has been to utilize commercial systems, often modifying their recognition algorithms to improve recognition accuracy, and then to use the enhanced systems to develop guidelines for the application of voice recognition systems in advanced rotorcraft.

One speech recognition system was tested in a Bell Jet Ranger helicopter in level cruise, sustained turn (that created blade slap noise), approach to VNE (that created additional vibration), and hover in-ground effect (high pilot workload). Each pilot trained the system individually to his voice for the 20-word vocabulary. Recognition accuracy was not affected by cockpit noise or vibration as much as might have been expected. However, increased pilot workload did degrade recognition accuracy. The results are summarized in Table 1.

Table 1: Automatic Speech Recognition Accuracy
During Four Flight Modes

	Average Noise Level (dbA)	Recognition Accuracy (% Correct)
Level Cruise	92.5	98.3
Sustained Turn	90.0	98.1
Approach to VNE	95.0	95.8
Hover (IGE)	91.0	95.8

In a separate research effort, the multiple resources model provided predictions about tasks for which speech recognition would (and would not) be appropriate. The success of the theory in predicting performance in laboratory research prompted several simulator comparisons of speech and manual control of different subtasks in the context of advanced, high-technology helicopter missions. The task requirements included cruise, hover, and air-to-ground engagements flown by current Army Apache pilots. Some missions were flown with all-manual cockpit controls. Others were flown with a combination of manual (flight path control and weapons firing) and speech controls (weapons selection, data-burst transmission, and countermeasure activation).

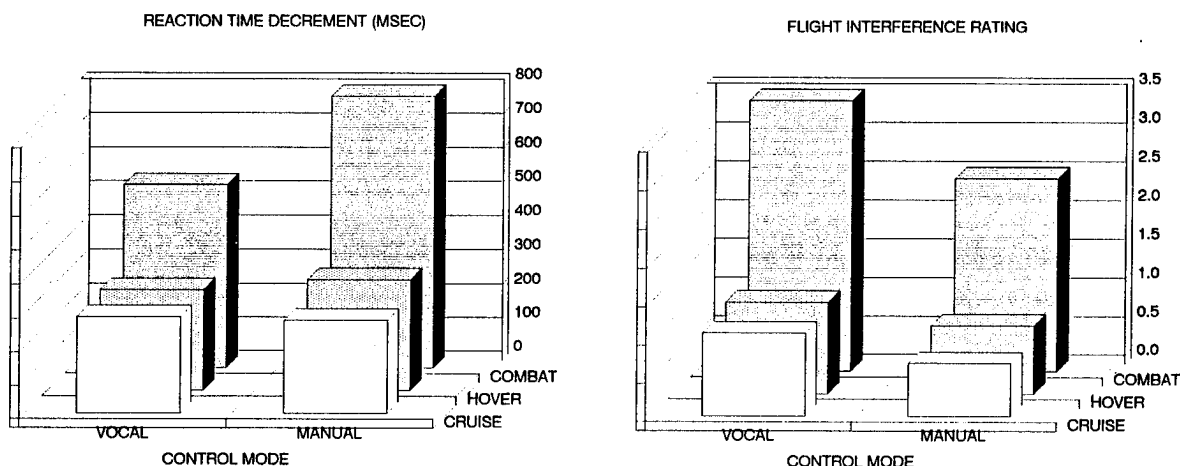


Figure 8: Comparison of speech and manual modes of entry for the selection of countermeasures

Predicted benefits (and drawbacks) of the two entry systems for different tasks (e.g., weapon selection, data burst transmission, countermeasure activation) and with different levels of automation were derived from the theoretical and laboratory research. It was expected (and found) that combat tasks, performed with no automation, would be sufficiently demanding to overload pilot's capacities for performing manual-control tasks. In this

case, an advantage for voice-interactive controls was found. However, this advantage was attenuated in the less demanding portions of the scenario. Speech controls did, in fact, improve performance by reducing competition for manual response resources. Interestingly, the performance benefit of speech controls was achieved despite pilot reports of higher workload (Figure 8). Uttering consistent voice commands to achieve adequate recognition accuracy by the voice input system demanded additional attention, as did the requirement to monitor feedback from the system (to ensure that the intended command was entered). The results of both laboratory and simulation research supported the predictions of the multiple resources theory and suggest the utility of speech controls in reducing competition for manual response resources. However, the current generation of voice recognition systems is not yet sufficiently robust or reliable to encourage their operational use for high-priority tasks. It is expected that the advantage of speech control will be further attenuated as increasing levels of automation are provided in future simulations, as they will reduce the need for continuous manual control activities.

VISUAL RESEARCH

Introduction

The major challenge that will be faced by pilots flying advanced technology helicopters will be the requirement for a single pilot to conduct military missions at night and in adverse weather. The visual demands of low-level flight already provide a significant source of workload for two-man crews flying current-technology helicopters under visual flight conditions. Much of the information required for flight-path control at very low altitudes is obtained by monitoring the environment, with only occasional reference to flight instruments. Therefore, transition to single-pilot operations will require technological advances to facilitate and enhance pilots' abilities to extract information from the environment for immediate flight-path control and geographical orientation.

Little is known about how humans extract information about vehicle state, motion parameters, and how they orient themselves to the immediate environment from direct visual cues in good visibility. In addition, technological advances have been introduced to aid pilot performance in low visibility (such as helmet-mounted displays of sensor imagery or computer-generated symbology), although basic knowledge about human perceptual capabilities in this area is seriously deficient. Thus, research was initiated in collaboration with the Army to establish pilot performance limitations with current and advanced helmet-mounted night vision systems, specify the minimum visual cues necessary for pilots to maintain situational awareness (e.g., perceive motion, estimate range, and identify objects), and develop guidelines for the design and use of such systems based on human perceptual and performance capabilities.

The near-term goal of this program element is to specify the visual requirements in and outside of the cockpit for flight-path control, to optimize display formats and symbologies, and to augment and enhance images provided by sensors to aid in the design of adequate helmet-mounted displays for pilots to use at night and in low visibility. The long-term goal is to provide the algorithms, based on a model of the human vision system, for a machine vision system to enable automated NOE flight. This goal is a key element in the Aircraft Automation Program at Ames, and will be performed in conjunction with researchers in other divisions in the Aerospace Directorate.

Cockpit Displays for Low-Visibility Operations

There are a number of ways that a pilot's visual information requirements might be met under low-visibility conditions. Each alternative poses a number of research questions, however. Current systems for providing pilots with visual information in low-visibility conditions include light-intensifying goggles and thermal imaging systems. Computer-generated symbology or other types of graphic displays are often superimposed on a remotely-sensed video image, creating problems of display clutter, background stimulation interfering with visual tasks in the fovea, and incompatibilities when the sensor is off-axis with respect to the direction of helicopter movement.

State-of-the-art helmet-mounted displays not only limit pilots' abilities to extract motion cues (due to their narrow field of view), but also require pilots to shift their attention among sensor images and computer-generated symbology presented on the same display, panel-mounted displays, and environmental cues visible to the unaided eye. A research program has been initiated to examine the cognitive and perceptual demands thus placed on the pilots, establish guidelines about the use of monocular, binocular, and binocular HMD formats, and to propose alternative training methods to improve pilots' abilities to use such devices.

Advances in technology might enable computer-generated enhancement and display of remotely-sensed visual information. This possibility requires research on image-processing techniques, such as holography and stereoscopic systems, and matching display characteristics to the properties of the human visual system. Other systems, such as one under development at Ames might provide a low-cost "virtual" environment in which a pilot could visually explore 360 deg of computer-generated or remotely sensed environmental information with a wide-angle (120 deg) stereo display. The system might be controlled by pilot body or head position, gesture, or voice. This technology, however promising, is several years from practical application, however. Even greater advances in technology and vision modeling might eventually create machine vision systems to enable automated NOE flight.

Computational Model of Visual Flow Fields

Software tools, developed at Ames, can represent the visual information reaching the pilot's eyes, model how this information is used, and generate velocity flow fields. These analytic tools can be used to: (1) analyze the visual scene requirements (based on rate of movement, height above the ground, field of view, and terrain features) for various phases of flight, (2) determine the resolution and field of view requirements of helmet-mounted displays and obstacle-avoidance systems, (3) develop guidelines for the placement and properties of sensors to provide optimal information for human users, (4) provide guidance and control algorithms, and (5) specify the visual information requirements for NOE flight in low visibility. In addition, display formats are being developed which can provide pilots with additional information when available visual cues are inadequate (e.g., hovering with a narrow-field-of-view, monocular display).

Visual Flight-Path Control

Models of visual perception developed at Ames and aviation accident reports suggest that pilots may use inappropriate visual cues to control altitude. For example, a model of human slant perception was developed that can predict the errors that will occur under conditions of low visibility or on relatively featureless terrain. Even for landings that occur at airfields, the absence of visually perceptible perspective lines converging on the targeted touchdown point early in the approach can contribute to "landing short" accidents. The problem is particularly acute for the steep angles of approach that helicopters are capable of flying. Additional research is being conducted to determine the information that is provided by motion cues (such as naturally occurring optical flow patterns or those simulated on a cockpit display) to extend the utility of the model.

A part-task simulation was conducted to determine how pilots extract and use vehicle motion cues (represented by stylized perspective displays such as depicted in Figure 9a). Horizontal perspective lines (orthogonal to the direction of flight) contributed to better altitude control than did perspective lines (parallel to the direction of flight). Optical motion associated with lateral translations was misinterpreted as altitude changes, further contributing to altitude-control errors (Figure 9b).

Additional research was conducted to examine how pilots extract cues from panel- and helmet-mounted displays to maintain visual control of altitude while tracking targets moving off-axis to the direction of flight. The performance envelopes for three-dimensional target tracking using visually-coupled devices was examined with impoverished (perspective grid displays) and high-fidelity (computer-generated terrain) visual scenes. A part-task simulation established range, azimuth, and elevation parameters. Optical velocities accounted for most of the tracking errors; velocities as low as 30-40 deg/sec resulted in degraded performance. As the slant range of a target was decreased, a constant ground error was represented by an increase in displayed error on the helmet-

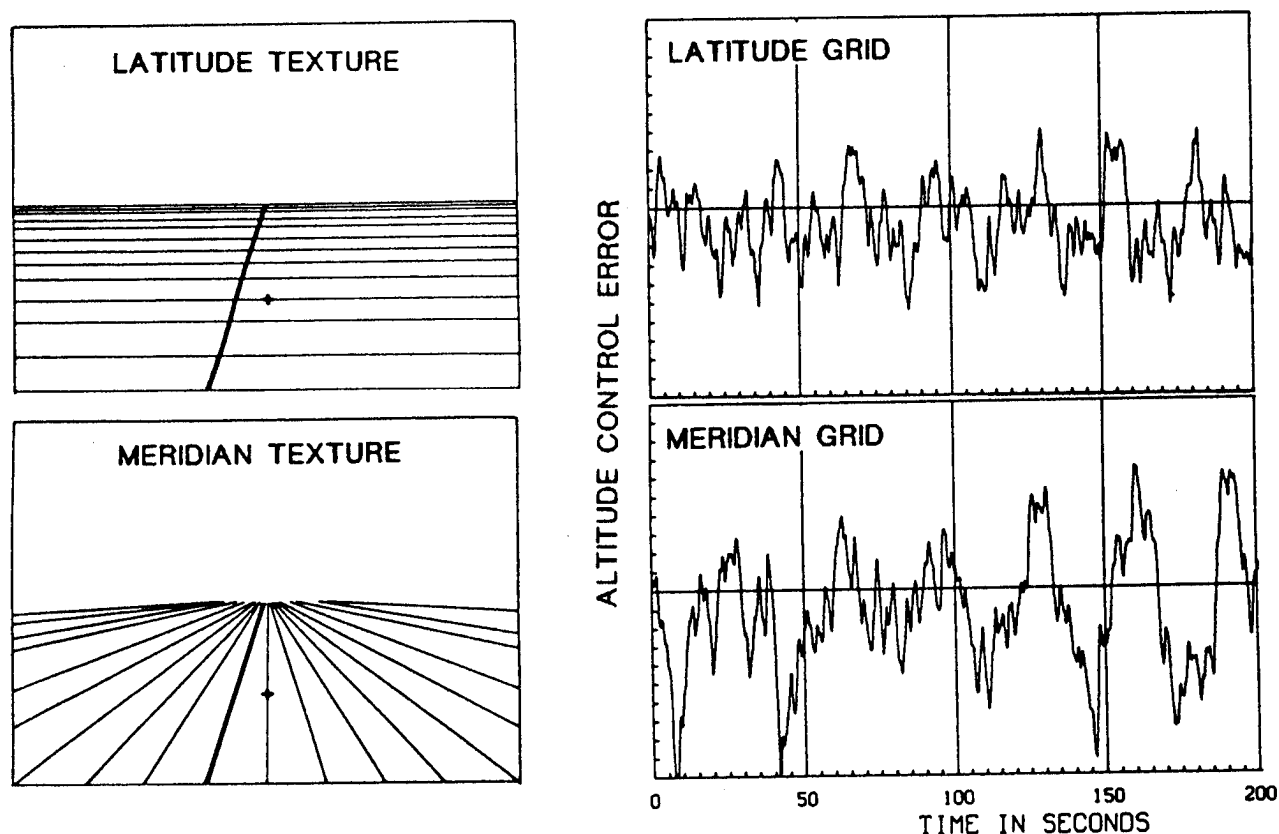


Figure 9: Altitude control performance using texture-augmented displays.

mounted display. Thus, line-of-sight errors projected onto the ground were minimized, rather than display error (the basic geometry is depicted in Figure 10).

A high-fidelity helicopter simulation evaluated the performance consequences of off-axis tracking in a more realistic setting. Army Apache pilots tracked moving targets from a hover or while in motion using information displayed on a Honeywell IHADSS. Target tracking was accomplished by the pilot-flying (Manual) or the pilot-not-flying (Automatic) under simulated day and night conditions. Preliminary analyses indicate that pilots had difficulty conducting simultaneous target tracking and aircraft control tasks. Again, optical velocity accounted for most of the tracking errors, ground errors remained relatively constant (although displayed error increased) as slant angle increased (Figure 11), and tracking performance was worse with curved flight paths than with straight.

Biodynamic Factors

The detrimental effects of vibration on visual acuity have been well documented for direct vision. They are even more severe with helmet-mounted displays where decrements are caused by relative motion between a displayed image (due to involuntary, vibration-induced head motions) and the eye. The normal vestibular-ocular reflex induces eye movements that oppose those of the head to maintain a stationary point of regard. While appropriate for viewing panel-mounted displays, it is not appropriate for helmet-mounted displays; relative motion is produced between the image on the head-coupled display and the eye, resulting in retinal blurring, increased errors and longer responses.

Based on a computer simulation of the vibration frequencies of helicopters, an adaptive noise-canceling technique has been developed at Ames, that minimizes the relative motion between viewed images and the eye by shifting displayed images in the same direction and magnitude as the induced reflexive eye movement. This filter stabilizes the images in space while still allowing the low-frequency voluntary head motions that are required for aiming accuracy.

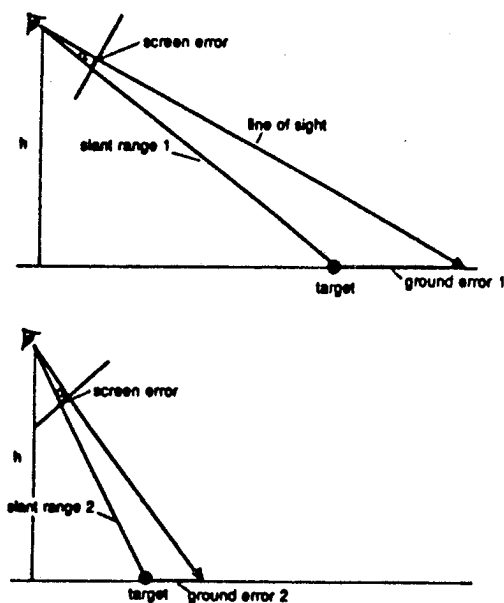


Figure 10: Screen error vs ground error: Basic Geometry

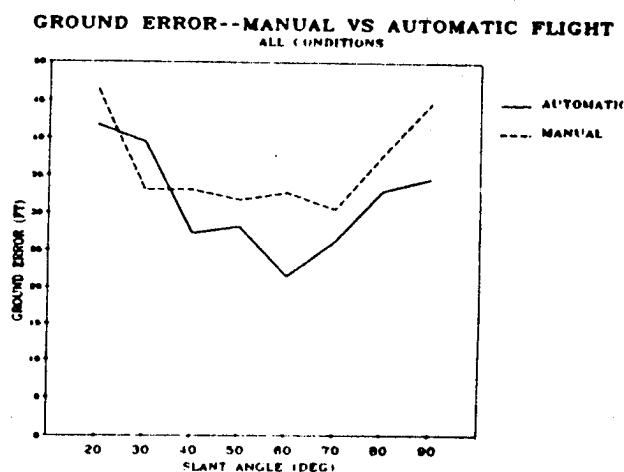
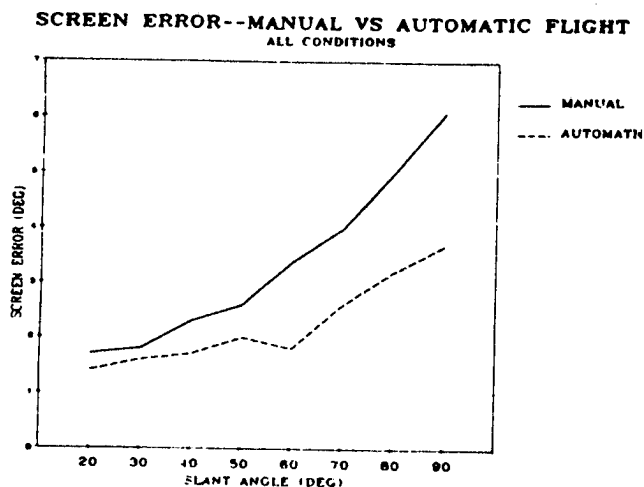


Figure 11: Manual vs automatic flight: Obtained screen error vs ground error.

Display Resolution

The problem of display resolution has been raised, particularly in conjunction with helmet-mounted pilot night vision systems. Research is required to determine whether the field of view is the key to enhancing the effectiveness of a night vision system, or rather the display resolution of the images, the addition of binocular cues, or other factors.

The computational model of human vision developed at Ames can be used to specify optimal spatial and temporal sampling procedures to enhance human visual performance using computer-generated displays, video displays provided by remote sensors, or computer-generated symbology superimposed on video displays. Depending on the display resolution available, accurate estimates can be made about visual information frequencies that can be displayed without distortion. In addition, by emulating the irregular sampling characteristics of the human vision system, the problem of aliasing can be avoided when generating visual displays.

Expert System for Symbology Evaluation

Most advanced helmet-mounted display designs include superimposed, computer-generated instrument displays. Although it is often possible to evaluate candidate symbologies empirically, a more effective method is to evaluate them in software. For example, an expert system has been developed by the Perception and Cognition

Group at Ames to automate the evaluation of helicopter display symbologies. The Ames Vision Model was used to compute the perceptual distances among alternative symbols and fonts to provide objective criteria for selecting perceptually distinct symbols.

TRAINING

The training research element includes theoretical development of optimal training strategies, application of these strategies in operational environments, and formulation of evaluation criteria for training programs. Our interest in training evolved from its apparent relationship with workload. Training is often proposed as a solution to workload problems, as it is assumed that both performance and workload are equally improved by training. However, the two research areas rarely, if ever, overlap and there is little empirical evidence to support such assumptions. In addition, the workload encountered by trainees must be monitored to ensure that: it is low enough to allow learning to take place, (2) training elements and promotion rules are derived logically, and (3) training time is optimized. Since the cost of training is escalating rapidly, low-cost, effective training methods are urgently needed.

NASA/Army Workshops

Ames co-sponsored two workshops with the U. S. Army to initiate this program element. The topic of the first workshop was the relationship between workload and training. The topic of the second workshop was individual differences in pilot selection, training, workload, and operational performance. Participants were invited from academia, industry and the government to discuss workload and training and their relationships in the context of advanced helicopter operations. The results of the workshop have been summarized in an Executive Summary and will be published in book form. The meeting was a great success in acquainting members of different research communities, revealing their problems, and discussing why there is such a limited flow of information and support among industry, academic and government research laboratories.

Theoretical Development

As a consequence of these two workshops, there has been a significant increase in research directed toward understanding the relationships among workload, training, and performance and in developing efficient and effective training strategies. Although training is essential in achieving acceptable levels of performance for complex systems, and it is often proposed as a solution for workload-related problems, the assumption that both performance and workload are improved equally by training appears to be unfounded. Furthermore, trainee workload must be monitored to ensure that it is low enough (for learning to take place), yet high enough to make optimal use of training resources.

Part-task training is one method by which acceptable levels of trainee workload can be achieved during the initial exposure to complex and difficult tasks. In part-task training, specific task elements are singled out for individual practice. The goal is to reduce the workload of these tasks (by achieving automatic performance) so they will not consume the cognitive resources required to learn the remainder of the task. A disadvantage is that these tasks must be re-integrated into the whole task to ensure that they can be performed collectively.

An alternative method has been suggested in which the whole task forms the basis of training, but priority instructions focus the trainee's attention on one element of the task at a time. This form of embedded part-task training achieves acceptable levels of workload by requiring that trainees learn and attend to only one element of the task at a time. Since the component tasks are presented in the context of the entire task, however, some time-sharing skills are developed during initial training, and integrating the component skills to promote efficient overall task performance presents less of a problem.

These and other training approaches have been evaluated in laboratory research and in the context of helicopter flight training. The goal is to identify which skills and task components are most likely to benefit from specific training strategies and to develop guidelines for developing training programs. Existing theoretical predictions form the basis of this research, although their applicability to complex skills, such as helicopter flight, had to be established. For example, laboratory research has suggested that performance and workload improvements would be found for "consistent" task components but not for "inconsistent" components. A consistent component is one for which specific information, display configurations, or system states are invariably associated with a specific response. By contrast, inconsistent components may require different responses each time they occur, and neither performance nor workload improvements occur as training progresses. This theory would predict that pilots would benefit from part-task training on target acquisition (a "consistent" task) but not from part-task training on vehicle-control training (a less consistent task). Alternatively, for tasks in which time-sharing is the most critical required skill, other theories would predict that part-task training methods would be less effective than whole-task training, because learning how to integrate or time-share two tasks that require common visual/manual resources can only be learned in the context of the whole task. To conduct this research element, an efficient method of performing task and skill analyses was developed to identify the specific skills that might be improved by either part-task or whole-task training methods. Several alternative training methods, including part-task, whole-task, and priority manipulation within a whole-task, have been examined in simulation research. For example, in a recent helicopter simulation, it was found that part-task training on more consistent task components (e.g., target acquisition) resulted in better vehicle-control performance in the integrated task than did part-task training on vehicle control *per se* (Figure 12). However, neither part-task training method was as effective as whole task training, as this whole-task training allowed pilots sufficient opportunity to develop necessary time-sharing skills in context. The results of this and other simulation research emphasize the importance of matching training procedures to the characteristics of individual task elements as well as to the structure of the integrated, target activity to achieve the most effective and efficient use of training time and facilities.

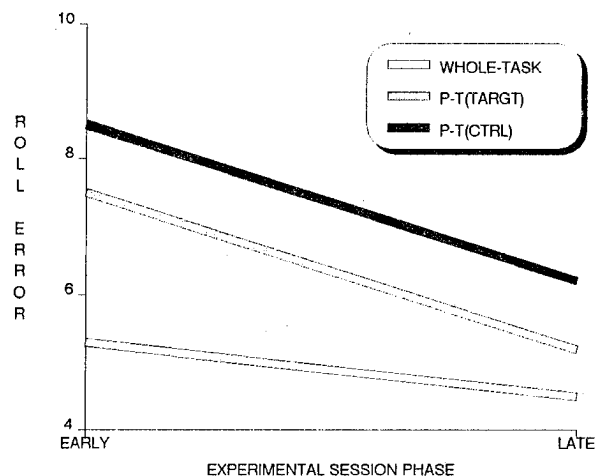


Figure 12: Comparison of three training methods in the

Training Procedures for Advanced Night-Vision Systems

Training pilots to use helmet-mounted, sensor-driven, night vision systems is one of the most demanding challenges faced by military and civilian users. Although these systems allow pilots to perform low-level missions at night and in low-visibility, they impose high workload and pilots are generally not able to achieve the same performance levels possible with direct vision. Furthermore, the cost of training is extremely high; training is currently conducted entirely in flight as adequate simulations do not yet exist. Thus, providing initial training in micro-processor-based, part-task simulators might provide an environment in which the perceptual and cognitive problems characteristic of this system could be resolved prior to the beginning of inflight training.

Pilots experience considerable difficulty during initial training with helmet-mounted pilot night vision systems. In addition, some of these difficulties persist even after many hours of use and skills degrade quickly if they are not used. A survey was conducted in which several key problem areas emerged: low resolution, reduced field of view, inadequate image definition, monocular display format, offset sensor location, superimposed HUD symbology, and helmet fit and weight. These system-related problems result in difficulties in detecting, identifying, and tracking objects, binocular rivalry (between the aided and unaided eyes), motion parallax, poor motion, depth, and range perceptions, and visual fatigue. These, in turn, limit performance and mission duration.

These results prompted research to identify the underlying perceptual and information processing mechanisms which must be addressed during training and to establish optimal learning strategies. The goal is to develop guidelines for a low-cost, microprocessor-based training program which will allow pilots to develop the skills necessary to use such systems effectively.

In parallel, a research program was established to evaluate the effectiveness of microprocessor-based training programs in the acquisition and performance of general flight-management skills. The goal is to evaluate the effectiveness of complex computer games in improving the acquisition and performance of flight management skills. The underlying rationale is that the strategies and cognitive skills learned by interacting with low-cost computer games can be generalized to the learning and performance of complex operational tasks. Cognitive skills training will be provided to half of the members of an incoming class of pilots during basic flight training. The total training times, flight school retention statistics, and flying performance of the two groups of pilots will be compared and a longitudinal study of their operational performance will be conducted.

To date, a task/skill analysis has been completed and the training program has been developed. Field tests began in October 1987 with a group of incoming pilot-trainees. Total training times, flight school retention statistics, and flying performance will be compared to those of pilots in the standard training program. If the cognitive-skills-training procedures prove to be effective, then a ground-based training system will be developed to improve pilot performance with night vision systems. This system will train pilots how to interpret superimposed symbology, focus and shift their visual attention, compensate for the loss of peripheral cues, and adapt to the distortions and resolution limitations of current (and projected) helmet-mounted, night vision systems.

SUMMARY

At each stage in the research process, information obtained in more realistic situations was used to refine theoretical models and provide the focus for well-controlled laboratory studies to address specific issues. By moving back and forth between the three research environments, the requirements of theoretical development can be balanced against the requirements of the "real world". Furthermore, operational relevance can be insured at the same time that the predictive advantages of a theoretical foundation can be maintained. If theoretical researchers cannot become familiar with applied problems (through participation in simulation and inflight research) and if designers, engineers, and operational test and evaluation personnel are not exposed to the advantages of experimental control, a theoretical foundation, and the use of validated measures, the advances made in none of these fields can be capitalized upon.

This is the unique role that a government research laboratory, such as Ames Research Center, can play. Here, scientists, engineers, and pilots work in close proximity to each other and can conduct collaborative research in which each can take advantage of the other's knowledge and tools to provide a strong research foundation that can be transferred to industry. If nothing else, this environment creates a unique opportunity for each group to learn the other's language. This provides a vehicle for translating the considerable data base available in academia and the pragmatic experiences of designers, engineers, and pilots into a useful body of knowledge.

ROTORCRAFT HANDLING-QUALITIES DESIGN CRITERIA DEVELOPMENT

Edwin W. Aiken, J. Victor Lebacqz, Robert T. N. Chen, and David L. Key,*

Ames Research Center

SUMMARY

Handling qualities are those qualities or characteristics of an aircraft that govern the ease and precision with which a pilot is able to perform those flight tasks required in support of an aircraft mission. These qualities include not only the basic vehicle stability and control characteristics but also the displays and controllers that comprise the pilot-vehicle interface. Joint NASA/Army efforts at Ames Research Center to develop rotorcraft handling-qualities design criteria began in earnest in 1975. At that time, primarily because of the need to simulate Army missions embodying the new doctrine of nap-of-the-Earth (NOE) operations and the emergence of Ames as the lead rotorcraft research center for NASA, the development of both ground-based and flight research facilities was initiated. Notable results of this effort were the UH-1H VSTOLAND variable stability helicopter, the VFA-2 camera-and-terrain-board simulator visual system, and the generic helicopter real-time mathematical model, ARMCOP. Using these facilities, an initial series of handling-qualities studies was conducted to assess the effects of rotor design parameters, interaxis coupling, and various levels of stability and control augmentation. In addition, the effects of the format and dynamics of electronic display symbols were investigated for NOE tasks conducted during night and adverse weather conditions.

Further improvements in the capability for rotorcraft handling-qualities research occurred in 1979, when the Vertical Motion Simulator became operational, and in 1982, with the addition of a multiwindow, computer-generated-imagery visual system. Using these new facilities, many noteworthy research efforts were, and are continuing to be, conducted. Included among these are investigations of the effects of side-stick controllers, roll-control requirements, directional-control requirements, and requirements for helicopter air combat agility and maneuverability. The capability of the current research facility to conduct moving-base simulations of near-terrain helicopter air combat is unmatched and is critical for this newly defined mission.

The ability to conduct in-flight handling-qualities research has been enhanced by the development of the NASA/Army CH-47 variable-stability helicopter. This

*Aircrew-Aircraft Systems Division, Army Aeroflightdynamics Directorate, Moffett Field, California.

facility allows the investigation of a wide range of control response and electronic display characteristics in the actual flight environment. Research programs conducted using this vehicle include vertical-response investigations, hover augmentation systems, and the effects of control-force characteristics.

The handling-qualities data base created by these and other experimental programs was judged to be sufficient to allow an update of the military helicopter handling-qualities specification, MIL-H-8501. That effort was initiated in 1982 and, by December 1985, a version was ready to be included as part of the request for proposals for the new Army Family of Light Helicopters, LHX.

This report summarizes these efforts, including not only the in-house experimental work but also contracted research and collaborative programs performed under the auspices of various international agreements. The report concludes by reviewing the topics that are currently most in need of work and the plans for addressing these topics.

INTRODUCTION

Handling qualities are "those qualities or characteristics of an aircraft that govern the ease and precision with which a pilot is able to perform the tasks required in support of the aircraft role" (ref. 1).

Handling qualities may, therefore, be thought of as being a measure of the degree to which the pilot is able to exploit the aircraft's inherent performance potential, with acceptable workload and training. The effect of inadequate handling qualities is less obvious than is an error in structural limit and weight or drag estimation. This situation occurs because handling-qualities involve the ability of the pilot to perform certain mission tasks, and pilots are very adaptable; moreover, the performance requirements for mission tasks are usually ill-defined. Thus, the tasks may still be performed even though the pilot is overworked and, perhaps, only marginally in control. Such shortcomings manifest themselves as high accident rates (pilot error is the most common cause of accidents), pilot fatigue, and excessive training required to develop and maintain proficiency.

A more obvious example in which better handling-qualities design capabilities may have avoided a problem is the redesign of the AH-64 Apache empennage from a T-tail to a low-mounted, horizontal stabilizer late in the development program. Similarly, better criteria and simulation capabilities may have avoided potential problems with the UH-60 Black Hawk stabilator, which even now is undergoing design changes. High-performance fixed-wing aircraft are replete with handling-qualities problems discovered at or after first flight, even though the data supporting fixed-wing handling-qualities criteria and specifications are better defined than they are for rotorcraft.

Many modern rotorcraft missions involve flight close to the ground or near obstacles such as ships. These missions demand a continual precision of control

that is necessary in other aircraft only during takeoff and landing or in formation flight. To perform these missions, the outside world has to be visible at all times, and yet the user wants to operate in poor weather and at night. As a result, vision aids have to be used, and, since it will be many years before vision aids provide anything close to the fidelity of looking out the window in visual meteorological conditions (VMC), the visual cues can be expected to be degraded and therefore to have a major effect on handling qualities.

Many of these low-altitude, low-speed mission tasks are performed relative to some ground-fixed reference, so even a constant wind is a complicating handling-qualities factor. Local objects, such as buildings, trees, or hills can disturb the airflow to make the task even more difficult. Another unique mission capability of rotorcraft is their ability to carry slung loads. This introduces many complications to the overall handling-qualities task. These mission characteristics not only make helicopter handling qualities very demanding and critical to mission accomplishment, but also very difficult to reproduce in a simulator for research, development, or training.

In addition to the missions performed by rotorcraft, the vehicles themselves have many unique characteristics with implications for handling-qualities needs and criteria development. Because of their complex aerodynamics, they are exceedingly difficult to represent mathematically for accurate analysis and simulation. For example, there are complex interactions between the main and tail rotors. When flying at low speed, the low dynamic pressure means that small perturbations in flight direction or wind can have large effects on the rotorcraft forces and moments. The kinematics are more predictable but still highly complex. The overall result is that considerable cross-coupling exists between longitudinal and lateral directional axes (pitch-to-roll, collective control to yaw, etc.); responses to control and disturbances are nonlinear, so that response to control is different to the left than to the right; and the responses change nonlinearly with the size of the disturbance. In addition, many of these effects are frequency-dependent.

Another ramification of these complexities that is important for handling qualities is the multiplicity of limits that the pilot has to observe. These limits tend not to be unique. For example, normal load-factor limit depends on the mix of longitudinal cyclic and collective control used to induce the load-factor excursion. Many limiting parameters are difficult to sense, and few limits are indicated to the pilot. As a result, pilots tend to give dangerous limiting conditions a wide berth so they stay well within the available performance envelope instead of exploiting the rotorcraft's full potential.

Finally, the critical factor in handling qualities, the pilot, is subjected to a unique environment of high noise, high vibration, and extreme temperatures. As a result, most old helicopter pilots are hard of hearing and have bad backs.

Methods of achieving good handling qualities are indicated in figure 1. Clearly, the cost of making any changes to correct deficiencies increases as the aircraft moves into the later development stages, so handling-qualities criteria and

specifications significantly affect development cost. Handling-qualities criteria and specifications can provide the following capabilities:

1. The ability for the Department of Defense (DOD) and the manufacturers to make intelligent, informed design trade-offs during aircraft design and development.

2. A central source of design guidance when the data are documented and compiled in a handling-qualities specification. This will help avoid repeating past mistakes each time a new aircraft is developed or an existing aircraft modified.

3. A method for DOD agencies to effectively monitor, guide, or evaluate the manufacturer's research and designs.

The current helicopter handling-qualities specification, MIL-H-8501, was written in 1952 with a minor revision in 1961. It has long been recognized as obsolete (refs. 1, 2). Table 1 indicates the primary deficiencies of MIL-H-8501 and also summarizes the characteristics of other proposed specifications. Despite these shortcomings, MIL-H-8501 is still being used for testing by the flight-test community; yet, it is ignored for mission-suitability assessment. A new specification is essential.

In 1975 the Army recognized these specification deficiencies and, in collaboration with NASA, started a major effort to develop a data base and design criteria that could eventually be integrated into a new specification. By 1982, sufficient progress had been made to justify initiating the development of a new specification. Army responsibility for helicopter specifications rests with the Aviation Systems Command (AVSCOM) Directorate of Engineering, but the effort to generate the new specification is being led by the Aeroflightdynamics Directorate of ARTA, with help from Ames Research Center. The work is monitored by a Technical Review Committee having representation from Army user organizations; Army test organizations; the Navy, through the Naval Air Development Center and the Naval Test Pilot School; the Air Force Wright Aeronautical laboratories; and the Federal Aviation Administration (FAA). Manufacturers have been involved at every step. A version oriented at LHX was developed and adopted by AVSCOM as an Airworthiness Design Standard (ADS-33) in December 1985. This standard was distributed with the LHX draft request for proposals in 1986. Since that time, efforts have been made to expand its coverage to other types of helicopters so that it can become a credible generic specification.

The purpose of this report is to review these Army/NASA efforts in rotorcraft handling qualities. First, the development of major ground and flight-research facilities is described; then ground-based and flight-based research are reviewed. The ground and flight research sections are divided into two parts: tasks conducted in VMC and tasks conducted in instrument meteorological conditions (IMC) or in night conditions for which displays and vision aids play a large role. Finally, the status of these efforts in providing a data base for the specification is assessed, and recommendations for future rotorcraft handling-qualities research are provided.

GROUND-BASED AND IN-FLIGHT SIMULATION FACILITIES

Ground-Based Simulation Facilities

In order to conduct handling-qualities research in an efficient and safe manner, a necessary element in the approach to that research is the use of ground-simulation facilities. These facilities can be very productive sources of handling-qualities data, and their use is mandatory for investigations of handling qualities under hazardous conditions such as exist at night, during adverse weather, or with equipment failures. However, the validity of these data is heavily dependent on the fidelity of the various components of the simulation environment, including the vehicle mathematical model, the system used to provide the visual cues from the outside world, and the cockpit motion simulation.

Over the past decade, a significant number of rotorcraft handling-qualities investigations, many of which are summarized herein, have been conducted using the Ames ground-simulation facilities. The requirements for these and other research programs have provided the impetus for continuing improvements in the piloted simulation capabilities at Ames. This capability to perform rotorcraft simulation has progressed from the use of fixed-base facilities with limited field-of-view, low-resolution, camera-and-terrain board visual systems to simulators with limited cockpit motion capabilities and later to large-amplitude, moving-base simulators with wide field-of-view, high-resolution, computer-generated visual displays. This progression is illustrated by the following summary of the attributes of three of the major Ames moving-base simulator facilities which have been heavily utilized in rotorcraft handling-qualities experimental research programs. A more detailed discussion of rotorcraft simulation technology at Ames is contained in reference 3.

The Six-Degree-of-Freedom Motion Simulator (fig. 2) became operational in 1964. Although the translational motion of this facility is limited to an 18-ft cube, it is an extremely useful tool for the investigation of precision hover handling qualities. In the cab configuration illustrated in figure 2, the pilot is provided with real-world visual cues, and the motion system is set up to reproduce the actual motions of the simulated aircraft within the physical limits of the motion system. Investigations of handling-qualities requirements for hover translational rate command systems have been conducted in this configuration. Alternatively, the cab may be covered, the motion system software altered, and visual cues provided by a single, black-and-white, TV monitor (fig. 3). This cab configuration was used in an investigation of control and display requirements for a night and adverse weather attack helicopter mission. In this experiment, the source of the visual cues was a camera-and-terrain board visual system suitable for NOE flight simulation. Superimposed on the terrain board imagery were selectable sets of symbols generated by a computer graphics system.

In 1969, the Flight Simulator for Advanced Aircraft (FSAA) became operational (fig. 4). This facility was originally designed for fixed-wing aircraft research and includes a capability for high-fidelity lateral motion cueing -- a total of 80 ft -- for the simulation of sideslip during landing approach or engine failure during

takeoff. Much of the initial work on NOE handling qualities and FAA rotorcraft certification requirements for IFR flight was conducted on this facility. Fundamental limitations of the FSAA for rotorcraft research simulations were the restricted field of view associated with the simulator visual system -- approximately 34° by 48° -- and the limited fidelity of the vertical motion cueing caused by the 8 ft of available vertical travel.

As a direct result of the burgeoning requirements for improved-fidelity rotorcraft simulations, the Vertical Motion Simulator (VMS) was designed and developed (fig. 5). Its 60 ft of available vertical travel allows an extremely high level of fidelity in vertical motion cueing. By rotating the cab about its vertical axis, the experimenter may tailor the motion system capabilities in the longitudinal and lateral axes to his own requirements; the available 40 ft of travel has been used in the lateral axis for experiments that evaluate the use of sideslip in air combat, for example, or in the longitudinal axis for investigations in areas such as the potential benefits of thrust-vector control for NOE flight. In addition, a wide-field-of-view, four-window, high-resolution, computer-generated-imagery system provides a significant improvement in the ability to supply the pilot with a compelling visual environment. One of the four visual channels may be used to represent the view from an independent eye point, thus allowing the simulation of an opponent aircraft in air combat or the representation of the image from a remote sensor. Since it became operational in 1979, the VMS has supported simulations of rotorcraft such as the UH-60 Black Hawk, the Rotor Systems Research Aircraft, the XV-15 and V-22 tilt-rotor aircraft, and the X-Wing. Simulated mission tasks include NOE flight, touchdown autorotations, shipboard landings, landing approaches to oil rigs, terrain-following/terrain-avoidance, and helicopter air combat.

Although marked improvements have been made in the ability to simulate rotorcraft flight in the near-Earth environment, it will likely never be economically feasible to duplicate that flight environment. Significant simulation deficiencies for handling-qualities research still exist. These shortcomings, which include items such as visual system computational-time delays and dynamic mismatches between simulated and real-world motion cues, cast some doubt on the absolute validity of handling-qualities data generated solely in piloted simulations and make mandatory the use of in-flight simulation using variable-stability rotorcraft to verify the simulation results. In addition, these research aircraft may be used as tools to assist in the efforts to improve the fidelity of rotorcraft simulation. Ground- and in-flight simulation, therefore, must be considered as integral elements of experimental handling-qualities research.

In-Flight Simulation Facilities

For experimental handling-qualities research, the validation of results from ground-based facilities in the actual flight environment is considered to be of fundamental importance. This requirement implies, for generic research not tied to a specific vehicle, that a flight facility with variable stability, control, and display capabilities be developed and used as an integral research tool. This need

has been filled for the NASA/Army handling-qualities research primarily by two vehicles: the modified UH-1H and the modified CH-47B helicopters.

The UH-1H helicopter was modified to provide an in-flight simulation capability by adding an avionics system called VSTOLAND (fig. 6). The system provides integrated navigation, guidance, display, and control functions through two flight digital computers; it may be operated with or without flight-director commands, in the modes of manual, control-stick steering (CSS), autopilot, or research. A block diagram of the system components is shown in figure 7; a more complete description of the system capabilities is given in references 4 and 5.

The flight-control portion of the VSTOLAND system uses a combination of a full-authority parallel servo and a limited-authority (20% to 30%) series servo in each control linkage. In addition, disconnect devices exist in the left cyclic controls to allow for a fly-by-wire mode through this research cyclic stick. The right stick, or safety pilot side, retains the standard UH-1H cyclic and cockpit instruments. Handling-qualities experiments are conducted in the research mode, with the software providing a set of flight-control laws with variable gains. A schematic diagram of one such control-law channel is shown in figure 8 to illustrate the operation of the system.

Although suitable for generic investigations of configurations not too dissimilar to that of a UH-1H, the VSTOLAND UH-1H implementation using limited-authority series servos, in combination with flight envelope restrictions imposed by the teetering rotor system and control authority of the basic machine, resulted in insufficient research flexibility to examine a broad range of rotorcraft flight-control and handling-qualities issues. Accordingly, the CH-47B, originally modified for the TAGS program (ref. 6) and subsequently used by NASA Langley for terminal-area investigations (ref. 7), was further modified and extended for NASA/Army handling-qualities and flight-control research at Ames

The CH-47B (fig. 9) is equipped with full-authority, electrohydraulic actuators in each of the four control axes: differential collective (pitch), lateral cyclic (roll), differential lateral cyclic (yaw), and collective (heave). These actuators receive position commands generated by control laws that are programmed in on-board digital and analog computers. Their output motion is transmitted to the flight-control system of the basic CH-47B through electrohydraulic rotary clutches, thereby causing the safety pilot's controls to move in parallel. Downstream from these clutches and their associated mechanical linkages, there are essentially no modifications to the basic flight-control system of the standard production CH-47B. Figure 10 shows the implementation of the electronic control system (ECS) for a typical axis. Electric control inputs from the evaluation pilot's controls (center-line or side-stick) are combined in the flight computers with data from the motion sensors to generate commands to the parallel ECS actuators that drive the basic CH-47B flight-control system.

The various controls, displays, sensors, and computers that make up the research system are shown schematically in figure 11. The CH-47B is equipped with a Sperry 1819A minicomputer; a Digital Equipment Corporation PDP 11/73 microcomputer;

and an Electronic Associates, Inc. TR-48 analog computer. To support instrument-flight tasks with the aircraft, a Sperry Flight Systems color electronic attitude director indicator (EADI) is also installed. Finally, unlike the UH-1H, the evaluation pilot's center stick has been modified to incorporate a programmable artificial feel and trim system manufactured by the Calspan Corporation; a right-hand, four-axis, small-displacement side-stick controller is also available for use in selectable combinations with the existing conventional collective and pedal controllers. A complete description of the facility is given in reference 8.

GROUND-BASED EXPERIMENTAL RESEARCH

Visual Meteorological Conditions

The major initial focus of the rotorcraft handling-qualities research performed by NASA and the Army was to ascertain requirements for near-terrain and NOE flight in visual conditions. The need for these new requirements resulted from evolving Army doctrines that emphasize low-level flight to enhance mission survival and effectiveness, and it was recognized that the existing data base was entirely inappropriate for the new tasks that were envisaged. Accordingly, a series of analyses, piloted ground-based simulations, and flight experiments involving terrain-flying tasks and low-altitude tactical missions was initiated.

Studies and experiments designed to examine the effect of aircraft design parameters, interaxis coupling, and levels of stability and control augmentation on the handling qualities and man-machine performance of the low-level flying tasks in VMC were performed initially to provide generic design information (refs. 9-15).

The first visual terrain-flight experiment was conducted on a fixed-based simulator to explore the effects on the handling characteristics of basic single-rotor helicopters of large variations in rotor design parameters, such as flapping-hinge offset, flapping-hinge restraint, blade inertia (or Lock number), and pitch-flap coupling (ref. 9). In the second ground-based simulation experiment, representative configurations from the first experiment were evaluated on a moving-base simulator (the FSAA) to examine the effect of motion cues (ref. 10) and the effects of various levels of stability and control augmentation (ref. 11). A more sophisticated stability and control augmentation system (SCAS) was also synthesized, using linear optimal control theory to meet a set of comprehensive performance criteria (ref. 12). This system, designed expressly for a hingeless-rotor helicopter, was subsequently evaluated in the third piloted ground-simulator experiment on the FSAA. A flight experiment (ref. 13) was conducted on the variable-stability UH-1H/VSTOLAND helicopter to verify some selected configurations from the first two ground experiments, to explore additional configuration variations, and to investigate the effect of field of view on helicopter handling qualities for NOE operations. To relate directly some of the results of these handling qualities experiments to the design parameters of the helicopter, an analytical study was conducted

to develop a design rule for the selection of some primary rotor parameters to decouple the longitudinal and lateral motions of the helicopter (refs. 14, 15).

Taken together, these experiments provide a significant design data base concerning the influence of basic helicopter characteristics on pilot acceptance of near-terrain tasks. For example, the influence of coupling from the collective control into pitch and yaw is illustrated for a hingeless rotor helicopter in figure 12; the importance of reducing these couplings can be seen by the improvement of the Cooper-Harper ratings (ref. 17) to "satisfactory" as the couplings are reduced. Similar results were obtained from experiments concerning pitch-roll coupling resulting from aircraft angular rate. In particular, a criterion with respect to the ratio of the roll moment caused by pitch rate to that caused by roll rate and design procedures to minimize this coupling were developed. Recent studies are expanding this information to include limits on the frequency dependency of the coupling (ref. 18).

Following this initial series of experiments that focused on design parameters, more specialized experiments were directed at particular responses of concern. The effects of thrust-response characteristics on rotorcraft handling qualities have been and are being investigated in both ground- and in-flight simulation programs at Ames. Thrust response to the pilot's collective inputs is a complex function of engine-governor dynamics, rotor inertia effects on energy stored in the rotor, excess thrust available, and aircraft vertical damping. A multiphase program is being conducted to study these effects on helicopter handling qualities in hover and during representative low-speed NOE operations. Three moving-base piloted simulations have been conducted on the VMS to provide criteria and substantiating data for the updated MIL-H-8501 specification (refs. 19, 20). The results of these investigations are summarized in reference 21.

Based on these experimental results, the proposed vertical-axis requirements include criteria for the time-constant of the altitude rate response to collective input, the shape of that same response, rotor angular speed limits, and vertical control power. The current VMS investigation focuses on three concerns associated with the proposed criteria: (1) conservative vertical damping requirements, (2) conservative control power requirements, and (3) the effects of the shape of the altitude-rate time-response to a collective input. Preliminary results indicate that, when the pilot has sufficient time to perform a bob-up task, satisfactory handling qualities are achieved with very low values of vertical damping (fig. 13); results from a dolphin task also support the need to relax the proposed boundaries. Similarly, the effects of low values of control power are only apparent when the constraints on time required to perform the maneuver are severe. The results from the investigation of the effects of the shape of the altitude-rate response generally support the current requirement but indicate a strong dependence on the details of the task being performed.

Another response-oriented major shortcoming in the current handling-qualities data base is the lack of roll-control effectiveness criteria. This fundamental requirement has a major effect on the basic design of a helicopter. Analyses and two VMS simulations have been conducted to determine a systematic approach to

specifying roll-control effectiveness requirements for maneuvering (ref. 22). The results of this program showed that control power requirements can be relaxed for large-amplitude maneuvers such as are required in air combat, and that satisfactory handling qualities are obtained when a sufficiently large margin exists between vehicle performance capability and the requirements of the task. The short-term roll response of the vehicle, determined by rotor stiffness and control-system characteristics and expressed as bandwidth, has a significant effect on handling qualities and performance; this effect is a strong function of task demands (fig. 14).

To compensate for a similar lack of mission-oriented handling-qualities data, a piloted simulation was conducted (ref. 23) to evaluate the effects of the following on the handling-qualities characteristics of various generic rotorcraft configurations including tilt-rotor, coaxial rotor, and no-tail-rotor designs: (1) mission task requirements, (2) basic yaw sensitivity and damping, and (3) directional gust sensitivity. The results of the experiment indicate that rotorcraft configurations with high directional gust sensitivity require more yaw damping to maintain satisfactory handling qualities during NOE tasks. Both yaw damping and control-response characteristics are critical parameters in determining handling qualities for an air-to-air target-acquisition and tracking task. Loss of directional control can occur at low airspeeds under certain wind conditions in which yaw damping is low and gust sensitivity is high.

The characteristics of the controllers to effect these vehicle responses are also important; they are highlighted by the recent trend toward side-stick controllers with multi-axis functions. The first real rotorcraft application of these new controllers was the U.S. Army's Advanced Digital/Optical Control System (ADOCS) program. For this program, a series of piloted simulations was conducted both at the Boeing Vertol facility and on the VMS to assess the interactive effects of side-stick controller (SSC) characteristics and stability and control augmentation on handling qualities (ref. 24). An initial experiment revealed that angular rate stabilization in pitch and roll was sufficient to provide satisfactory handling qualities when a two-axis SSC was used for control of these axes; however, when a rigid three- or four-axis device (which added directional and directional-plus-collective control, respectively to the SSC) was used, attitude stabilization was required to maintain adequate handling qualities (ref. 25). These results were substantiated and expanded upon by the experiment reported in reference 26, which demonstrated that a four-axis, small-deflection SSC yielded satisfactory handling qualities for NOE tasks when it was integrated with a SCAS that incorporated higher levels of augmentation; however, separated controllers were required to maintain satisfactory handling qualities for the more demanding control tasks or when reduced levels of stability and control augmentation were provided (fig. 15).

A summary of the effects of SSC characteristics on terrain flight handling qualities based primarily on the ADOCS results is contained in reference 27. The general approach to these experiments provided the basis for the structure of the proposed updated version of MIL-H-8501 according to control-response types. In addition, the results of this program have had a significant effect on the types of

control systems and cockpit controllers currently being developed for the candidate LHX designs in the Advanced Rotorcraft Technology Integration program.

Very recently, the use of rotorcraft in the air-to-air combat environment has become a major new mission requirement for future vehicles. To define handling-qualities capabilities that are necessary for this new role, the Army and NASA initiated modifications to the VMS facility that would permit simulations of air-to-air combat in the near-terrain environment, with good duplication of both visual and motion cues. The initial experiment emphasized the development of this facility capability and included an initial investigation of generic influences of rotor type and stability/control augmentation (ref. 28).

On this basis, the second experiment included a systematic investigation of maneuvering envelope size (normal load factor, sideslip) and directional axis dynamics, using a simplified generic helicopter model (ref. 29). Figure 16 illustrates the aggregate use of sideslip and normal acceleration envelopes in this experiment for three levels: one representative of an AH-1, one of a UH-60, and one expanded for a projected new helicopter LHX. These results indicate that a lower load-factor limit of -0.5 g may be adequate--a value lower than -1.0 g was never achieved. One design implication, of course, is that rotor systems that do not permit any negative g are not suitable for this role. In addition, maximum load factors greater than that achievable with present helicopter designs were often used by the pilots, and the limits presented to the pilot were at times exceeded for all of the configurations. Automatic envelope limiting may be required to use an expanded capability successfully. It was also found that the most successful pilots used aircraft sideslip performance to significant advantage, with an envelope representative of current utility helicopters being adequate; a potential trade-off of this characteristic with a turreted gun will be examined in an upcoming experiment.

In addition to experiments aimed at defining specific handling-qualities characteristics, such as those described above, more general investigations have been conducted which both exploit and examine the ability of ground simulation to address questions that might be difficult to deal with in flight. One example is the study of autorotation requirements and the simulator capabilities required to investigate this flight phase (ref. 30). Among the variables considered in the experiment was the level of vertical-motion cueing being provided in the simulation; four values ranging from fixed-base up to the full ability of the VMS were investigated.

Figure 17 shows representative plots of collective control use as a function of allowable vertical-axis travel for one pilot. In general, this pilot exercised the proper control technique with the full VMS motion. As the motion performance degraded, the pilot's collective technique changed. Many landing flares with degraded motion performance showed signs of ballooning, stair-stepping, and overcontrol in the collective time-histories. Not all pilots were so affected, and even with full VMS motion, some pilots would show some of the poor control techniques illustrated in figure 17. However, the trend shown did occur for several pilots. It is suggested that, when the control technique used in the simulator is significantly different from that used in flight, confidence in simulator-based research results or in flight-training transfer is reduced.

The issues of transfer of training also become important in the new environment of single-pilot operations in high workload environments. With the exception of research for single-pilot IFR in the civil/FAA context (to be reviewed later in this paper), single-crew concepts had not been considered in helicopter flight-control research. However, the advent of the Army's desire for a single-crew scout/attack helicopter called Light Helicopter Family (LHX) puts more emphasis on single-crew workload. In such a situation, the pilot has to not only control the flight path of the rotorcraft but also perform innumerable other tasks associated with navigation, communications, and threat avoidance or attack. Two experiments, Single Pilot Advanced Cockpit Engineering Simulation (SPACES I and II), were performed on the VMS to investigate these effects (ref. 31). The objective was to determine the SCAS configuration that, when combined with appropriate cockpit displays and controls, would allow adequate mission performance.

The simulation used a highly integrated glass cockpit with helmet-mounted displays, multi-axis side-stick controllers, voice input/output (I/O) systems, moving map displays, programmable switching, sophisticated sensors and detectors, and limited artificial intelligence (expert systems) to improve pilot-vehicle performance.

These tests showed that superimposing the mission management tasks on flight-path management tasks results in degraded handling qualities. Of the configurations investigated, only the SCAS with heading, altitude and airspeed hold, plus turn coordination was rated satisfactory (Level 1) by Army test pilots for single-pilot NOE flight operation at tested conditions. Each axis was augmented sufficiently so that attention to flight-path tasks could be reduced, allowing additional time for accomplishment of mission management tasks.

For two reasons, the pilots considered altitude hold to be the single most important feature in NOE flight: (1) it allowed the pilot to use his left hand for mission management tasks, and (2) it provided terrain avoidance when the pilot could not constantly monitor altitude because of other duties.

Instrument Meteorological Conditions

The requirement that rotorcraft operations be conducted at night and under other conditions of limited visibility has given impetus to research programs designed to investigate the interactive effects of vision aids and displays on handling qualities.

In a program conducted to support the development of the Advanced Attack Helicopter (AAH), various levels of stability and control augmentation together with variations in the format and dynamics of the symbols provided on the Pilot Night Vision System (PNVS) (fig. 18) were investigated in a piloted simulation (ref. 32). It was found that the handling qualities of the baseline control-display system were unsatisfactory and required improvement; recommendations for alterations to the PNVS symbol dynamics and the implementation of a velocity-command system for a hover/bob-up/weapon-delivery task were made to the Army AAH program manager. The

velocity-command type of control system was subsequently incorporated into the AH-64 flight-control systems as a selectable hover augmentation system. The approach taken in the design of this experiment heavily influenced the methods used in the ADOCS simulator investigations and the structure of the control laws designed and investigated in those experiments.

An investigation involving the simulation of a less complex night vision aid was conducted to support the Army Helicopter Improvement Program (AHIP) (ref. 33). In that simulation, the effects of presenting the PNVIS flight symbols on a panel-mounted display (PMD) versus a head-up display (HUD) were compared for a nighttime scout helicopter mission in which the pilot was provided with night-vision goggles. As a consequence of the experimental results, the OH-58D now includes a pilot's HUD which provides information complementary to that which is available on the instrument panel.

The state-of-the-art night-vision system for combat helicopters includes a visually coupled helmet-mounted display of infrared imagery and superimposed symbols: the Integrated Helmet and Display Sight System (IHADSS) (fig. 19). This system was used in two simulator investigations designed to assess the effects of reduced visibility conditions on the ADOCS visual flight simulation results cited previously (refs. 34, 35). Significant degradations in handling qualities occurred for most tasks flown with the IHADSS relative to the identical tasks flown under visual flight conditions (fig. 20). In general, higher levels of stability augmentation were required to achieve handling qualities comparable to those achieved for the visual flight tasks.

These simulation results have substantiated the highly interactive effects of vision-aid/display characteristics and control-response types on handling qualities requirements under IMC. In recognition of these effects, the proposed update to MIL-H-8501 incorporates a scheme for determining required control-response types based, in part, on the type and quality of the visual cues available to the pilot from vision aids and displays during IMC missions.

Research has also been conducted to ascertain IFR approach requirements for helicopters operating with simpler SCAS and display systems. This work has been aimed at both military and civilian instrument operating conditions and was performed as part of a joint NASA/FAA/CAA program. Six experiments were conducted; they had the following general objectives:

1. First experiment (ground simulation, ref. 36): develop generic models of current helicopters having three different rotor types; explore SCAS concepts and influence of longitudinal static stability; and determine relative influence of IFR compared with VFR approaches.

2. Second experiment (ground simulation, refs. 36, 37): determine suitability of requirements on cockpit control position; examine efficacy of several SCAS concepts; and explore influence of turbulence.

3. Third experiment (ground simulation, ref. 38): determine influence of crew-loading (single pilot versus dual pilot); determine influence of three-cue flight director displays; and examine suitability of additional SCAS concepts.

4. Fourth experiment (flight, ref. 39): validate selected results of ground-simulation experiments in flight concerning static longitudinal stability, level of SCAS, and flight director displays.

5. Fifth experiment (ground simulation, ref. 40): examine influences of unstable static control gradients, angle-of-attack stability, and pitch-speed coupling; and examine influence of failed SCAS.

6. Sixth experiment (ground simulation, ref. 41): investigate SCAS requirements for decelerating instrument approach; explore influence of electronic display format; and examine influence of approach geometry and deceleration profile.

One set of results from these experiments is shown in figure 21, which compares Cooper-Harper ratings for similar stability and control characteristics and displays as a function of the task considered. It should be noted in particular that the difference between the dual-pilot and single-pilot task considered in experiment 3 resulted in a change of almost one pilot rating, justifying, in principle, a division of criteria depending on crew-loading. It may also be seen that a decelerating instrument approach leads to a reduced capability relative to constant-speed approaches; however, the use of appropriate augmentation and flight director displays still permits clearly adequate pilot ratings, with desired performance attainable. The results of this series of experiments have recently formed the basis for an FAA Notice of Proposed Rulemaking (ref. 42) in which the IFR criteria are modified to allow decelerating approaches.

Terminal-area research was also extended to the case of rotorcraft with a thrust-vectoring capability--specifically, tilt-rotors (ref. 43). This class of vehicles introduces a variety of additional operational and handling-qualities concerns to the terminal-area problem, revolving primarily around the change from aerodynamic to thrust-supported lift, or vice versa, and the effect of combinations of speed, descent angle, and thrust-vector angle (conversion corridor) during the conversion. In the experiment, variations in the conversion-corridor, handling-qualities coupling, and levels of SCAS and display assistance given to the pilot, were examined.

Some of the results are shown in figure 22, which illustrates the influence of visual conditions, SCAS type, and conversion procedure on Cooper-Harper pilot ratings. On the basis of these results, the general influence of the conversion profile is as follows. Performing all the conversion before glide-slope acquisition (profile A) led to nearly desired performance when an attitude SCAS was implemented and to a clearly adequate capability with a rate SCAS; this method, which allows glide-slope tracking in a fixed configuration, shows results that are generally consistent with those for helicopters. Performing part of the conversion before acquiring the glide-slope and part after acquiring it (profile B) led to degraded pilot ratings for instrument approaches, particularly with the rate SCAS. This

degradation was due primarily to conversion-induced pitch and heave coupling. The advantage of performing part of the conversion early in the approach, allowed more time at a fixed configuration to get stabilized before breakout. Finally, performing all conversion while descending on the glide slope (profile C) was considered adequate in visual flight but marginally inadequate on instruments; there was little benefit from the attitude SCAS for instrument approaches. These results indicate the need for additional assistance in augmentation or display sophistication or both for a task in which the aircraft configuration is continually varying during a crucial period.

FLIGHT-BASED EXPERIMENTAL RESEARCH

The use of ground-simulation facilities affords a significant capability to examine efficiently a wide variety of handling-qualities problems, and the improved motion and visual cueing devices used in the NASA simulation facilities, as discussed earlier, provide reasonably high fidelity for several types of rotorcraft missions. Nonetheless, a fundamental requirement exists to validate simulator results in the flight environment, and a basic precept of the NASA/Army handling-qualities research program has been to conduct selected research experiments in flight.

Both of the extensive series of experiments discussed earlier investigating basic handling-qualities parameters in visual flight for near-terrain missions and control and display parameters for instrument operations in the terminal area included one flight-validation experiment using the UH-1H (refs. 44, 45). In the near-terrain experiment, the flight investigation concentrated on validating the influences of roll damping and control sensitivity for a slalom task. Figure 23 compares these flight results (labeled EXP IV) with ground simulation. Because of the limited inherent capability of the VSTOLAND UH-1H, the flight results are limited to one value of control sensitivity and a small range of damping. Nonetheless, the correspondence of flight and simulator data is generally good for this specific task. Similarly, figure 24 compares results from the flight-validation experiment (experiment 4) with ground-simulation data for the helicopter IFR program. Again, the correspondence is good for this task, particularly since one of the simulated configurations had baseline characteristics similar to those of the UH-1H (experiments 3, 5). For both of these relatively benign tasks, therefore, the flight experiments provided the validation necessary to extend the confidence region for the ground-simulation data.

As the demand for more capability from the helicopter/pilot system increases, however, limitations in simulator fidelity become of more concern, and the appropriateness of the UH-1H VSTOLAND as a valid flight research capability becomes limited because of the rotor design and the controls implementation. To address these concerns with flight validation, it has been necessary to use helicopters from other research facilities, as well as the NASA/Army CH-47B.

An initial example of the use of other facilities for flight validation of the NOE research was a collaborative effort with the German Aerospace Research Establishment (DFVLR) Institute for Flight Mechanics, which was conducted under the auspices of a memorandum of understanding between the U.S. Army and the German Ministry of Defense. In this experiment, unmodified UH-1D and BO-105 helicopters were flown over NOE slalom courses to assess the effects on handling qualities of basic rotor characteristics for this task and to provide correlation for the UH-1H VSTOLAND experiment results obtained previously (ref. 44). This flight program, documented in reference 45, demonstrated the superiority of the basic hingeless rotor system of the BO-105 when the task "bandwidth" was increased, thereby indicating the bounds of usefulness of the UH-1H VSTOLAND results. One outgrowth of this collaborative effort has been the development, in Germany, of a variable-stability BO-105 helicopter to provide a practical flight research platform for the more demanding tasks that are representative of current helicopter mission requirements.

Another in-flight simulation facility is the Bell 205 operated by the National Aeronautical Establishment (NAE) of Canada. This facility is described in reference 46, and a summary of much of the handling-qualities research performed under contract to the Army is contained in reference 47. References 48 and 49 discuss some detailed results. One of the major issues of concern is that, for some tasks, such as precision hover, the ground-simulator results predict more stringent control-system requirements than are observed in flight. Figure 25 (from ref. 46) illustrates some preliminary results concerning this discrepancy. As can be seen, pitch/roll bandwidths of the order of 3.0 rad/sec were predicted to be required to achieve Cooper-Harper pilot ratings in the Level 1 region from VMS results, whereas an equivalent level of acceptability was found in the Bell 205 in-flight simulator for a bandwidth of only 2.0 rad/sec. Similar discrepancies appear to occur for vertical-axis dynamic characteristics (ref. 48). It is emphasized that some of these results are still preliminary; nonetheless, it is of fundamental importance to understanding the underlying reasons, and current research is beginning to address this problem (e.g., ref. 49). Clearly, it is also of fundamental importance to have an in-flight simulation capability as the research facility for use when ground-simulation data are suspect.

To assist in this regard, the NASA/Army CH-47B is currently used to provide flight validation of selected ground-simulation results. This aircraft serves as a complementary facility to the NAE Bell 205 and affords the capability of back-to-back comparisons with ground-simulation experiments conducted at the Ames facilities. Reference 50 describes a recent experiment to extend previous VTOL ground and flight-simulation results to the helicopter bob-up task; in addition, previous simulation helicopter bob-up configurations were implemented for flight evaluation. Figure 26 illustrates the comparison of flight and simulation results for different simulated engine-governor response characteristics. In general, the flight results yielded slightly improved pilot ratings as compared with those of the ground simulator, although the differences are not significant and are within expected rating scatter. The one large difference that occurs with the slow engine-governor indicates a possible unrealistic requirement for rpm monitoring present in the ground simulation.

Both the Bell 205 and the CH-47B flight results have had major effects on draft versions of the revised handling-qualities specification because of the reduced system requirements for a given level of pilot acceptance. Neither of these aircraft, however, has sufficient inherent levels of agility and maneuverability to address properly new tasks consistent with more demanding missions such as air-to-air combat. In addition, although they both incorporate some form of head-down electronic display, neither is currently equipped to examine the interaction of visually coupled (e.g., helmet-mounted) displays with various aircraft stability and control characteristics. For these new in-flight investigations, it will be necessary to develop a new rotorcraft in-flight simulator with increased agility and maneuverability.

RESEARCH CHALLENGES

One measure of the success of the Army/NASA rotorcraft handling-qualities efforts reviewed in the previous sections is the level of completeness of the proposed MIL-H-8501 (ref. 51), because the generation of this specification has been based largely on these results. Although the specification structure follows the philosophy generated for MIL-F-8785B and C, and used in MIL-F-83300, the details of the requirements are considerably different, many of the methods of specifying the requirements are different, and several innovations have been introduced. Most notable of these is the attempt to recognize and accommodate the effects of degraded visual cues resulting from using displays and vision aids at night and in poor weather; the specification requires different response types and different response bandwidths for near-Earth tasks in degraded visual cues.

The heart of the specification, of course, is the adequacy of the quantitative requirements. The specification is based largely on data from Army/NASA rotorcraft program experiments and from several programs of international collaboration at the NAE of Canada, the DFVLR, and the British Royal Aircraft Establishment. Currently, there are still many topics that have not been addressed because of a lack of data. In addition, some of the requirements rely on data that were generated on ground-based simulators with no flight validation. Because the magnitude of the task of generating the needed handling-qualities data is so large (fig. 27), full use must be made of ground-based simulators to do the broad parameter investigations. However, despite considerable investment in simulation facilities by NASA and the Army (refs. 52-54), the fidelity of current ground-based simulation for helicopter research in the region of low speed and hover limits the confidence with which quantitative handling-qualities boundaries can be developed. The predicted trends are usually representative, but because of sensory cue deprivation, the simulator often predicts worse handling qualities than exist in flight.

Figure 28 an example. It is suspected that the visual systems are to blame for deficiencies during small-amplitude maneuvering and that the limited-motion systems are the major contributors in more aggressive tasks. Unfortunately, though several efforts have been made to come to grips with this problem (refs. 49, 55-58), those

studies have so far been unsuccessful, and currently there is no focused research effort to determine the basic requirements for an acceptable simulation of the low-speed and hover flight regimes.

Work needs to be performed on both the engineering fidelity, the primary ingredient of which is the mathematical model representing the rotorcraft, and the perceptual fidelity, the primary contributors to which are the visual and motion cues. Methods have to be developed for systematically assessing simulation fidelity and for improving deficient aspects. A major contribution toward improving engineering fidelity could be made by improving the interactional aerodynamic prediction methods which would result in improved simulation mathematical models. Better low-altitude atmospheric disturbance models are also required.

Although much can be achieved with ground-based simulators, for the foreseeable future there will still be a need for flight verification. Although some flight verification can be obtained by comparison with existing aircraft, there is a need for an in-flight simulator, or variable-stability rotorcraft, so that parameters can be varied systematically for a range of tasks and for new configurations as they evolve. Aside from the CH-47 variable-stability research helicopter at Ames Research Center, which is not agile enough and will have to be returned to the Army in 1988, there is no in-flight rotorcraft simulator available for basic research in the United States.

Because advances in ground-based and in-flight simulation tools benefit the designer also, all four major helicopter manufacturers have, or are developing, extensive helicopter simulator facilities as part of their Light Helicopter Family (LHX) pre-design efforts. They will be faced with the same problems of simulation validation that exist in the government. They need improvements in simulator fidelity to be able to use them as credible design tools. Training simulators suffer from similar problems. Both Black Hawk and Apache training simulators are known to have deficiencies that can induce a negative transfer of training.

Some of the topics that need more work are listed in table 2. Some have not been addressed at all; for example, slung loads, response to upsets as distinguished from response to control, multi-mode control blending and nonlinear control characteristics, and digital implementation of high-gain stability and control augmentation systems. Of the topics that have been addressed, and for which data are documented in the Background Information and Users' Guide (BIUG), are side-stick controllers, cross-coupling, and thrust-response dynamics and margins. The topics that need more work are broad-based and pervade the whole specification; for example, the effects of visual-cue degradation and the mission task element definition and performance benefits. Another class of topics needing work has to do with specific missions such as air-to-air combat; these include the uses of thrust-vectoring and maneuver envelope enhancement.

CONCLUSION

The foregoing reflects the dynamic character of rotorcraft technology. As the vehicle capabilities evolve, the mission complexity increases. When MIL-H-8501 was generated (1961 revision), helicopters were underpowered, unstable, and used sedate maneuvering in VMC. When the current Army/NASA research efforts to review this specification started (1975), the doctrine of NOE flying had evolved, with the concurrent need for high agility and maneuverability close to the ground. This requirement later evolved into NOE flight at night and in poor weather, thus bringing in different handling-qualities considerations. The latest evolving rotorcraft mission is that of air-to-air combat (1986). This mission raises agility and maneuverability needs and is clearly dominated by handling-qualities considerations. However, for certain mission requirements that have existed for years, such as shipboard recovery, the criteria are still not adequate; the desired all-weather operational capability has yet to be realized.

Although the work done on rotorcraft handling qualities in the last 12 years is a major contribution, much more remains to be done. The proposed update of MIL-H-8501 is a considerable advance over the existing MIL-H-8501A, but many deficiencies need to be addressed. It is hoped that in another 12 years we will have solved many of these problems, but it is also anticipated that rotorcraft missions and technology will have further evolved, thus providing more challenges to the handling-qualities community.

REFERENCES

1. Key, D. L.: Handling Qualities Specifications for U.S. Military Helicopters. AIAA Paper 80-1592, 1980. (Also, AIAA J. Aircraft, vol. 19, no. 2, Feb. 1982.)
2. Key, D. L.: The Status of Military Helicopter Handling Qualities Criteria. AGARD Conference Proceedings CP-333, 1982.
3. Bray, R. S.: Helicopter Simulation Technology: An Ames Research Center Perspective. NASA CP-2219, 1982.
4. Liden, S.: V/STOLAND Digital Avionics System for UH-1H. NASA CR-152179, 1978.
5. Baker, F. A.; Jaynes, D. N.; et al.: VSTOLAND Avionics System Flight Test Data on a UH-1H Helicopter. NASA TM-78591, 1980.
6. Tactical Aircraft Guidance System Advanced Development Program Flight Test Phase Report. USAAMRDL TR-73-89, U.S. Army Air Mobility Research and Development Laboratory, Fort Eustis, Va., Apr. 1974.

7. Kelly, J. R.; and Niessen, F. R.: Navigation, Guidance, and Control for Helicopter Automatic Landings. NASA TP-1649, 1980.
8. Hindson, W. S.; Hilbert, K. B.; et al.: New Capabilities and Recent Research Programs of the NASA/Army CH-47B Variable-Stability Helicopter. 42nd Annual National Forum of the American Helicopter Society, Washington, D.C., June 1986.
9. Chen, R. T. N.; and Talbot, P. D.: An Exploratory Investigation of the Effects of Large Variations in Rotor System Dynamics Design Parameters On Helicopter Handling Characteristics in Nap-of-the-Earth Flight. Paper No. 77.34-41, 33rd Annual National Forum of the American Helicopter Society, Washington, D. C., May 1977.
10. Talbot, P. D.; Dugan, D. C.; Chen, R. T. N.; and Gerdes, R. M.: Effects of Rotor Parameter Variations on Handling Qualities of Unaugmented Helicopters in Simulated Terrain Flight. NASA TM-81890, 1980.
11. Chen, R. T. N.; Talbot, P. D.; Gerdes, R. M.; and Dugan, D. C.: A Piloted Simulator Investigation of Augmentation Systems to Improve Helicopter Nap-of-the-Earth Handling Qualities. Paper No. 78-29, 34th Annual National Forum of the American Helicopter Society, Washington, D.C., May 1978.
12. Miyajima, K.: Analytical Design of a High-Performance Stability and Control Augmentation System for a Hingeless Rotor Helicopter. Paper No. 78-27, 34th Annual National Forum of the American Helicopter Society, Washington, D.C., May 1978.
13. Corliss, L. D.; and Carico, G. D.: A Preliminary Flight Investigation of Cross-Coupling and Lateral Damping for Nap-of-the-Earth Helicopter Operations. Paper No. 81-28, 37th Annual National Forum of the American Helicopter Society, New Orleans, La., May 1981.
14. Chen, R. T. N.: Effects of Primary Rotor Parameters on Flapping Dynamics. NASA TP-1431, 1980.
15. Chen, R. T. N.: Selection of Some Rotor Parameters to Reduce Pitch-Roll Coupling of Helicopter Flight Dynamics. Paper No. I-6, American Helicopter Society National Specialists' Conference on Rotor Systems Design, Philadelphia, Pa., Oct. 1980.
16. Chen, R. T. N.: Unified Results of Several Analytical and Experimental Studies of Helicopter Handling Qualities in Visual Terrain Flight. NASA CP-2219, 1982, pp. 59-74.
17. Cooper, G. E.; and Harper, R. P.: The Use of Pilot Ratings in the Evaluation of Aircraft Handling Qualities. NASA TN D-5153, 1969.

18. Watson, D. C.; and Aiken, E. W.: An Investigation of the Effects of Pitch-Roll Coupling on Helicopter Handling Qualities for Terrain Flight. AIAA Conference on Guidance, Navigation, and Control, Monterey, Ca., Aug. 1987.
19. Corliss, L. D.; and Blanken, C. L.: A Simulation Investigation of the Effects of Engine- and Thrust-Response Characteristics on Helicopter Handling Qualities. Paper 62, 9th European Rotorcraft Forum, 1983.
20. Corliss, L. D.; and Blanken, C. L.: Effects of Rotor Inertial and RPM Control on Helicopter Handling Qualities. AIAA Paper 83-2070, 1983.
21. Key, D. L.; and Aiken, E. W.: Aircrew-Aircraft Integration: A Summary of U.S. Army Research Programs and Plans. Vertica, vol. 10, no. 314, 1986, pp. 299-313.
22. Heffley, R. K. et al.: Study of Helicopter Roll Control Effectiveness Criteria. NASA CR-177404, 1986. (Also, USAAVSCOM TR 85-A-5.)
23. Bivens, C. C.: Directional Handling Qualities Requirements for Nap-of-the-Earth Tasks. J. Am. Helicopter Soc., vol. 31, no. 1, Jan. 1986, pp. 37-42.
24. Landis, K. H.; and Glusman, S. I.: Development of ADOCS Controllers and Control Laws. NASA CR-177339, 1985. (Also, USAAVSCOM TR 84-A-7.)
25. Aiken, E. W.: Simulator Investigations of Various Side-Stick Controller/Stability and Control Augmentation Systems for Helicopter Terrain Flight. AIAA paper 82-1522, 1983.
26. Landis, K. H.; Dunford, P. J.; Aiken, E. W.; and Hilbert, K. B.: Simulator Investigations of Side-Stick Controller/Stability and Control Augmentation Systems for Helicopter Visual Flight. J. Am. Helicopter Soc., Apr. 1985, pp. 3-13.
27. Aiken, E. W.: A Review of the Effects of Side-Stick Controllers on Rotorcraft Handling Qualities. J. Am. Helicopter Soc., vol. 31, no. 3, July 1986, pp. 27-34.
28. Lewis, Michael S.; and Aiken, Edwin W.: Piloted Simulation of One-on-One Helicopter Air Combat at NOE Flight Levels. NASA TM-86686, 1985.
29. Lewis, M. S.; Mansur, M. H.; and Chen, R. T. N.: A Simulator Investigation of Parameters Affecting Helicopter Handling Qualities in Air Combat (HAC II). NASA TM in preparation.
30. Decker, W. A.; Adam, C. F.; and Gerdes, R. M.: Pilot Use of Simulator Cues for Autorotation Landings. 42nd Annual National Forum of the American Helicopter Society, Washington, D.C., June 1986.

31. Haworth, L. A.; Bivens, C. C.; and Shively, J.: An Investigation of Single-Piloted Advanced Cockpit and Control Configurations for Nap-of-the-Earth Helicopter Combat Mission Tasks. 36th Annual National Forum of the American Helicopter Society, May 1980.
32. Aiken, E. W.; and Merrill, R. K.: Results of a Simulator Investigation of Control System and Display Variations for an Attack Helicopter Mission. Paper 80-28, 36th Annual National Forum of the American Helicopter Society, May 1980.
33. Carico, D.; Blanken, C. L.; Bivens, C. C.; and Morris, P. M.: Fixed-Based Simulator Investigation of Display/SCAS Requirement for Army Helicopter Low-Speed Tasks. Paper A-83-39-40-4000, 39th Annual National Forum of the American Helicopter Society, May 1983.
34. Landis, K. H.; and Aiken, E. W.: Simulator Investigations of Side-Stick Controller/Stability and Control Augmentation Systems for Night Nap-of-the-Earth Flight. J. Am. Helicopter Soc., vol. 29, no. 1, Jan. 1984, pp. 56-65.
35. Aiken, E. W.; Hilbert, K. B.; Landis, K. H.; and Glusman, S. I.: An Investigation of Side-Stick Controller/Stability and Control Augmentation System Requirements for Helicopter Terrain Flight under Reduced Visibility Conditions. AIAA Paper 84-0235, 1984.
36. Forrest, R. D.; Chen, R. T. N.; et al.: Piloted Simulator Investigation of Helicopter Control Systems Effects on Handling Qualities during Instrument Flight. Paper No. 79-26, 35th Annual National Forum of the American Helicopter Society, Washington, D.C., May 1979.
37. Lebacqz, J. V.; and Forrest, R. D.: A Piloted Simulator Investigation of Static Stability and Stability/Control Augmentation Effects on Helicopter Handling Qualities for Instrument Approaches. Paper No. 80-30, 36th Annual National Forum of the American Helicopter Society, Washington, D. C., May 1980.
38. Lebacqz, J. V.; Forrest, R. D.; and Gerdes, R. M.: A Piloted Simulator Investigation of Static Stability and Stability/Control Augmentation Effects on Helicopter Handling Qualities for Instrument Approach. NASA TM-81188, 1980.
39. Lebacqz, J. V.; Forrest, R. D.; Gerdes, R. M.; and Merrill, R. K.: Investigation of Control, Display, and Crew-Loading Requirements for Helicopter Instrument Approach. AIAA Paper 81-1820, 1981.
40. Lebacqz, J. V.; Weber, J. M.; and Corliss, L. D.: A Flight Investigation of Static Stability, Control Augmentation, and Flight Director Influences on Helicopter IFR Handling Qualities. Paper No. 81-25, 37th Annual National Forum of the American Helicopter Society, New Orleans, La., May 1981.

41. Lebacqz, J. V.; Forrest, R. D.; and Gerdes, R. M.: A Ground Simulator Investigation of Helicopter Longitudinal Flying Qualities for Instrument Approach. NASA TM-84225, 1982.
42. Notice of Proposed Rulemaking. U.S. Federal Aviation Administration, Federal Register, June 12, 1986.
43. Lebacqz, J. V.; and Scott, B. C.: Ground Simulation Investigation of VTOL Airworthiness Criteria for Terminal Area Operations. J. Guidance, Control, and Dynamics, vol. 8, no. 6, Nov.-Dec. 1985, pp. 761-767.
44. Gerdes, R. M.: A Pilot's Assessment of Helicopter Handling-Quality Factors Common to Both Agility and Instrument Flying Tasks. NASA TM-81217, 1980.
45. Pausder, H. J.; and Gerdes, R. M.: The Effects of Pilots Stress Factors on Handling Qualities Assessments during U. S./German Helicopter Agility Flight Tasks. NASA TM-84294, 1982.
46. Morgan, J. M.: Airborne Simulation at the National Aeronautical Establishment of Canada. AGARD Conference Proceedings CP-408, Oct. 1985.
47. Mitchell, D. G.; and Hoh, R. H.: Preliminary Results of Flight Tests Conducted in Support of MIL-H-8501 Upgrade. STI Working Paper 1194-100-2, Systems Technology, Inc., Hawthorne, Calif., Sept. 1985.
48. Baillie, S. W.; and Morgan, J. M.: Investigation of Vertical Axis Handling Qualities for Helicopter Hover and NOE Flight. AGARD Flight Mechanics Panel Conference, Amsterdam, Netherlands, Oct. 1986.
49. Hoh, R. H.: Handling Qualities Criterion for Very Low Visibility Rotorcraft NOE Operations. AGARD Flight Mechanics Panel Conference, Amsterdam, Netherlands, Oct. 1986.
50. Hindson, W. S.; Tucker, G. E.; Lebacqz, J. V.; and Hilbert, K. B.: Flight Evaluation of Height Response Characteristics for the Hover Bob-up Task and Comparison with Proposed Criteria. 42nd Annual National Forum of the American Helicopter Society, Washington, D.C., June 1986.
51. Hoh, R. H., et al: Mission-Oriented Flying Qualities Requirements for Military Rotorcraft. Report No. 1194, Systems Technology, Inc., Hawthorne, Calif., Dec. 1985.
52. Statler, I. C.; Key, D. L.: Simulation Requirements for Rotorcraft. Paper No. 32, 4th European Rotorcraft Forum, Sept. 1978.
53. Key, D. L.; Odneal, B. L.; and Sinacori, J. B.: Mission Environment Simulation for Army Rotorcraft Development--Requirements and Capabilities. AGARD Conference Proceedings CP-249, Apr. 1978.

54. Deel, A.; and Key, D. L.: SFTS R&D Hard at Work on the Future. Army Aviation, Sept. 1983.
55. Key, D. L.; Hansen, R. S.; Cleveland, W. B.; and Abbott, W. Y.: Helicopter Simulation Validation Using Flight Data. AGARD Conference Proceedings, CP-339, Oct. 1982.
56. Clement, W. F.; Cleveland, W. B.; and Key, D. L.: Assessment of Simulation Fidelity Using Measurements of Piloting Technique in Flight. AGARD Conference Proceedings CP-359, May 1984.
57. Bray, R. S.,: Visual and Motion Cueing in Helicopter Simulation. AGARD Conference Proceedings CP-408, Oct. 1985.
58. Decker, W. A.; Adam, C. F.; and Gerdes, R. M.: Pilot Use of Simulator Cues for Autorotation Landing. Paper Presented at the 42nd Annual National Forum of the American Helicopter Society, June 1986.

TABLE 1.- CURRENT HELICOPTER HANDLING-QUALITIES SPECIFICATIONS

SPECIFICATION	DATE	APPLICATION	COMMENTS
MIL-H-8501	1952	HELICOPTERS	SPECIFICALLY HELICOPTERS SPARSE COVERAGE CRITERIA INADEQUATE FOR ARMY MISSIONS LACKS TREATMENT OF ENVELOPES AND FAILURES BASICALLY FOR VMC
MIL-H-8501A	1961	MINOR REVISION	
AGARD 408	1962	V/STOL	
MIL-F-83300	1970	V/STOL (AND HELICOPTERS USAF ONLY)	BROAD COVERAGE SYSTEMATIC STRUCTURE CRITERIA INADEQUATE FOR ARMY MISSIONS BASED ON V/STOL DATA BASICALLY FOR VMC
UTTAS PIDS	1971	UTTAS	BASED ON 8501A MANEUVERING CRITERIA ADDED
AAH PIDS	1973	AAH	
AGARD 577	1973	V/STOL	
8501B (PROPOSED)	1973	HELICOPTERS	MANY NEW UNSUBSTANTIATED REQUIREMENTS
AHIP SPEC	1981	INTERIM SCOUT	BASICALLY 8501A

TABLE 2.- ROTORCRAFT HANDLING-QUALITIES RESEARCH NEEDS IN THE NEAR TERM

- SLUNG LOADS – INCLUDING TWIN LIFT
- THRUST VECTORING POSSIBILITIES AND POTENTIAL
- VISUAL CUE DEGRADATION EFFECTS AND QUANTIFICATION
- RESPONSE TO COMMAND VERSUS STABILIZATION OF UPSETS
- DIGITAL IMPLEMENTATION OF HIGH GAIN SCAS
- SINGLE PILOT SCAS
- GUIDANCE FOR FAILURE WARNING AND TRANSIENTS
- CROSS COUPLING
- SIDE STICK CONTROLLERS
- MANEUVER ENVELOPE ENHANCEMENT BY LIMITING AND CUEING
- THRUST RESPONSE DYNAMICS AND MARGINS
- CONTROL MODE BLENDING
- NONLINEAR CONTROL BLENDING
- MISSION TASK ELEMENT DEFINITION AND PERFORMANCE BENEFITS
- AIR-AIR COMBAT VEHICLE VERSUS WEAPONS

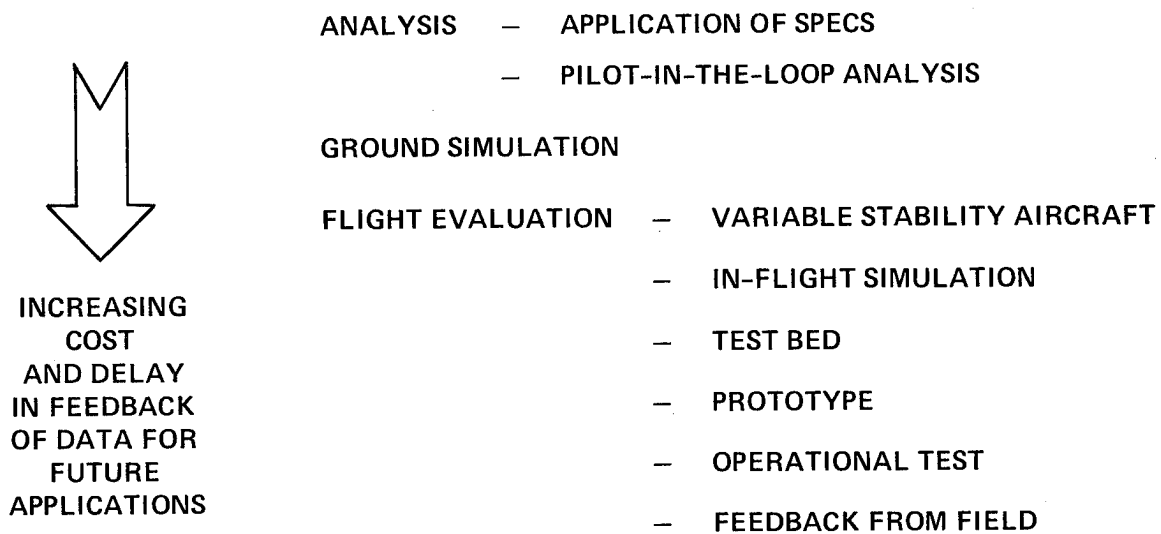


Figure 1.- Methods of achieving good handling qualities.

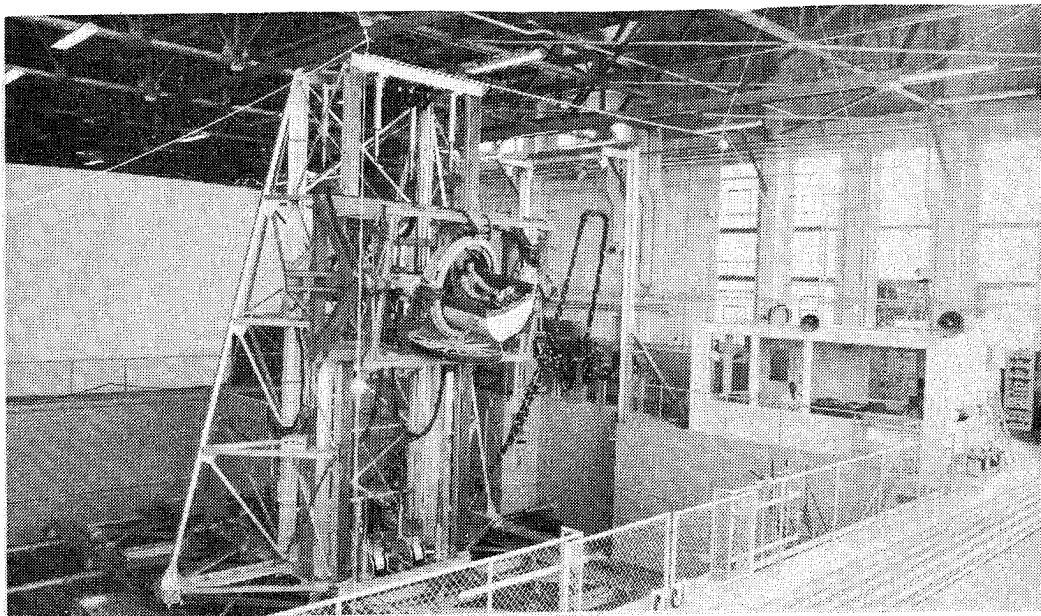


Figure 2.- Six-degree-of-freedom motion simulator.



Figure 3.- Cab configuration for control-display investigation.

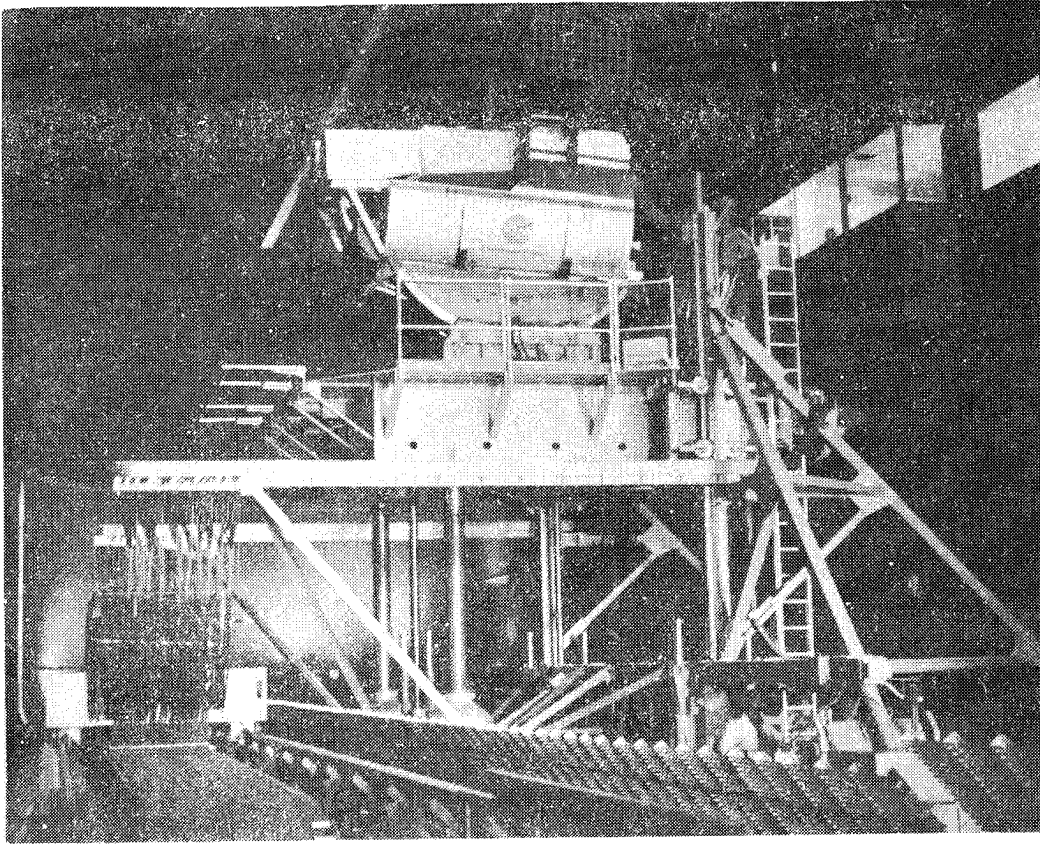


Figure 4.- Flight simulator for advanced aircraft.

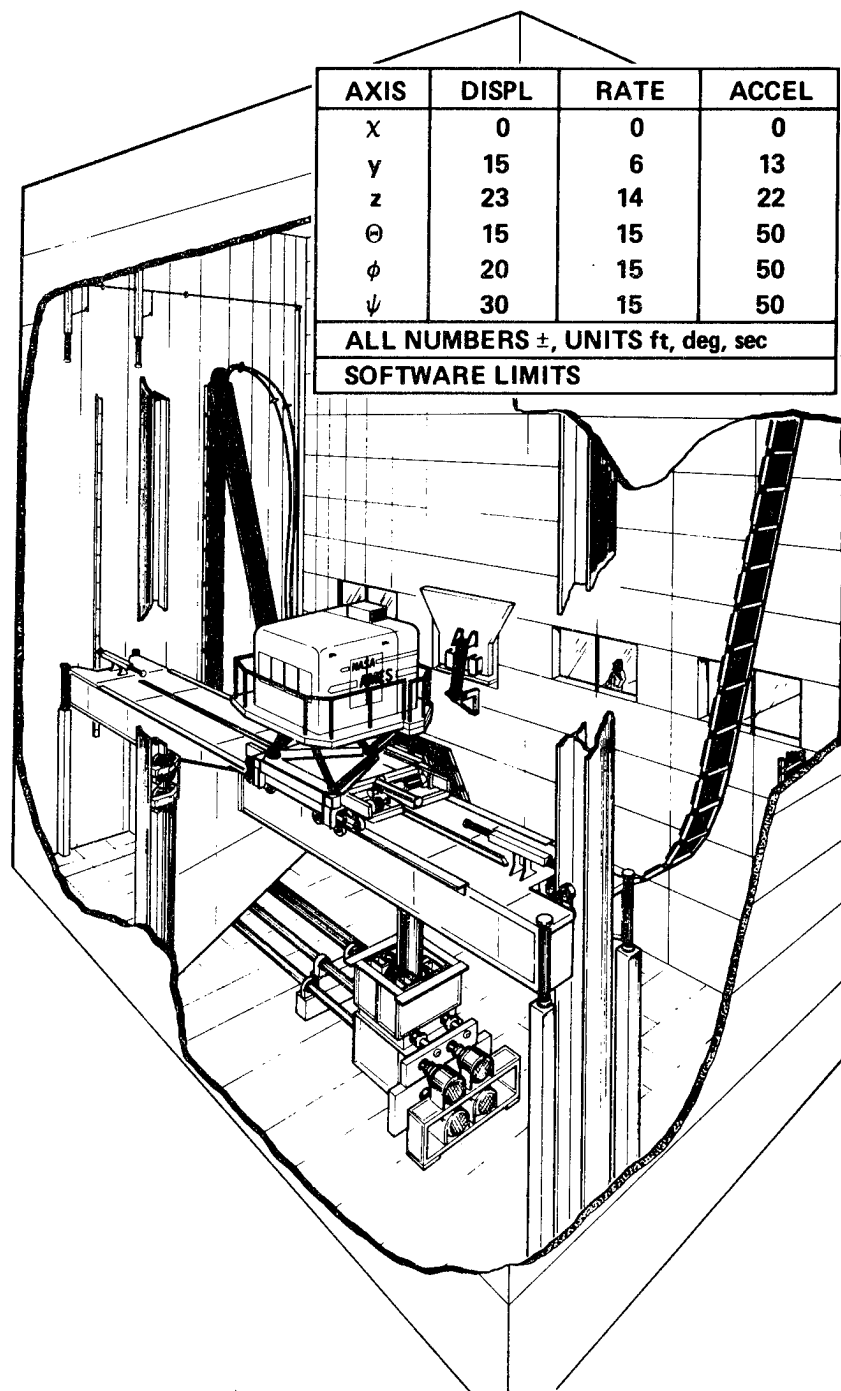


Figure 5.- Vertical motion simulator.

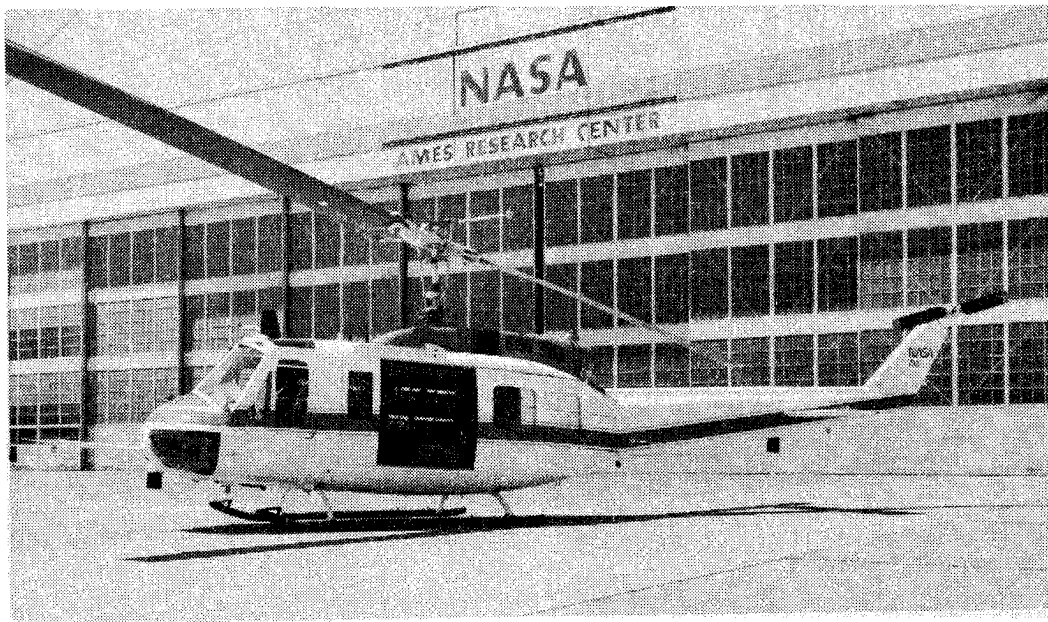


Figure 6.- UH-1H VSTOLAND aircraft.

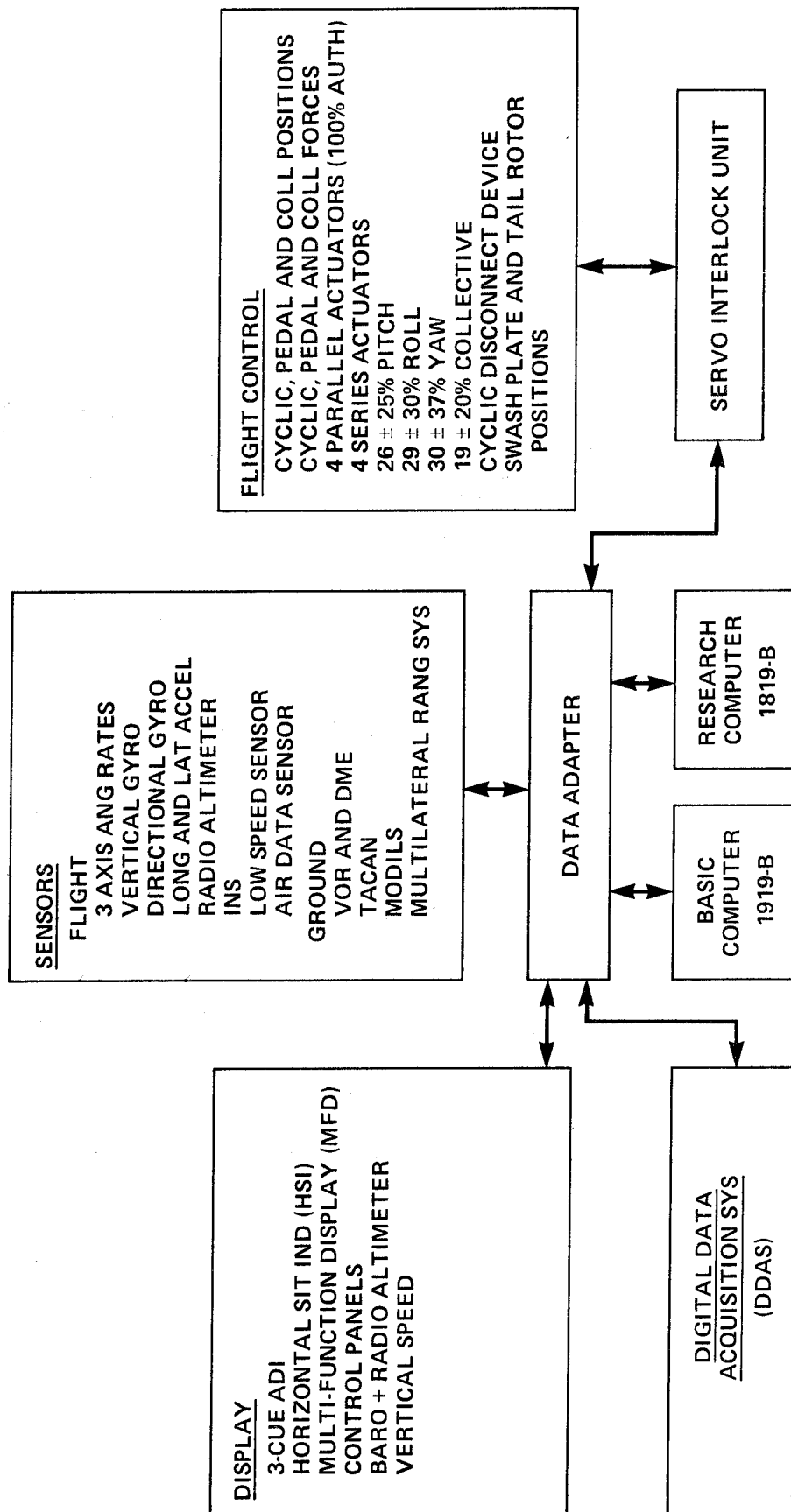


Figure 7.- UH-1H VSTOLAND system components.

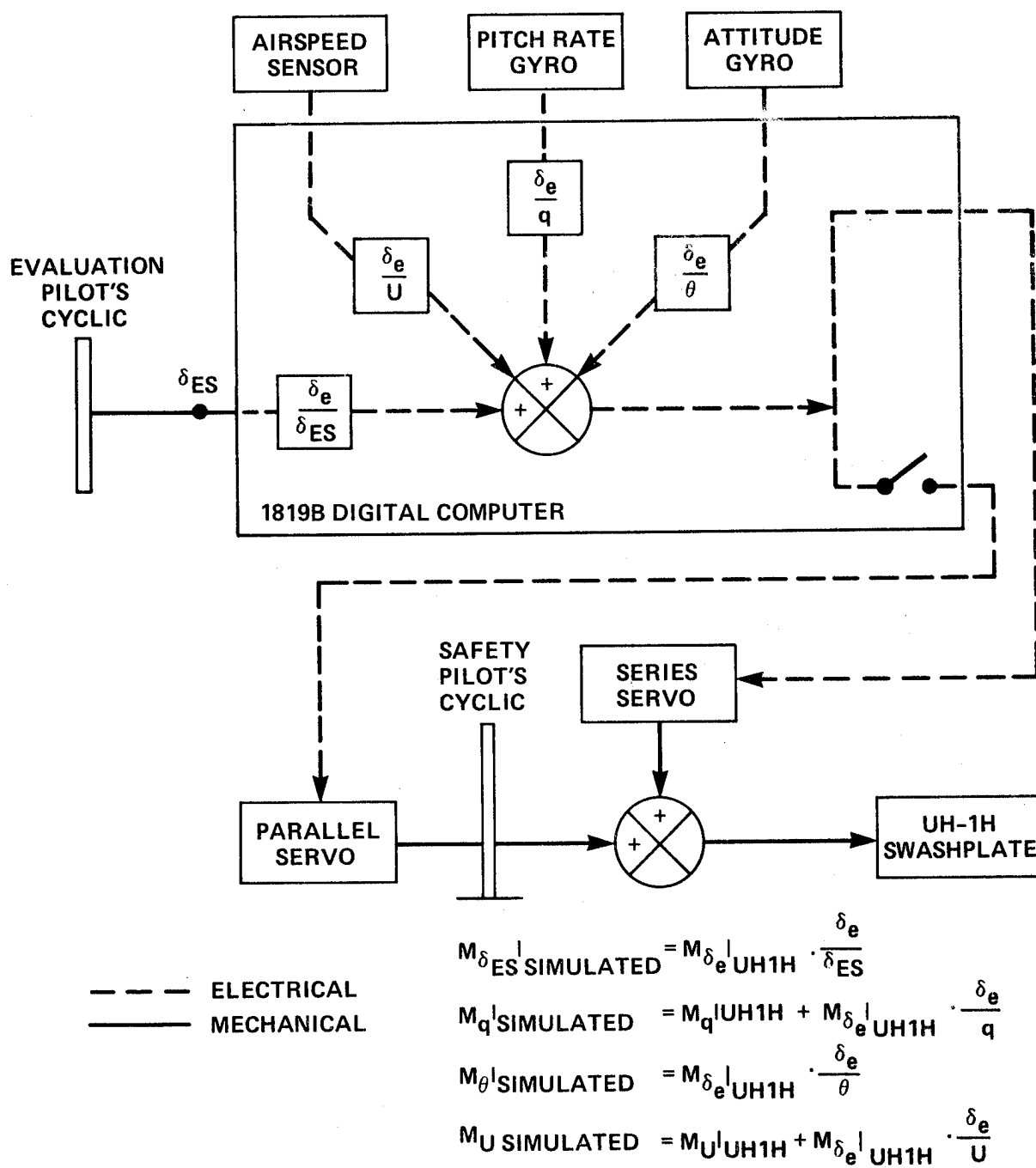


Figure 8.- VSTOLAND control-law channel.

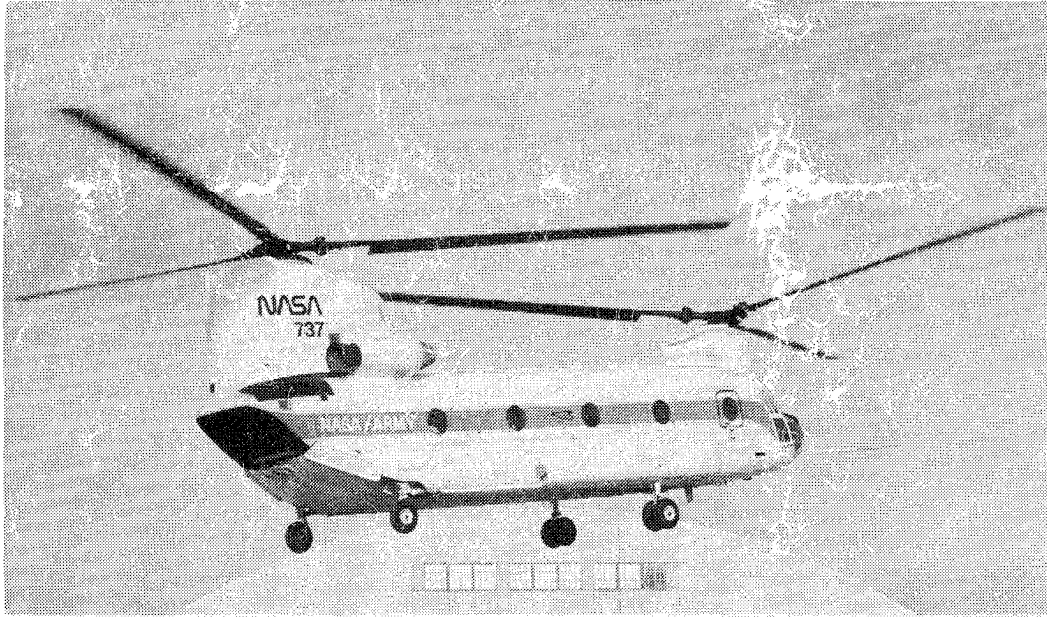


Figure 9.- CH-47B variable stability helicopter.

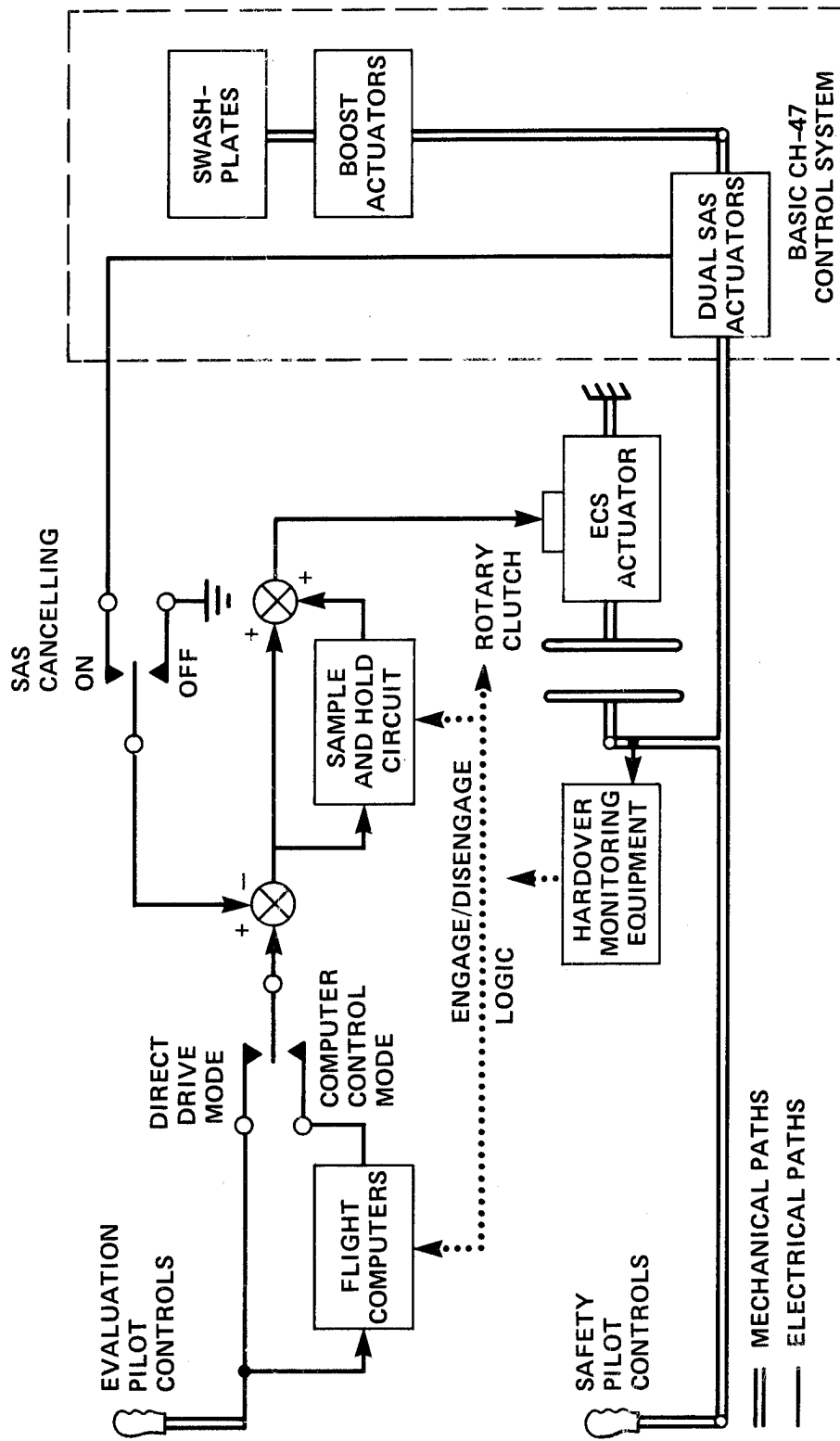


Figure 10.- CH-47B electronic control system.

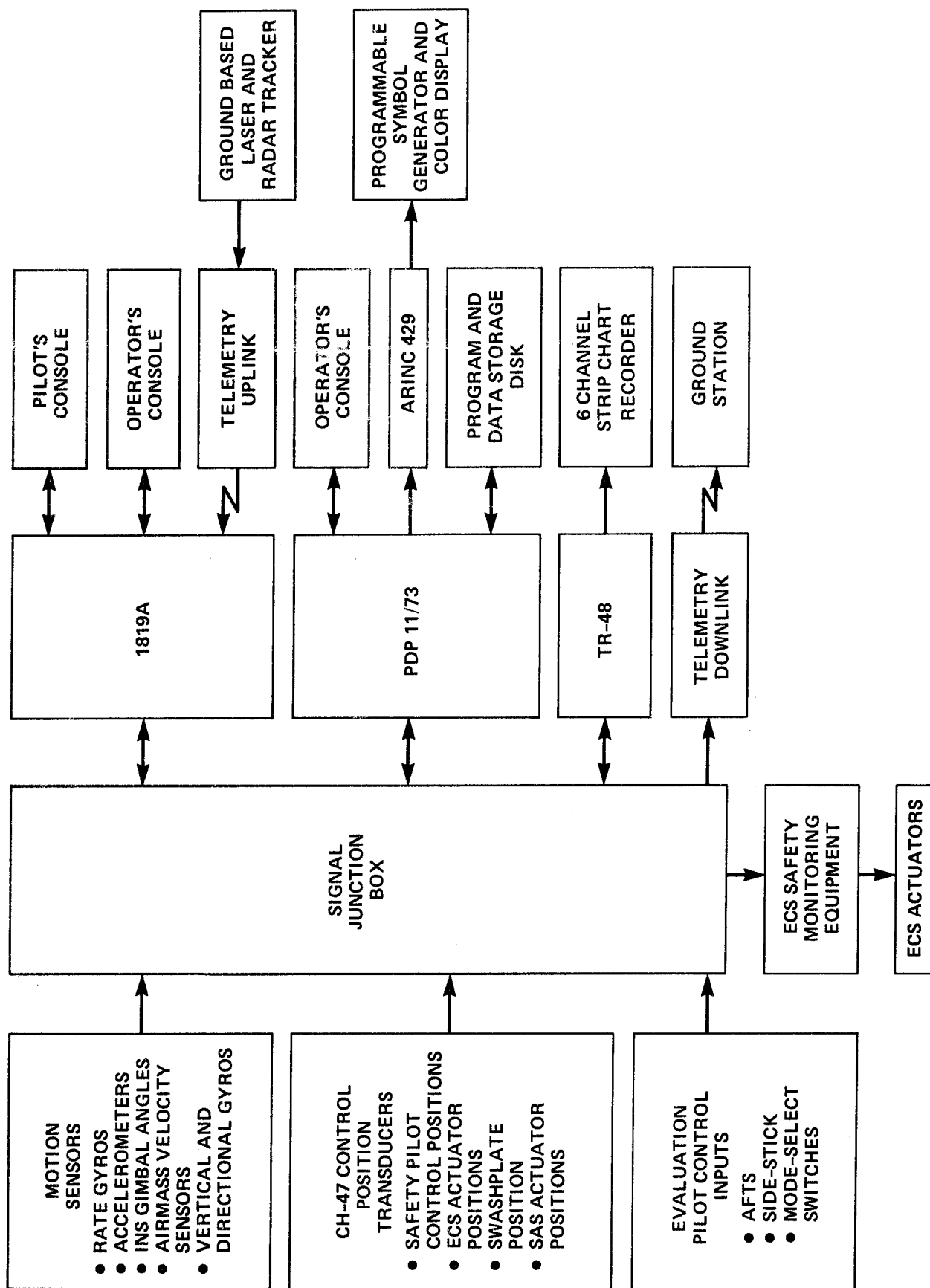


Figure 11.- CH-47B research system.

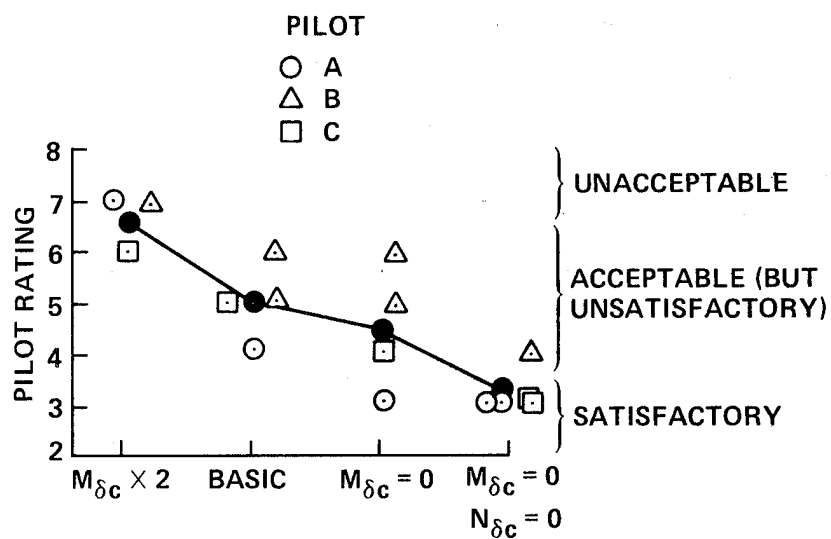


Figure 12.- Effect of pitch and yaw response to collective input.

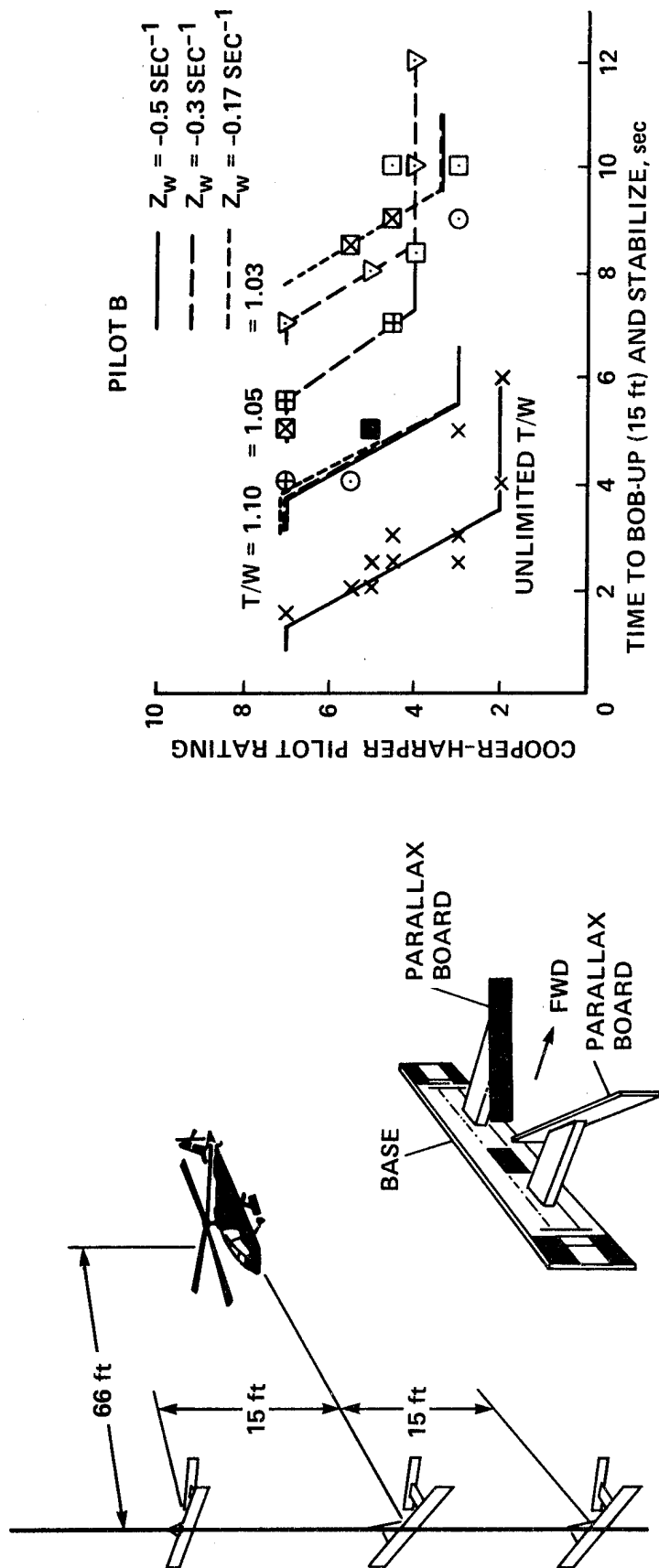


Figure 13.- Effects of time-constraints and vertical damping on bob-up handling qualities.

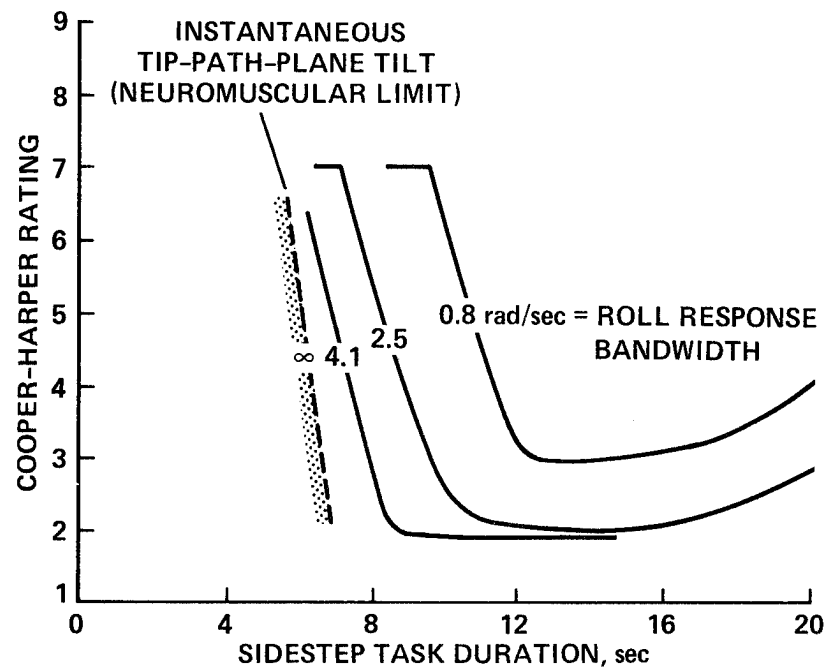


Figure 14.- Effects of short-term roll response as a function of time-constraints.

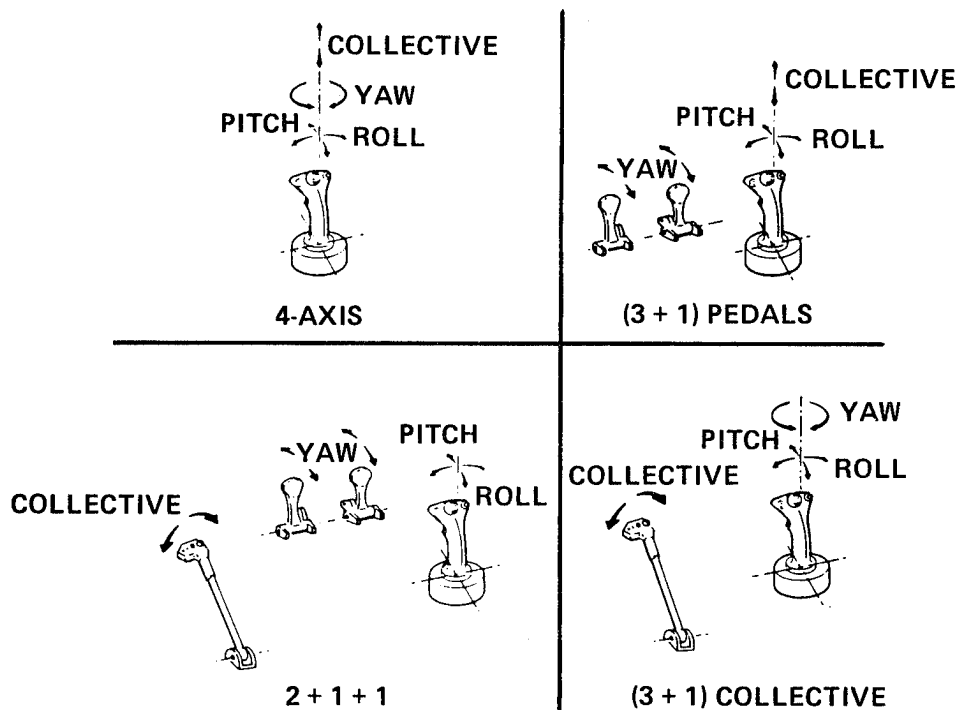


Figure 15.- ADOCS controller configurations.

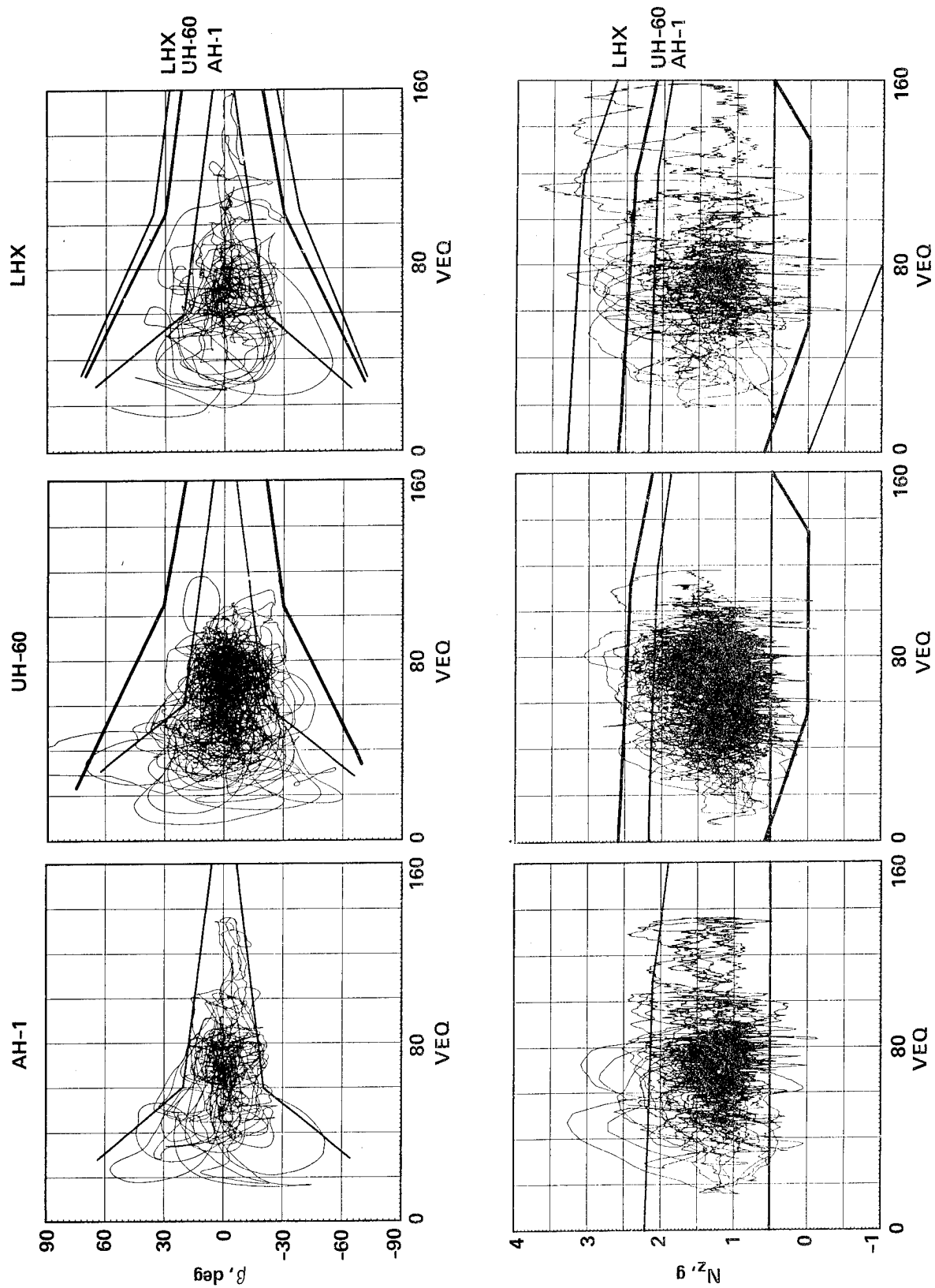


Figure 16.- Use of sideslip and normal acceleration in helicopter air combat simulation.

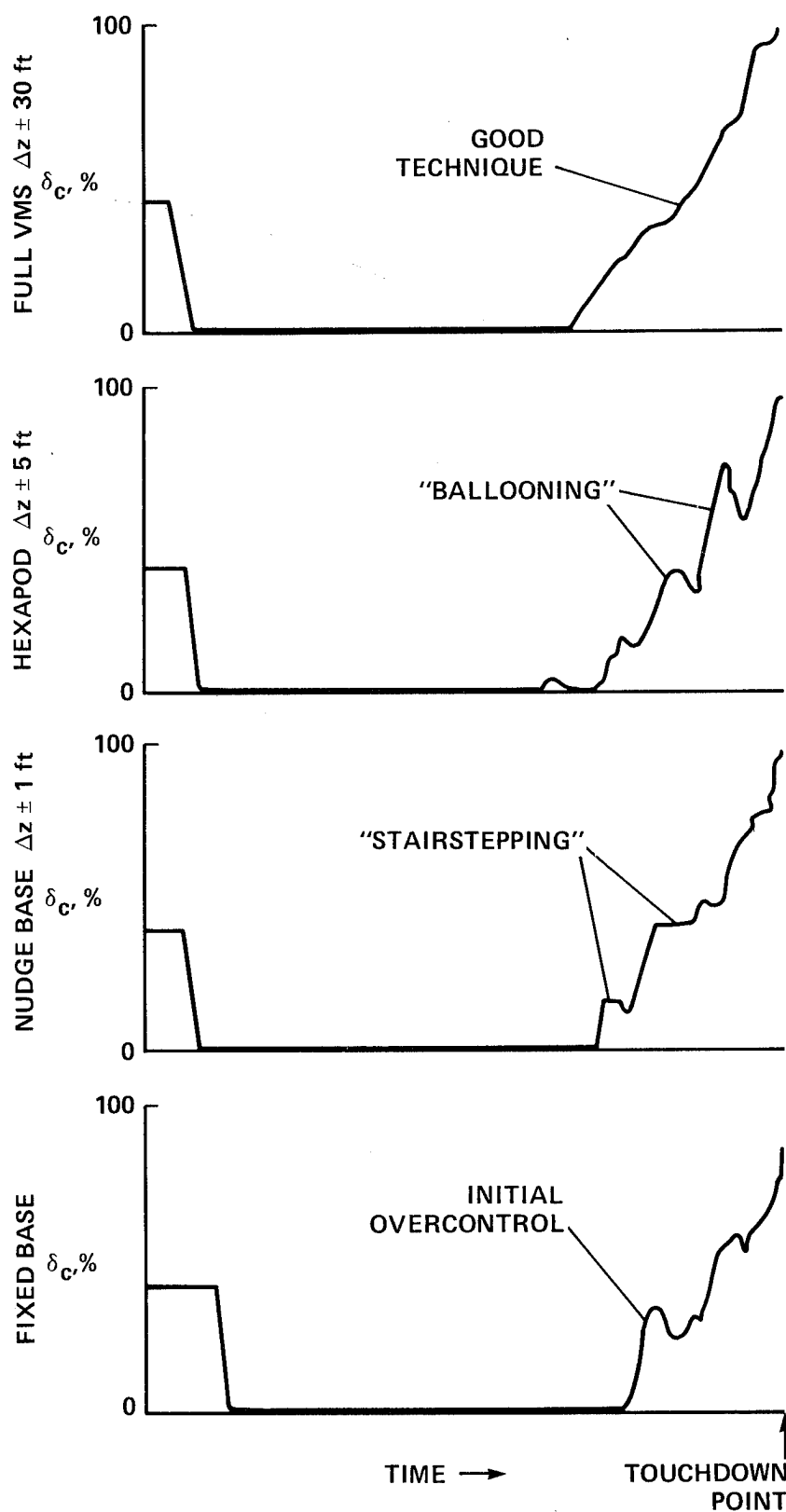


Figure 17.- Effect of motion system characteristics on collective use during simulated autorotations.

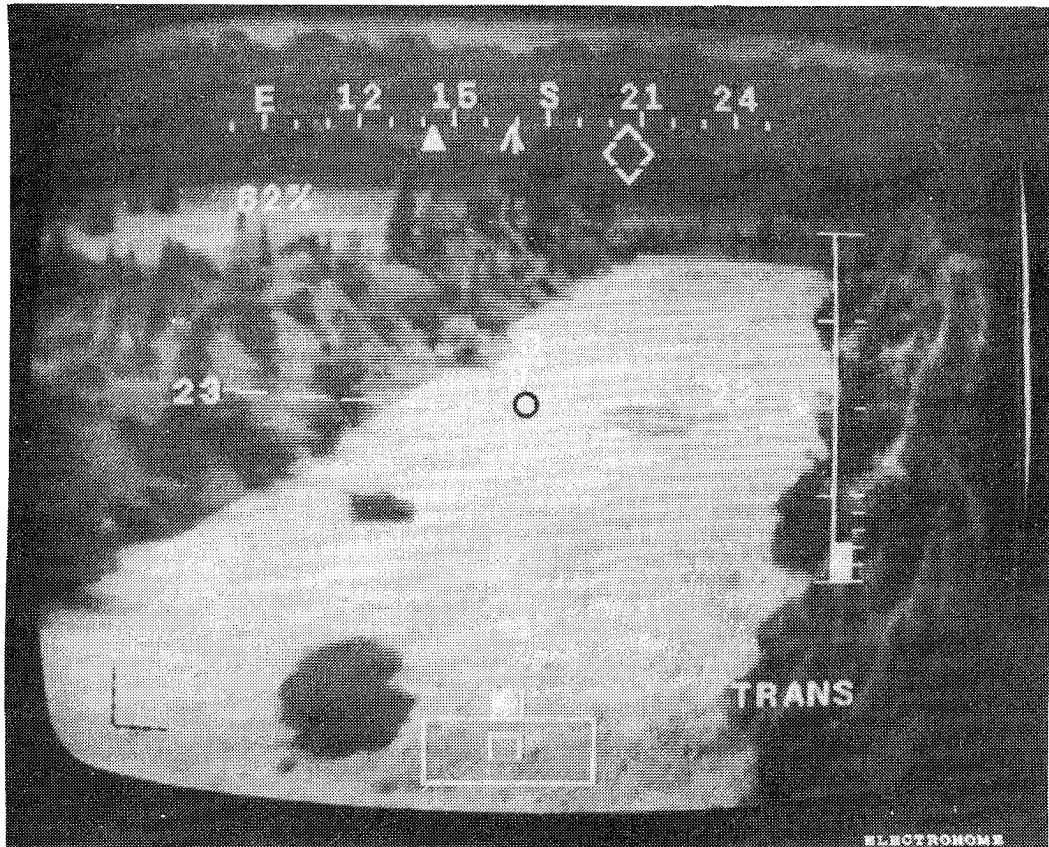


Figure 18.- Pilot night vision system symbols.



Figure 19.- Integrated helmet and display sight system.

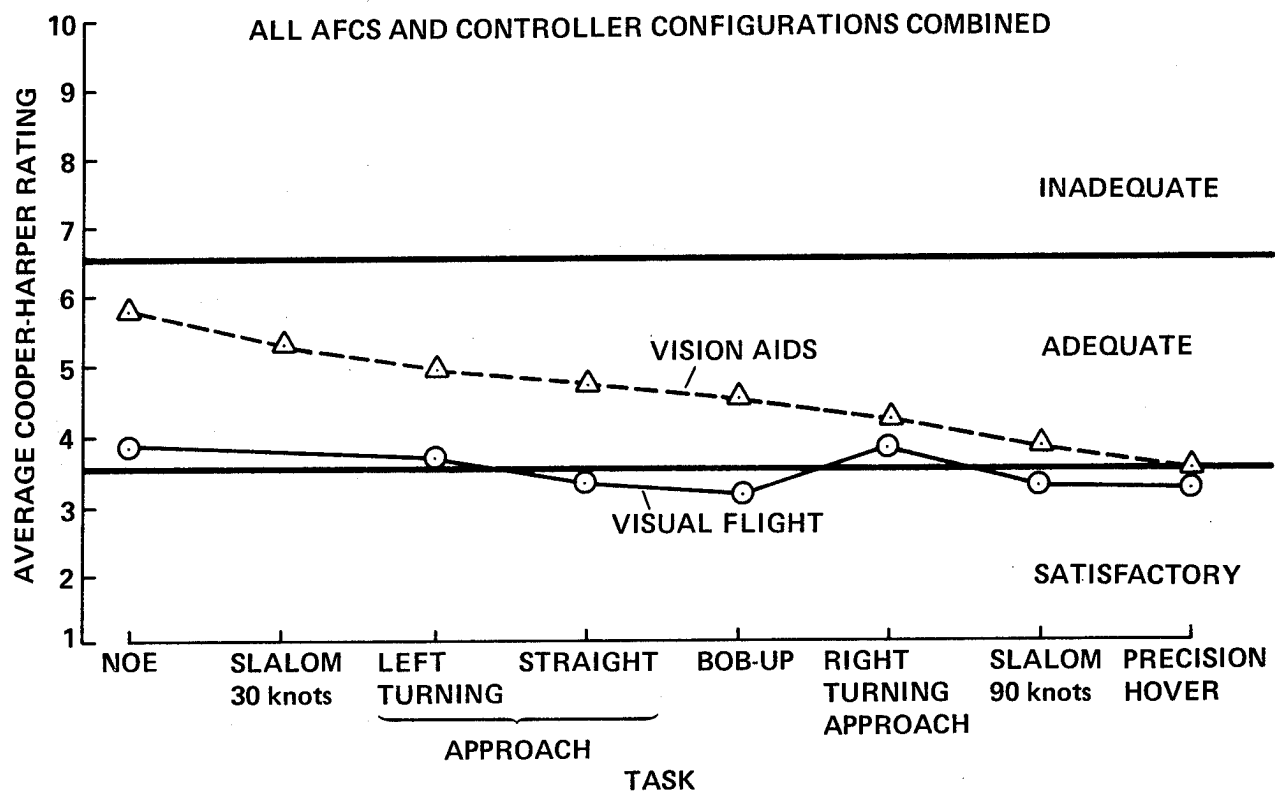


Figure 20.- Effect of reduced visibility conditions on handling qualities.

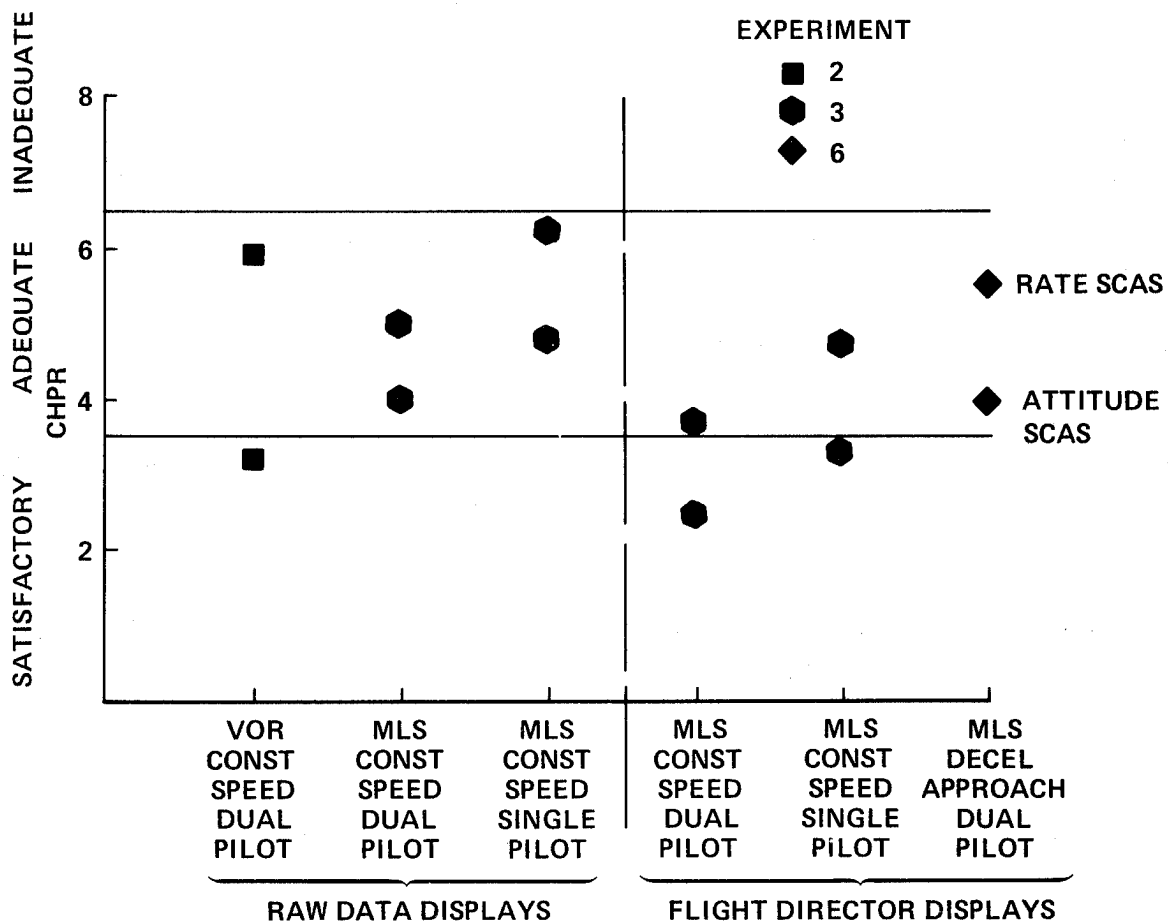


Figure 21.- Influence of task on IFR handling qualities.

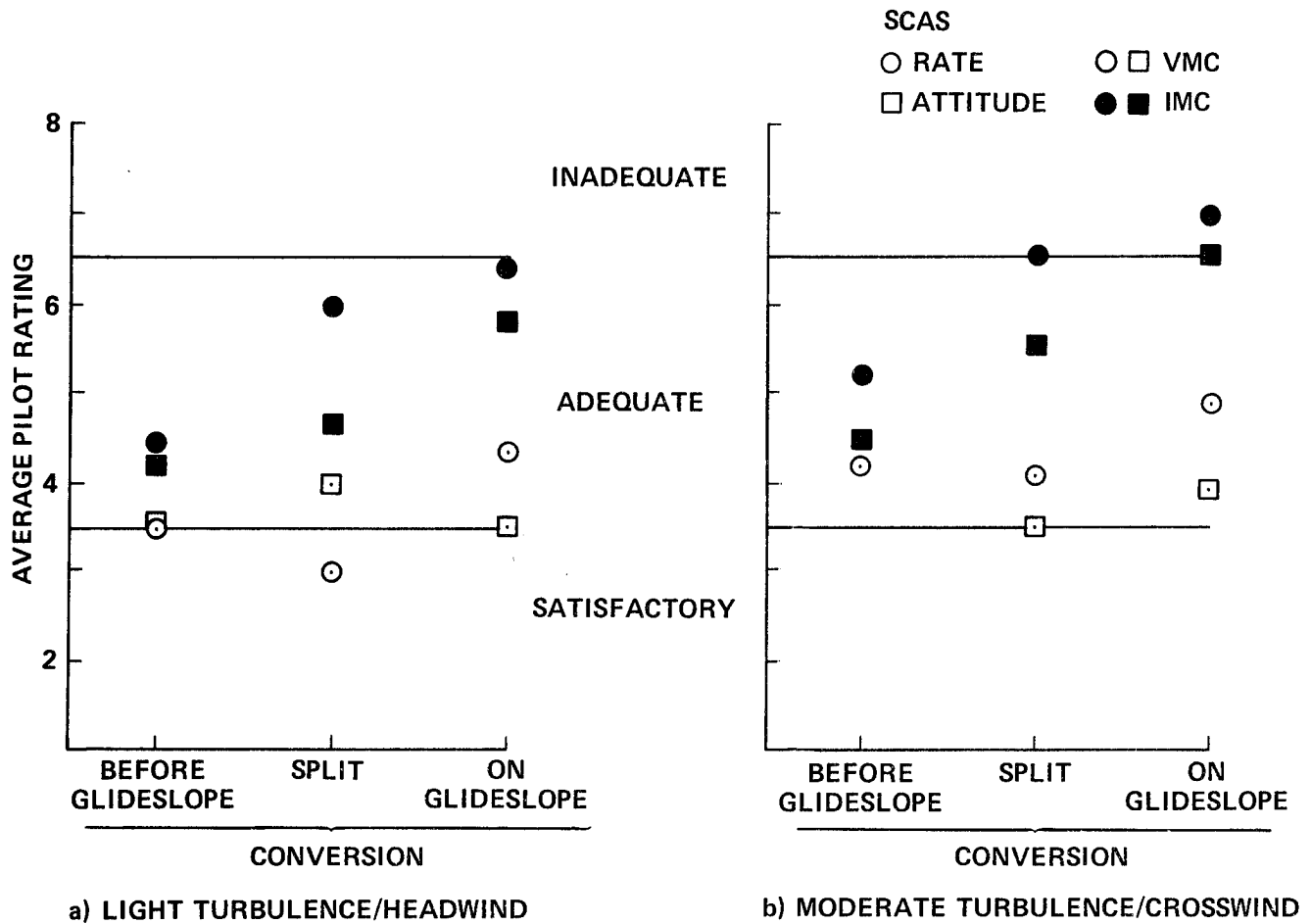


Figure 22.- Influence of conversion procedure, SCAS, and visual conditions on tilt-rotor handling qualities.

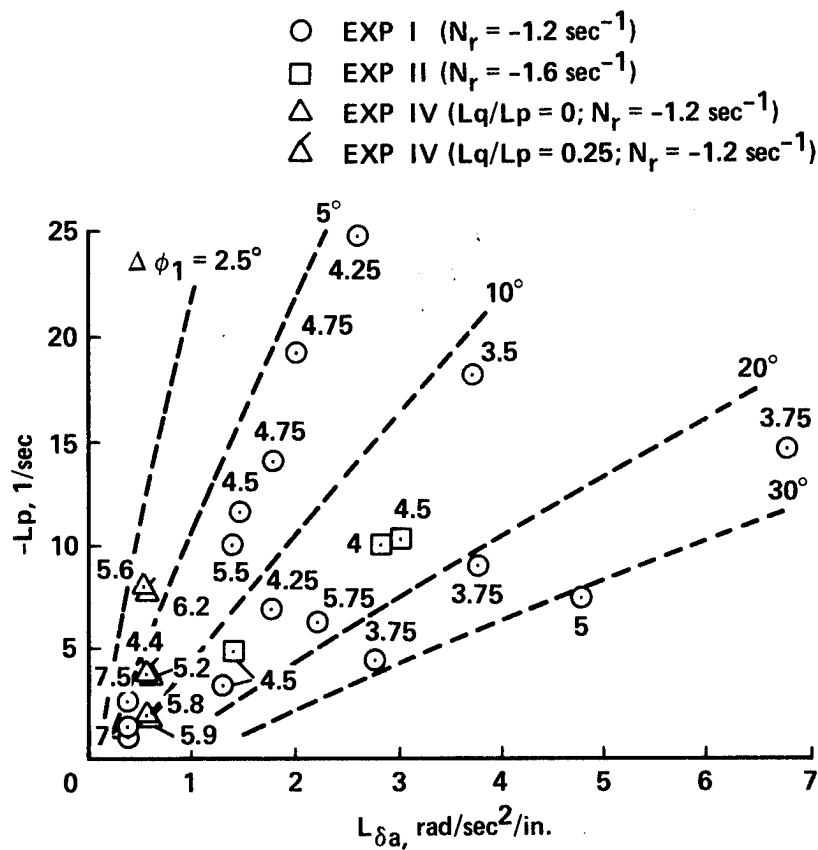


Figure 23.- Ground and in-flight simulation results: roll control requirements for a slalom task.

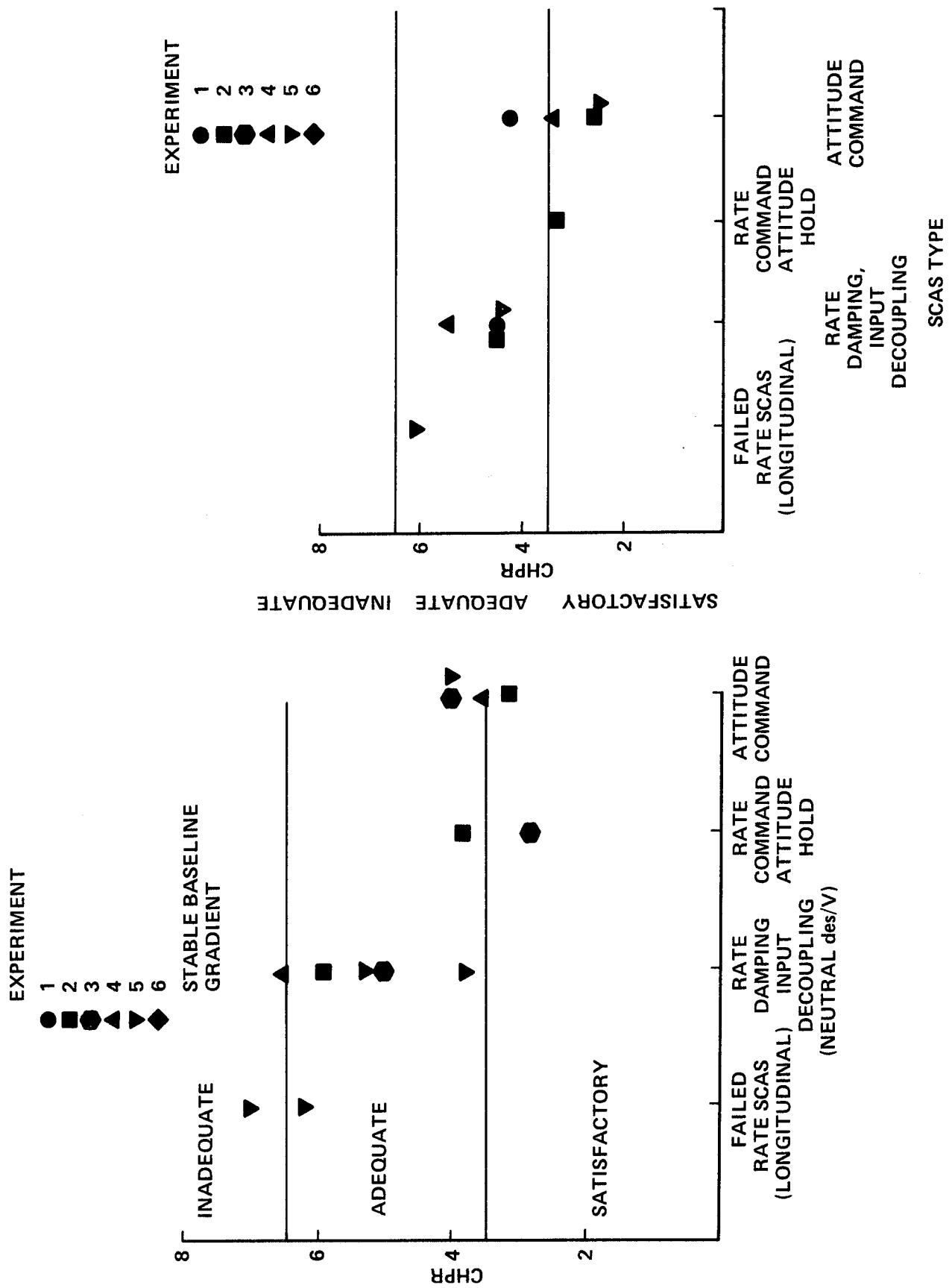


Figure 24.- Ground and in-flight simulation results: helicopter IFR program.

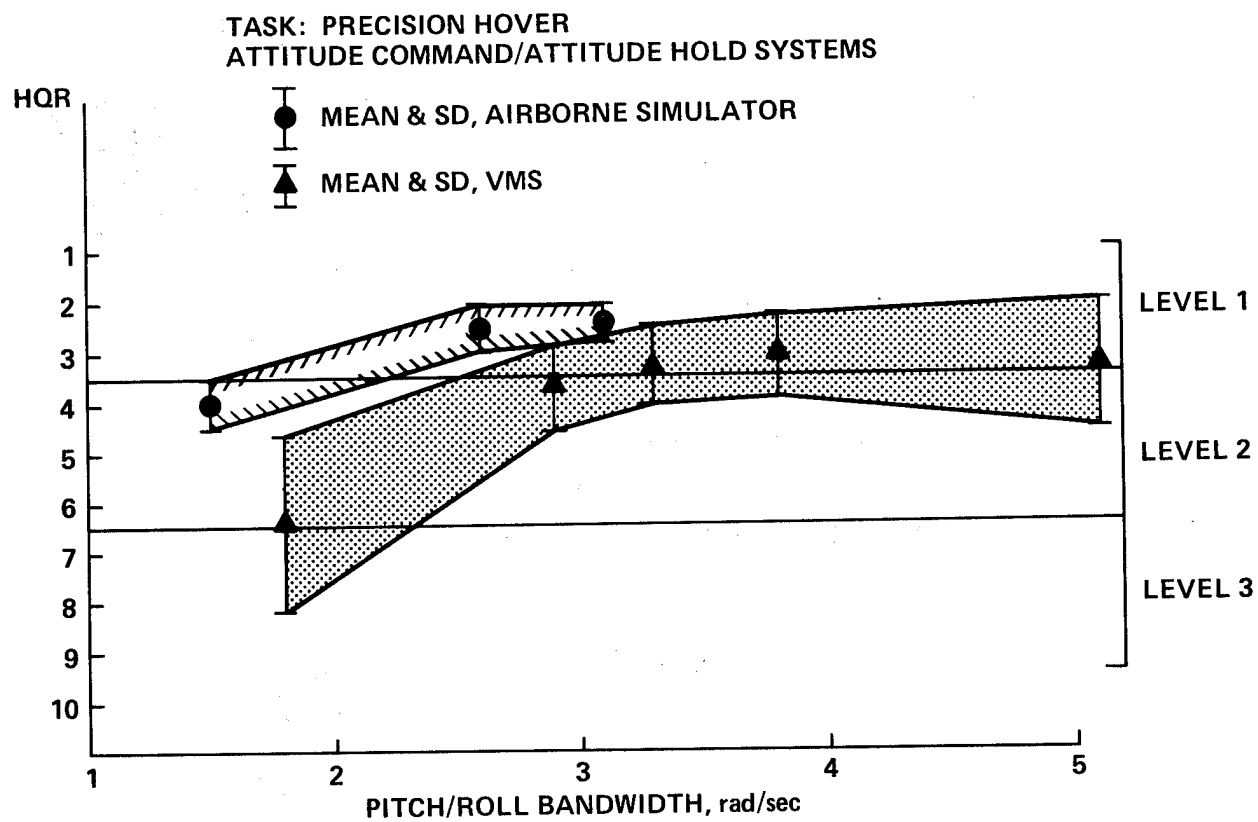


Figure 25.- Ground and in-flight simulation results: precision hover tasks.

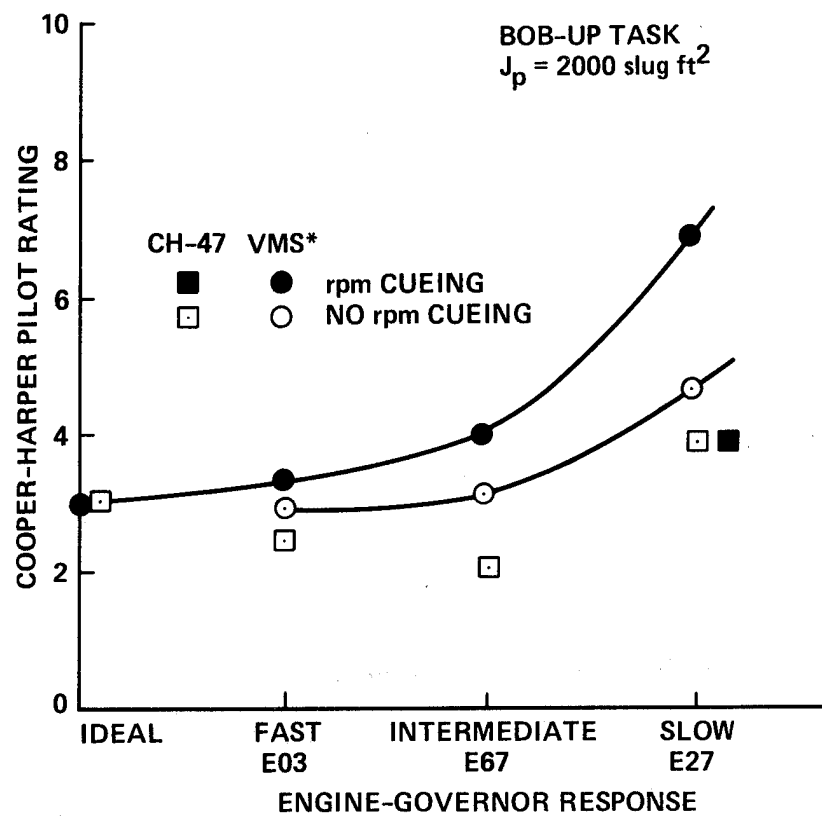


Figure 26.- Ground and in-flight simulation results: engine-governor response.

CHARACTERIZE HELICOPTER:

	u	v	w	p	q	r	δ_e	δ_a	δ_r	δ_c		
X											LINEAR 10 X 6	60
Y											ENGINE	4
Z											CONTROLLERS δ &F	6
L											PARAMETERS	70
M												
N												

TASKS

HOVER	VERTICAL HORIZONTAL; LONG, LAT, DIR COMBINED	12
FORWARD FLIGHT	SHIPBOARD, SLUNG LOADS (V \geq 45 kt) MANEUVERING – LONG, LAT, DIR, AIR-AIR APPROACH AND LANDING	

ENVIRONMENT

VMC/IMC/NIGHT DISPLAYS/VISION AIDS WIND, SHEAR, TURBULENCE	10
---	----

EXPERIMENT

5 PARA X 4 VALUES = 5X5X5X5 = 625 2 TASKS, 2 ENVIR X 2 PILOTS (50% REPEAT) = 12	7600 EVALS
--	------------

SIMULATION TIME

15 MIN/EVAL X 20 HOURS/WEEK X 5 WEEKS =	400/SIMULATIONS
---	-----------------

Figure 27.- Scope of rotorcraft handling-qualities problem.

SYM	REF	RESPONSE TYPE	AIRCRAFT (FLIGHT/SIM)	TASK(S)	ω_{BW_θ}	TURB
◇	5	RATE	UH-60A (VMS)	SIDESTEP	2.3	LIGHT
◆	5	RATE	UH-60A (FLIGHT)	SIDESTEP	2.1	LIGHT
○	13	RATE	V/STOL (FSAA)	SHIPBOARD LDG	2.3	LIGHT
◇	14	RCAH	ADOCS (VERTOL SIM)	NOE	2.6	NONE
△	14	RCAH	ADOCS (VMS)	NOE	2.8	NONE
△	14	RCAH	ADOCS (VMS)	PRECISION HOVER	2.8	MOD
◆	45	RCAH	XV-15 (FLIGHT)	HOVER TRANSL	2.9	LIGHT
◆	45	RATE (SAS OFF)	XV-15 (FLIGHT)	HOVER TRANSL	0.4	LIGHT
■	46	RATE	AV-8A (FLIGHT)	HOVER (DAY)	2.3 (EST)	LIGHT
△	48	RATE	V/STOL (VMS)	SHIPBOARD LDG	1.8	LIGHT
▲	NCR	RCAH AND RATE ($\tau_p \leq 0.14$ sec)	UH-1H (FLIGHT)	LANDING	1.5-2.8	LIGHT

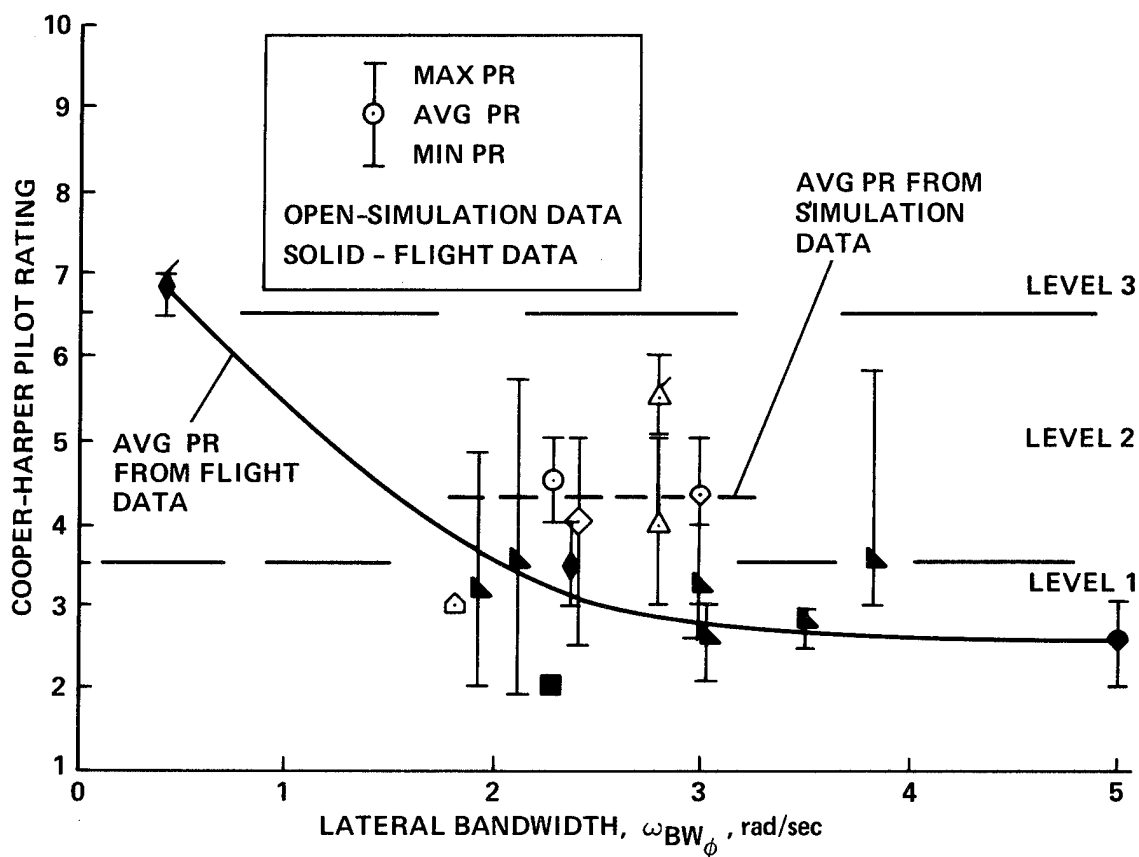


Figure 28.- Comparison of flight and simulation results for rate-response types.

ACOUSTICS

Session Cochairmen:

Otis S. Childress, NASA

Yung H. Yu, Department of the Army

ACOUSTICS SESSION

SUMMARY

Session Co-chairman Childress opened the session pointing out the tremendous growth in rotorcraft acoustic technology over the past decade. A short history leading to the formulation of the joint Government/Industry Rotorcraft Noise Reduction Program emphasizing the factors that drive the technology development was given. These factors also have driven the increased in-house sponsored research of both the government and industry. The four papers presented in this session discussed these expanded acoustic research programs of the government.

Mr. H. G. Morgan presented a paper entitled "Recent Langley Helicopter Acoustics Contributions." He focussed his remarks on the resolution of noise scales or metric issues for certification; status of the helicopter system noise prediction program (ROTONET); highlights of research on source noise mechanisms of the rotating systems, blade rotation, blade-vortex interaction, and broadband noise sources; and finally contributions to the interior noise problems.

Dr. John Coy presented a paper entitled "Identification and Proposed Control of Helicopter Transmission Noise at the Source." This paper dealt with identification of the source(s) within the transmission of the noise transmitted to the interior of the aircraft. The paper concludes with a discussion of a continuing research program focussed on reducing the noise sources and blocking transmission of the noise to the interior.

Dr. F. H. Schmitz presented a paper entitled "A Decade of Aeroacoustics Research at NASA-Ames." He gave an overview of accomplishments in the last decade in the following areas: acoustic flight and ground tests; wind-tunnel acoustic measurements; rotorcraft aeroacoustic scaling (definition of guidelines); theoretical predictions; and application of computational fluid dynamics to acoustic predictions.

Dr. Y. H. Yu presented a paper entitled "Aeroacoustic Research Programs in the Army." The thrust of Dr. Yu's paper was a discussion of theoretical and experimental work related to the understanding of helicopter impulsive noise.

RECENT LANGLEY HELICOPTER ACOUSTICS CONTRIBUTIONS

H. G. Morgan, S. P. Pao, and C. A. Powell

National Aeronautics and Space Administration
Langley Research Center

SUMMARY

The helicopter acoustics program at NASA Langley has included technology for elements of noise control ranging from sources of noise to receivers of noise. This paper discusses the scope of Langley contributions for about the last decade. Specifically, it reviews the resolution of two certification noise quantification issues by subjective acoustics research, the development status of the helicopter system noise prediction program ROTONET, and presents highlights from research on blade rotational, broadband, and blade vortex interaction noise sources. Finally, research contributions on helicopter cabin (or interior) noise control are presented. A bibliography of publications from the Langley helicopter acoustics program for the past 10 years is included.

INTRODUCTION

Acoustics research at Langley Research Center covers sources of noise, propagation of noise, and receivers of noise. That portion of acoustics research aimed at helicopters has the same total scope and begins with understanding, predicting, and reducing noise generated by the most important sources, considers propagation of noise from source to receiver through the atmosphere or vehicle structure, and includes technology to determine criteria for controlling the impact of noise on receivers. Two classes of helicopter receiver problems are being addressed. The first class of research concerns the control of noise impacting residents in heliport communities--the "exterior" noise problem. The second class of concerns relates to the control of the noise environment of helicopter passengers and crew--the "interior" noise problem.

Helicopter acoustics research at Langley Research Center has been ongoing for about three decades. The level of activity was relatively small until the last decade when national and international concerns with the environment and quality of life resulted in proposals for noise certification of helicopters. The stimulus of impending noise certification requirements led to the recognition of limitations of existing noise control technology and to a push to expand the noise control technology base. Therefore, beginning in the late 70's, Langley helicopter acoustics research expanded significantly to respond to this need. The thrust of the expanded program has been to create the capability to design to a noise goal in order to make U.S. helicopters more competitive in the world-wide civil marketplace. Most of the effort has gone

into the exterior, or community, noise problem at which noise certification is directed. A lesser, but still significant effort has gone towards control of the interior noise environment of passengers and crew.

An appreciation for the scope of acoustics research necessary to create design-to-a-certification-noise-goal capability comes from considering the complexity of helicopters as noise sources. This complexity is illustrated conceptually in figure 1 which shows a helicopter noise spectrum to be made up of contributions from several different noise sources. Sound at lower frequencies tends to be dominated by blade rotational tones arising from rotor loading and thickness. At higher frequencies, the sound becomes broadband in character and is generated by mechanisms that involve turbulence inflow or the rotor blade boundary layer. Of course, these sources exist on both main and tail rotors which generate noise at differing frequencies due to different shaft speeds. In intermediate frequency ranges, interaction noise sources tend to dominate the spectrum. Probably the most significant is blade vortex interaction (BVI) which occurs when the tip vortex shed from one blade is intersected by a following blade. Another such source is main rotor-tail rotor (MR-TR) interaction occurring when the tail rotor is loaded by the unsteady downwash field of the main rotor. The relative levels and frequencies of the various sources shift with operating condition, forward speed, and observer location relative to the vehicle. To determine which of the noise sources are in most need of research, the end goal of noise certification must be considered. The noise scale used for designing and certifying helicopters is the Effective Perceived Noise Level, or EPNL, that incorporates the A-weighted filter to approximate the response of the human ear and reflect people's perception of noise. The filter provides greatest weight to sound energy in the 1000 to 5000 Hz frequency range and filters out much of the low frequency sound energy associated with blade rotational noise. The filtered noise spectra is shown to be much "flatter" than the unfiltered spectra and to increase the relative importance of higher frequencies. For this reason, civil helicopter noise research must include the higher frequency sources even though their absolute noise levels are significantly less than the noise levels in the lower frequency range.

This paper will discuss the most significant of Langley's recent contributions to the technology of helicopter noise control. The first section describes research to resolve international issues associated with noise measurement for quantifying noise during helicopter certification and during heliport operations. Then, the program to develop design-for-noise capability centered on the ROTONET noise prediction system will be described. The research to understand, predict, and reduce the most important individual noise sources follows. The last section of the paper shifts attention from exterior to interior noise concerns and discusses Langley research on cabin environment. Finally, a bibliography is included which lists Langley helicopter acoustics research publications of the past decade.

NOISE MEASUREMENT SCALES

The prime requirement for noise measurement scales, or a noise metric, for noise certification or for assessing impact of noise on communities is

that the scale adequately quantify those characteristics of the noise which influence human perception. During the past decade, NASA Langley has conducted a number of subjective acoustic studies to answer specific questions related to the ability of noise scales to quantify helicopter noise. Two studies which have had major impact on FAA and ICAO noise certification procedures (FAR-Part 36) and community noise assessment regulations (FAR-Part 150) are described in the following sections.

Noise Certification

A major concern in choosing a measurement scale for helicopter noise certification was the need for an impulse correction to account for the blade-slap phenomenon. Prior to the formulation of the ICAO noise certification rule and FAA notice of proposed rule making (NPRM), some laboratory studies had indicated that the standard aircraft noise certification scale, effective perceived noise level (EPNL), underestimated the annoyance due to helicopter noise containing appreciable blade-slap. As a consequence, an impulse correction was proposed which would have significantly complicated the EPNL calculation procedure and which would have severely penalized some U.S. manufactured helicopters. To provide data in a realistic setting, the FAA requested that Langley conduct a flight experiment using a jury of people to evaluate actual helicopter overflight sounds.

In the experiment conducted at NASA Wallops Flight Facility in the spring of 1978 and reported in reference 1, 91 people made judgments on the noise of 72 helicopter and propeller airplane flyovers. Some of them were located inside houses and others were out-of-doors during the tests. A photograph of the outdoor subjects and the test area is presented in figure 2. The impulsive characteristics of one of the two helicopter types was systematically varied by changing the main rotor speed while maintaining a constant airspeed and holding other characteristics of the noise relatively constant.

Results from the experiment indicated that, at equal noise levels as measured by EPNL, the more impulsive helicopter was judged less annoying than the less impulsive helicopter. This result is illustrated in figure 3 where the average annoyance rating given by the outdoor listeners is plotted against EPNL for the two helicopter types and the propeller airplane. Least square linear regression fits to the data for the impulsive and non-impulsive helicopters are indicated by the solid and dashed lines respectively. The more impulsive helicopter was judged very similar to the propeller airplane. These and other results from the experiment indicated that the proposed impulse correction did not improve the annoyance prediction ability of EPNL. Based on these results and a number of additional carefully controlled laboratory studies conducted at Langley or under NASA contract, the United States delegation convinced the ICAO to drop the impulse correction requirement for helicopter certification.

Community Impact

The total community impact of aircraft or helicopter noise is generally considered to depend on the number of overflights as well as the noise level from each overflight. The equivalent noise level (LEQ) scale, which integrates or sums the noise from a number of overflights on an energy basis, has been shown by both community surveys and laboratory studies to effectively quantify the total noise impact around large airports or along major roads with a large number of noise events per day. However, does LEQ adequately reflect annoyance around the growing number of heliports with a low number (1 to 10) of flights per day? Because of the difficulty in obtaining sufficient statistical accuracy, standard community survey techniques applied to naturally occurring heliport environments are inappropriate for answering this question. In addition, the necessity for testing very low numbers of events for extended time periods made the validity of laboratory experimentation questionable. With the support of the FAA, a new methodology was used to address this issue that combined the home environment with controlled noise exposures, reference 2.

The survey was conducted by telephone in a community near Fort Eustis, Virginia that is normally exposed to helicopter noise. The participants were repeatedly surveyed on evenings following days in which the helicopter noise levels and number of flights were closely controlled by arrangement with Army heliport officials. Noise exposure was controlled by using two different types of helicopters on different days in the tests. A UH-1H helicopter provided a relatively impulsive noise exposure and a UH-60A provided a relatively low impulsive exposure. On any given day overflights were made at either 500 ft. or 1500 ft. to provide nominal peak noise levels of 85 dB(A) or 75 dB(A). The number of planned flights per day varied from 1 to 32. Noise measurements were made at a number of locations in the community on test days to ensure accurate noise exposure estimates. The community residents participating in the survey were paid an honorarium to maintain interest but were told only of a general interest in transportation noise and given no hint of the true purpose of the test. A total of 338 residents were interviewed on each of 17 controlled exposure days.

Results from the survey indicate that community residents could discriminate days with noise exposures resulting from a very low number of flights per day from days with only a few more flights per day. Average annoyance scores for days with different noise exposures are shown in figure 4 on the noise scale sound exposure level (SEL) with number of flights as a parameter. SEL is a measure of the noise exposure of a single flight which includes A-weighting for frequency content and is corrected for the duration of the flight. An increase in annoyance with exposure is seen over the range of both noise level and number of flights. The data were also examined to determine the applicability of single number noise exposure indexes to quantify the respondents' annoyance. Results for LEQ, the scale used to assess airport noise exposure in the FAR-Part 150 and by the EPA for any type of community noise exposure, is shown in figure 5. Except for the very lowest noise exposure condition, a linear increase in annoyance with exposure is evident, thus demonstrating that the LEQ scale is indeed applicable to heliport community situations with low numbers of flights per day.

Although not illustrated in this paper, several other interesting findings were obtained in the survey. One, consistent with the results of the field study described previously, was that impulsive helicopters are not inherently more annoying than non-impulsive helicopters when their noise is measured on a scale corrected for duration and noise level.

ROTONET

The aim of noise certification is to force the incorporation of the best available noise control technology in new helicopter designs. For this to happen in a rational manner, manufacturers must be able to conduct sensitivity analyses that predict, with confidence, the effects of design variables on the noise generated under certification conditions. As pointed out earlier, this requires methodology for determining noise from several helicopter noise sources and then predicting their combined effects in certification measurement units under specified conditions. ROTONET is a modular testbed computer program that predicts noise at a specified receiver location of a helicopter system that aims to meet this need. The elements of ROTONET are depicted in figure 6. Inputs include the configuration variables (such as rotor and tail rotor geometry and rotational speeds), flight path (such as level flyover or landing descent), and observer location (such as certification measurement sites). The ROTONET computer program itself has three major functional computer code groups. The first, rotor performance, predicts the airfoil section and rotor force coefficients for isolated main and tail rotors and generates aerodynamic loads and motions for inputs to source noise prediction. The second code grouping contains several source noise modules that are required to account for all contributors such as blade rotational noise, broadband noise, and blade vortex interaction. Finally, the propagation cluster of modules accounts for effects such as source to observer geometry, atmospheric absorption, spherical spreading, and ground reflection and attenuation, and computes the noise on any desired scale such as overall sound pressure level (OASPL), A-weighted sound pressure level (L_A), and effective perceived noise level (EPNL).

The modular approach to ROTONET permits the newest technology to be incorporated in the computer system. The prediction procedure for any given noise source may be analytical or empirical and can be replaced by a better procedure that subsequently becomes available. A user's proprietary method can be incorporated by meeting well defined interface requirements. A phased development of ROTONET is being followed, with each phase representing a more complete and advanced modeling of the helicopter noise prediction problem. The Phase I baseline system described in reference 3 is operational and contains blade rotational and broadband noise modules. The Phase II version now being evaluated adds better broadband source noise capability, accounts for non-uniform inflow, uses a prescribed wake, expands the harmonic range of the blade rotational source module, and generally improves utility. The Phase III version under development is building towards including a BVI capability and a rotor free wake along with other improvements. In addition to operating on Langley's mainframe CDC computers, ROTONET operates on VAX minicomputers and in that form has been delivered to all four major helicopter companies.

At least three of the companies have exercised the Phase I and Phase II systems, have verified that proprietary modules can be interfaced and operated with ROTONET, and are planning to evaluate the more advanced versions.

Initial applications of ROTONET indicate the kinds of results that are possible. Table I, from reference 3, compares predictions with measurement of EPNL for a Bell 222 in level flyover for four combinations of speed and altitude. The prediction with just rotational noise sources is directly from the Phase I system and is uniformly low compared to measurement by about 6-7 EPNdB. The broadband source module used in the second prediction is a partial version of the full broadband source module in Phase II. The addition of the broadband source significantly improves the overall agreement with measurement, bringing it to within 3-4 EPNdB. This comparison demonstrates that the broadband source is a significant contributor when noise is measured on the EPNL scale. However, it also shows that system noise prediction must be further improved before it can be routinely applied with confidence. The goal continues to be to predict EPNL to within +1.5 EPNdB. For the case presented, addition of the BVI source is believed to be necessary for further significant improvement in prediction.

While the EPNL predictive ability just discussed is the desired product of ROTONET, determination and assessment of weak links in prediction of the complex quantity EPNL is extremely difficult. The comparison with data just discussed relates output for a given input but gives no information on the efficacy of the myriad of intervening steps. Therefore, a series of helicopter flight tests are underway to obtain a data base that not only relates input (flight condition) to output (EPNL) but also permits assessment of the intervening steps. This data base will be used to validate the predictive ability of ROTONET, develop confidence in its utility, and identify improvement needs.

The first test in the series has been completed at Wallops Flight Facility and was conducted cooperatively with McDonnell-Douglas Helicopters using the 500E helicopter shown in figure 7. The configurations tested had a 5-blade main rotor, either 2- or 4-blade tail rotors, and sometimes included an engine exhaust muffler to insure uncontaminated main and tail rotor noise. A specially designed rotor head telemetry system transmitted rotor blade data for on-board recording along with other vehicle data, thus eliminating slip rings for obtaining high frequency data off the rotor. Laser radar tracking provided precise helicopter position and velocity data. Microphone array techniques, time correlated with the on-board data, were used to measure a hemispherical far field noise directivity pattern underneath the vehicle with a high level of statistical confidence. A typical result from the May 1986 test is illustrated in figure 8 and compared with a ROTONET prediction. In this case, the 1/3 octave band noise spectrum radiated from near the overhead position is shown. The prediction of the details of the spectrum are reasonable at low frequencies, very good at mid-frequencies, and poor at higher frequencies. However, EPNL (which makes use of the spectrum time history throughout the flyover) is predicted to within 1.7 EPNdB, illustrating the forgiving nature of the EPNL scale. Such detailed spectral information shows clearly that improved noise source models must be included in the system model. The acoustic data from the MD 500E flight test will include EPNL and

narrow band spectra as well as 1/3 octave spectra such as this for measurement locations beneath the helicopter covering nearly a hemisphere. The data base will also include operating and dynamic state data and layered atmospheric weather data and will be available to the industry for comparison with company prediction methods as well as ROTONET.

NOISE SOURCES

Helicopter external noise is generated by a large number of distinctively different sources and mechanisms. Among the most important are high speed impulsive noise associated with transonic rotor tip speeds, tonal rotational noise from main and tail rotors, broadband noise of various types, blade-vortex interaction noise, main rotor-tail rotor interaction noise, and engine noise. With the exception of engine noise, all these sources are related to moving aerodynamic surfaces of helicopters. Therefore, their intensity and spectral characteristics are functions of system configuration, flight speed, maneuvers, and rotor dynamics. Thus, the analysis, prediction, and measurement of individual source components, which are needed as part of the total helicopter system noise prediction in ROTONET, are complex and difficult. However, significant progress has been made in the quantitative understanding of the most important source mechanisms. Research to understand the high speed impulsive noise source has been led by the Army Aeromechanics Directorate at Ames Research Center. Langley Research Center's most significant accomplishments are related to three important sources for civil noise certification, blade rotational noise, broadband noise, and blade vortex interaction noise.

Rotational Noise Theory

The generation of noise by bodies in arbitrary motion is governed by the Ffowcs Williams Hawkins (FW-H) equation which may be derived from first principles of mass and momentum conservation. It can be simply interpreted as a wave equation with three source terms commonly identified as the thickness, loading, and quadrupole noise sources. At Langley, Farassat obtained and reported a general solution to the FW-H equation and adapted it to rotor noise prediction, reference 4. His analytical development is unique in several ways. Mathematics aside, perhaps most important is that the solution is obtained in the time domain, rather than the frequency domain, as an acoustic pressure time history. The solution is expressed in an integral form that can be numerically evaluated and permits full description of rotor blade geometry and kinematics. Since the noise spectrum is obtained by Fourier transform of the time history, the method predicts amplitudes of the fundamental and all its harmonics and is not limited to predicting only one or two tones. More recent developments have shown that the time domain solution can also be adapted for linearized unsteady aerodynamic analysis, reference 5, and extended to obtain a practical solution for supersonic tip speed propeller noise analysis, reference 6.

A comparison between prediction by the Farassat formulation and measured noise data from the Operations Loads Survey (OLS) Bell helicopter were conducted and reported in references 7 and 8 to evaluate the prediction capability. Typical results from that validation study are shown in figures 9 and 10. Shown are noise spectra measured and predicted ahead of the helicopter, near the plane of the rotor. Figure 9 is at relatively low speed, 66 fps, and 8.5 degrees below the rotor plane. The fundamental rotor tone and 16 harmonics are illustrated. Three tail rotor tones are also identified over the frequency range. For the predictions, measured aerodynamic loads were used as inputs. The results demonstrate that full scale rotor rotational noise can be predicted with good accuracy at modest forward speeds using only thickness and loading source components, if aerodynamic loading is known with confidence. Figure 10 is a result at higher flight speed, 200 fps, 13.3 degrees below the rotor plane. At this higher speed, the amplitudes of the fundamental tone and lower harmonics were underpredicted, indicating the need to consider quadrupole sources, transonic aerodynamics near the advancing blade tip, or nonlinear effects. This particular methodology for predicting rotational noise, demonstrated to work very well except at high forward speeds, is part of the Phase I ROTONET system described earlier.

Recently, substantial effort has been devoted to improving the computational codes for rotor blade rotational noise prediction. The theory has been reformulated to permit faster and more accurate computations. Other improvements in the numerical algorithms and geometrical modeling have improved speed and robustness. The complete, updated version of the blade rotational noise prediction code, known as the Brentner-Farassat code or WOPWOP, is described in reference 9 and has been distributed to the industry. Two results using the code from a recent validation effort in reference 10 are shown in figures 11 and 12. The comparisons are with wind tunnel data for a 1/4 scale UH-1 helicopter. The noise code was coupled to an existing rotor performance code, C-81 from Ames Research Center, to generate input data. Figure 11 shows the acoustic pressure time history and spectrum for a case where thickness noise dominates. Agreement in time history and for a broad frequency range are felt to be good and of the same order of agreement obtained with earlier codes. Figure 12, however, is the time history for a flight condition where loading noise is dominant and BVI occurs. Agreement is not good for this case for two reasons--first, BVI prediction is not included in the analysis, and secondly, the aerodynamic loads from C-81 are inadequate. This highlights the necessity of using the best available aerodynamic loading information if blade rotational noise is to be predicted for arbitrary locations and flight conditions. The robustness, high resolution, and stability of the new code make it ideal for studying noise effects of detailed rotor dynamics, such as lead-lag and random impulsive blade loads, and rotor geometry variations. Therefore, Langley efforts are directed at coupling the noise code to newer and better aerodynamic codes including Ames' CAMRAD and TFAR codes.

Broadband Noise

Broadband noise is of concern for its contributions to total noise measured on the certification scale EPNL at higher frequencies. It is

especially important for large, low rotor-speed rotor systems. Numerous broadband sources and generating mechanisms have been identified. Unsteady, non-deterministic loading on the rotor produces the random part of blade rotational noise. Of more concern at higher frequencies is the self-noise generated by a rotor blade and its boundary layer and shed vortices. Dominant broadband source mechanisms recognized in the survey of reference 11 are turbulence ingestion, trailing edge-turbulence interaction, trailing edge bluntness, separated flows, and blade tip vortex shedding.

The Langley program has addressed these sources over the past decade so that the relative importance of each is understood. An example of this research from reference 12 is illustrated in figures 13 and 14. As seen in the photograph, relatively small models were tested at low velocities in Langley's Quiet Flow Facility. Most tests were two-dimensional and varied Reynolds numbers over a wide range by changing both velocity and airfoil chord. The data show how the scaled noise level for the trailing edge-boundary layer interaction source collapses into a single curve through the boundary layer laminar to turbulent transition flow region. Such measurements were a key in developing an empirical prediction method for the broadband sources that has been incorporated into ROTONET.

An opportunity to assess broadband prediction methods occurred during the joint NASA/DFVLR/FAA rotor noise test in the DNW wind tunnel in the Netherlands during May 1986. Figure 15 shows the 40% scale B0-105 rotor being tested in that facility. The unique DNW aeroacoustic wind tunnel is the only facility in the world with an acoustic environment permitting broadband noise to be measured on a model of realistic size. Noise was measured with microphones above the rotor plane and external to the flow. Prior to tunnel entry, the broadband noise for each test condition had been predicted using the newly developed method for ROTONET. One of the best comparisons from reference 13 is presented in figure 16. Four 50 Hz bandwidth measured spectra are shown for constant thrust coefficient, C_T , and advance ratio, μ . The parameter, angle of attack of the tip path plane, α_{Tpp} , is a measure of rate of descent which is known to be major variable in blade vortex interaction, or BVI. The broadband noise prediction in the figure uses all of the previously mentioned source mechanisms except trailing edge bluntness which is not important for this case. As expected, at low frequencies where rotational and blade vortex interaction noise dominate, the prediction falls far below the measured spectra. However, at high frequencies, the prediction agrees remarkably well with experiment. While complete data from the experiment are still being analyzed, this early result is very encouraging and suggests that the prediction procedure truly incorporates the important noise generation mechanisms. The agreement is surprising when considering the 2-dimensional basis for the prediction method. However, the availability of data from a carefully conducted basic research experiment, even though 2-dimensional, is the key to the good prediction.

At intermediate frequencies, up to about 6000 Hz model scale, noise levels in figure 16 change drastically with the parameter α_{Tpp} , thus indicating interaction is dominating the noise at these frequencies. The state of understanding of the interaction noise is still poor, and is the focus for on-going research, some of which is discussed in the next section.

Blade-Vortex Interaction Noise

Blade vortex interaction (BVI) noise arises from the impulsive load when a rotor blade intersects or passes near the tip vortex shed by a preceeding blade. It depends on operating conditions, observer position, and frequency range. As just pointed out on figure 16, it's energy usually shows in the spectrum between lower frequency blade rotational noise and higher frequency broadband noise. Research on this very complex noise source is not nearly as advanced as on the other sources discussed. Langley's approach to the problem has been to study it in a very fundamental way with 2-dimensional experiments and analysis as well as to conduct wind tunnel experiments on rotating blade systems. Figure 17, from reference 14, shows a 2-dimensional flow visualization experiment in the Langley Quiet Flow Facility which examined details of vortex interaction with an airfoil and determined the bounds of three zones of interaction for BVI. A distributed vortex may deflect its trajectory but will retain its shape if it is more than one chord length away from the airfoil. When the encounter distance is within a half chord, the vortex will deform as well as deflect. If the encounter distance is within an airfoil thickness, collision occurs and viscous interaction splits the incident vortex and may induce secondary vortices. Parallel computational acoustic studies using an Euler Code to model the interaction process are reported in reference 15 and illustrated in figure 18. A vortex is injected 1.5 chord lengths upstream from and 0.5 chord lengths below the airfoil leading edge and then tracked as it washes downstream. It both distorts and accelerates as it passes a lifting airfoil and these processes generate the noise. The predicted acoustic pressure time history is seen to closely approximate the familiar impulse noise of BVI.

Such fundamental studies provide insights into the fluid mechanics that generate BVI. However, experiments with rotating blade models are necessary to develop noise prediction capability and noise reduction approaches. The most recent such Langley experiment on BVI was conducted jointly with the broadband noise experiment in the DNW wind tunnel in May 1986. The test configuration for BVI noise testing is shown in figure 19 and is reported in reference 16. In this case, an array of microphones is mounted on a traversing carriage beneath the rotor, with the microphones inside the wind tunnel flow, to map the BVI noise on a plane beneath the rotor. A typical result is shown in figure 20 for a rotor tip-path-plane angle of 2.3° . The contours are constant peak-to-peak BVI pressure on a plane 2.1 m beneath the 4-meter diameter rotor. The area covered by the rotor disk is shaded. The unsymmetric character of the BVI radiated noise is immediately apparent, with the most intense noise appearing under the advancing side of the rotor. This is believed to result from a vortex interaction with an advancing rotor blade in the aft quadrant. On that basis, the square shaded area is the noise source shadow cast by the fuselage which makes BVI noise levels in the shadow questionable. The very steep gradients of acoustic pressure demonstrate the sensitivity of microphone placement in any experimental assessment of BVI. Data from this experiment are being used to evaluate prediction methods for the BVI source which are urgently needed in the ROTONET noise prediction system.

CABIN ENVIRONMENT

The final section of this paper will discuss recent Langley contributions toward understanding and controlling the noise and vibration environment in cabins of helicopters. The interior noise and vibration levels of current helicopters are very high relative to other air and ground transportation systems due to proximity of the crew and passenger spaces with the rotor gearbox which is the dominant interior noise and vibration source. The result of the high noise and vibration levels is poor passenger acceptance compared to other aircraft and, in the case of military helicopters in particular, possible degradation in pilot performance and increased risk of hearing loss. The Langley program has included numerous studies of ride quality due to noise and vibration in helicopters and other transportation systems as well as a number of studies for predicting and controlling helicopter interior noise. The model developed for predicting ride quality due to combined interior noise and vibration will be described first, followed by a discussion of two helicopter interior noise studies.

Ride Quality Model

A series of experimental studies that used Langley's Passenger Ride Quality Apparatus (PRQA), figure 21, and over 3000 test subjects generated a data base from which a comprehensive model for estimating discomfort/acceptance of passengers exposed to complex interior noise and vibration was developed. The model, reference 17, accounts for multi-degree of freedom vibrations combined with interior noise. The basic outputs of the model are numerical indices representing total absolute discomfort (or acceptance) of a given environment as well as indices representing the relative contributions of noise and vibration to total discomfort. The indices are measured on a ratio scale, called DISC's, such that $DISC = 2$ corresponds to twice the discomfort as $DISC = 1$, etc. The absolute value of $DISC = 1$ represents a threshold level rated uncomfortable by 50 percent of the subjects tested. The model has been incorporated into a commercially available device, called the Ride Quality Meter, which samples the noise and vibration environment and reads out the numerical discomfort indices, reference 18.

A recent study to assess the validity of the ride quality model is reported in reference 19. The study was conducted in the PRQA using measured helicopter interior noise and vibration as inputs and experienced military pilots as test subjects. The interior of the simulator was configured to resemble a modern jet transport with four first class seats. The noise and vibration inputs were measured on OH-58C, UH-1H, AH-1S, UH-60A and CH-47C helicopters. Military pilots (35 from Fort Eustis, VA and Naval Air Station, Norfolk, VA) served as passengers who rated each of 120 different ride conditions. The noise conditions represented levels and spectra inside current flight helmets.

Typical results from the study are shown in figure 22 for the range of noise and vibration simulated for the OH-58C helicopter. Average discomfort rating, in DISC's, is plotted versus interior A-weighted noise level for low,

moderate, and high vibration conditions. Open symbols represent mean discomfort ratings given by pilots, and closed symbols show predicted discomfort ratings from the NASA model. The agreement is good over the range of conditions and the data show the typical interactions between noise and vibration that determine total discomfort. Because of the good agreement between predicted and actual ratings in this and other studies, the U.S. Army Aviation System Command has recently incorporated the NASA ride quality model into the human factors vibration requirement of their Aeronautical Design Standard ADS-27.

Interior Noise Prediction and Control

NASA Langley Research Center has conducted several programs to investigate aspects of helicopter interior noise control. In one early program, the Civil Helicopter Research Aircraft (CHRA), the modified CH-53A shown in figure 23, was outfitted with a 16-seat passenger cabin and state-of-the-art noise control treatment. Acoustic measurements, reference 20, were made over a wide range of operating conditions before and after the installation of the acoustic treatment. A comparison of the noise environment in the treated and untreated interior volume is shown in figure 24. Both before and after treatment, the subjectively dominant noise sources were identified as first-stage planetary and main bevel/tail take-off gear clash. Although acoustic treatment reduced interior noise levels about 30 dB, the levels were still considerably in excess of current jet transports. Subsequent flight demonstrations confirmed that interior noise remained excessive.

The experiences from the Civil Helicopter Program demonstrated the shortcomings of helicopter interior noise control technology. Langley has since contracted with Sikorsky to develop advanced, but practical, helicopter interior noise predictive techniques and control concepts. Extensive flight and laboratory measurements of cabin noise and structural vibrations at acoustic frequencies have been made on a modern helicopter, figure 25, and are reported in reference 21. These measurements were used to validate a statistical energy analysis (SEA) model of the directly radiated and structure-borne interior noise originating from the gearbox which dominates the cabin noise. In the SEA model, the S-76 fuselage is represented by 95 subsections (35 frames, 53 panels, and 7 acoustic spaces) and 235 junctions. The only main elements not modeled are the propulsion system, tail cone and landing gear.

A comparison of the predicted and measured in-flight cabin noise is presented in figure 26 for the four subjectively most important octave bands centered at 500, 1000, 2000 and 4000 Hz. Also shown is the Speech Interference Level (SIL), a noise scale which sums the energy in these bands and which is frequently used for specifying cabin noise levels. The maximum and minimum noise measured at various locations in the cabin as well as the data averaged over the cabin is presented. Excellent agreement was found between the predicted and measured interior noise for SIL and for each octave band when experimental data were averaged over measurement locations. Since the

SEA model provides a volume average of the acoustic energy level, the averaging of the levels at many locations is appropriate and demonstrates that predictive tools are available for this class of problems.

Analytical studies using the SEA model have shown that the most efficient interior noise reduction for this vehicle can be achieved with high frequency vibration isolation between the gear box and the fuselage. Therefore, a resilient, load-limiting, fail-safe isolator has now been designed and will be evaluated in ground experiments in the final phase of the contract to complete the cycle of noise prediction, diagnosis, and reduction.

CONCLUDING REMARKS

This paper summarizes the major helicopter acoustics research activities of Langley Research Center over the last decade. Individual projects are described that address a variety of issues covering the span of acoustics disciplines from noise generation by individual sources to the propagation of noise and the effects of noise on receivers. Most of this research has been driven by civil sector requirements for noise certification and heliport operations.

Langley research was a major factor in resolving national and international issues on noise measurement scales used to quantify helicopter noise. Certification issues involving a "penalty" for blade slap noise proposed by U.S. competitors were resolved, and, in another case, the ability of LEQ to quantify community environmental impact around heliports with very limited numbers of operations was demonstrated.

The ROTONET testbed helicopter noise prediction computer system has become a reality with operational codes delivered to the four major manufacturers for evaluation during 1986. This prediction capability includes blade rotational and broadband sources and operates at each company on VAX computers. However, confidence must be established in prediction ability before ROTONET is widely used. A series of validation flight tests are planned to acquire the data for this purpose, but only the first test using a MD-500E helicopter has been completed. In addition, Phase III ROTONET is under development to improve prediction capability by including additional, as well as improved, source noise models.

Langley research on individual helicopter noise sources is focused on the requirements for ROTONET. Rotor blade rotational source noise theory is highly developed but needs to be expanded to include quadrupole sources and nonlinear effects to treat higher tip speeds. A big increment in blade rotational noise prediction ability will come from improved high frequency unsteady aerodynamic load predictions, expected to come from CFD codes, which are a main ingredient in noise prediction. Excellent progress in defining and developing semi-empirical predictions for broadband noise has also been made in the last 5 years. This technology has been made available to the industry through ROTONET. Progress on interaction noise is urgently needed but is coming much slower. The interaction noise generation mechanisms are extremely

complicated and are the subject of studies by Langley and other research groups. As results become available, the technology will be included in ROTONET.

The internal noise and vibration environment in helicopter cabins has been studied less extensively. A ride quality model has been developed which predicts passenger and crew acceptability of combined noise and vibration environments. Recently, this model was incorporated in the Army Aviation System Command's aeronautical design standards. On-going research on interior noise control has resulted in an interior noise prediction methodology which provides, for the first-time, a tool for design sensitivity analyses. Combined with new materials and concepts, an opportunity now exists for significant progress in this difficult area.

REFERENCES

1. Powell, C. A.: Subjective Field Study of Response to Impulsive Helicopter Noise. NASA TP 1833, April 1981.
2. Fields, J. M.; and Powell, C. A.: A Community Survey of Helicopter Noise Annoyance Conducted under Controlled Noise Exposure Conditions. NASA TM 86400, March 1985.
3. Golub, R. A.; Weir, D. S.; and Tracy, M. B.: Application of the Baseline ROTONET System to the Prediction of Helicopter Tone Noise. AIAA Preprint No. 86-1904, July 1986.
4. Farassat, F.: Theory of Noise Generation from Moving Bodies with an Application to Helicopter Rotors. NASA TR R-451, 1975.
5. Farassat, F.: A New Aerodynamic Integral Equation Based on an Acoustic Formula in the Time Domain. AIAA Journal, vol. 22, p. 1337, 1984.
6. Nystrom, P. A.; and Farassat, F.: A Numerical Technique for Calculation of the Noise of High-Speed Propellers with Advanced Blade Geometry. NASA TP 1662, 1980.
7. Succi, G. P.: Validation of Helicopter Noise Prediction Techniques. NASA CR 165715, 1981.
8. Farassat, F.; and Succi, G. P.: The Prediction of Helicopter Rotor Discrete Frequency Noise. Vertica, vol. 7, pp. 309-320, 1983.
9. Brentner, K. S.: Prediction of Helicopter Rotor Discrete Frequency Noise a Computer Program Incorporating Realistic Blade Motions and Advanced Acoustic Formulation. NASA TM 87721, 1986.
10. Brentner, K. S.: A Prediction of Helicopter Rotor Discrete Frequency Noise for Three Scale Models Using a New Acoustic Program. AIAA Paper No. 87-0252, presented at the 25th AIAA Aerospace Sciences Meeting, Reno, Nevada, January 12-15, 1987.

11. Brooks, T. F.; and Schlinker, R. H.: Progress in Broadband Noise Research. Vertica, vol. 7, pp. 287-307, 1983.
12. Brooks, T. F.; Marcolini, M. A.; and Pope, D. S.: Airfoil Trailing-Edge Flow Measurements. AIAA Journal, vol. 24, pp. 1245-1251, 1986.
13. Brooks, T. F.; Marcolini, M. A.; and Pope, D. S.: Model Rotor Broadband Noise Study in DNW. Paper presented at the AHS National Specialists' Meeting on Aerodynamics and Aeroacoustics, Arlington, TX, February 1987.
14. Booth, E. R., Jr.; and Yu, J. C.: Two-Dimensional Blade-Vortex Flow Visualization Investigation. AIAA Journal, vol. 24, pp. 1468-1473, 1986.
15. Hardin, J. C.; and Lamkin, S. L.: An Euler Code Calculation of Blade-Vortex Interaction Noise. ASME Paper 86-WA/NCA-3, presented at the ASME Winter Annual Meeting, Anaheim, CA, December 7-12, 1986.
16. Martin, R. M.; and Splettstoesser, W.: Initial Acoustic Results from the BVI Test of a 40 Percent Model Rotor in the DNW. Presented at the AHS National Specialists' Meeting on Aerodynamics and Aeroacoustics, Arlington, TX, February 25-27, 1987.
17. Leatherwood, J. D.; Dempsey, T. K.; and Clevenson, S. A.: A Design Tool for Estimating Passenger Ride Discomfort within Complex Ride Environments. Human Factors, vol. 22, no. 3, pp. 291-312, June 1980.
18. Wood, J. J.; and Leatherwood, J. D.: A New Ride Quality Meter. Presented at the SAE Vehicle Noise and Vibration Conference, May 15-17, 1985, Traverse City, Michigan. In Proceedings of Vehicle Noise and Vibration Conference, Paper No. 850981, pp. 177-183.
19. Leatherwood, J. D.; Clevenson, S. A.; and Hollenbaugh, D. D.: Evaluation of Ride Quality Prediction Methods for Helicopter Interior Noise and Vibration Environments. NASA TP 2261, AVSCOM TR-84-D-2, March 1984.
20. Howlett, J. T.; Clevenson, S. A.; Rupf, J. A.; and Snyder, W. J.: Interior Noise Reduction in a Large Civil Helicopter. NASA TN D-8477, July 1977.
21. Yoerkie, C. A.; Gintoli, P. J.; and Moore, J. A.: Development of Rotorcraft Interior Noise Control Concepts; Phase II, Full Scale Testing. NASA CR 172594.

Altitude (ft)	Speed (kts)	EPNL (EPNdB)		
		Predicted rotational only	Predicted rotational & broadband	Measured
404	137	88.0	90.1	92.5
417	123	85.6	88.4	91.6
452	110	83.0	86.7	90.4
977	123	79.4	82.1	85.8

Notes: Overhead flyover

Microphone 4 feet above ground

TABLE I.- EFFECTIVE PERCEIVED NOISE FOR HELICOPTER IN LEVEL FLYOVER

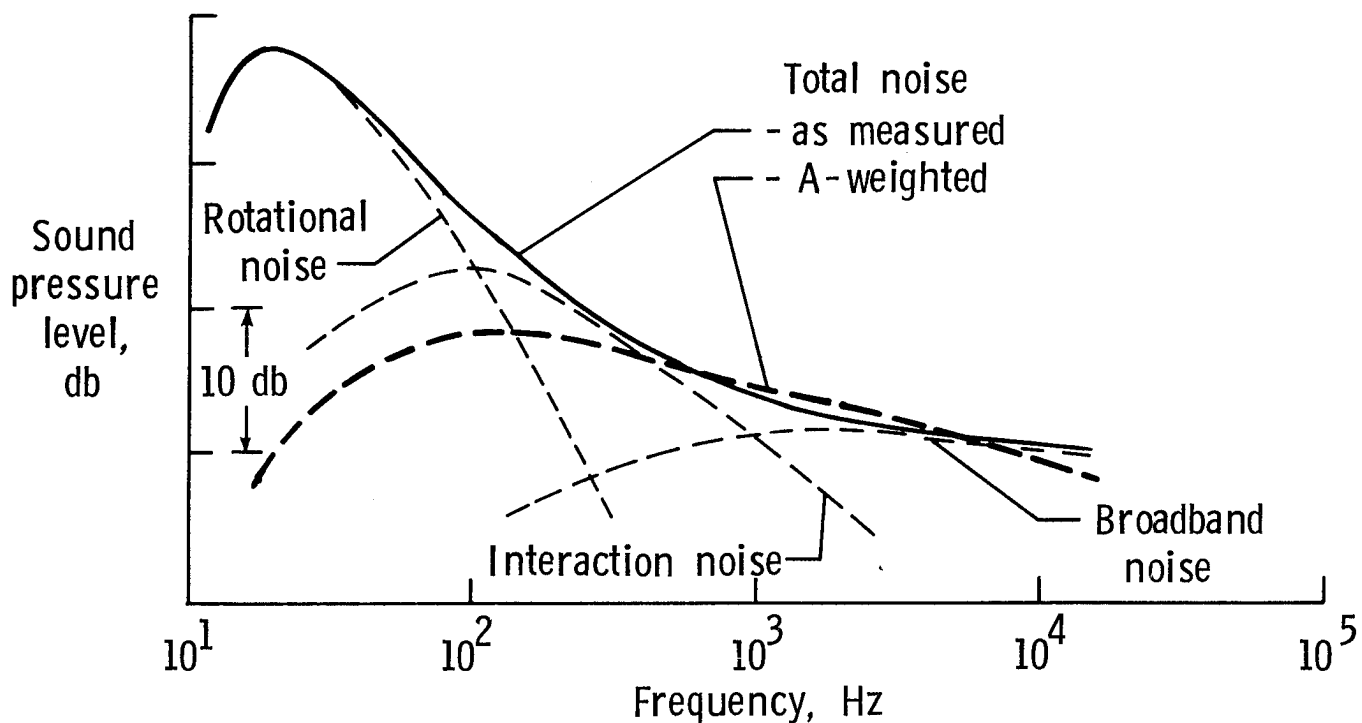


Figure 1.- Typical helicopter noise spectrum.



Figure 2.- Outdoor listening site for helicopter overflight experiment.

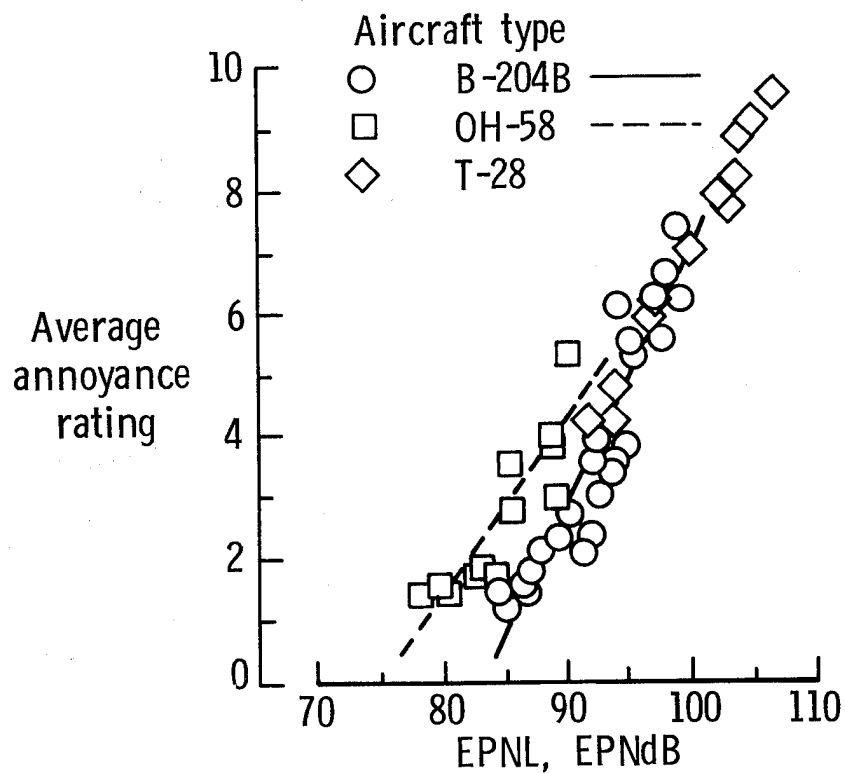


Figure 3.- Average noise annoyance ratings of outdoor listeners during helicopter overflights.

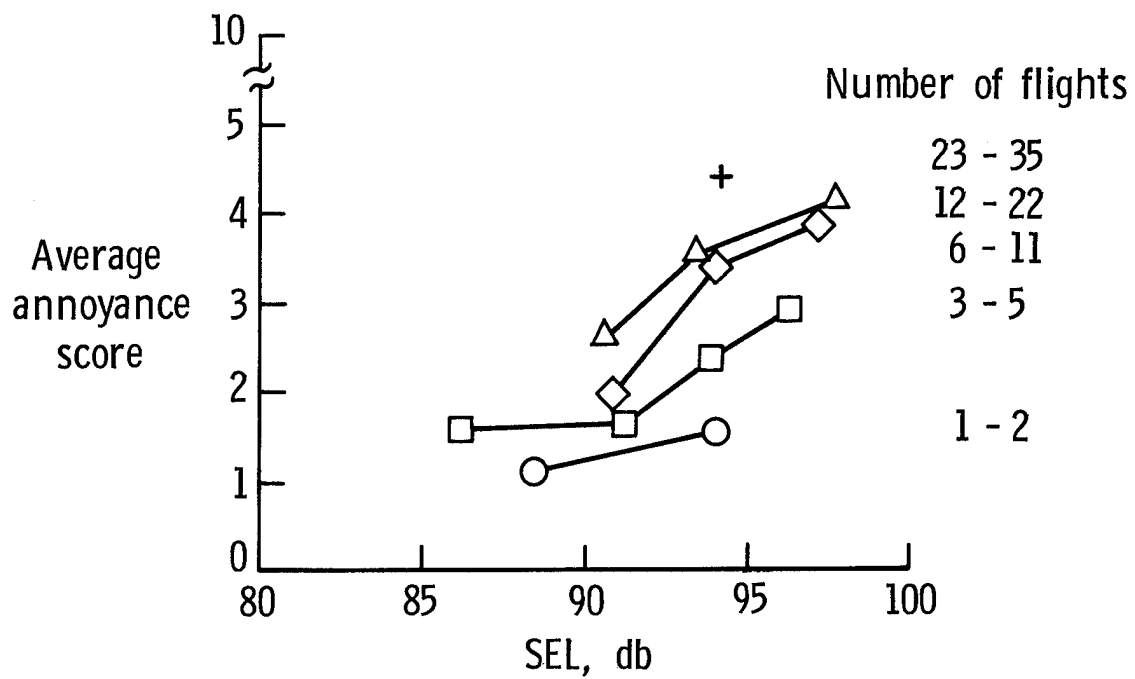


Figure 4.- Effect of noise level and number of flights on annoyance.

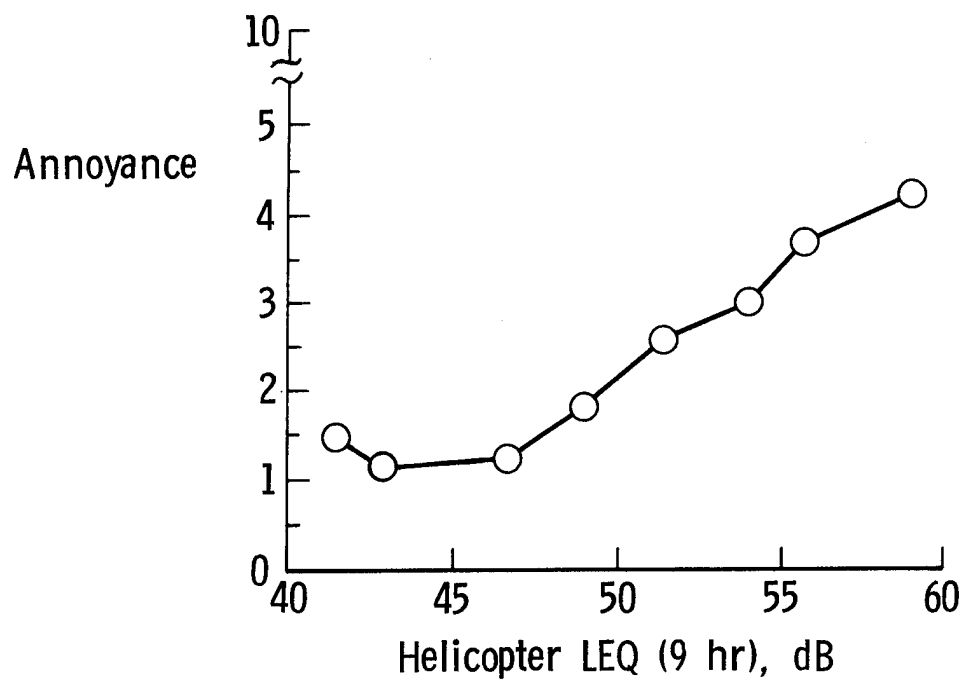


Figure 5.- Relationship between annoyance and Equivalent Noise Level (LEQ).

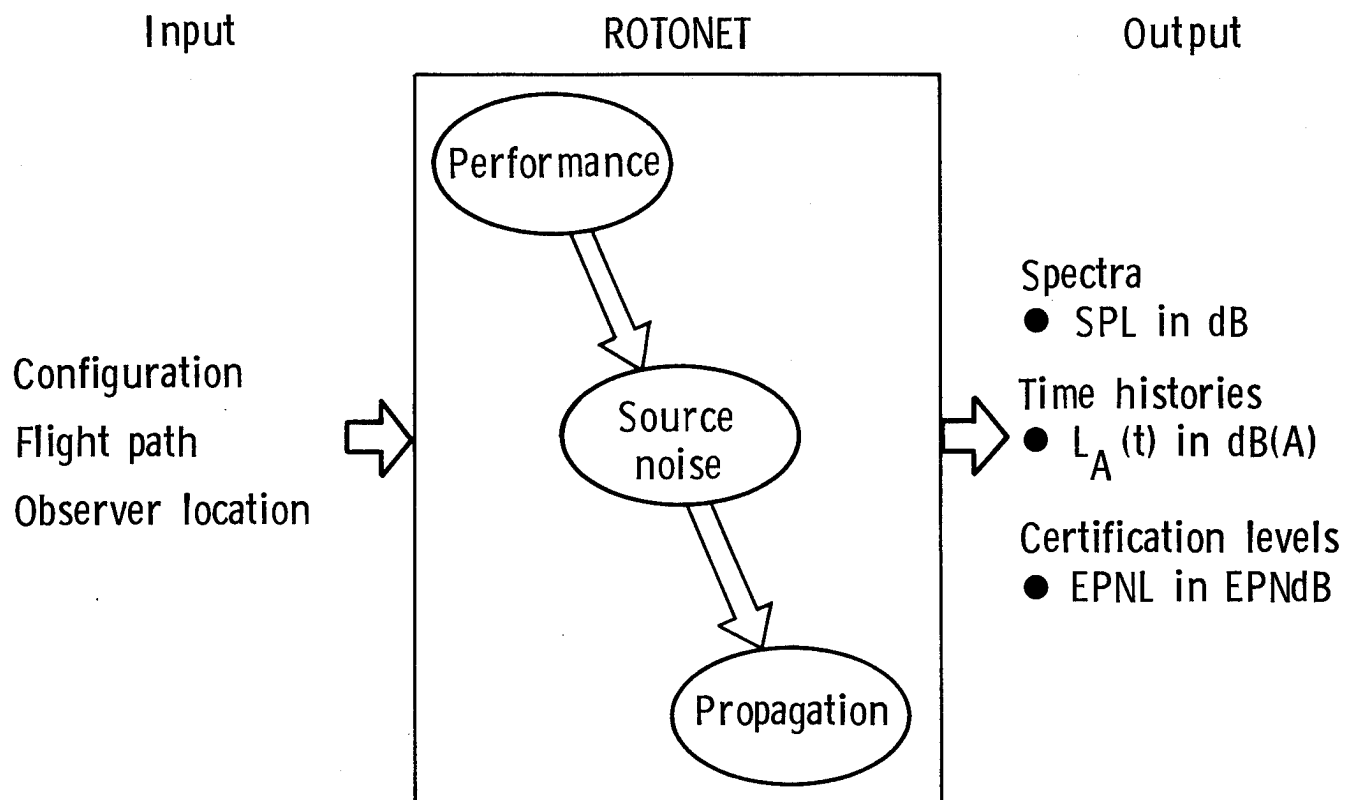


Figure 6.- ROTONET computer program for helicopter system noise prediction.

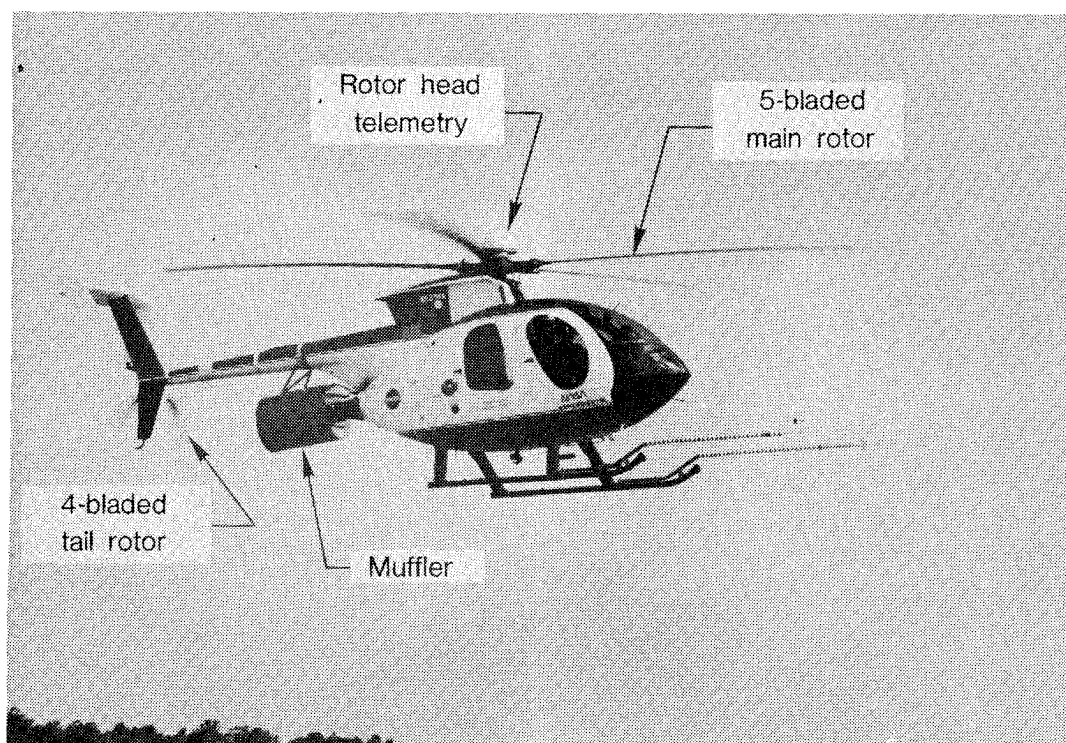


Figure 7.- Experimental helicopter used in noise prediction validation flight test.

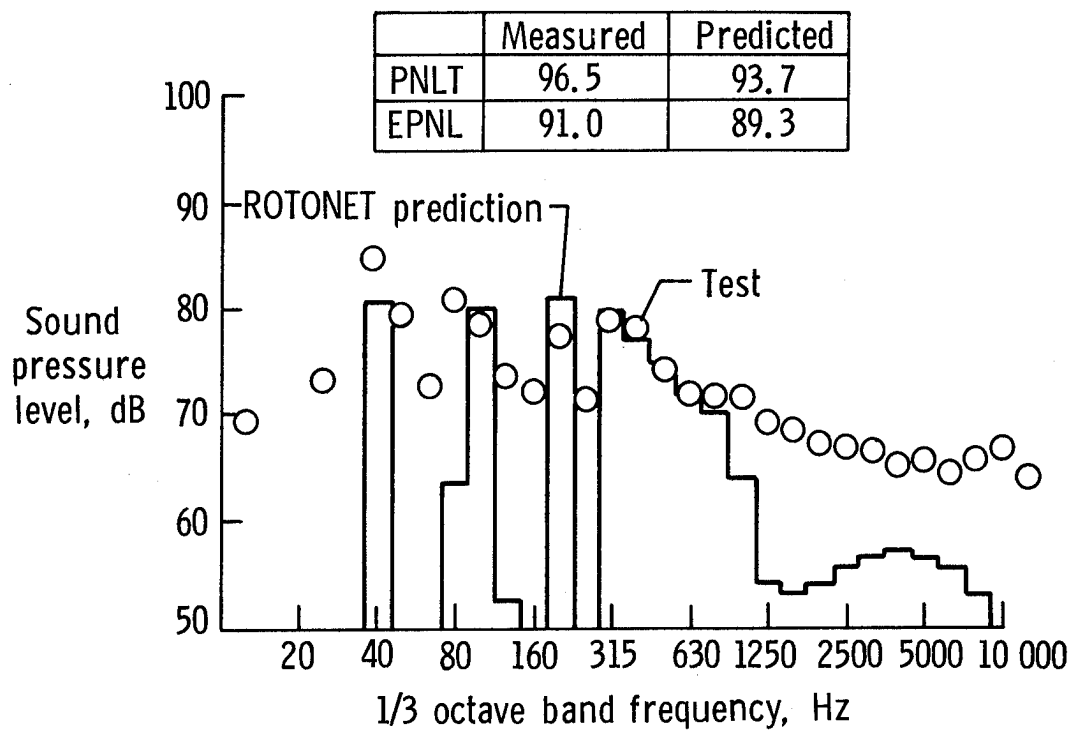


Figure 8.- Noise spectrum during overhead flyover at peak tone-corrected perceived noise level (PNLT), 95 knots flight speed, 250 ft. altitude, 2-blade tail rotor.

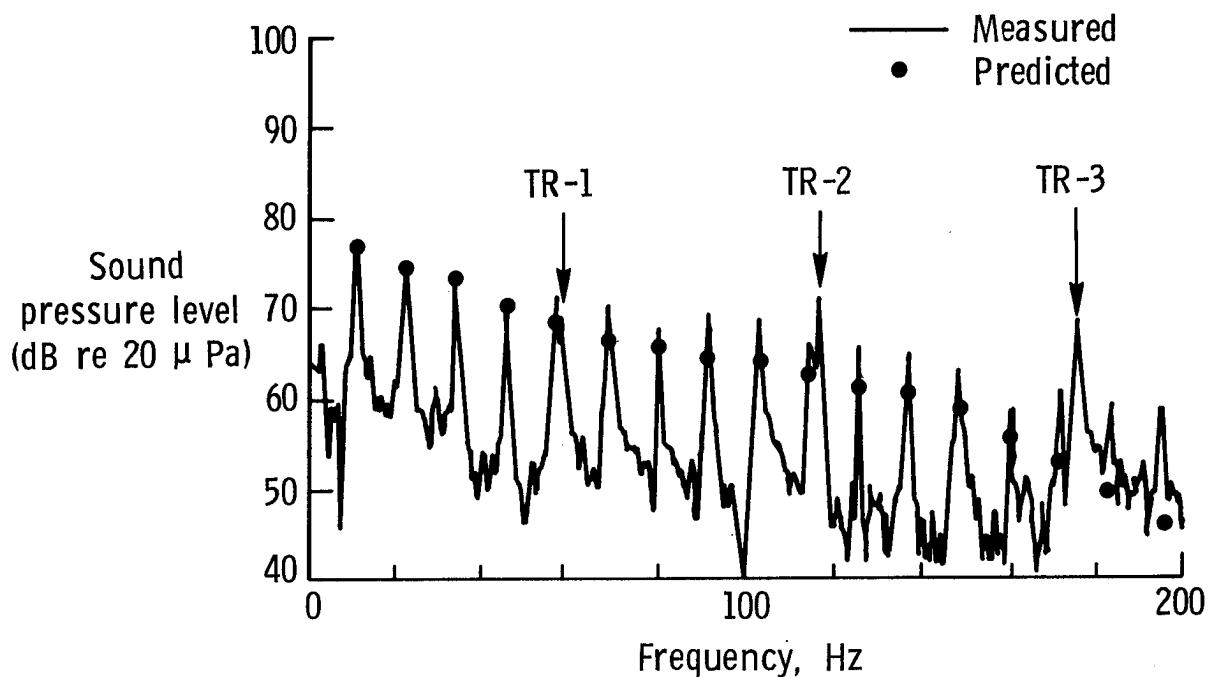


Figure 9.- Noise spectrum of OLS helicopter, 66 fps flight speed, 8.5° emission angle from rotor plane.

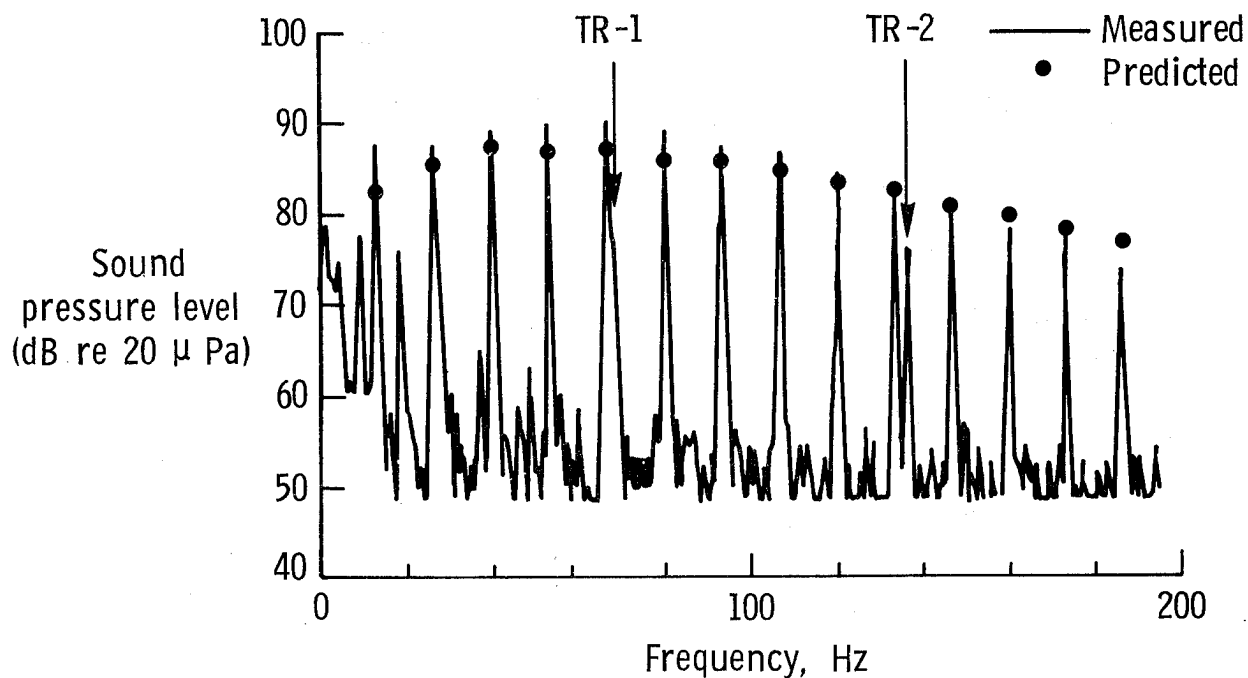


Figure 10.- Noise spectrum of OLS helicopter, 220 fps flight speed, 13.3° emission angle from rotor plane.

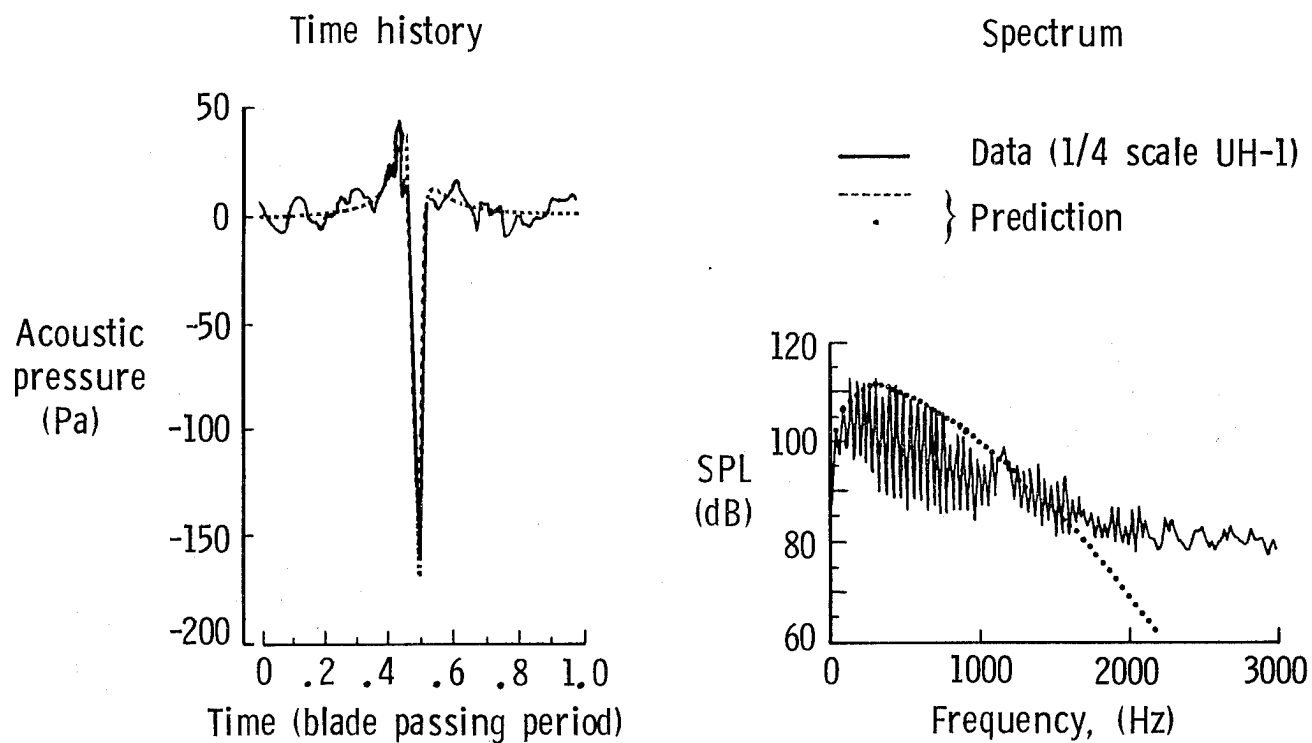


Figure 11.- Noise prediction for 1/4-scale UH-1 model when thickness noise dominates, tip Mach Number = 0.86, 100 knots, 140° azimuth in tip path plane.

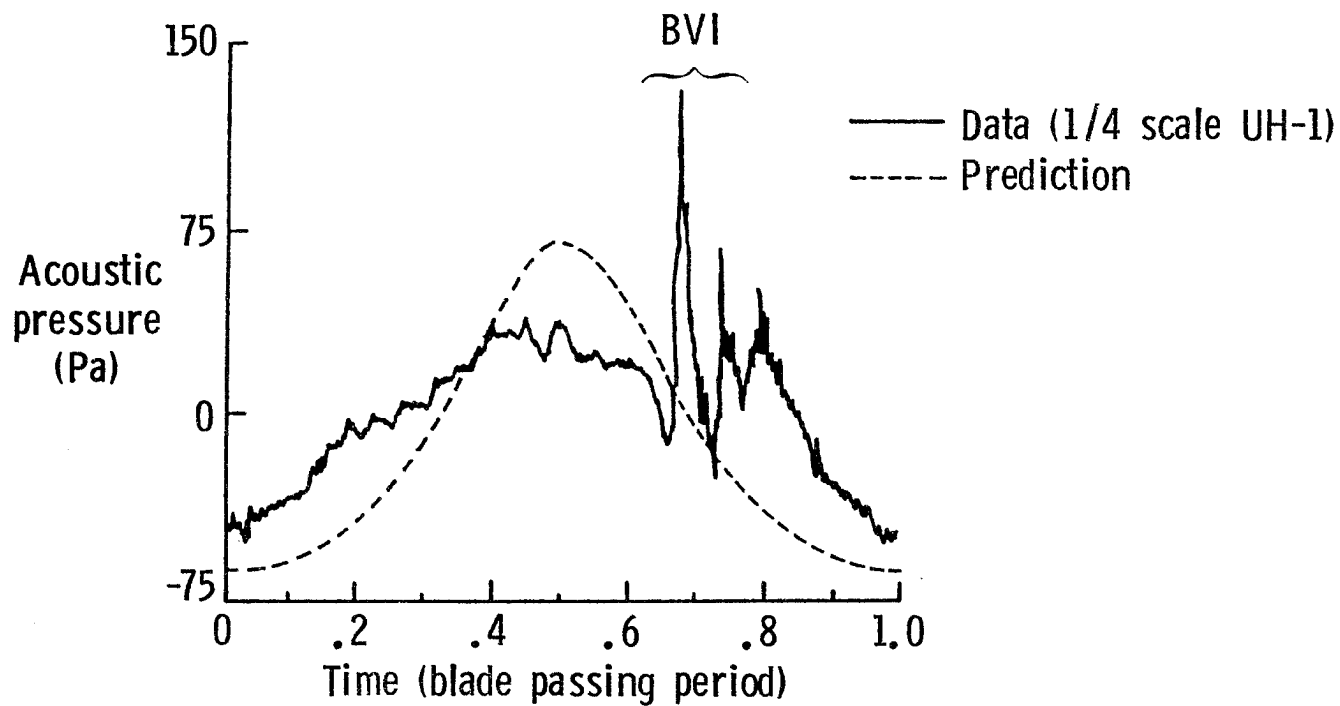


Figure 12.- Noise prediction for 1/4-scale UH-1 model when loading noise dominates, tip Mach Number = 0.82, 60 knots, 140° azimuth in tip path plane.

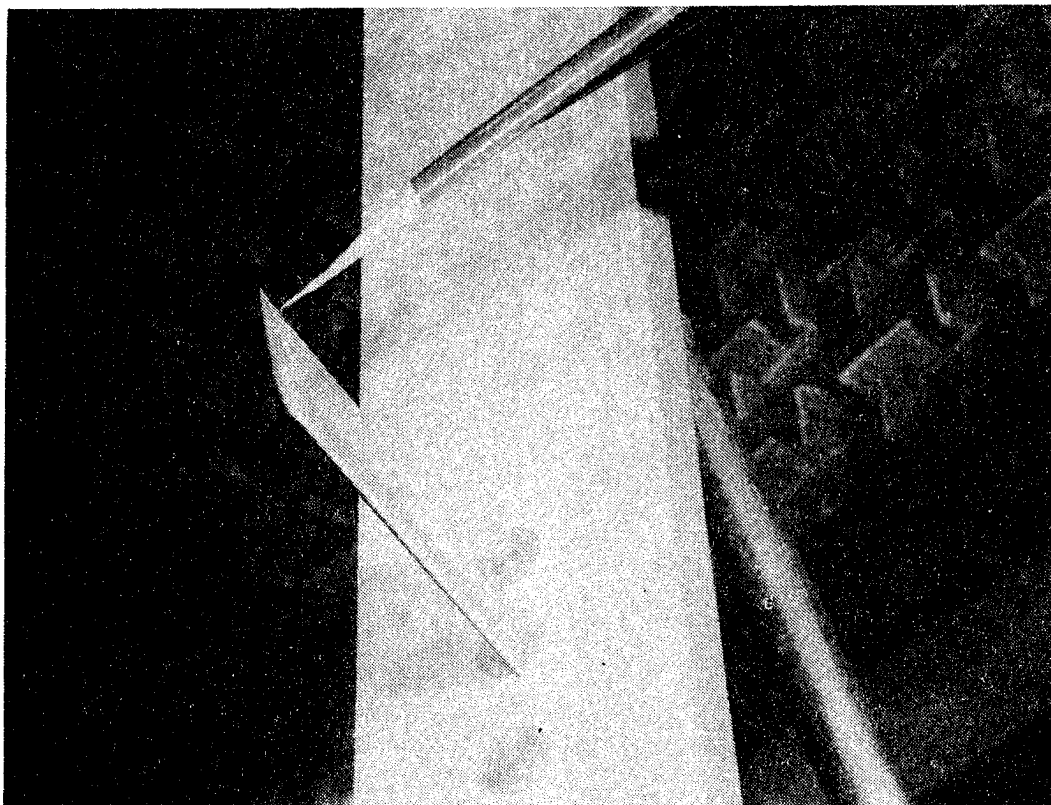


Figure 13.- Broadband noise experiment in Langley Quiet Flow Facility.

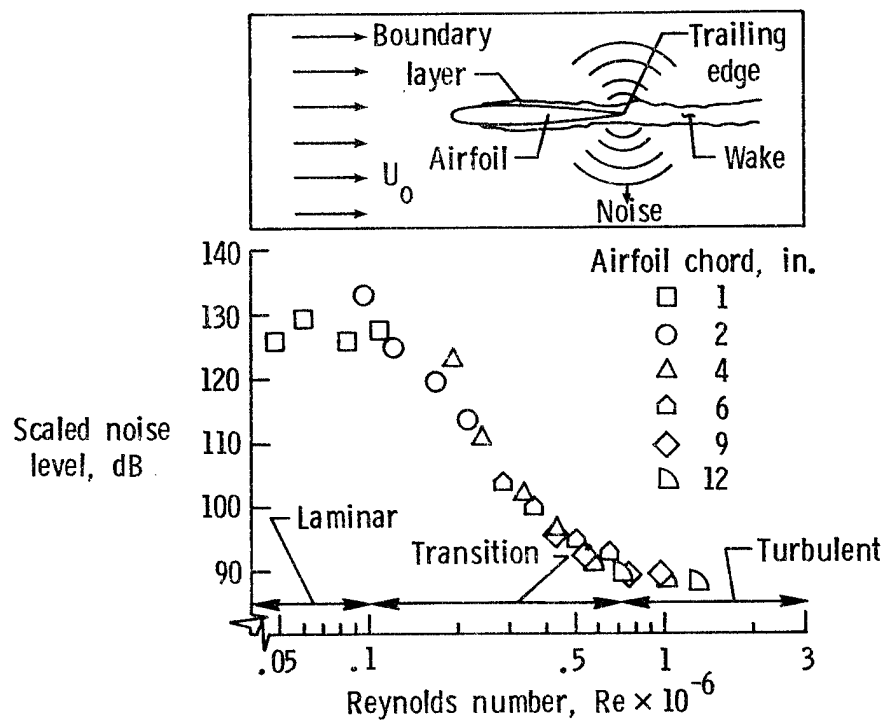


Figure 14.- Scaled level of trailing edge-boundary layer interaction noise through boundary layer transition region.

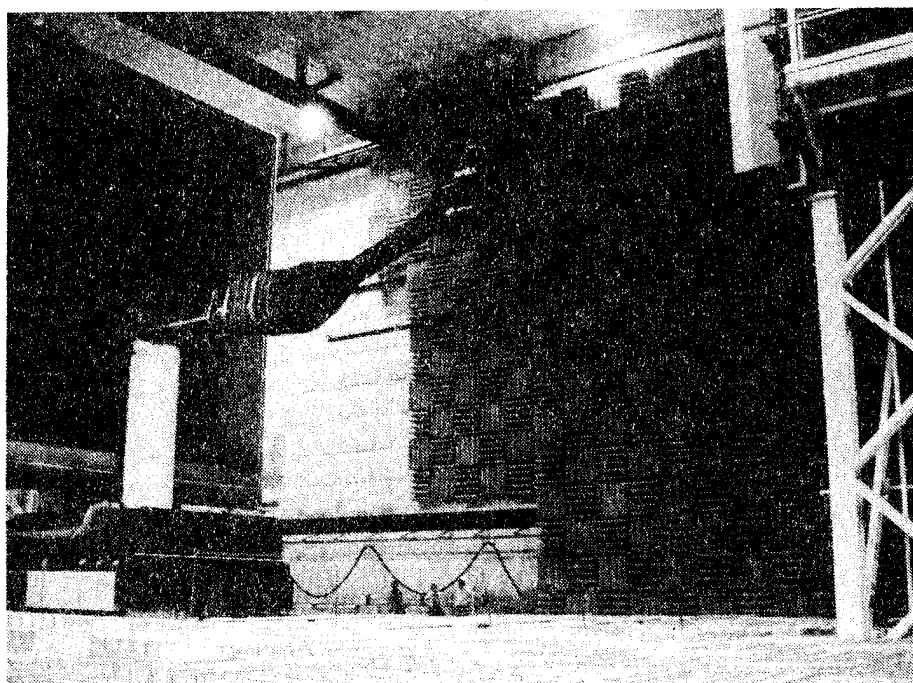


Figure 15.- Rotor broadband noise experiment in the DNW wind tunnel.

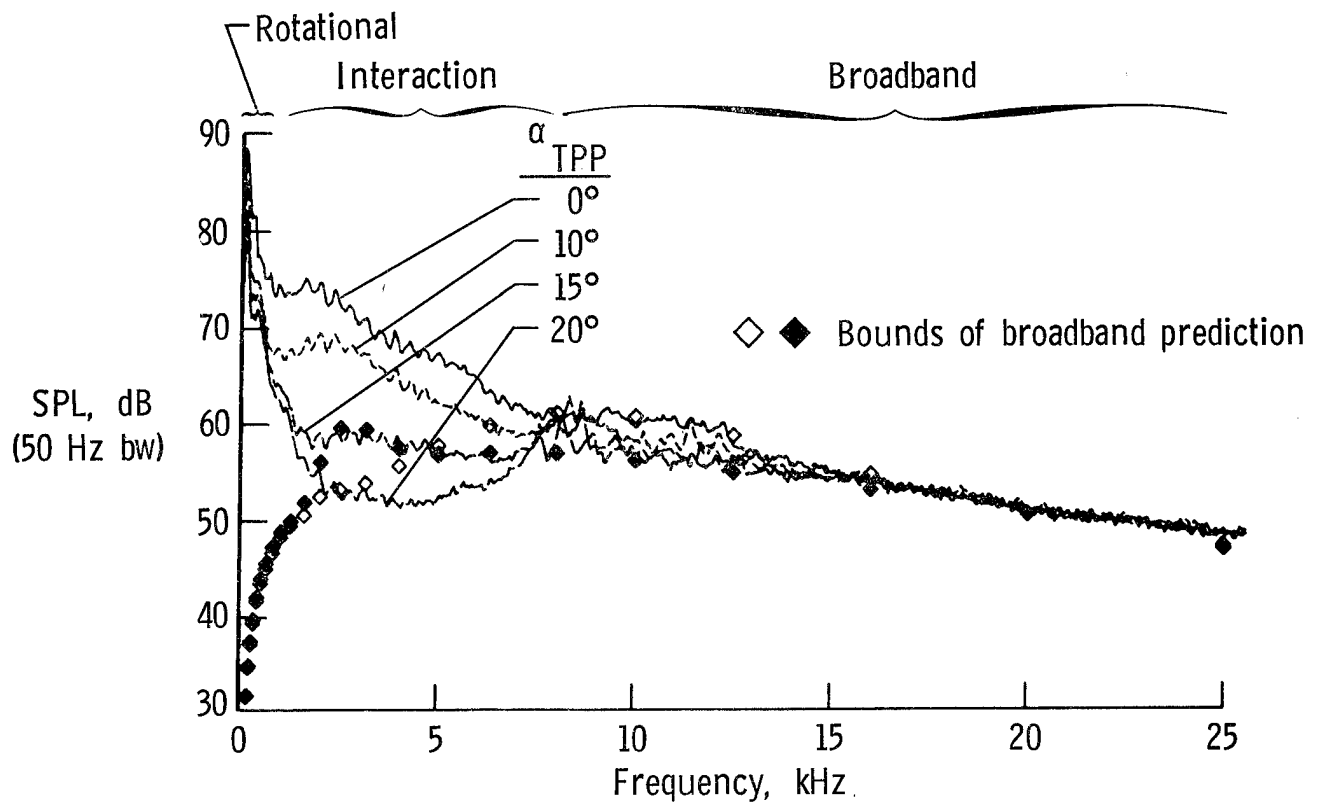


Figure 16.- Rotor broadband noise spectra from DNW test for varying rotor tip path plane angles, 40% scale rotor, $C_T = 0.0044$, $\mu = 0.086$, 1050 rpm.

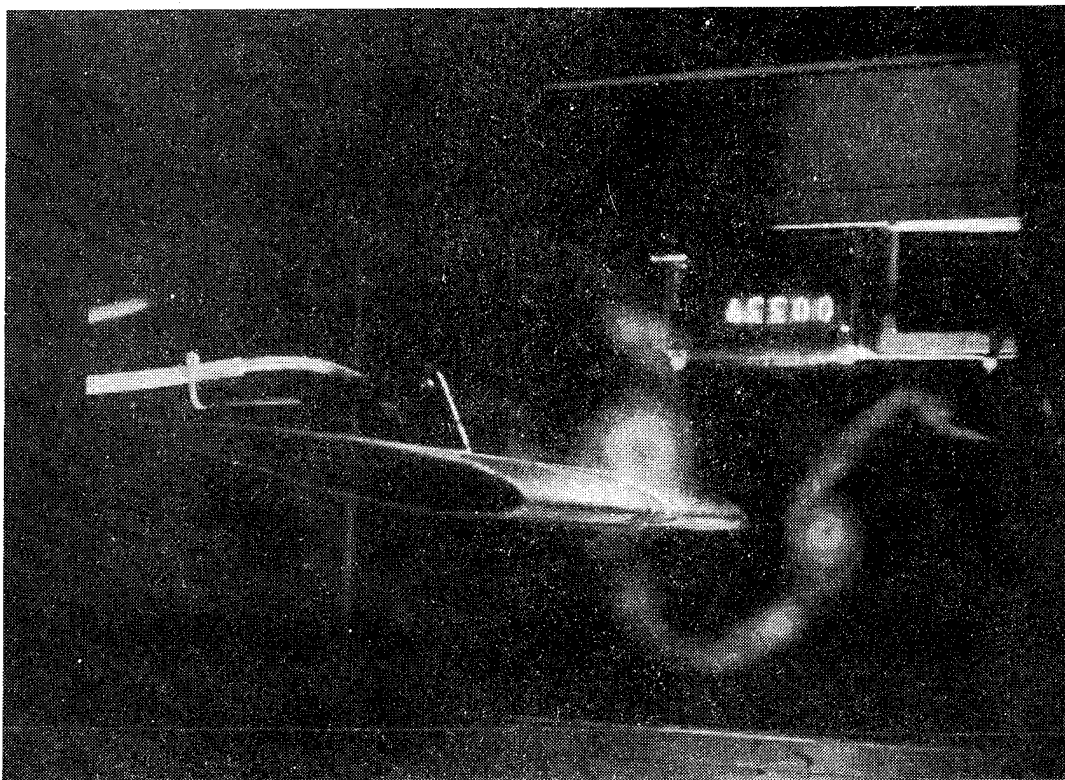


Figure 17.- Two-dimensional airfoil-vortex interaction experiment in the Quiet Flow Facility.

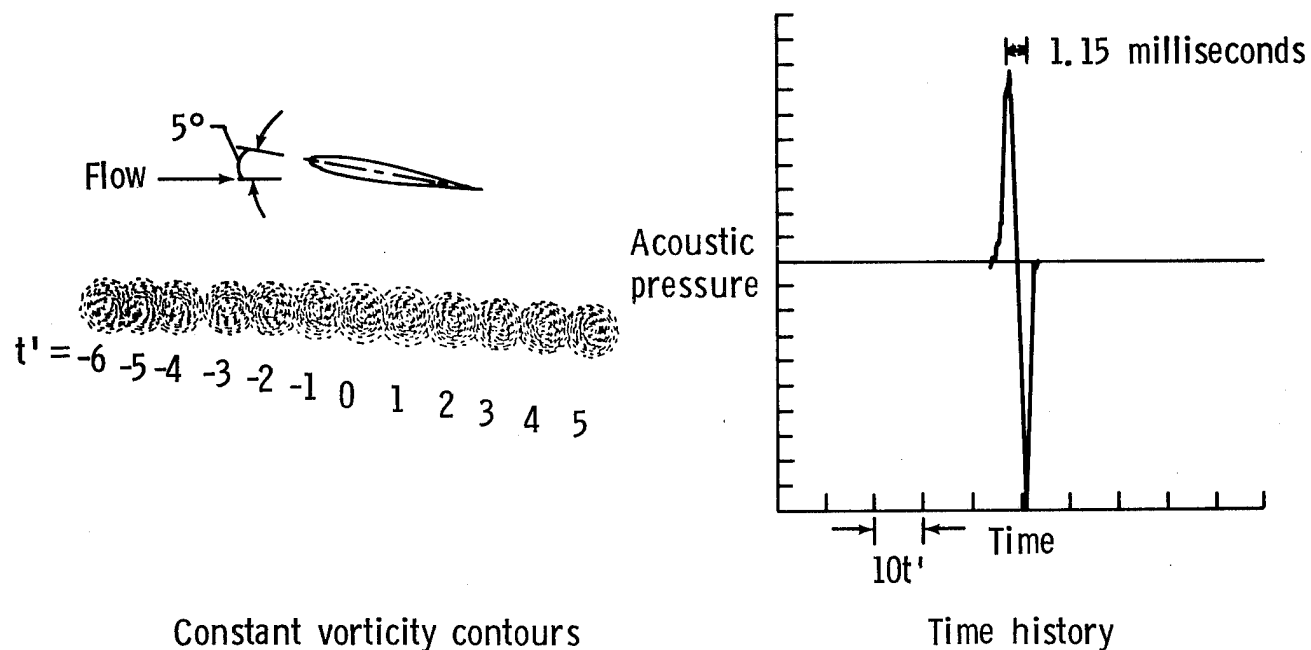


Figure 18.- Computational acoustics model of blade vortex interaction noise.

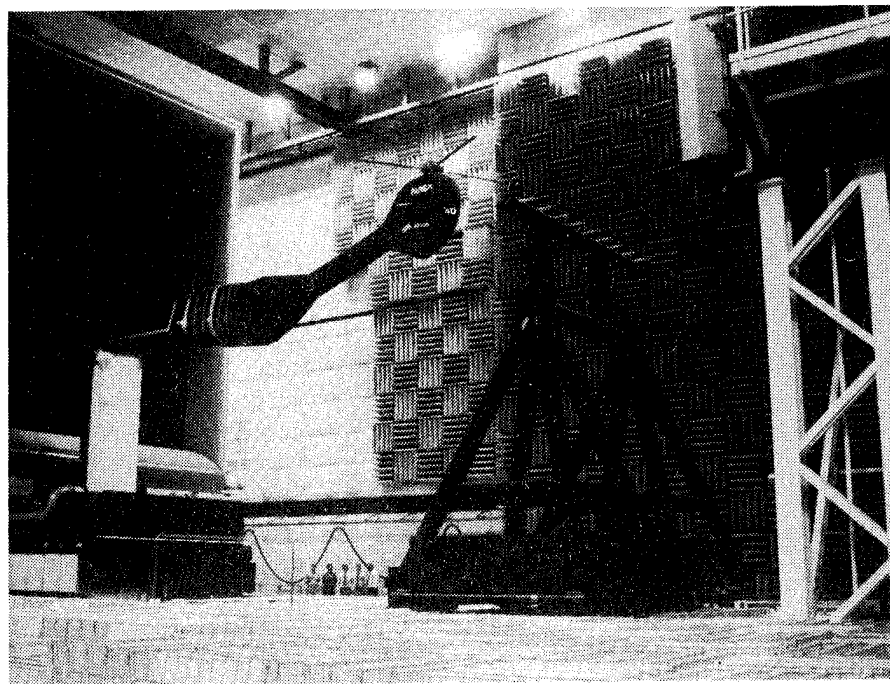


Figure 19.- Blade vortex interaction noise experiment in the DNW wind tunnel.

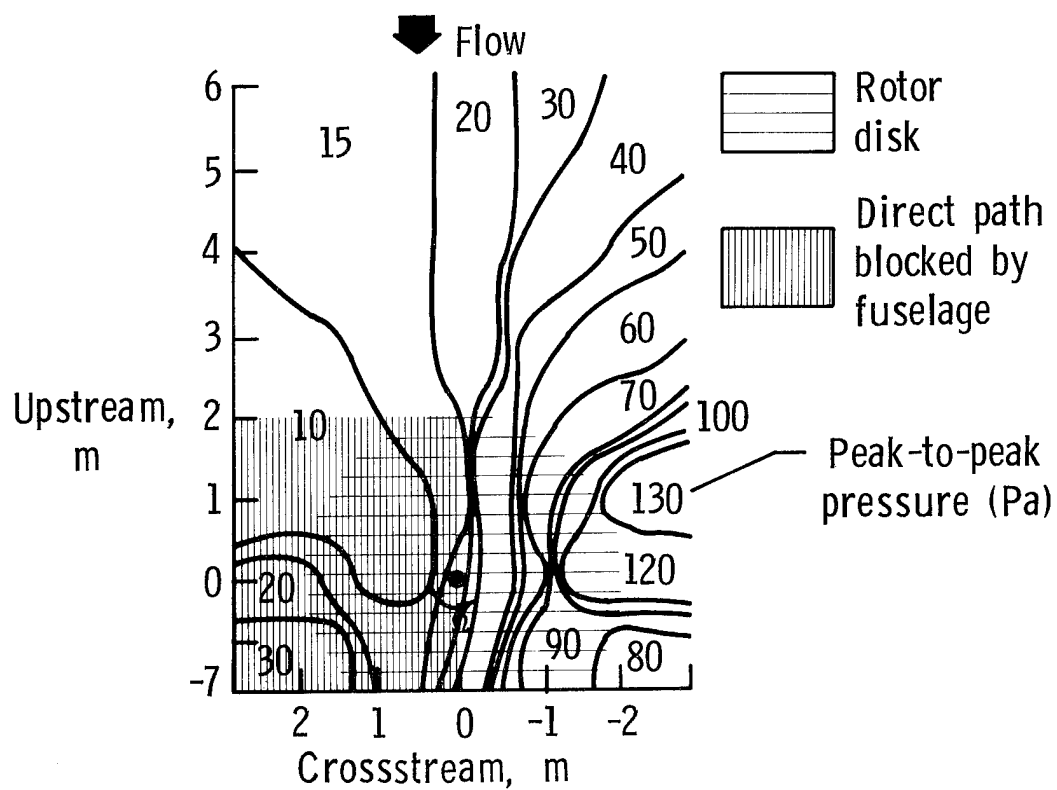


Figure 20.- Contours of constant impulsive noise beneath the rotor due to blade vortex interaction, $\alpha_{\text{TPP}} = 2.3^\circ$, 60 knots.

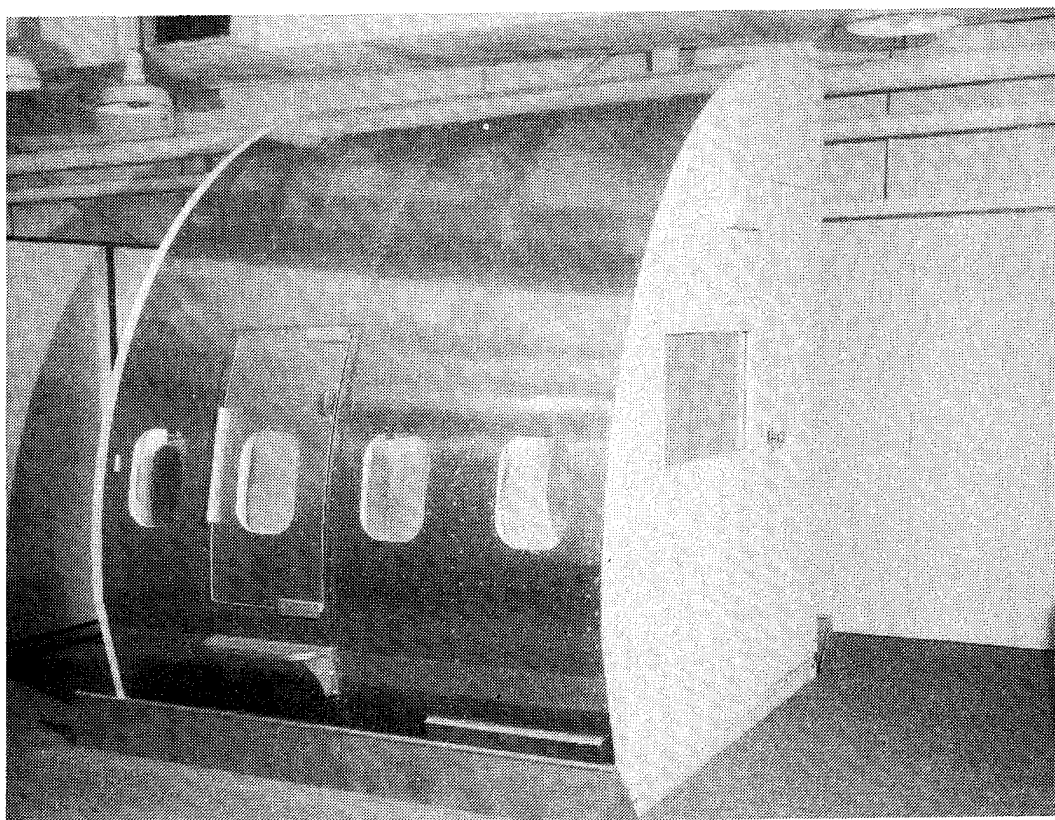


Figure 21.- Ride Quality Simulator

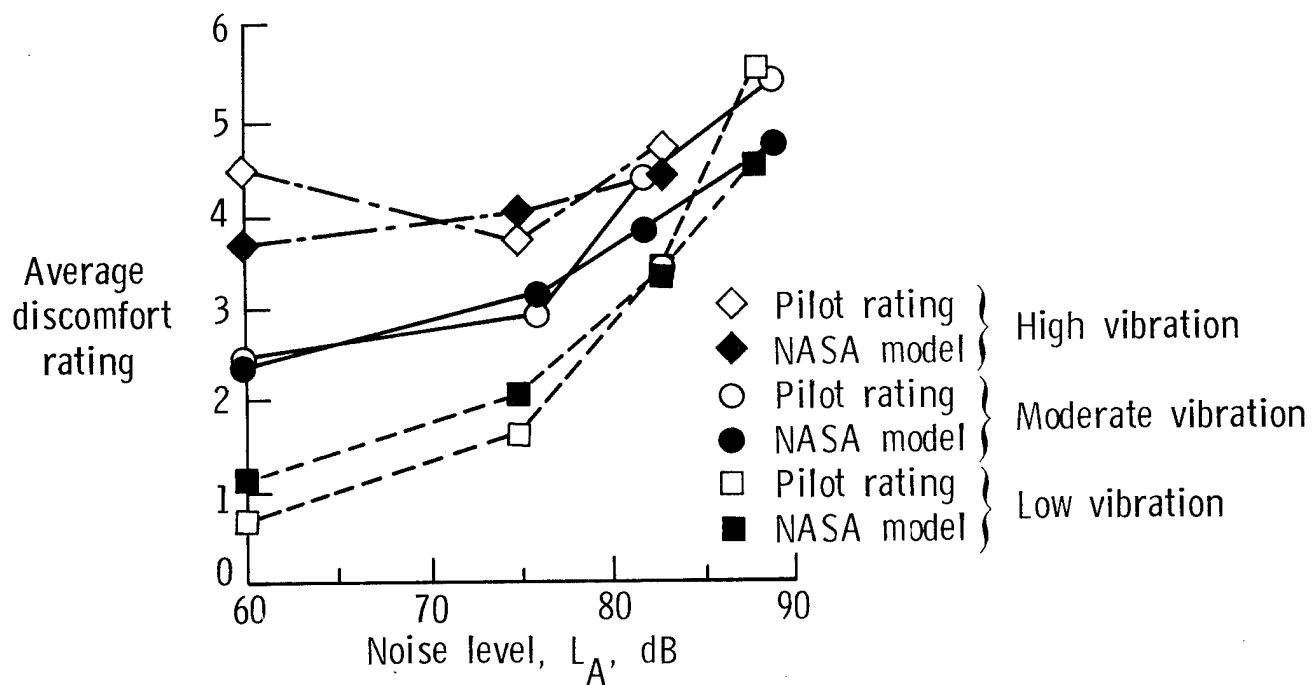


Figure 22.- Effect of noise and vibration level on pilot discomfort.

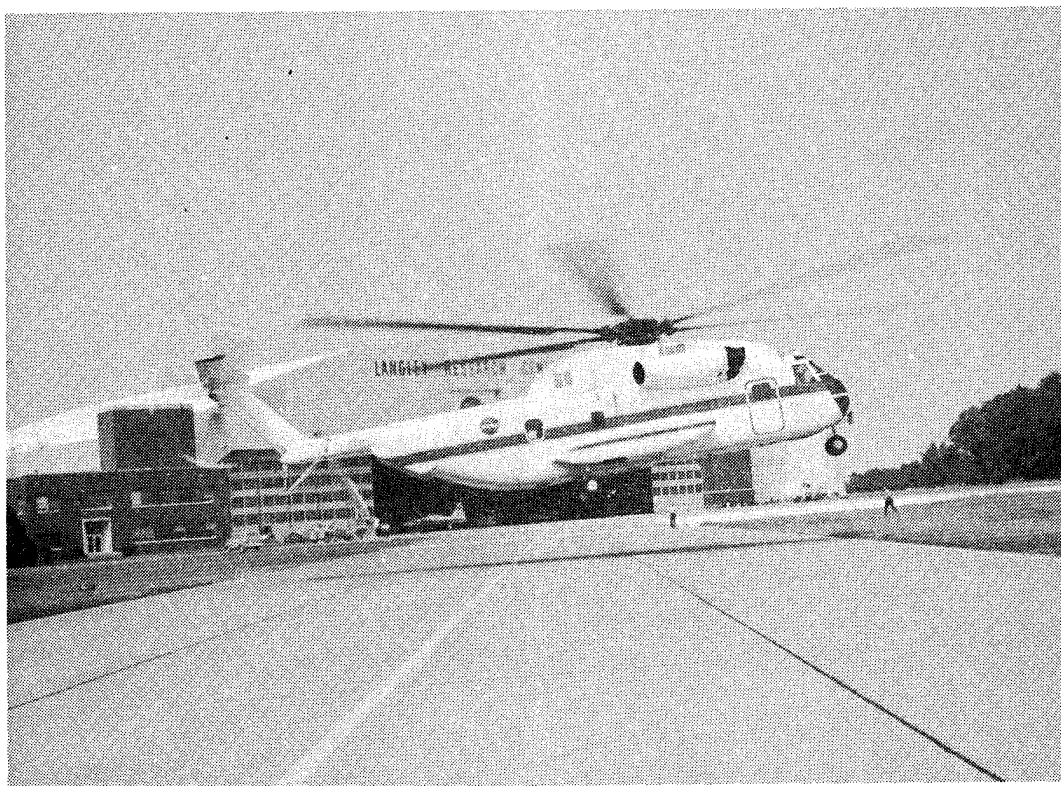


Figure 23.- Civil helicopter research aircraft (CHRA).

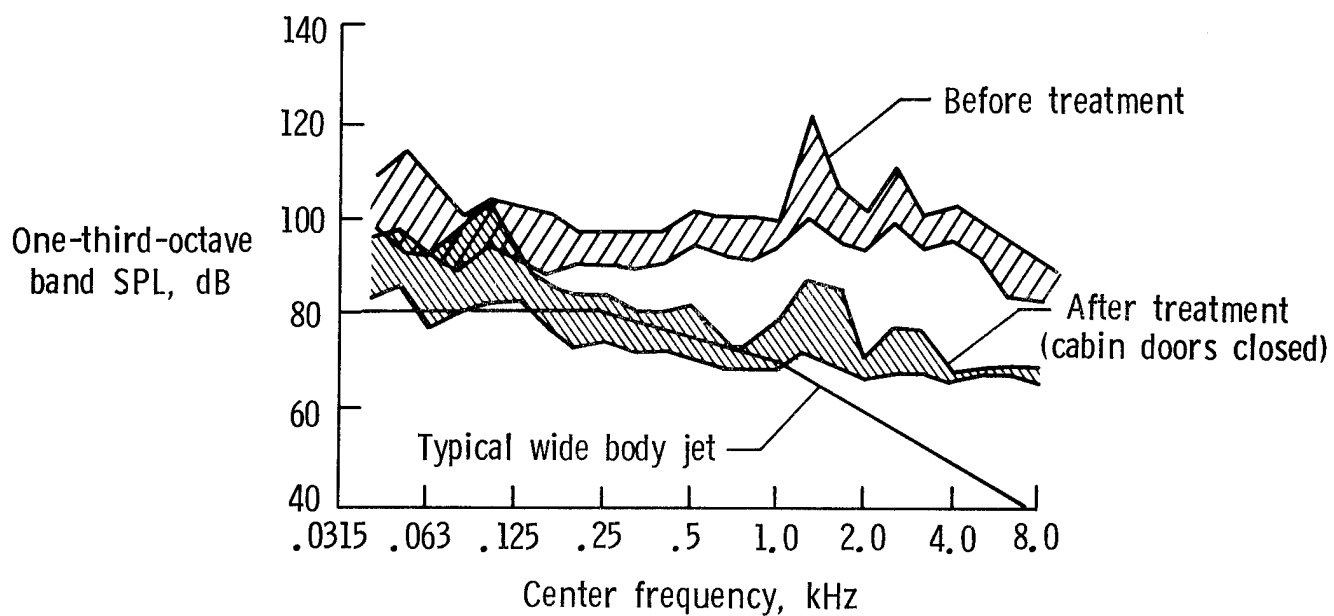


Figure 24.- Effect of acoustic treatment on interior noise in civil helicopter research aircraft.

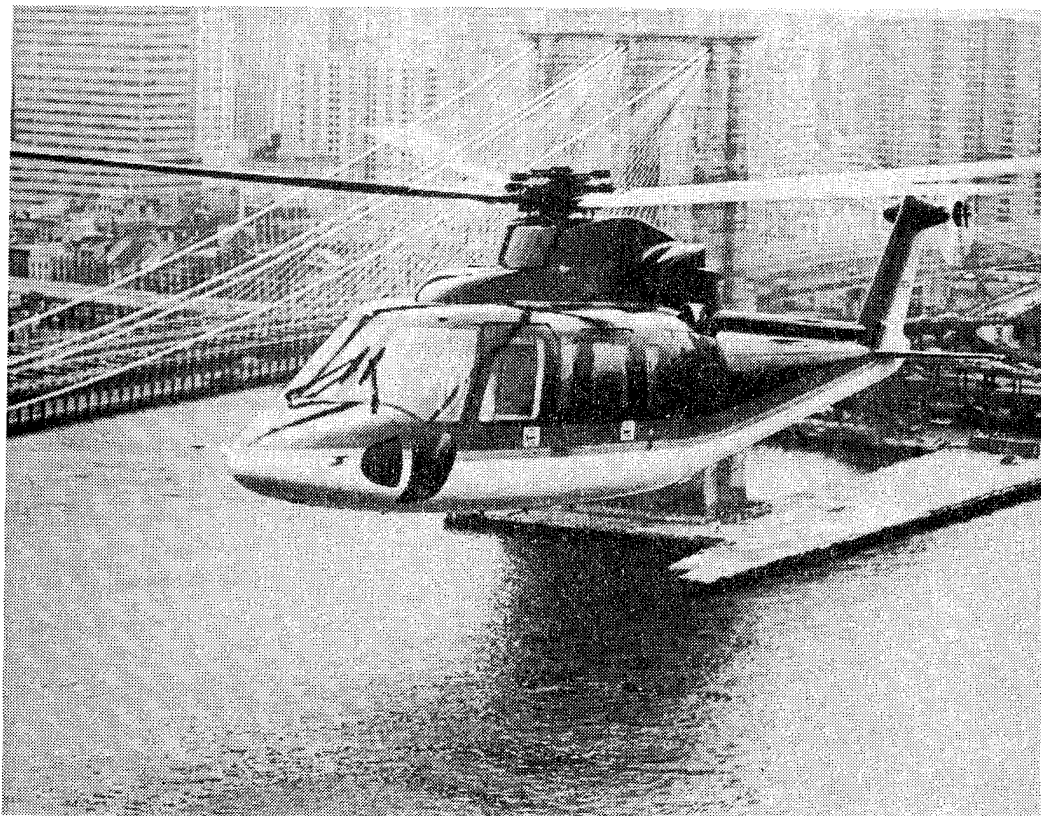


Figure 25.- Interior noise test helicopter.

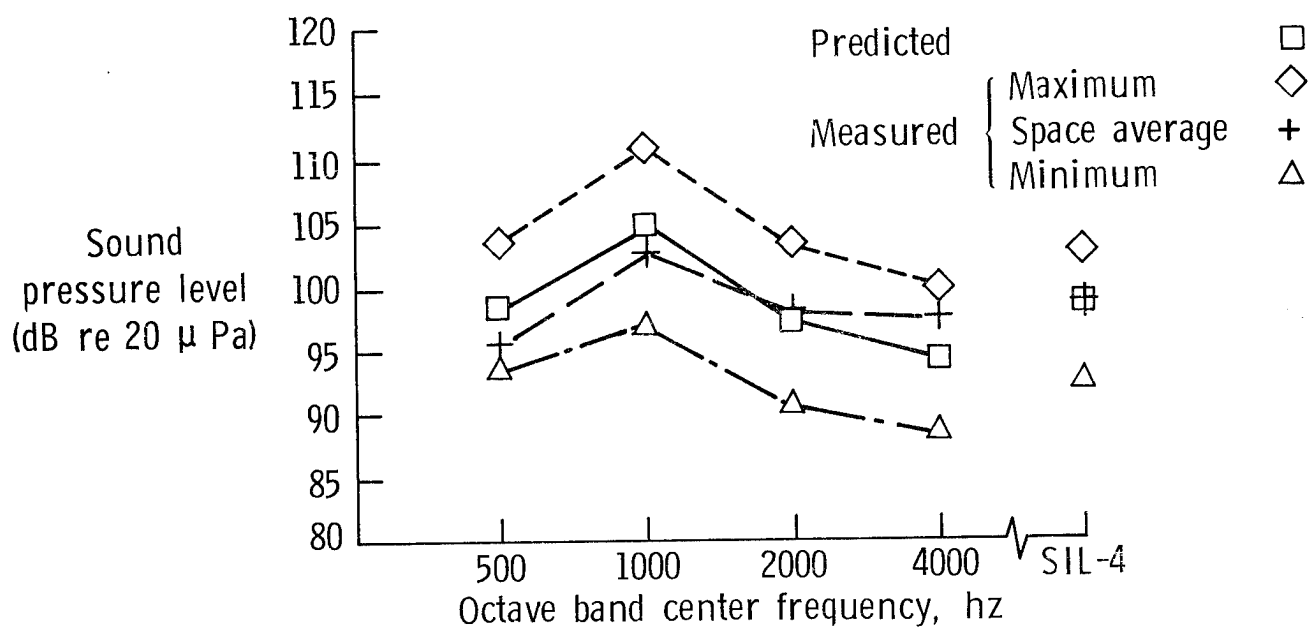


Figure 26.- Measured and predicted inflight sound pressure levels in test helicopter.

BIBLIOGRAPHY

PUBLICATIONS: 1976-1987

NASA Reports

1. Mall, G. H.; and Farassat, F.: A Computer Program for the Determination of the Acoustic Pressure Signature of Helicopter Rotors Due to Blade Thickness. NASA TM X-3323, 1976.
2. Ramakrishnan, Ramani; Randall, Donald; and Hosier, Robert N.: A Computer Program to Predict Rotor Rotational Noise of a Stationary Rotor from Blade Loading Coefficients. NASA TM X-3281, 1976.
3. Lawton, Ben W.: Subjective Assessment of Simulated Helicopter Blade-Slap Noise. NASA TN D-8359, 1976.
4. Leatherwood, Jack D.; and Dempsey, Thomas K.: Psychophysical Relationships Characterizing Human Response to Whole-Body Sinusoidal Vertical Vibration. NASA TN D-8188, 1976.
5. Dempsey, Thomas K.; and Leatherwood, Jack D.: Prediction of Passenger Ride Quality in a Multifactor Environment. NASA TM X-72945, 1976.
6. Dempsey, Thomas K.; Leatherwood, Jack D.; and Clevenson, Sherman A.: Noise and Vibration Ride Comfort Criteria. NASA TM X-73975, 1976.
7. Dempsey, Thomas K.; Leatherwood, Jack D.; and Drezek, Arlene B.: Passenger Ride Quality Within a Noise and Vibration Environment. NASA TM X-72841, 1976.
8. Pegg, Robert J.: Insights Into the Nature and Control of Rotor Noise. Presented at the NASA Conference on Aircraft Safety and Operating Problems, October 1976. NASA SP 416.
9. Farassat, F.; and Brown, T. J.: A New Capability for Predicting Helicopter Rotor and Propeller Noise Including the Effect of Forward Motion. NASA TM X-74037, June 1977.
10. Howlett, J. T.; Clevenson, S. A.; Rupf, J. A.; and Snyder, W. J.: Interior Noise Reduction in a Large Civil Helicopter. NASA TN D-8477, July 1977.
11. Farassat, F.; Nystrom, P. A.; and Brown, T. J.: Bounds on Thickness and Loading Noise of Rotating Blades and the Favorable Effect of Blade Sweep on Noise Reduction. Presented at the AHS-NASA/Army Specialists Meeting on Helicopter Acoustics, Hampton, Virginia, May 1978. NASA CP 2052.

12. Hilton, David A.; Henderson, Herbert R.; Maglieri, Domenic, J.; and Bigler, William B., III: On the Effects of Operations on the Ground Noise Footprints Associated with a Large-Multi-Bladed Nonbanging Helicopter. Presented at the AHS/NASA/Army Specialists Meeting on Helicopter Acoustics, Hampton, Virginia, May 1978. NASA CP 2052.
13. Pegg, Robert J.; and Shidler, Phillip A.: Exploratory Wind Tunnel Investigation of the Effect of the Main Rotor Wake on Tail Rotor Noise. Presented at the AHS/NASA/Army Specialists Meeting on Helicopter Acoustics, Hampton, Virginia. NASA CP 2052, May 1978.
14. Mantay, Wayne; Shidler, Phillip A.; and Campbell, Richard L.: Full-Scale Testing on an OGEE Tip Rotor. Presented at the AHS/NASA/Army Specialists Meeting on Helicopter Acoustics, Hampton, Virginia. NASA CP 2052, May 1978.
15. Hoad, Danny R.; and Greene, George, C.: Helicopter Noise Research at the Langley V/STOL Tunnel. Presented at the AHS/NASA/Army Specialists Meeting on Helicopter Acoustics, Hampton, Virginia. NASA CP 2052, May 1978.
16. Powell, Clemans A.: A Subjective Field Study of Helicopter Blade-Slap Noise. NASA TM 78738, July 1978.
17. Morris, C. E. K., Jr.; Farassat, F.; and Nystrom, P. A.: An Evaluation of Linear Acoustic Theory for a Hovering Rotor. NASA TM 80059, February 1979.
18. Clevenson, S. A.; and Leatherwood, J. D.: Effects of Noise Spectra and a Listening Task Upon Passenger Annoyance in a Helicopter Interior Noise Environment. NASA TP-1590, November 1979.
19. Fields, James M.: The Relative Importance of Noise Level and Number of Events on Human Reactions to Noise: Community Survey Findings and Study Methods. NASA TM-81795, March 1980.
20. Clevenson, Sherman A.; and Shepherd, William T. (Editors): Time-of-Day Corrections to Aircraft Noise Metrics. NASA CP-2135, June 1980.
21. Key, Kelli F.; and Powell, Clemans A.: Effects of Conversation Interference on Annoyance Due to Aircraft Noise. NASA TP-1712, August 1980.
22. Powell, Clemans A.: Annoyance Due to Multiple Airplane Noise Exposure. NASA TP-1706, August 1980.
23. Powell, Clemans A.: Subjective Field Study of Response to Impulsive Helicopter Noise. NASA TP-1833, April 1981.

24. Yu. James C.: Mean-Flow and Turbulence Measurements in the Vicinity of the Trailing Edge of an NACA 63₁-012 Airfoil. NASA TP-1845, May 1981.
25. Hammond, C. E.; Hollenbaugh, D. D.; Clevenson, S. A.; and Leatherwood, J. D.: An Evaluation of Helicopter Noise and Vibration Ride Qualities Criteria. NASA TM-83251, December 1981.
26. Conner, David A.; and Hoad, Danny R.: Reduction of High-Speed Impulsive Noise by Blade Planform Modification of a Model Helicopter Rotor. NASA TM-84553, AVRADCOM TR 82-B-6, December 1982.
27. Huston, Robert J. (Compiler): Rotorcraft Noise. NASA CP-2234, July 1982.
28. Powell, Clemans A.; and McCurdy, David A.: Effects of Repetition Rate and Impulsiveness of Simulated Helicopter Rotor Noise on Annoyance. NASA TP-1969, February 1982.
29. Willshire, William L., Jr.: Rye Canyon X-Wing Noise Test: One-Third Octave Band Data. NASA TM-84602, January 1983.
30. Clevenson, Sherman A.; Leatherwood, Jack D.; and Hollenbaugh, Daniel D.: Interior Noise and Vibration Measurements on Operational Military Helicopters and Comparisons with Various Ride Quality Criteria. NASA TM-84664, AVRADCOM TR 83-D-21, August 1983.
31. Long, Lyle N.: The Compressible Aerodynamics of Rotating Blades Based on an Acoustic Formulation. NASA TP-2197, December 1983.
32. Conner, D. A.; and Hoad, D. R.: Experimental Blade Vortex Interaction Noise Characteristics of a Utility Helicopter at 1/4 Scale. NASA TM-84653, AVSCOM TM-83-B-1, January 1984.
33. Childress, O. S., Jr. (Compiler): Helicopter Noise Reduction Program - 1983. NASA CP-2308, May 1984.
34. Kryter, K. D.: Physiological, Psychological, and Social Effects of Noise. NASA RP-1115, July 1984.
35. Leatherwood, J. D.; and Barker, L. M.: A User-Oriented and Computerized Model for Estimating Vehicle Ride Quality. NASA TP-2299, April 1984.
36. Leatherwood, J. D.; Clevenson, S. A.; and Hollenbaugh, D. D.: Evaluation of Ride Quality Prediction Methods for Helicopter Interior Noise and Vibration Environments. NASA TP-2261, AVSCOM TR 84-D-2, March 1984.
37. Leatherwood, J. D.: Combined Effect of Noise and Vibration on Passenger Acceptance. NASA TM-86284, August 1984.

38. Fields, J. M.; and Powell, C. A.: A Community Survey of Helicopter Noise Annoyance Conducted Under Controlled Noise Exposure Conditions. NASA TM 86400, March 1985.
39. Willshire, W. L., Jr.: Long Range Downwind Propagation of Low-Frequency Sound. NASA TM 86409, April 1985.
40. Childress, O. S., Jr. (Compiler): Helicopter Noise Reduction Program--1984. NASA CP 2375, June 1985.
41. Parrott, T. L.; Schein, D. B.; and Gridley, D.: Analytical Study of Acoustic Response of a Semireverberant Enclosure with Application to Active Noise Control. NASA TP-2472, December 1985.
42. Booth, E. R., Jr.; and Yu, J. C.: New Technique for Experimental Generation of Two-Dimensional Blade-Vortex Interaction at Low Reynolds Numbers. NASA TP-2551, March 1986.
43. Brentner, K. S.: Prediction of Helicopter Rotor Discrete Frequency Noise--A Computer Program Incorporating Realistic Blade Motions and Advanced Acoustic Formulation. NASA TM 87721, October 1986.
44. Childress, O. S., Jr. (Compiler): Helicopter Noise Reduction Program--1985. NASA CP-2415, April 1986.
45. Hardin, J. C.: Introduction to Time Series Analysis. NASA RP-1145, March 1986.
46. Martin, R. M.; and Burley, C. L.: Power Cepstrum Technique with Application to Model Helicopter Acoustic Data. NASA TP-2586, June 1986.
47. Martin, R. M.; and Connor, A. B.: Wind-Tunnel Acoustic Results of Two Rotor Models with Several Tip Designs. NASA TM 87698, July 1986.
48. Mueller, A. W.; Smith, C. D.; Shepherd, K. P.; and Sullivan, B. M.: A New Version of the Helicopter Aural Detection Program--ICHIN. NASA TM 87745, July 1986.
49. Yu, J. C.; and Abrahamson, A. L.: Acoustic Treatment of the NASA Langley 4- by 7-Meter Wind Tunnel: A Feasibility Study. NASA TP-2563, August 1986.
50. Brentner, K. S.: Prediction of Helicopter Rotor Discrete Frequency Noise. NASA TM 87721, October 1986.

Contractor Reports

1. Davis, S. Jon; and Egolf, T. Alan: An Evaluation of a Computer Code Based on Linear Acoustic Theory for Predicting Helicopter Main Rotor Noise. NASA CR-159339, 1980.
2. JanakiRam, D. S.: Experimental Evaluation of Active and Passive Means of Alleviation Rotor Impulsive Noise in Descent Flight. NASA CR-159188, December 1979 (Released 1980).
3. Bennett, Ricarda L.; and Pearsons, Karl S.: Handbook of Aircraft Noise Metrics. NASA CR-3406, March 1981.
4. Hubbard, H. H.; Shepherd, K. P.; and Grosveld, F. W.: Broad Band Sound From Wind Turbine Generators. NASA CR-165810, November 1981.
5. Schlinker, Robert H.; and Amiet, Roy K.: Helicopter Rotor Trailing Edge Noise. NASA CR-3470, November 1981.
6. Succi, George P.: Validation of Helicopter Noise Prediction Techniques. NASA CR-165715, April 1981.
7. Gridley, Doreen: Program for Narrow-Band Analysis of Aircraft Flyover Noise Using Ensemble Averaging Techniques. NASA CR-165867, March 1982.
8. Molino, John A.: Should Helicopter Noise be Measured Differently from Other Aircraft Noise? - A Review of the Psychoacoustic Literature. NASA CR-3609, November 1982.
9. Ollerhead, J. B.: Laboratory Studies of Scales for Measuring Helicopter Noise. NASA CR-3610, November 1982.
10. Pearsons, Karl S.; and Horonjeff, Richard D.: Measurement of Speech Levels in the Presence of Time Varying Background Noise. NASA CR-3547, April 1982.
11. Sullivan, B. M.; and Mabry, J. E.: A Study of Noise Metric and Tone Correction Accuracy. NASA CR-165910, April 1982.
12. Schlinker, Robert H.; and Amiet, Roy K.: Rotor-Vortex Interaction Noise. NASA CR-3744, October 1983.
13. Succi, George P.: Limits on the Prediction of Helicopter Rotor Noise Using Thickness and Loading Sources: Validation of Helicopter Noise Prediction Techniques. NASA CR-166097, April 1983.
14. Yoerkie, C. A.; Moore, J. A.; and Manning, J. E.: Development of Rotorcraft Interior Noise Control Concepts - Phase I: Definition Study. NASA CR-166101, May 1983.

15. George, A. R.; and Chou, S-T.: Broadband Rotor Noise Analyses. NASA CR-3797, April 1984.
16. Hayden, R. E.: Comparison of Options for Reduction of Noise in the Test Section of the NASA Langley 4 x 7M Wind Tunnel Including Reduction of Nozzle Area. NASA CR-172446-2, September 1984.
17. Hayden, R. E.; and Wilby, J. F.: Sources, Paths, and Concepts for Reduction of Noise in the Test Section of the NASA Langley 4 x 7M Wind Tunnel. NASA CR-172446-1, September 1984.
18. Howe, M. S.: On the Long Range Propagation of Sound Over Irregular Terrain. NASA CR-3862, December 1984.
19. Abrahamson, A. L.: An Evaluation of Proposed Acoustic Treatments for the NASA LaRC 4- x 7-Meter Wind Tunnel. NASA CR-172577, April 1985.
20. Anderson, G. S.; Hayden, R. E.; Thompson, A. R.; and Madden, R.: Evaluation of the Feasibility of Scale Modeling to Quantify Wind and Terrain Effects on Low-Angle Sound Propagation. NASA CR-172488, January 1985.
21. Burton, D. E.; Schlinker, R. H.; and Shenoy, R. K.: The Status of Analytical Helicopter Noise Prediction Methods. NASA CR-172606, August 1985.
22. Hellman, R. P.: Contribution of Tonal Components to the Overall Loudness, Annoyance, and Noisiness of Noise: Relation Between Single Tones and Noise Spectral Shape. NASA CR-3892, May 1985.
23. Huff, D. L.; and Shenoy, R. K.: Investigation of the Transonic Blade-Vortex Interaction Characteristics of Airfoil Sections Using ATRAN-2 and Euler Codes. NASA CR-172604, July 1985.
24. Liu, N-S.; and Shamroth, S. J.: On the Application of a Hairpin Vortex Model of Wall Turbulence to Trailing Edge Noise Prediction. NASA CR-177938, August 1985.
25. Reich, F. R.; and Coleman, W. J.: Feasibility of an Optical Slip-Ring for High-Density-Data Communication Links. NASA CR-172611, July 1985.
26. Shepherd, K. P.: Detection of Low Frequency Impulsive Noise from Large Wind Turbine Generators. NASA CR-172511, January 1985.
27. Shepherd, K. P.; and Hubbard, H. H.: Sound Propagation Studies for a Large Horizontal Axis Wind Turbine. NASA CR-172564, March 1985.
28. Yates, J. E.: Analysis of the Surface Load and Radiated Sound of a Vibrating Airfoil with Application to the Experiment of Brooks. NASA CR-3864, January 1985.

29. Foss, J. F.; Klewicki, C. L.; and Disimile, P. J.: Transverse Vorticity Measurements Using an Array of Four Hot-Wire Probes. NASA CR-178098, May 1986.
30. Simonich, J. C.; Amiet, R. K.; Schlinker, R. H.; and Greitzer, E. M.: Helicopter Rotor Noise Due to Ingestion of Atmospheric Turbulence. NASA CR-3973, May 1986.
31. Yoerkie, C. A.; Gintoli, P. J.; and Moore, J. A.: Development of Rotorcraft Interior Noise Control Concepts, Phase II: Full Scale Testing. NASA CR-172594, February 1986.

Journal Articles and Other Publications

1. Farassat, F.; Pegg, R. J.; and Hilton, D. A.: Thickness Noise of Helicopter Rotors at High Tip Speeds. AIAA Progress in Astronautics and Aeronautics, 1976, vol. 44, pp. 601-613.
2. Dempsey, T. K.; Leatherwood, J. D.; and Clevenson, S. A.: Development of Noise and Vibration Ride Comfort Criteria. Journal of the Acoustical Society of America, vol. 65, no. 1, pp. 124-132, January 1979.
3. Leatherwood, Jack D.; Dempsey, Thomas K.; and Clevenson, Sherman A.: A Design Tool for Estimating Passenger Ride Quality Within Complex Ride Environments. Journal of the Human Factors Society, vol. 22, no. 3, June 1980, p. 291-312.
4. Brooks, T. F.: Trailing Edge Noise Prediction Using Amiet's Method. Journal of Sound and Vibration, vol. 77, no. 1, September 1981, p. 437-439.
5. Brooks, Thomas F.; and Hodgson, Thomas H.: Trailing Edge Noise Prediction Using Measured Surface Pressures. Journal of Sound and Vibration, vol. 77, no. 4, August 22, 1981, p. 69-117.
6. Farassat, F.: Linear Acoustic Formulas for Calculation of Rotating Blade Noise. AIAA Journal, vol. 19, no. 9, September 1981, p. 1122-1130.
7. Farassat, F.; and Martin, R. M.: A Note on the Tip Noise of Rotating Blades. Journal of Sound and Vibration, vol. 86, February 8, 1983, p. 449-453.
8. Brooks, T. F.; and Schlinker, R. H.: Progress in Rotor Broadband Noise Research. Vertica, vol. 7, no. 4, 1983, p. 287-307.
9. Farassat, F.: Comments on "Derivation of the Fundamental Equation of Sound Generated by Moving Aerodynamic Surfaces" by Hans R. Aggarwal. AIAA Journal, vol. 22, no. 8, August 1984, p. 1183-1184.

10. Farassat, F.: A New Aerodynamic Integral Equation Based on an Acoustic Formula in the Time Domain. AIAA Journal, vol. 22, no. 9, September 1984, p. 1337-1340.
11. Farassat, F.: Solution of the Wave Equation for Open Surfaces Involving a Line Integral Over the Edge. Journal of Spacecraft and Rockets, vol. 95, no. 1, July 1984, p. 136-141.
12. Farassat, F.; and Succi, G. P.: The Prediction of Helicopter Rotor Discrete Frequency Noise. Vertica, vol. 7, no. 4, 1983, p. 309-320.
13. Fields, J. M.: The Effect of Numbers of Noise Events on People's Reactions to Noise: An Analysis of Existing Survey Data. The Journal of the Acoustical Society of America, vol. 75, no. 2, February 1984, p. 447-467.
14. Leatherwood, J. D.; Clevenston, S. A.; and Hollenbaugh, D. D.: Evaluation of Ride Quality Prediction Methods for Operational Military Helicopters. Journal of the American Helicopter Society, vol. 29, July 1984, p. 11-18.
15. Raney, J. P.; and Hoad, D. R.: Creating Competitive Rotorcraft Noise Technology. Aerospace America, vol. 22, February 1984, p. 60-63.
16. Brooks, T. F.; and Marcolini, M. S.: Scaling of Airfoil Self-Noise Using Measured Flow Parameters. AIAA Journal, vol. 23, no. 2, February 1985, p. 207-213.
17. Farassat, F.; and Myers, M. K.: Some Qualitative Results on the Thickness and Loading Noise of Rotating Blades. Journal of Sound and Vibration, vol. 101, no. 2, 1985, p. 262-266.
18. Hardin, J. C.; and Mason, J. P.: A New Look at Sound Generation by Blade/Vortex Interaction. Journal of Vibration, Acoustics, Stress, and Reliability and Design, vol. 107, April 1985, p. 224-228.
19. Vaicaitis, R.; and Mixson, J. S.: Theoretical Design of Acoustics Treatment for Noise Control in a Turboprop Aircraft. Journal of Aircraft, vol. 22, no. 4, April 1985, pp. 318-324.
20. Beyer, T.; Powell, C.; Daniels, E.; and Pope, L.: Effects of Acoustic Treatment on the Interior Noise of a Twin Engine Propeller Airplane. Journal of Aircraft, vol. 22, no. 9, September 1985, pp. 784-788.
21. Martin, R. M.; Brooks, T. F.; and Hoad, D. R.: Reduction of Background Noise Induced by Wind Tunnel Jet Exit Vanes. AIAA Journal, vol. 23, no. 10, October 1985, p. 1631-1632.

22. Wood, J. J.; and Leatherwood, J. D.: Meter Measures Ride Comfort. Automotive Engineering--Testing and Instrumentation Issue, vol. 93, no. 6, June 1985, p. 50-56.
23. Booth, E. R., Jr.; and Yu, J. C.: Two-Dimensional Blade-Vortex Flow Visualization Investigation. AIAA Journal, vol. 24, no. 9, September 1986, p. 1468-1473.
24. Brooks, T. F.; and Marcolini, M. A.: Airfoil Tip Vortex Formation Noise. AIAA Journal, vol. 24, no. 2, February 1986, p. 246-252.
25. Farassat, F.: Prediction of Advanced Propeller Noise in the Time Domain. AIAA Journal, vol. 24, no. 4, April 1986, pp. 578-584.
26. Brooks, T. F.; Marcolini, M. A.; and Pope, D. S.: Airfoil Trailing-Edge Flow Measurements. AIAA Journal, vol. 24, no. 8, August 1986, p. 1245-1251.
27. Martin, R.; Elliott, J.; and Hoad, D.: Experimental and Analytical Predictions of Rotor Blade-Vortex Interaction. AHS Journal, vol. 31, no. 4, October 1986, pp. 12-20.
28. Brooks, T.; Marcolini, M.; and Pope, D.: A Directional Array Approach for the Measurement of Rotor Noise Source Distributions with Controlled Spatial Resolution. Journal of Sound and Vibration, vol. 112, no. 1, January 1987, pp. 192-197.

Meeting Presentations

1. Brown, Thomas J.; and Farassat, Fereidoun: A New Capability for Predicting Helicopter Rotor Noise in Hover and in Flight. Presented at the 1976 Army Science Conference, June 1976. Conference Proceedings, vol. II.
2. Farassat, F.; and Brown, T. J.: Development of a Noncompact Source Theory with Applications to Helicopter Rotors. Presented at the AIAA 3rd Aeroacoustics Conference, July 1976. AIAA Paper No. 76-563.
3. Brooks, T. F.; and Hodgson, T. H.: Prediction and Comparison of Trailing Edge Noise Using Measured Surface Pressures. Presented at the AIAA 6th Aeroacoustics Conference, June 4-6, 1980, Hartford, Connecticut. AIAA Paper No. 80-0977.
4. Farassat, F.: A Collection of Formulas for Calculation of Rotating Blade Noise--Compact and Noncompact Source Results. Presented at the AIAA 6th Aeroacoustics Conference, June 4-6, 1980, Hartford, Connecticut. AIAA Paper No. 80-0996.

5. Greene, George C.; and Raney, John P.: An Overview of NASA's Propeller and Rotor Noise Research. Presented at the AIAA 6th Aeroacoustics Conference, June 4-6, 1980, Hartford, Connecticut. AIAA Paper No. 80-0992.
6. Brooks, Thomas F.; and Marcolini, Michael A.: Airfoil Self Noise - Effect of Scale. Presented at the AIAA 8th Aeroacoustics Conference, April 11-13, 1983, Atlanta, Georgia. AIAA Paper No. 83-0785.
7. Clevenson, Sherman A.; Leatherwood, Jack D.; and Hollenbaugh, Dan D.: Operational Military Helicopter Interior Noise and Vibration Measurements with Comparisons to Ride Quality Criteria. Presented at the AIAA/AHS 1983 Aircraft Design, Systems, and Operations Meeting and Technical Display, October 17-19, 1983, Fort Worth, Texas. AIAA Paper No. 83-2526.
8. Booth, E. R., Jr.; and Yu, J. C.: Two Dimensional Blade-Vortex Interaction Flow Visualization Investigation. Presented at the AIAA/NASA 9th Aeroacoustics Conference, October 15-17, 1984, Williamsburg, Virginia. AIAA Paper No. 84-2307.
9. Brooks, T. F.; and Marcolini, M. A.: Airfoil Tip Vortex Formation Noise. Presented at the AIAA/NASA 9th Aeroacoustics Conference, October 15-17, 1984, Williamsburg, Virginia. AIAA Paper No. 84-2308.
10. Brooks, T. F.; Marcolini, M. A.; and Pope, D. S.: Airfoil Trailing Edge Flow Measurements and Comparison with Theory Incorporating Open Wind Tunnel Corrections. Presented at the AIAA/NASA 9th Aeroacoustics Conference, October 15-17, 1984, Williamsburg, Virginia. AIAA Paper No. 84-2266.
11. Hardin, J. C.; and Lamkin, S. L.: Aeroacoustic Interaction of a Distributed Vortex with a Lifting Joukowski Airfoil. Presented at the AIAA/NASA 9th Aeroacoustics Conference, October 15-17, 1984, Williamsburg, Virginia. AIAA Paper No. 84-2287.
12. Hardin, J. C.; and Mason, J. P.: A New Look at Sound Generation by Blade/Vortex Interaction. Presented at the 1984 ASME Winter Annual Meeting, December 9-14, 1984, New Orleans, Louisiana. Paper No. 84-041.
13. Martin, R. M.: Comparison of Noise Prediction for the X-Wing System and a Conventional Rotor in Hover. Presented at the AHS 40th Annual Forum and Technical Display, May 16-18, 1984, Crystal City, Virginia. AHS Paper No. A-84-40-03-D000. In Proceedings, p. 9-17.
14. Martin, R. M.; Elliott, J. W.; and Hoad, D. R.: Comparison of Experimental and Analytic Predictions of Rotor Blade-Vortex Interactions Using Model Scale Acoustic Data. Presented at the AIAA/NASA 9th Aeroacoustics Conference, October 15-17, 1984, Williamsburg, Virginia. AIAA Paper No. 84-2269.

15. Powell, C. A.; and Fields, J. M.: Community Annoyance Due to Controlled Helicopter Noise Exposures. Presented at the 4th Congress of the Federation of Acoustical Societies of Europe, August 21-24, 1984, Sandefjord, Norway. In Proceedings, FASE '84, p. 313-316.
16. Willshire, W. L., Jr.; and Martin, R. M.: Noise and Performance Characteristics of a Model Scale X-Wing Rotor System in Hover. Presented at the AIAA 22nd Aerospace Sciences Meeting, January 9-12, 1984, Reno, Nevada. AIAA Paper No. 84-0337.
17. Grosveld, F. W.; and Metcalf, V. L.: Random Response and Noise Transmission of Composite Panels. Presented at the AIAA, ASME, et al., 26th Structures, Structural Dynamics, and Materials Conference, April 15-17, 1985, Orlando, Florida. AIAA Paper No. 85-0789-CP
18. Metcalf, V. L.; and Grosveld, F. W.: Noise Transmission Characteristics of Aircraft Type Composite Panels. Presented at the 1985 SAE General Aviation Aircraft Meeting and Exposition, April 15-19, 1985, Wichita, KS. SAE Paper No. 850878.
19. Silcox, R. J.; and Elliott, S. J.: Applicability of Superposition and Source Impedance Models of Active Noise Control Systems. Presented at the International Institute of Noise Control Engineering International Conference on Noise Control Engineering, September 18-20, 1985, Munich, Germany. In Proceedings, vol. 1, 1985, p. 587-590.
20. Willshire, W. L., Jr.: Long Range Downwind Propagation of Low Frequency Noise. Presented at the University of Mississippi Symposium/Workshop on the Physics of Long Distance Sound Propagation and Coupling Into the Ground, February 13-16, 1985, New Orleans, Louisiana. In Proceedings, vol. 1, p. 176-194.
21. Wood, J. J.; and Leatherwood, J. D.: A New Ride Quality Meter. Presented at the SAE Vehicle Noise and Vibration Conference, May 15-17, 1985, Traverse City, Michigan. In Proceedings of Vehicle Noise and Vibration Conference, Paper No. 850981, p. 177-183.
22. Booth, E. R., Jr.: Surface Pressure Measurement During Low Speed Two-Dimensional Blade-Vortex Interaction. Presented at the AIAA 10th Aeroacoustics Conference, July 9-11, 1986, Seattle, Washington. AIAA Paper No. 86-1856.
23. Farassat, F.; and Myers, M. K.: Aerodynamics Via Acoustics: Application of Acoustic Formulas for Aerodynamic Calculations. Presented at the AIAA 10th Aeroacoustics Conference, July 9-11, 1986, Seattle, Washington. AIAA Paper No. 86-1877.

24. Lester, H.; and Fuller, C.: Active Control of Propeller Induced Noise Fields Inside a Flexible Cylinder. Presented at the AIAA 10th Aeroacoustics Conference, July 9-11, 1986, Seattle, Washington. AIAA Paper No. 86-1957.
25. Farassat, F.; and Myers, M. K.: The Moving Boundary Problem for the Wave Equation: Theory and Application. Presented at the First IMACS Symposium on Computational Acoustics, August 6-8, 1986, New Haven Connecticut. Proceedings pending.
26. Golub, R. a.; Weir, D. S.; and Tracy, M. B.: Application of the Baseline ROTONET System to the Prediction of Helicopter Tone Noise. Presented at the AIAA 10th Aeroacoustics Conference, July 9-11, 1986, Seattle, Washington. AIAA Paper No. 86-1904.
27. Grosveld, F. W.; and Beyer, T. B.: Modal Characteristics of a Stiffened Composite Cylinder with Open and Closed End Conditions. Presented at the AIAA 10th Aeroacoustics Conference, July 9-11, 1986, Seattle, Washington. AIAA Paper No. 86-1908.
28. Hardin, J. C.; and Lamkin, S. L.: Concepts for Reduction of Blade-Vortex Interaction Noise. Presented at the AIAA 10th Aeroacoustics Conference, July 9-11, 1986, Seattle, Washington. AIAA Paper No. 86-1855.
29. Martin, R. M.; and Burley, C. L.: Application of Cepstrum to Remove Echoes from Rotor Acoustic Spectra. Presented at the AHS 42nd Annual Forum & Technology Display, June 2-4, 1986, Washington, DC. In Proceedings.
30. Zorumski, W. E.; and Willshire, W. L., Jr.: The Acoustic Field of a Point Source in a Uniform Boundary Layer Over an Impedance Plane. Presented at the AIAA 10th Aeroacoustics Conference, July 9-11, 1986, Seattle, Washington. AIAA Paper No. 86-1923.
31. Hardin, J. C.; and Lamkin, S. L.: An Euler Code Calculation of Blade-Vortex Interaction Noise. Presented at the ASME Winter Annual Meeting, December 7-12, 1986, Anaheim, California. ASME Paper No. 86-WA/NCA-3.
32. Martin, R.; and Hardin, J.: The Spectral Characteristics of Rotor Blade-Vortex Interaction Noise: Experimental and Mathematical Results. Presented at the AIAA 25th Aerospace Sciences Meeting, January 12-15, 1987, Reno, Nevada.
33. Brentner, K. S.: A Prediction of Helicopter Rotor Discrete Frequency Noise for Three Scale Models Using a New Acoustic Program. Presented at the AIAA 25th Aerospace Sciences Meeting, January 12-15, 1987, Reno, Nevada. AIAA Paper No. 87-0252.

34. Brooks, T. F.; Marcolini, M. A.; and Pope, D. S.: Model Rotor Broadband Noise Study in DNW. Paper presented at the AHS National Specialists' Meeting on Aerodynamics and Aeroacoustics, February 25-27, 1987, Arlington, Texas.
35. Martin, R. M.; and Splettstoesser, W.: Initial Acoustic Results from the BVI Test of a 40 Percent Model Rotor in the DNW. Presented at the AHS National Specialists' Meeting on Aerodynamics and Aeroacoustics, February 25-27, 1987, Arlington, Texas.
36. Farassat, F.; and Brentner, K. S.: The Uses and Abuses of the Acoustic Analogy in Helicopter Rotor Noise Prediction. Presented at the AHS National Specialists' Meeting on Aerodynamics and Aeroacoustics, February 25-27, 1987, Arlington, Texas.
37. Golub, R.; and Weir, D.: The Phase II ROTONET System. Presented at the AHS National Specialists' Meeting on Aerodynamics and Aeroacoustics, February 25-27, 1987, Arlington, Texas.

IDENTIFICATION AND PROPOSED CONTROL OF HELICOPTER

TRANSMISSION NOISE AT THE SOURCE

John J. Coy, Robert F. Handschuh, and David G. Lewicki
Propulsion Directorate
U.S. Army Research and Technology Activity - AVSCOM
Lewis Research Center
Cleveland, Ohio 44135

Ronald G. Huff, Eugene A. Krejsa, and Allan M. Karchmer
National Aeronautics and Space Administration
Lewis Research Center
Cleveland, Ohio 44135

SUMMARY

Helicopter cabin interiors require noise treatment which is expensive and adds weight. The gears inside the main power transmission are major sources of cabin noise. This paper describes work conducted by the NASA Lewis Research Center in measuring cabin interior noise and in relating the noise spectrum to the gear vibration of the Army's OH-58 helicopter. Flight test data indicate that the planetary gear train is a major source of cabin noise and that other low frequency sources are present that could dominate the cabin noise. Companion vibration measurements were made in a transmission test stand, revealing that the single largest contributor to the transmission vibration was the spiral bevel gear mesh. Our current understanding of the nature and causes of gear and transmission noise is discussed. The authors believe that the kinematical errors of the gear mesh have a strong influence on the noise. This paper summarizes completed NASA/Army sponsored research that applies to transmission noise reduction. The continuing research program is also reviewed.

INTRODUCTION

Helicopter interior noise and vibration are of concern because of passenger comfort and the effect on pilot and crew efficiency. The military is most concerned with pilot workload and efficiency, while the commercial arena is interested to attract passengers who are expecting jet smooth and quiet transportation with the convenience of a vertical takeoff from congested areas. In current helicopters the excessive interior noise causes annoyance, disrupts crew performance and requires ear protection equipment to be worn (fig. 1). Most experts agree that the major source of the annoying noise in the cabin originates from the gearing in the main transmission which is commonly mounted to the cabin ceiling. The sound and vibration energy is propagated through the structure or through the air directly to excite the cabin walls.

In the past, a major goal of transmission design was to reduce the weight, and as weight decreased, the noise has increased (ref. 1). This may be due to the increased flexibility of the transmission housing that accompanies a weight reduction. Also, the noise increases with the power and size of the helicopter.

The objective of this paper is to identify the applicable tools and techniques that have been developed during the years of NASA/Army cooperation and to present them in one place. A second objective is to present some conclusions based on the relevant work of the past in summary form. The third objective is to describe the NASA/Army transmission noise program so that industry, government, and universities can work together to achieve quieter helicopter transmissions.

This paper will present and discuss noise and vibration measurements taken on the U.S. Army OH-58 helicopter transmission. Measurements were taken in the NASA Lewis Transmission Laboratory, and in flight at the Ohio National Guard Facility at Akron-Canton Airport. Our current understanding of the nature and causes of gear and transmission noise is discussed, followed by a summary of the past work sponsored by the Army Propulsion Directorate and NASA Lewis that is applicable to the noise and vibration problem. Now there is a focussed attention on helicopter noise; current activity and plans for future work on helicopter noise are presented.

OH-58 HELICOPTER & TRANSMISION

The OH-58C Helicopter is the Army's Light Scout/Attack helicopter, which has a single two-bladed rotor and is powered by a 236 kW (317 rated output shp) gas turbine engine. The gross vehicle weight is 14.2 kN (3200 lb). The main transmission has a reduction ratio of 17.44:1, dry weight of 0.467 kN (105 lb), and is engine output rated for 201 kW (270 hp) continuous duty. The Army began receiving the OH-58's from Bell Helicopter Company in 1969. The OH-58 is a derivative of the Bell Model 206. The most recent Army upgrade of this helicopter is the OH-58 D model, rated at 339 kW (455 hp) at the main rotor. The commercial family of 206 versions has several models.

The Noise Problem

Historically, helicopters have been plagued by internal noise problems. Noise levels range from 100-120 dBA in the cabin. The sound can be from many sources, such as the transmission gear noise, the turbine engine compressor and exhaust noise, the rotor blades, and air turbulence. The transmission is a particularly troublesome source and is believed to be the main source of annoying noise in the helicopter cabin. The noise from the transmission enters the cabin following two paths, structure borne radiation and direct radiation (fig. 2). The magnitude of the direct radiation is a function of the acoustic power radiated from the transmission case, transmitted acoustically to the cabin outer walls, and transferred through to the cabin. Of course if there are any small openings in the wall between the transmission compartment and the cabin the sound will directly enter the cabin. The structure borne path is particularly hard to block because the transmission case and its mounts are an integral part of the lift-load bearing path. The transmission mounts must be strong and rigid: strong enough to support the entire helicopter by transferring the lift-load from the rotor blades to the air frame; and rigid enough for stable control of the helicopter. The stiff mounts pass the gear vibrations exceedingly well to the airframe, and the sound transmits to the cabin directly.

OH-58 Investigations

The measurement experience reported here was limited to the OH-58 helicopter (fig. 3). Vibration measurements of the transmission were previously reported for the OH-58 helicopter (refs. 2 and 3) and for two larger sized helicopters (refs. 4 and 5). The in-flight measurements of cabin noise were performed in a National Guard helicopter at the Akron-Canton Airport. Measurements of the in-flight vibration and noise are presented here for the first time.

OH-58 Transmission.

The test transmission is described in reference 2 and is shown in figure 4. It is rated for use where the engine output is 201 kw (270 hp) continuous duty and 236 kw (317 hp) at takeoff for 5 min. The input shaft, turning at 6180 rpm, drives a 19 tooth spiral bevel pinion meshing with a 71 tooth bevel gear. The input shaft is mounted on triplex ball bearings and one roller bearing. The 71 tooth bevel gear shaft is mounted on duplex ball bearings and one roller bearing. The bevel gear shaft drives a floating sun-gear which has 27 teeth. The power is taken out through the planet carrier. There are three planet gears of 35 teeth which are mounted on spherical roller bearings. The ring gear (99 teeth) is splined to the top case and therefore is stationary. The overall gear reduction ratio is 17.44:1.

NASA LEWIS TEST STAND

Figure 5 shows the NASA 500 hp helicopter transmission test stand, which was used to run the self-excited vibration tests (ref. 3). The test stand operates on the "four-square" or torque regenerative principle, where mechanical power is recirculated around the closed loop of gears and shafting, passing through the test transmission. A 149 kW (200 hp) variable speed dc motor is used to power the test stand and control the speed. Since the torque and power are recirculated around the loop, only the losses due to friction have to be replenished.

An 11 kW (15 hp) variable speed dc motor driving against a magnetic particle clutch is used to set the torque in the test stand. The output of the clutch does not turn continuously, but only exerts a torque through the speed reducer gearbox and chain drive to the large sprocket on the differential gear unit. The large sprocket is the first input to the differential. The second input is from the upper shaft which passes concentrically through the hollow upper gear shaft in the closing-end gearbox. The output shaft from the differential gear unit is the previously mentioned hollow upper gear shaft of the closing-end gearbox. The torque in the loop is adjusted by changing the electrical field strength at the magnetic particle clutch. The input and output shafts to the test transmission are equipped with speed sensors, torque meters, and slip rings.

NOISE AND VIBRATION MEASUREMENTS

The transmission was instrumented with accelerometers with a flat frequency response up to 10 kHz, installed in the test stand and operated at 6060 rpm and load of 224 kW (300 hp). After reaching an equilibrium operating temperature of approximately 93 °C (200 °F), the accelerometer signals were recorded on a 14 channel FM tape recorder and later processed with a digital signal processor to get the vibration spectra.

Test Cell Measurements

Vibration spectra have been extensively measured for the OH-58 transmission in test rigs at the Corpus Christi Army Depot and at NASA Lewis (refs. 2 and 3). Measurements were made for a matrix of test conditions and thus it was determined that transmission speed had a significant effect while torque had a small effect on vibration amplitude. The highest magnitude of vibration consistently occurred at the spiral bevel gear mesh frequency for a variety of accelerometer locations. A typical spectrum is shown in figure 6, where the accelerometer was located in the plane of the planetary gear stage, just above the split-line between the top and bottom halves of the transmission housing.

In-flight Measurements

In-flight measurements were made in an Ohio National Guard OH-58 helicopter at the Akron-Canton Airport. Data records were recorded on FM magnetic tape and later analyzed using a spectrum analyzer. Microphone and accelerometer transducers were used. One of the accelerometers was placed near the split line of the transmission upper and lower housing in the approximate location that was used to obtain the result shown in figure 6. The objective of placing the accelerometer was to have a comparison with data collected in the test cell. A second accelerometer was placed on the transmission support base at the cabin roof. The purpose of this was to characterize the structure borne vibration by measuring the vibrations on the airframe at a point in the path of propagation. Figure 7 shows the results from spectrum analysis of the accelerometer measurements. Microphones were placed head-high in the vicinity of the copilot station and the aft cabin. The objective was to measure the noise perceived by passengers and, with the accelerometer signals in hand, thereby determine the severity of the noise components due to the transmission. Figure 8 shows the results from spectrum analysis of the noise measurements.

DISCUSSION OF RESULTS

In general, the vibration spectra contain many discrete frequencies where there is significant concentrated vibrational energy. The frequencies are identified with the gear mesh frequencies and the higher harmonics at integer multiples of the mesh frequencies. From the measurements in the test cell it was found that the single largest contributor to the transmission housing vibration was the spiral bevel gear mesh (fig. 6). The flight data were consistent with these findings (fig. 7(a)), except for some additional vibrational contributions, which have not yet been identified.

Analysis of the flight and test rig data indicates that the highest amplitude of transmission vibration occurs at the bevel gear clash frequency. However, for transducer locations other than directly on the transmission, the flight data presented some different conclusions regarding the effect of transmission vibration on the cabin noise. Flight data (fig. 7(b)) from accelerometers on the transmission mount at the cabin attachment point show that the vibration at the bevel and planetary gear mesh frequencies are equal to one another and to the peak amplitude of the bevel gear vibration measured on the transmission case (fig. 7(a)). It now becomes apparent that the transfer function from the housing to the mounting point has increased the relative significance the planetary gear vibration. This could be due to structural resonance or to vibration from the planetary gear and bevel gear being transferred along different paths resulting in an apparent increase of the planetary gear vibration at the transmission/cabin interface. Based on this observation, one might expect the planetary and bevel gears to contribute equally to the cabin noise.

The noise generated in the cabin by the transmission vibration is a function of the transfer function between the transmission and the cabin interior and the acoustic efficiency of the process. Since the process is unknown at this time, it is necessary to rely on the data provided by the cabin microphones (fig. 8). The noise spectra from the microphone measurements show a trend of decreasing amplitude as the frequency increases. This is because the higher frequency noise waves are more easily absorbed and dissipated in the acoustic transmission process. The spectra at the two locations (figs. 8(a) and (b)) differ only slightly, possibly due to standing wave patterns in the cabin.

The transmission related noise in the cabin is dominated by the planetary gear mesh frequency. This indicates that reducing the vibration generated by the planetary gears could significantly decrease the cabin noise level. Attention should also be directed to identification and reduction of the noise source that exists at frequencies below 400 Hz. Therefore it appears that the most troublesome noise in the cabin is the lowest frequency gear noise as well as other low frequency noise the source of which is unknown at this time. In the cabin, the bevel gear noise is significantly below the planetary gear noise. It may be concluded that if the large amplitude of vibration for the bevel gear had occurred at the lower frequency of the planetary gear mesh frequency there would be even higher level of transmission noise in the cabin.

NATURE AND CAUSES OF TRANSMISSION NOISE

Noise generated by gears is due to many mechanisms such as mechanical impact of gear teeth, ejection of air and oil from between the gear teeth, the time varying stiffness of the gear mesh, movement of the load on the gear tooth, and errors in gear tooth geometry (refs. 6 to 10). Many of these mechanisms are inherent to transmissions and their elimination as a noise source is impossible. It is believed that kinematic error is the most significant source of noise and vibration in gearboxes. Kinematic errors are particularly troublesome for spiral bevel gears. The spiral bevel gears in a helicopter transmit high power at high speed, so elimination of kinematic errors can reduce the noise and vibration.

Kinematic Errors

Kinematic errors are defined as the deviations from a constant rate of turning of the driven gear while the driving gear turns at a constant rate (fig. 9). If a set of gears transmits motion without kinematic errors then they are said to have conjugate motion (horizontal dashed line of fig. 9). Each parabolic curve shown in the figure represents the kinematic error for one gear tooth as it moves through mesh. Intersection of the parabolic curves is where the load is transferred to the next gear tooth. It is this varying gear ratio that provides a source of vibration (noise) excitation to the gear system.

Conjugate Motion

Conjugate motion results if the vector normal to the gear tooth surfaces at the point of contact passes through the pitch point during the process of meshing (fig. 10). This requirement is satisfied for spur gears of involute tooth profile under very light load; when the load is high, the elastic deflection of the gear teeth upsets the condition of conjugacy. The involute system of tooth shapes for spur and helical gears can be described by simple mathematical expressions. In contrast to spur gears, there is no equation for describing the surface of a spiral bevel gear tooth. The surface coordinates of the points on the tooth must be calculated, based on the generating motions of the grinding machine.

As currently manufactured, spiral bevel gears do not have conjugate action. Spiral bevel gears with conjugate action were examined many years ago. It was found that if the gears had line contact between the teeth then they were very sensitive to shaft misalignment. This resulted in very poor performance: for even slight misalignment, the tooth contact moved to the edge of the tooth, causing very high contact stress, noise and poor life. To compensate for this sensitivity, the gears had to be made with something called "mismatch", which is a crowning of the tooth profile in both the lengthwise and profilewise directions. This reduced the sensitivity to misalignments but it also compromised noise, because conjugate action was lost.

The process of grinding teeth on a spiral bevel gear is a function of many different settings on the gear grinding machine. Nominally similar gears may result from several different sets of machine settings. Usually the machine settings are chosen, the gear and pinion are made, and the gear and pinion are tested in a fixture to see what kind of contact pattern exists between the teeth. Then the machine settings are adjusted to improve the contact pattern between the teeth, and the gears are ground again. The process may have to be repeated several times.

It is possible to determine the contact pattern and kinematic errors, based on a given set of machine settings. This procedure is extremely complicated and must be done using a computer (refs. 11 and 12). The basis for the mathematical methods is vector analysis and differential geometry.

The way of visualizing how the meshing of spiral bevel gears with zero kinematical errors takes place is similar to the spur gear example (refs. 13 and 14). Recall from the spur gear example (fig. 10), that the surface normal

at the contact point always passes through a fixed point in space--the pitch point. For the bevel gears, which can be imagined as two pitch cones rolling against one another at a pitch line (fig. 11), the normal to the tooth surfaces at the contact point should pass through a fixed line in space,--the pitch line.

If we require that the tooth surface normal vector always passes through the pitch line, and if we require that the tooth surface normal be constrained to move parallel to itself as the contact point shifts across the tooth, then the gears will have zero kinematic errors. The problem becomes one of how to achieve this type of motion by the intelligent selection of the machine settings for the gears to be manufactured. This has been accomplished through the kinematic modelling of the manufacturing process (ref. 15), which results in a set of nonlinear equations that must be solved simultaneously using numerical methods.

AVAILABLE SUPPORTING TECHNOLOGY

Helicopter cabin noise is significantly affected by the transmission and in particular the gears in the transmission. Gears are a source of high vibration and have been the subject of study for years in research investigations too numerous to mention here. There has also been a significant amount of NASA/Army sponsored research that is pertinent. For that work to be truly useful, it must be brought to the attention of gear and transmission designers and researchers. The work falls into the categories of Dynamic Load Analysis, Tooth Profile Modification, and Measurement Tools.

Dynamic Load Analysis

Dynamic load is defined as the load on the gear tooth as a function of time and position as the gear rotates. Dynamic loads are caused by the interaction of the mass of the gear and driven elements and the stiffness of the gear tooth. Usually the gear system is modelled with second order differential equations with time varying stiffness parameters. The stiffness changes because the number of gear teeth in mesh varies as the gears rotate. The average number of teeth in mesh is called the contact ratio. The Hamilton Standard division of United Technologies, under a NASA contract has developed two computer programs for the calculation of gear dynamic loads (refs. 16 and 17). Computer program GRDYSNG is for a single pair of spur gears in mesh. The model includes two rotational degrees of freedom, and time varying tooth stiffness. Contact ratios between one and three are possible, and variations of the tooth from involute form are possible. An option permits a buttress form tooth, which has a lesser pressure angle on the drive side than the coast side. Computer program GRDYNMLT extends the capability of GRDYSNG to include multiple gear mesh conditions such as present in a planetary gear stage.

The Cleveland State University has developed computer program PGT which calculates dynamic loads on planetary gear trains. The dynamic model has 9° of freedom, and is able to analyze a planetary gear train with three planet gears. A variable mesh stiffness is used, including the effects of planet phasing and location errors. The analysis can be used to study static and dynamic load sharing among planets, tooth errors and intentional profile

modifications (ref. 18). The computer programs PGT and GRDYNMLT have been compared with each other and with experimental data from full scale transmission experiments (ref. 19).

The gear tooth stiffness that is modelled in most gear dynamic computer programs is static tooth stiffness. A more realistic stiffness model has the load moving across the profile of the tooth as the gears rotate; the effect becomes very significant at high speeds. The influence of moving load was investigated under a NASA sponsored grant at Michigan Technological University (ref. 20). The University of Cincinnati investigated the effect on involute and straight tooth forms (ref. 21) and developed a computer program to study the effects of parametric variations on gear dynamic load (refs. 22 to 23).

Computer program TELSGE was developed by Northwestern University, where the gear tooth stiffness was determined by finite elements. The model is for a simple spur gear mesh with 2° of freedom, and includes the effect of the thin film of lubricant between the gear teeth (ref. 24). The problem of dynamic loads in spiral bevel gears is extremely complex due to the tooth geometry and the additional degrees of freedom necessary for even a simple mesh of two gears. In reference 25 the concepts of reference 24 were extended to the case of spiral bevel gears using 12° of freedom. The study was for a particular pair of gears and the results are not generally applicable to all spiral bevel gear pairs. There is continuing work at Bolt Beranek and Newmann to investigate the noise generating mechanism for bevel gears (NASA contract NAS3-23703).

Tooth Profile Modification

Tooth profile modification, especially tip relief is a commonly used method to control the amplitude of dynamic load in gears. There is no consensus among researchers on what is the best or optimum shape of tooth profile modification. A study of the problem was conducted by Bolt Beranek and Newmann using a conventional modification consisting of linear tip relief, in comparison to a new profile that was determined on the basis of minimum vibration excitation (ref. 26). Significant differences in the dynamic forces transmitted by the teeth are predicted for the two cases. In contrast to all the methods reviewed so far, the Bolt Beranek and Newmann approach uses the frequency domain, rather than integrating equations of motion in the time domain.

The noise from spiral bevel gears is thought to come primarily from the kinematic errors that are inherent in the manufacture of the gear teeth. A study to determine a way to manufacture the gears eliminating the kinematic errors was conducted by Litvin at the University of Illinois (ref. 27). The result of the analysis is to provide new settings for the bevel gear grinder so that the gears are manufactured with a conjugate tooth shape.

Measurement Tools

The measurement of gear noise is usually performed using accelerometers placed on the gearbox housing. As the measurements have shown in this paper, the highest contributor to noise can best be found under realistic conditions of running the gearbox, while using a microphone. The conditions in a test cell are not conducive for exacting microphone measurements due to the presence

of other machinery and accessories in the test cell that contribute to the noise. In addition, the noise field is complex and a single microphone in the test cell may not be definitive. The element of personal safety in the test cell often precludes manual movement of microphones during a test run. The problem of test cell measurements was studied by Flanagan and Atherton (ref. 28) and their solution was to use a robot-held acoustic intensity probe. Acoustic intensity measurements are made with two closely spaced microphones which measure the sound power passing a stationary point. The total sound power emanating from a source (the gearbox) can be obtained by measuring the intensity around the source and integrating over the surface enclosing the source. Since intensity is a vector quantity, sources external to the gearbox will make a net zero contribution. The advantage of the intensity method is that a specially treated anechoic chamber is not needed. The robotic acoustic intensity measurement system (RAIMS) is shown in figure 12.

Kinematic error has been explained previously. The theoretical aspect of kinematic error is well appreciated by gear theoreticians but there is currently no practical machine to measure the kinematic error of gears while the gears are loaded. A design study for such a machine was conducted by Houser (ref. 29). Until such a machine is built, progress in gear noise reduction will be limited because of our incomplete understanding of the influence of transmission errors and gear tooth flexibility on noise.

These tools need to be exploited and further developed to improve their usefulness in specific application to solving noise and vibration problems in helicopter transmissions.

CURRENT RESEARCH APPROACH

There are three general fronts on which we can attack the helicopter cabin noise problem: by using acoustic treatments in the cabin, by using isolation methods, and by reducing the source of noise excitation (fig. 13). The acoustic treatment approach has generally worked in the past but at the expense of added weight as well as added cost. New methods such as advanced lightweight sound treatments, and optimum usage of those treatments should be investigated. The work should emphasize a minimum weight penalty for the necessary noise reduction. The isolation approach can be used to manage the energy paths of the vibration and noise and prevent them from efficiently passing the energy to the cabin interior. New approaches to isolation can result from structural modification with special attention to the acoustic/dynamic coupling. Vibration absorbers should also be investigated. These could be active or passive and placed anywhere in the energy path. Reduction of the noise by reducing the vibration at the gear mesh is attractive because it could have benefits of increased life and reliability as well. The gear mesh dynamics could be improved with new tooth forms for low noise. Increased damping mechanisms within the gearbox could absorb the energy being transmitted to the cabin. An improvement of the overall transmission system dynamics could be achieved with new design techniques for housings, bearings, gears, and shafts based on dynamic and vibrational criterion. Advanced bearing mounts, and damper pads could result in lower dynamic loads.

The role of NASA Lewis and Langley Research Centers will be to cooperatively research the cabin noise problem, to concentrate in the traditional

areas of their respective expertise, and to provide the enabling technology to the industry for use in effectively reducing cabin noise.(fig. 14). Langley will concentrate in areas such as cabin noise characterization, structural modification and advanced treatments. NASA Lewis will investigate ways of quieting the gearbox. The gear mesh will be studied for ways to reduce dynamic loads with new tooth forms and tooth profile modification. Damping techniques, detuning, and system optimization will be investigated.

CONCLUDING REMARKS

This paper has described work conducted by NASA Lewis in measuring cabin interior noise and in relating the noise spectrum to the gear vibration for the Army's OH-58 helicopter. Noise and vibration data were collected and analyzed from flight tests and from ground-based tests in a transmission test stand. Our current understanding of the nature and causes of gear and transmission noise was discussed. This paper summarized NASA/Army sponsored research that applies to transmission noise reduction. The continuing research program was also reviewed. The following remarks summarize the important conclusions.

1. During the last 20 yr helicopter cabin noise due to the gear train has continued to increase with the power-to-weight ratio of the transmissions. This has required that additional sound treatment material be added, causing a weight penalty to the total helicopter system.

2. A large portion of the cabin noise is contained in discrete frequencies associated with gear mesh behavior. It is believed that significant reductions of noise can be achieved if gear vibrations within the transmission are reduced. The single largest contributor to the transmission vibration is the spiral bevel gear mesh and the planetary gear train is a major source of cabin noise. The authors believe that the kinematical errors of the gear mesh have a strong influence on the noise.

3. Several analytical design tools have been developed that will be useful in reducing gear noise excitation, viz., minimum excitation gear profile design techniques and dynamic load analysis computer codes. Also, the robotic acoustic intensity system (RAIMS) for measuring noise in a noisy test cell environment will be a valuable tool for measuring and comparing the relative noisiness of advanced components and transmission systems compared to baseline technology levels. These tools need to be exploited and further developed to improve their usefulness in specific applications.

4. NASA Lewis and Langley Research Centers with the cooperation of the collocated Army Research Centers are continuing to perform focussed research for reducing the cabin noise of future helicopters. This will be accomplished by developing the enabling technology for reduced gear noise, reduced noise propagation to the cabin and advanced acoustical treatments of the cabin interiors.

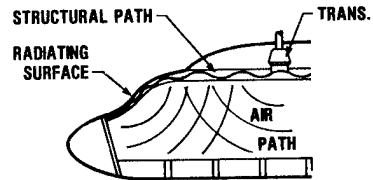
REFERENCES

1. Weden, G. J. and Coy, J. J.: "Summary of Drive-Train Component Technology in Helicopters", Gears and Power Transmission Systems for Helicopters and Turboprops, AGARD CP 369, pp 2-1 to 2-17, 1985.
2. Townsend, D. P., Coy, J. J. and Hatvani, B. R.: "OH-58 Helicopter Failure Analysis", NASA TM-X-71867, 1976.
3. Lewicki, D. G. and Coy, J. J.: "Vibration Characteristics of the OH-58A Helicopter Main Rotor Transmission", NASA TP (in process).
4. Mitchell, A. M., Oswald, F. B. and Schuller, F. T.: "Testing of YUH 61A Helicopter Transmission in NASA Lewis 2240 KW (3000 HP) Facility", NASA TP-2538, 1986.
5. Mitchell, A. M., Oswald, F. B. and Coe, H. H.: "Testing of UH 60A Helicopter Transmission in NASA Lewis 2240 KW (3000 HP) Facility", NASA TP-2626, 1986.
6. Coy, J. J., Townsend, D. P. and Zaretsky, E. V.: "Gearing", NASA RP-1152, AVSCOM TR 84-C-15, (Chapter 38 in Mechanical Design and Systems Handbook, H. Rothbart, ed., McGraw-Hill, 1985.
7. Mark, W. D.: "Analysis of Vibratory Excitation of Gear Systems as a Contributor to Aircraft Interior Noise -- Helicopter Cabin Noise", NASA CR-159088, 1979.
8. Mark, W. D.: "Gear Noise Origins", Gears and Power Transmission Systems for Helicopters and Turboprops, AGARD CP 369, pp 30-1 to 30-14, 1985.
9. Litvin, F. L. and Coy, J. J.: "Spiral Bevel Geometry and Gear Train Precision", Advanced Power Transmission Technology, G. K. Fischer, ed. NASA CP-2210, pp 335-344, 1983.
10. Litvin, F. L.: "The Theory of Gearing", 2nd ed, Nauka, Moscow, 1968. (The new edition (in English), revised and completed, sponsored by NASA, is in press).
11. Litvin, F. L., Rahman, P. and Goldrich, R. N.: "Mathematical Models for the Synthesis and Optimization of Spiral Bevel Gear Tooth Surfaces", NASA CR-3553, 1982.
12. Litvin, F. L., Hayasaka, M. S., Rahman, P. and Coy, J. J.: "Synthesis and Analysis of Spiral Bevel Gears". Design and Synthesis, H. Yoshikawa, ed., North Holland, New York, pp 302-305, 1985.
13. Litvin, F. L., Tsung, W-J. and Coy, J. J.: "Generation of Spiral Bevel Gears with Zero Kinematical Errors and Computer Aided Simulation of their Meshing and Contact", Computers in Engineering, R. Raghavan and S. M. Rohde, eds., Vol. 1, ASME, New York, 1985.
14. Litvin, F. L., Tsung, W-J., Coy, J. J. and Heine, C.: "Method for Generation of Spiral Bevel Gears with Conjugate Gear Tooth Surfaces", USAAVSCOM TR 86-C-27, ASME Paper 86-DET-3, 1986.

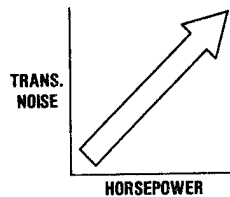
15. Litvin, F. L., Tsung, W-J., Coy, J. J., Handschuh, R. F. and Tsay C-B. P.: "New Generation Methods for Spur, Helical, and Spiral-Bevel Gears", USAAVSCOM TR 86-27, NASA TM-88862, 1986.
16. Pike, J.A.: "Interactive Multiple Spur Gear Mesh Dynamic Load Program", NASA CR-165514, 1982
17. Boyd, L.S., and Pike, J. A. "Multimesh Gear Dynamics Program Evaluation and Enhancements" NASA CR 174747, 1985.
18. August, R., Kasuba, R., Frater, J. L. and Pintz, A.; "Dynamics of Planetary Gear Trains", NASA CR-3793, 1984.
19. Choy, F. K., Townsend, D. P., and Oswald, F. B.: "Dynamic Analysis of Multi-Mesh Helicopter Gear Transmission Systems, NASA TP (in process).
20. Shuey, L.W.: "An Investigation of the Dynamic Response of Spur Gear Teeth with Moving Loads", M. S. Thesis, Michigan Technological University, 1983.
21. Lin, H. H. , Huston, R. L., and Coy J. J.: "Dynamic Analysis of Straight and Involute Tooth Forms, ASME Paper 84-DET-226, 1984.
22. Lin, H. H.: "Computer Aided Design and Analysis of Spur Gear Dynamics", PhD Dissertation, University of Cincinnati, 1985.
23. Lin, H.-H. and Huston, R. L.: "Dynamic Loading on Parallel Shaft Gears", NASA CR 179473.
24. Wang, K. L. and Cheng, H.S.: "Thermal Elastohydrodynamic Lubrication of Spur Gears", NASA CR 3241, 1980.
25. Chao, C. H-C.: "A Computer Solution for the Dynamic Load, Lubricant Film Thickness and Surface Temperatures in Spiral Bevel Gears", PhD Dissertation, Northwestern University, 1982.
26. Mark, W. D.: "The Transfer Function Method for Gear System Dynamics Applied to Conventional and Minimum Excitation Gearing Designs", NASA CR-3626, 1982.
27. Litvin, F. L., Tsung, W-J., Coy, J. J. and Heine, C.: "Generation of Spiral Bevel Gears with Zero Kinematical Errors and Computer Aided Tooth Contact Analysis", NASA TM 87273, USAAVSCOM TR 86-C-2, 1986.
28. Flanagan, P. M. and Atherton, W. J., "Investigation on Experimental Techniques to Detect, Locate and Quantify Gear Noise in Helicopter Transmissions", NASA CR-3847, 1985.
29. Bassett, D. E. and Houser, D. R.: "The Design and Analysis of Single Flank Transmission Error Tester for Loaded Gears", NASA CR (in process).

EXCESSIVE INTERNAL NOISE LEVELS IN CURRENT HELICOPTERS

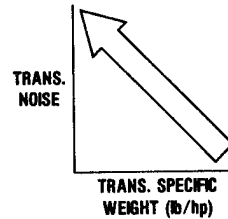
- DISCOMFORT, ANNOYANCE, AND FATIGUE OF CREW AND PASSENGERS
- VOICE COMMUNICATIONS ARE DISRUPTED
- CREW PERFORMANCE IS DEGRADED
- PERMANENT HEARING LOSS



- TRANSMISSION IS THE MAJOR SOURCE OF INTERNAL NOISE



- TRANSMISSION NOISE INCREASES WITH LARGER HELICOPTERS



- TRANSMISSION NOISE INCREASES WITH NEWER, LIGHT WEIGHT TRANSMISSIONS

FIGURE 1. - THE HISTORIC TREND FOR THE PAST 20 YR WAS HIGHER POWER, GREATER POWER-TO-WEIGHT RATIO AND INCREASING TRANSMISSION NOISE.

TRANSMISSION NOISE PATHS

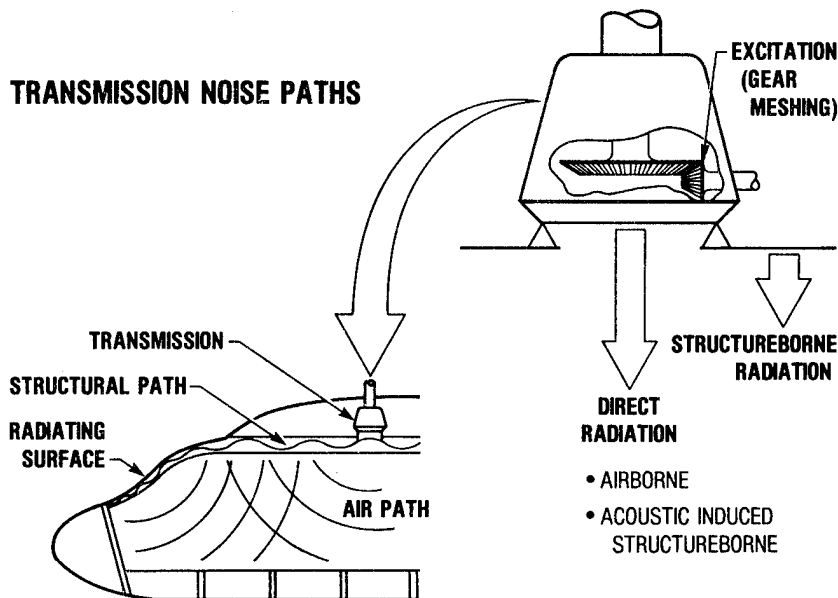


FIGURE 2. - THE NOISE FROM THE TRANSMISSION TRAVELS VIA STRUCTURAL-BORNE AND DIRECT AIR-BORNE PATHS TO THE CABIN WALLS AND IS RADIATED TO THE CABIN INTERIOR.

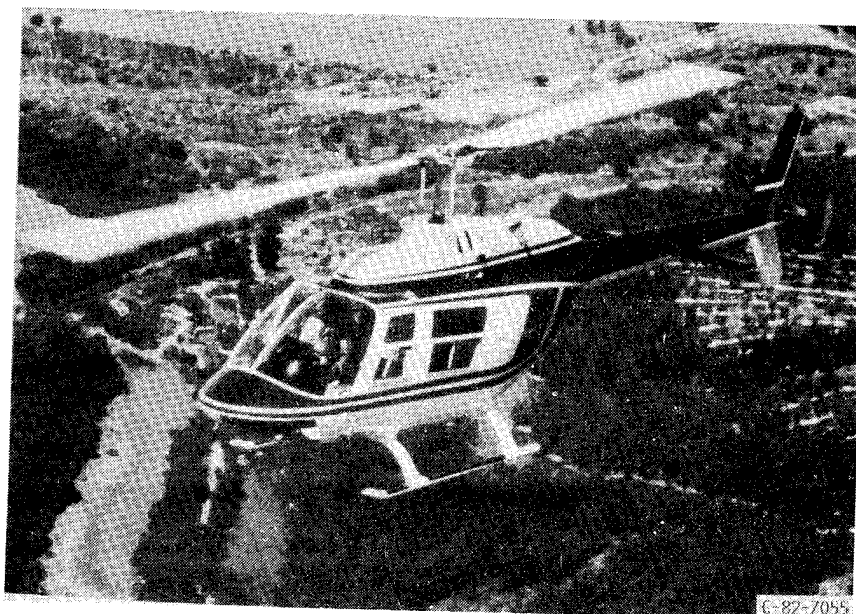
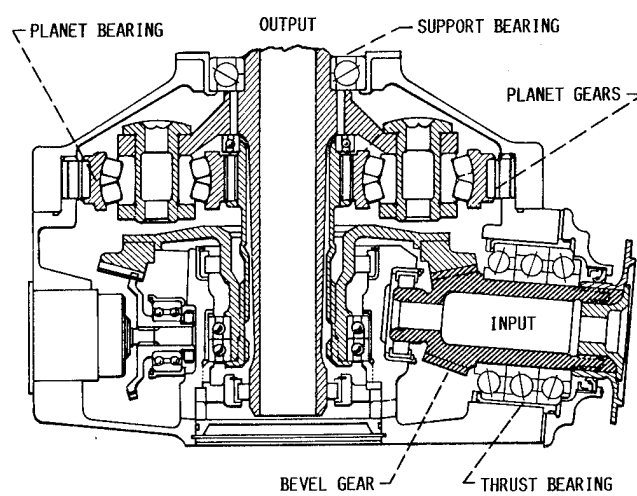


FIGURE 3. - THE OH 58 IS THE ARMY'S LIGHT OBSERVATION HELICOPTER. THE CIVIL VERSION (SHOWN) IS THE MODEL 206.



CD-82-12990

FIGURE 4. - OH 58 HELICOPTER TRANSMISSION.

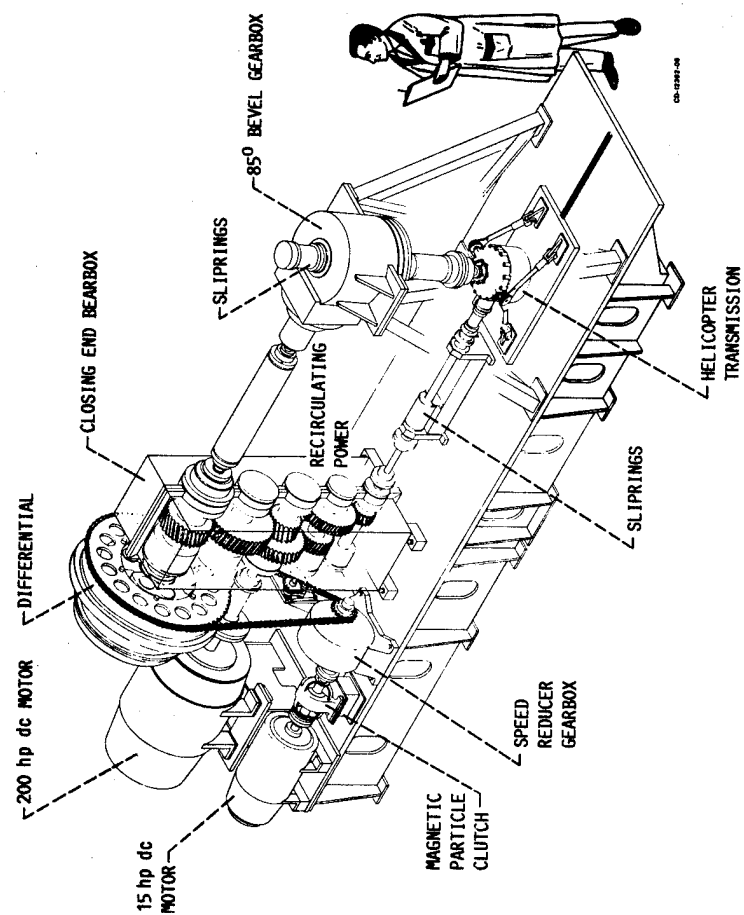


FIGURE 5. - THE NASA LEWIS 500 hp HELICOPTER TRANSMISSION TEST STAND.

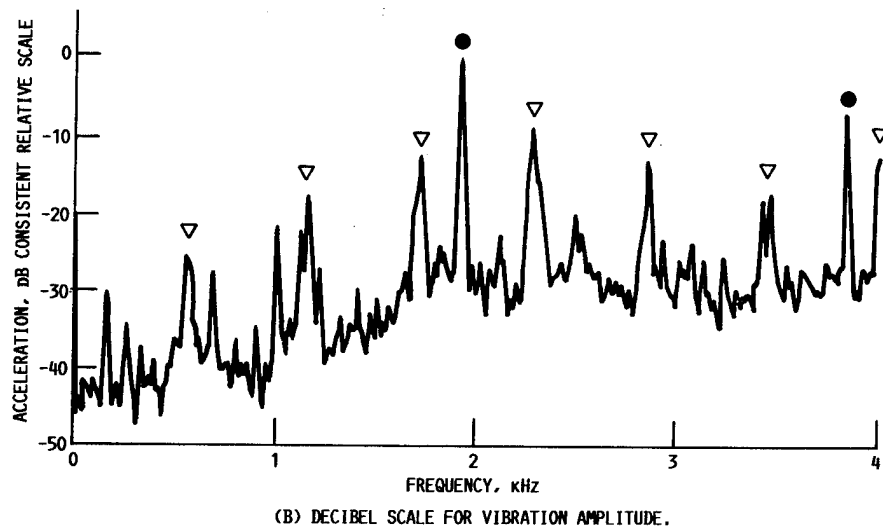
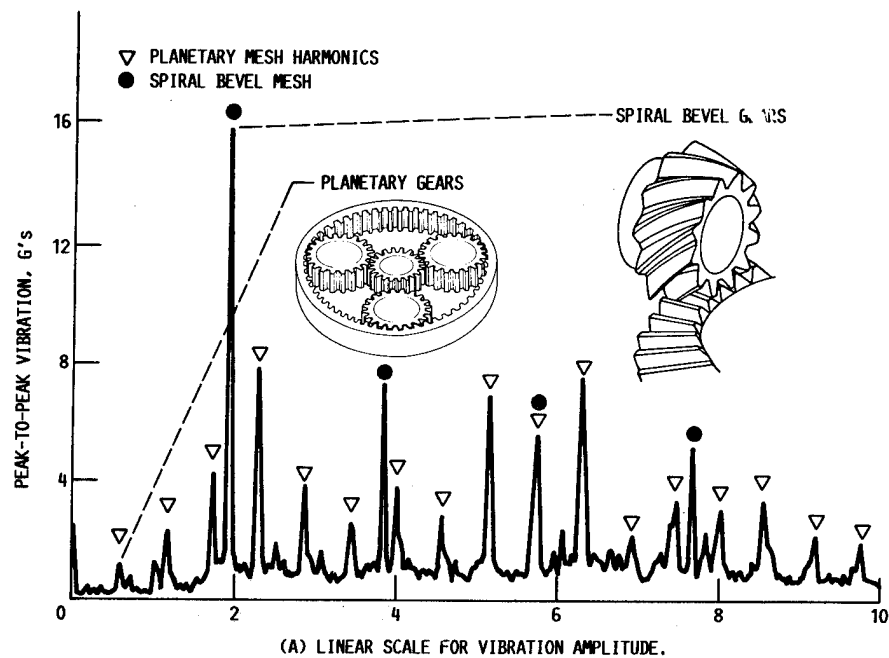


FIGURE 6. - VIBRATION SPECTRUM OF AMPLITUDE VERSUS FREQUENCY AS MEASURED IN NASA TEST STAND. ACCELEROMETER MOUNTED ON CASE NEAR RING GEAR. NOTE THAT VIBRATION ENERGY IS CONCENTRATED AT THE GEAR MESHING FREQUENCIES AND THEIR HIGHER HARMONICS.

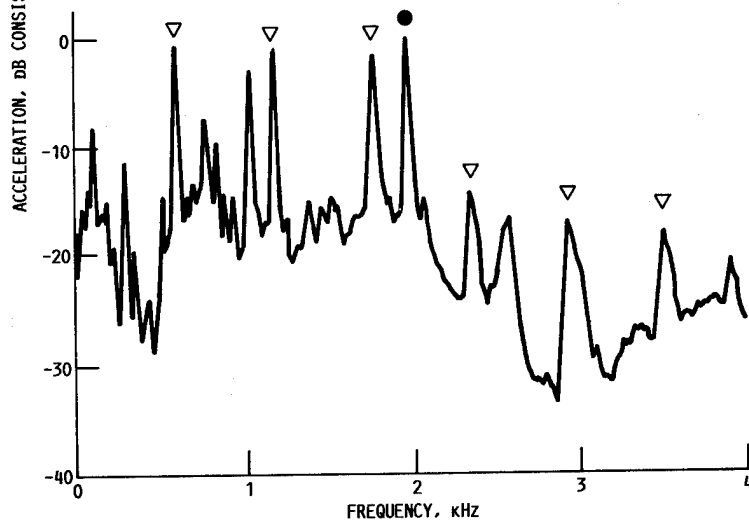
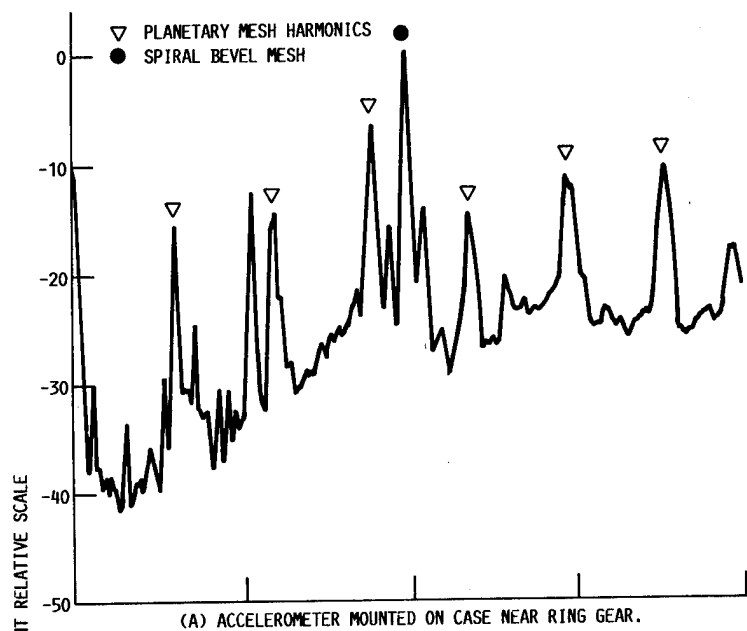


FIGURE 7. - VIBRATION SPECTRUM OF AMPLITUDE VERSUS FREQUENCY AS MEASURED IN FLIGHT. VIBRATION ENERGY IS CONCENTRATED AS A FEW DISCRETE FREQUENCIES AND THEIR HIGHER HARMONICS. NATURE OF THE SPECTRUM IS SIMILAR TO TEST CELL MEASURED DATA.

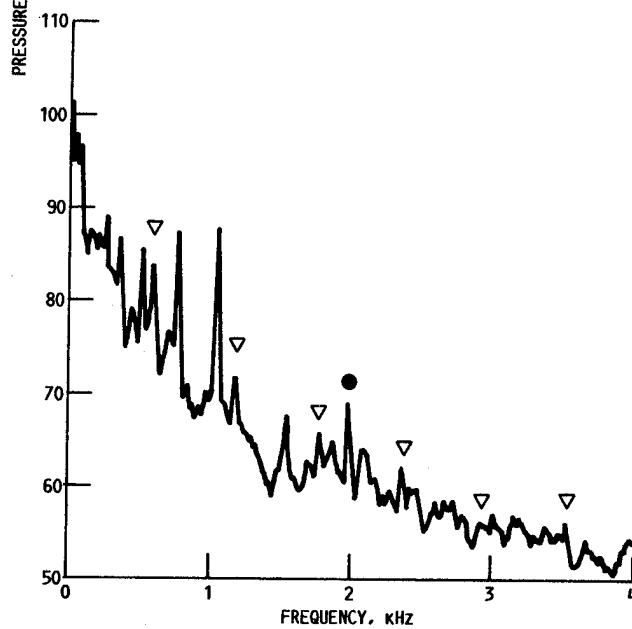
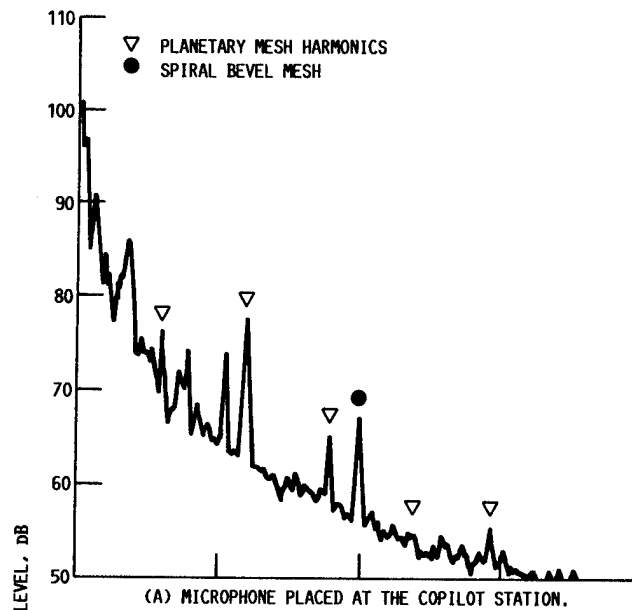


FIGURE 8. - NOISE SPECTRUM OF SOUND PRESSURE LEVEL VERSUS FREQUENCY MEASURED DURING FLIGHT. PEAKS IN THE SPECTRUM HAVE BEEN IDENTIFIED AS TRANSMISSION ORIGINATED. THE HIGHER FREQUENCIES ARE ATTENUATED.

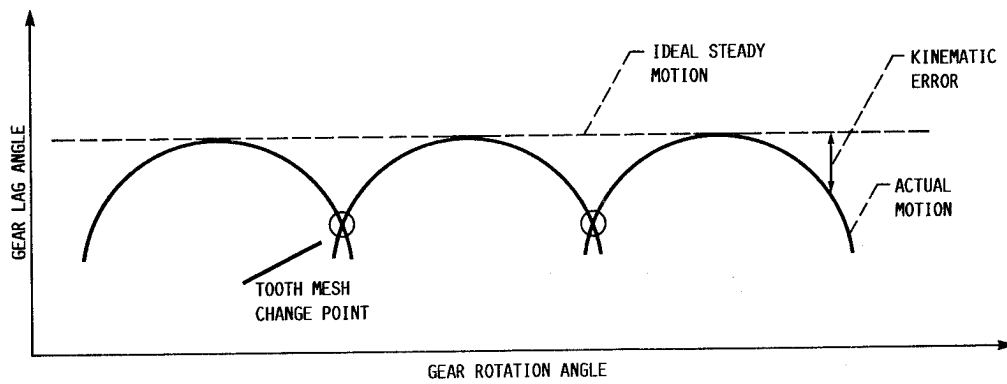


FIGURE 9. - TYPICAL TRANSMISSION ERRORS AS A FUNCTION OF GEAR ROTATIONAL ANGLE.

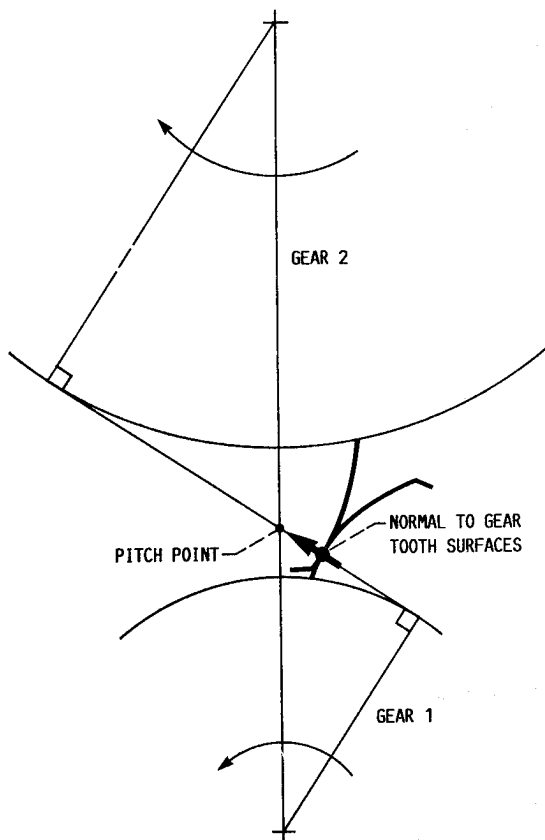


FIGURE 10. - CROSS SECTION OF SPUR GEAR TEETH IN MESH. THE KINEMATIC ERRORS ARE ZERO IF THE NORMAL TO THE TEETH AT THE CONTACT POINT PASSES THROUGH THE PITCH POINT AS THE GEARS ROTATE.

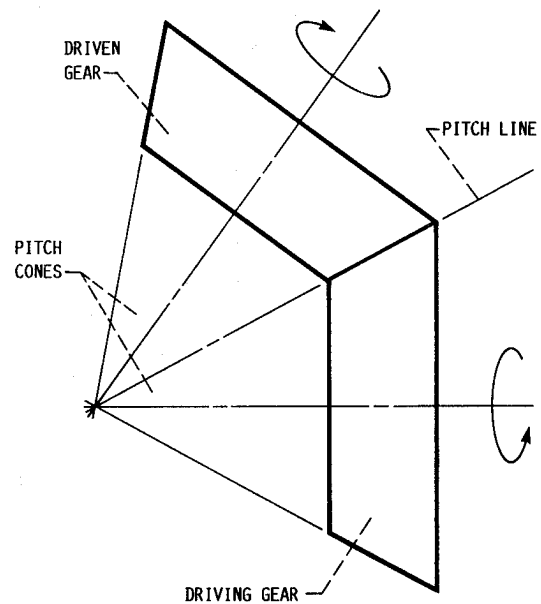


FIGURE 11. - BEVEL GEARS ARE REPRESENTED BY THEIR PITCH CONES IN ROLLING CONTACT. THE PITCH LINE IS THE CORRESPONDENT TO PITCH POINT FOR SPUR GEARS.

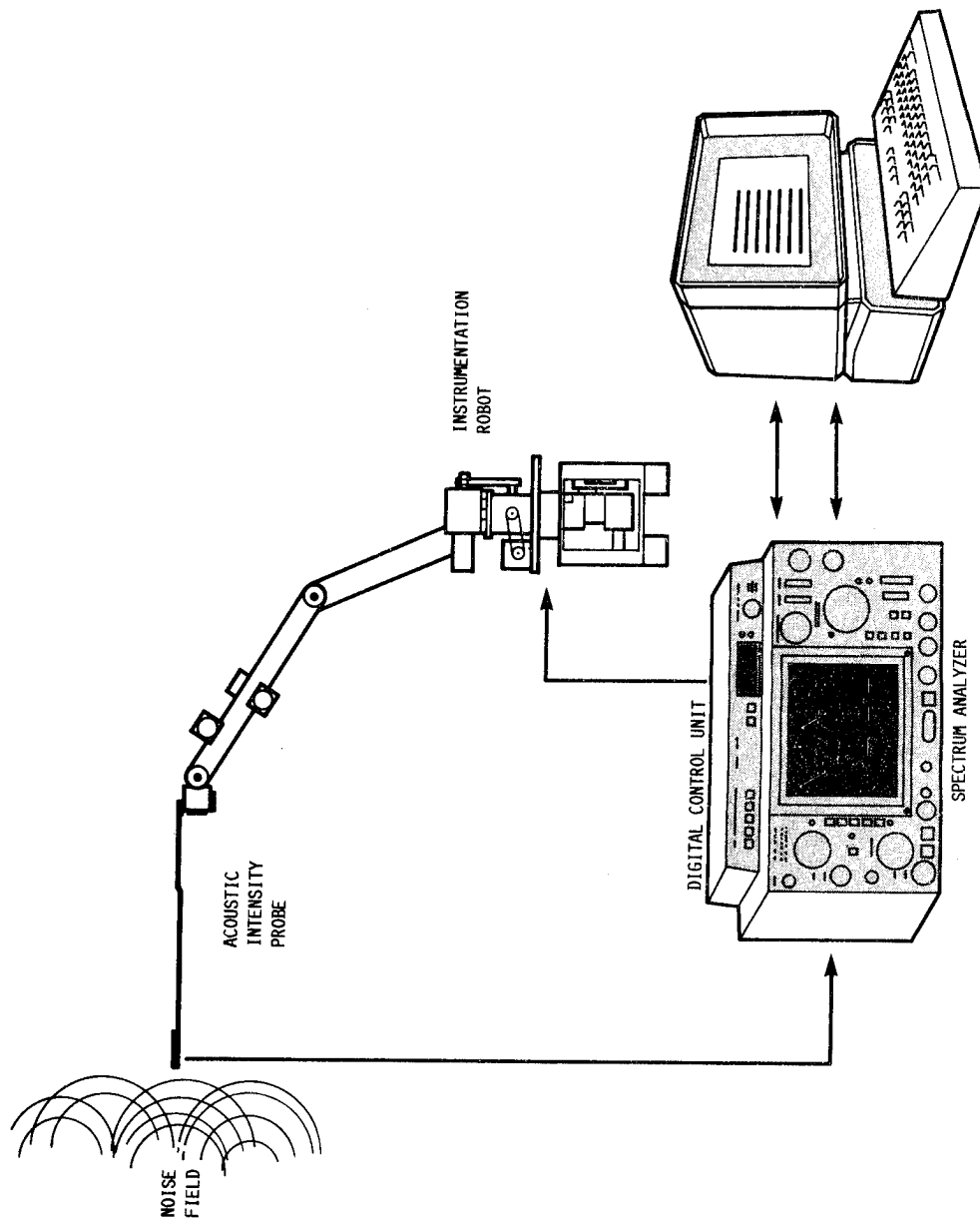


FIGURE 12. - SCHEMATIC OF RAIMS (ROBOTIC ACOUSTIC INTENSITY MEASUREMENT SYSTEM).

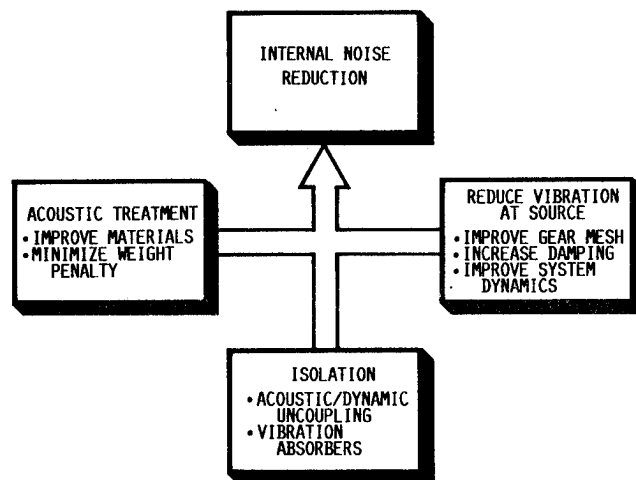


FIGURE 13. - NOISE REDUCTION CAN BE ACHIEVED BY USING ACOUSTIC TREATMENTS, ISOLATION TECHNIQUES, AND REDUCING THE SOURCE. LEWIS WILL CONCENTRATE ON REDUCING THE SOURCE.

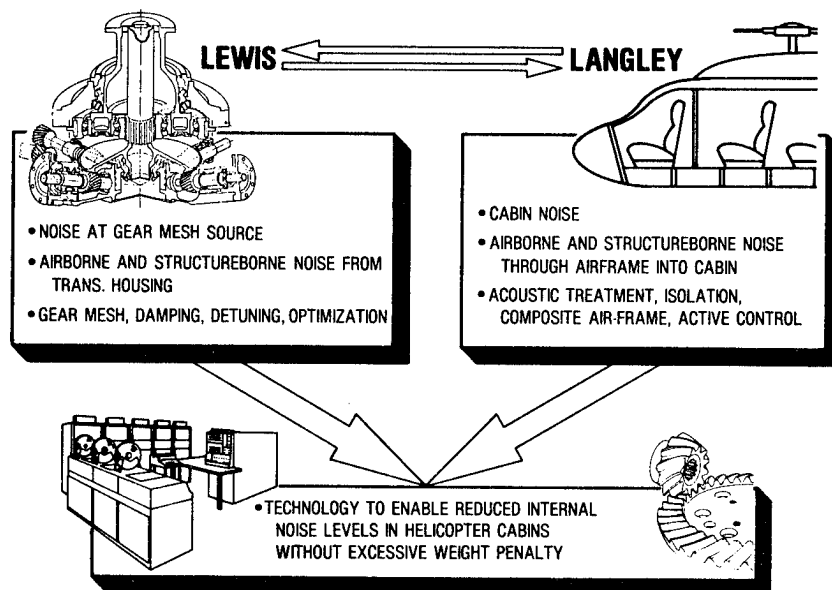


FIGURE 14. - THE ROLE OF LEWIS AND LANGLEY IS TO FOCUS ON THE AREAS OF THEIR EXPERTISE AND COOPERATIVELY PROVIDE ADVANCED TECHNOLOGY TO THE INDUSTRY FOR USE IN EFFECTIVELY REDUCING CABIN NOISE.

A DECADE OF AEROACOUSTIC RESEARCH AT NASA AMES RESEARCH CENTER

F. H. Schmitz, M. Mosher, C. Kitaplioglu, J. Cross, and I. Chang

Ames Research Center

SUMMARY

The rotorcraft aeroacoustic research accomplishments of the past decade at Ames Research Center are reviewed. These include an extensive sequence of flight, ground, and wind-tunnel tests that have utilized unique facilities to guide novel and pioneering theoretical research. Many of these experiments were of benchmark quality. They have been used to isolate the inadequacies of linear theory in high-speed impulsive noise research, have led to the development of new theoretical approaches, and have guided the emerging discipline of computational fluid dynamics to rotorcraft aeroacoustic problems. The results reported here have been achieved by a dedicated team of NASA researchers with, in many cases, the cooperation and assistance of personnel at the co-located Army rotorcraft center.

INTRODUCTION

Within its role of lead center for rotorcraft, NASA Ames Research Center (ARC) has had an active role in rotorcraft aeroacoustic research for the past 10 years. The major contributions have involved and drawn upon an extensive implicit knowledge of the integrated disciplines of the helicopter itself--including rotary-wing aerodynamics, performance, and dynamics. This knowledge, which resides at Ames because of its interdisciplinary rotorcraft research programs, has had a profound influence on rotorcraft acoustics. Significant advances have been made in theory development as well as in the utilization and development of unique acoustic testing techniques. In many cases, NASA researchers have worked with researchers of the Aeroflightdynamics Directorate, U.S. Army Research and Technology Activity, which is co-located at Ames Research Center. In effect, this close working arrangement substantially augmented the net effort in acoustic research--helping make it a very productive cooperative effort. The results presented here, were accomplished for the most part by NASA researchers. A companion paper addressing the Army contributions, with NASA support, is also presented at this conference.

Understanding, predicting, and reducing helicopter noise is important to both the civilian and military communities. For civilian operation, noisy helicopters limit the acceptability of their operation in many locations, thus limiting the commercial market for them. For military operations, loud detectable helicopters are easy to locate by even the most unsophisticated enemy. Early research into mechanisms that could produce the loud characteristic noises of helicopters yielded many hypotheses--even some remarkable theoretical approaches that attempted to

quantify different parts of the composite noise picture. Frequency-based methods were most often used to characterize rotor noise, dividing it into two general classes: harmonic and broadband noise sources (ref. 1). Little attention was paid to the phase of the resulting spectral analysis for either source of noise. In effect, noise levels were often compared with measured harmonics to decide if the mechanism being predicted matched the measured data.

Unfortunately, this frequency-domain approach (without phase information) did not lead to a complete understanding of the governing noise mechanisms. In hindsight, it turns out that many different sources of noise can combine to yield what appear to be acceptable theoretical-experimental comparisons of harmonic levels. In a great many cases, a more thorough comparison would have shown that theory and experiment did not really agree if the relative phases of the harmonic noise sources were included in the comparison. This was especially true for "impulsive noise sources"--unquestionably some of the most important sources of rotorcraft noise.

ACOUSTIC FLIGHT AND GROUND TESTING

In 1974, a new method of measuring helicopter noise was conceived (ref. 2) and implemented in a joint program with the Army Aeroflightdynamics Directorate, the Army Aviation Engineering Flight Activity, and ARC. A relatively quiet fixed-wing aircraft (OV-1C) was equipped with a tail-mounted microphone and an on-line data acquisition system to measure and record the in-flight external noise. Conditions known to produce helicopter noise were first established by the quiet fixed-wing aircraft, and the helicopter was then flown, at selected positions relative to it, in a station-keeping mode (fig. 1). Data gathered in this manner yielded the first undistorted picture of many helicopter noise sources. Using a simple plot of acoustic pressure time-histories it was possible to distinctly trace the various noise sources. The absence of ground reflections and Doppler shifts that are inherent in ground-measured data made the quantification of theoretical approaches possible.

This in-flight measurement technique was enhanced by the selection of the Lockheed YO-3A aircraft as the replacement for the OV-1. The YO-3A had been designed for use as a low-altitude observation aircraft during the Vietnam era and was, by design, an extremely quiet aircraft. The initial testing with a YO-3A, provided and supported by the Federal Bureau of Investigation (FBI), involved measuring the radiated noise of both the two UTTAS (YUH-60 and 61) and the two AAH (YAH-63, -64) prototypes during the Army's competitive evaluation. For these series of tests, the YO-3A was outfitted with three microphones and an in-flight data acquisition system. As a result of these early successes, in 1977 ARC acquired its own YO-3A acoustic research aircraft (fig. 2) and dedicated it to the task of measuring the acoustic emissions of low-speed flying vehicles--especially rotorcraft.

Over the past 8 years, ARC has operated this unique facility in a variety of acoustic research programs. These have included in-flight measurements of the new composite "747" main rotor blades for the AH-1 series helicopter, both tapered-tip

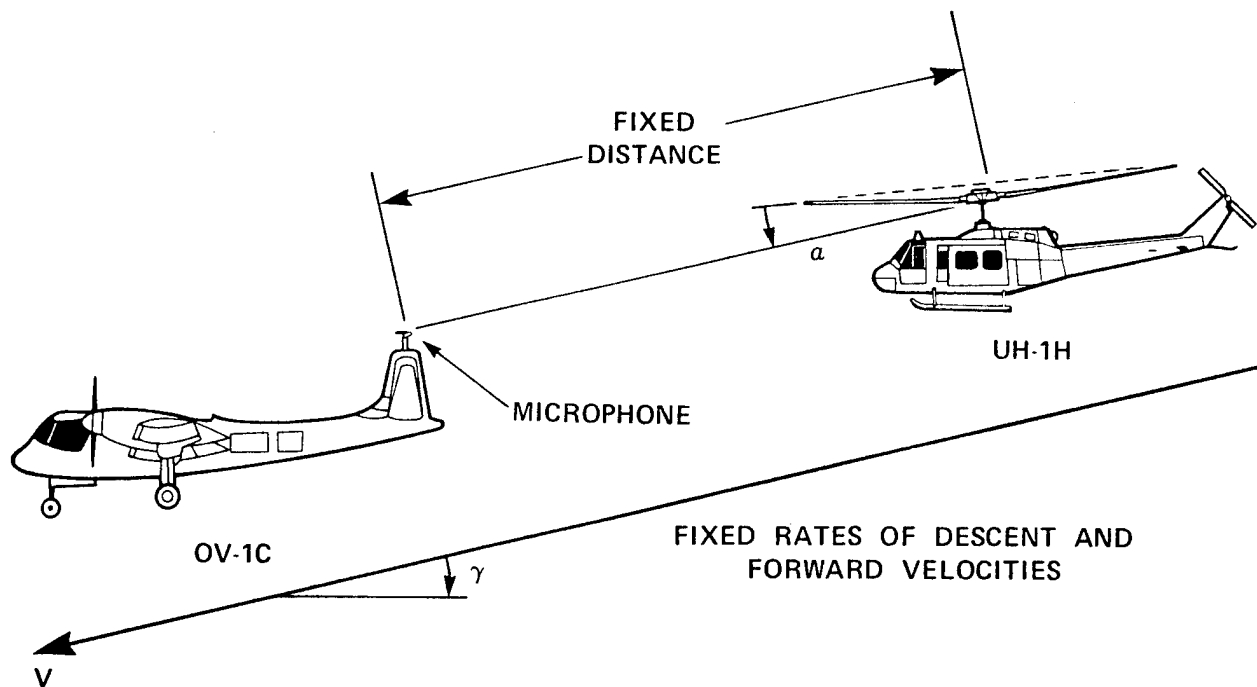


Figure 1.- Schematic of in-flight far-field measurement technique (from ref. 2).

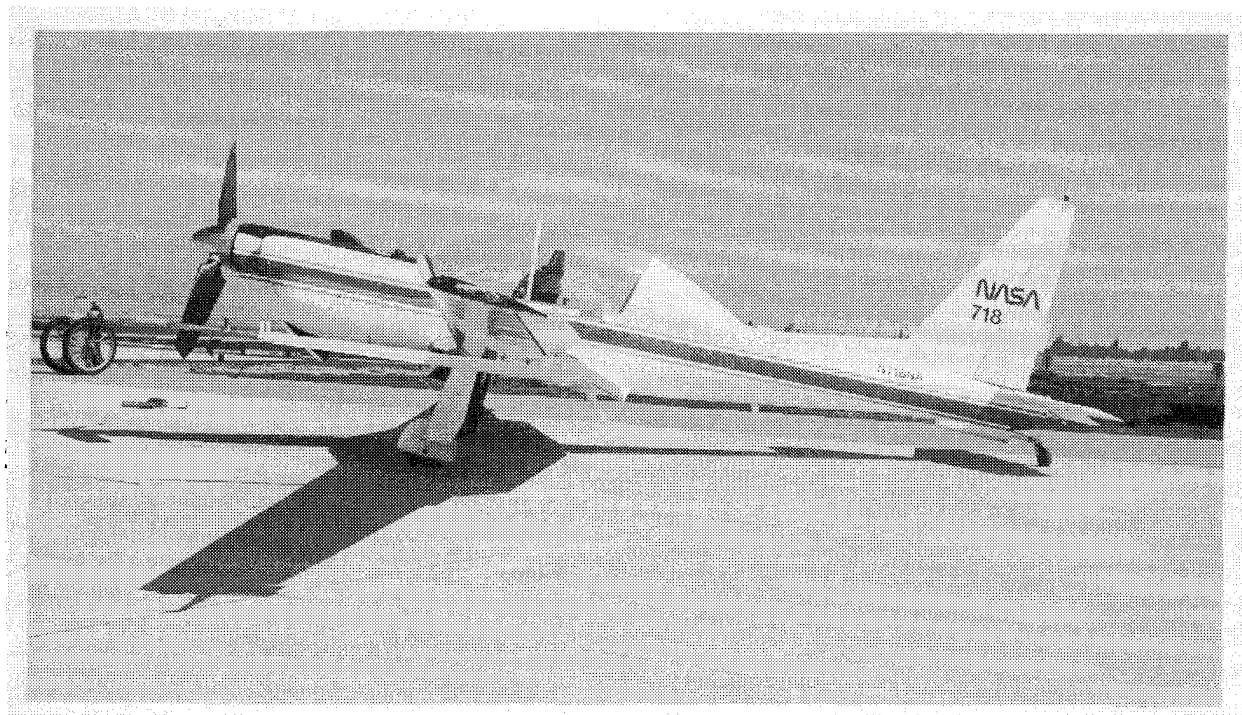


Figure 2.- Ames YO-3A quiet aircraft noise-measurement platform.

(fig. 3) and ogee-tip designs (refs. 3 and 4), 500-D four-bladed and two-bladed tail-rotor measurements, AH-1G pressure instrumented rotor blades (ref. 5), the AH-64 production baseline rotor, and the UH-60 production baseline rotor. In several of these programs, acoustic measurements were also made on ground arrays, using traditional flyover measurement techniques. During the 500-D and AH-1G tests, the flyover testing was done while flying in formation with the YO-3A, thereby completely documenting the emission characteristics of the subject helicopter. These two tests were conducted with assistance from NASA Langley Research Center (LRC), the lead center for acoustic research.

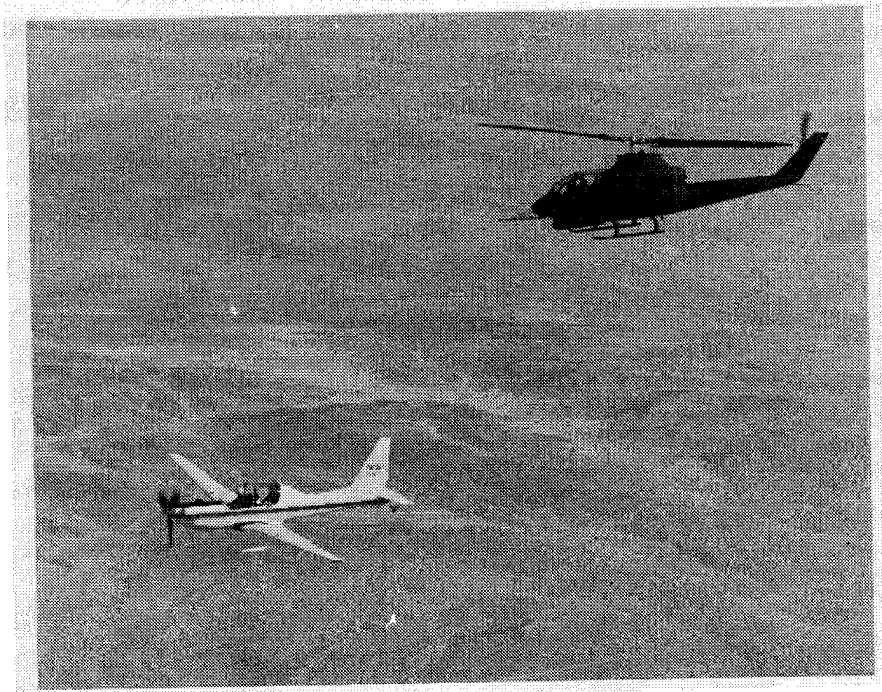


Figure 3.- YO-3A in-flight acoustic measurements of AH-1S helicopter with 747 taper-tipped fiberglass main-rotor blades.

The YO-3A Acoustic Research Aircraft will continue to be a vital facility for future aeroacoustic research programs. To enhance the capabilities of the YO-3A, measurement and station-keeping equipment are currently being upgraded. A helicopter acoustics laser positioning system (HALPS), is designed to give the precise position of the test aircraft relative to the YO-3A, and to measure the test aircraft's azimuth, elevation, and range to the YO-3A. The HALPS displays these values to the flight engineer aboard the YO-3A, and transmits them to the test aircraft, where a glide-slope indicator displays the information for the pilot, allowing him to establish and maintain precise formation flight. The flight-test engineer sets the desired aircraft formation with the use of a hand-held terminal. The accuracy of the system during bench testing has been of the order of ± 1 ft. Although HALPS has yet to be used to acquire flight data, it promises a significant improvement over the current optical ranging system. HALPS offers the additional benefit of having the range data recorded, along with the measured acoustic data, on the on-board tape recorder for use during postflight analysis.

The large number of different types of rotorcraft at Ames has facilitated many static and flyover noise-measurement programs, including the Rotor Systems Research Aircraft (RSRA) and XV-15 Tilt Rotor Research Aircraft. Acoustic measurements over microphone ground arrays and during tie-down tests led to both a near- and a far-field acoustic description of the XV-15 tilt-rotor aircraft (fig. 4). These near-field measurements were instrumental in demonstrating that cabin noise in the XV-15 cockpit was not a serious problem. Acoustic measurements taken at the Outdoor Aerodynamic Research Facility (OARF) have evaluated new higher-performance and lower-noise rotor blades for tilt-rotor aircraft (ref. 6). Some of these experimental findings have enhanced the knowledge base that has been used in the design of the Navy's V-22 Osprey--the world's first operational tilt-rotor aircraft.

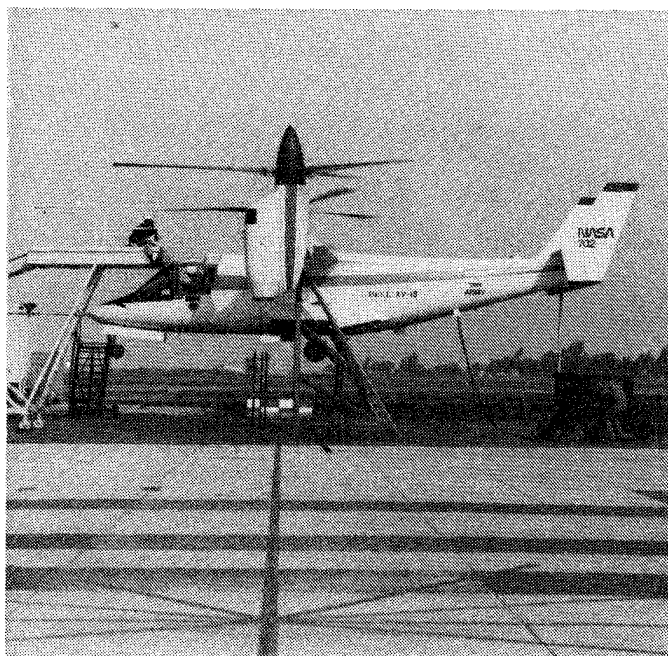


Figure 4.- XV-15 tilt rotor tie-down noise tests.

WIND-TUNNEL ACOUSTIC MEASUREMENTS

The NASA Ames 40- by 80-Foot Wind Tunnel, or 40 x 80, has been the free world's largest low-speed wind tunnel. Before the 1980 upgrade, it had been used to gather important research data, including acoustic measurements on many full-scale rotorcraft systems. Because of the acoustically hard metal walls of the 40 x 80 test section, the acoustic measurements taken before the 1980 wind tunnel modification are not entirely representative of free-field data. The absolute sound levels are noticeably distorted by the reverberant characteristics of the test section. This distortion precludes detailed understanding of the acoustic field; however, comparison of overall noise levels is still possible. These early measurements were important because they were able to show the trends of sound levels with key parametric

changes. They were also used to assess gross noise level differences between new rotorcraft concepts.

One of the first attempts at measuring noise in the 40 x 80 was made in 1967 (ref. 7). A two-bladed Bell UH-1D helicopter was tested, in a standard and in a thin-tipped rotor blade configuration, at advancing-tip Mach numbers of 0.7 through Mach 1.0. Two microphones, which were placed in the test section about 1.1 and 1.4 diam upstream of the rotor, successfully recorded very loud impulsive noise levels at high advancing-tip Mach numbers. Although the absolute levels were contaminated by tunnel-reverberation effects, the noise level trends were basically correct, showing that impulsive noise harmonics increase dramatically with advancing-tip Mach numbers and that thin-tipped rotor blades can substantially reduce high-speed impulsive noise.

In the spring of 1977, the 44-ft-diam Sikorsky S-76 main rotor with four interchangeable tips (rectangular, swept, tapered, and swept-tapered) was tested in the 40 x 80 (refs. 8 and 9). This rotor system, shown in figure 5, mounted in the test section of the 40 x 80 incorporated state-of-the-art aerodynamics and represented Sikorsky Aircraft's design for the executive helicopter commuter market. The test envelope was extensive, spanning tunnel speeds of 30 to 175 knots, advance ratios of 0.075 to 0.4, advancing-tip Mach numbers of 0.64 to 0.97, rotor lift coefficients divided by solidity of 0.0 to 0.14, and rotor shaft angles of -10° to $+10^{\circ}$. Considerable data were acquired for simulated high-speed flight conditions of the S-76 rotor system. Above advancing-tip Mach numbers of 0.9 where transonic phenomena control the amplitude and waveform of the radiated impulsive noise, the swept-tapered (production) tip produced the lowest noise levels. These data showed that



Figure 5.- S-76 main rotor mounted in 40 x 80 tunnel test section.

sweep and taper both help to reduce high-speed noise levels while at the same time improving the high-speed performance of the rotor.

Several entirely new rotorcraft configurations were also tested in the 40 x 80 for aerodynamics, dynamics, and noise. The XV-15 tilt-rotor research aircraft (forerunner of the multi-service V-22 Osprey aircraft) was tested with the rotors operating in a horizontal (helicopter mode) and in the vertical (airplane mode) plane. In the airplane mode (fig. 6) with the rotors operating at reduced cruise rpm, discrete harmonic noise levels were about 15 dB quieter than those measured in the helicopter mode (ref. 10). The higher rotational tip speeds and the unsteady aerodynamics of the rotors in the helicopter configuration were responsible for most of the increased noise levels.

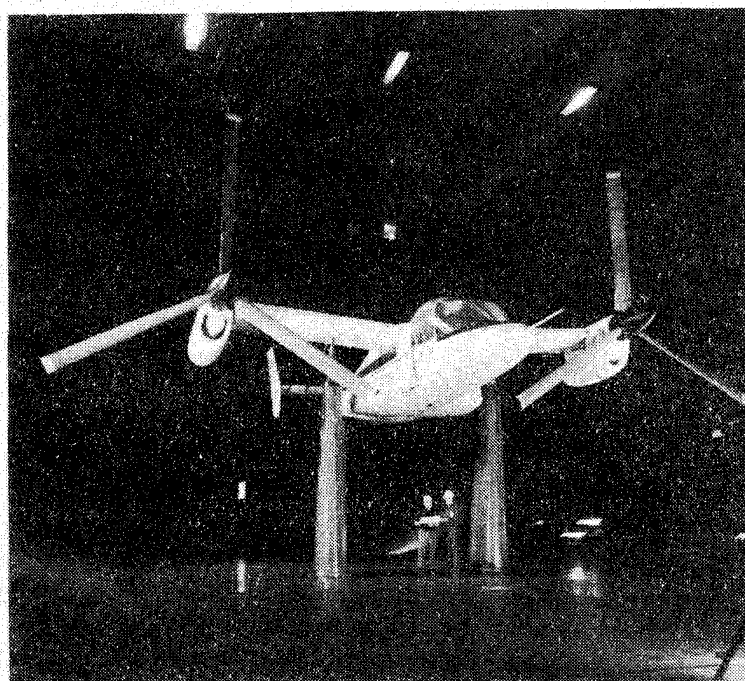


Figure 6.- XV-15 Tilt Rotor Research Aircraft mounted in the propeller mode in the 40 x 80 tunnel.

The use of "blowing" to control the lift of the main rotor was tested in two separate programs. In the summer of 1978, noise was measured on a 44-ft-diam four-bladed main rotor which used circulation control for collective and cyclic lift control (refs. 11-13). Mechanical controls also set the collective pitch of the blades; so collective lift depended on mechanical and pneumatic settings. Noise measurements in the 40 x 80, which were made from hover to 140 knots, showed that sound levels depended more on maximum jet-blowing velocity than on mechanical collective. Sound levels increased with increased blowing velocities. This increase was broadband in character, centered at about 2000 Hz, and believed to be a result of the blowing itself. At 60 knots the noise levels of this rotor were about 15 dB higher than those of a conventional rotor of similar performance, whereas at

140 knots the levels were about 2 dB higher. Blowing was also used successfully in the spring of 1979 to control a 25-ft-diam circulation control, X-Wing rotor as it performed its first transition from helicopter to fixed-wing aircraft in a 40 x 80 tunnel test (fig. 7). The stoppable rotor had a circulation-control symmetrical airfoil with both leading- and trailing-edge slots to control cyclic and some of the collective lift. By carefully controlling the amount of blowing out of the slots, it was possible to transition the rotor to a stopped condition in forward flight while maintaining the lift and controlling moments on the rotor system. The measured sound levels of the rotor depended primarily on the jet-blowing velocity and secondarily on the forward speed. No characteristic impulsive noise was measured in this aircraft in the rotating (helicopter) configuration, although the test matrix included regions where blade-vortex interaction noise is present on conventional rotors. The sound levels, which were quite high at jet-blowing Mach numbers of about 0.7, decreased with either increased or decreased blowing.

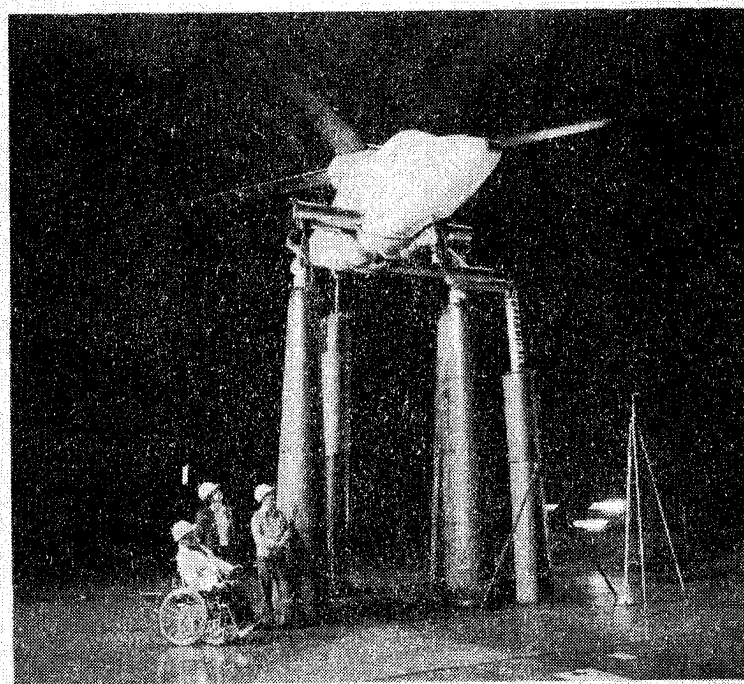


Figure 7.- X-Wing rotor mounted in the 40 x 80 tunnel.

Just before the 40 x 80 tunnel was shut down for extensive modifications and upgrading in the summer of 1980, the advancing-blade concept (ABC) rotor was tested (ref. 14). The ABC demonstrator was a coaxial helicopter with counterrotating rotors that were 36 ft in diameter. The measured rotor sound levels were about 5 dB higher than for a conventional helicopter rotor (i.e., S-76 without a tail rotor) and in general exhibited more impulsive noise--probably because the rotors operate close to a more complex wake pattern. There is some indication that a part of this additional noise could be reduced by altering the lift distribution between rotor systems.

In mid-1980 an extensive upgrade of the 40 x 80 wind tunnel was begun which included re-powering the fan drive unit so the tunnel, in a closed-circuit operation, would reach a top speed of 300 knots and adding a new open-circuit 80- by 120-ft leg for large-scale low-speed testing (top speed approaching 100 knots). A lower maximum drive fan tip speed of 377 ft/sec plus a 6-in. fiberglass acoustic lining for the closed circuit test section were two major acoustic improvements. The 6-in. acoustic liner (fig. 8) was mounted behind a perforated plate to give near-anechoic (without echoes) conditions above 500 Hz in the test section. There was an unfortunate structural failure of the tunnel in 1982, which will delay operational testing until the spring of this year. Preliminary calibration measurements of the flow quality and background-noise levels to date are encouraging (as of February 1987 the tunnel has attained a top speed of 295 knots) and do ensure the 40 x 80 an important role in the rotorcraft acoustic testing world. The 80 x 120 leg of the 40 x 80 also may be useful for acoustic testing. Its enormous test section will be treated with 6 in. of acoustic material on the floor and ceiling and 10 in. on the sidewalls to help reduce the noise radiated to the surrounding community. A significant benefit of this treatment is an improvement in the test section acoustical properties, making it possible to make far-field noise measurements of model-scale and some full-scale rotor systems in the test section.

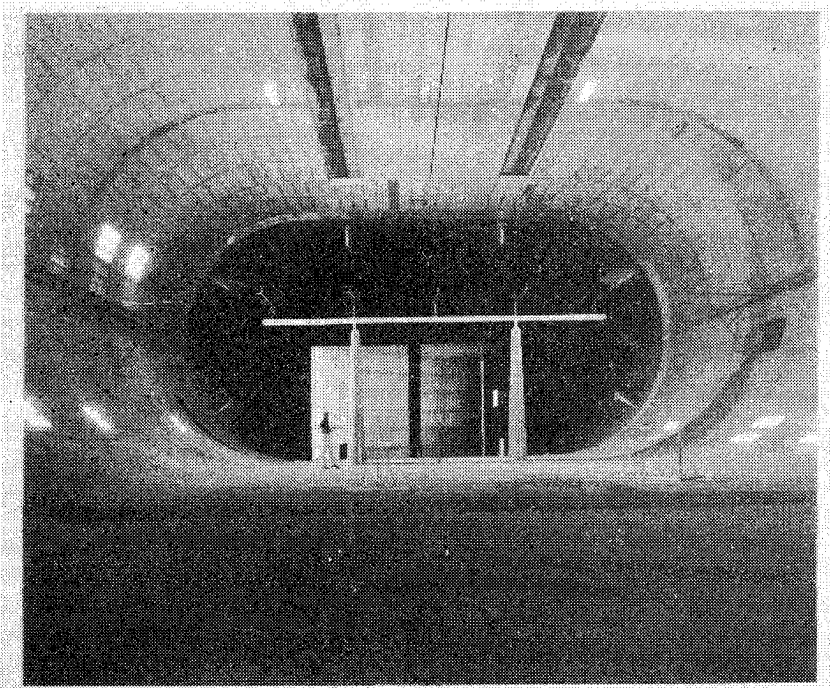


Figure 8.- 40- by 80-ft test section with acoustical liner.

Studies are also under way to investigate whether the size of the 80 x 120 and the low fan-drive noise can be used in a further modification of the 80 x 120 test section to make it the world's largest anechoic wind tunnel (ref. 15). The inherently large size of this modified facility would allow near-anechoic properties at low frequencies and large distances--factors that are important in source-noise reduction for acoustic detection of rotorcraft.

ROTORCRAFT SCALING

Although prediction of a rotorcraft's noise levels from a first-principle approach is the ultimate goal of much of the acoustic research done in the United States, a more immediate practical goal is the use of small-scale model-rotor testing to assess the effect of design changes on the radiated noise. Scale-model testing offers the advantages of easier tunnel access (because of the availability of more wind tunnels which can test small-scale models), and a more anechoic environment (because the scaling raises the frequencies of the rotorcraft noise sources allowing them to be more easily absorbed by acoustic wall treatment). However, it first must be conclusively demonstrated that the model-scale results accurately represent the full-scale acoustic phenomena of interest. To this end, much of the work in industry and at ARC has been to try to quantify how well full-scale acoustic phenomena can be duplicated in model scale. Unfortunately, no really clear general picture has emerged, although the researchers who are involved are still optimistic.

Over the years, small-scale models of rotor systems have been used to assess differences in performance and noise of competing configurations (refs. 16-19). The best results have been obtained when the model test has been run to investigate the effects of geometric changes on a previously isolated noise source, that is, high-speed impulsive noise or blade-vortex interaction noise. It is hoped that the differences in noise levels that were measured in model scale are similar to those that would have been measured on the full-scale rotorcraft. Unfortunately, many of the documented tests showing that these model-scale results do represent full-scale noise levels are not very convincing. If the data were taken in non-anechoic measurement halls, it must be corrected for reverberation effects. Adjustments are made to the measured sound-pressure levels in frequency bands (usually 1/3 octaves) resulting in levels that are corrected to free-field data. The full-scale data, on the other hand, are usually corrected for ground or wall reflections, and wind and temperature effects. It is not unusual to have differences between model and full-scale data in these adjusted levels of about 6 dB (ref. 19). This is not an adequate verification that the rotor noise sources have been faithfully reproduced in model scale. Differences of 6 dB translate into possible aerodynamic source-level differences of 100%.

More definitive scale-model rotor testing is under way. Research performed under contract to Ames by the United Technologies (ref. 20), as well as scale-model testing by Ames researchers (ref. 21), has yielded mixed results. The 1/6-scale model S-76 rotor (fig. 9) did not faithfully match full-scale data. In conditions simulating forward-flight descents typical of a landing approach, sound-pressure differences of up to 10 dB were shown between model- and full-scale wind tunnel data. The 1/20-scale models of reference 20 have shown even poorer correlation with full-scale data.

It is tempting to conclude that model-scale tests do not reproduce full-scale phenomena, but other researchers have shown more promising results (refs. 22 and 23). Under certain operating conditions, high-speed impulsive and blade-vortex

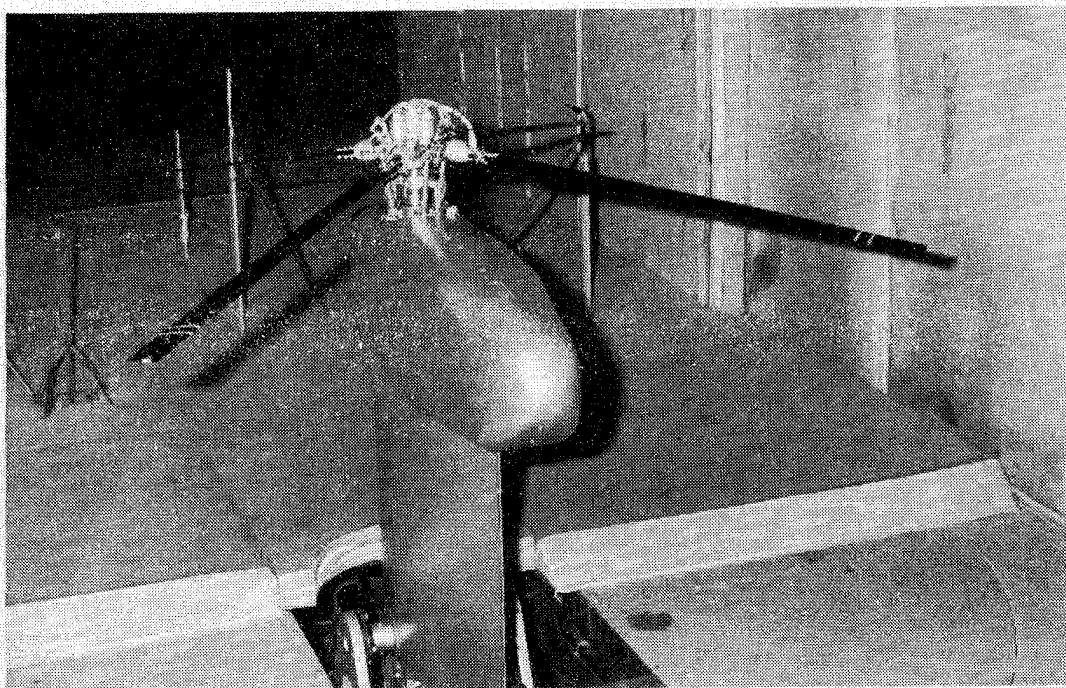


Figure 9.- One-sixth-scale S-76 model rotor mounted in Ames acoustically treated 7- by 10-ft wind tunnel.

interaction noise were reproduced quite faithfully in model scale. Why then are there such mixed results?

Part of the answer may lie in the extreme difficulty of doing carefully controlled model-scale and full-scale acoustic testing. Aside from the corrections for the non-ideal acoustic environment, the operating conditions known to produce much of the terminal-area approach noise, which is due to blade-vortex interaction, are quite sensitive to the separation distances between the rotor blades and the closely passing tip vortices. Thus, it is very important that all model-scale and full-scale trim conditions be matched exactly. The most difficult condition to match is the actual tip-path-plane angle measured with respect to the local velocity vector. This angle is influenced by wind-tunnel wall corrections--something not accounted for in several of the less successful tests reported here. It is probable that a better match between model- and full-scale data is possible. New testing comparing scaled rotors under more controlled and definitive conditions in environments that do not substantially alter the measured sound-pressure levels is currently under way.

THEORETICAL PREDICTIONS

An important goal of the acoustic research efforts of the past 10 years has been to more accurately predict, from first principles, helicopter noise. Ames has

played a key role in this effort by demonstrating the strengths and weaknesses of current theoretical efforts. This has, in many cases, led to new theoretical approaches or methods for predicting the radiated noise.

For several reasons, large, comprehensive, multidisciplinary mathematical models for predicting far-field rotorcraft noise have not been emphasized at Ames. First, very simple controlled experiments of isolated noise sources (refs. 24 and 25) have shown that existing linear theory does not predict the radiated noise to within ± 3 -6 dB. One cannot expect the accuracy of a comprehensive mathematical model to be any better than any of its components. Secondly, the noise radiation field is very sensitive to the aerodynamic flow field surrounding the blade, which is not known to the degree necessary to predict the global acoustic field. The comprehensive aerodynamic-dynamic models that are considered to be state-of-the-art (e.g., C-81, CAMRAD) are known to be inadequate for noise-prediction purposes by themselves. They cannot predict the higher harmonic air-load flow-field environment of the operational helicopter. The aeroacoustic researchers at Ames have chosen a different approach. Emphasis has been placed on developing those theories or models that isolate key aerodynamic and acoustic phenomena that can be verified with simple, straightforward model-scale or full-scale experiments, in flight, in static tests, or in wind tunnels.

One of the first efforts in this regard was that of Arndt and Borgman (ref. 26). Using measured acoustic data taken in the 40×80 tunnel of a rotor operating at high tip speed, they showed that the radiated noise could be attributed to the increasing drag rise caused by shock waves on the advancing side of the rotor disk. Because only sound-pressure levels were directly compared in the theory-experiment, the results did look encouraging. If actual time-histories had been compared under these conditions, the comparison would not have been as favorable. This was verified in some of the in-flight measurements that were flown a few years later and discussed earlier in this paper. Nevertheless, these early researchers showed that noise levels grew tremendously as the rotor's advancing-tip Mach number approached 1--an experimental observation noted in the early 40×80 acoustic testing. However, their theory never could explain why the high-speed impulsive noise levels were not sensitive to thrust variations, a key finding of these earlier experiments.

Another attempt to predict rotorcraft noise was made in 1978 (ref. 27). A simple theoretical linear-thickness monopole model was developed that was used to generate waveforms of the Sikorsky S-76 rotor system in high-speed flight. These calculations were compared with averaged time-domain S-76 data taken in the 40×80 tunnel. Comparison with experiment was generally encouraging because the pulse shapes looked similar to the measured data. However, quantitative comparisons were difficult because of the reverberant environment in the untreated test section in these early tests. Nevertheless, the importance of blade-thickness effects on the radiated noise was clearly shown by these early computations.

The usefulness of using linear acoustic models to describe the radiated acoustic field of helicopter rotors in high-speed flight was called into question by some fundamental high-tip-speed model-scale data (ref. 24). Large discrepancies in level

and pulse shape between theory and experiment were shown by using data from these very controlled fundamental experiments. The discrepancies were tied to transonic aerodynamic effects which are represented as quadrupole source terms in the acoustic analogy formulation (ref. 28). Including these nonlinear terms improved the correlation with experiment in these benchmark hover computations and showed that predicting high-speed impulsive noise was impossible unless the nonlinear effects of the noise generation and radiation process were modeled (ref. 19). Therefore, the acoustic analogy approach was not vigorously pursued for this source of impulsive noise. Instead, computational fluid dynamic (CFD) codes were adopted and expanded to address the high-speed acoustic problem, as well as the transonic aerodynamic problem. In essence, acoustics and aerodynamics were directly linked, implying that further improvements in high-speed far-field noise prediction were dependent on the accurate prediction of the local transonic flow over the blade.

Another significant theoretical development was recently made by Mosher (refs. 30-32). Mosher developed a new, very general method to examine the effects of wind-tunnel walls on discrete frequency noise, such as the low-frequency harmonic noise typical of rotorcraft. The theoretical model consists of an arbitrary, known harmonic acoustic source of finite dimension inside an infinite duct of constant cross-sectional area (representing the tunnel test section) with uniform subsonic flow (see fig. 10). An impedance boundary condition on the duct wall allows the wall to absorb some of the incident acoustic energy. Numerical solutions are found by matching an acoustic panel method in a control volume around the helicopter rotor to a modal series representation of sound in the duct far from the rotor. Because this scheme allows arbitrary duct shapes and arbitrary sources, sound in a complicated system may be analyzed.

Some representative results from this new theory are shown in figure 11 for a horizontal plane that is 0.4 of a radius below the rotor. Contour levels of the fundamental rotor harmonic peak amplitudes are modified by the test section of the wind tunnel at these very low frequencies. Very close to the rotor, the sound field

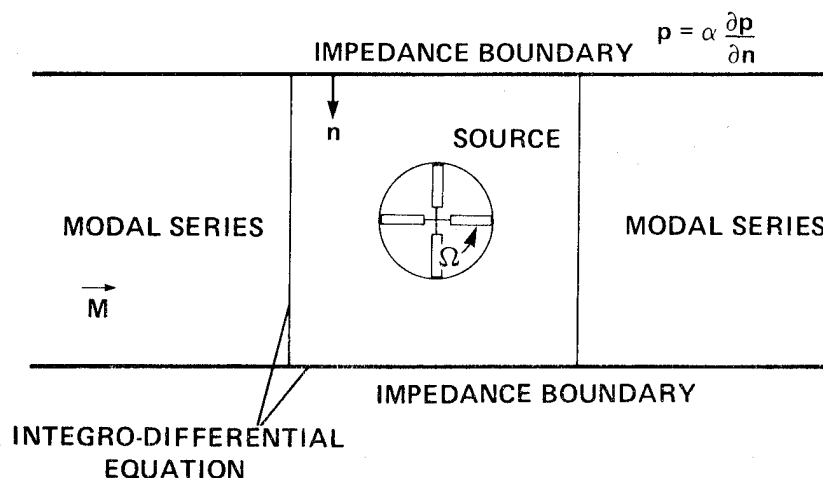


Figure 10.- Computational model of a rotor in a wind tunnel.

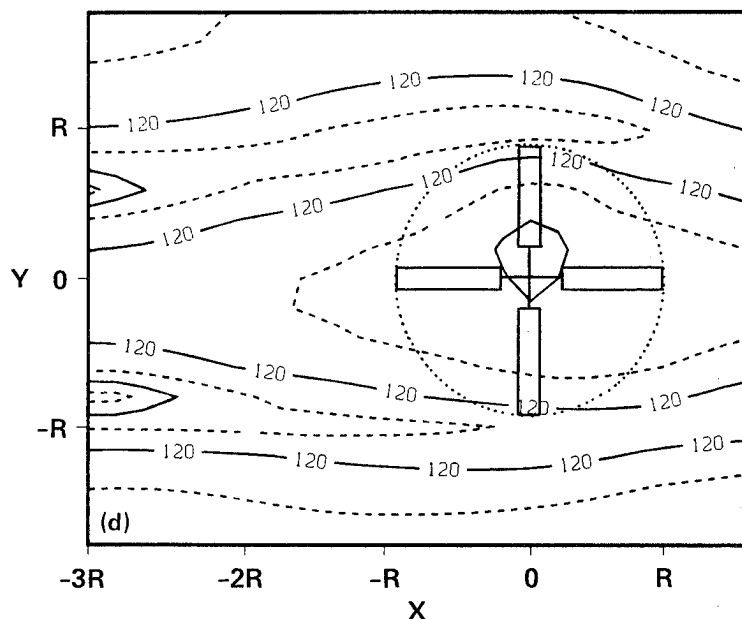


Figure 11.- Representative results: contours of sound-pressure levels in a horizontal plane $0.4 R$ below the rotor plane.

in the wind tunnel resembles the sound field in unbounded space. However, at distances required for mid- to far-field noise measurements, the sound field has characteristics that are predominantly determined by modal propagation in the duct. Wind-tunnel test-section wall acoustic characteristics and the relative size of the rotor disk in relation to the test-section dimensions determine how far from the rotor useful acoustic measurements can be made that closely match free-field conditions. The reverberation problem is most severe at the lower blade passage frequencies where it is very difficult to have good tunnel-wall absorption.

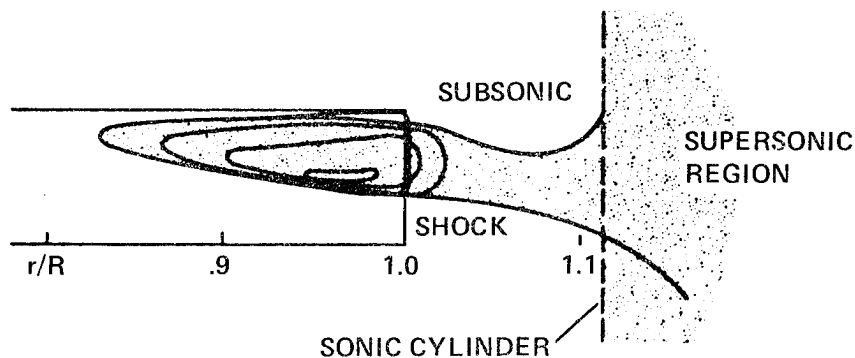
The implications of this work are significant. Once the theoretical model has been verified experimentally, it can be used to pick measurement positions in existing wind tunnels to minimize duct wall effects, to determine how to acoustically treat existing wind tunnels to measure rotorcraft noise in a specific frequency range, and to help modify existing wind tunnels to enhance their measurement properties. The method is computationally efficient at low frequencies--where the reverberation problem is most severe for all existing wind tunnels.

COMPUTATIONAL FLUID DYNAMICS

Ames has pioneered the application of computational fluid dynamics (CFD) to helicopter aerodynamic and acoustic problems. The close connection between aerodynamics and acoustics as they relate to impulsive noise was first made in some benchmark hover experiments performed by the Army in 1978 (ref. 28). A model-scale UH-1H rotor was tested in an anechoic hover chamber while far-field acoustics and local

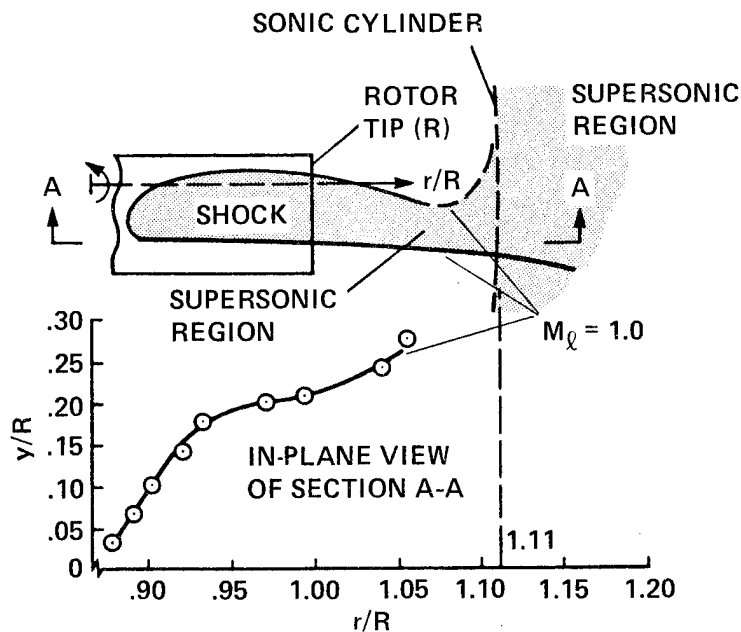
blade-flow measurements were made simultaneously. At hover tip Mach numbers approaching 0.9, local shock waves, which first appeared at lower subsonic tip Mach numbers at about 90% radius, "delocalized" to the acoustic far-field. In effect, localized nonlinear aerodynamic effects were directly propagated to the acoustic far-field--helping explain why linear acoustic analogies could not adequately predict the rotor's acoustic radiation. It was shown (ref. 29) that the criterion for acoustic "delocalization" was the local flow Mach number, as viewed by an observer in a coordinate system rotating with the blade, must be equal to or greater than 1 in the continuous region from just in-board of the rotor tip to the microphone located in the acoustic far-field.

The Army and ARC already had significant CFD efforts under way to predict the potential flow field of high-speed rotorcraft (refs. 33 and 34). These efforts were modified to predict the entire flow field in the vicinity of the rotor to estimate regions where delocalization might occur. A first attempt at predicting this phenomenon was reported in reference 35 and is shown in figure 12(a). Experimental measurements of the same rotor (fig. 12(b)) show that these CFD methods predict the transonic acoustic field quite well (ref. 28). These particular computations were done by Bell Helicopter using the NASA Ames ROT-22 full-potential quasi-steady code. This same code has been used extensively at Bell, with NASA assistance, to help in the design of new tip shapes to avoid the loud impulsive noise associated with the delocalization phenomenon. In the past 4 years, new full-potential and Euler finite difference codes have been integrated with integral rotor-wake models to predict the full, unsteady, high-speed aerodynamic and acoustic near-fields (refs. 36-38). A comparison of the full-potential code results with local blade-surface pressures for a nonlifting rotor operation at high advance ratios and at high advancing-tip Mach numbers is shown in figure 13 (ref. 36). The good agreement between the unsteady computations and experimental pressure distribution measurements are typical of both full-potential and Euler codes for the nonlifting rotor. Shock positions and strength are predicted quite well on the rotor's advancing side. The importance of using unsteady computational results can also be seen in the same figure. The quasi-steady results (dotted curves) do not predict shock locations well at angles other than 90°.



(a) Theory.

Figure 12.- Theory-experiment comparison of delocalization of shock waves to the acoustic far field of a hovering rotor.



(b) Experiment

Figure 12.- Concluded.

A similar comparison for the lifting rotor is shown in figure 14 for the high advancing-tip Mach numbers at high advance ratios. In this case, the rotor's trailed tip-vortex system is modeled in the computational procedure. At these high advance ratios, this wake system is fairly far from the advancing rotor. Under this condition, agreement between the full-potential (ref. 37) and experiment (ref. 39) is generally good, as shown. However, at lower advance ratios when the wake system is close to the advancing blade, good agreement between computation and experiment is less likely. Additional work is under way to more accurately model the rotor-wake system in these cases.

It should be noted that because the flow field is highly nonlinear, there is virtually no method of predicting the flow field of a high-speed rotor other than the CFD approach. The introduction of CFD methods to this problem by Ames researchers has provided the helicopter industry with powerful new tools to help design high-speed rotorcraft that are efficient and quiet. An example of the use of CFD in this regard is the aerodynamic and acoustic design of the main rotor blades for the Bell OH-58 advanced helicopter improvement program. Bell engineers, using the ARC developed ROT-22 full-potential code (ref. 34), designed a new OH-58 main rotor that yielded increased high-speed performance and less noise. Local blade section and planform characteristics near the tip of the advancing rotor were carefully chosen to avoid "delocalization," and hence avoid impulsive noise radiation in high-speed flight.

The impulsive noise caused by blade-vortex interaction (BVI) has also been seriously addressed by NASA and the Army using CFD techniques over the past few

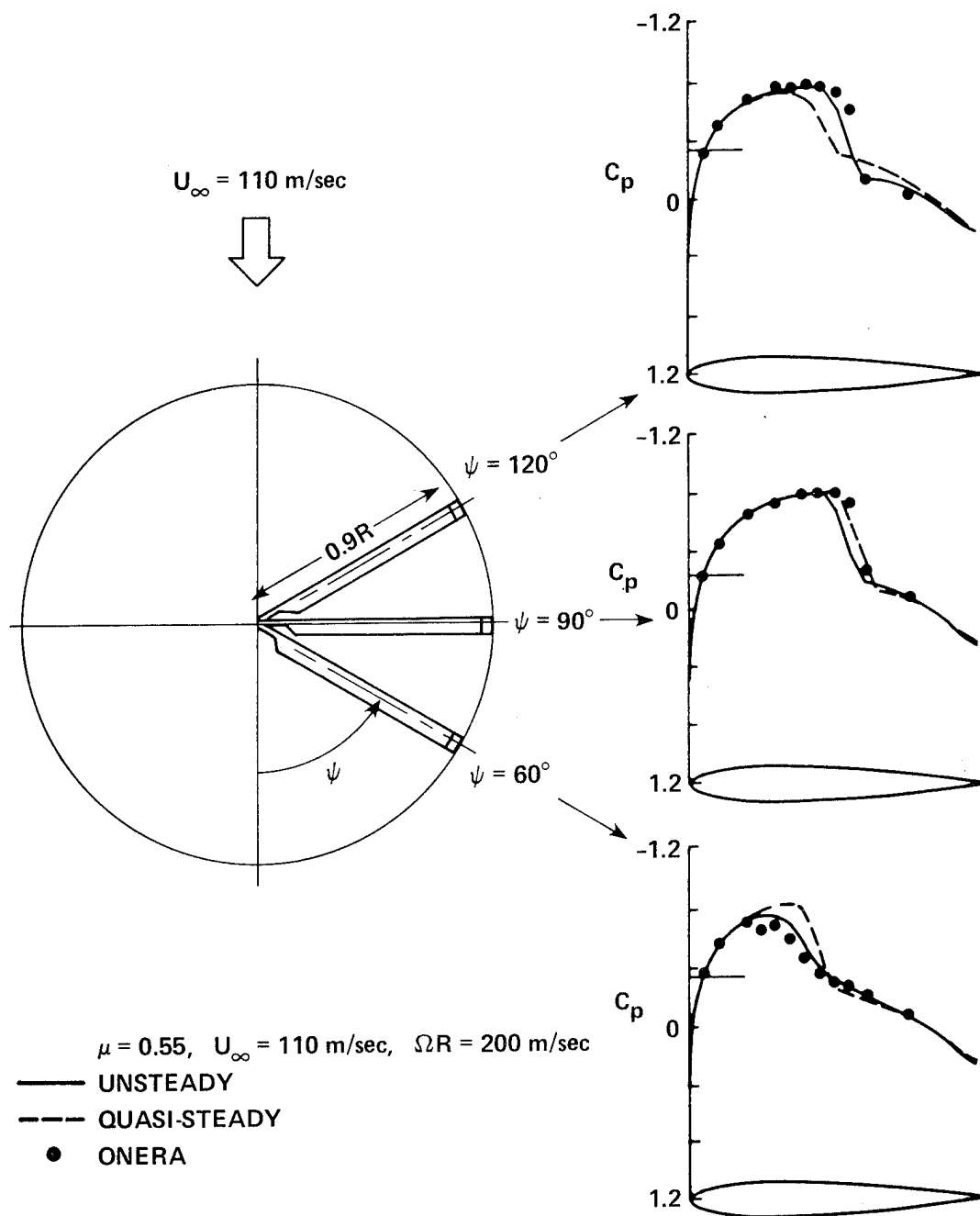


Figure 13.- Comparison of full potential CFD computations with experimental measurements for a high-speed nonlifting rotor in forward flight.

years. Experimental findings have suggested that part of the problem can be represented in two dimensions by considering a two-dimensional blade section interacting with a two-dimensional vortex. The first studies, which utilized an ARC-developed small-perturbation potential code with coarse grids (ref. 40), clearly showed the aerodynamic details of the interaction process near the two-dimensional blade section. However, the acoustic waves that radiated away from the airfoil were weak and

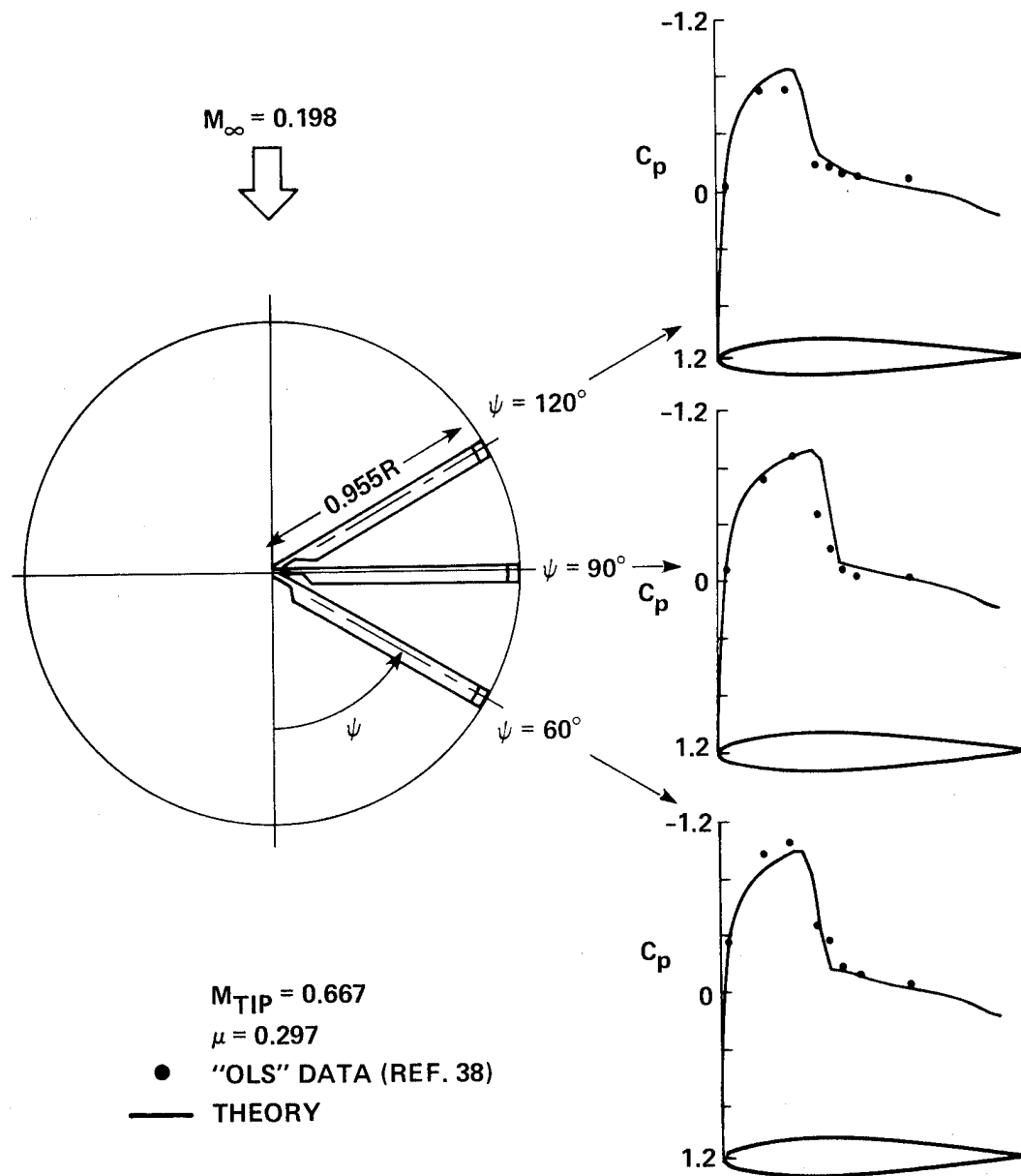


Figure 14.- Comparison of full potential CFD computations with experimental measurements for a high-speed lifting rotor.

were subject to grid-smearing by the CFD process itself. Nevertheless, it was possible to trace acoustic waves radiating to the boundaries of the computation field. Several authors have since pursued this two-dimensional CFD problem with more powerful CFD codes and cleverer ways of looking for radiating acoustic waves (ref. 41). These codes have also been installed on industry computers and used to help design airfoils that reduce the shock-like disturbances that can occur near the leading edge of the airfoil during BVI. Sikorsky Aircraft, using an ARC-developed code (LTRAN2-HI), developed the 1095 RN airfoil to help reduce the impulsive noise that is radiated during blade-vortex interaction (BVI). The airfoil has a specially

designed leading-edge contour that according to CFD computations, reduces the local shock waves during BVI. However, there is still some uncertainty about the effectiveness of these leading-edge design changes in reducing the radiated far-field noise. New theoretical computations and experiments are planned to help ascertain whether these near-field acoustic results are indicative of what happens in the acoustic far-field.

An extremely interesting and complete representation of the two-dimensional BVI problem was recently given by Rai (ref. 42). Using a very high-order CFD scheme on the Cray X-MP computer, he was able to capture the unfolding acoustic radiation problem in great detail (fig. 15). His method used the Navier-Stokes equations and did not describe, a priori, the trajectory or the unfolding structure of the vortex. Instead, the entire unsteady transonic BVI problem was simulated and solved in a very accurate manner. As computers become faster and larger in the next few years, it will be possible to design airfoils and hence complete rotor systems to reduce the noise radiated by rotorcraft.

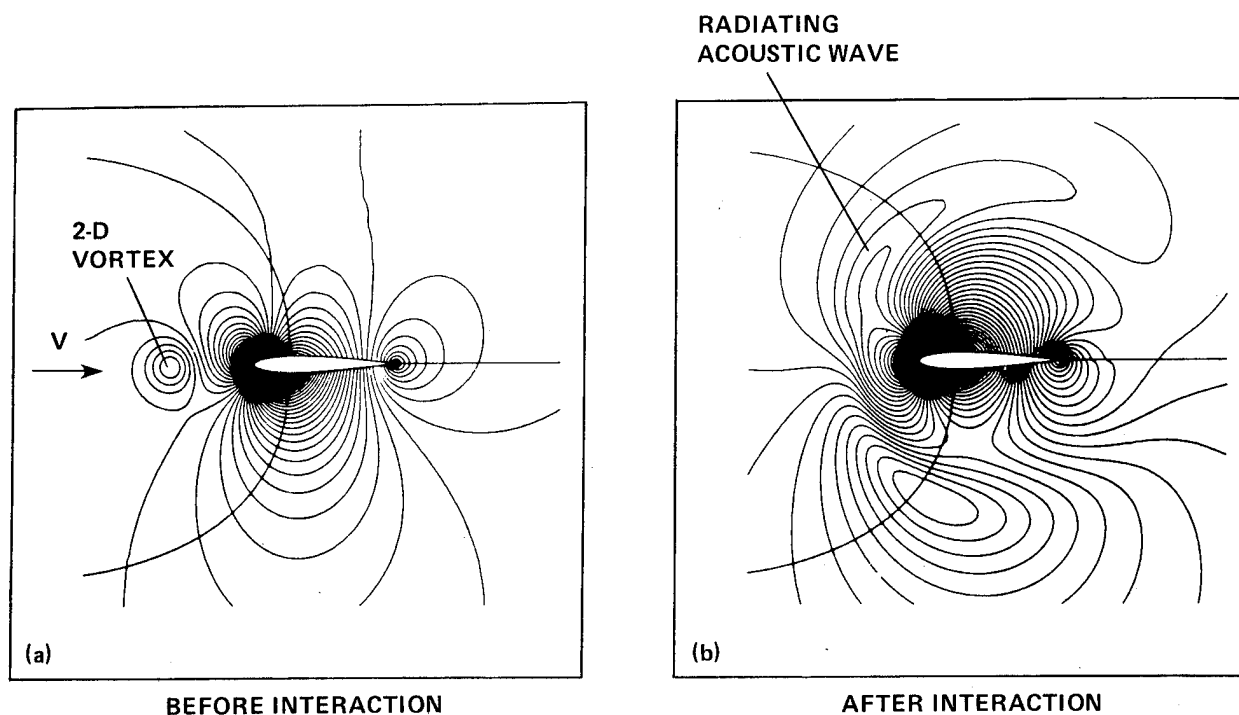


Figure 15.- An acoustic wave radiating from a 2-D airfoil during blade-vortex interaction.

CONCLUDING REMARKS

This paper has reviewed the important rotorcraft aeroacoustic advances that have been made at Ames Research Center over the past decade. On a fundamental research level, there have been some key experimental, as well as theoretical breakthroughs. It is very difficult to clearly separate the advances into two distinct

classes because theory and experiment have been integrated in most rotorcraft programs. Nevertheless, it's probably fair to say that the findings of a few key experiments have helped change the understanding of the important rotorcraft noise-generating mechanisms and have led to the development of new and fruitful theoretical approaches. In particular, the following accomplishments stand out.

1. The development of the YO-3A quiet aircraft as an in-flight acoustic measurement platform. It has been used to measure the radiation characteristics of many research and prototype aircraft.

2. The development of the National Full-Scale Aerodynamics Complex (NFAC) ($40 \times 80 \times 120$), the world's largest aeroacoustic testing facility. The low fan-drive tip speed, the approximately 300-knots forward-speed capability, and the extremely large test sections make the complex unique for rotorcraft aeroacoustic research at model- and full-scale.

3. A new theoretical method for predicting the effect of wind-tunnel walls on the radiation patterns of low-frequency rotorcraft noise. The method will be used to help design appropriate testing techniques and tunnel treatment for low-frequency noise--the most important contributor to rotorcraft signature reduction efforts.

4. The discovery of the causes and the mechanisms of impulsive noise radiation. Through extensive wind-tunnel and flight testing, improved theoretical approaches were developed and verified that more accurately described the impulsive noise phenomena. An important finding of the improved prediction techniques was that it was necessary to compare amplitude and phase (or compare time-histories) of the measured and predicted acoustic radiation.

5. The application of computational fluid dynamics (CFD) to rotorcraft acoustic problems. A new CFD capability has been developed and transferred to United States industry to help solve high-speed and blade-vortex interaction impulsive noise problems.

Besides providing the tools, techniques, and facilities, Ames Research Center has been working with industry to try to reduce rotorcraft noise through design. One notable example of these efforts is the design of the rotor blades for the Bell OH-58 advanced helicopter improvement program. Knowledge of the delocalization mechanism, together with a direct application of CFD to the high-speed acoustic problem, led to rotor tips that were designed for increased performance and reduced noise. Another example of the application of this new technology is the design of the SC-1095 RN airfoil. Working with a CFD code that was developed at Ames, and using the knowledge acquired in fundamental research programs, Sikorsky Aircraft engineers have developed an airfoil section that promises to reduce rotorcraft blade-vortex interaction noise. Experimental efforts are now planned to verify the theory in a full-scale aeroacoustic test in the 40×80 tunnel.

Many of these results have been transferred to industry through the normal publication process and through cooperative and contracted programs with other government agencies and industry. Of particular significance in this regard is the

excellent cooperative research efforts that have existed between the U.S. Army Aeroflightdynamics Directorate and ARC. In some of the Ames research accomplishments it is very difficult to sort out the contributions of the Army and Ames scientists. Also of note is the positive role that the NASA/AHS/Industry National Rotorcraft Noise Reduction program has had on the level of support for rotorcraft aeroacoustic research within the government and United States industry. This program has funded the engineers who are responsible for applying these advances to the design and operational problems of the rotorcraft industry, thereby expediting the technology transfer from the government research laboratories to industry.

Acknowledgments

The authors would like to acknowledge the contributions of many other NASA researchers at Ames Research Center who have added to the knowledge of rotorcraft acoustics over the past decade. In particular, Dr. Charles Smith, Mr. Paul Soderman, Dr. Albert Lee, Dr. Wayne Johnson, Mr. Mike Tauber, Mr. Jerry Shockey, and Mr. Mike Watts, are to be commended for their efforts.

REFERENCES

1. Lowson, M. V.: Helicopter Noise: Analysis-Prediction and Methods of Reduction. AGARD Report LS-63, 1973.
2. Schmitz, F. H.; and Boxwell, D. A.: In-Flight Far-Field Measurement of Helicopter Impulsive Noise. J. Am. Helicopter Soc., vol. 21, no. 1, 1976, pp. 2-16.
3. Boxwell, D. A.; and Schmitz, F. H.: In-Flight Acoustic Comparison of the 540 and K747 Main Rotors for the AH-1S Helicopter. Appendix, U.S. Army Aviation Engineering Flight Activity Report 77-33, Edwards Air Force Base, Calif., 1979.
4. Boxwell, D. A.; and Schmitz, F. H.: Full-Scale Measurements of Blade-Vortex Interaction Noise. J. Am. Helicopter Soc., vol. 27, no. 4, 1982, pp. 11-27.
5. Cross, J. L.; and Watts, M. E.: Tip Aerodynamics and Acoustics Test--A Report and Data Survey. NAS research report in preparation.
6. Maisel, M.; and Harns, D.: Hover Tests of the XV-15 Tilt Rotor Research Aircraft. AIAA Paper 81-2501, 1981.
7. Cox, C. R.: Full-Scale Helicopter Rotor Noise Measurements in Ames 40- by 80-Foot Wind Tunnel. Technical Data Report 576-099-052, Bell Helicopter Co., Sept. 1967.
8. Lee, A.; and Mosher, M.: A Study of the Noise Radiation for Four Helicopter Rotor Blades. Symposium on Helicopter Acoustics, NASA CP-2052, May 1978.
9. Mosher, M.: Acoustic Measurements of a Full-Scale Rotor with Four Tip Shapes. NASA TM-85878, 1984.
10. Lee, A.; and Mosher, M.: An Acoustical Study of the XV-15 Tilt Rotor Research Aircraft. AIAA Paper 79-0612, Seattle, Wash., 1979.
11. Lee, A.: An Acoustical Study of Circulation Control Rotor. NASA CR-152209, 1979.
12. Mosher, M.: Acoustics of Rotors Utilizing Circulation Control. AIAA J. Aircraft, vol. 20, no. 11, Nov. 1983, pp. 946-952.
13. Mosher, M.: Acoustic Measurements of the X-Wing Rotor. NASA TM-8429, 1983.
14. Peterson, R. L.; and Mosher, M.: Acoustic Measurements of a Full-Scale Coaxial, Hingeless Rotor Helicopter. NASA TM-84349, 1983.

15. Snyder, C. T.; and Presley, L. L.: Current Wind Tunnel Capability and Planned Improvements at NASA Ames Research Center. AIAA Paper 86-0729-CP, West Palm Beach, Fla., 1986.
16. Hubbard, J. E., Jr.; Humbad, N. G.; Bauer, P.; and Harris, W. L.: Parametric Studies of Model Helicopter Rotor Blade Slap at Low Tip Speeds. Report No. 79-1, Fluid Dynamics Research Laboratory, Massachusetts Institute of Technology, Cambridge, Mass., Feb. 1979.
17. Hoad, D. R.: Helicopter Model-Scale Results of Blade-Vortex Interaction Impulsive Noise as Affected by Tip Modification. Paper No. 80-62, National Forum of the American Helicopter Society, Washington, D.C., May 1980.
18. Shenoy, R.: Role of Scale Models in the Design of Low BVI Noise. Presented at the 41st Annual National Forum of the American Helicopter Society, Fort Worth, Tex., May 16, 1985.
19. Sternfield, H.; and Schaeffer, E.: An Investigation of Rotor Harmonic Noise by the Use of Small-Scale Wind Tunnel Models. NASA CR-166,388, 1982.
20. Shenoy, R. K.; Kohlhepp, F. W.; and Leighton, K. P.: Acoustic Characteristics of 1/20-Scale Model Helicopter Rotors. NASA CR-177,355, 1986.
21. Kitaplioglu, C.; and Shinoda, P.: Hover and Forward Flight Acoustics and Performance of a Small-Scale Helicopter Rotor System. Paper No. 98, 11th European Rotorcraft Forum, London, England, Sept. 1985.
22. Schmitz, F. H.; Boxwell, D. A.; Splettstoesser, W. R.; and Schultz, K. J.: Model Rotor High-Speed Impulsive Noise-Full-Scale Comparisons and Parametric Variations. Vertica, vol. 8, no. 4, 1984.
23. Boxwell, D. B.; Schmitz, F. H.; Splettstoesser, W. R.; and Schultz, K. J.: Helicopter Model Rotor Blade Vortex Interaction Impulsive Noise: Scalability and Parametric Variations. J. Am. Helicopter Soc., Jan. 1987.
24. Boxwell, D. A.; Yu, Y. H.; and Schmitz, F. H.: Hovering Impulsive Noise: Some Measured and Calculated Results. NASA CP-2052, 1978. (Also, Vertica, vol. 3, no. 1, 1979.)
25. Farassat, F.; Nystrom, P. A.; and Morris, C. E. K., Jr.: A Comparison of Linear Acoustic Theory with Experimental Noise Data for a Small-Scale Hovering Rotor. AIAA Paper 79-0608, Seattle, Wash., 1979.
26. Arndt, R. E.; and Borgman, D. C.: Noise Radiation from Helicopter Rotors Operating at High Tip Mach Numbers. J. Am. Helicopter Soc., vol. 16, 1971, pp. 36-45.

27. Johnson, W.; and Lee, A.: Comparison of Measured and Calculated Helicopter Rotor Impulsive Noise. NASA TM-78473, 1978.
28. Yu, Y. H.; Caradonna, F. X.; and Schmitz, F. H.: The Influence of the Transonic Flow Field on High-Speed Helicopter Impulsive Noise. Presented at the 4th European Rotorcraft and Powered Lift Aircraft Forum, Sept. 1978.
29. Schmitz, F. H.; and Yu, Y. H.: Transonic Rotor Noise-Theoretical and Experimental Comparisons. Vertica, vol. 5, 1981, pp. 55-74.
30. Mosher, M.: An Outflow Acoustic Boundary Condition for Internal Duct Flows. NASA TM-86798, Feb. 1986.
31. Mosher, M.: The Influence of Wind-Tunnel Walls on Discrete Frequency Noise. Ph.D. Thesis, Stanford University, Stanford, Calif., June 1986.
32. Mosher, M.: Effect of a Wind Tunnel on the Acoustic Field from Various Aeroacoustic Sources. AIAA Paper 86-1897, Seattle, Wash., July 1986.
33. Caradonna, F.; and Isom, M.: Numerical Calculations of Unsteady Transonic Potential Flow over Helicopter Rotor Blades. AIAA J., vol. 14, no. 4, 1976, pp. 482-488.
34. Tauber, M.; and Hicks, R.: Computerized Three-Dimensional Aerodynamic Design of a Lifting Rotor Blade. Proceedings of the 36th Annual National Forum of the American Helicopter Society, Washington, D.C., 1980.
35. Shenoy, K. R.: Semiempirical High-Speed Rotor Noise Prediction Technique. Presented at the 38th Annual National Forum of the American Helicopter Society, 1982.
36. Chang, I.: Transonic Flow Analysis for Rotors, Part 2, Three-Dimensional, Unsteady, Full-Potential Calculation. NASA TP-2375, 1985.
37. Chang, I.; and Tung, C.: Numerical Solution of the Full-Potential Equation for Rotors and Oblique-Wings Using a New Wake Model. AIAA Paper 85-0268, 1985.
38. Chang, I.; and Tung, C.: Euler Solution of the Transonic Flow for a Helicopter Rotor. AIAA Paper 87-0523, Jan. 1987.
39. Boxwell, D. A.; Schmitz, F. H.; Splettstoesser, W. R.; and Schultz, K. J.: Model Helicopter Rotor High-Speed Impulsive Noise: Measured Acoustics and Blade Pressures. NASA TM-85850, 1983.
40. George, A. R.; and Chang, S. B.: Noise Due to Transonic Blade-Vortex Interactions. Presented at the 39th Annual National Forum of the American Helicopter Society, May 1983.

41. Baeder, J.; McCroskey, W.; and Srinivasan, G.: Acoustic Propagation Using Computational Fluid Dynamics. Presented at the 42nd Annual Forum of the American Helicopter Society, June 1986.
42. Rai, M. M.: Navier-Stokes Simulations of Blade-Vortex Interaction Using High-Order Accurate Upwind Schemes. AIAA Paper 87-0543, Jan. 1987.

AEROACOUSTIC RESEARCH PROGRAMS AT THE ARMY AVIATION RESEARCH
AND TECHNOLOGY ACTIVITY

Yung H. Yu,* Fredric H. Schmitz,† and H. Andrew Morse‡
Fluid Mechanics Division
Aeroflightdynamics Directorate
U.S. Army Research and Technology Activity (AVSCOM)
Moffett Field, California

ABSTRACT

The Army rotorcraft aeroacoustic programs are reviewed, highlighting the theoretical and experimental progress made by Army researchers in the physical understanding of helicopter impulsive noise. The two impulsive noise sources addressed over this past decade are high-speed impulsive noise and blade-vortex interaction noise, both of which have had and will continue to have an increasing influence on Army rotorcraft design and operations. The advancements discussed are in the areas of in-flight data acquisition techniques, small-scale-model tests in wind tunnels, holographic interferometry/tomographic techniques, and the expanding capabilities of computational fluid dynamics in rotorcraft acoustic problems. Current theoretical prediction methods are compared with experimental data, and parameters that govern model scaling are established. The very successful cooperative efforts between the Army, NASA, and industry are also addressed.

1. INTRODUCTION

Noise generated by a helicopter has been a difficult scientific problem for many years. It has many different origins, most of which are related to aerodynamic phenomena around rotor blades and the fuselage. Over the past decades, many major analytical and experimental developments were made by the Army research efforts. Some of the most notable are comprehensive acoustic prediction codes for high-speed impulsive noise, an in-flight acoustic measurement technique, and a joint government/industry test program in a world-class anechoic wind tunnel. In many cases these developments led to the discovery of many important rotorcraft acoustic characteristics and aerodynamic phenomena related to impulsive noise. In the

*Division Chief, Fluid Mechanics, Aeroflightdynamics Directorate.

†Currently Division Chief, Full-Scale Aerodynamics Research Division, NASA Ames Research Center.

‡Senior Staff Scientist, Aeroflightdynamics Directorate.

following text, two different impulsive noise-generating mechanisms are reviewed; high-speed impulsive noise and blade-vortex interaction (BVI) noise.

2. HIGH-SPEED IMPULSIVE NOISE

Over the past 10 years, an in-flight method of gathering helicopter impulsive noise data has been developed by the Aeroflightdynamics Directorate (ARTA, AVSCOM) (ref. 1). A quiet, fixed-wing aircraft (OV-1C and later the YO-3A) was instrumented with microphones and flown in formation with the subject helicopter, as shown in figure 1. Because these aircraft are relatively quiet and the impulsive signals are intense, good-quality acoustic data were acquired. The major advantages of gathering data in this manner are (1) there are no ground reflections; (2) there are long and steady data samples; and (3) helicopter flight conditions and directivity profiles are easily explored. From data taken during high-speed level flight, a strong negative pressure peak, called high-speed impulsive noise, is observed and has been shown to be caused by blade thickness and transonic effects. It is at a maximum near the tip-path plane of the rotor and falls off with increasing lateral directivity angles. As a consequence, the pilot cannot identify this large acoustic energy radiation from inside the helicopter. Furthermore, at high tip Mach numbers an extremely sharp positive pressure rise follows this sharp expansion wave, resulting in very intense radiated noise levels which shock indicate that this rapid increase in pressure is associated with a radiating shock wave.

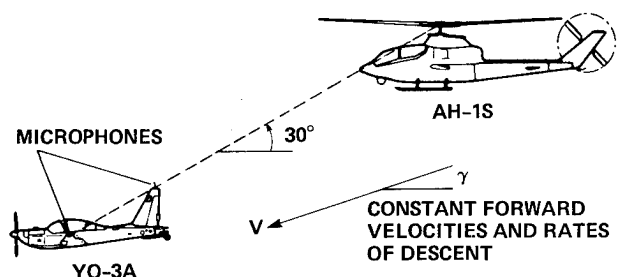


Figure 1.- In-flight technique.

In order to study more closely this interesting phenomenon of a sharp positive acoustic pressure rise observed in a full-scale flight test, both small-scale-model wind tunnel tests and hover tests have been carried out with the following questions in mind:

1. Can high-speed impulsive noise be scaled, and if so, what are the scaling parameters?
2. Can high-speed impulsive noise be scaled in hover (i.e., how important are the unsteady effects)?
3. How accurately can high-speed impulsive noise be predicted? What degree of modeling is required?

4. How does a local shock wave radiate to the acoustic far field?

In order to duplicate the full-scale acoustic phenomena with small-scale models, several wind tunnel tests were carried out in the Ames 7 x 10 ft wind tunnel, CEPRA-19 anechoic wind tunnel, and DNW anechoic wind tunnel. The typical comparison of acoustic data of a 1/7-scaled AH-1/OLS model in the DNW tunnel with AH-1 full-scale flight test data is shown in figure 2. Negative peak pressure levels and waveform shapes are plotted as a function of advancing tip Mach number, which has been proven to be the most important nondimensional parameter of high-speed impulsive noise. (Further comparison of model acoustic data in the DNW and CEPRA-19 wind tunnels with AH-1 full scale flight test data can be found in refs. 2-4.) From the comparisons, it is clear that high-speed impulsive noise can be scaled and that the primary scaling parameters are geometry and the advancing tip Mach number.

The interesting aspect of high-speed helicopter noise is the development of the saw-toothed waveform at high advancing-tip Mach numbers as shown in figure 3. A near-symmetrical pulse is observed in case A ($M_T = 0.867$), while the symmetrical pulse becomes saw-tooth in character (case B, $M_T = 0.9$). This sudden change of the waveform is called delocalization and the corresponding tip Mach number is called the delocalization Mach number. This is a very unique phenomenon peculiar to a rotating blade, which will be discussed further in the later section. At still higher advancing tip Mach numbers (case C, $M_T = 0.925$), the peak negative pressure becomes very large, and the sudden rise in pressure becomes nearly instantaneous. The noise generated by this latter waveform is rich in higher harmonics and can be subjectively classified as harsh and extremely intense. The exact same phenomena were also observed in hover as shown in figure 4 (details in ref. 5). The most remarkable observation about the model-hovering rotor data is their pulse shape similarity to the model-scale acoustic data taken in forward flight. Although the hovering amplitudes are higher than the forward flight amplitudes, the delocalization process is duplicated quite well. This implies that the unsteady aerodynamic effects of forward flight play a secondary role in the delocalization process. The high-speed impulsive noise signatures generated by full- and model-scale forward flight tests can be studied to first order in hover and the scaling parameter is the advancing tip Mach number.

The theoretical analysis is based on the well-known integral equation derived by Ffowcs Williams and Hawkings (ref. 6).

$$4\pi a_0^2 \rho'(\bar{x}, t) = \frac{\partial}{\partial t} \int_S \left[\frac{\rho_0 v_n}{r|1 - M_r|} \right] ds - \frac{\partial}{\partial x_i} \int_S \left[\frac{p_{ij} n_j}{r|1 - M_r|} \right] ds + \frac{\partial^2}{\partial x_i \partial x_j} \int_V \left[\frac{T_{ij}}{r|1 - M_r|} \right] d\bar{V} \quad (1)$$

Far-field acoustic pressure is explicitly expressed in terms of integrals over the blade surface (monopoles and dipoles) and over the surrounding volume (quadrupoles). A comparison between linear thickness calculations, first term in equation (1) versus the experimental data for hover, is shown in figure 5 for several different tip Mach numbers. The striking features of the comparison between theory

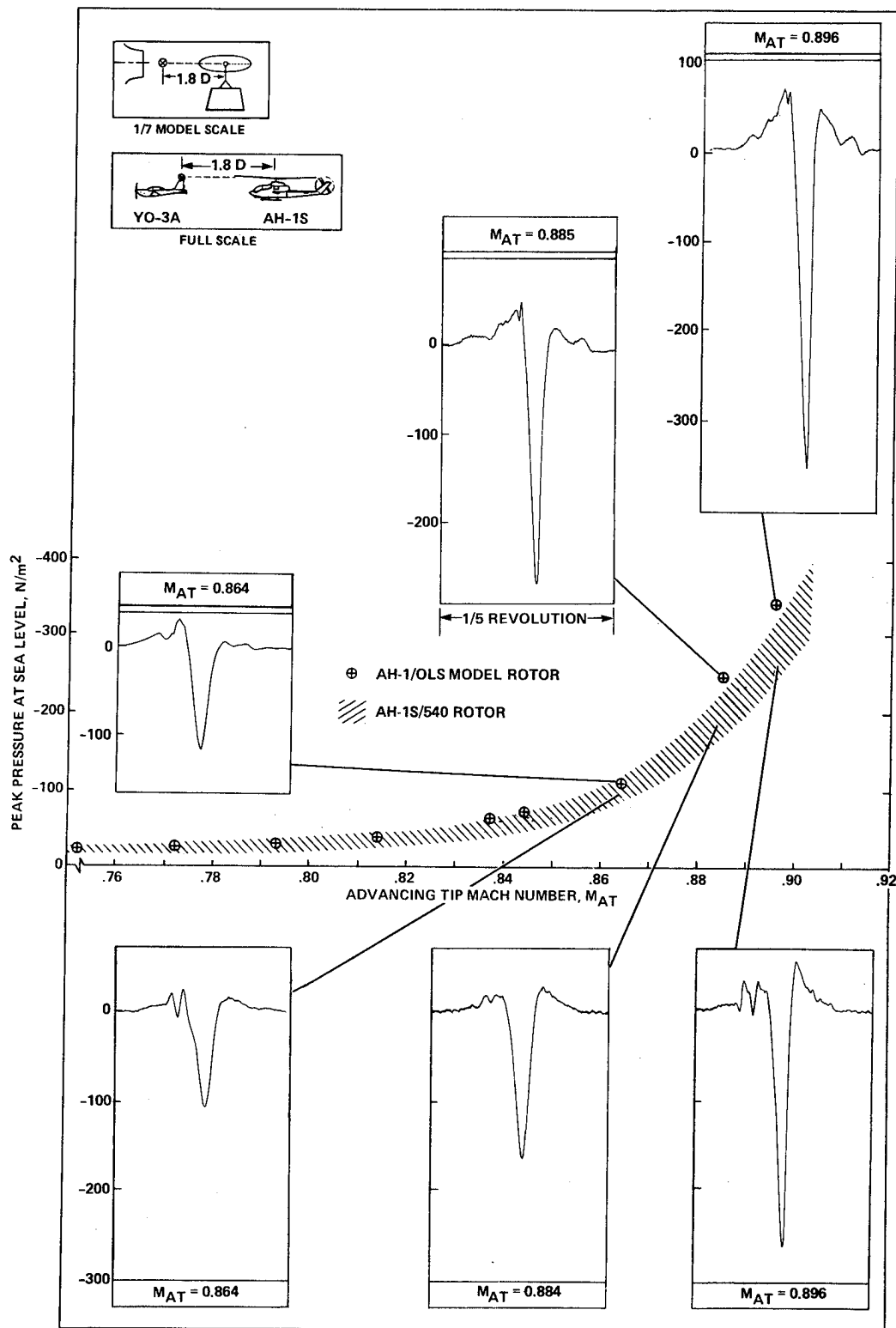


Figure 2.- Comparison of model and full-scale acoustic waveforms for an in-plane microphone 1.8 rotor diameters ahead.

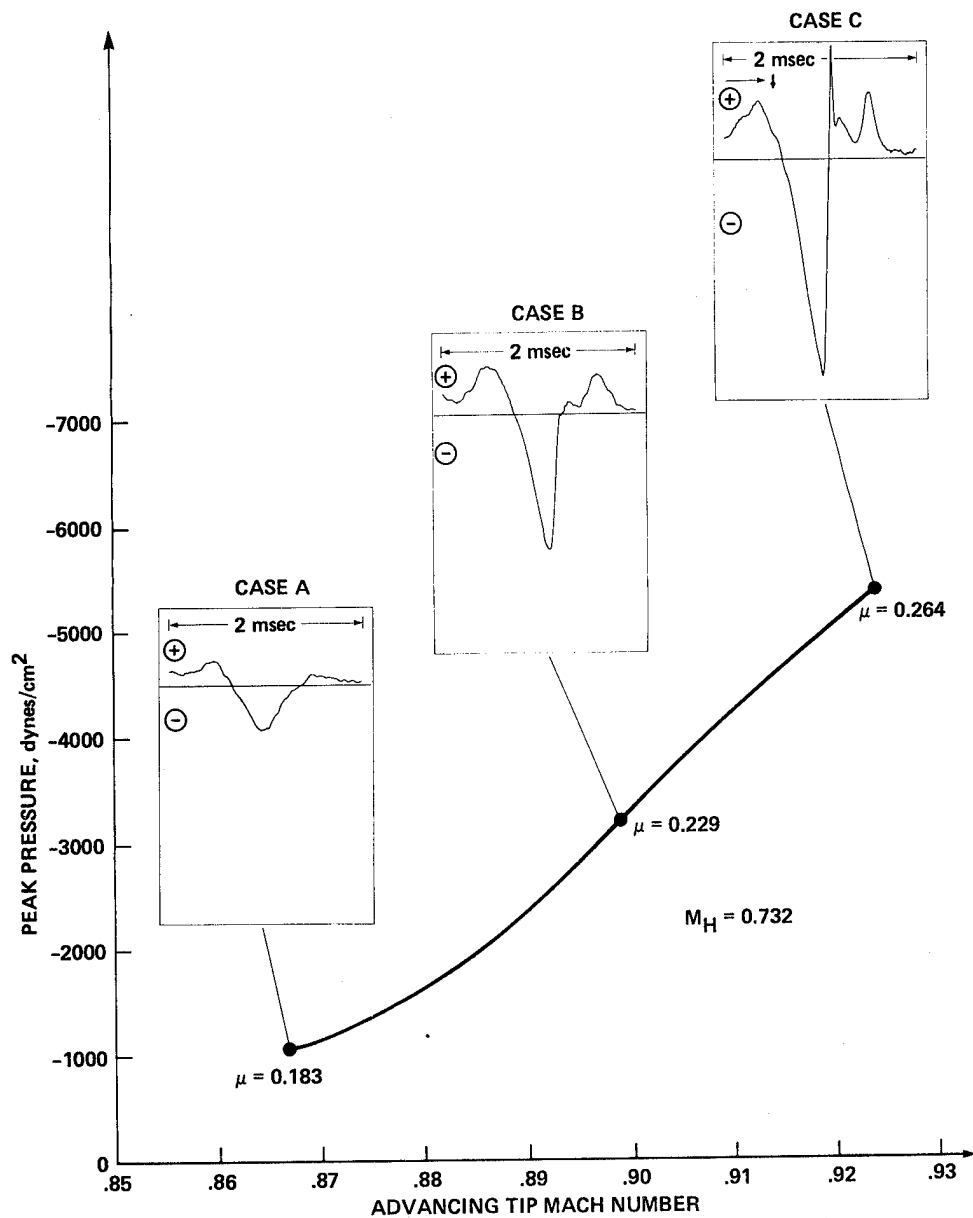


Figure 3.- Waveform shape versus advancing-tip Mach number.

and experiment at the tip Mach number less than 0.9 are the similarity in pulse shape and underprediction of the theory in negative peak levels by a factor of about 2. At hover tip Mach number of 0.9, the amplitude of the peak negative pressure pulse is again underpredicted by a factor of 2, but there is also a dramatic change in the waveform of the experimental data which is not predicted by the linear

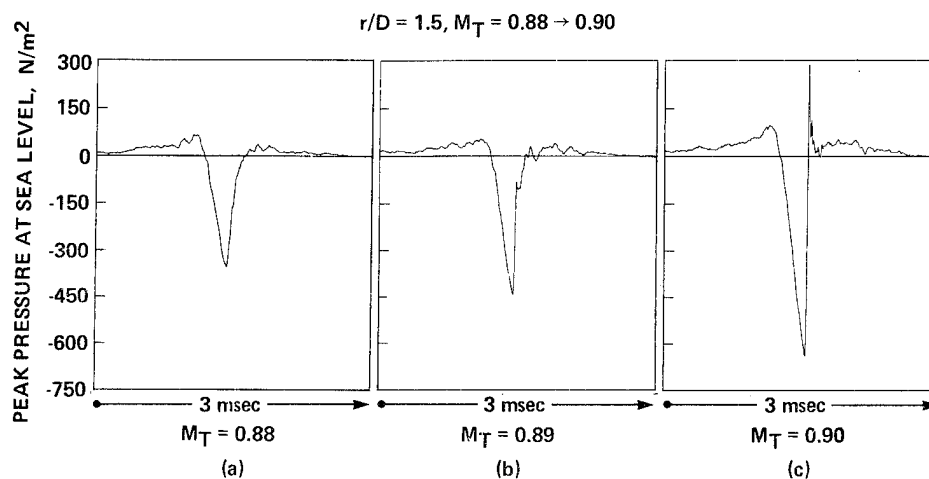


Figure 4.- Waveform transition; the development of a radiating discontinuity, in-plane, $r_H/D = 1.5$, $M_T = 0.90$.

theory.¹ The discrepancy between the linear theory and experimental data can be explained by nonlinear flow phenomena around the blade tip and can be lessened by adding the quadrupoles term of the governing equation. In order to incorporate the near aerodynamic nonlinear flow field into the quadrupole term of the equation, the governing potential equation was transformed (ref. 7) to blade-fixed cylindrical coordinates as follows:

$$\left\{ \omega^2 - \frac{a_0^2}{r^2} - (\gamma + 1) \frac{\omega}{r^2} \phi_\theta \right\} \phi_{\theta\theta} - 2\omega \phi_r \phi_{r\theta} - 2\omega \phi_z \phi_{z\theta} = \{ a_0^2 + (\gamma - 1) \omega \phi_\theta \} \left(\phi_{rr} + \frac{1}{r} \phi_r + \phi_{zz} \right) \quad (2)$$

This transonic equation governs the delocalization phenomenon and also helps explain the influence of the transonic flow field on the acoustic far field signatures. The coefficient of $\phi_{\theta\theta}$ determines the propagation behavior of the local shock depending on its sign. Below the local sonic Mach number, the coefficient becomes a negative sign and the equation (2) behaves like an elliptic-type equation in which no wave-like behavior is possible. In this case, the local shock structure does not propagate into the acoustic far field. However, above a local sonic Mach

¹The remaining linear dipole term [second term in the eq. (1)] was included in reference 8 and the results were almost indistinguishable from those of the monopole calculations. Also, similar conclusions were drawn in reference 9 for a high-speed rotor in forward flight. In addition, most of the experimental data suggested that the high-speed noise phenomenon was not dependent on thrust or torque at a constant Mach number.

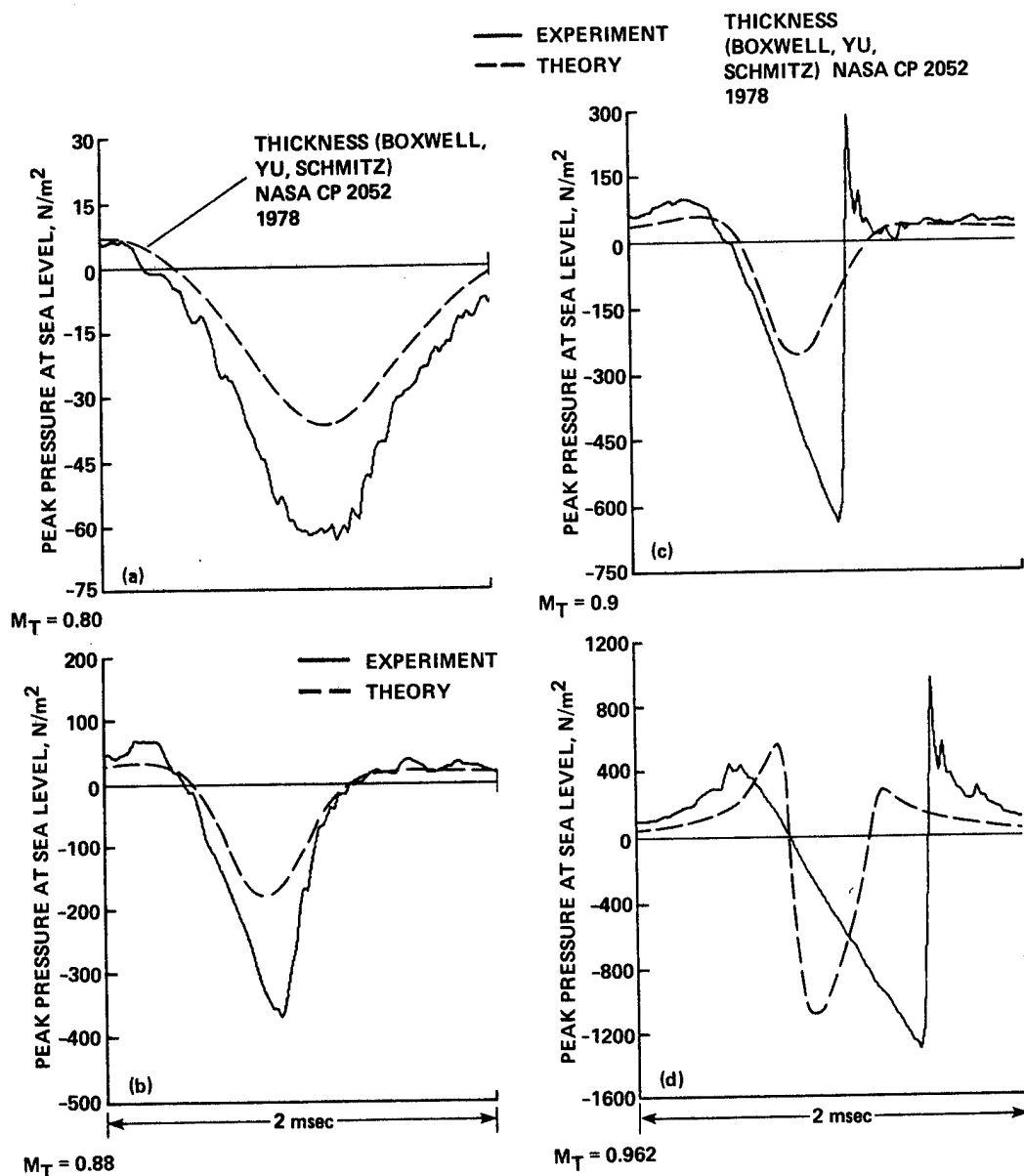


Figure 5.- Comparison of theory with experimental pressure time-history, in-plane, $r_H/D = 1.5$. (a) $M_T = 0.8$; (b) $M_T = 0.88$; (c) $M_T = 0.9$; (d) $M_T = 0.962$.

number, the coefficient becomes positive and equation (2) becomes hyperbolic. Local shock waves then propagate into the acoustic far field without interruption and generate strong shock characteristics in the acoustic signatures. This phenomenon is called the delocalization. Since this delocalization phenomenon is directly related to the acoustic far field, a logical step in the prediction of acoustic field is the incorporation of the near-field aerodynamic nonlinearities into the acoustic formulation. The accuracy of the acoustic far-field calculation is totally dependent on the detailed knowledge of the near-field aerodynamic nonlinearities surrounding the blade. The comparison of acoustic waveform calculations with a three-dimensional transonic numerical code (ref. 10) against the experimental data is shown in figure 6.

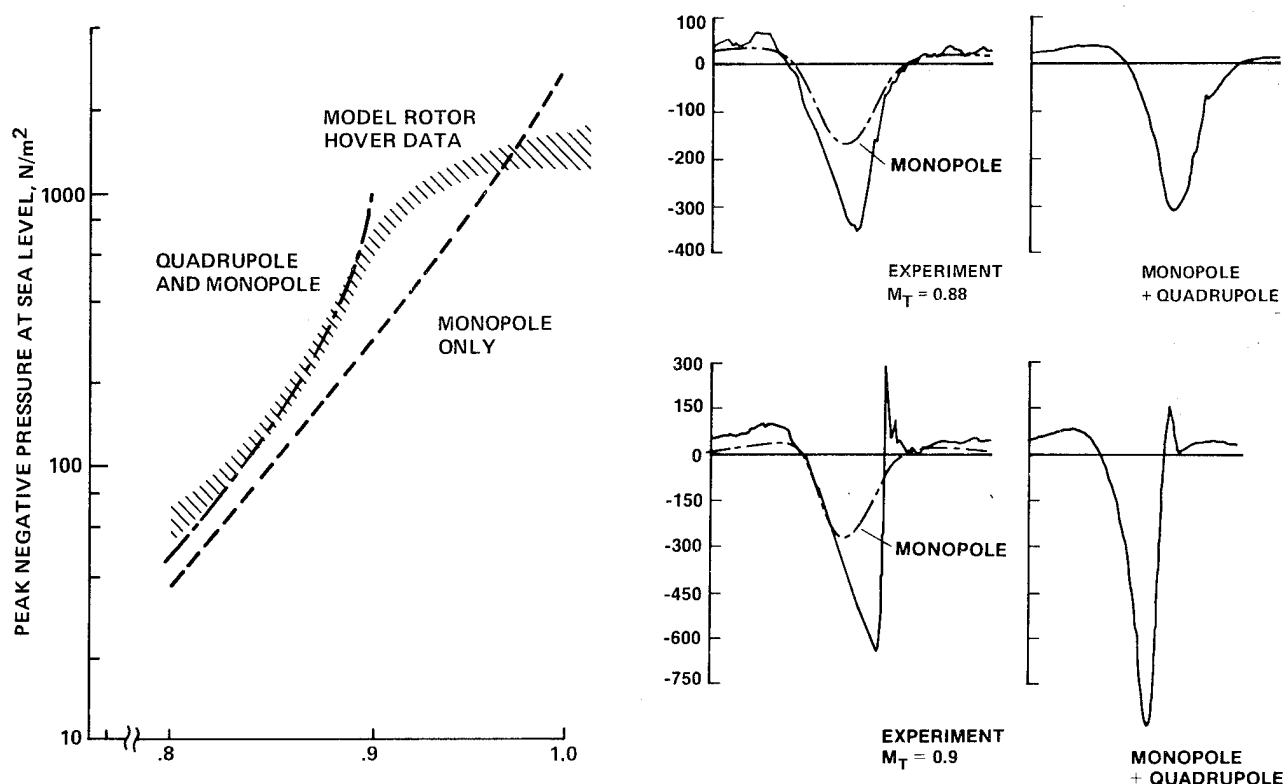


Figure 6.- Comparison of theory and experiment in hover, in-plane, $r/D = 1.5$.

At Mach numbers below the delocalization Mach number (0.9 for the NACA 0012 airfoil with a rectangular planform), the waveform shape is basically symmetrical and good correlation in amplitude and waveform shape is observed. At the tip Mach number of 0.90, the nonlinear quadrupole term changes waveform shape dramatically and increases in amplitude, leading to good agreement in pulse shape. This is a reflection of the fact that local shocks are propagating from the surface of the airfoil to the acoustic far field. However, in these comparisons, the amplitude is now overpredicted at or above a tip Mach number of 0.9 even though the waveform changes from the symmetric to saw-tooth shapes at the correct Mach number as shown in the experimental data. This has suggested several areas where improvements can be made, and they are discussed in the following sections.

The experimental verification of this computational code is less satisfactory because of a lack of high quality near-field experimental data. In order to improve this situation, a new experimental technique, called optical holographic interferometry/computerized tomography, has been developed. A powerful pulsed ruby laser recorded 40 interferograms with a 2-ft view field around the model rotor blade tip operating at a tip Mach number of 0.9 (see fig. 7). After digitizing interferograms and extracting fringe-order functions, the computerized tomography code reconstructed the flow field, providing pressure coefficient contours in several planes as shown in figure 8 (refs. 11-13). The results from this holographic technique give very good agreement with previously obtained numerical computations and laser

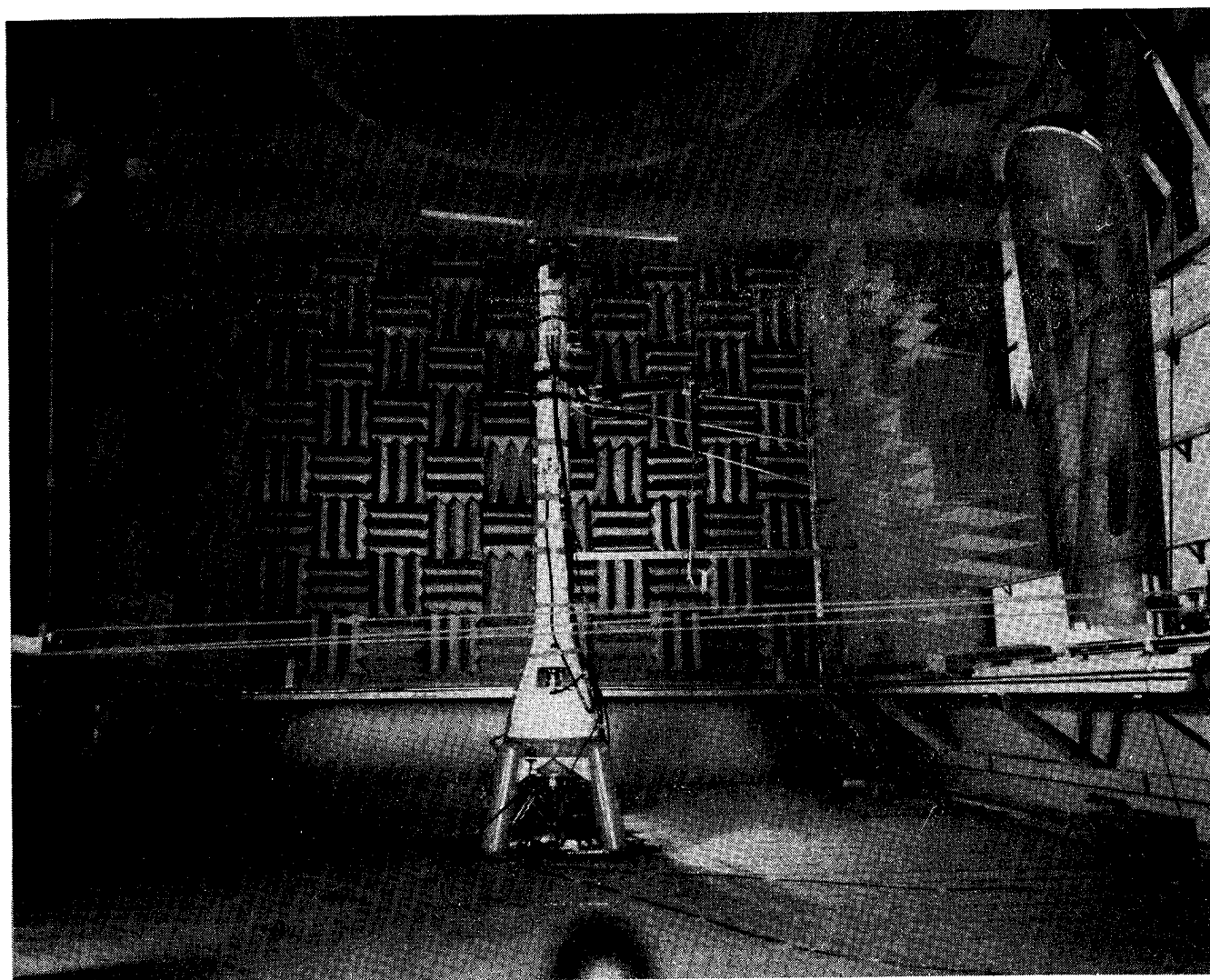


Figure 7.- Holographic interferometry setup.

velocimeter measurements of the aerodynamic flow field surrounding the rotor. Several important features of the holographic technique are (1) the lack of geometrical constraints in the optical system leads to the ability to conduct large-scale, nonlaboratory tests, (2) a single photo film contains a large volume of instantaneous three-dimensional flow information, providing a substantial reduction in test time, and (3) the reconstruction procedure can be performed in a laboratory, not in the test section where interferograms are recorded.

Therefore, the holographic technique with the computerized tomography proved to be a highly effective way to measure the large volume of the instantaneous three-dimensional, transonic flow field surrounding a rotor blade.

Another potential acoustic prediction method has been developed for the high-speed impulsive noise phenomenon using the methods of geometrical acoustics and computational fluid dynamics (CFD). With the geometrical acoustics approximation,

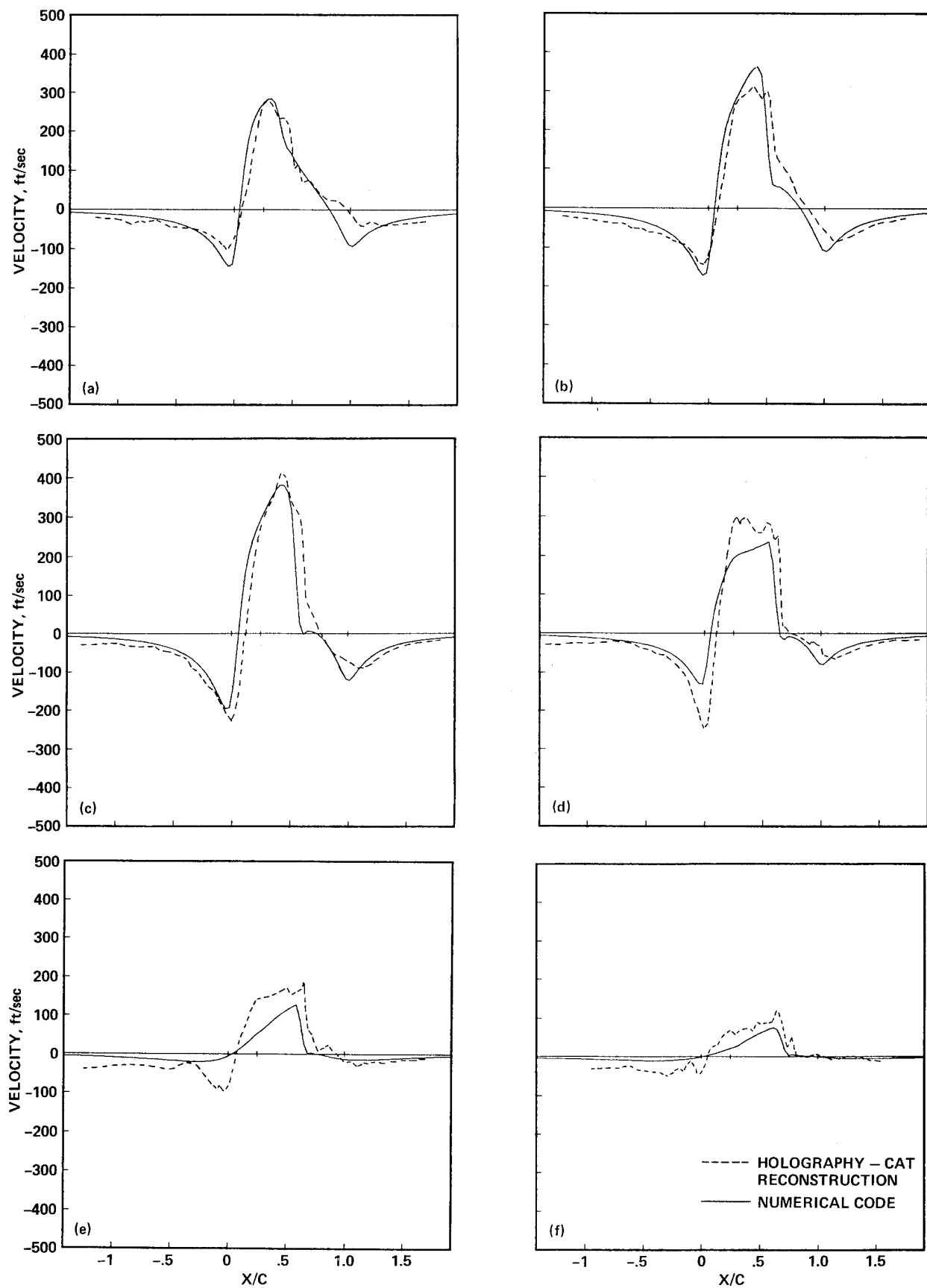


Figure 8.- Perturbation velocity distributions at six radial locations for $Y/C = 0.8$ above blade centerline. (a) $R/R_0 = 0.88$; (b) $R/R_0 = 0.92$; (c) $R/R_0 = 0.96$; (d) $R/R_0 = 1.00$; (e) $R/R_0 = 1.04$; (f) $R/R_0 = 1.08$.

the new Kirchhoff formula was developed by Isom (ref. 14), in which the quadrupole volume integral in the Ffowcs Williams and Hawkings formulation is reduced to a surface integral over the plane tangent to the sonic cylinder. Then, the initial data on the sonic cylinder are obtained from a transonic CFD code that solves the full potential equation in the near aerodynamic nonlinear field. Since CFD codes are less successful in the far field, this new approach combines the near-field aerodynamic calculation from a CFD code with the geometrical acoustic approximation in the acoustic far field (ref. 15).

3. BLADE-VORTEX INTERACTION (BVI) NOISE

The physical understanding of blade-vortex interaction noise is not as complete as is that of high-speed impulsive noise. Although there have been many experimental and theoretical efforts which have shown progress in understanding the generating mechanisms, only a few qualitative design changes have resulted. Similar to questions raised about high-speed impulsive noise, the following questions will be discussed:

1. Can BVI noise be scaled, and if so, what are the scaling parameters?
2. What are the known physical origins of BVI noise?
3. How accurately can BVI noise be predicted?

A comparison of the acoustic signatures of the Operational Loads Survey (OLS) model tests in both the CEPRA-19 and DNW anechoic wind tunnels with the 540 rotor full-scale flight test is shown in figure 9. A microphone is located approximately 30° beneath the plane of the rotor tips. This relative orientation of the microphone is known to maximize the blade-vortex interaction noise and reduce the magnitude of high-speed impulsive noise. The average time history of acoustic signatures from the model- and full-scale rotor systems become strikingly similar when the four important nondimensional scaling parameters are matched: advancing tip Mach number, advanced ratio, $C_{T/\sigma}$, tip-path-plane angle. (A more complete picture of the comparison of model- and full-scale blade vortex interaction noise is shown in ref. 16.) Good general agreement in amplitude as well as pulse shapes between model- and full-scale tests is apparent at all descent conditions at low advance ratios ($\mu \leq 0.2$). At high advance ratios, the BVI phenomenon was not well scaled. The reasons for this are not known at the present time.

There were several tests performed to simultaneously measure the acoustic and aerodynamic field so that the aerodynamic data could be used as input to acoustic prediction codes. A major full-scale experiment was carried out by a joint U.S. Army/Bell Helicopter program, called the Operational Loads Survey (OLS). Several small scale OLS-model wind tunnel tests were also performed in the 14 x 22 Foot Wind Tunnel (ref. 17) and CEPRA-19 and DNW anechoic wind tunnels (refs. 18 and 19). From these tests, one of the most important findings was that the BVI phenomenon was seen to be concentrated near the very leading edge of the blade chord. Furthermore, the

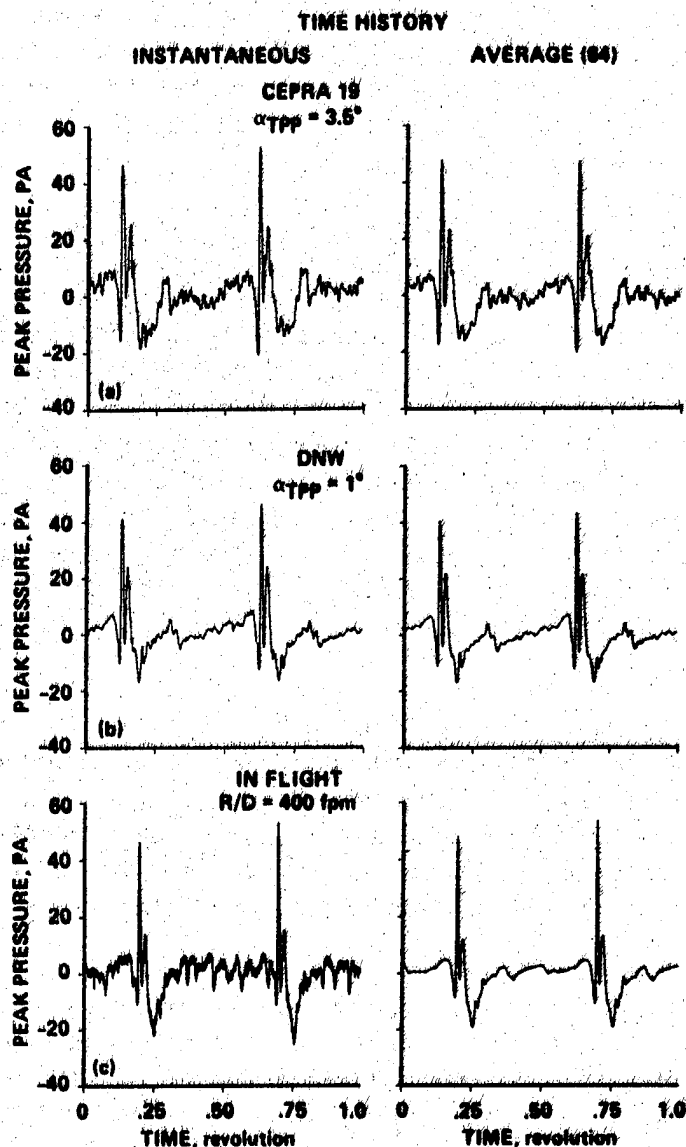


Figure 9.- Rotor acoustic comparisons, 30° below rotor-plane microphone: $\mu = 0.164$, $M_{AT} = 0.772$, $C_T = 0.0054$. (a) CEPRA 19 time-history, $\alpha_{Tpp} = 3.5^\circ$; (b) DNW time-history, $\alpha_{Tpp} = 1.0^\circ$; (c) full-scale time-history, R/D = 400 ft/min.

interaction of $3/2$ revolution old vortex and the blade in the advancing side appears a strong contributor on the acoustic field, in which the vortex and the blade are positioned almost parallel. Because of the local transonic flow around the leading edge generated by the nearby vortex, the near-discontinuous acoustic pressure propagation was observed in some Schlieren pictures of advancing-side BVI on a small-model rotor in a wind tunnel (ref. 20).

To predict the acoustic pressure measurements, equation (1) can be used where only the pressure term (acoustic dipole sources) is used. A computer model of the BVI phenomenon from the measured pressure data was constructed which carefully fit the measured data and kept track of the interaction loci. The comparison of the

measured OLS and computed acoustic waveforms are shown in figure 10 (ref. 21). The general waveform was well predicted in the right wing and nose-boom microphones; however, the peak amplitudes are underestimated and the pulse widths overestimated. These discrepancies may be traced to experimental frequency response limitations of the data measurement system, analytical modeling of the measured pressure data, or possibly to the omission of quadrupole sources caused by transonic flow.

Based on the model- and full-scale experiments, it is thought that compressibility plays a significant role in the aerodynamics of BVI. The local transonic flow field which exists during BVI has initially been simplified to a two-dimensional (2-D) encounter with the vortex passing by a stationary airfoil. The governing computational fluid dynamic (CFD) equations are then numerically solved to yield both the aerodynamic forces and the radiated noise. The transonic small disturbance equation was used with a concentrated potential (irrotational) vortex structure to investigate the unsteady pressure fluctuation on the airfoil surface and the propagation of acoustic waves to the far field. The propagating wave and its structure is clearly visible in figure 11 where much more energy is seen to propagate in the upstream direction (ref. 22). It is clear that the computational technique can be used to gain insight into the highly complex nonlinear blade vortex interaction phenomena.

In order to validate computational codes and to improve the physical understanding, other experimental techniques are being developed under the Army supervision to help understand the basic mechanisms of BVI. In one such experiment, an airfoil was placed in a shock tube in the wake of a vortex generator in which the 2-D airfoil-vortex interaction phenomenon was simulated. The event was measured with pressure transducers, high-speed Mach-Zehnder interferometry (ref. 23), and holographic interferometry (ref. 24).

This pioneering computational and experimental work is in the beginning stages of development. These preliminary results are encouraging and reaffirm the importance of leading-edge blade geometry on the BVI problem. In the near future, this work should be able to suggest leading-edge geometries that tend to minimize the airfoil pressure disturbances leading to generation of less BVI acoustic energy that is radiated to the far field.

Because of the importance of the trailing tip vortex strength, blade tip planform should have an important effect on BVI noise. A test was carried out in the NASA Langley 14 x 22 Foot Wind Tunnel to evaluate the potential benefits of tip-shape modification in alleviating blade-vortex interaction noise as shown in figure 12. The results of the program (ref. 25) showed that a tip shape can be designed such that a modest improvement can be achieved in the blade-vortex interaction noise propagation characteristics as compared to a rectangular tip shape. Furthermore, a test program of an advanced blade design for the Army's UH-1 helicopter fleet was also carried out in the 14 x 22 Foot Wind Tunnel to determine the performance benefits provided by rotor blade planform taper as shown in figure 13. It appeared that the advanced rotor design did not significantly reduce the blade-vortex interaction noise, while high-speed impulsive noise could be reduced substantially (about 8 or 9 dB reduction) (refs. 26 and 27).

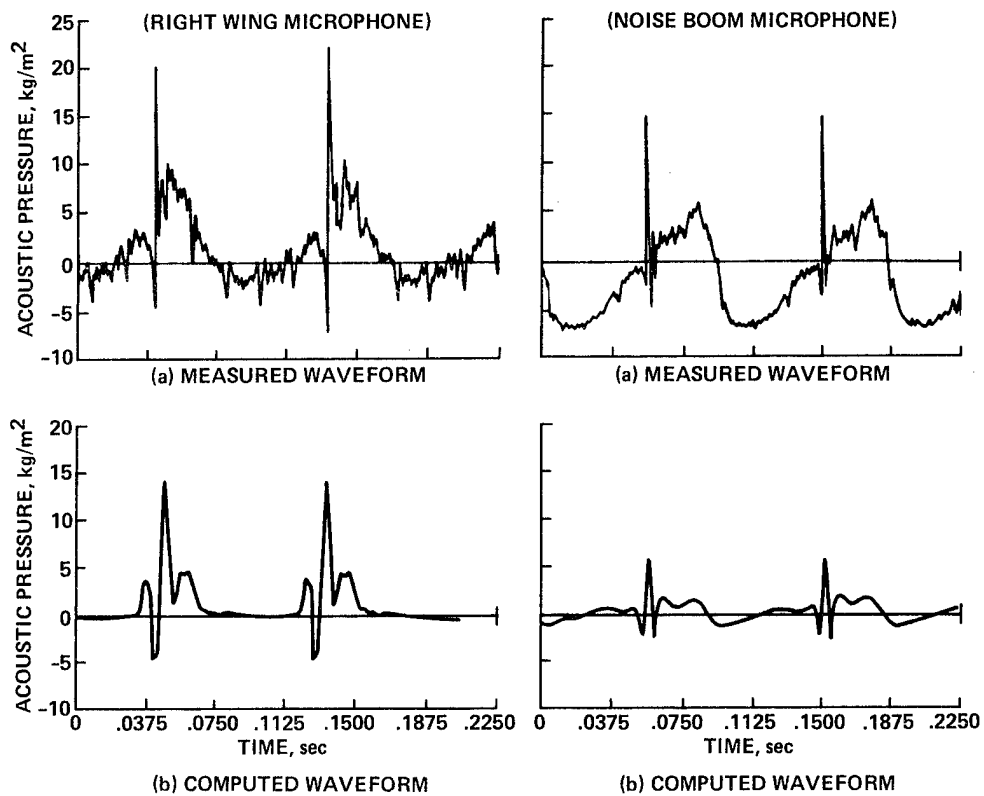
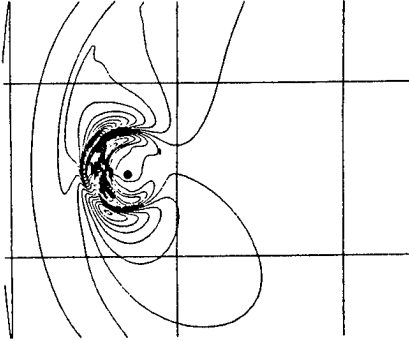


Figure 10.- Comparison of acoustic waveform between measurement and computation.

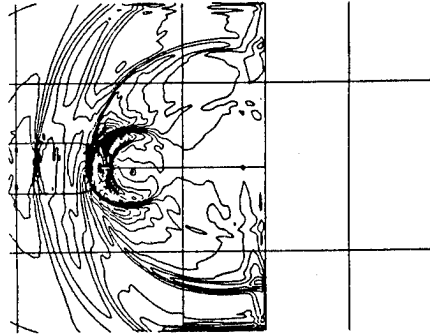
ATRAN 2

NAVIER-STOKES SOLVER

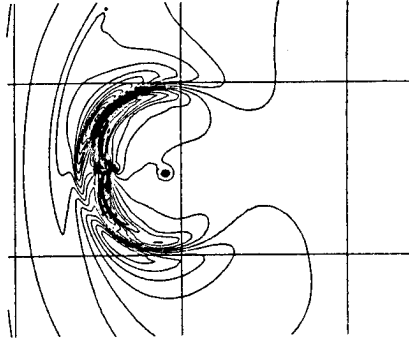
$X_v = 2.00$



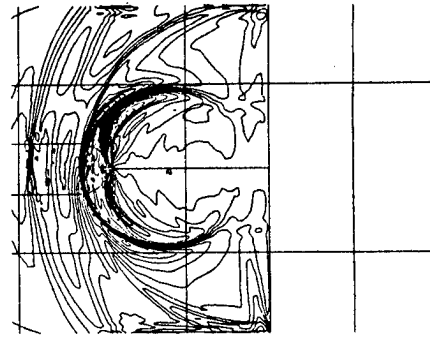
$X_v = 2.00$



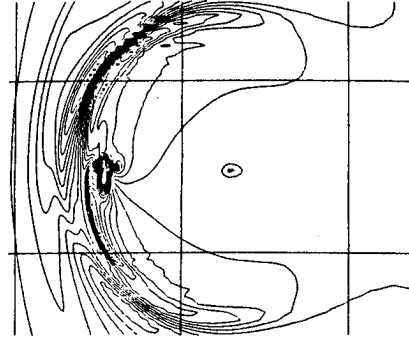
$X_v = 4.00$



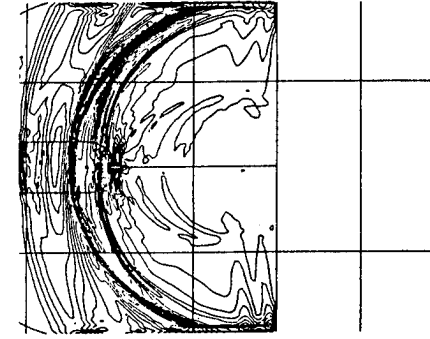
$X_v = 4.00$



$X_v = 8.00$



$X_v = 8.00$



$(C_p - C_{pi}) \cdot \sqrt{R}$

$(C_p - C_{pi}) \cdot \sqrt{R}$

Figure 11.- Wave propagation due to blade-vortex interaction.

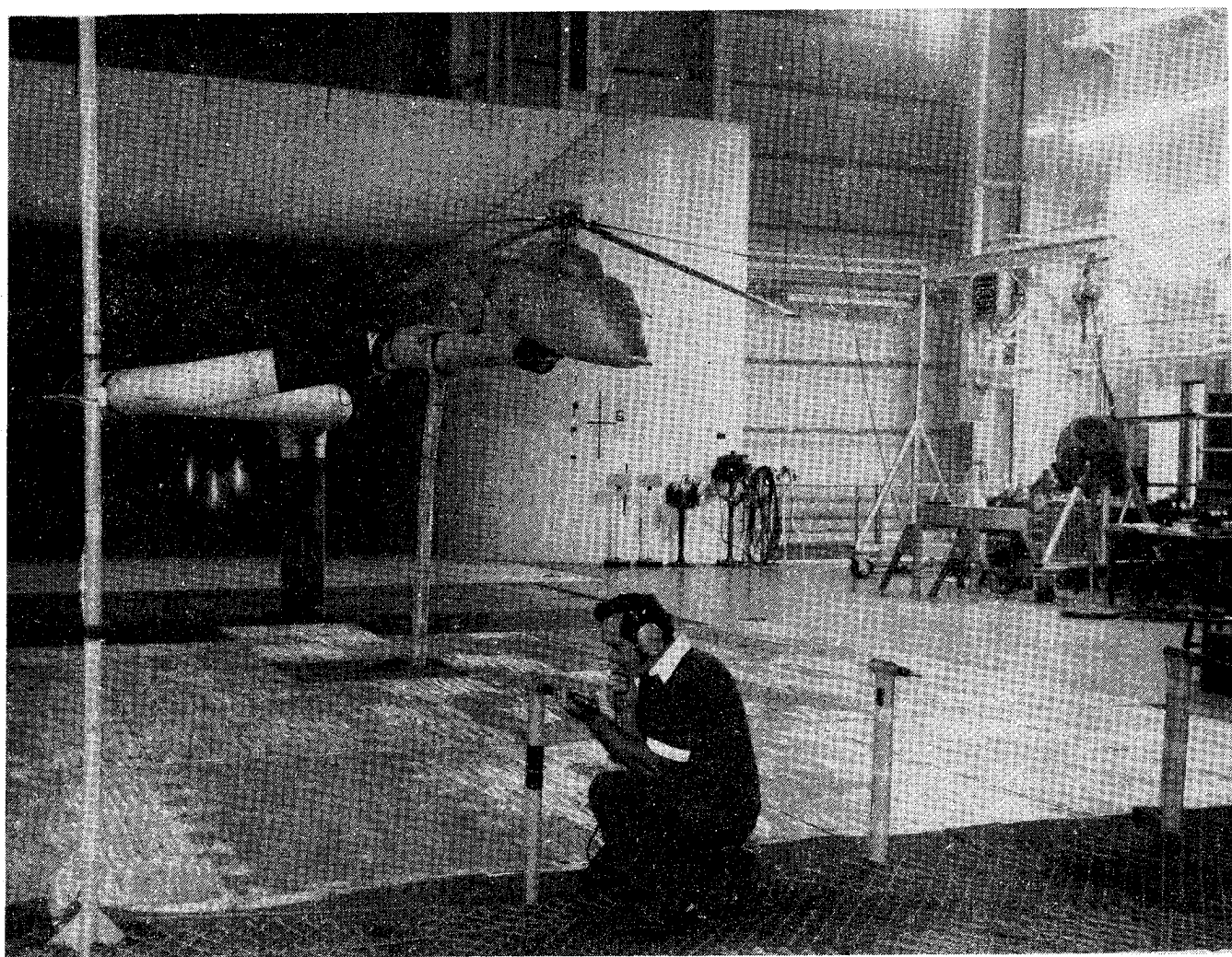


Figure 12.- UH-1 acoustic test at NASA Langley 14 x 22 Foot Wind Tunnel.

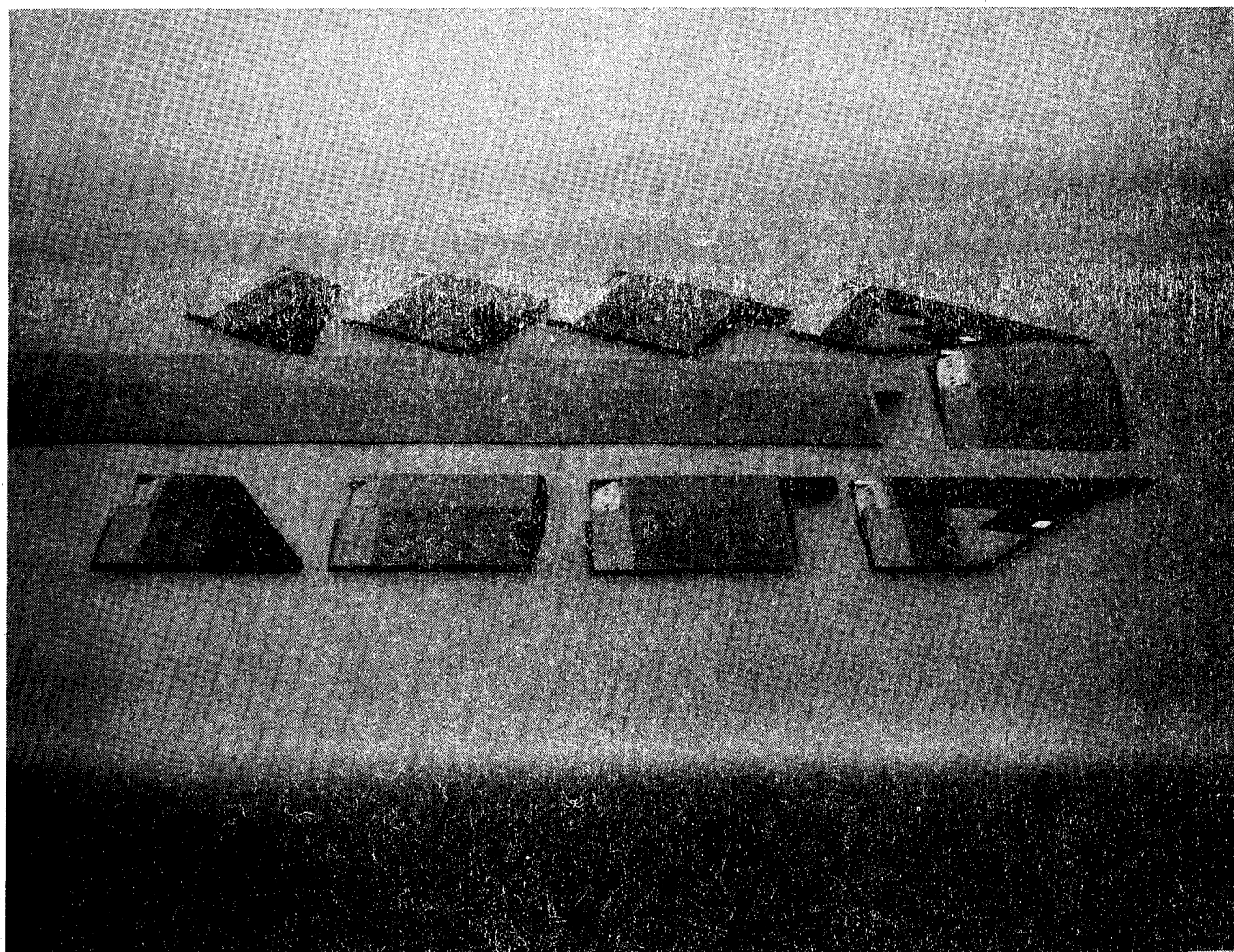


Figure 13.- Tip-shape generic rotor test.

4. ACOUSTIC AND AERODYNAMIC TEST OF A MODEL ROTOR (AATMR) PROGRAM

A new joint program between the Army and the rotorcraft industry has been initiated to take acoustic and aerodynamic measurements in the DNW wind tunnel with advanced, dynamically scaled, pressure instrumented model rotor systems to relate the important aerodynamic phenomena to the near- and far-field acoustic radiation. In particular, high-speed impulsive noise, blade-vortex interaction noise, and low-frequency harmonic noise are being studied. Particular test objectives are (1) to verify existing analytical prediction codes for acoustics and aerodynamics with dynamically flexible blades, (2) to compare the measured data with full-scale flight data and full-scale wind tunnel data and develop scaling parameters, and (3) to improve blade design capabilities.

A first test was performed this past summer under a joint research agreement with the Aeroflightdynamics Directorate (ARTA) and Boeing Vertol. Boeing Vertol furnished a 1/5 dynamically scaled, pressure instrumented model of the BV 360 rotor in the DNW wind tunnel (fig. 14) which was tested by the Army/Boeing-Vertol with NASA's assistance. During the test, the on-line digital data acquisition and processing system gathered extremely accurate acoustic and pressure signatures of the rotor. In addition, very low-speed shadowgraph photographs were taken to define the epicycloid patterns of tip vortex trajectories and a photogrammetry technique was also attempted to measure the live twist distributions of the highly elastic BV 360 rotor blades. The data reduction process is under way and results will be available shortly (ref. 28).

5. CONCLUDING REMARKS

This paper reviews the progress made in helicopter aerodynamically generated impulsive noise by Army researchers over the past decade. From full-scale flight tests and several small-scale model wind tunnel tests, it is clear that high-speed impulsive noise can be scaled and the primary scaling parameter is the advancing tip Mach number. Also improved basic physical understanding of the high-speed impulsive noise generating mechanism and of the delocalization phenomenon has been substantially achieved for use in the design of advanced blades for reduced noise. In the case of blade-vortex interaction (BVI) noise, the physical understanding of the noise generating mechanism is not as complete as that of high-speed impulsive noise. However, the BVI noise can be scaled for low advance ratios and the scaling parameters are advancing tip Mach number, advance ratio, $C_{T/\sigma}$, and tip-path-plane angle. Because of the compressibility effect on BVI aerodynamics, CFD techniques are now emerging for understanding the basic mechanisms of BVI and the associated radiated noise mechanisms. The preliminary results are very encouraging and CFD techniques should help to design a blade for reduced noise. The cooperative programs between the Army, NASA, and industry have been very successful and will be continued.

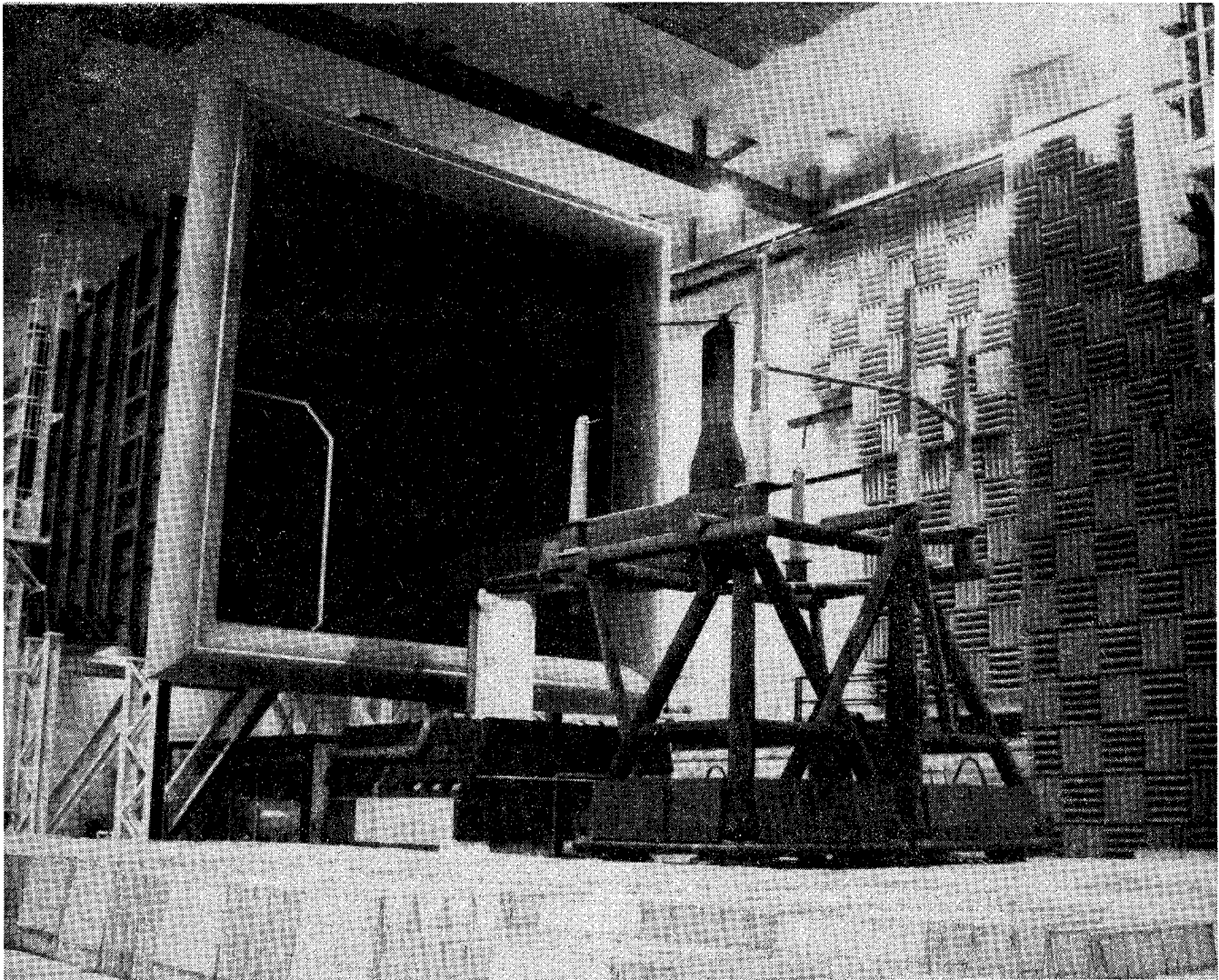


Figure 14.- BV-360 rotor system at the DNW wind tunnel.

6. ACKNOWLEDGMENTS

The authors wish to acknowledge support and contributions of our many friends and colleagues at the Aeroflightdynamics Directorate and Aerostructures Directorate; in particular, Mr. Andrew W. Kerr, Director; Mr. Donald Boxwell; Dr. Francis Caradonna; Mr. Danny Hoad; and Professor Morris Isom. Also, sincere appreciation goes to our many colleagues at the U.S. Army Research Office (ARO), ONERA, DNW, DFVLR, NLR, NASA, and U.S. helicopter manufacturers for their talents and enthusiastic support.

7. REFERENCES

1. Schmitz, F. H.; and Boxwell, D. A.: In-Flight Far-Field Measurement of Helicopter Impulsive Noise. *Journal of the American Helicopter Society*, vol. 21, 1976, pp. 2-16.
2. Boxwell, D. A.; Schmitz, F. H.; Splettstoesser, W. R.; Schultz, K. J.; Lewy, S.; and Caplot, M.: A Comparison of the Acoustic and Aerodynamic Measurements of a Model Rotor Tested in Two Anechoic Wind Tunnels. NASA TM 88364, 1986.
3. Splettstoesser, W. R.; Schultz, K. J.; Schmitz, F. H.; and Boxwell, D. A.: Model Rotor High-Speed Impulsive Noise--Parametric Variations and Full-Scale Comparisons. Presented at the 39th Annual Forum of the American Helicopter Society, May 1983.
4. Boxwell, D. A.; Schmitz, F. H.; Splettstoesser, W. R.; and Schultz, K. J.: Model Helicopter Rotor High-Speed Impulsive Noise: Measured Acoustics and Blade Pressures. Presented at the Ninth European Rotorcraft Forum, Paper 17, Stresa, Italy, Sept. 1983.
5. Boxwell, D. A.; Yu, Y. H.; and Schmitz, F. H.: Hovering Impulsive Noise: Some Measured and Calculated Results. *Vertica*, vol. 3, 1978, pp. 35-45.
6. Ffowes Williams, J. E.; and Hawkings, D. L.: *Philosophical Transactions of the Royal Society London, Series A*, vol. 264, 1969, pp. 321-342.
7. Isom, M. P.: Some Non-Linear Problems in Transonic Helicopter Acoustics. Report 79-19, Department of Mechanical and Aerospace Engineering, Polytechnic Institute of New York, 1979.
8. Farassat, F.; Nystrom, P. A.; and Morris, C. E. K.: A Comparison of Linear Acoustic Theory with Experimental Noise Data for a Small Scale Hovering Rotor. Paper 79-0608, AIAA Aeroacoustic Conference, Seattle, Washington, 1979.
9. Schmitz, F. H.; and Yu, Y. H.: Helicopter Impulsive Noise: Theoretical and Experimental Status. *Journal of Sound and Vibration*, vol. 109, no. 3, 1986, pp. 361-422.
10. Caradonna, F. X.: The Transonic Flow on a Helicopter Rotor. Ph.D. dissertation, Dept. of Aeronautics and Astronautics, Stanford University, 1978.
11. Yu, Y. H.; and Kittleson, J. K.: Reconstruction of a Three-Dimensional Transonic Rotor Flow Field from Holographic Interferograms. *AIAA Journal*, vol. 25, no. 2, Feb. 1987, pp. 300-305.

12. Becker, F.; and Yu, Y. H.: Digital Fringe Reduction Techniques Applied to the Measurements of Three-Dimensional Transonic of Flow Fields. Optical Engineering, vol. 24, no. 3, May/June 1985, pp. 429-434.
13. Kittleson, J. K.; and Yu, Y. H.: Transonic Rotor Flow-Measurement Technique Using Holographic Interferometry. Journal of American Helicopter Society, Oct. 1985, pp. 3-10.
14. Isom, M. P.: Geometrical Acoustics and Transonic Helicopter Noise. Annual Contract Report, NASA Ames Contract NCC 2-172, 1987.
15. Purcell, T. W.; Strawn, R. C.; and Yu, Y. H.: Prediction of High-Speed Rotor Noise with a Kirchhoff Formula, presented at the AHS Specialists' Meeting on Aerodynamics and Aeroacoustics, Arlington, Texas, 1987.
16. Boxwell, D. A.; and Schmitz, F. H.: Full-Scale Measurements of Blade-Vortex Interaction Noise. Paper 80-61, presented at the 36th Annual Forum of the American Helicopter Society, Washington, D.C., May 1980.
17. Hoad, D. R.; and Greene, G. C.: Helicopter Noise Research at the Langley V/TOL Tunnel, NASA CP-2052, 1978.
18. Splettstoesser, W. R.; Schultz, K. J.; Boxwell, D. A.; and Schmitz, F. H.: Helicopter Model Rotor-Blade Vortex Interaction Impulsive Noise: Scalability and Parametric Variations. Paper 18, presented at the Tenth European Rotorcraft Forum, The Hague, The Netherlands, Aug. 1984.
19. Schmitz, F. H.; Boxwell, D. A.; Lewy, S.; and Dahan, C.: A Note on the General Scaling of Helicopter Blade-Vortex Interaction Noise. Presented at the 38th Annual National Forum of the American Helicopter Society, 1982.
20. Tangler, J. L.: Schlieren and Noise Studies of Rotors in Forward Flight. Paper 77, presented at the 33rd Annual National Forum of the American Helicopter Society, Washington, D.C., 1977.
21. Nakamura, Y.: Prediction of Blade-Vortex Interaction Noise from Measured Blade Pressure. Presented at the Seventh European Rotorcraft and Powered Lift Aircraft Forum, Partenkirchen, Garmisch, Germany, 1981.
22. Baeder, J. D.; McCroskey, W. J.; and Srinivasan, G. R.: Acoustic Propagation Using Computational Fluid Dynamics. Presented at the 42nd Annual Forum of the American Helicopter Society, Washington, D.C., June 1986.
23. Meier, G. E. A.: Transonic Noise Generation by Duct and Profile Flow. Technical Report, Max Planck Institut fur Stromungsforschung, Gottingen, Germany, 1984.

24. Mandella, M.; and Bershader, D.: Quantitative Study of the Compressive Vortex: Generation, Structure and Interaction with Airfoils. Presented at the AIAA Aerospace Science Meeting, Reno, Nev., Jan. 1987.
25. Hoad, D. R.: Helicopter-Model Scale Results of Blade-Vortex Interaction Impulsive Noise as Affected by Tip Modifications. Paper 80-62, presented at the AHS 36th Annual Forum, Washington, D.C., 1980.
26. Hoad, D. R.: Evaluation of Helicopter Blade Vortex Interaction Noise for Five Tip Configuration. NASA TP 1608, 1979.
27. Martin, R. M.; Elliot, J. W.; and Hoad, D. R.: Comparison of Experimental and Analytic Predictions of Rotor Blade-Vortex Interactions Using Model Scale Acoustic Data. Paper 84-2269, presented at the AIAA/NASA 9th Aeroacoustics Conference, Williamsburg, Va., Oct. 1984.
28. Dadone, L.; Dawson, S.; Boxwell, D. A.; and Ekquist, D.: Model 360 Rotor Test at DNW---Review of Performance and Blade Airload Data. Presented at the 43rd Annual Forum of the American Helicopter Society, St. Louis, Mo., May 1987.



Report Documentation Page

1. Report No. NASA CP-2495		2. Government Accession No.		3. Recipient's Catalog No.	
4. Title and Subtitle NASA/Army Rotorcraft Technology Volume II - Materials and Structures, Propulsion and Drive Systems, Flight Dynamics and Control, and Acoustics				5. Report Date February 1988	
				6. Performing Organization Code RJ	
7. Author(s)				8. Performing Organization Report No.	
				10. Work Unit No.	
9. Performing Organization Name and Address Office of Aeronautics and Space Technology National Aeronautics and Space Administration				11. Contract or Grant No.	
				13. Type of Report and Period Covered Conference Publication	
12. Sponsoring Agency Name and Address National Aeronautics and Space Administration Washington, DC 20546				14. Sponsoring Agency Code	
15. Supplementary Notes The conference was jointly sponsored by the National Aeronautics and Space Administration and the Department of the Army, with the participation of industry coordinated by the American Helicopter Society, Inc.					
16. Abstract The 1987 NASA/Army Rotorcraft Technology Conference was held at Ames Research Center, Moffett Field, California, March 17-19, 1987. The Conference Proceedings is a compilation of over 30 technical papers presented at this milestone event which reported on the advances in rotorcraft technical knowledge resulting from NASA, Army, and industry rotorcraft research programs over the last 5 to 10 years. The Conference brought together over 230 government, industry, and allied nation conferees to exchange technical information and hear invited technical papers by prominent NASA, Army, and industry researchers covering technology topics including aerodynamics, dynamics and aeroelasticity, propulsion and drive systems, flight dynamics and control, acoustics, systems integration, and research aircraft.					
17. Key Words (Suggested by Author(s)) helicopter flight dynamics rotor aerodynamics and control rotor dynamics propulsion acoustics				18. Distribution Statement Unclassified - Unlimited Subject Category 01	
19. Security Classif. (of this report) Unclassified		20. Security Classif. (of this page) Unclassified		21. No. of pages 585	
				22. Price A25	